SYNTHESIS, KINETICS, AND MECHANISM OF CATALYTICALLY ACTIVE AMINIC RADICAL-TRAPPING ANTIOXIDANTS

&

DEVELOPMENT OF THE FLUOROMETRIC AND SPECTROPHOTOMETRIC TOOLS USED IN THEIR ANALYSIS

By

Evan Haidasz

A thesis submitted to the Department of Chemistry and Biomolecular Sciences
in conformity with the requirements for the degree of Doctor of Philosophy in Chemistry

University of Ottawa
Ottawa, Ontario, Canada
March 2017

Abstract

Amine and nitroxide based radical-trapping antioxidants (RTAs) have long been known to display remarkable efficacy as inhibitors of hydrocarbon autoxidation. Their unique ability to catalytically trap the chain-carrying peroxyl radicals responsible for oxidative degradation of organic materials has led to their widespread use in petroleum-derived materials. While a great deal of research has been done to understand and expand upon this reactivity, little improvement in the chemistry behind diarylamine and nitroxide RTAs has emerged.

In recent years our group has established that heterocyclic analogues of phenolic and diarylaminic RTAs are more stable to one-electron oxidation than the equivalent phenyl derivatives. This has allowed substitution of these RTAs with strong electron donating groups without compromising their stability to oxidation, and has led to the development of some of the most effective RTAs ever reported – compounds which often have reactivities *ca.* 200-fold greater than the current industrial standards. Herein, we describe the development of novel fluorometric and spectrophotometric methods to measure the reactivities of these RTAs, which replace more traditional approaches that are often laborious and require highly specialised equipment. Co-autoxidations with the highly absorbent probes PBD-BODIPY and STY-BODIPY allow for rapid and convenient measurement of RTA activity under a wide variety of conditions by UV/Vis spectrophotometry. Similarly, the high temperature activity of these RTAs can be measured in heavy hydrocarbon autoxidations, where hydroperoxide formation is monitored through the use of a pro-fluorescent phosphine.

The key step in Korcek's proposed diarylamine catalytic cycle has been studied and found to proceed through different mechanisms depending on the structure of the intermediate *N*,*N*-diarylalkoxyamine. While unactivated alkoxyamines widely react through N-O homolysis/disproportionation to regenerate the diarylamine RTA, activation of either the aryl or alkyl fragments allows regeneration through a more efficient, pericyclic retro-carbonyl-ene (RCE) reaction. Additionally, the mechanism behind the high temperature RTA activity of dialkylnitroxides

– key intermediates in the activity of hindered amine light stabilizers (HALS) – has been evaluated and found to be dependent on *in situ* formation of carboxylic acids. Upon protonation by these acids, dialkylnitroxides become potent RTAs capable of trapping oxygen-centered radicals. The oxoammonium ions arising from this reaction then oxidize alkyl radicals competitively with O_2 addition to regenerate the nitroxide.

Lastly, we have extended the strategy used for heterocyclic phenols and diarylamines to the development of highly reactive azaphenoxazine and azaphenothiazine RTAs. While synthesis of these compounds is complicated by the presence of a favorable smiles rearrangement, synthesis of the 'correct' isomers yields *extremely* potent RTAs, capable of trapping peroxyl radicals under diffusion control. Applying these compounds in both ambient and high temperature autoxidations reveals that they may be some of the most effective RTAs ever reported, outperforming even the most reactive of the heterocyclic diarylamines previously studied.

Acknowledgements

Over my time here, I have been extremely fortunate to work alongside a group of hard-working, dedicated, and incredibly knowledgeable people. I would like to thank my supervisor Derek Pratt for his expert advice, guidance, support, and the many things I have learned working for him over the years. I would also like to thank Keith Ingold for his insight into much of the chemistry I've worked with, and all of his helpful advice over the years.

Thank you to all the members of the Pratt Group (past and present). There are way too many people to mention them all, but a particular thank you goes to JP Chauvin, Markus Griesser, Ron Shah, Zosia Zielinski, Omkar Zilka, Kareem Harrison, Pierre Faudot-dit-Bel, Jia-Fei Poon, Luke Farmer, Anthony Van Kessel, and Derek Meng. I am also very grateful for the help of Jay Hanthorn who taught me a great deal about chemistry during my Honours project and early years of graduate school.

I also want to give a huge thank you to everyone in my family. This would likely have been impossible without the overwhelming support I received from my parents, grandparents, aunts, uncles, and siblings.

Statement of Originality

I hereby certify that all of the work described in this thesis is the original work of the author, with exceptions for work performed by collaborators noted in the preface to each chapter. The work in this thesis draws upon a great deal of previously published research. Any published (or unpublished) work by others is cited and fully acknowledged within the references.

Evan Haidasz

Table of Contents

List of Schemes

List of Figures

List of Tables

List of Abbreiviations

α-TOC	α-tocopherol
AAPH	2,2'-azobis-(2-amidinopropane) monohydrochloride
AIBN	azobisisobutyronitrile
BDE	bond dissociation enthalpy
BHA	butylated hydroxyanisole (2,6-di-*t*-butyl-4-methoxyphenol)

BHT	butylated hydroxytoluene (2,6-di-*t*-butyl-4-methylphenol)
CV	cyclic voltametry
DKIE	deuterium kinetic isotope effect
DPA	diphenylamine
DPPH	2,2-diphenyl-1-picrylhydrazyl
DPV	differential pulse voltametry
DMF	dimethylformamide
DMSO	dimethylsulfoxide
DTA	ditolylamine
EDG	electron donating group
EPR	electron paramagnetic resonance
GC	gas chromatography
HALS	hindered amine light stabilizers
HOMO	highest occupied molecular orbital
HPLC	high-pressure liquid chromatography
IP	ionization potential
KSE	kinetic solvent effect
LUMO	lowest unoccipied molecular orbital
NHE	normal hydrogen electrode
PCET	proton coupled electron transfer
PET	photoinduced electron transfer
RCE	retro-carbonyl-ene
RTA	radical trapping antioxidant
SOMO	singly occupied ,olecular orbital
TEMPO	(2,2,6,6-tetramethylpiperidin-1-yl)oxyl
TFA	trifluoroacetic acid
THF	tetrahydrofuran
TS	transition state

CHAPTER 1: Background and Significance

1.1 Hydrocarbon Autoxidation

Autoxidation is the spontaneous, radical-mediated oxidative degradation of hydrocarbons (RH). All hydrocarbon materials exposed to an aerobic atmosphere are susceptible to this to varying degrees – from the saturated hydrocarbons predominant in petroleum-derived consumer products, to the lipids which comprise the biological membranes in living organisms.[1,2] Not only does autoxidation convert the hydrocarbon substrate to its corresponding hydroperoxide (ROOH), but the hydroperoxide products themselves often decompose to yield further mixtures of alcohols, aldehydes, ketones, esters, and/or carboxylic acids,[3-5] many of which are toxic and have unwanted physical or chemical properties.

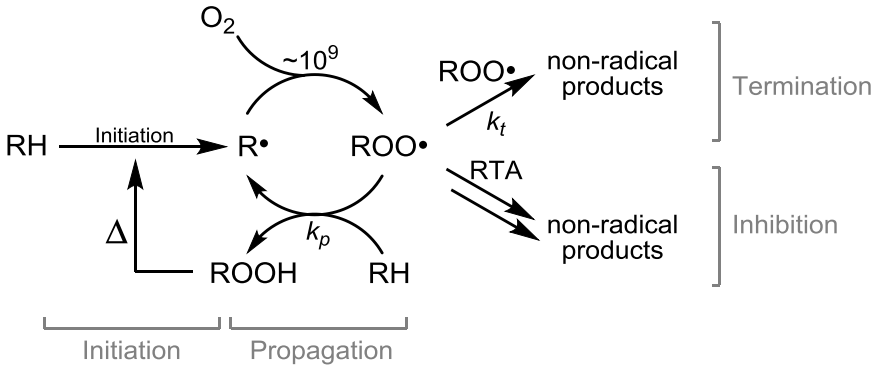

Scheme 1.1. Radical chain mechanism of hydrocarbon autoxidation.

Since the late 1950s, a great deal of effort has been devoted to understanding and controlling autoxidation due to its importance both in extending the lifetime of hydrocarbon materials, and its implication in many degenerative diseases. The different reactions involved in autoxidation can be broadly categorized into four separate classes: initiation, propagation, termination, and inhibition (Scheme 1.1).[1,2] Initiation reactions are those processes which generate radical species within the reaction. Propagation reactions encompass the chain carrying steps in autoxidation, and are

responsible for the majority of hydroperoxide formation. Termination and inhibition reactions both remove chain-propagating radicals from the reaction – either by the self-reaction of two substrate-derived radicals (termination), or by their reaction with other compounds known as radical-trapping antioxidants (inhibition).

1.1.1 Initiation

The radical species which initiate autoxidation are often generated by either thermal or photochemical processes acting on a weak bond present in the mixture (e.g. photooxidation of trace aldehydes[6,7]). Homolysis of these weak bonds yields two initiator-derived radicals (In•) which then react with the hydrocarbon substrate to form carbon centered radicals (eqs 1.1 and 1.2).[1,2]

$$In_2 \xrightarrow{R_i} 2\ In\bullet \qquad (1.1)$$

$$In\bullet + RH \longrightarrow InH + R\bullet \qquad (1.2)$$

The hydroperoxides produced as a product of autoxidation are also radical initiating species. Upon photolysis or thermolysis, hydroperoxides produce alkoxyl and hydroxyl radicals (RO•/HO•) which rapidly abstract H-atoms from the substrate and initiate radical chains.[8] Since each hydroperoxide produced in a chain reaction can subsequently initiate two additional chains, the rate of initiation (R_i) in the reaction increases as hydroperoxides are produced, and autoxidation in these systems is autocatalytic.[9] Furthermore, autocatalytic behaviour isn't limited to high temperatures where thermolysis of hydroperoxides is rapid. In the presence of low-valent metals/metal ions (e.g. Fe^{II} in biological systems, or metal components in mechanical systems), reductive heterolysis of the hydroperoxides by Fenton-type reactions will also yield radicals capable of starting a chain ($RO\bullet/HO^-$ *or* $RO^-/HO\bullet$).[10] In autoxidation experiments run at or near ambient temperatures, initiation from these sources is typically slow; as such, small amounts of a radical initiator, such as 2,2'-azo bis(2-methylpropionitrile) (AIBN), are added to the reaction in order to generate radicals at a constant rate.

1.1.2 Propagation

Propagation of the chain reaction is responsible for the vast majority of hydroperoxide formation during autoxidation. In the first step, oxygen adds rapidly to a substrate-derived alkyl radical (k_{O2} ~ 3 × 10^9 $M^{-1}s^{-1}$)[11] to yield the corresponding peroxyl radical (eq 1.3). This radical then abstracts a H-atom from another molecule of substrate, yielding a hydroperoxide and a new substrate-derived alkyl radical (eq 1.4).

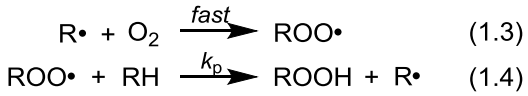

The second-order rate constant for this reaction (k_p) is related to the C-H bond dissociation enthalpy (BDE) of the most activated bond(s) in the substrate. For example, while saturated alkanes autoxidize quite slowly under ambient conditions,[12] more activated substrates such as those bearing benzylic, allylic, or α-alkoxy substituents react considerably faster (Figure 1.1).[13,14]

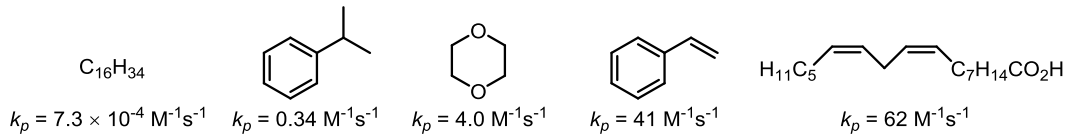

Figure 1.1. Structures and propagation rate constants (k_p) of representative hydrocarbon substrates.

Autoxidation of alkenyl aromatic substrates, such as styrene or indene, is propagated largely by addition of peroxyl radicals across the alkene, with the resulting benzylic radicals undergoing O_2 addition to yield another peroxyl radical.[13] In these cases, rather than producing hydroperoxides directly, the primary products are oxygen-substrate co-polymers (Scheme 1.2). However, the kinetic behaviour of the autoxidation and its inhibition by radical-trapping antioxidants (RTAs) remains the same.[15,16]

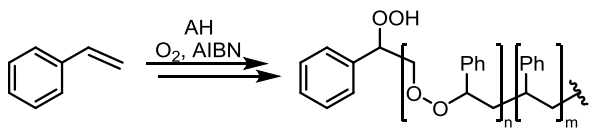

Scheme 1.2. Formation of oxygen-substrate copolymers in the autoxidation of styrene.

1.1.3 Termination

Termination reactions occur between two substrate-derived radicals, eliminating both from the reaction to yield non-radical products. While termination reactions can occur between any two chain-carrying radicals in the reaction (eqs 1.5-1.7), the rapid addition of O_2 to alkyl radicals (*vide supra*) reduces the steady state of R• such that termination between two ROO• (eq 1.7) is the predominant pathway under most conditions.

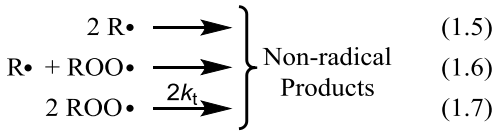

The mechanism of peroxyl radical termination depends on the structure of the radical.[17] Tertiary peroxyls, such as ^{t}BuOO• and CumylOO•, undergo termination followed by fragmentation and in-cage recombination of alkoxyl radicals, yielding di-*tert*-alkyl peroxides (Scheme 1.3).[18] Alternatively, primary and secondary peroxyl radicals undergo termination through a similar mechanism to that first proposed by Russell,[19] although recent computational studies by Coote[20] suggest that this reaction proceeds by the same asymmetric cleavage as *tert*-alkyl peroxyls, and forms the triplet ketone as the immediate product.

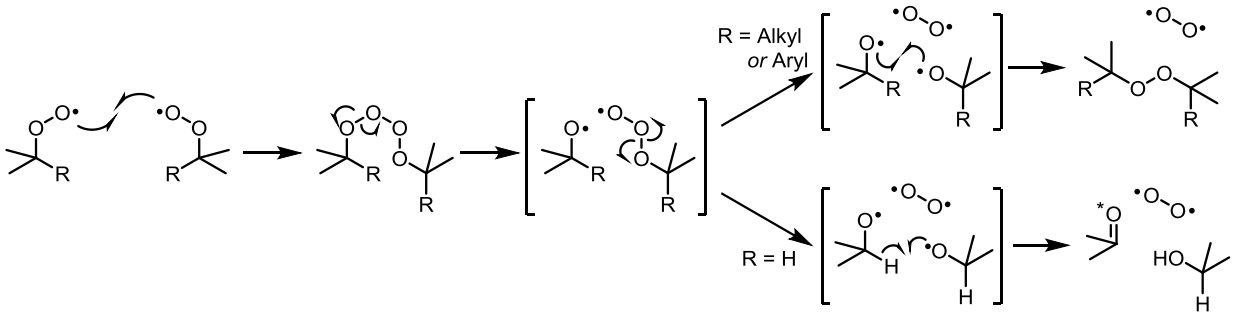

Scheme 1.3. Mechanisms for the termination of *tert*-alkylperoxyl or *sec*-alkylperoxyl radicals.

The second-order rate constants for the peroxyl radical termination (k_t) differ significantly between even similar secondary and tertiary radicals (e.g. $k_t = 2.0 \times 10^7$ vs. 2.3×10^4 $M^{-1}s^{-1}$, for ethylbenzene[13] and cumene,[21] respectively), since those in the latter case cannot undergo α-H-atom

transfer, and instead escape of the alkoxyl radicals from the solvent cage is a more likely outcome.[20] Despite the rapid k_t for reactions between peroxyl radicals, the low steady state concentration of radicals in the reaction means that termination remains quite slow, and the autoxidation can have very long kinetic chain lengths (producing many equivalents of hydroperoxides) before the radicals terminate. For an uninhibited autoxidation with a constant R_i, and assuming a steady state concentration of peroxyl radicals, the rate of hydroperoxide formation (and/or oxygen consumption) can be determined by eq 1.8.[2]

$$\frac{d[\mathrm{ROOH}]}{dt} = \frac{-d[\mathrm{O_2}]}{dt} = \frac{k_\mathrm{p}[\mathrm{RH}]\sqrt{R_\mathrm{i}}}{\sqrt{2k_\mathrm{t}}} \quad (1.8)$$

1.2 Inhibiting Autoxidation

Antioxidants are compounds which inhibit the autoxidative degradation of hydrocarbons. Preventative antioxidants are compounds which slow initiation, often by decomposing hydroperoxides and/or other initiating species (e.g. phosphines and sulfides which reduce ROOH to ROH).[1,2] Radical-trapping antioxidants (RTAs) inhibit autoxidation by trapping chain-carrying radicals and shortening/eliminating the chain reaction. The most effective RTAs target the chain-carrying peroxyl radicals due to their much higher abundance under most conditions.[1,2] While in theory the alkyl radicals can also be trapped by sufficiently reactive RTAs – for example, by nitroxides which react with alkyl radicals at *ca.* 10^8 $M^{-1}s^{-1}$, but are believed not to react directly with peroxyl radicals[22-24] – however, this often requires very high concentrations of RTA in order to be kinetically competitive with O_2 addition.[25]

The rate at which the RTAs trap the propagating radicals is key to their efficacy. More reactive RTAs trap peroxyl radicals faster, shortening the chain length of the reaction, resulting in slower accumulation of hydroperoxides and an extended lifetime of the material. Under autocatalytic

conditions, this also means that R_i will also be kept lower as the reaction progresses, and further consumption of the RTA slower as a result.

1.2.1 Phenolic and Diarylaminic Antioxidants

Phenols and diarylamines (e.g. BHT and diphenylamine, Scheme 1.4) are among the most common RTAs used industrially.[1,2] Both trap peroxyl radicals by proton coupled electron transfer (PCET)[26,27] from their activated O-H or N-H bond, with inhibition rate constants of *ca.* 10^4 $M^{-1}s^{-1}$ for the two examples shown in Scheme 1.4.

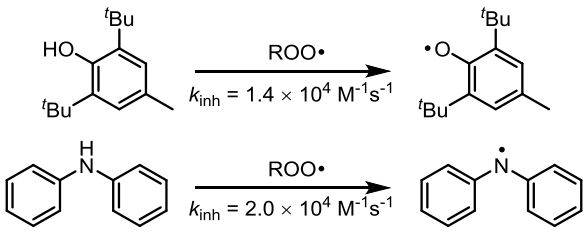

Scheme 1.4. Reaction of BHT and diphenylamine with peroxyl radicals, and their associated rate constants.

The BDEs of the O-H and N-H bonds are among the most important factors for determining the reactivity of the RTAs towards radicals. Evans-Polanyi relationships exist between the BDEs of the reactive bonds and $\log(k_{inh})$ for their inhibition reactions, indicating that compounds with weaker bond trap peroxyl radicals faster (for reactions with similar steric demand).[28,29] Similarly, the BDEs follow positive Hammett correlations versus σ_P^+ (i.e. the reactive bonds are weakened by electron donating groups) – a result of stabilizing the electron-deficient RTA-derived radical.[30,31] Taken together, these relationships predict that RTAs bearing EDGs in the *para*-position on their aromatic rings will have enhanced reactivity towards peroxyl radicals via weaker reactive N-H or O-H bonds. This prediction is verified by experiments showing that $\log(k_{inh})$ for the inhibition reaction also varies linearly versus σ_P^+, with reaction constants, ρ = -1.58 and -1.59 for phenols[31,32] and diarylamines,[28] respectively – consistent with EDGs increasing the rate of the reaction by stabilizing a transition

state that is more electron-poor than its ground state. Furthermore, computational and experimental results confirm that both of these trends also hold true for substituted phenothiazines.[30,33]

Under conditions with a constant R_i, the kinetic behavior of an inhibited autoxidation can be described by eq 1.9, which arises from assuming a steady state concentration of peroxyl radicals, and that all peroxyl radicals are (eventually) trapped via inhibition reactions.[2] The rate constant for the inhibition reaction (k_{inh}) can then be determined from the initial rate of hydroperoxide formation in the inhibited region of an autoxidation reaction.

$$\frac{d[\mathrm{ROOH}]}{dt} = \frac{-d[\mathrm{O_2}]}{dt} = \frac{k_p[\mathrm{RH}]R_i}{nk_{inh}[\mathrm{RTA}]} \quad (1.9)$$

The other important consideration for RTA efficacy is the stoichiometry of the inhibition reaction – how many radicals does an RTA trap? In an inhibited autoxidation with a known R_i, the stoichiometric number, n – defined as the average number of radicals trapped per molecule of RTA – can be determined from the inhibition time, t_{inh}, via equation 1.10.[2]

$$R_i = \frac{n[\mathrm{AH}]}{t_{inh}} \quad (1.10)$$

Under ambient conditions, most phenols have n = 2,[34] first from trapping a peroxyl radical by PCET from the O-H bond, followed by termination of the phenoxyl radical by a second peroxyl (Scheme 1.5). As the temperature is increased, the stoichiometry of phenols decreases (e.g. n = 1.2, for BHT at 160°C),[35] likely due to increased non-productive reactions of the phenoxyl radicals, and/or bond homolysis and initiation by the dialkylperoxide products.[36] It is important to note that the stability of the intermediate RTA-derived radical is essential for effective inhibition. In cases where these radicals can abstract a H-atom from either the substrate or ROOH, the compound would be an ineffective inhibitor and instead would function as a chain transfer agent.[37]

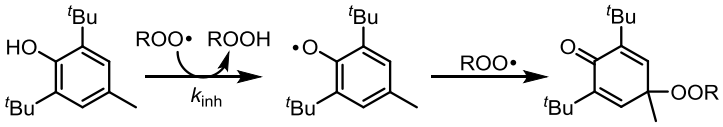

Scheme 1.5. Inhibition mechanism for trapping of peroxyl radicals by a phenolic RTA (BHT).

Diphenylamines, much like phenols, have $n \sim 2$, at ambient temperatures,[38,39] however, upon heating to temperatures >120°C, very high stoichiometric numbers have been observed (e.g. $n = 41$, for diphenylamine at 130°C), implying that products from the initial inhibition reactions retain RTA activity.[40] During their study of this reactivity, Korcek *et. al.* found that in autoxidizing hexadecane at 160°C, bis(4-octylphenyl)nitroxide was converted back to the corresponding amine in up to 70% yield.[41] Furthermore, heating a mixture of O-alkyl bis(4-octylphenyl) alkoxyamines returned the amine in 64% yield. Based on these results, they proposed that diarylamine RTAs proceed through the catalytic cycle depicted in Scheme 1.6 – accounting for the turnover of the amine and the high stoichiometric numbers observed at these temperatures.

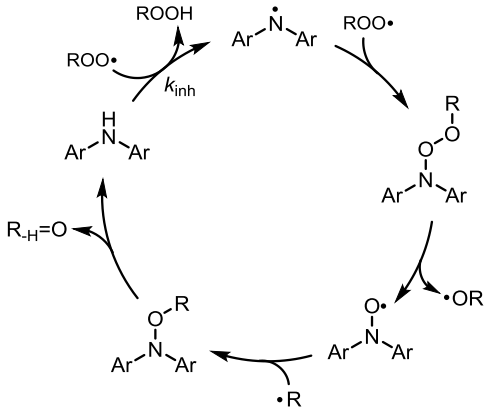

Scheme 1.6. Proposed mechanism for the catalytic activity of diarylamine RTAs (Korcek cycle).

The key step in the transformation is the rate-limiting decomposition of the *N*,*N*-diarylalkoxyamine to regenerate the amine. The reaction is thought to proceed through N-O homolysis (necessitating elevated temperatures to cleave the bond), followed by in-cage disproportionation of the resulting diarylaminyl and alkoxyl radicals.[41] In essence, this pathway

would make use of the *substrate* as the stoichiometric reductant, providing a readily available means to regenerate the diarylamine RTA from its oxidation products.

Based on this mechanism, a path towards further optimization of diarylamine RTAs could be suggested. Substitution of EDGs onto the aromatic rings stabilizes the RTA-derived aminyl radical, weakening the N-H bond and increasing k_{inh} for the inhibition reaction. Similarly, the N-O bond is also weakened by the inclusion of EDGs, which would improve turnover, and bring about an increase in the stoichiometry of the RTA. As such, highly electron rich diarylamines might be expected to offer improved performance over the 4,4'-dialkyldiphenylamines used industrially. However, the oxidation potentials of the RTAs (both phenols and diarylamines) are also greatly reduced by the addition of EDGs – consistent with the expectation that they will stabilize the radical cation arising from one-electron oxidation of the RTA.[28,42] In addition to the radical cation, one-electron oxidation of the RTAs generates other radical species as well, either superoxide (which forms HOO• upon protonation) from the direct reaction with O_2, or RO•/HO• from heterolytic decomposition of hydroperoxides (Scheme 1.7). As such, highly electron rich RTAs tend to produce radicals within an autoxidation rather than trap them – a fact which has largely precluded their development and use.

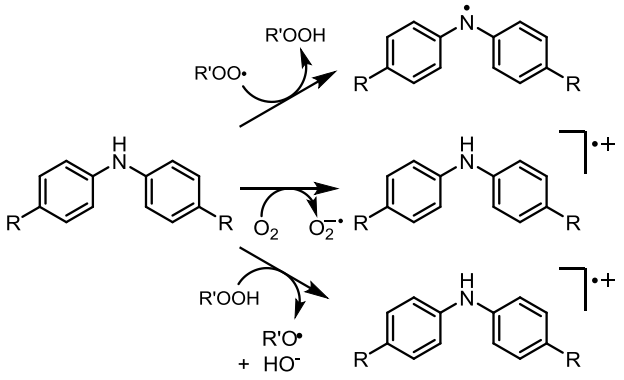

Scheme 1.7. Competing antioxidant and oxidation reactions on substituted diarylamies.

A solution to this problem was advanced some time ago by Pratt *et. al.* when they found that incorporation of heteroatoms into the aromatic rings of phenols greatly increased their oxidation

potentials (E^0) relative to their O-H BDEs (and resulting k_{inh}).[42] This effect was rationalized based on greater destabilization of the positively charged radical cation (arising from one-electron oxidation) by the electronegative heteroatoms relative to the neutral phenoxyl radical. Substituting these more stable pyridinols and pyrimidinols with EGDs yielded incredibly reactive RTAs – capable of trapping peroxyl radicals at nearly diffusion-controlled rates – without compromising their stability to oxidation (Figure 1.2).[42-45]

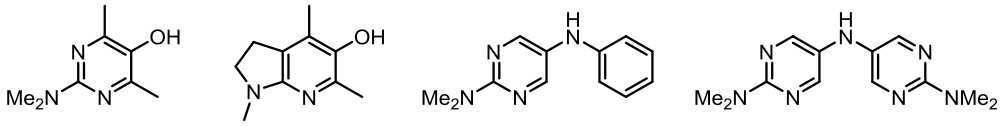

k_{inh} ($M^{-1}s^{-1}$):	8.8×10^6	2.8×10^8	3.0×10^6	1.8×10^7
E^0 ($V_{vs.\ NHE}$):	0.55	n.d.	0.81	0.65

Figure 1.2. Inhibition rate constants (k_{inh}) and oxidation potentials (E^0) of selected heterocyclic RTAs.

This approach was subsequently applied to the synthesis of heterocyclic diarylamines,[46] some of which were found to possess reactivities *ca.* 200-fold greater than industrially standard dialkyldiphenylamines.[28] However, at the time of their initial publication, the high temperature reactivity of these RTAs had yet to be explored.

1.2.2 Phenothiazine and Phenoxazine Antioxidants

Phenothiazines have long been known to be potent RTAs,[47-49] and have been used as inhibitors in petroleum-derived products, including lubricating oils, rubbers, and fuels. Much like the diarylamines from which they are derived, they react with peroxyl radicals by PCET from their N-H bond, and their reactivity to peroxyl radicals (k_{inh}) can be controlled in much the same way.[30,33] Phenoxazine, although not as commonly used as an RTA, is also highly reactive to peroxyl radicals. Both phenothiazine and phenoxazine have incredibly weak N-H bonds – a result of the EDG directly incorporated into the tricyclic structure and the enforced planarity of the rings, which further

stabilizes the RTA-derived aminyl radicals.[33] These compounds are highly reactive inhibitors, trapping peroxyl radicals with k_{inh} = 8.8 × 10^6 and 2.9 × 10^7 $M^{-1}s^{-1}$,[33] for phenothiazine and phenoxazine, respectively, approximately 440- and 1450-fold more reactive than the parent diphenylamine (Figure 1.3).

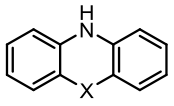

X	N-H BDE (kcal/mol)	k_{inh} ($M^{-1}s^{-1}$)
H,H'	85.8	2.0×10^4
S	79.3	8.8×10^6
O	77.2	2.9×10^7

Figure 1.3. N-H BDEs and inhibition rate constants (k_{inh}) of diphenylamine, phenothiazine, and phenoxazine.

Moreover, despite their high reactivity to peroxyl radicals, phenothiazine and phenoxazine are particularly stable to one-electron oxidation, with E^0 = 0.85 and 0.87 V (vs. NHE),[50] respectively, (Figure 1.4). Furthermore, Lucarini *et. al.* report that phenoxazine is capable of trapping radicals with n = 5 in styrene at 50°C, implying at least some turnover even at moderate temperatures.[33] This seemingly unique balance of reactivity and stability suggests that phenothiazine and phenoxazine present ideal scaffolds for further optimizing the reactivity of aminic RTAs.

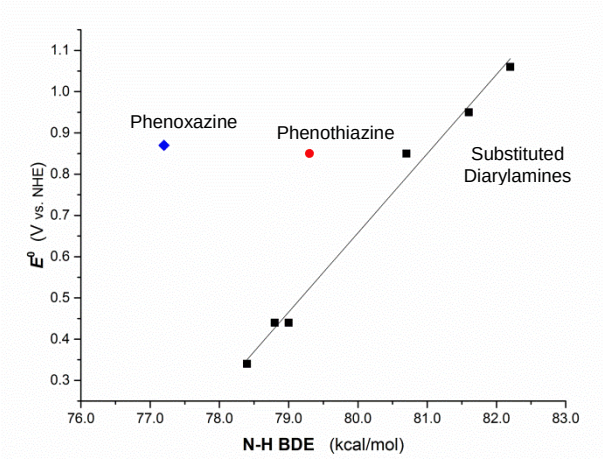

Figure 1.4. Oxidation potential (E^0) vs. N-H BDE for phenothiazine (red), phenoxazine (blue), and a series of diarylamine RTAs (black). The diphenylamines, listed in order of decreasing N-H BDE, are di-*p*-tolylamine, bis(6-methoxypyrdin-3-yl)amine, bis(4-methoxyphenyl)amine, N^5-(4-(dimethylamino) phenyl)-N^2,N^2-dimethylpyrimidine-2,5-diamine, N^5-(6-(dimethylamino)pyridin-3-yl)-N^2,N^2-dimethyl-pyridine-2,5-diamine, and bis (4-dimethylaminophenyl)amine.[28]

1.2.3 Hindered Amine Light Stabilizers

Hindered amine light stabilizers (HALS) are a third class of RTA, and are key additives to plastics, as well as other petroleum-derived products.[2] Dialkylnitroxides are key to the reactivity of HALS, and are formed upon oxidation of the hindered 2° or 3° amines that are initially added to the polymer/hydrocarbon substrate. Hindered nitroxides (e.g. 2,2,6,6-tetramethylpiperidine-*N*-oxyl, TEMPO) have been reported to trap hundreds of radicals per molecule of nitroxide (e.g. n = 510, for TEMPO in paraffin oil at 130°C).[40] Despite the exceptional reactivity of HALS, the mechanism of their action is not nearly as well understood as that of diarylamine RTAs, and is usually described in a general scheme referred to as the 'Denisov Cycle' (Scheme 1.8).

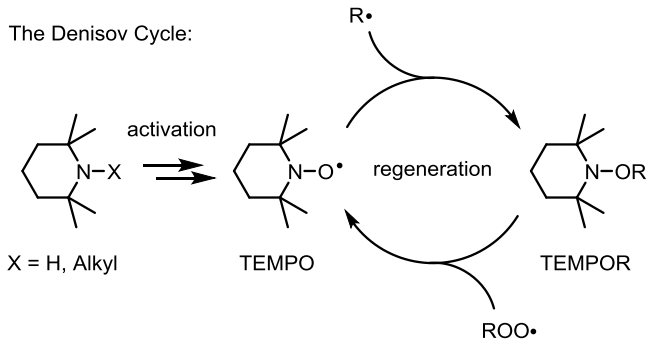

Scheme 1.8. General scheme for the catalytic activity of hindered amine light stabilizers.

Given the well-established results which demonstrate that nitroxides (such as TEMPO) are unreactive to peroxyl radicals,[22] but highly reactive to alkyl radicals ($k_{inh} \sim 10^8$ $M^{-1}s^{-1}$),[23,24] this cycle is generally suggested to involve trapping of an alkyl radical by the nitroxide, followed by regeneration of the nitroxide from its alkoxyamine (e.g. TEMPOR). While many alternative mechanism have been invoked to account for the regeneration of the nitroxide, the most reasonable suggestion involves H-atom abstraction from the alkoxyamine, followed by rapid β-fragmentation of the resulting carbon centered radical, and subsequent oxidation of the hindered aminyl radical (Scheme 1.9).[51]

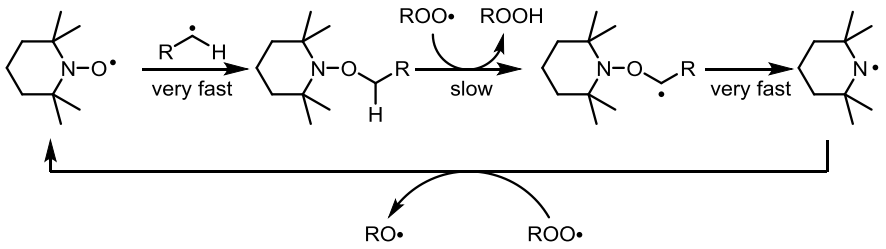

Scheme 1.9. Proposed turnover mechanism for HALS antioxidant activity.

Our group has previously shown that in the presence of acids nitroxides become very potent RTAs capable of trapping oxygen centered radicals at rates approaching diffusion control.[52] Furthermore, in the presence of weak acids, such as acetic or benzoic acid, the nitroxides inhibited for extended periods of time – consistent with incredibly high stoichiometric numbers, such as those measured by Bolsman, Blok, and Frijns at 130°C.[40] It was further found that the nitroxide was not consumed over the course of the reaction, despite the fact that many radicals were being trapped. While nitroxides are known to undergo disproportionation reactions under acidic conditions to produce an oxoammonium ion and a hydroxylamine (k_{inh} = 2.4 × 10^6 $M^{-1}s^{-1}$), the reactivity of the nitroxides under these conditions (e.g. k_{inh} = 7.0 ×10^8 $M^{-1}s^{-1}$, with 4.3 mM TFA) was much greater.[52] Instead, the small amount of protonated nitroxide in the solution was found to function as the formal H-atom donor (via proton-coupled electron transfer), and the oxoammonium ion formed from the inhibition reaction was then being reduced back to the nitroxide by an unknown reductant responsible for the catalytic turnover of the RTA (Scheme 1.10).

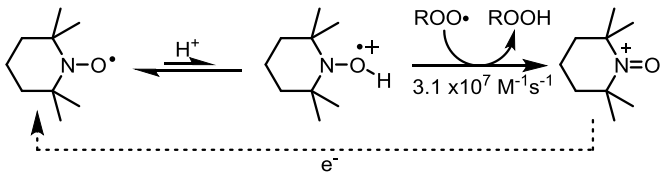

Scheme 1.10. Proposed mechanism for the acid-catalyzed RTA activity of nitroxides.

At the time, the identity of the reductant was unknown, as was the reason that turnover was possible in the presence of weak acids, but not strong ones.

1.3 Techniques for Measuring RTA Activity

The efficacy of an antioxidant is directly related to its reactivity towards peroxyl and (occasionally) alkyl radical species. Over the years many approaches have been developed to attempt to measure the relative activities of different RTAs. A pair of recent reviews discuss many of the advantages and limitations of these different approaches,[53,54] however, a brief discussion will be given here.

1.3.1 Inhibited Autoxidations

The most reliable way to measure the reactivity of RTAs involves kinetic studies of inhibited autoxidations – where the reaction progress of an autoxidation (and its inhibition by an RTA) is directly followed.[53] In these cases the RTA reacts directly with peroxyl radicals carrying an autoxidative chain, and their reactivity is determined based on the competition between propagation and inhibition of the reaction. The autoxidations can be monitored either through consumption of the starting materials (typically O_2) or formation of the hydroperoxide products. The initial rate in the 'inhibited phase' of the reaction and the inhibition time t_{inh} can be used to calculate the stoichiometry and second-order rate constant for the inhibition reaction (n and k_{inh}), through the use of eqs 1.9 and 1.10.[2] In cases involving more complex kinetic behaviour in the reaction (e.g the *in situ* formation of a sulfenic acid RTA from a thiosulfinate precursor),[55] numerical integration using kinetic modeling software can also be used to solve for these vlues.[56]

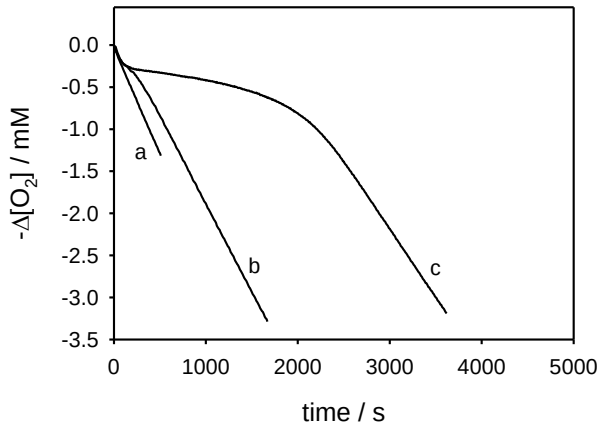

Figure 1.5. Representative oxygen consumption trace. [a)] Uninhibited. [b)] Inhibited by a poorly reactive RTA. [c)] Inhibited by a highly reactive RTA.

Oxygen consumption measurements (Figure 1.5) are among the most general methods for inhibited autoxidation experiments, and can be carried out with a variety of substrates and conditions. In these cases the autoxidation reaction is performed in a sealed flask connected to a differential pressure transducer, which monitors the pressure in the flask relative to a completely inhibited reference reaction.[57] As O_2 is consumed in the reaction, the pressure in the flask decreases and reaction progress is monitored by the pressure differential between the two flasks. Unfortunately, this method necessitates specialized equipment and often requires very high R_i in order to ensure a measurable change in the partial pressure of O_2 above the reaction. The rotating sector technique is a variation on this approach wherein the light source for a photoinitiated autoxidation is regularly interrupted by a rotating sectored disk.[16,32] This modification allows separation of the propagation and termination reactions within the autoxidation by effectively measuring the chain propagation after the (photo)initiation has been stopped.

Alternatively, inhibited autoxidations can be monitored by formation of the oxidation products. In these cases HPLC or GC analysis can used to quantify the oxidation products following reduction of the hydroperoxides by triphenylphosphine. This limits the range of usable substrates to those compounds which produce comparatively few different hydroperoxide products (e.g.

ethylbenzene, tetralin, methyl linoleate, etc.),[58,59] furthermore, substrates which produce polymeric oxidation products (e.g. styrene, indene) cannot be easily analysed.

In cases where complex mixtures of hydroperoxides are produced (e.g. high temperature autoxidation of saturated alkanes),[3] analytical methods that do not directly depend on the structure of the hydroperoxide become necessary. Iodometric titration is the most common technique for analysis of these mixtures; this consists of treating the hydroperoxide sample with I^-, and titrating the resulting I_2 (and I_3^-) with a reducing agent, usually thiosulfate (eqs 1.11-1.13).[53,60]

$$2\,I^- + ROOH + 2\,H^+ \longrightarrow I_2 + ROH + H_2O \qquad (1.11)$$

$$I_2 + I^- \rightleftharpoons I_3^- \qquad (1.12)$$

$$I_3^- + 2\,S_2O_3^{2-} \longrightarrow 3\,I^- + S_4O_6^{2-} \qquad (1.13)$$

This technique is quite laborious as each sample requires individual titrations to determine [ROOH]. Furthermore, it is not specific to hydroperoxides and any oxidizing or reducing agents in the sample that are capable of reacting with I^- or I_2 will influence the results.[53]

1.3.2 Peroxyl Radical Clocks

Radical clocks are a convenient means to determine the kinetics of radical reactions via the competition between a unimolecular reaction with a known rate constant (e.g. intramolecular cyclization, β-fragmentation, etc.),[61] and the bimolecular reaction in question (e.g. H-atom transfer).[62] In the case of peroxyl radical clocks, the competition is often between trapping and β-fragmentation of a peroxyl radical (Scheme 1.11), where the ratio of kinetic and thermodynamic products from the reaction is used to derive k_{inh}.[62,63] Peroxyl radical clocks have been developed based on product ratios in the autoxidation of polyunsaturated fatty acids[62,63] and from decomposition of perester precursors[64,65] – both have been used to measure k_{inh} of phenolic[62] and diarylamine RTAs.[28]

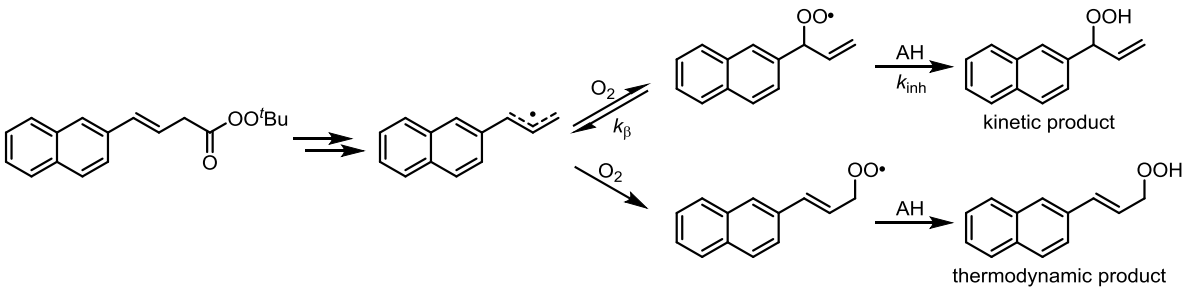

Scheme 1.11. Kinetic competition between trapping and *β*-fragmentation of a peroxyl radical clock.

While clocking experiments provide a practical means to directly determine the kinetics of the reaction between RTAs and peroxyl radicals, no stoichiometric data is gleaned from these experiments, and no information on the fate of the RTA-derived radicals or their behaviour in an autoxidation can be determined.

1.3.3 Antioxidant 'Assays'

Given that many of the methods outlined above require specialized equipment or laborious analyses, it is no surprise that many attempts at more accessible and/or rapid alternatives have been developed.[53] These include, but are not limited to the DPPH assay,[66-68] galvinoxyl assay,[69] TROLOX equivalent antioxidant capacity (TEAC),[70] ferric reducing antioxidant power (FRAP),[71] and cupric reducing antioxidant capacity (CUPRAC).[72] These 'antioxidant assays' are generally based on spectrophotometric determination of a reaction (often an equilibrium) between an oxidant and the RTA as a reductant. Many of these assays do not serve as good (or even adequate) models for peroxyl radicals due to the metal (or organic) ions which function as oxidizing agents, and are only effective in measuring the total reducing equivalents of an electron donor in the solution.[2,53] The kinetics of the reaction between the RTAs and peroxyl radicals – *which are vital to RTA efficacy* – are generally not measured in these assays. Even DPPH, which is isoelectronic with ROO•,[68] reacts with phenolic antioxidants roughly 1000-fold slower than peroxyl radicals (Scheme 1.12) – unless the reaction is in a protic solvent, where the reaction is greatly accelerated due to a change in the

mechanism, namely electron transfer from the trace amounts of the phenoxide anion, followed by protonation of the resulting DPPH anion.[73]

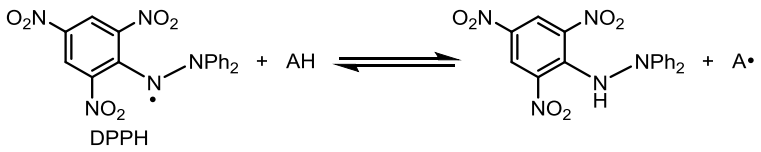

Scheme 1.12. Radical equilibrium between DPPH and an H-atom donor.

While inhibited autoxidations afford the most reliable kinetic and stoichiometric data on the reactivity of RTAs, the convenience of these assays has nonetheless lead to their comparatively widespread (mis)use. The ideal approach would be to develop a method to rapidly carryout inhibited autoxidation experiments, while maintaining the simplicity and convenience of these spectrophotometric assays.

1.4 Research Objectives

1.4.1 A Fluorometric Assay for Quantification of Mixtures of Hydroperoxides

Initially, we were interested in studying the reactivity and turnover of our group's heterocyclic diarylamine RTAs in high temperature autoxidation of heavy hydrocarbons. However, given the difficulty in analysing the complex mixtures of oxidation products arising from the reactions, and the problems associated with iodometric titration of individual samples from each time point, we first sought to develop a more convenient and accurate approach to analyse these reactions. While there are many examples of fluorescent probes for the detection of reactive oxygen species and oxidation products, there has not been an effective method for *quantification* of hydroperoxides. Taking inspiration from the pro-fluorescent phosphine probes used by Bertozzi to monitor progress in the Staudinger ligation,[74] we envisioned a phosphine-conjugated fluorophore where, in its reduced state, the phosphine lone pair would quench the fluorescence of the probe by photoinduced electron

transfer. However, upon oxidation of the phosphine by ROOH, the fluorescence of the probe would increase, and could be used to quantify [ROOH].

The objectives of this project were to:

1. Synthesize a phosphine-conjugated fluorophore which exhibits significant fluorescence enhancement upon oxidation of the phosphine.
2. Characterize the reactivity of the probe with a model secondary hydroperoxide, such that the fluorescence enhancement could be used to quantify [ROOH] in unknown samples from the autoxidation of *n*-hexadecane.
3. Apply this methodology to monitor the high temperature autoxidation of *n*-hexadecane (160°C, based on the work of Mahoney[3]), and inhibition of the autoxidation by RTAs – including the highly reactive heterocyclic diarylamines previously developed by our group.

1.4.2 A Spectrophotometric Approach to Inhibited Autoxidations

The ideal approach to determine the reactivity of RTAs involves kinetic studies of inhibited autoxidations – often by oxygen uptake experiments. The inaccessibility of these experiments (due to both the effort and specialized equipment required) has led to the use of dubious 'antioxidant assays' to measure the 'reactivity' of RTAs. In an effort to simplify the methodology behind inhibited autoxidations and streamline measurements on the activity of RTAs, we sought to develop a spectrophotometric approach to these reactions.

Inspired by BODIPY$^{581/591}$-C_{11}, a probe used for the visualization of cellular lipid peroxidation by confocal microscopy,[75,76] we considered that co-autoxidation of an oxidizable substrate with a more easily accessed fluorometrically or spectrophotometrically distinct probe would allow continuous monitoring of inhibited autoxidations by standard laboratory equipment.

Furthermore, this methodology would be highly versatile, and could be applied in a variety of substrates under a range of conditions, for both kinetic and mechanistic experiments.

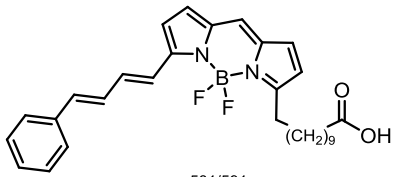

$BODIPY^{581/591}$-C_{11}

The objectives of this project were to:

1. Synthesize a greatly simplified version of $BODIPY^{581/591}$-$C_{11.}$
2. Characterize the kinetics of its reactions with peroxyl radicals in inhibited and uninhibited co-autoxidations, such that methodology could be developed to measure k_{inh} and n of added radical trapping antioxidants.
3. Verify this methodology against a range of RTAs reported in the literature and confirm that mechanistic experiments (e.g. kinetic isotope effects, kinetic solvent effects, and co-antioxidant behaviour) are accurately reproduced using this methodology.

1.4.3 Mechanistic Investigation into the Decomposition of *N,N*-Diarylalkoxyamines

The ability of diarylamine RTAs to regenerate within high temperature autoxidations has led to their widespread use in petroleum-derived materials. While the key step in this process has been postulated to proceed through an N-O homolysis/disproportionation reaction, there had been no mechanistic studies to verify that this is the case. Furthermore, it is unknown how this reaction might be optimized to improve turnover of the RTA, and what other reactions may be detrimental to this process. For these reasons, we sought to undertake a computational and experimental study in order to provide insight into the mechanism and behaviour of the key regeneration reaction. Initially the entire catalytic cycle proposed by Korcek,[41] and several potential off-cycle reactions, could be modeled using the highly accurate CBS-QB3 methodology.[77] These computations could then be

supplemented with mechanistic experiments performed with authentic *N*,*N*-diarylalkoxyamines – prepared from diarylamines and strained endoperoxides by the method of Kelly.[78]

The objectives of this project were to:

1. Computationally model the proposed catalytic cycle for diarylamine regeneration, including any potentially detrimental off-cycle reactions. Identify alternative mechanisms that could be invoked in the key steps in the catalytic cycle.
2. Synthesize authentic samples of *N*,*N*-diarylalkoxyamines, varying the structures of both the amine and alkoxide fragments of the molecule.
3. Study the decomposition of the alkoxyamines upon heating to elevated temperatures. Measure the Arrhenius parameters for the regeneration reaction and perform deuterium isotope effect studies. Optimize the structure of the alkoxyamines to improve the rate and yield of the regeneration reaction.

1.4.4 Mechanistic Investigations into the RTA Activity of Dialkylnitroxides

Despite their widespread use, the lack of a definitive mechanism for the RTA activity of HALS (and their derived nitroxides) has likely hindered development of more effective RTAs of this type. The discovery that HALS-derived nitroxides can effectively trap oxygen-centered radicals in the presence of acids has introduced a previously unknown reactivity that may be involved in their efficacy as RTAs. Our recent observation that dialkylnitroxides (such as TEMPO) trap peroxyl radicals rapidly and *catalytically* in the presence of weak carboxylic acids (e.g. acetic/benzoic acid), implies that much of the originally reported activity of HALS could be attributable to this pathway, since carboxylic acids are known to be major by-products of hydrocarbon autoxidation at elevated temperatures.[40,79] However, many questions remain; what is the mechanism for nitroxide turnover in

the presence of acid? Why can this happen in the presence of weak acids, but not strong? Can this mechanism be relevant in high temperature autoxidations and HALS activity in general?

We suspected that electron transfer from chain-carrying alkyl radicals could be responsible for the reduction of the HALS-derived oxoammonium salts (which arise from the reaction between protonated nitroxides and ROO•).[52] However, whether oxoammonium salts are capable of oxidizing alkyl radicals, and if the rate of this reaction could be competitive with addition of O_2 to R•, was unknown.

The objectives of this project were to:

1. Determine the viability of an electron transfer reaction between an alkyl radical and a hindered oxoammonium salt. Measure the rate of this reaction to reveal if it could be kinetically competitive with the addition of O_2 to alkyl radicals.
2. Examine the role of weak/strong acids in the turnover mechanism.
3. Determine the viability of this mechanism in high temperature autoxidations of heavy hydrocarbons.

1.4.5 Synthesis and Kinetics of Azaphenoxazine and Azaphenothiazine RTAs

Understanding the structure-activity relationships which govern the reactivity of phenolic and diarylaminic antioxidants has led to the development of many of the most reactive RTAs ever reported.[2] Substitution of the RTAs with EDGs weakens the reactive bond, but can destabilize the molecule towards direct one-electron oxidation.[30,31] This effect can be balanced by incorporating heterocyclic rings into the RTA structure, increasing the oxidation potential of the compound, while maintaining the high reactivity offered by the weak N-H or O-H bond.[42]

The exceptional RTA activity seen by phenoxazines and phenothiazines, coupled with their inherent stability towards oxidation suggests that they may be the most promising scaffold yet for the

development of RTAs. We sought to apply the same strategy that was used for phenols and diarylamines to these compounds, hoping to produce highly electron-rich air-stable RTAs.

Due to the fixed structure of the phenoxazine and phenothiazine rings, a single nitrogen atom could be incorporated at either the 1-, 2-, 3-, or 4-positions in a single ring. While nitrogen atoms in the diarylamines could be incorporated in similar positions, the most effective positions for increasing E^0 were the 3- and/or 5-positions on the ring (equivalent to the 2- and 4- positions on phenothiazine, Figure 1.6).[80] This pattern has the added advantage of leaving the *para*-position (or 3-position on phenothiazines/phenoxazines) available for substitution of EDGs in conjugation with the central nitrogen atom.

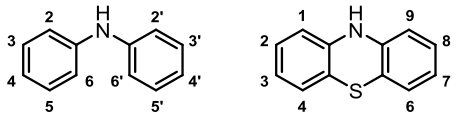

Figure 1.6. General structure of diphenylamine and phenothiazine.

Although there has been some interest in aza-derivatives of phenothiazine and phenoxazine,[81-84] the 2-aza, 4-aza, and 2,4-diaza derivatives are generally underrepresented. This can in part be attributed to their considerably more difficult syntheses. Whereas the 1-aza, and 3-aza compounds can be synthesized by comparatively straightforward nucleophilic substitution of a disubstituted pyridine by 2-amino(thio)phenol (Scheme 1.13), the 2-aza, and 4-aza derivative often require multi-step syntheses in order to circumvent an intramolecular Smiles rearrangement which would eventually lead to the wrong isomer being produced (Scheme 1.14).[85,86]

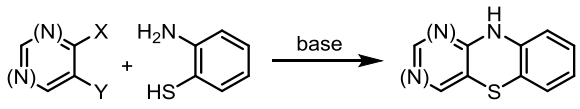

Scheme 1.13. General synthesis of 1-aza and 3-azaphenothiazine.

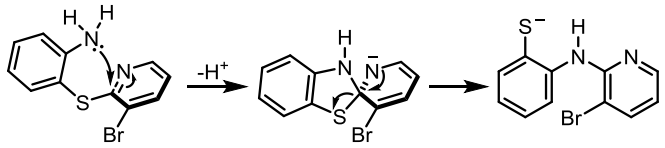

Scheme 1.14. Smiles rearrangement of a 2-aminophenyl pyridyl sulfide.

Similarly, the syntheses of 2,4-diazaphenothiazine derivatives are complicated by the same problem.[87] However, reports by Bakavoli *et. al.* state that certain 3-amino-2,4-diazaphenothiazine compounds can be made by in good yield over 3 steps, from commercially available meterials.[88-91] To the best of our knowledge, 2,4-diazaphenoxazines have not previously been prepared.

Given that the exceptionally weak N-H bonds in the phenoxazine and phenothiazine precursors will be weakened further by inclusion of EDGs onto the structure, it is expected that these compounds will have amongst the weakest N-H bonds – and among the highest k_{inh}'s – of any antioxidants previously reported. It is further expected that N-O bonds within the diarylalkoxyamines formed in (high temperature) autoxidations will be similarly weakened, and as a result, catalytic turnover of these RTAs in high temperature autoxidations will be greatly improved. Moreover, weakening the N-O bonds may also facilitate catalytic turnover of these compounds at temperatures much lower than normally required for diphenylamine RTAs.

The objectives of this project were to:

1. Synthesize a range of heterocyclic azaphenoxazines and azaphenothiazines, including both mono- and diaza- derivatives, and bearing EDGs in the 3-position on the rings. Develop a synthetic route to 2,4-diazaphenoxazines.
2. Measure the reactivity and turnover of these RTAs at ambient (37°) and elevated (160°C) temperatures, using the newly developed procedures outlined above. Develop conditions to measure the RTA activity between 70-100°C, in order to study catalytic turnover at moderate temperatures.

1.5 References

(1) Ingold, K. U. *Chem. Rev.* **1961**, *61*, 563–589.

(2) Ingold, K. U.; Pratt, D. A. *Chem. Rev.* **2014**, *114*, 9022–9046.

(3) Jensen, R. K.; Korcek, S.; Mahoney, L. R.; Zinbo, M. *J. Am. Chem. Soc.* **1979**, *101*, 7574–7584.

(4) Pryor, W. A.; Porter, N. A. *Free Radic. Biol. Med.* **1990**, *8*, 541–543.

(5) Schneider, C.; Tallman, K. A.; Porter, N. A.; Brash, A. R. *J. Biol. Chem.* **2001**, *276*, 20831–20838.

(6) Cooper, H. R.; Melville, H. W. *J. Chem. Soc.* **1951**, 1984–1993.

(7) Cooper, H. R.; Melville, H. W. *J. Chem. Soc.* **1951**, 1994–2002.

(8) Avila, D. V.; Brown, C. E.; Ingold, K. U.; Lusztyk, J. *J. Am. Chem. Soc.* **1993**, *115*, 466–470.

(9) Jensen, R.; Korcek, S.; Zinbo, M.; Johnson, M. *Int. J. Chem. Kinet.* **1990**, *22*, 1095–1107.

(10) Fenton, H. J. H. *J. Chem. Soc., Trans.* **1894**, *65*, 899–910.

(11) Maillard, B.; Ingold, K. U.; Scaiano, J. C. *J. Am. Chem. Soc.* **1983**, *105*, 5095–5099.

(12) Jensen, R. K.; Korcek, S.; Zinbo, M. *Int. J. Chem. Kinet.* **1994**, *26*, 673–680.

(13) Howard, J.; Ingold, K. *Can. J. Chem.* **1967**, *45*, 793–802.

(14) Howard, J. A.; Ingold, K. U. *Can. J. Chem.* **1969**, *47*, 3809–3815.

(15) Mayo, F. R.; Miller, A. A.; Russell, G. A. *J. Am. Chem. Soc.* **1958**, *80*, 2500–2507.

(16) Howard, J. A.; Ingold, K. U. *Can. J. Chem.* **1962**, *40*, 1851–1864.

(17) J. A. Howard, in Peroxyl Radicals, ed. Z. B. Alfassi, Wiley, New York, **1997**, 283–334.

(18) Howard, J. A.; Adamic, K.; Ingold, K. U. *Can. J. Chem.* **1969**, *47*, 3793–3795.

(19) Russell, G. A. *J. Am. Chem. Soc.* **1957**, *79*, 3871–3877.

(20) Lee, R.; Gryn'ova, G.; Ingold, K. U.; Coote, M. L. *Phys. Chem. Chem. Phys.* **2016**, *18*, 23673–23679.

(21) Enes, R. F.; Tomé, A. C.; Cavaleiro, J. A. S.; Amorati, R.; Fumo, M. G.; Pedulli, G. F.; Valgimigli, L. *Chem. - A Eur. J.* **2006**, *12*, 4646–4653.

(22) Brownlie, I. T.; Ingold, K. U. *Can. J. Chem.* **1967**, *45*, 2427–2432.

(23) Bowry, V. W.; Ingold, K. U. *J. Am. Chem. Soc.* **1992**, *114*, 4992–4996.

(24) Sobek, J.; Martschke, R.; Fischer, H. *J. Am. Chem. Soc.* **2001**, *123*, 2849–2857.

(25) Haidasz, E. A.; Meng, D.; Amorati, R.; Baschieri, A.; Ingold, K. U.; Valgimigli, L.; Pratt, D. A. *J. Am. Chem. Soc.* **2016**, *138*, 5290–5298.

(26) Mayer, J. M.; Hrovat, D. A.; Thomas, J. L.; Borden, W. T. *J. Am. Chem. Soc.* **2002**, *124*, 11142–11147.

(27) DiLabio, G. A.; Johnson, E. R. *J. Am. Chem. Soc.* **2007**, *129*, 6199–6203.

(28) Hanthorn, J.; Amorati, R.; Valgimigli, L.; Pratt, D. *J. Org. Chem.* **2012**, *77*, 6895–6907.

(29) Amorati, R.; Valgimigli, L. *Org. Biomol. Chem.* **2012**, *10*, 4147.

(30) Pratt, D. A.; DiLabio, G. A.; Valgimigli, L.; Pedulli, G. F.; Ingold, K. U. *J. Am. Chem. Soc.* **2002**, *124*, 11085–11092.

(31) Pratt, D. A.; DiLabio, G. A.; Mulder, P.; Ingold, K. U. *Acc. Chem. Res.* **2004**, *37*, 334–340.

(32) Howard, J. A.; Ingold, K. U. *Can. J. Chem.* **1963**, *41*, 1744–1751.

(33) Lucarini, M.; Pedrielli, P.; Pedulli, G. F.; Valgimigli, L.; Gigmes, D.; Tordo, P. *J. Am. Chem. Soc.* **1999**, *121*, 11546–11553.

(34) Burton, G. W.; Ingold, K. U. *J. Am. Chem. Soc.* **1981**, *103*, 6472–6477.

(35) Igarashi, J.; Jensen, R. K.; Lusztyk, J.; Korcek, S.; Ingold, K. U. *J. Am. Chem. Soc.* **1992**, *114*, 7727–7736.

(36) Lerchová, J.; Nikiforov, C. A.; Pospíšil, J. *J. Polym. Sci. Polym. Symp.* **2007**, *57*, 249–253.

(37) Mahoney, L. R. *Angew. Chemie Int. Ed.* **1969**, *8*, 547–555.

(38) Brownlie, I. T.; Ingold, K. U. *Can. J. Chem.* **1966**, *44*, 861–868.

(39) Thomas, J. R.; Tolman, C. A. *J. Am. Chem. Soc.* **1962**, *84*, 2930–2935.

(40) Bolsman, T.; Blok, A.; Frijns, J. *Recl. des Trav. Chim. des Pays-Bas* **1978**, *97*, 310–312.

(41) Jensen, R. K.; Korcek, S.; Zinbo, M.; Gerlock, J. L. *J. Org. Chem.* **1995**, *60*, 5396–5400.

(42) Pratt, D. A.; DiLabio, G. A.; Brigati, G.; Pedulli, G. F.; Valgimigli, L. *J. Am. Chem. Soc.* **2001**, *123*, 4625–4626.

(43) Valgimigli, L.; Brigati, G.; Pedulli, G. F.; DiLabio, G. A.; Mastragostino, M.; Arbizzani, C.; Pratt, D. A. *Chem. - A Eur. J.* **2003**, *9*, 4997–5010.

(44) Wijtmans, M.; Pratt, D. A.; Valgimigli, L.; DiLabio, G. A.; Pedulli, G. F.; Porter, N. A. *Angew. Chemie Int. Ed.* **2003**, *42*, 4370–4373.

(45) Wijtmans, M.; Pratt, D. A.; Brinkhorst, J.; Serwa, R.; Valgimigli, L.; Pedulli, G. F.; Porter, N. A. *J. Org. Chem.* **2004**, *69*, 9215–9223.

(46) Hanthorn, J. J.; Valgimigli, L.; Pratt, D. A. *J. Org. Chem.* **2012**, *77*, 6908–6916.

(47) Murphy, C. M.; Saunders, C. E. *Pet. Refin.* **1947**, *26*, 479–484.

(48) Murphy, C. M.; Ravner, H.; Smith, N. L. *Ind. Eng. Chem.* **1950**, *42*, 2479–2489.

(49) West, H. L. *J. Inst. Pet.* **1948**, *34*, 774.

(50) Values from Chapter 7.

(51) Gryn'ova, G.; Ingold, K. U.; Coote, M. L. *J. Am. Chem. Soc.* **2012**, *134*, 12979–12988.

(52) Amorati, R.; Pedulli, G. F.; Pratt, D. A.; Valgimigli, L. *Chem. Commun.* **2010**, *46*, 5139–5141.

(53) Amorati, R.; Valgimigli, L. *Free Radic. Res.* **2015**, *49*, 633–649.

(54) Li, B.; Pratt, D. A. *Free Radic. Biol. Med.* **2015**, *82*, 187–202.

(55) Amorati, R.; Lynett, P. T.; Valgimigli, L.; Pratt, D. A. *Chem. - A Eur. J.* **2012**, *18*, 6370–6379.

(56) Hoops, S.; Sahle, S.; Gauges, R.; Lee, C.; Pahle, J.; Simus, N.; Singhal, M.; Xu, L.; Mendes, P.; Kummer, U. *Bioinformatics* **2006**, *22*, 3067–3074.

(57) Lucarini, M.; Pedulli, G. F.; Valgimigli, L.; Amorati, R.; Minisci, F. *J. Org. Chem.* **2001**, *66*, 5456–5462.

(58) Howard, J. A.; Ingold, K. U. *Can. J. Chem.* **1966**, *44*, 1119–1130.

(59) Xu, L.; Davis, T. A.; Porter, N. A. *J. Am. Chem. Soc.* **2009**, *131*, 13037–13044.

(60) Spickett, C. M.; Wiswedel, I.; Siems, W.; Zarkovic, K.; Zarkovic, N. *Free Radic. Res.* **2010**, *44*, 1172–1202.

(61) Beckwith, A. L. J.; Bowry, V. W.; Ingold, K. U. *J. Am. Chem. Soc.* **1992**, *114*, 4983–4992.

(62) Roschek, B.; Tallman, K. A.; Rector, C. L.; Gillmore, J. G.; Pratt, D. A.; Punta, C.; Porter, N.

A. *J. Org. Chem.* **2006**, *71*, 3527–3532.

(63) Pratt, D. A.; Tallman, K. A.; Porter, N. A. *Acc. Chem. Res.* **2011**, *44*, 458–467.

(64) Jha, M.; Pratt, D. A. *Chem. Commun.* **2008**, *9*, 1252–1254.

(65) Hanthorn, J.; Pratt, D. *J. Org. Chem.* **2012**, *77*, 276–284.

(66) Blois, M. S. *Nature* **1958**, *181*, 1199–1200.

(67) Huang, D.; Ou, B.; Prior, R. L. *J. Agric. Food Chem.* **2005**, *53*, 1841–1856.

(68) Foti, M. C. *J. Agric. Food Chem.* **2015**, *63*, 8765–8776.

(69) Tai, A.; Sawano, T.; Yazama, F.; Ito, H. *Biochim. Biophys. Acta - Gen. Subj.* **2011**, *1810*, 170–177.

(70) Re, R.; Pellegrini, N.; Proteggente, A.; Pannala, A.; Yang, M.; Rice-Evans, C. *Free Radic. Biol. Med.* **1999**, *26*, 1231–1237.

(71) Benzie, I. F.; Strain, J. J. *Anal. Biochem.* **1996**, *239*, 70–76.

(72) Apak, R.; Güçlü, K.; Özyürek, M.; Karademir, S. E. *J. Agric. Food Chem.* **2004**, *52*, 7970–7981.

(73) Litwinienko, G.; Ingold, K. U. *Acc. Chem. Res.* **2007**, *40*, 222–230.

(74) George A. Lemieux; de Graffenried, C. L.; Bertozzi, C. R. *J. Am. Chem. Soc.* **2003**, *125*, 4708–4709.

(75) Kang, H. C.; Haugland, R. P. Long Wavelength Chemically Reactive Dipyrrometheneboron Difluoride Dyes and Conjugates. US5451663 A, 1993.

(76) Drummen, G. P. .; van Liebergen, L. C. .; Op den Kamp, J. A. .; Post, J. A. *Free Radic. Biol. Med.* **2002**, *33*, 473–490.

(77) Montgomery, J. A.; Frisch, M. J.; Ochterski, J. W.; Petersson, G. A. *J. Chem. Phys.* **1999**, *110*, 2822.

(78) Kelly, D.; Bansal, H.; Morgan, J. *Tetrahedron Lett.* **2002**, *43*, 9331–9333.

(79) Jalan, A.; Alecu, I. M.; Meana-Pañeda, R.; Aguilera-Iparraguirre, J.; Yang, K. R.; Merchant, S. S.; Truhlar, D. G.; Green, W. H. *J. Am. Chem. Soc.* **2013**, *135*, 11100–11114.

(80) Hanthorn, J.; Valgimigli, L.; Pratt, D. *J. Am. Chem. Soc.* **2012**, *134*, 8306–8309.

(81) Ito, Y.; Hamada, Y. *Chem. Pharm. Bull. (Tokyo).* **1978**, *26*, 1375–1383.

(82) Takahashi, T.; Yoneda, F. *Chem. Pharm. Bull. (Tokyo).* **1958**, *6*, 46–49.

(83) Takahashi, T.; Yoneda, F. *Chem. Pharm. Bull. (Tokyo).* **1958**, *6*, 378–381.

(84) Petrow, V. A.; Rewald, E. L. *J. Chem. Soc.* **1945**, 313–315.

(85) Takahashi, T.; Maki, Y. *Chem. Pharm. Bull. (Tokyo).* **1958**, *6*, 369–373.

(86) Bonvicino, G. E.; Yogodzinski, L. H.; Hardy, R. A. *J. Org. Chem.* **1962**, *27*, 4272–4280.

(87) Pluta, K.; Morak-Młodawska, B.; Jeleń, M. *J. Heterocycl. Chem.* **2009**, *46*, 355–391.

(88) Bakavoli, M.; Nikpour, M.; Rahimizadeh, M.; Saberi, M. R.; Sadeghian, H. *Bioorg. Med. Chem.* **2007**, *15*, 2120–2126.

(89) Bakavoli, M.; Sadeghian, H.; Tabatabaei, Z.; Rezaei, E.; Rahimizadeh, M.; Nikpour, M. *J. Mol. Model.* **2008**, *14*, 471–478.

(90) Pooryaghoobi, N.; Bakavoli, M.; Alimardani, M.; Bazzazan, T.; Sadeghian, H. *Iran. J. Basic Med. Sci.* **2013**, *16*, 784–789.

(91) Nikpour, M.; Mousavian, M.; Davoodnejad, M.; Alimardani, M.; Sadeghian, H. *Med. Chem. Res.* **2013**, *22*, 5036–5043.

CHAPTER 2: A Versatile Fluorescence Approach to Kinetic Studies of Hydrocarbon Autoxidations and their Inhibition by Radical-Trapping Antioxidants

2.1 Preface

We have developed a simple coumarin–triarylphosphine conjugate that undergoes significant fluorescence enhancement upon oxidation of the phosphine. This assay has been used to quantify the complex mixtures of hydroperoxides arising from autoxidation of *n*-hexadecane (at 160 °C) and measure its inhibition by radical-trapping antioxidants (RTAs). This chapter is comprised of sections of a publication in Chemical Communications (*Chem*. *Commun*., **2012**, *48*, 10141-10143). This has been supplemented with a following publication in the Journal of the American Chemical Society (*J. Am. Chem. Soc.*, **2015**, *137*, 2440–2443) where the methodology is used to measure the reactivities of novel heterocyclic diarylamine RTAs at 160 °C – conditions representative of those found in many industrial applications. The carboxylic acids produced from *β*-hydroperoxy ketones produced in the autoxidation deactivate these more basic RTAs. However, addition of tri-tert-butylpyridine as a sacrificial base leads to dramatic improvement in the activity of these compounds – outperforming the industrial standard diphenylamine RTAs by up to a factor of 12.5 – efficacies that are unprecedented in the decades of academic and industrial research in this area. Development of the pro-fluorescent phosphine probe was carried out in conjunction with fellow graduate students Jay Hanthorn and Paul Gebhardt who are responsible for the synthesis of the different coumarin-conjugated phosphines. The studies on the high-temperature reactivity of diarylamine RTAs were carried out with fellow graduate student Ron Shah, who is responsible for the synthesis of some of the heterocyclic diarylamines and a significant share of the high temperature autoxidation data with them.

2.2 Introduction

Autoxidation, the radical-mediated peroxidation of hydrocarbons (RH, Scheme 2.1),[1,2] is responsible for oxidative degradation in organic materials from polymers, lubricating oils and other petroleum-derived products to the lipids present living organisms. Understanding this process – and its inhibition – has been the focus of a great deal of research over the past decades due to its impact on the lifetimes of both industrial and biological materials, as well as its supposed involvement in the pathogenesis of degenerative diseases.

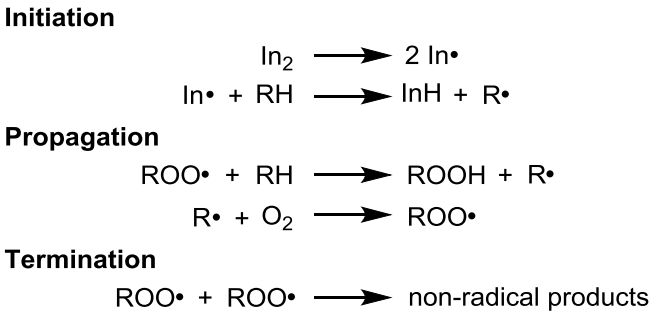

Scheme 2.1. Radical chain mechanism of hydrocarbon autoxidation.

Autoxidation reactions – comprising an oxidizable substrate, radical initiator, and (often) an antioxidant, under an aerobic atmosphere – are followed either by consumption of O_2 or formation of the hydroperoxide products (ROOH). O_2 consumption experiments are generally preferred since they can be done in real time by differential pressure measurements,[3] while the latter are discontinuous assays often carried out by either iodometric titration or laborious HPLC/GC analyses.[4] Recently, several (pro-)fluorescent molecular probes (e.g. diphenyl-1-pyrenylphosphine (DPPP, **2.1**)[5,6] and Spy-LHP (**2.2**)[7]) have been developed to detect ROOH formation in real time in solution and/or cells. These probes generally feature known fluorophores whose fluorescence is quenched via photoinduced electron transfer (PeT) from a conjugated phosphine. Upon oxidation of the phosphine by ROOH (precluding PeT from the phosphine to the fluorophore), the fluorescence of the probe is restored, leading to an enhanced signal.

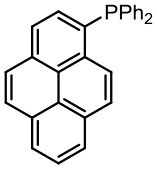

2.1

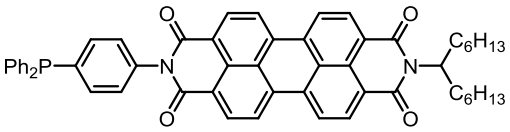

2.2

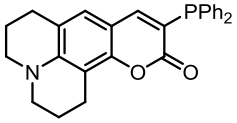

2.3

We sought to use this approach in a microplate assay to measure hydroperoxide formation in inhibited autoxidation reactions, but quickly learned that these compounds (and their synthetic precursors) are highly insoluble in organic solution and are generally very expensive.[8]

2.3 Results and Discussion

2.3.1 Synthesis and Characterization of Pro-Fluorescent Phosphines

Inspired by the work of Bertozzi and co-workers,[9] Xian *et al.*[10] developed the more accessible and soluble coumarin-based dye **2.3** for the determination of *S*-nitrosothiols. However, oxidation of **2.3** by hydroperoxides is quite slow ($k < 0.1\ M^{-1}\ s^{-1}$), and background oxidation by O_2 can be problematic. Since triphenylphosphine reacts more rapidly with hydroperoxides,[11] we opted to include a phenyl spacer between the phosphine and coumarin moieties. Given the simplicity of synthesizing the 7-substituted coumarin precursors (by Knoevenagel condensation or Wittig olefination and *in situ* lactonization of the cinnamate), we elected to focus on structures containing this core. We initially synthesized the structures shown in Scheme 2.2, attempting to optimize for both rate of oxidation by ROOH and fluorescence enhancement upon oxidation.

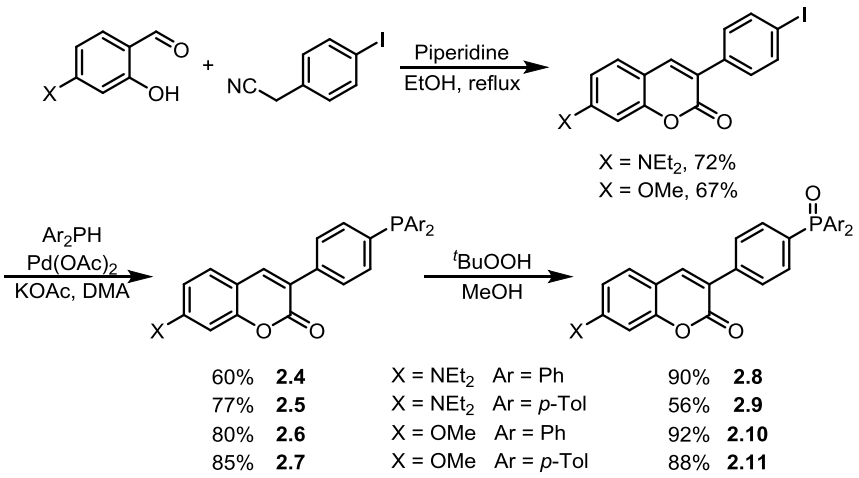

Scheme 2.2. Synthesis of coumarin–triarylphosphine conjugates.

The quantum yields of the dialkylamino-substituted phosphines (**2.4**, **2.5**) and phosphine oxides (**2.8**, **2.9**) ($\Phi_{f,ox}$ and $\Phi_{f,red}$, Table 2.1), were quite low in comparison to **2.3** ($\Phi_{f,ox}$ = 0.79).[10] Moreover, the quantum yields of both the oxidized and reduced forms of the probes has similar quantum yields, indicating a lack of any significant quenching by the phosphine moiety and implying a mismatch between the energy of the phosphine lone pair and coumarin excited state HOMOs. When the dialkylamino-substituent was exchanged for a methoxy group, a significant increase in quantum yield was observed. Additionally, the 2.4-fold increase in quantum yield upon oxidation of **2.6** to **2.10**, indicated a better match between the energies of the phosphine and coumarin. Substituting the more electron-rich di(*p*-tolyl)phosphine improved the fluorescence enhancement upon oxidation further ($\Phi_{f,ox}/\Phi_{f,red}$ = 10.6). Moreover, **2.7** was indefinitely stable in air at 25 °C in non-protic solvents, and underwent negligible oxidation in protic solvents over several hours.

Table 2.1. Relevant spectral parameters of coumarin–phosphine conjugates **2.4**–**2.7**, and phosphine oxides (**2.8**–**2.11**) at 298 K in MeOH.

	λ_{ex} (nm)	λ_{em} (nm)	$\Phi_{f,red}$[a]	$\Phi_{f,em}$[a]	$\Phi_{f,ox}/\Phi_{f,red}$
2.4, **2.8**	408	486	0.17	0.21	1.2
2.5, **2.9**	406	486	0.15	0.17	1.3
2.6, **2.10**	345	426	0.20	0.48	2.4
2.7, **2.11**	343	422	0.05	0.52	10.6

[a]Determined versus sodium difluorescein in methanol (Φ_f = 0.92).[12]

Since the reaction of triarylphosphines with hydroperoxides are too slow for determination of ROOH concentration based on a single 'end-point' fluorescence measurement (*e.g.* k = 1.3, 1.0 and 0.4 M^{-1} s^{-1} for reactions of *n*-, *sec*-, and *tert*-BuOOH, respectively, with triphenylphosphine in EtOH at 25 °C),[11,13] the second order rate constant for the reaction of **2.7** and a model secondary hydroperoxide was determined. The initial rates of the reaction between **2.7** (20μM) and varying concentration of tetralin hydroperoxide (TetOOH, chosen as a model secondary hydroperoxide because it is stable and can be recrystallized to very high purity)[14] are shown in Figure 2.1. From this, the second order rate constants were determined to be, k = 9.1 and 1.2 M^{-1} s^{-1} in MeOH at 37 °C and *t*-amyl alcohol (*t*-AmOH) at 25 °C, respectively. With these rate constants in hand, the hydroperoxide concentration within unknown samples can be determined from their initial rates of their reactions with **2.7**.

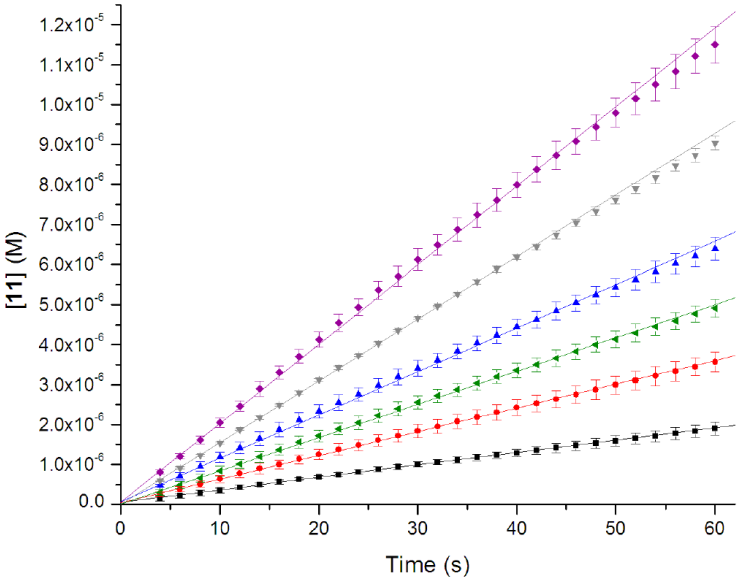

Figure 2.1. Formation of **2.11** as a function of time from reaction of **2.7** with varying concentrations (600, 1200, 1800, 2400, 3600 and 4800 μM) of tetralin hydroperoxide in *t*-amyl alcohol at 25°C.

2.3.2 Analysis of Hexadecane Autoxidations

Although the fluorimetric determination of [ROOH] could potentially be used for the determination of autoxidation/inhibition kinetics at ambient temperatures, its versatility is best demonstrated by its application to the complex mixtures of hydroperoxides which arise from autoxidation of saturated hydrocarbons at elevated temperatures. These are impossible to study by conventional O_2 uptake approach since the solutions must be continuously oxygenated to prevent mass transfer of O_2 from becoming rate-limiting, and fragmentation of the hydrocarbon chains (*vide infra*) produces volatiles which can interfere with the differential pressure measurements.[4] Heavy hydrocarbon autoxidations are typically monitored by iodometric titration or HPCL/GC analyses of reaction products,[4,15] both of which are laborious can suffer from poor reproducibility. Enabled by this methodology we were able to monitor the autoxidation of *n*-hexadecane and its inhibition by the common industrial antioxidant BHT (2,6-di-*tert*-butyl-4-methylphenol) simply by removing aliquots from a stirred flow reactor, and analysing them by a microplate assay with **2.7**. Since autoxidations containing inhibitor were very

slow, tetralin hydroperoxide (8 mM) was added as a radical initiator in order to increase the rate of the reaction (see Supporting Information).The results are shown in Figure 2.2.

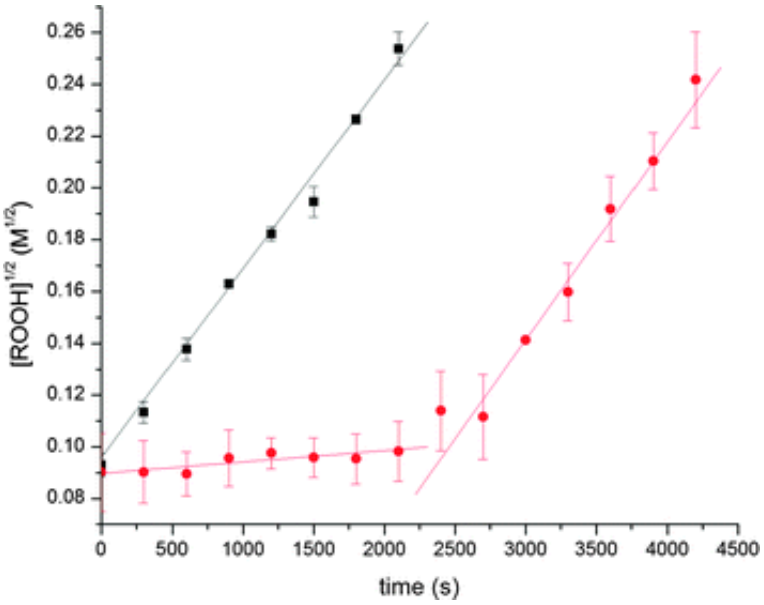

Figure 2.2. Autoxidation of neat hexadecane initiated with 8 mM TetOOH (■), and its inhibition with 1 mM of BHT (●) at 160 °C.

The uninhibited rate of hexadecane autoxidation (7.3×10^{-5} $M^{1/2}$ s^{-1}) measured under these conditions is in satisfactory agreement with that reported under similar conditions by Igarashi *et al.* (15×10^{-5} $M^{1/2}s^{-1}$),[15,16] as is the length of the inhibited period observed with added BHT (~2500 s for 1 mM BHT *vs.* ~2600 s for 1.2 mM BHT).[15]

3.3.3 Diarylamine-Inhibited Hexadecane Autoxidations

Diarylamine RTAs (Ar_2NH) are important additives to many types of petroleum-derived products due to their ability to trap peroxyl radicals catalytically.[1,2] Much like phenols, diarylamines inhibit autoxidation by formal H-atom transfer from an activated X-H bond to the chain carrying peroxyl radical (eq 2.1). The diarylaminyl radical is subsequently oxidized to a nitroxide (eq 2.2), which can either react with another radical through one of the aryl rings or combine with an alkyl radical to

give an alkoxyamine (eq 2.3). In either event, a total of two radicals have been trapped (stoichiometric factor, $n = 2$); at ambient temperatures the RTAs cannot react further.

$$Ar_2NH + ROO\bullet \longrightarrow Ar_2N\bullet + ROOH \quad (2.1)$$
$$Ar_2N\bullet + ROO\bullet \longrightarrow Ar_2NO\bullet + RO\bullet \quad (2.2)$$
$$Ar_2NO\bullet + R\bullet \longrightarrow Ar_2NOR \quad (2.3)$$
$$Ar_2NOR \longrightarrow Ar_2NH + R_{\text{-H}}=O \quad (2.4)$$

At elevated temperatures commonly seen in industrial applications (e.g. those where engine lubricants are used or at which polymers are processed), however, the alkoxyamine product can undergo further chemistry to regenerate the diarylamine RTA. Although the catalytic activity of aminic RTAs had been recognized for decades (e.g. in 1978 Bolsman, Blok and Frijns reported a stoichiometric factor of 52 was for 4,4′-dialkyldiphenylamine in paraffin oil at 130 °C),[17] the mechanism for the catalytic cycle was first suggested in 1995 by Korcek and co-workers.[18] The key transformation, which occurs either by N–O dissociation and in-cage disproportionation[18] or a retro-carbonyl–ene reaction,[19] regenerates the diarylamine from the substrate-derived alkoxyamine (eq 2.4).

Our group has previously demonstrated that the incorporation of nitrogen atoms into the aromatic rings of phenolic[20-24] and diphenylamine[25-27] RTAs stabilizes them to direct oxidation by O_2 or background hydroperoxides. This enables their substitution with strong electron donating groups, weakening the reactive N-H or O-H bond and providing exceptional reactivity toward peroxyl radicals (i.e., $\Delta H_1^{\ddagger} \approx 0$). While previous studies on these more reactive RTAs were largely based on results at ambient temperatures, using the above methodology with **2.7** has provided a reliable means to study their reactivity at elevated temperatures where they are expected to be catalytically active. Since the efficacy of these electron rich RTAs is highly dependent on the balance between their reactivity (given by k_{inh}) and stability (given by E^0), the diarylamines in Chart 2.1 were selected to provide a range from the most reactive, but most oxidizable (**2.12**) to the least reactive, but most stable compound (**2.17**).[25-27] These RTAs are similar to those previously reported by our group, but

are substituted with longer alkyl chains in order to ensure their solubility in heavy hydrocarbon solvents (see the Supporting Information for their preparation). In order to compare **2.12**-**2.17** with industrially relavent RTAs, compound **2.18** was selected as a model 4,4'-dialkyldiphenylamine.

Chart 2.1. Some Diarylamines and Their Relevant Properties[28]

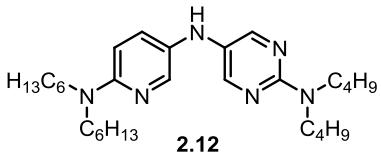

2.12

k_1 (37°C) = 3.1×10^7 $M^{-1}s^{-1}$

E^0 = 0.50 V

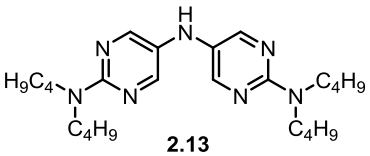

2.13

k_1 (37°C) = 1.8×10^7 $M^{-1}s^{-1}$

E^0 = 0.65 V

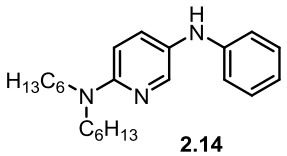

2.14

k_1 (37°C) = 1.1×10^7 $M^{-1}s^{-1}$

E^0 = 0.60 V

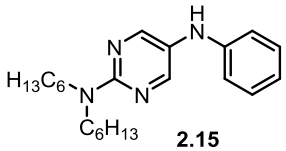

2.15

k_1 (37°C) = 3.0×10^6 $M^{-1}s^{-1}$

E^0 = 0.81 V

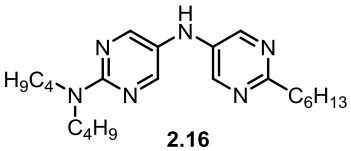

2.16

k_1 (37°C) = 2.4×10^6 $M^{-1}s^{-1}$

E^0 = 0.84 V

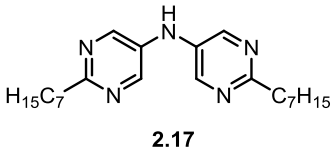

2.17

k_1 (37°C) = 3.0×10^4 $M^{-1}s^{-1}$

E_{pa} = 1.55 V

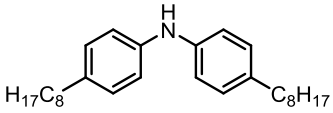

2.18

k_1 (37°C) = 1.8×10^5 $M^{-1}s^{-1}$

E_{pa} = 1.02 V

Returning to the *n*-hexadecane autoxidations described above, the activities of **2.12**–**2.18** were measured at 160°C using the same approach,[4,15] and analyzed by microplate assay with fluorogenic phosphine **7**.[29] Representative results are shown in Figure 2.3. In the uninhibited autoxidation, [ROOH] increases at an exponential rate due to the autocatalytic nature of the reaction (i.e. thermolysis of product hydroperoxides is the primary source of new chain-initiating radicals).[4] After 80-90mM of hydroperoxides accumulate in the reaction (*ca* 3% of the substrate) their concentration begins to decrease as hydroperoxides decompose to form a complex mixture of ketones, alcohols, carboxylic acids, and esters.[4] For this reason, the autoxidations were typically monitored for the first *ca.* 2% of the reaction.

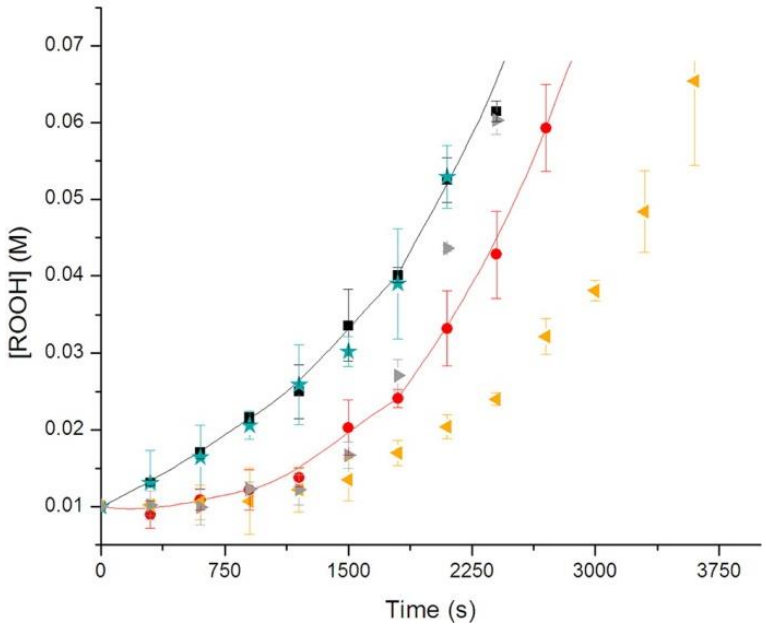

Figure 2.3. Hydroperoxide formation in the autoxidation of *n*-hexadecane at 160 °C initiated by 10 mM TetOOH in the absence of RTA (black ■) or in the presence of 40 μM of **2.15** (◂), **2.16** (▸), **2.17** (★), or **2.18** (●).

4,4'-dioctyldiphenylamine **2.18** inhibits the autoxidation for *ca*. 530 s,[38] after which a profile similar to the uninhibited autoxidation is observed. Of the heterocyclic diarylamines, however, only **2.13** (not shown) and **2.15** (Figure 2.3) appear to inhibit the autoxidation more effectively than the industrial standard, **2.18**. Compound **2.16** inhibits the autoxidation well for *ca*. 1500s before it is completely consumed, while compounds **2.12**, **2.14**, and **2.17**, seem to display little to no inhibitory effect. The remarkable improvement in reactivity between **2.12**-**2.16** and **2.18** at 37°C is difficult to reconcile with their poor performance at elevated temperatures. Since the inhibition reaction (eq 2.1) have very small activation enthalpies, the inhibition rate constant k_{inh} should be relatively invariant with temperature (e.g., k_{inh} for **2.18**, for which log A = 6.9 and E_a = 2.5 kcal/mol,[27] will only increase by a factor of 2.4 upon heating from 37 to 160 °C). Furthermore, the activation enthalpies of the more reactive RTAs should be smaller, and thus, have even less influence from the temperature. Given this, it was expected that the trends seen between the RTAs should translate to elevated temperatures.

2.3.4 Formation of Carboxylic Acids in Hexadecane Autoxidations

Considering the unexpectedly poor performance of the RTAs upon heating, we next examined their stability to oxidation at elevated temperatures. Solutions of **2.12**-**2.16** in *n*-hexadecane were heated to 160°C under at atmosphere of O_2 and samples taken over 1h. While the most oxidizable compounds (**2.12**, **2.13**, **2.14**) did decompose gradually (see Supporting Information for data), this slow decomposition is inconsistent with the data in Figure 2.3, which show virtually no inhibition from the initial stages of the reaction.

Since carboxylic acids are known to be a by-product of hydrocarbon autoxidation, we next wondered if the more basic heterocyclic RTAs might be sensitive to acids produced *in situ*. Korcek and co-workers suggested that these acids arise from fragmentation of *β*-hydroperoxy ketones formed from sequential intramolecular H-atom abstraction on the hydrocarbon chain (Scheme 2.3). This mechanism was subsequently studied by Green, Truhlar, and co-workers.[30] Indeed, analysis of the autoxidation samples by electrospray mass spectrometry showed significant concentrations of carboxylic acids arising from fragmentation between C_8 and C_{14} on the hydrocarbon chain (Figure 2.4, shorter chain carboxylic acids are likely volatilized as a result of the high temperatures). Quantifying these revealed that the acid concentration approached *ca.* 25% of the hydroperoxide concentration over the first 2400s of the reaction (~15 mM vs ~60 mM; Figure 2.5).

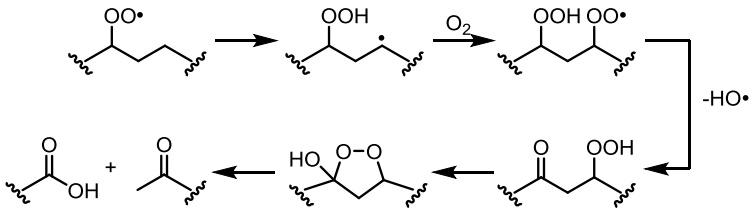

Scheme 2.3. Proposed mechanism of acid formation in the early stages of hydrocarbon autoxidations.

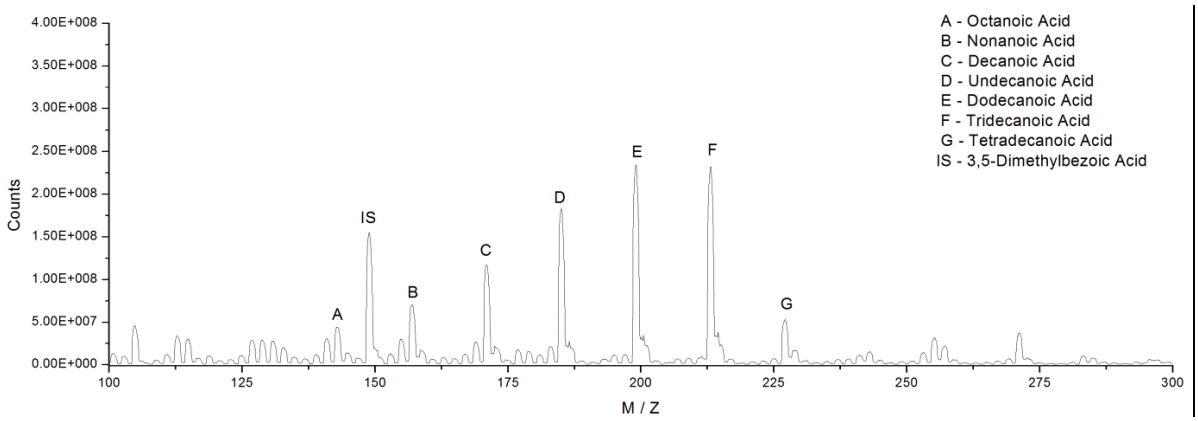

Figure 2.4. Mass spectrum of 50μL autoxidation sample (t = 1800s) diluted with 4.95mL 20% iPrOH, 80% MeOH containing 10.5 μM 3,5-dimethylbenzoic acid.

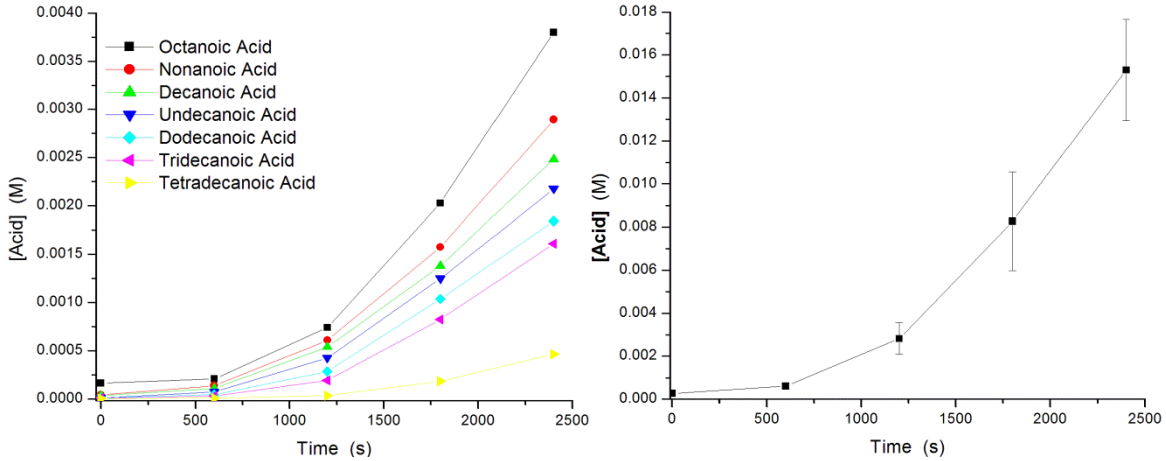

Figure 2.5. Total production of alkyl carboxylic acids in uninhibited hexadecane autoxidation at 160°C, initiated by 10 mM tetralin hydroperoxide.

Since diarylaminyl radicals are inherently electron poor,[31,32] protonation of the diarylamine would strengthen the reactive N-H bond, reducing its reactivity to peroxyl radicals. Calculating the BDE of **2.15** using the reliable CBS-QB3 method[33] showed that the bond strength increases from 81.8 to 86.0 kcal/mol upon protonation of the ring,[34] consistent with a nearly 100-fold reduction k_{inh} at 160°C.

To confirm this effect, 1mM of palmitic acid, a nonvolatile saturated carboxylic acid, was added to autoxidations inhibited by **2.15** and **2.18** (Figure 2.6). The presence of even a small amount

of acid was found to be detrimental to the efficacy of the heterocyclic RTA, while that of the less basic diphenylamine **2.18** was unchanged.

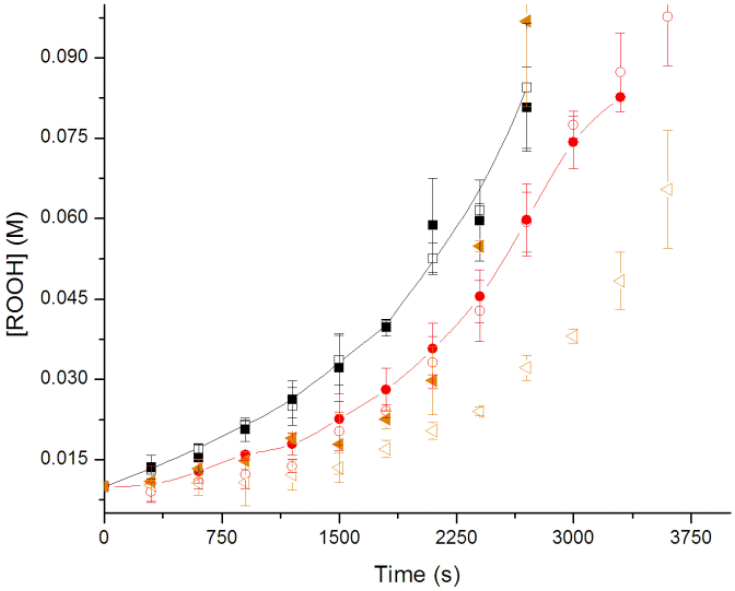

Figure 2.6. Hydroperoxide formation in the autoxidation of hexadecane at 160°C initiated by 10 mM tetralin hydroperoxide (■) and inhibited by 40 μM of either **2.18** (●) or **2.15** (◀) in the presence of palmitic acid (1 mM). Empty symbols depict autoxidations carried out in the absence of acid.

2.3.5 Addition of Base to Inhibited Hexadecane Autoxidations

Reasoning that addition of base should "rescue" the RTA activity of **2.15**, 1mM of the non-volatile non-nucleophilic base 2,4,6-tri-*tert*-butylpyridine (TTBP) was added to the reactions. Gratifyingly, upon addition of the base diarylamine **2.15** displayed unprecedented inhibitory activity (Figure 2.7), inhibiting the autoxidation for *ca*. 6600s relative to the uninhibited reaction – a 12.5-fold increase over industrial standard **2.18** ($t_{2\%}$ = 534s). The activity of diphenylamine **2.18** was also unaffected by the addition of base, consistent with the above results suggesting that buildup of acids doesn't affect its reactivity. Importantly, when TTBP was exchanged for cesium carbonate or a *tert*-alkyl primary amine (Primene 81-R) the effect of the base was maintained – further confirming that the

buildup of acid is responsible for inactivation of the heterocyclic RTAs (see the Supporting Information for data).[35]

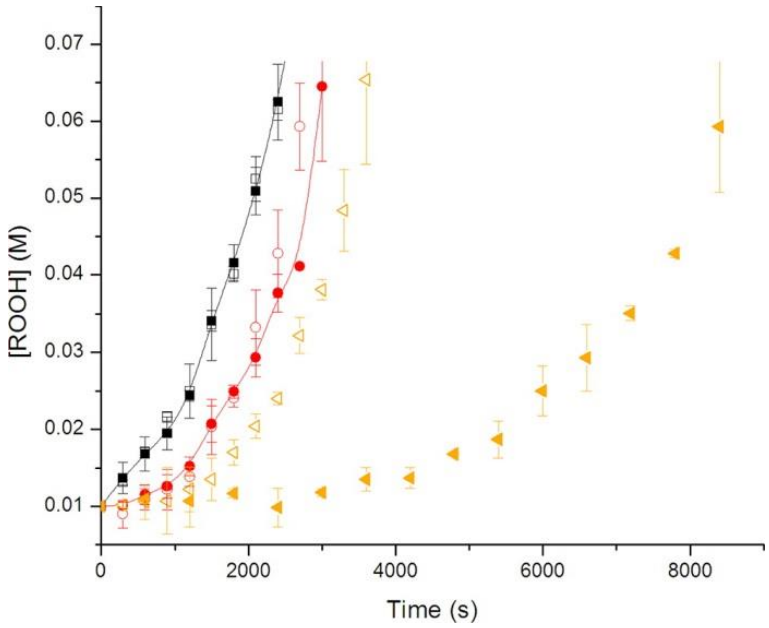

Figure 2.7. Hydroperoxide formation in the autoxidation of *n*-hexadecane at 160 °C initiated by 10 mM tetralin hydroperoxide in the absence of RTA (■) or inhibited by 40 μM **2.15** (◂) or **2.18** (red ●) in the presence of TTBP (1 mM). Open symbols correspond to the data in Figure 2.3 (i.e., in the absence of TTBP).

Measuring the pK_a's of the conjugate acids of each of the RTAs confirmed that **2.12**-**2.16** (pK_a = 8.2-9.8, see Supporting Information) were considerably more basic than diphenylamine **2.18** (pK_a = 4.6).[36] Consequently, accumulation of carboxylic acids would affect **2.12**-**2.16** to a much greater extent than **2.18**. When autoxidations were carried out on **2.12**-**2.14**, and **2.16** in the presence of 1mM added TTBP, each of these were found to greatly outperform **2.18** (Figure 2.8). Even the diarylamines which were found to decompose over the course of the reaction (**12**-**14**, *vide supra*) were found to be superior to **2.18**,[37] likely because the remaining material is still highly reactive. The pyrimidine-containing compounds **2.15**, and **2.16** performed the best of all the RTAs tested – presumably as a result of the improved stability of these compounds (E^0 = 0.81-0.84V, *cf.* Chart 2.1) relative to the similarly reactive pyridine derivatives (E^0 = 0.50-0.60V).

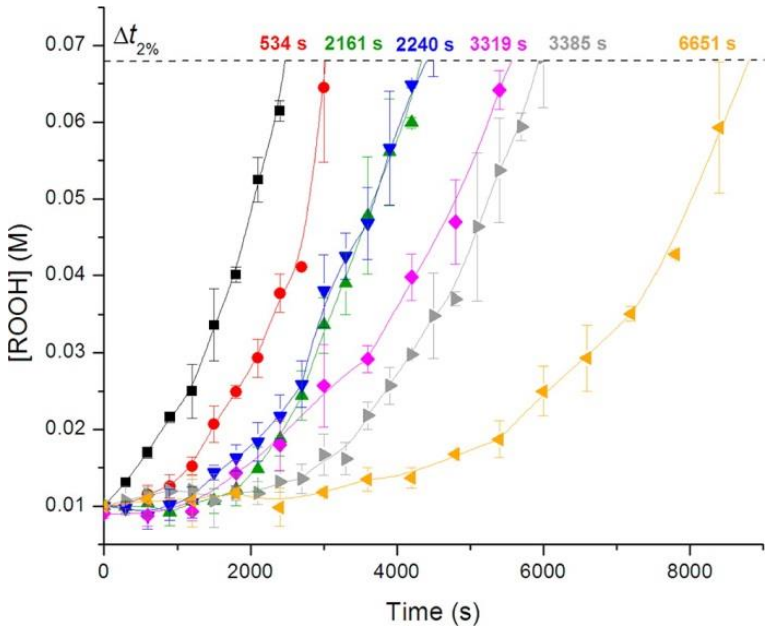

Figure 2.8. Hydroperoxide formation in the autoxidation of *n*- hexadecane at 160 °C initiated by 10 mM tetralin hydroperoxide in the absence of RTA (black ■) or inhibited by 40 of μM **2.12** (▼), **2.13** (◆), **2.14** (▲), **2.15** (◀), **2.16** (▶), or **2.18** (●) in the presence of TTBP (1 mM). The delay in the time required to reach [ROOH] = 68 mM (=2%) in the presence of each of **12**–**16** or **18** is given as $\Delta t_{2\%}$.

The incredible efficacy seen by these diarylamines is presumably a result of both their higher inherent reactivity to peroxyl radicals (given by k_{inh}) and improved turnover through their catalytic cycle. Since, at elevated temperatures, the rate of initiation (R_i) increases as hydroperoxides accumulate, RTAs which better inhibit hydroperoxide formation (i.e. faster k_{inh}) also act preventatively, slowing the growth of R_i in the reaction. Since consumption of the antioxidants in the reaction is dependent on R_i, this has the added effect of slowing further consumption of the RTA and extending the inhibition of the reaction.

The more reactive RTAs are also expected to have improved through their catalytic cycle. In our recent investigation into the catalytic activity of diarylamine RTAs,[19] we found that the key step in the cycle (eq 2.4) proceeds through either a N-O homolysis/diaproportionation pathway, or a retro-carbonyl-ene reaction depending on the structure of the reactants. In either of these cases, the alkoxyamine N-O bond is broken as the reaction proceeds. Much like the N-H bond, stabilizing the

diarylaminyl radical weakens the N-O bond and lowers the energy required for this reaction. CBS-QB3[33] calculations suggest that alkoxyamines derived from **2.15** have N-O BDEs *ca.* 2.3 kcal/mol weaker than those from **2.18**, consistent with a ~14-fold improvement in turnover at 160°C. Furthermore, stabilization of the diarylaminyl radical is would also be expected to improve turnover by increasing the reversibility of off-cycle reactions (such as radical coupling through the aryl rings), and funneling more of the material through the productive pathways.

2.4 Conclusions

The capability to determine [ROOH] and measure RTA activity at elevated temperatures is particularly useful as it simulates the conditions encountered by lubricants and polymers in industrially relevant applications. The approach developed with pro-fluorescent phosphine **2.7**, has provided a simple and convenient means to analyse the complex mixtures of hydroperoxides arising from the autoxidation of heavy hydrocarbons. This methodology has allowed us to study the reactivity of a series of novel diarylamine RTAs at elevated temperatures where their catalytic activity is key to their performance. Although accumulation of carboxylic acids as a by-product of autoxidation is highly detrimental to their activity, addition of small amounts of base can uncover this reactivity – revealing their unprecedented efficacy as radical trapping antioxidants. Moreover, bases are already almost universally added to lubricating oils and other petroleum derived materials which are designed to be in contact with metal surfaces.

These results have important implications in both the design and use of the next generation of diarylamine RTAs. Achieving the correct balance of reactivity and stability is key to improved efficacy of these RTAs. Furthermore, a keen understanding of the interaction between all of the components in an autoxidizing mixture (whether derived from the autoxidation itself or as further additives) is necessary to maximize the performance of the RTA and the material as a whole.

2.5 References

(1) Ingold, K. U. *Chem. Rev.* **1961**, *61*, 563–589.

(2) Ingold, K. U.; Pratt, D. A. *Chem. Rev.* **2014**, *114*, 9022–9046.

(3) Burton, G. W.; Ingold, K. U. *J. Am. Chem. Soc.* **1981**, *103*, 6472–6477.

(4) Jensen, R. K.; Korcek, S.; Mahoney, L. R.; Zinbo, M. *J. Am. Chem. Soc.* **1979**, *101*, 7574–7584.

(5) Akasaka, K.; Suzuki, T.; Ohrui, H.; Meguro, H. *Anal. Lett.* **1987**, *20*, 731–745.

(6) Akasaka, K.; Suzuki, T.; Ohrui, H.; Meguro, H. *Anal. Lett.* **1987**, *20*, 797–807.

(7) Soh, N.; Ariyoshi, T.; Fukaminato, T.; Nakajima, H.; Nakano, K.; Imato, T. *Org. Biomol. Chem.* **2007**, *5*, 3762–3768.

(8) For example, Dojindo Molecular Technologies Inc. offer **2** for $206 per mg ($M_w$ 832.96, 90% purity).

(9) George A. Lemieux; de Graffenried, C. L.; Bertozzi, C. R. *J. Am. Chem. Soc.* **2003**, *125*, 4708–4709.

(10) Pan, J.; Downing, J. A.; McHale, J. L.; Xian, M. *Mol. Biosyst.* **2009**, *5*, 918–920.

(11) Hiatt, R.; Smythe, R. J.; McColeman, C. *Can. J. Chem.* **1971**, *49*, 1707–1711.

(12) Zhang, X.-F.; Liu, Q.; Wang, H.; Fu, Z.; Zhang, F. *J. Photochem. Photobiol. A Chem.* **2008**, *200*, 307–313.

(13) Soh *et al.* report k = 6400 M^{-1} s^{-1} for the reaction of **2** and methyl linoleyl hydroperoxides in EtOH at 37 °C.[7] It is unclear why this reaction is almost four orders of magnitude faster than the reaction of PPh_3 and *sec*-butyl hydroperoxides in EtOH (k = 1.0 M^{-1} s^{-1} at 25 °C)[10].

(14) Knight, H. B.; Swern, D. *Org. Synth.* **1954**, *34*, 90.

(15) Igarashi, J.; Jensen, R. K.; Lusztyk, J.; Korcek, S.; Ingold, K. U. *J. Am. Chem. Soc.* **1992**, *114*, 7727–7736. These autoxidations were self-initiated, so R_i was estimated based on [ROOH] ~ 10 mM at t = 10 min.

(16) The kinetics of the ROOH-initiated autoxidation of hexadecane obey $d[ROOH]^{1/2}/dt = ½[R–H]k_p\{2k_i/2k_t\}^{1/2}$ at low conversion, see ref. 15.

(17) Bolsman, T.; Blok, A.; Frijns, J. *Recl. des Trav. Chim. des Pays-Bas* **1978**, *97*, 310–312.

(18) Jensen, R. K.; Korcek, S.; Zinbo, M.; Gerlock, J. L. *J. Org. Chem.* **1995**, *60*, 5396–5400.

(19) Haidasz, E. A.; Shah, R.; Pratt, D. A. *J. Am. Chem. Soc.* **2014**, *136*, 16643–16650.

(20) Pratt, D. A.; DiLabio, G. A.; Brigati, G.; Pedulli, G. F.; Valgimigli, L. *J. Am. Chem. Soc.* **2001**, *123*, 4625–4626.

(21) Valgimigli, L.; Brigati, G.; Pedulli, G. F.; DiLabio, G. A.; Mastragostino, M.; Arbizzani, C.; Pratt, D. A. *Chem. - A Eur. J.* **2003**, *9*, 4997–5010.

(22) Wijtmans, M.; Pratt, D. A.; Valgimigli, L.; DiLabio, G. A.; Pedulli, G. F.; Porter, N. A. *Angew. Chemie Int. Ed.* **2003**, *42*, 4370–4373.

(23) Nam, T.; Rector, C. L.; Kim, H.; Sonnen, A. F. P.; Meyer, R.; Nau, W. M.; Atkinson, J.; Rintoul, J.; Pratt, D. A.; Porter, N. A. *J. Am. Chem. Soc.* **2007**, *129*, 10211–10219.

(24) Li, B.; Harjani, J. R.; Cormier, N. S.; Madarati, H.; Atkinson, J.; Cosa, G.; Pratt, D. A. *J. Am. Chem. Soc.* **2013**, *135*, 1394–1405.

(25) Hanthorn, J.; Valgimigli, L.; Pratt, D. *J. Am. Chem. Soc.* **2012**, *134*, 8306–8309.

(26) Hanthorn, J. J.; Valgimigli, L.; Pratt, D. A. *J. Org. Chem.* **2012**, *77*, 6908–6916.

(27) Hanthorn, J.; Amorati, R.; Valgimigli, L.; Pratt, D. *J. Org. Chem.* **2012**, *77*, 6895–6907.

(28) The data shown are from ref 14 and were obtained with RTAs bearing methyl side chains, except for the data for **16**, which have been measured using the same methodology and are reported for the first time here (see Supporting Information).

(29) Hanthorn, J.; Haidasz, E.; Gebhardt, P.; Pratt, D. *Chem. Commun.* **2012**, *48*, 10141–10143.

(30) Jalan, A.; Alecu, I. M.; Meana-Pañeda, R.; Aguilera-Iparraguirre, J.; Yang, K. R.; Merchant, S. S.; Truhlar, D. G.; Green, W. H. *J. Am. Chem. Soc.* **2013**, *135*, 11100–11114.

(31) Pratt, D. A.; DiLabio, G. A.; Valgimigli, L.; Pedulli, G. F.; Ingold, K. U. *J. Am. Chem. Soc.* **2002**, *124*, 11085–11092.

(32) Pratt, D. A.; DiLabio, G. A.; Mulder, P.; Ingold, K. U. *Acc. Chem. Res.* **2004**, *37*, 334–340.

(33) Montgomery, J. A.; Frisch, M. J.; Ochterski, J. W.; Petersson, G. A. *J. Chem. Phys.* **1999**, *110*, 2822.

(34) Protonation of the ring would also be expected to slow the regeneration of the amine from the corresponding alkoxyamine (i.e., eq 2.4) by strengthening the N–O bond. CBS-QB3 calculations predict that the N-O bond in the alkoxyamine derived from **15** is 4.2 kcal/mol stronger upon protonation of the ring (39.0 vs. 43.2 kcal/mol).

(35) Addition of more base did not extend the inhibited period.

(36) For reference, the pK_a of diphenylamine in water is 0.79. See: Pankratov, A. N.; Shchavlev, A. E. *J. Anal. Chem.* **2001**, 56, 123.

(37) Addition of base did not improve the activity of bis(2-alkylpyrimidine)amine **2.17**, consistent with the fact that its conjugate acid (pK_a = 4.2 ± 0.1) is stronger than the conjugate acid of **2.18** (pK_a = 4.6 ± 0.3).

(38) Unfortunately, it is not possible to accurately determine the stoichiometry of the reaction of the diarylamines with peroxyl radicals at this temperature since the autocatalytic nature of the reaction means that R_i changes as the reaction proceeds. As a result, we have "quantified" the efficacy of the inhibition of the heterocyclic diarylamines relative to the industry standard **2.7** simply by comparing the times required for 2% of the substrate to be autoxidized ($\Delta t_{2\%}$).

2.6 Supporting Information

Syntheses of phosphines **2.4**-**2.6**, and phosphine oxides **2.8**-**2.10** are provided in the Supporting Information section of the publication in Chemical Communications (*Chem. Commun.*, **2012**, *48*, 10141-10143). Control experiments for inhibited hexadecane autoxidations, diarylamine pKa measurements, as well as clocking experiments for diarylamine **2.16** are provided in the Supporting

Information section of the publication in The Journal of the American Chemical Society (*J. Am. Chem. Soc.*, **2015**, *137* (7), pp 2440–2443).

2.6.1 General Experimental

Reagents were purchased from commercial suppliers and used without further purification, unless otherwise indicated. The diarylamines (**2.12-2.17**) were synthesized according to our previously published report[S1] with slight modifications. Column chromatography was carried out using flash silica gel (40-63 μm, 230-400 mesh). ^{1}H and ^{13}C NMR were recorded on a Bruker AVANCE spectrometer at 400MHz and 100MHz respectively, unless specified otherwise. High resolution mass spectra were obtained on a Kratos Concept Tandem mass spectrometer.

2.6.2 General Procedure for Hexadecane Autoxidations

n-Hexadecane (100 mL) was thoroughly degassed with argon and then heated to 160°C while argon was continuously bubbled through the liquid. Once the temperature stabilized, 0.04 mmol of inhibitor (**2.12-2.18**) and 164 mg (1.0 mmol) of tetralin hydroperoxide were added to the solution and the flow of argon was replaced with O_2. Aliquots (0.5 mL) were removed every 5 minutes, and allowed to cool to room temperature for analysis. Four duplicates (30 μL) of each sample were loaded into separate wells of a 96-well microplate and the automated reagent dispenser of the microplate reader was used to dilute each sample with *tert*-amyl alcohol (200 μL) and a solution of a fluorgenic phosphine dye solution (20 μL of a 250 μM stock solution in acetonitrile) immediately before reading. The plate was stirred for 8 seconds, and allowed to rest for 2 more seconds, and the fluorescence of each well was measured every second for 60 seconds (absorption 340; emission 425). The concentration of hydroperoxide was determined from the rate of phosphine oxidation

using the rate constant for the reaction of the dye with secondary hydroperoxides in *tert*-amyl alcohol (k = 1.2 $M^{-1}s^{-1}$) assuming pseudo-first-order kinetics.

2.6.3 Synthesis of Pro-Fluorescent Phosphine 2.7 and Phosphine Oxide 2.11

3-(4-Iodophenyl)-7-methoxy-2H-chromen-2-one. A solution of 4- iodophenylacetonitrile (4.33 g, 17.8 mmol), 2-hydroxy-4-methoxybenzaldehyde3 (3.38 g, 17.5 mmol) and piperidine (1.52 g, 17.8 mmol) in 35 mL EtOH was heated to reflux until reaction completion, determined by TLC. The reaction was quenched by addition to 150 mL H_2O and extracted 3x with EtOAc. Organics were washed with brine and dried over $MgSO_4$ to afford a red oil. Purification by column chromatography (EtOAc/Hexanes 1:4) to obtain a peach-coloured solid. Yield: 67% brown solid. ^{1}H NMR (Actone-d_6, 400 MHz) δ ppm 8.13 (s, 1H), 7.81 (d, J = 8.5 Hz, 2H), 7.66 (d, J = 8.5 Hz, 1H), 7.58 (d, J = 8.5 Hz, 2H), 6.98-6.93 (m, 2H), 3.94 (s, 3H). ^{13}C NMR (Actone-d_6, 100 MHz) δ ppm 165.0, 161.5, 157.4, 142.4, 139.1, 137.0, 132.2, 131.5, 124.8, 115.1, 114.5, 102.0, 95.2, 57.3. HRMS (EI) m/z calculated 377.9753, found 377.9767.

3-(4-(Di-p-tolylphosphino)phenyl)-7-methoxy-2H-chromen-2-one (**2.7**). To a solution of the aryl iodide (4.0 mmol) in 4.0 mL N,N-dimethylacetamide (freshly distilled over BaO) was added $Pd(OAc)_2$ (2 mg, 4 µmol), KOAc (471 mg, 4.8 mmol) and di-*p*-tolylphosphine (781 mg, 4.2 mmol). The reaction was stirred at 100 °C until completion, as determined by TLC. Quenched by addition to H_2O and extraction with CH_2Cl_2. Washed with brine and dried over $MgSO_4$. Purified by column chromatography, eluting with EtOAc/Hexanes, followed by recrystallization to analytical purity. Yield: 85% off white solid. ^{1}H NMR (Actone-d_6, 400 MHz) δ ppm 8.12 (s, 1H), 7.76 (d, J = 8.0 Hz, 2H), 7.65 (d, J = 8.4 Hz, 1H), 7.32 (m, 2H), 7.23 (m, 8H), 6.94 (m, 2H), 3.94 (s, 3H), 2.34 (s, 6H). ^{13}C NMR ($CDCl_3$, 100 MHz) δ ppm 164.9, 161.6, 157.3, 142.3, 140.7, 137.5, 135.7, 135.6, 135.4, 134.9, 134.7, 131.4, 131.2, 131.2, 130.3, 130.2, 125.4, 115.2, 114.4, 102.0, 57.3, 22.2. HRMS (EI) m/z calculated 464.1541, found 464.1540.

3-(4-(Di-p-tolylphosphoryl)phenyl)-7-methoxy-2H-chromen-2-one (**2.11**): To a solution of **7** (1.0 mmol) in 5 mL MeOH was added tertbutylhydroperoxide (1.0 mmol) at room temperature. Once oxidation was complete, the phosphine oxide was passed through a small silica column eluting with EtOAc, followed by recrystallization to analytical purity. Yield: 88% white solid. ^{1}H NMR (Actone-d_6, 400 MHz) δ ppm 8.20 (s, 1H), 7.91 (dd, J = 8.1, 2.0 Hz, 2H), 7.76-7.67 (m, 3H), 7.61 (d, J = 8.0 Hz, 2H), 7.58 (d, J = 8.0 Hz, 2H), 7.37-7.35 (m, 4H), 6.95-6.96 (m, 2H), 3.95 (s, 3H), 2.41 (s, 6H). ^{13}C NMR ($CDCl_3$, 100 MHz) δ ppm 165.1, 161.5, 157.5, 144.1 (d, J = 2.8 Hz), 143.2, 140.6 (d, J = 2.8 Hz), 136.1, 135.0, 133.7, 133.6, 133.5, 133.4, 132.8, 131.8, 131.6, 131.1, 130.9, 130.2, 130.1, 124.8, 115.0, 114.6, 102.0, 57.4, 22.5. HRMS (EI) m/z calculated 480.1490, found 480.1474.

2.6.4 General Method for the Preparation of 5-Bromo-*N*,*N*-Dialkylaminopyri(mi)dines

To a solution of 5-bromo-2-aminopyri(mi)dine (1.0 mmol) in dry THF (2 mL) at 50°C, NaH (2.2mmol) was added slowly and the mixture was stirred until H_2 evolution ceased. Alkylbromide (2.1 mmol) was then added and the reaction was refluxed overnight. The reaction was cooled, quenched with MeOH and extracted with Et_2O. The combined organics were washed with brine and dried over $MgSO_4$. The oil obtained was passed through a plug of silica (Et_2O/Hexanes) to obtain pure products.

5-Bromo-N,N-dihexylpyridin-2-amine: Yield: quantitative, Colourless Oil. ^{1}H NMR (400 MHz; $CDCl_3$): δ 8.12 (s, 1H), 7.40 (dd, *J* = 9.1, 2.6 Hz, 1H), 6.31 (d, *J* = 9.1 Hz, 1H), 3.37 (t, *J* = 7.6 Hz, 4H), 1.56 (s, 4H), 1.31 (d, *J* = 1.3 Hz, 12H), 0.91-0.88 (m, 6H). ^{13}C NMR (100 MHz; $CDCl_3$): δ 156.5, 148.6, 139.1, 106.9, 105.0, 49.0, 31.8, 27.5, 26.9, 22.8, 14.1, HRMS: m/z Calc: $C_{17}H_{29}BrN_2$: 340.1514 Found: 340.1515.

5-Bromo-N,N-dibutylpyrimidin-2-amine: Yield: 92%, Colourless Oil. ^{1}H NMR (400 MHz; $CDCl_3$): δ 8.20 (s, 2H), 3.46 (t, *J* = 7.5 Hz, 4H), 1.57-1.49 (m, 4H), 1.30 (dt, *J* = 14.6, 7.3 Hz, 5H), 0.90 (dd, *J* = 7.2, 6.5 Hz, 7H). ^{13}C NMR (100 MHz; $CDCl_3$): δ 159.7, 157.6, 104.6, 77.4, 77.1, 76.7, 47.8, 29.8, 20.2, 14.0, HRMS: m/z Calc: $C_{12}H_{20}BrN_3$: 285.0840 Found: 285.0841.

5-Bromo-N,N-dihexylpyrimidin-2-amine: Yield: 92%, Colourless Oil. ^{1}H NMR. (400 MHz; $CDCl_3$): δ 8.24 (s, 2H), 3.48 (t, *J* = 7.6 Hz, 4H), 1.57 (s, 5H), 1.30 (t, *J* = 3.3 Hz, 12H), 0.89 (d, *J* = 2.5 Hz, 6H). ^{13}C NMR (100 MHz; $CDCl_3$): δ 159.8, 157.7, 104.7, 48.2, 31.8, 27.6, 26.8, 22.8, 14.2, HRMS: m/z Calc: $C_{16}H_{28}BrN_3$: 340.1466 Found: 340.1466.

2.6.5 Method for the Preparation of 5-Bromo-2-Hexylpyrimidine

Hexylmagnesiumbromide was prepared prior to use. Mg (1.0 mmol) in dry THF was activated 4x with I_2. Hexylbromide (1.0 mmol) in dry THF (10 mL) was added slowly to maintain the solution at near reflux. After addition was complete the reaction was heated to 60°C for 1hr. $ZnCl_2$ (1.25 mmol) solution was added dropwise to Hexylmagnesiumbromide (1.0 mmol) in THF (12.5 mL) and stirred for 10 minutes. 5-bromo-2-iodopyrimidine (0.5 mmol) and $Pd(PPh_3)_4$ was added and stirred overnight. The reaction quenched with water, and extracted with Et_2O. The combined organics were washed with brine, and dried over $MgSO_4$. Column chromatography (10% Et_2O/Hexanes eluent) afforded pure product. Yield: 61%, White Powder. ^{1}H NMR (400 MHz; $CDCl_3$): δ 8.69 (s, 2H), 2.90 (t, *J* = 7.7 Hz, 2H), 1.78 (dt, *J* = 14.7, 7.5 Hz, 2H), 1.31 (dd, *J* = 5.9, 3.6 Hz, 7H), 0.87 (t, *J* =

7.0 Hz, 3H). ^{13}C NMR (100 MHz; $CDCl_3$): δ 170.0, 157.7, 117.7, 39.0, 31.7, 29.1, 28.7, 22.7, 14.2, HRMS: m/z Calc: $C_{10}H_{15}BrN_2$: 242.0418 Found: 242.0419.

2.6.6 Cu-Catalyzed Benzylamination of 5-Bromo-N,N-Dibutylpyrimidin-2-Amine

To a sealed tube were added 5-bromo-N,N-dihexylpyridin-2-amine (1.0 mmol), CuI (0.2 mmol), L-proline (0.4 mmol), and K_2CO_3 (1.5 mmol). The flask was filled with argon before DMSO (1.5 mL) and Water (1.0 % v/v) was added. After a few minutes of stirring, $BnNH_2$ (1.8 mmol) was added and the reaction was heated to 80°C until completion, as determined by TLC. The reaction was cooled, quenched with water, and extracted with Et_2O. The combined organics were washed twice with water, washed with brine, and dried over $MgSO_4$. Column chromatography (40% Et_2O/Hexanes eluent) afforded pure products. The compound was recrystallized from hexanes to analytical purity. Yield: 83%, Yellow Needles. ^{1}H NMR (400 MHz; $CDCl_3$): δ 7.91 (s, 2H), 7.35-7.26 (m, 5H), 4.23 (s, 2H), 3.47 (t, *J* = 7.5 Hz, 4H), 1.59-1.51 (m, 4H), 1.33 (dq, *J* = 15.1, 7.5 Hz, 4H), 0.93 (t, *J* = 7.3 Hz, 6H). ^{13}C NMR (100 MHz; $CDCl_3$): δ 157.3, 145.1, 139.3, 132.5, 128.8, 127.72, 127.52, 77.5, 77.2, 76.8, 50.1, 47.8, 30.3, 20.4, 14.2, HRMS: m/z Calc: $C_{23}H_{36}N_4$: 368.2940 Found: 368.2939.

2.6.7 Deprotection of N^5-Benzyl-N^2,N^2-Dibutylpyrimidine-2,5-Diamine

To a solution of 13 (1.0 mmol) in degassed MeOH (5 mL) were added 10% Pd/C (10 wt %) and ammonium formate (3.0 mmol). The flash was backfilled with argon and the solution was heated to reflux until completion, as determined by TLC. When complete, the solution was cooled and filtered through a pad of celite. The solvent was evaporated and the resulting solid was re-dissolved in a 40% Et_2O/hexanes solution. The precipitate formed was filtered off through another pad of celite and washed with ether. The solvent was evaporated to obtain the desired compound without any residual

ammonium formate. No further purification was attempted because of oxidative instability and difficulty associated with chromatographing this compound.

2.6.8 General Procedure for Synthesis of Diarylamines

To a flame-dried Schlenk flask were Pd_2dba_3 (0.01mmol) and BippyPhos (Pd/L = 1:4). The flask was evacuated and backfilled with argon before *tert*-amylalcohol (1 mL) was added, followed by KOH (1.5 mmol) and H_2O (1.0% v/v) the solution was stirred for 20 minutes. After 20 min, ArBr (1.0 mmol) and $ArNH_2$ (1.1 mmol) were added, and the reaction was heated to 110°C. Once complete, the mixture was evaporated under vacuum and loaded on a silica column. Column chromatography (Et_2O/hexanes eluent with 1−5% Et_3N added depending on substrate) afforded pure products.

N^2,N^2-dibutyl-N^5-(6-(dihexylamino)pyridin-3-yl)pyrimidine-2,5-diamine (**2.12**)**:** Yield: 67%, Brown Oil. ^{1}H NMR (300 MHz; $CDCl_3$): δ 8.09 (s, 2H), 7.83 (d, *J* = 2.7 Hz, 1H), 7.07 (dd, *J* = 9.0, 2.9 Hz, 1H), 6.35 (d, *J* = 8.9 Hz, 1H), 4.75 (s, 1H), 3.58 (q, *J* = 7.0 Hz, 4H), 3.36 (t, *J* = 7.6 Hz, 4H), 1.57-1.52 (m, 4H), 1.29-1.26 (m, 20H), 1.17 (t, *J* = 7.0 Hz, 6H), 0.87 (t, *J* = 6.7 Hz, 6H). ^{13}C NMR (75 MHz; $CDCl_3$): δ 157.9, 154.2, 151.0, 138.9, 130.6, 129.0, 128.8, 106.0, 49.1, 42.2, 32.0, 29.7, 29.5, 27.9, 27.3, 22.8, 14.2, 13.3, HRMS: m/z Calc: $C_{29}H_{50}N_6$: 482.4097 Found: 482.4098.

N^2,N^2-dibutyl-N^5-(2-(dibutylamino)pyrimidin-5-yl)pyrimidine-2,5-diamine (**2.13**)**:** Yield: 65%, Yellow Powder. ^{1}H NMR (300 MHz; $CDCl_3$): δ 7.95 (s, 4H), 3.47 (t, *J* = 7.5 Hz, 8H), 1.60-1.50 (m, 9H), 1.33 (dt, *J* = 15.0, 7.4 Hz, 9H), 0.92 (t, *J* = 7.3 Hz, 12H). ^{13}C NMR (75 MHz; $CDCl_3$): δ 157.7, 147.0, 129.4, 47.8, 30.2, 20.4, 14.2, HRMS: m/z Calc: $C_{24}H_{41}N_7$: 427.3423 Found: 427.3422.

N^2,N^2-Dihexyl-N^5-phenylpyridine-2,5-diamine **(2.14):** Yield: 74%, Brown Oil. ^{1}H NMR (400 MHz; $CDCl_3$): δ 8.03 (d, *J* = 2.7 Hz, 1H), 7.31 (dd, *J* = 9.0, 2.8 Hz, 1H), 7.19-7.15 (m, 2H), 6.78-6.75 (m, 3H), 6.43 (d, *J* = 9.0 Hz, 1H), 5.25 (s, 1H), 3.42 (t, *J* = 7.7 Hz, 4H), 1.62-1.56 (m, 4H), 1.35-1.32 (m,

12H), 0.90 (t, *J* = 6.8 Hz, 6H). ^{13}C NMR (100 MHz; $CDCl_3$): δ 14.2, 22.8, 27.0, 27.8, 31.9, 49.1, 105.7, 114.2, 118.7, 126.6, 129.4, 134.3, 144.4, 147.0, 155.5, HRMS: m/z Calc: $C_{23}H_{35}N_3$: 353.2831 Found: 353.3428.

N^2,N^2-Dihexyl-N^5-phenylpyrimidine-2,5-diamine **(2.15):** Yield: 81%, Brown Oil. ^{1}H NMR (400 MHz; $CDCl_3$): δ 8.22 (s, 2H), 7.20-7.16 (m, 2H), 6.79 (t, *J* = 7.3 Hz, 1H), 6.72 (d, *J* = 7.6 Hz, 2H), 5.13 (s, 1H), 3.54 (t, *J* = 7.6 Hz, 4H), 1.63-1.58 (m, 4H), 1.33 (d, *J* = 3.7 Hz, 12H), 0.90 (t, *J* = 6.6 Hz, 6H). 13-C NMR (100 MHz; $CDCl_3$): δ 159.5, 155.4, 146.8, 129.5, 124.9, 119.1, 114.0, 48.2, 31.9, 27.9, 26.9, 22.8, 14.2, HRMS: m/z Calc: $C_{22}H_{34}N_4$: 354.2783 Found: 354.2790.

N^2,N^2-dibutyl-N^5-(2-hexylpyrimidin-5-yl)pyrimidine-2,5-diamine (**2.16):** Yield: 84%, Yellow Powder. ^{1}H NMR (400 MHz; $CDCl_3$): δ 8.19 (s, 2H), 8.15 (s, 2H), 5.23-5.16 (m, 1H), 3.53 (t, *J* = 7.5 Hz, 4H), 2.83 (t, *J* = 7.7 Hz, 2H), 1.74 (quintet, *J* = 7.1 Hz, 2H), 1.59 (quintet, *J* = 7.3 Hz, 4H), 1.37-1.29 (m, 10H), 0.94 (t, *J* = 7.3 Hz, 6H), 0.86-0.84 (m, 3H). 13-C NMR (100 MHz; $CDCl_3$): δ 162.4, 159.8, 155.4, 142.7, 138.6, 123.1, 48.0, 38.6, 31.8, 30.0, 29.18, 29.11, 22.7, 20.4, 14.20, 14.16, HRMS: m/z Calc: $C_{22}H_{36}N_6$: 384.3001 Found: 384.3099.

2.6.9 Reaction of 2.7 with Tetralin Hydroperoxide

Stock solution of the appropriate amount of tetralin hydroperoxide in *t*-amyl alcohol (30 µL) were loaded into separate wells of a 96-well microplate and the automated reagent dispenser of the microplate reader was used to dilute each sample with *tert*-amyl alcohol (200 µL) and a solution of a fluorgenic phosphine dye solution (20 µL of a 250 µM stock solution in acetonitrile) immediately before reading. The plate was stirred for 8 seconds, and allowed to rest for 2 more seconds, and the fluorescence of each well was measured every second for 60 seconds (absorption 340; emission 425).

2.6.10 Initial Rates of the Reaction of 2.7 with TetOOH

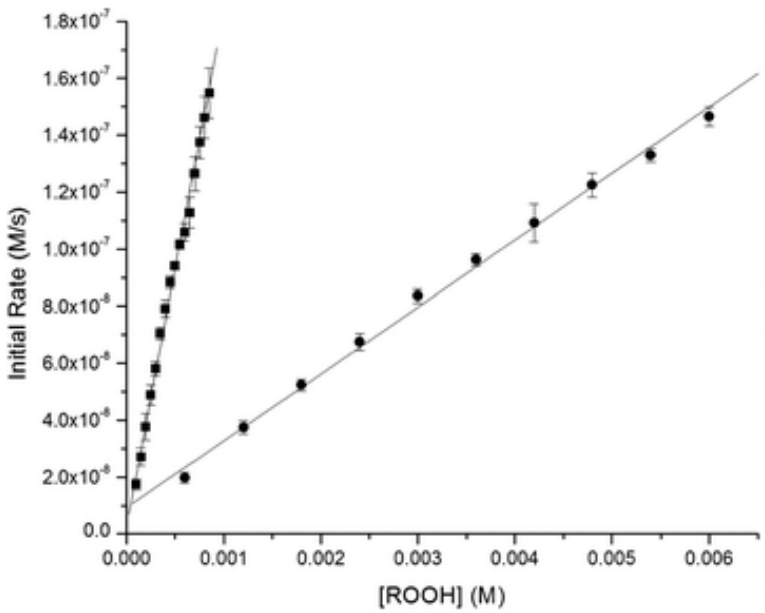

Figure S2.1. Initial rates for the reaction of **2.7** (20 μM) with TetOOH in MeOH (■) at 37 °C and *t*-AmOH (●) at 25 °C.

2.6.11 Hexadecane Autoxidation in the Presence of Carbonate and Amine Bases

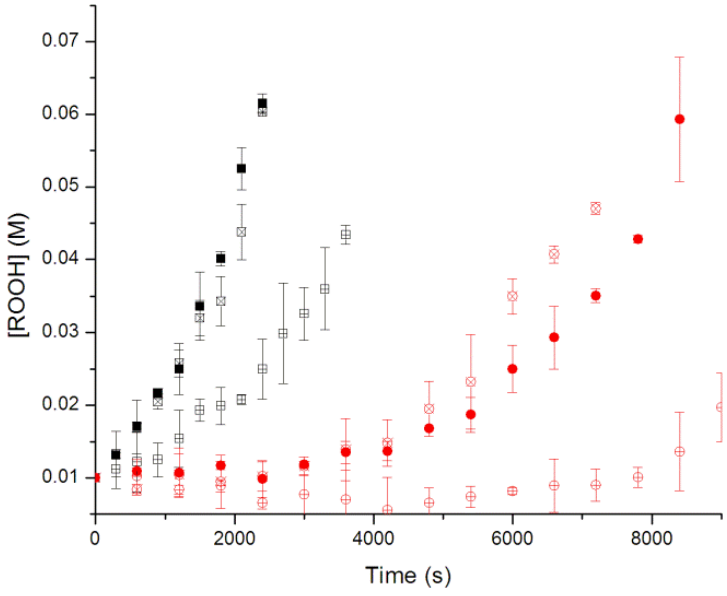

Figure S2.2. Hydroperoxide formation in the autoxidation of *n*-hexadecane at 160°C initiated by 10 mM tetralin hydroperoxide, uninhibited in the presence of 1.0 mM TTBP (■), 1.0 mM Cs_2CO_3 (⊠),

ca. 1.0 mM DOW Primene 51 (⊞) and inhibited by 40 μM of **2.15** in the presence of 1.0 mM TTBP (●), 1.0 mM Cs_2CO_3 (⊠), *ca.* 1.0 mM DOW Primene 51 (⊕).

2.6.12 Carboxylic Acid Measurements

Samples were taken from uninhibited hexadecane autoxidations (as described above). 50μL of the sample was diluted into 4.95 ml of a 20% iPrOH in MeOH solution containing 10.5 μM 3,5-dimethylbenzoic acid. The samples were infused directly onto the TQ Detector of a Waters Acuity H-Class UPLC-MS. The mass spectrum (from 50-400 M/Z) of each sample was recorded three times, for 2 minutes per read, with a scan time of two seconds. (Negative ion mode, Capillary voltage = 3.2 kV, Cone voltage = 40V, Extractor voltage = 3V, Source T = 150°C, Desolvation T = 250°C, Desolvation Gas flow = 500 l/hr, Cone gas flow = 50 l/hr).

Standards were prepared from 2.0 mM solutions of octanoic, nonanoic, decanoic, undecanoic, dodecanoic, tridecanoic, and tetradecanoic acids (in the same hexadecane solution), and diluted in the same way as described above.

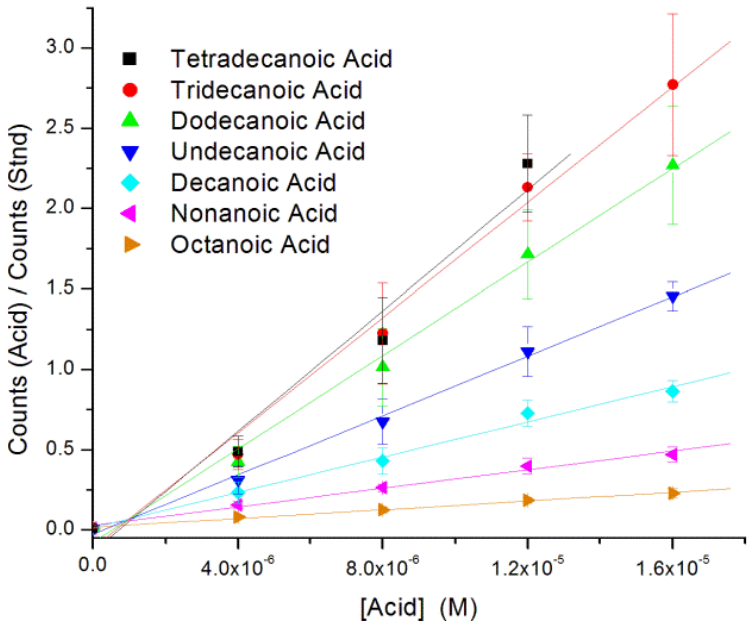

Figure S2.3. Standard curve for alkyl carboxylic acids vs 10.5 μM 3,5-dimethylbenzoic acid.

CHAPTER 3: A Continuous Visible Light Spectrophotometric Approach to Accurately Determine the Reactivity of Radical-Trapping Antioxidants

3.1 Preface

Inhibited autoxidations – monitored either by O_2 consumption or hydroperoxide formation – are the most reliable way to obtain kinetic and stoichiometric information on the activity of radical-trapping antioxidants (RTAs). While many comparatively simple "antioxidant assays" (e.g., the DPPH assay) have supplanted these in popularity, they are generally very poor substitutes since they often do not employ peroxyl radicals as the oxidant and do not account for both the kinetics and stoichiometry of the radical-trapping reaction(s). In an effort to improve upon the traditional approaches for inhibited autoxidations – and making them as simple as the more popular "antioxidant assays" – we have developed a spectrophotometric approach for monitoring reaction progress in these reactions. The approach employs easily prepared 1-phenylbutadiene-conjugated or styrene-conjugated BODIPY chromophores (PBD-BODIPY or STY-BODIPY, respectively) as signal carriers that co-autoxidize along with a hydrocarbon substrate.

We show that inhibition rate constants (kinh) are accurately determined for a range of phenolic and diarylamine RTAs using this approach, and that mechanistic experiments, such as kinetic isotope effects and kinetic solvent effects, are equally easily carried out. Moreover, synergistic interactions between RTAs, as well as the unconventional activity of diarylamine RTAs, are captured using this methodology. Lastly, we show that the approach can be employed for monitoring reactions in aqueous solution. This chapter is presented as it was published in the Journal of Organic Chemistry (*J. Org. Chem.*, **2016**, 81, 737-744). This work was performed in conjunction with Anthony Van Kessel, who as an undergraduate student under my supervision at the time, was responsible for the experiments with STY-BODIPY, both in aqueous and organic solution.

3.2 Introduction

Autoxidation, the radical-mediated chain reaction that converts hydrocarbons to hydroperoxides (eqs 3.1 and 3.2), can be inhibited by the addition of radical-trapping antioxidants (RTAs). The relevant inhibition reactions for phenolic RTAs are shown in eqs 3.3 and 3.4.

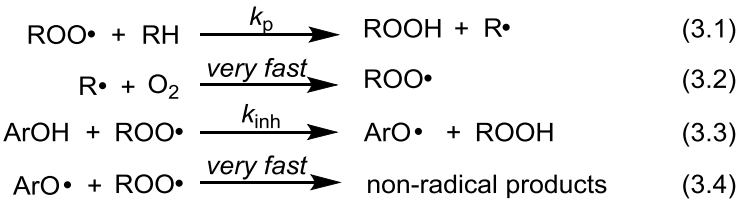

The inherent reactivity of an RTA is characterized by the rate constant for its reaction with peroxyl radicals (also known as the inhibition rate constant, k_{inh}) since this is the reaction that competes with the rate-determining propagation step of the chain reaction (eq 3.1). An additional, but equally important, consideration is the stoichiometry of the RTA-peroxyl reaction (n), which is generally 2 for phenols due to the reactions in eqs 3.3 and 3.4.[1,2]

Given the importance of RTAs in the preservation of petroleum-derived materials and consumer products, as well as their putative role in maintaining human health and promoting longevity, many methods have been developed to study RTAs. The best approaches comprise kinetic studies of inhibited autoxidations, where reaction progress is followed either by consumption of one of the starting materials (O_2) or the formation of products (hydroperoxides).[3–5] The former approach is preferred as it can be carried out continuously, but it involves specialized equipment to accurately assess the pressure differential between inhibited and uninhibited autoxidations carried out in parallel. The latter approach is a discontinuous assay where hydroperoxides are determined in aliquots removed from the reaction mixture. This is usually done by laborious iodometric titrations or time-consuming chromatographic analyses. Recently developed fluorogenic probes are attractive alternatives, but the fact remains that these are discontinuous assays.[6]

Over the years, the desire for more accessible and/or rapid alternatives to inhibited autoxidations has prompted the development of a myriad of assays of "antioxidant activity". Some of the most common include TROLOX equivalent antioxidant capacity (TEAC),[7] ferric reducing antioxidant power (FRAP),[8] and DPPH• quenching (eq 3.5).[9–11]

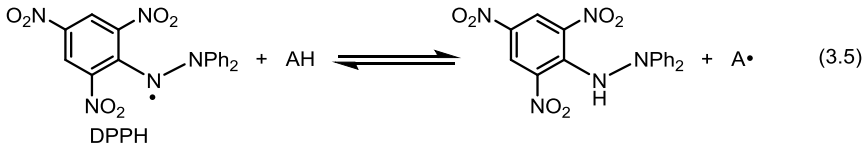

(3.5)

These approaches are generally based on spectrophotometric determination of the position of the equilibrium between a test antioxidant (a reducing agent) and an oxidizing agent that possesses a good absorbance and/or fluorescence.[3–5] It must be emphasized that *peroxyl radicals are often not employed as the oxidizing agent* in these experiments and that they are generally carried out in highly polar (alcoholic) solvents that are necessary to solubilize the reagents. *Such solvents are poor models for either the confines of the lipid bilayer or petroleum derived materials wherein RTA activity is most important*. In fact, these reactions can be subject to kinetic solvent effects owing to either H-bonding of the RTA or the contributions of electron transfer reactions from the conjugate base of the RTA.[12] The ideal approach to determine the reactivity of RTAs would incorporate the desirable features of the above methods; it would be rapid, operationally simple, utilize standard laboratory equipment, *and most importantly* be capable of providing accurate kinetic and stoichiometric information for reactions of RTAs with peroxyl radicals.

C11-BODIPY581/591 is a popular compound for monitoring lipid oxidation in cell culture.[13,14] Its fluorescence is shifted significantly (from 595 to 520 nm) upon reaction with peroxyl radicals – presumably as a result of reduced conjugation due to peroxyl radical addition to the 4-phenyl-1,3-butadienyl (PBD) unit followed by O_2 addition to the resultant carbon-centered radical as shown in Scheme 3.1 (although this has not been studied in detail).

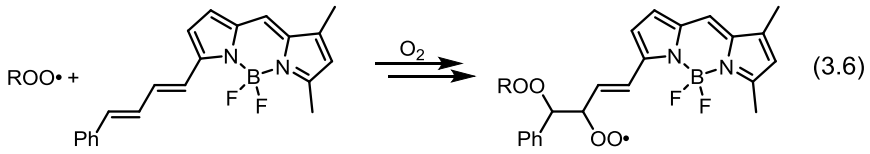

Scheme 3.1. Propagation steps in the autoxidation of C11-BODIPY$^{581/591}$.

Niki[15] demonstrated that C11-BODIPY581/591 is oxidized in azo-initiated co-autoxidations with methyl linoleate and that an added antioxidant (2,6-di-tert-butyl-4-methylphenol, BHT) can slow this process. Accordingly, we wondered if an assay based upon the competitive oxidation of C11-BODIPY$^{581/591}$ (or a suitable inexpensive analogue thereof) and an appropriate organic substrate (to ensure that the process is a radical chain reaction) could be developed to enable the accurate determination of the inhibition rate constants (k_{inh}) and stoichiometry (n) of reactions of RTAs with peroxyl radicals. Our successful efforts are described below.

3.3 Results and Discussion

3.3.1 Monitoring Styrene Autoxidations

Since the undecanoic acid substitution in C11-BODIPY$^{581/591}$ simply provides fatty acid-like physical properties for phospholipid bilayer solubility, the solution-based experiments described here were performed with the simpler BODIPY-substituted 1-phenylbutadiene (hereafter PBD-BODIPY). This compound is much more easily prepared (Scheme 3.2)[16,17] and manipulated than the commercially available (but exceedingly expensive) C11-BODIPY$^{581/591}$. The spectroscopic properties of PBD-BODIPY have been described by others[16,17] and are highly similar to that of C11-BODIPY$^{581/591}$,[18] in particular, the absorption spectrum, which features a maximum at 591 nm and emission spectrum with corresponding maximum at 608 nm.[4]

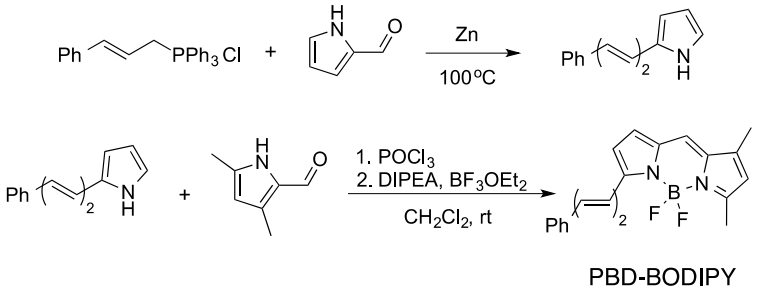

Scheme 3.2. Synthesis of PBD-BODIPY.

Under conditions similar to those commonly used in O_2 consumption experiments, the AIBN-initiated (see Chart 3.1) co-autoxidation of styrene (4.3 M in chlorobenzene) and PBDBODIPY (10 μM) at 37°C, produced a linear increase in fluorescence at 515 nm with time (λ_{ex} = 485 nm, data not shown). However, since PBD-BODIPY is expected to oxidize in a similar manner to styrene – via addition of a peroxyl radical to the phenylbutadienyl unit followed by O_2 addition to the resultant alkyl radical to afford a new peroxyl radical (as shown for C11-BODIPY$^{581/591}$ in eq 3.6)[19] – the fluorescent product is incorporated into a styrene-oxygen copolymer in solution, precluding standardization of the signal.[20] Therefore, we elected to monitor the kinetics of PDB-BODIPY oxidation and its inhibition by added RTAs using absorbance. Representative examples are shown in Figure 3.1.

Chart 3.1. Free radical initiators, AIBN and AAPH.

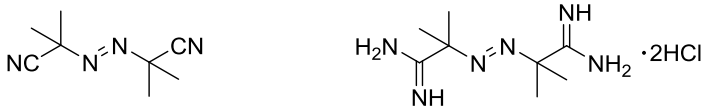

The reaction profiles in Figure 3.1 are strikingly reminiscent of those obtained from inhibited autoxidations monitored by O_2 consumption.[3–5] Inhibition by the representative phenolic RTAs **3.1**−**3.4** followed the expected trend, where pyrimidinol **3.4** was most reactive to peroxyl radicals, suppressing PBD-BODIPY oxidation to the greatest extent, followed closely by 2,2,5,7,8-pentamethylchroman-6-ol (PMC, **3.3**) and then 3,5-di-tert-butyl-4-hydroxyanisole (**3.2**) and, last, 3,5-di-tert-butyl-4-hydroxytoluene (BHT, **3.1**).

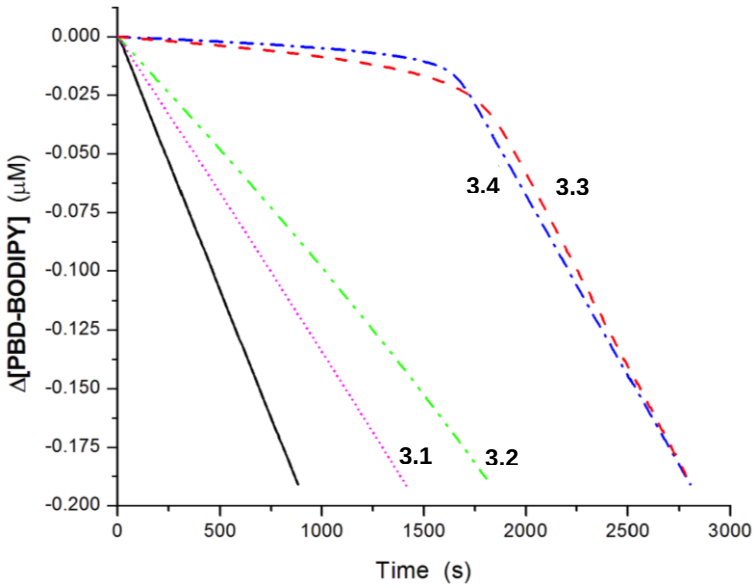

Figure 3.1. Co-autoxidation of styrene (4.3 M) and PBD-BODIPY (10 μM) initiated by AIBN (6 mM) in PhCl at 37 °C (solid line) and inhibited by 2 μM BHT (**3.1**), BHA (**3.2**), PMC (**3.3**), and 2-(N,N-dimethylamino)-4,6-dimethyl-5-pyrimidinol (**3.4**). Reaction progress was monitored by absorbance at 591 nm (ε = 139,000 $M^{-1}cm^{-1}$).

Although a simple comparison of the initial rates of PBD-BODIPY consumption in the presence of the different RTAs provides a good qualitative assessment of their relative RTA activity, we sought to develop a method to obtain quantitative data, i.e., the inhibition rate constant (k_{inh}) for reaction of an RTA with peroxyl radicals. In order to do so, the rate constant for the competing reaction of PBD-BODIPY with peroxyl radicals ($k_{PBD\text{-}BODIPY}$) must be known. This was easily determined by measuring its rate of consumption in co-autoxidations with variable concentrations of PBD-BODIPY (assuming a steady-state concentration of peroxyl radicals) via eq 3.7.[3–5]

$$\frac{-\delta[\text{PBD}-\text{BODIPY}]}{\delta t} = \frac{k_{\text{PBD}-\text{BODIPY}}}{\sqrt{2k_t}}\sqrt{R_i}[\text{PBD} - \text{BODIPY}] \qquad (3.7)$$

Thus, plotting the rate of PBD-BODIPY consumption versus its concentration (as in Figure 3.2) yields a line where the slope is given by a combination of $k_{PBD\text{-}BODIPY}$, $\sqrt{R_i}$, and $\sqrt{2k_t}$ (eq 3.7).

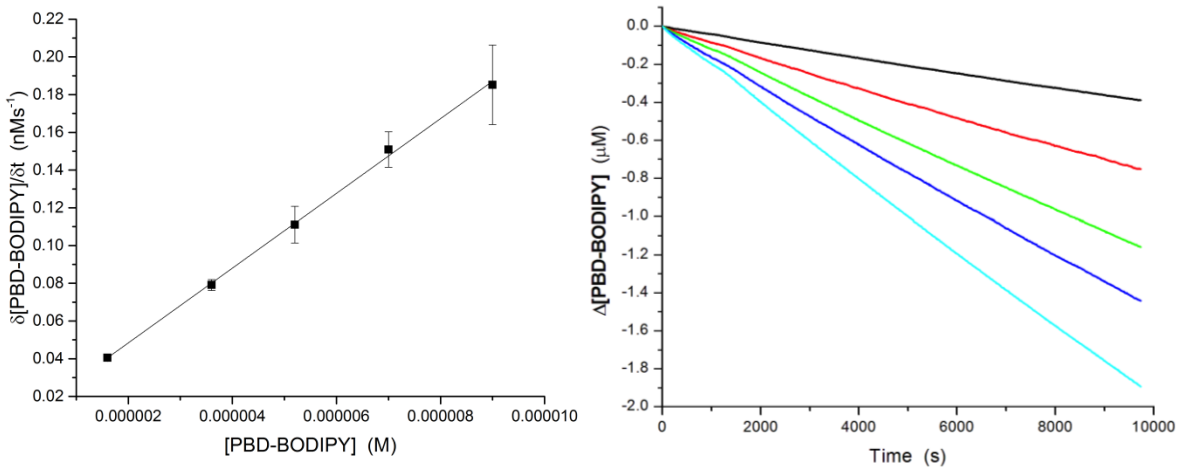

Figure 3.2. Rate of PBD-BODIPY consumption as a function of PBD-BODIPY concentration in AIBN-initiated (6 mM) co-autoxidations of PBDBODIPY and styrene (4.3 M) in PhCl at 37 °C (left) and the corresponding representative raw data (right). Reaction progress was monitored by absorbance at 591 nm (ε = 139,000 $M^{-1}cm^{-1}$).

The rate of initiation, R_i, can be estimated from literature data to be 2.0 × 10^{-9} M s^{-1} at 37 °C. Alternatively, it can be determined readily under the exact experimental conditions simply from the length of the inhibition period, t_{inh}, of an inhibited autoxidation with a known amount of inhibitor AH, provided its stoichiometric number (n) is known, as in eq 3.8.

$$R_i = \frac{n[AH]}{t_{inh}} \qquad (3.8)$$

Doing so with **3.3** (e.g., using the data in Figure 3.1), which is well-known to have n = 2, we obtain R_i = 2.2 × 10^{-9} M s^{-1} corresponding to ek_d = 1.9×10^{-7} s^{-1}. Although there are three possible peroxyl−peroxyl radical termination reactions that may occur (eqs 3.9−3.11), we can assume that eq 3.9 dominates since styrylperoxyl radicals react very rapidly with each other (k_t = 2.1 × 10^7 M^{-1} s^{-1})[23,24] and styrene is present in a great excess compared to PBD-BODIPY.

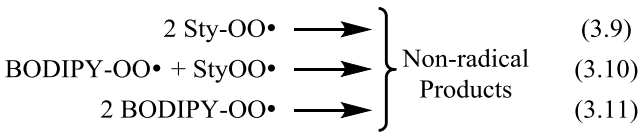

Using these values of R_i and k_t, the rate constant for the reaction of PBD-BODIPY and peroxyl radicals can be calculated as $k_{PBD\text{-}BODIPY} = 2720\ M^{-1}\ s^{-1}$. With this key value in-hand, the data in Figure 3.1 can be analyzed using the well-established kinetic expressions for inhibited hydrocarbon autoxidations,[3–5] where k_{inh} for the RTAs can be determined from the initial rate of PBD-BODIPY consumption as in eq 3.12 and n from t_{inh} as in eq 3.13.[51]

$$\frac{-\delta[\mathrm{PBD-BODIPY}]}{\delta t} = \frac{k_{\mathrm{PBD-BODIPY}}[\mathrm{PBD-BODIPY}]R_i}{nk_{inh}[\mathrm{RTA}]} \qquad (12)$$

$$n = \frac{t_{inh}R_i}{[\mathrm{RTA}]} \qquad (13)$$

Doing so for RTAs **3.2**–**3.4** yields rate constants that are within experimental error of those determined by O_2 consumption (see Table 3.1) and which are characterized by stoichiometric numbers of $n \sim 2$, as expected (vide supra). RTA **3.1** (BHT) was too slow to effectively compete with PBD-BODIPY oxidation, precluding determination of its corresponding k_{inh} value (more on this later).

Table 3.1. Inhibition Rate Constants and Stoichiometries Determined for Various RTAs Determined by Co-Autoxidations of PBD-BODIPY and Styrene[a]

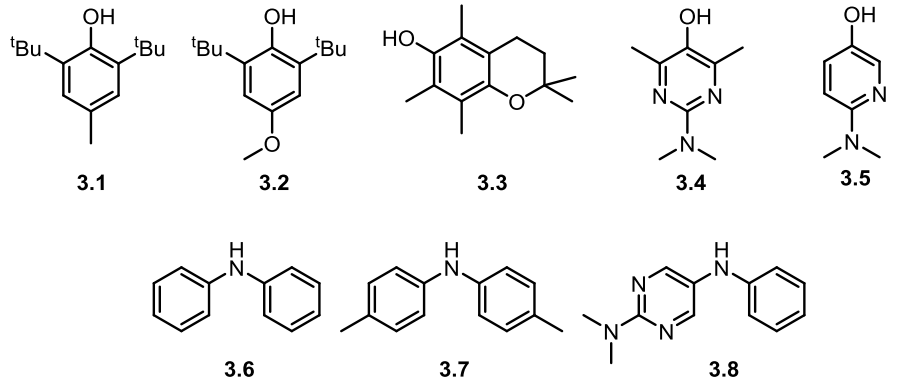

RTA	*n*	k_{inh} ($M^{-1}s^{-1}$)	Literature k_{inh} ($M^{-1}s^{-1}$)
3.1	---	*too slow*	1.4×10^4 (30 °C)[24]
3.2	1.8 ± 0.2	$(1.6 \pm 0.2) \times 10^5$	1.1×10^5 (30 °C)[24]
3.3	2.0	$(3.8 \pm 0.2) \times 10^6$	3.8×10^6 (30 °C)[24]
3.3[b]	1.9 ± 0.1	$(8.1 \pm 0.8) \times 10^5$	7.5×10^5 (30 °C)[d]
3.3[c]	2.0	$(6.6 \pm 0.4) \times 10^5$	6.8×10^5 (30 °C)[25]
3.4	1.8 ± 0.1	$(9.9 \pm 2.3) \times 10^6$	7.4×10^6 (30 °C)[26]
3.5	2.0 ± 0.2	$(4.4 \pm 0.6) \times 10^6$	3.6×10^6 (30 °C)[26]
3.6	---	*too slow*	2.0×10^4 (65 °C)[27]
3.7	3.1 ± 0.2	$(3.7 \pm 0.2) \times 10^5$	1.8×10^5 (37 °C)[28]
3.8	3.9 ± 0.2	$(9.9 \pm 0.6) \times 10^5$	3.0×10^6 (37 °C)[28]

[a]Determined by co-autoxidation of styrene (4.3 M) and PBD-BODIPY (10 μM) initiated by AIBN (6 mM) in PhCl at 37 °C and inhibited by 1−2 μM RTA. [b]Same as above, but containing 1% MeOD. The corresponding value for 1% MeOH was kinh = $(3.6 \pm 0.2) \times 10^6$ M^{-1} s^{-1}. The literature value was determined for 1% D_2O/H_2O. [c]Measured in CH_3CN. [d]Calculated from literature data.[24,29]

To demonstrate the utility of the approach for carrying out mechanistic studies, we determined example kinetic isotope effects (KIE) and kinetic solvent effects for the well-known reaction of **3.3**. The KIE for the reaction of **3.3** with peroxyl radicals was obtained by the addition of 1% MeOH/MeOD to an inhibited autoxidation. While MeOH had only a slight effect on the inhibition rate constant, $k_{inh}^{PhCl} / k_{inh}^{PhCl+MeOH}$ = 1.1, addition of MeOD substantially lowered it, i.e. $k_{inh}^{PhCl+MeOH} / k_{inh}^{PhCl+MeOD}$ = k_H/k_D = 4.4, in good agreement with the literature value of 5.1[29] and consistent with significant O−H bond cleavage in the transition state of the reaction of phenols with peroxyl radicals (eq 3.3). When the autoxidation was carried out in acetonitrile in lieu of chlorobenzene, $k_{inh}(CH_3CN) = 6.6 \times 10^5$ M^{-1} s^{-1} was obtained − a kinetic solvent effect of k_{PhCl}/k_{MeCN} = 5.8, in good agreement with the literature value of 5.6,[24,25] and consistent with the existence of a hydrogen-bonded pre-equilibrium.[12]

In order to further validate the current approach to assessing RTA activity, we also sought to reproduce an example of synergy between RTAs since this is often not picked up in simple antioxidant assays.[30] We chose an example from a recent investigation on antioxidant synergism carried out with our collaborators:[26] the combination of a highly reactive pyridinol RTA (**3.5**) with a

much less reactive hindered phenol (**3.2**). The data are shown in Figure 3.3, and are fully consistent with results obtained by O_2 consumption measurements.[26] That is, although the pyridinol is a fine RTA on its own, the hindered phenol can only retard oxidation of PBD-BODIPY. However, when the two RTAs are used together, their performance is much better than their additive contributions. This arises because the less reactive hindered phenol regenerates the more reactive pyridinol *in situ*, as in eq 3.14. This equilibrium is favorable since the O−H bond in pyridinol **3.5** is stronger than the O−H bond in hindered phenol **3.2** (by 2.4 kcal/mol).[26]

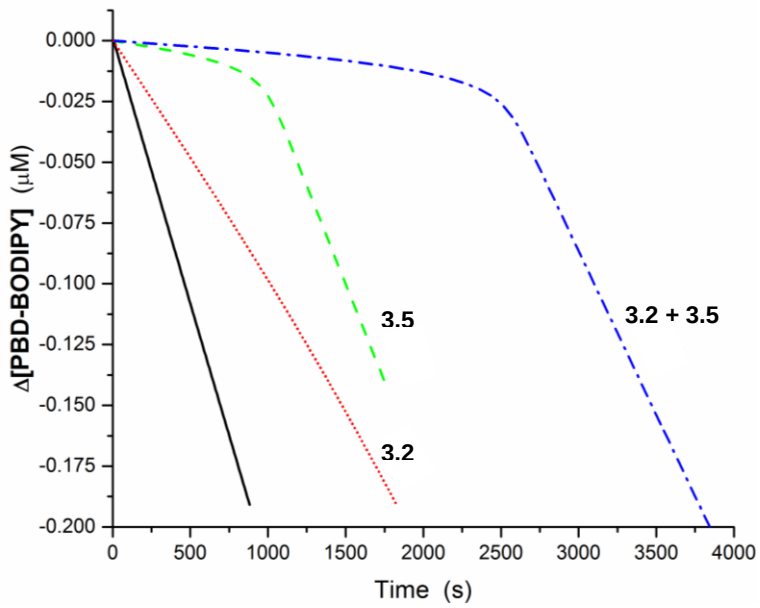

Figure 3.3. Co-autoxidation of styrene (4.3 M) and PBD-BODIPY (10 μM) initiated by AIBN (6 mM) in PhCl at 37 °C (solid line) and inhibited by **3.2** (2 μM), **3.5** (1 μM), or **3.5** + **3.2** (1 μM+2 μM). Reaction progress was monitored by absorbance at 591 nm (ε = 139,000 M^{-1} cm^{-1}).

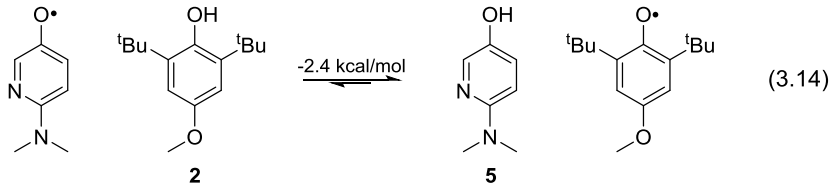

(3.14)

Diarylamine RTAs were also considered in our method validation. Representative inhibited autoxidation traces are shown in Figure 3.4. Like BHT, diphenylamine was too slow to effectively inhibit PBD-BODIPY oxidation. 4,4′-Dimethyldiphenylamine (**3.7**), representative of the industrial

standard dialkylated diphenylamines, displayed a pronounced inhibited period, as did the recently described heteroaryl-containing diarylamine **3.8**.[28] The rate constants obtained from fitting the data were in good agreement with the literature values (see Table 3.1).[31] Interestingly, the stoichiometric numbers from these experiments (n = 3.1 for **7** and n = 3.9 for **3.8**) suggest that more than two peroxyl radicals are trapped by each molecule of RTA, consistent with previous inhibited autoxidations monitored by O_2 consumption.[28] The basis of this behavior remains unclear, but is likely to be related to the catalytic behavior exhibited by diarylamines at elevated temperatures.[32,33]

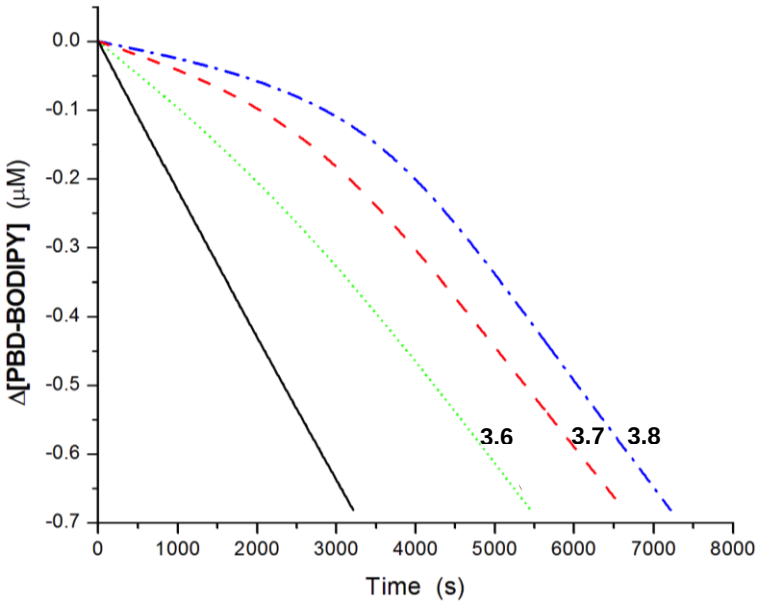

Figure 3.4. Co-autoxidation of styrene (4.3 M) and PBD-BODIPY (10 μM) initiated by AIBN (6 mM) in PhCl at 37 °C (solid line) and inhibited by 2 μM of **3.6**, **3.7** and **3.8**. Reaction progress was monitored by absorbance at 591 nm (ε = 139,000 M^{-1} cm^{-1}).

3.3.2 Monitoring Slower Autoxidations

Since PBD-BODIPY reacts too quickly with chain-carrying peroxyl radicals to be able to report on the potency of moderately reactive (and widely used) RTAs such as BHT and diphenylamine, we sought to develop a slightly less reactive analogue. We surmised that the removal of one of the unsaturations in the 1-phenylbutadiene sidechain in PBD-BODIPY should decrease its reactivity to

peroxyl radical addition significantly. We therefore prepared the styryl analogue, STY-BODIPY, for use as the signal carrier in an analogous co-autoxidation procedure employing cumene (k_p = 0.34 M^{-1} s^{-1}).[16]

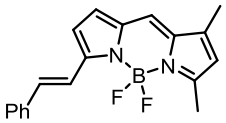

STY-BODIPY

Cumylperoxyl radicals undergo significantly slower termination reactions than styrylperoxyl radicals (i.e., k_t = 2.3 × 10^4 M^{-1} s^{-1} vs. 2.1 × 10^7 M^{-1} s^{-1}),[34] resulting in a higher steady state concentration of radicals and a concomitant increase in the rate at which STY-BODIPY is consumed. However, slower termination of chain-carrying radicals implies that cross-termination between cumylperoxyl radicals and secondary peroxyl radicals derived from STY-BODIPY will contribute significantly to the steady-state concentration of radicals in the autoxidation. Therefore, the direct determination of $k_{\text{STY-BODIPY}}$ could not be carried out as we did to obtain $k_{\text{PBD-BODIPY}}$. Instead, $k_{\text{STY-BODIPY}}$ was determined from the inhibited co-autoxidation of STY-BODIPY and cumene (Figure 3.5).

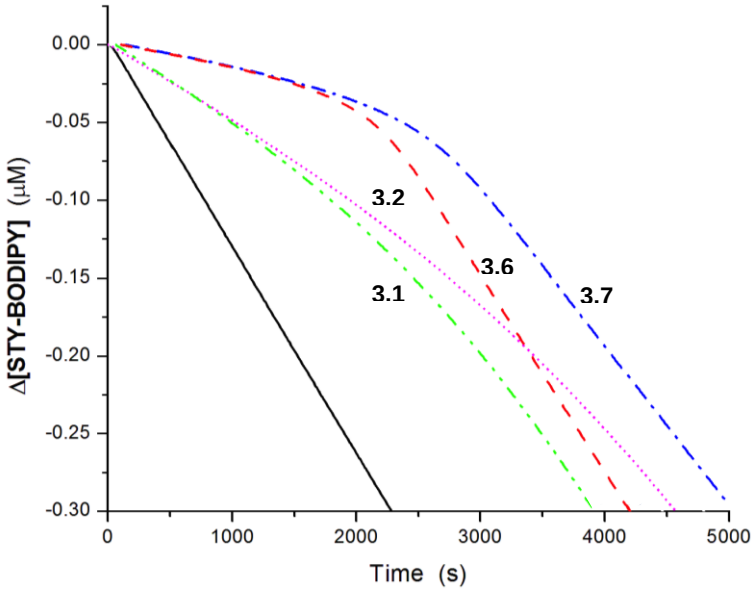

Figure 3.5. Co-autoxidation of cumene (3.6 M) and STY-BODIPY (10 μM) initiated by AIBN (6 mM) in PhCl at 37 °C (solid line) and inhibited by 2 μM of phenols **3.1** and **3.2**, and diarylamines **3.6** and **3.7**. Reaction progress was monitored by absorbance at 571 nm (ε = 128,000 M^{-1} cm^{-1}).

Since **3.2** is known to have k_{inh} = 1.1 × 10^5 M^{-1} s^{-1} and a stoichiometric number of n = 2,[24] the rate constant could be obtained simply by fitting the data to the standard kinetic scheme for inhibited autoxidations modified to include the contribution of chain propagation from the reaction of STYBODIPY with peroxyl radicals (see the Supporting Information for complete details). Fitting of this data yields $k_{STY\text{-}BODIPY}$ = 141 M^{-1} s^{-1}. This rate constant indicates that STY-BODIPY is significantly less reactive than PBD−PODIPY (recall $k_{PBD\text{-}BODIPY}$ = 2720 M^{-1} s^{-1}) – as expected – but still more reactive than styrene itself (k_p = 41 M^{-1} s^{-1}) and much more reactive than cumene (k_p = 0.34),[23] its co-autoxidation substrate.

Co-autoxidations of STY-BODIPY and cumene were well behaved and yielded inhibition rate constants for test RTAs that were in very good agreement with values obtained from O_2 consumption.[35] As expected, the slower rate of probe oxidation enabled the determination of rate constants for the slower RTAs BHT (**3.1**) and diphenylamine (**3.6**), which did not yield discernible inhibited periods in the autoxidation of the more reactive probe, PBD-BODIPY (*cf*. Figures 3.1 and 3.4, respectively).[36] Some representative data are shown in Table 3.2.

Table 3.2. Inhibition Rate Constants and Stoichiometries Determined for Various RTAs Determined by Co-autoxidations of STY-BODIPY and Cumene[a]

RTA	n	k_{inh} ($M^{-1}s^{-1}$)	Literature k_{inh} ($M^{-1}s^{-1}$)
3.1	2.2 ± 0.1	(2.1 ± 0.2) × 10^4	1.4 × 10^4 (30 °C)[24]
3.2	2.1 ± 0.1	1.1 × 10^5 [b]	1.1 × 10^5 (30 °C)[24]
3.6	2.5 ± 0.1	(1.7 ± 0.2) × 10^4	2.0 × 10^4 (65 °C)[27]
3.7	2.4 ± 0.1	(1.1 ± 0.1) × 10^5	1.8 × 10^5 (37 °C)[28]

[a]Determined by inhibited co-autoxidation of cumene (3.6 M) and STY-BODIPY (10 μM) initiated by AIBN (6 mM) in PhCl at 37 °C and inhibited by 2 μM antioxidant. [b]Assumed in order to derive $k_{STY\text{-}BODIPY}$.

3.3.3 Autoxidations in Water

Although PBD-BODIPY and STY-BODIPY are highly lipophilic, the very small concentrations used in the styrene and cumene co-autoxidations prompted us to consider if they would be useful for monitoring the kinetics of inhibited autoxidations in aqueous media. Kinetic data for the reactions of peroxyl radicals in water are relatively sparse despite their purported importance in vivo. Most data are the reactions of RTAs with methylperoxyl, and more often the highly reactive trichloromethylperoxyl, radicals have been determined.[37]

Co-autoxidations of STY-BODIPY and THF as a 40% (by volume) solution in water[38] initiated by the water-soluble azo initiator AAPH were very well behaved and consumption of STY-BODIPY was expectedly inhibited by the water-soluble antioxidants, Trolox (**3.9**) and ascorbate (**3.10**), see Figure 3.6.

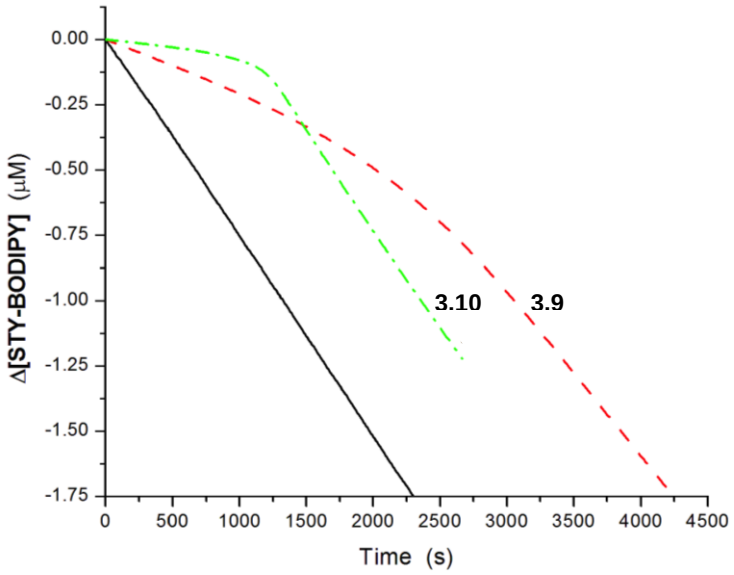

Figure 3.6. Co-autoxidation of THF (4.9 M) and STY-BODIPY (10 μM) initiated with AAPH (1 mM) in water at 37 °C (solid line) and inhibited by 2 μM of **3.9** or 20 μM of **3.10**. Reaction progress was monitored by absorbance at 562 nm (ε = 147,000 M^{-1} cm^{-1}).

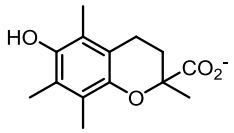

3.9

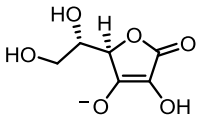

3.10

As was the case in the foregoing experiments, determination of inhibition rate constants in this system requires knowledge of the rate constant for reaction of STY-BODIPY with THF-derived peroxyl radicals ($k_{\text{STY-BODIPY}}$). Accordingly, data from ascorbate inhibited autoxidations were fit to the standard kinetic scheme for inhibited autoxidations of THF (k_p = 4.4 M^{-1} s^{-1})[39–41] modified to include the contribution of chain-propagation from reaction of STY-BODIPY with the THF-derived peroxyl radicals. Using the literature rate constant for the reaction of ascorbate and methylperoxyl radical obtained by pulse radiolysis measurements (2.4 × 10^6 M^{-1} s^{-1}),[42] a value of $k_{\text{STY-BODIPY}}$ = 7.9 × 10^3 M^{-1} s^{-1} was calculated.[43] Using this value, the inhibition rate constant for Trolox was measured to be k_{inh} = 2.2 × 10^5 M^{-1} s^{-1}, in very good agreement with the value predicted for α-tocopherol (4.9 × 10^5 M^{-1} s^{-1}) using the relationship developed by Ingold and co-workers for kinetic solvent effects on H-atom transfer reactions (eq 3.15) and the constants k^0_{inh} = 7.2 ×10^6 M^{-1} s^{-1}, α_2^H(α-TOH) = 0.37 and β_2^H(H_2O) = 0.38.[12,44]

$$\log k^S_{inh} = \log k^0_{inh} - 8.3\alpha_2^H\beta_2^H \qquad (15)$$

Under the reaction conditions, the stoichiometry of the ascorbate/peroxyl reaction was found to be only ~0.1. Although ascorbate can, in principle, reduce two peroxyl radicals to form dehydroascorbic acid (as in eqs 3.16 and 3.17), low stoichiometric numbers are commonly observed for ascorbate – either alone (n → 0 as [ascorbate] → ∞)[45] or when used in a synergistic combination with a lipid-soluble compound such as α-TOH.[46] The lower than ideal stoichiometry has been ascribed to the autoxidation of ascorbate and/or the reaction of the ascorbyl radical (anion) with O_2 to yield a chain carrying hydroperoxyl radical (superoxide, eq 3.18) in competition with the reaction of the ascorbyl radical (anion) with another peroxyl radical.[45,46] The methods described herein may

prove useful in delineating this reaction mechanism as well as others that have yet to be studied in detail in aqueous media.

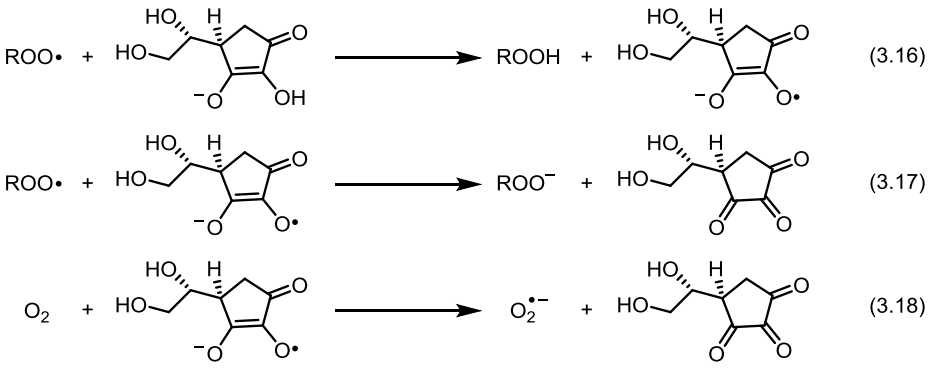

3.4 Conclusion

We have developed a novel, accurate, and operationally simple method for the study of antioxidant reactivity by the inhibited autoxidation approach. Reaction progress is monitored continuously by following the consumption of an easily synthesized BODIPY-conjugated probe by visible light spectrophotometry. The inhibition rate constants measured for several phenol and diarylamine RTAs using this approach are in excellent agreement with literature values. The method describes the co-antioxidant behavior of RTA mixtures and also the enhanced stoichiometry of suitably reactive diarylamines. The method can be calibrated for use in solvents of different polarities and/or H-bonding properties, allowing measurements of kinetic solvent effects. Furthermore, deuterium kinetic isotope effects are easily measured by the addition of 1% MeOD/MeOH to the co-autoxidations. Overall, the approach enables any researcher with access to a conventional UV−vis spectrophotometer to carry out inhibited hydrocarbon autoxidations to obtain invaluable kinetic and stoichiometric data on RTAs. It is our hope that this method will supplant popular assays based on spectroscopic determinations of equilibria between RTAs and persistent radicals or similarly dubious assessments of “antioxidant activity”.

3.5 Experimental

3.5.1 General Methods

All chemicals and solvents were purchased from commercial suppliers and used without further purification. Styrene and cumene were purified in batches. Styrene was extracted three times with 1 M NaOH(aq) and washed with water before drying with $MgSO_4$ and filtering. It was then fractionally distilled under vacuum, percolated through a column of silica, and stored under nitrogen at −20 °C (it could be stored for up to 3−4 days prior to use). It was further percolated through a column of ∼1/3 silica gel layered on top of ∼2/3 basic alumina immediately prior to use. Cumene was purified by the same method. Commercially available phenolic antioxidants BHT, BHA, and PMC (**3.1**, **3.2**, and **3.3**) were recrystallized prior to use. 6-(Dimethylamino)-3-pyridinol (**3.4**), 2-(dimethylamino)-4,6-dimethyl-5-pyrimidinol (**3.5**), and N^2,N^2-dimethyl-N^5-phenylpyrimidine-2,5-diamine (**3.8**) were synthesized by the reported procedures.[47,48] Diphenylamine (**3.6**) and di-p-tolylamine (**3.7**) were purchased and used without further purification. UV−vis spectra and kinetics were measured on a UV−vis spectrophotometer equipped with a temperature controller unit and a thermostated 6 × 6 multicell holder.

3.5.2 Synthesis of PBD- and STY-BODIPY

Both compounds were synthesized by literature procedures.[16,17] Briefly, a solid mixture of pyrrole-2-carboxaldehyde[49] (1.0 g, 10.5 mmol), zinc dust (0.69 g, 10.5 mmol), and either cinnamyl triphenylphosphonium chloride or benzyl triphenylphosphonium bromide (4.3 or 4.5 g, 10.5 mmol) was heated to 100 °C under an inert atmosphere and stirred overnight. The mixture was allowed to cool before it was diluted with $CHCl_3$ (25 mL) and filtered. The filtrate was washed once with water and once with brine before drying with $MgSO_4$. Following filtration and concentration under reduced pressure, the product was purified by column chromatography on silica gel using a gradient of

20−30% $CHCl_3$ in hexanes. The product phenylbutadienyl- or styryl-substituted pyrrole (0.53 or 0.46 g, 2.7 mmol) was then combined with 3,5-dimethylpyrrole-2- carboxaldehyde (0.34g, 2.7 mmol) in dry CH_2Cl_2 (135 mL) under an inert atmosphere. $POCl_3$ (0.27 mL, 2.9 mmol) was then added dropwise over several minutes, and the reaction was stirred overnight in the dark at room temperature. Diisopropylethylamine (2.0 mL, 11.5 mmol) was then added slowly, and the reaction was stirred for another 10 min, followed by dropwise addition of $BF_3{-}OEt_2$ (1.4 mL, 11.2 mmol). The reaction was stirred at room temperature until complete (∼1 h, as judged by TLC), poured into a separatory funnel, and washed twice with water and then a small amount of brine. The organic phase was dried with $MgSO_4$ and filtered and the solvent evaporated. Column chromatography (100% CH_2Cl_2) removed the major impurities. A second column (60% CH_2Cl_2 in hexanes) afforded pure product. Due to the oxidizability of both PBD-BODIPY and STY-BODIPY, 2.0 mM stock solutions of each compound were prepared in either 1,2,4-trichlorobenzene or DMSO (depending on whether they are for use in organic or aqueous solutions) and stored under nitrogen, frozen at −20 °C. When stored in this manner, there was minimal background oxidation of the either compound over several months.

4,4-Difluoro-5,7-dimethyl-3-(4-phenyl-1,3-butadienyl)-4-bora-3a,4a-diaza-s-indacene ***(PBD-BODIPY)***. Yield: 81 mg (9%). ^{1}H NMR (400 MHz; acetone-d_6): δ 7.65 (d, J = 7.3 Hz, 2H), 7.51 (s, 1H), 7.43−7.32 (m, 5H), 7.21−7.15 (m, 2H), 7.06 (d, J = 4.7 Hz, 1H), 6.94 (d, J = 14.9 Hz, 1H), 6.30 (s, 1H), 2.58 (s, 3H), 2.33 (s, 3H). ^{19}F NMR (377 MHz; acetone-d_6, $PhCF_3$ standard): δ −143.16 (dd, J =65.6, 32.8 Hz). HRMS (EI - magnetic sector): calcd for $C_{21}H_{19}BF_2N_2$ 348.1609, found 348.1582. λ_{max} (PhCl) = 591 nm, ε = 139162 M^{-1} cm^{-1}. The poor solubility of PBD-BODIPY in either $CDCl_3$, DMSO, acetone, or benzene, combined with its high oxidizability, prevented the acquisition of a well-resolved 13C NMR spectrum.

4,4-Difluoro-5,7-dimethyl-3-(2-phenylethenyl)-4-bora-3a,4adiaza- s-indacene (***STY-BODIPY***).

Yield: 128 mg (15%). 1H (400MHz; acetone-d_6): δ7.64 (t, J = 10.9 Hz, 3H), 7.52 (t, J= 8.2 Hz, 2H), 7.44 (t, J = 7.5 Hz, 2H), 7.36 (t, J = 7.3 Hz, 1H), 7.15(d, J = 4.3 Hz, 1H), 7.08 (d, J = 4.4 Hz, 1H), 6.29 (s, 1H), 2.57 (s,3H), 2.31 (s, 3H). ^{13}C NMR (75 MHz; acetone-d_6): δ 159.2, 153.0, 143.6, 136.7, 135.3, 135.0, 128.93, 128.85, 128.71, 127.0, 123.2, 120.2, 119.0, 115.2, 14.0, 10.4. ^{19}F-NMR (377 MHz; acetone-d_6): δ −143.00 (dd, J = 69.6 Hz, 34.8 Hz). HRMS (EI - magnetic sector): calcd for $C_{19}H_{17}BF_2N_2$ 322.1453, found 322.1434. λ_{max} (PhCl) = 571 nm, ε = 128,141 M^{-1} cm^{-1}.

3.5.3 Inhibited Co-autoxidations: Styrene/Cumene

Freshly purified styrene or cumene (1.25 mL) was loaded into a 3 mL cuvette along with 1.18 mL of PhCl. The cuvette was placed into the thermostated sample holder of a UV−vis spectrophotometer and allowed to equilibrate to 37 °C. A small aliquot (12.5 μL) of a 2.0 mM solution of the BODIPY probe in 1,2,4-trichlorobenzene was added, followed by 50 μL of 0.3 M solution of AIBN in PhCl, and the solution was thoroughly mixed. The absorbance at either 591 nm (PBD-BODIPY) or 571 nm (STY-BODIPY) was monitored for 40−60 min to ensure that the reaction was proceeding at a constant rate, after which 10 μL of a 500 μM solution of the test antioxidant was added. The solution was thoroughly mixed and the absorbance readings resumed.

3.5.4 Inhibited Co-autoxidations: THF/H_2O

Unstabilized THF (1.0 mL) was loaded into a 3 mL cuvette along with 1.43 mL of H2O. The cuvette was placed into the thermostated sample holder of a UV−vis spectrophotometer and allowed to equilibrate to 37 °C. A small aliquot (12.5 μL) of a 2.0 mM solution of the BODIPY probe in DMSO was added, followed by 50 μL of 0.05 M solution of AAPH in H2O, and the solution was thoroughly mixed. The absorbance at 562 nm was monitored for 10−20 min to ensure that the reaction was

proceeding at a constant rate, after which 10 μL of a 500 μM solution of the test antioxidant was added. The solution was thoroughly mixed, and the absorbance readings were resumed.

3.6 References

(1) Ingold, K. U. *Chem. Rev*. **1961**, 61, 563−589.

(2) Ingold, K. U.; Pratt, D. A. *Chem. Rev*. **2014**, 114, 9022−9046.

(3) Valgimigli, L.; Pratt, D. A. In Encyclopedia of Radicals in Chemistry, Biology and Materials; Chatgilialoglu, C., Studer, A., Eds.; John Wiley & Sons,: Chichester, UK, **2012**.

(4) Li, B.; Pratt, D. A. *Free Radical Biol. Med*. **2015**, 82, 187−202.

(5) Amorati, R.; Valgimigli, L. *Free Radical Res*. **2015**, 49, 633−649.

(6) Hanthorn, J. J.; Haidasz, E.; Gebhardt, P.; Pratt, D. A. *Chem. Commun*. **2012**, 48, 10141−10143.

(7) Re, R.; Pellegrini, N.; Proteggente, A.; Pannala, A.; Yang, M.; Rice-Evans, C. *Free Radical Biol. Med*. **1999**, 26, 1231−1237.

(8) Benzie, I. F.; Strain, J. *J. Anal. Biochem*. **1996**, 239, 70−76.

(9) Blois, M. S. *Nature* **1958**, 181, 1199−1200.

(10) Huang, D.; Ou, B.; Prior, R. L. *J. Agric. Food Chem*. **2005**, 53,1841−1856.

(11) Foti, M. *J. Agric. Food Chem*. **2015**, 63, 8765−8776.

(12) Litwinienko, G.; Ingold, K. U. *Acc. Chem. Res*. **2007**, 40, 222−230.

(13) Kang, H. C.; Haugland, R. P. Long Wavelength Chemically Reactive Dipyrrometheneboron Difluoride Dyes and Conjugates. US5451663 A, **1993**.

(14) Drummen, G. P.; van Liebergen, L. C.; Op den Kamp, J. A.;Post, J. A. *Free Radical Biol. Med*. **2002**, 33, 473−490.

(15) Yoshida, Y.; Shimakawa, S.; Itoh, N.; Niki, E. *Free Radic. Res*. **2003**, 37, 861−872.

(16) Kang, H. C.; Haugland, R. P. Ethenyl-Substituted Dipyrrometheneboron Difluoride Dyes and Their Synthesis. US5187288, **1993**.

(17) De Cremer, G.; Roeffaers, M. B. J.; Bartholomeeusen, E.; Lin, K.; Dedecker, P.; Pescarmona, P. P.; Jacobs, P. A.; De Vos, D. E.; Hofkens, J.; Sels, B. F. *Angew. Chem., Int. Ed.* **2010**, 49, 908−911.

(18) Naguib, Y. M. *Anal. Biochem*. **1998**, 265, 290−298.

(19) DFT calculations using the B3LYP/CBSB7 method indicate that the most favorable position for peroxyl addition is adjacent to the phenyl ring, yielding an allyl-BODIPY radical at least 7.4 kcal/mol more stable than those radicals derived from addition of the peroxyl radical at any of the other three positions of the 1-phenylbutadiene

moiety. See the Supporting Information for further details.

(20) Moreover, in some preliminary inhibited co-autoxidations the fluorescence intensity was significantly suppressed even when no/minimal inhibition was expected to take place. This was likely the result of fluorescence quenching by some RTAs and/or their oxidation products.

(21) Hammond, G. S.; Sen, J. N.; Boozer, C. E. *J. Am. Chem. Soc*. **1955**, 77, 3244−3248.

(22) Van Hook, J. P.; Tobolsky, A. V. *J. Am. Chem. Soc*. **1958**, 80, 779−782.

(23) Howard, J.; Ingold, K. *Can. J. Chem*. **1967**, 45, 793−802.

(24) Burton, G. W.; Doba, T.; Gabe, E.; Hughes, L.; Lee, F. L.; Prasad, L.; Ingold, K. U. *J. Am. Chem. Soc*. **1985**, 107, 7053−7065.

(25) Valgimigli, L.; Amorati, R.; Petrucci, S.; Pedulli, G. F.; Hu, D.; Hanthorn, J. J.; Pratt, D. A. *Angew. Chem., Int. Ed*. **2009**, 48, 8348−8351.

(26) Valgimigli, L.; Bartolomei, D.; Amorati, R.; Haidasz, E.; Hanthorn, J. J.; Nara, S. J.; Brinkhorst, J.; Pratt, D. A. *Beilstein J. Org. Chem*. **2013**, 9, 2781−2792.

(27) Brownlie, I. T.; Ingold, K. U. *Can. J. Chem*. **1966**, 44, 861−868.

(28) Hanthorn, J. J.; Amorati, R.; Valgimigli, L.; Pratt, D. A. *J. Org. Chem*. **2012**, 77, 6895−6907.

(29) Burton, G. W.; Ingold, K. U. *J. Am. Chem. Soc*. **1981**, 103, 6472−6477.

(30) Equilibrium methods (such as those used in many of the most common "antioxidant activity" assays) only reflect the reaction stoichiometry and show only additive relationships between multiple antioxidants.

(31) The literature value for **3.8**[28] was determined using a peroxyl radical clock approach,[50] which was found to overestimate the rate constants for some of the more reactive diarylamines relative to data obtained from inhibited autoxidations (by a factor of 2−3).[28]

(32) Jensen, R. K.; Korcek, S.; Zinbo, M.; Gerlock, J. L. *J. Org. Chem.* **1995**, 60, 5396−5400.

(33) Haidasz, E. A.; Shah, R.; Pratt, D. A. *J. Am. Chem. Soc*. **2014**, 136, 16643−16650.

(34) Enes, R. F.; Tomé, A. C.; Cavaleiro, J. A. S.; Amorati, R.; Fumo, M. G.; Pedulli, G. F.; Valgimigli, L. *Chem. - Eur. J.* **2006**, 12, 4646−4653.

(35) Diarylamine **3.7** showed reduced stoichiometry in these experiments relative to the PBD-BODIPY/styrene co-autoxidations (n = 2.4 vs 3.1). Secondary alkyl radicals (or the alkoxyamines derived from their combination with diarylnitroxides) are necessary for either the retro-carbonyl-ene or homolysis/dis-proportionation reaction to complete the catalytic cycle.[27,28] Similarly, the more reactive diarylamine **3.8** completely inhibited the reaction and had a stoichiometric number, n = 2.3, also down considerably from 3.9 in the PBD-BODIPY/styrene co-autoxidations.

(36) The more reactive RTAs **3.3**−**3.5** and **3.8** completely inhibited the co-autoxidation reaction, precluding determination of the inhibition rate constants.

(37) von Sonntag, C.; Schuchmann, H.-P. *Angew. Chem., Int. Ed*. **1991**, 30, 1229−1253. Neta, P.; Huie, R. E.; Ross, A. B. *J. Phys. Chem. Ref. Data* **1990**, 19, 413−513.

(38) The selection of this system was inspired by the work of Valgimigli and Amorati communicated at the 2014 International Congress on Hydrogen Atom Transfer (Rome).

(39) Howard, J. A.; Ingold, K. U. *Can. J. Chem*. **1969**, 47, 3809−3815.

(40) Howard, J. A. *Adv. Free Radical Chem*. **1972**, 4, 49−173.

(41) The propagation rate constant in THF/H_2O was assumed to be the same as in neat THF. R_i was determined from t_{inh} in the autoxidation inhibited by Trolox and assuming n = 2. See ref 24.

(42) Alfassi, Z. B.; Huie, R. E.; Kumar, M.; Neta, P. *J. Phys. Chem*. **1992**, 96, 767−770.

(43) The rate constant for the reaction of STY-BODIPY with THF-derived peroxyl radicals is significantly higher than that of STY-BODIPY with cumylperoxyl radicals also in chlorobenzene,

where it was measured to be 2.0×10^3 $M^{-1}s^{-1}$ (versus 141 $M^{-1}s^{-1}$ for cumylperoxyls). The difference (13.8-fold) can be rationalized by the greater electrophilicity of the THF-derived peroxyl radical compared to the cumylperoxyl radical and the significant polar effects known to operate in the transition states of radical additions to alkenes. For a discussion, see: Russell, G. A. In *Free Radicals*; Kochi, J. K., Ed.; Wiley: New York, **1973**; Vol. 1, pp 275−332.

(44) Snelgrove, D. W.; Lusztyk, J.; Banks, J. T.; Mulder, P.; Ingold, K. U. *J. Am. Chem. Soc*. **2001**, 123, 469−477.

(45) See: Wayner, D. D. M.; Burton, G. W.; Ingold, K. U. *Biochim. Biophys. Acta, Gen. Subj*. **1986**, 884, 119−123 and references cited therein.

(46) Doba, T.; Burton, G. W.; Ingold, K. U. *Biochim. Biophys. Acta, Lipids Lipid Metab*. **1985**, 835, 298−303. Barclay, L. R. C.; Locke, S. J.; MacNeil, J. M. *Can. J. Chem*. **1983**, 61, 1288−1290.

(47) Nam, T.-G.; Nara, S. J.; Zagol-Ikapitte, I.; Cooper, T.; Valgimigli, L.; Oates, J. A.; Porter, N. A.; Boutaud, O.; Pratt, D. A. *Org. Biomol. Chem*. **2009**, 7, 5103−5112.

(48) Hanthorn, J. J.; Valgimigli, L.; Pratt, D. A. *J. Org. Chem*. **2012**, 77, 6908−6916.

(49) Ryskiewicz, R. M.; Silverstein, E. E.; Willard, C. *Org. Synth*. **1956**, 36, 74.

(50) Hanthorn, J. J.; Pratt, D. A. *J. Org. Chem*. **2012**, 77, 276−284.

(51) Alternatively, the data in Figure 3.1 can be fit numerically to the standard kinetic scheme for inhibited autoxidations[3–5] modified to include the contribution of chain propagation from the reaction of PBD−BODIPY with peroxyl radicals in order to derive kinh for the RTAs (see the Supporting Information for complete details). The two approaches yield indistinguishable data.

3.7 Supporting Information

Information on the kinetic modeling / parameter fitting using COPASI software, as well as the optimized geometries and energies (Gaussian 09) of the computationally calculated structures are provided in the Supporting Information section of the publication in the Journal of Organic Chemistry (Haidasz, E. A.; Van Kessel, A. T. M.; Pratt, D. A.; *J. Org. Chem.*, **2016**, 81(3), 737-744).

3.7.1 UV –Vis Spectra and Extinction Coefficients for PBD-BODIPY and STY-BODIPY

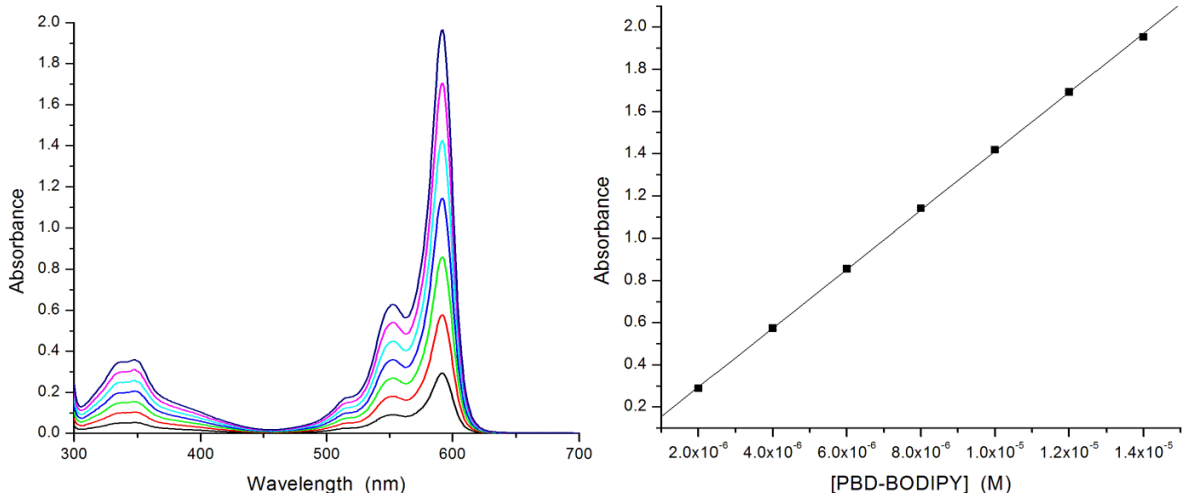

Figure S3.1. (A) Uv-Vis spectra for 2-14 μM PBD-BODIPY. (B) Extinction coefficient for PBD-BODIPY in 50% v/v styrene/PhCl, λ_{max} = 591 nm, ε = 139,163 $M^{-1}cm^{-1}$. Average of three measurements (error bars are too small to be resolved from the data points).

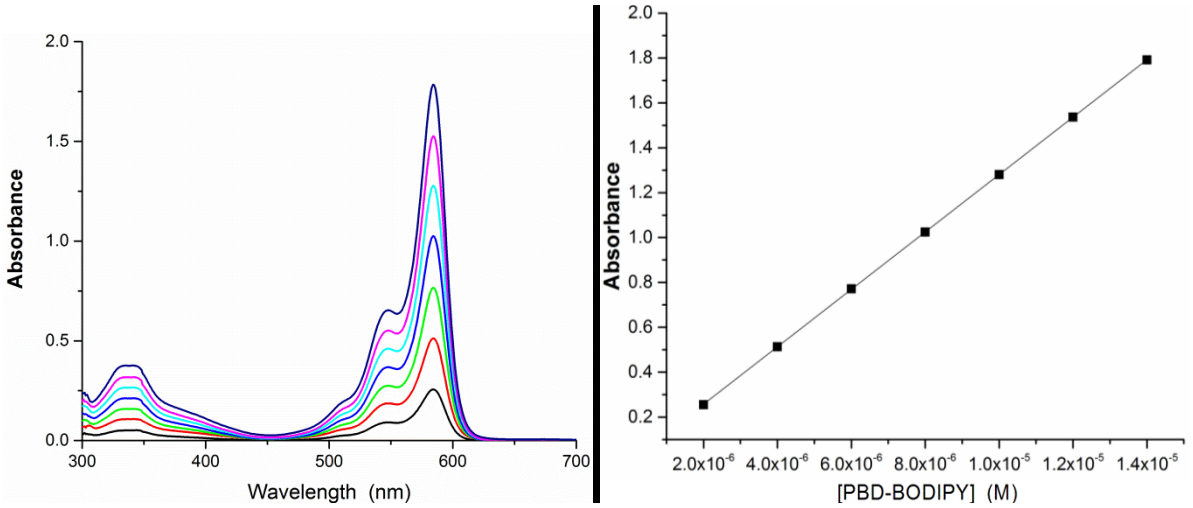

Figure S3.2. (A) Uv-Vis spectra for 2-14 μM PBD-BODIPY. (B) Extinction coefficient for PBD-BODIPY in 50% v/v styrene/MeCN, λ_{max} = 585 nm, ε = 127,860 $M^{-1}cm^{-1}$. Average of three measurements (error bars are too small to be resolved from the data points).

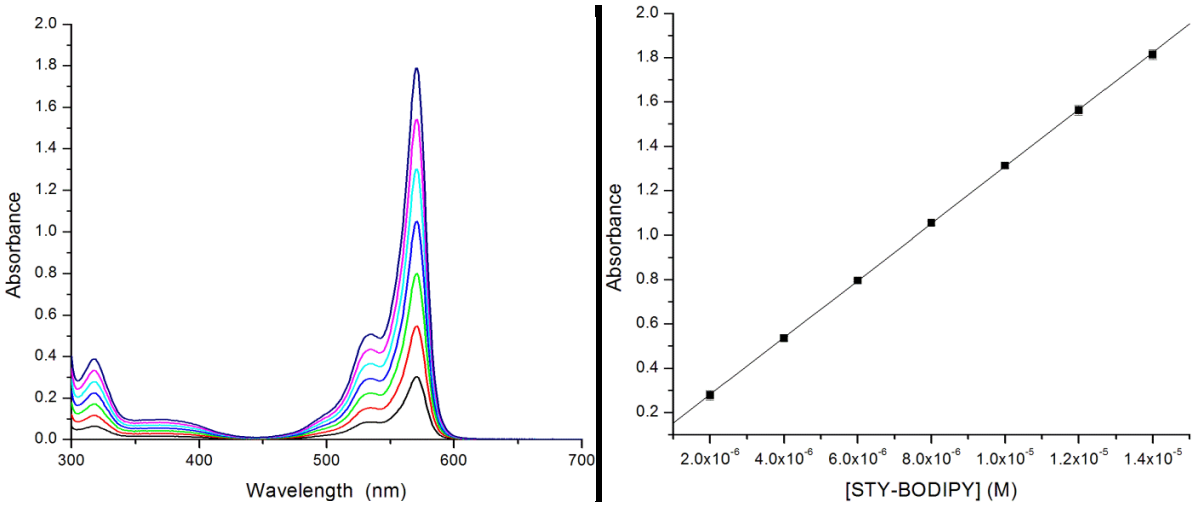

Figure S3.3. (A) Uv-Vis spectra for 2-14 μM STY-BODIPY. (B) Extinction coefficient for STY-BODIPY in 50% v/v styrene/PhCl, λ_{max} = 571 nm, ε = 128,141 $M^{-1}cm^{-1}$. Average of three measurements (error bars are too small to be resolved from the data points).

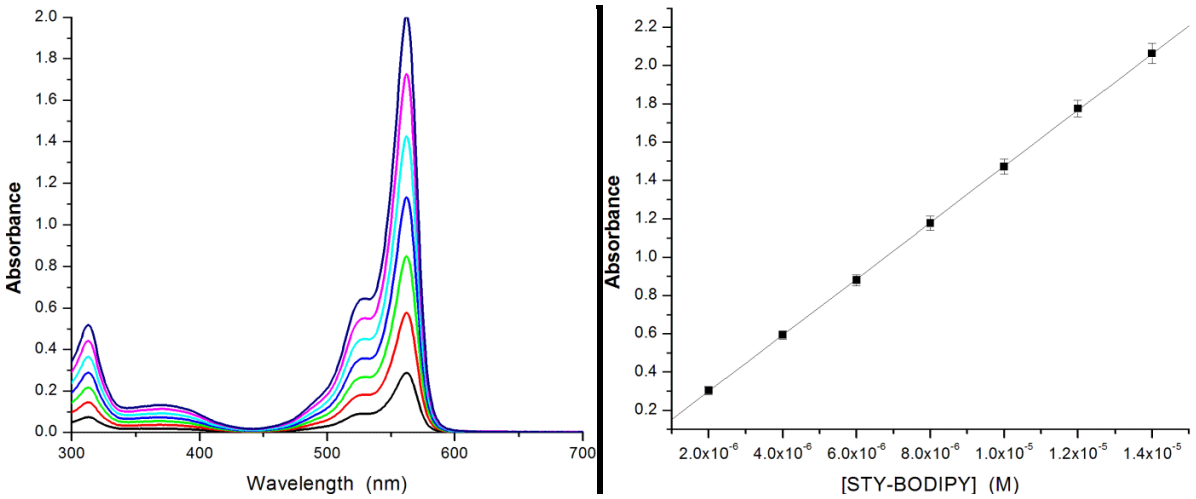

Figure S3.4. (A) Uv-Vis spectra for 2-14 μM STY-BODIPY. (B) Extinction coefficient for STY-BODIPY in 40% v/v THF/H_2O, λ_{max} = 562 nm, ε = 147,156 $M^{-1}cm^{-1}$. Average of three measurements.

3.7.2 Characterization Data for STY-BODIPY and PBD-BODIPY

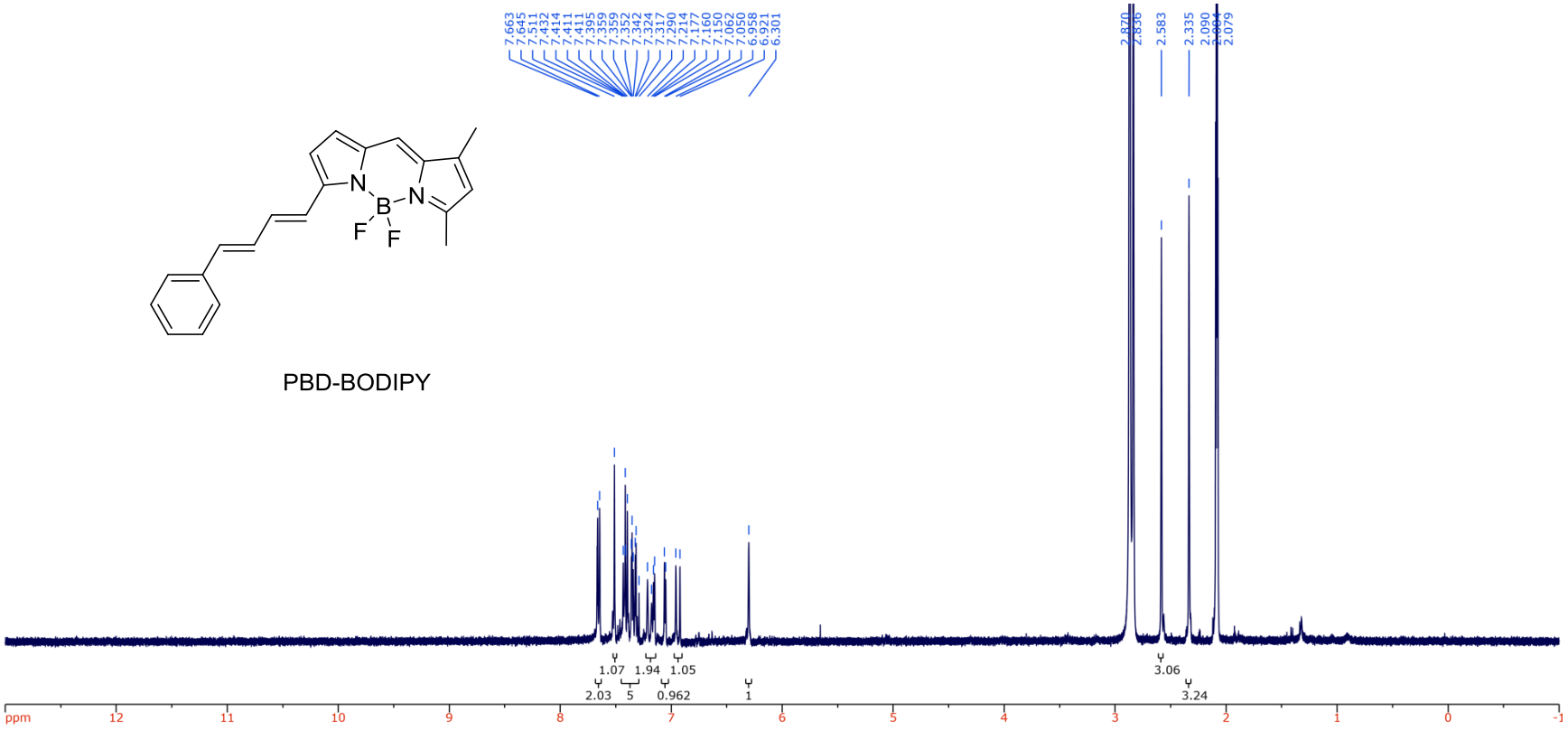

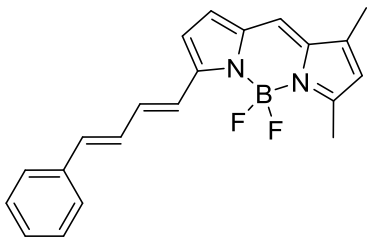
N
B
N
F
F

PBD-BODIPY

-63.720
-143.038
-143.125
-143.212
-143.299
ppm
-0
-20
-40
-60
-80
-100
-120
-140
-160
-180
-200

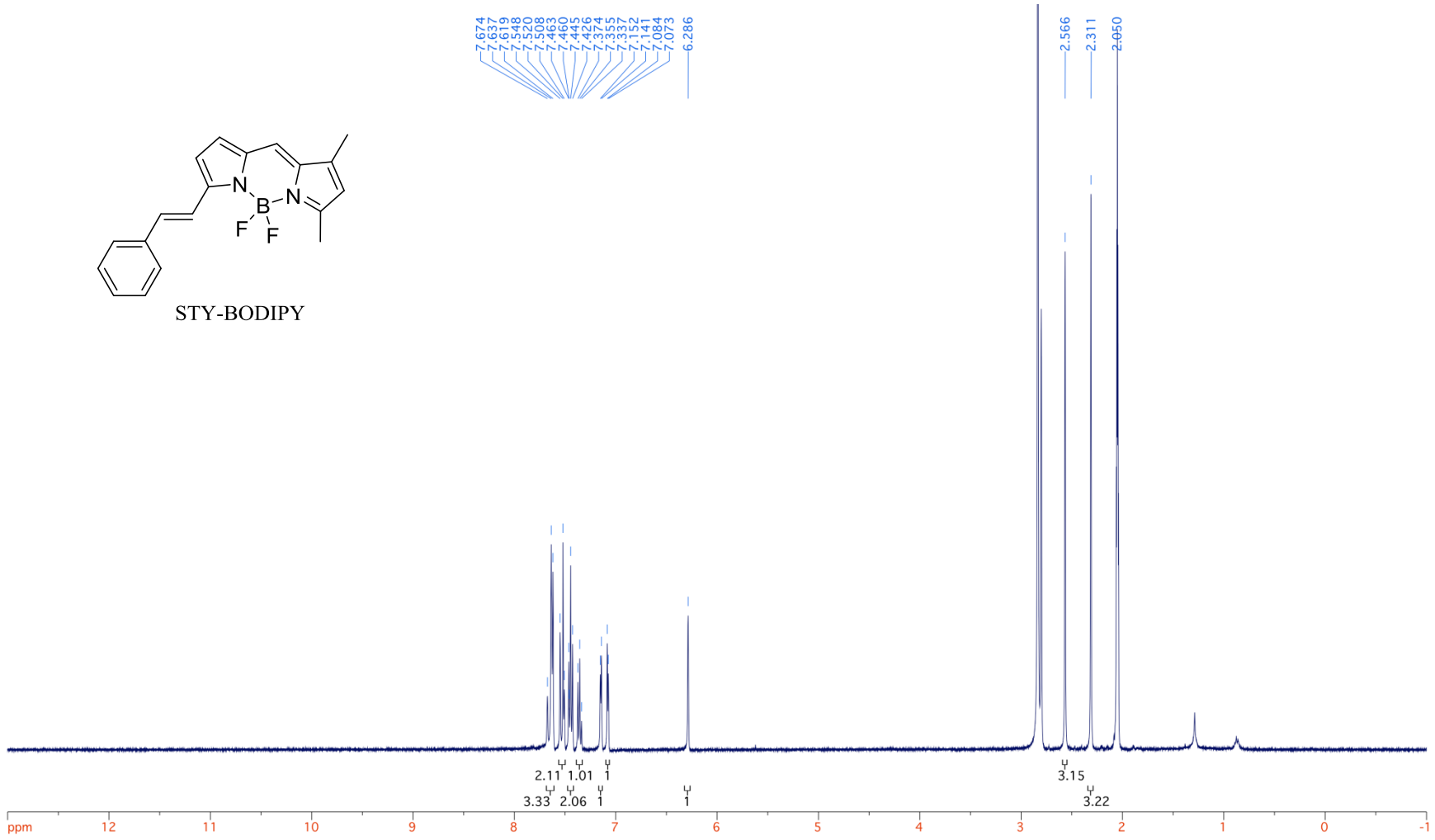
7.674
7.637
7.619
7.548
7.520
7.508
7.463
7.460
7.445
7.426
7.374
7.355
7.337
7.152
7.141
7.084
7.073
6.286
2.566
2.311
2.050
N
B
N
F
F
2.11
1.01
1
3.33
2.06
1
1
3.15
3.22
ppm
12
11
10
9
8
7
6
5
4
3
2
1
0
-1

STY-BODIPY

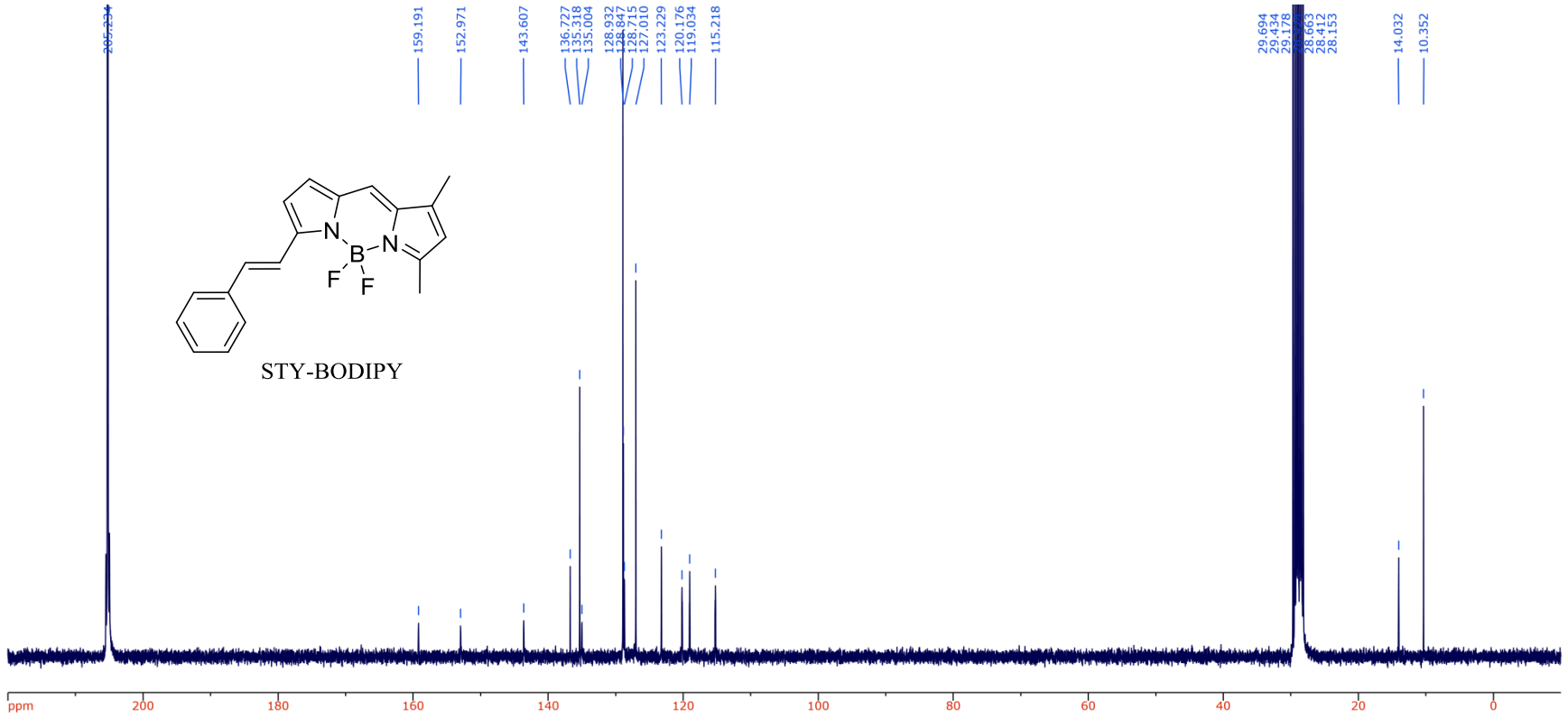
159.191
152.971
143.607
136.727
135.318
135.004
128.932
128.847
128.715
127.010
123.229
120.176
119.034
115.218
29.694
29.434
29.178
28.663
28.412
28.153
14.032
10.352
N
B
N
F
F
ppm
200
180
160
140
120
100
80
60
40
20
0

STY-BODIPY

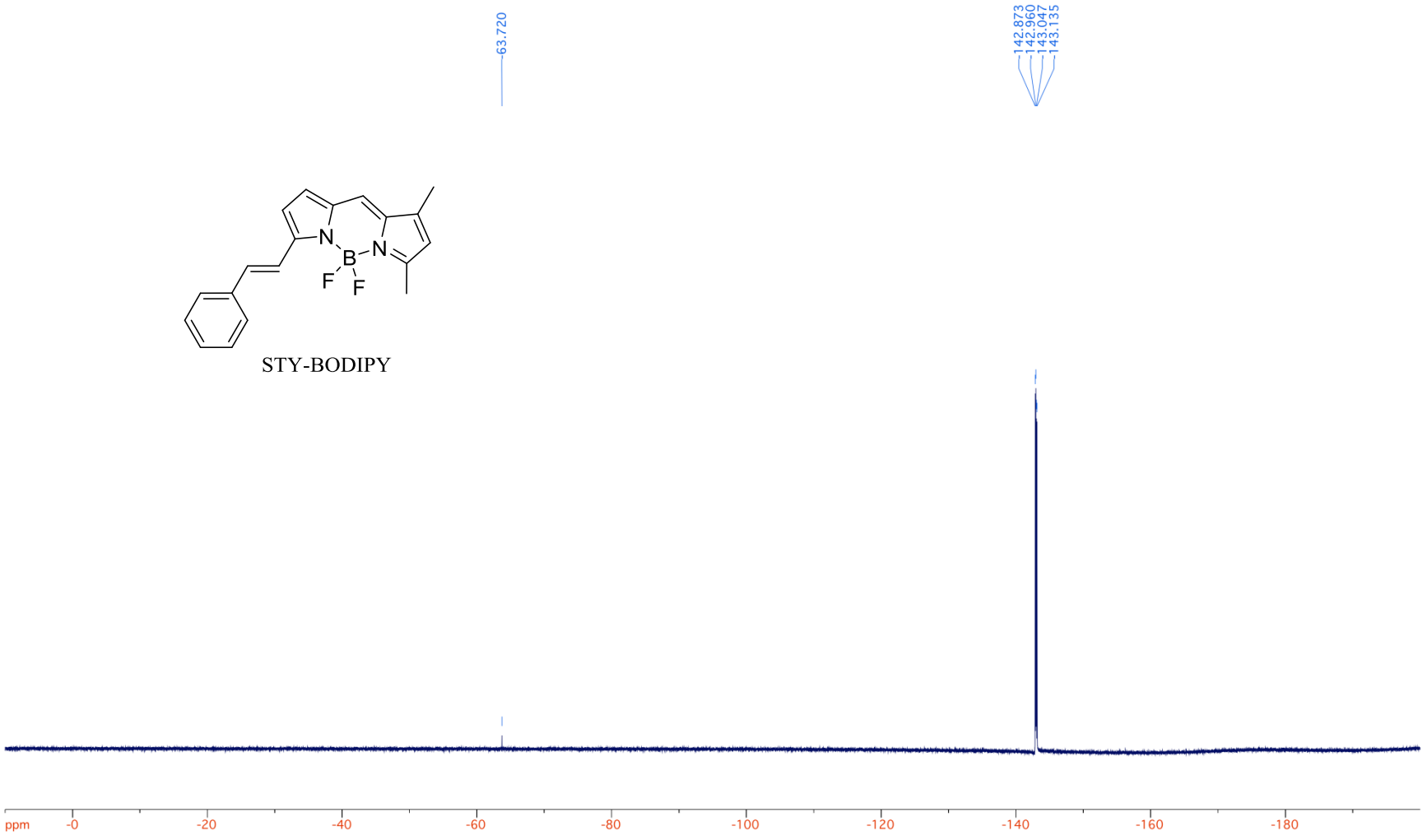
63.720
142.873
142.960
143.047
143.135
N
B
N
F
F
ppm
-0
-20
-40
-60
-80
-100
-120
-140
-160
-180

STY-BODIPY

CHAPTER 4: The Catalytic Mechanism of Diarylamine Radical-Trapping Antioxidants

4.1 Preface

Diarylamine radical-trapping antioxidants are important industrial additives, finding widespread use in petroleum-derived products. They are uniquely effective at elevated temperatures due to their ability to trap multiple radicals per molecule of diarylamine. Herein we report the results of computational and experimental studies designed to elucidate the mechanism of this remarkable activity. We find that the key step in the proposed catalytic cycle – decomposition of the alkoxyamine derived from capture of a substrate-derived alkyl radical with a diarylamine-derived nitroxide − proceeds by different mechanisms depending on the structure of both the substrate and the diarylamine. *N*,*N*-Diarylalkoxyamines derived from saturated substrates and diphenylamines decompose by N−O homolysis followed by disproportionation. Alternatively, those derived from unsaturated substrates and diphenylamines, or saturated substrates and *N*-phenyl-*β*-naphthylamine, decompose by an unprecedented concerted retro-carbonyl-ene reaction. The alkoxyamines that decompose by the concerted process inhibit hexadecane autoxidations at 160 °C to the same extent as the corresponding diarylamine, whereas those alkoxyamines that decompose by the N−O homolysis/disproportionation pathway are much less effective. This suggests that the competing cage escape of the alkoxyl radicals following N−O homolysis leads to significantly less effective regeneration of diarylamines and implies that the catalytic efficiency of diarylamine antioxidants is substrate-dependent. The results presented here have significant implications in the future design of antioxidant additives: diarylamines designed to yield intermediate alkoxyamines that undergo the retro-carbonyl-ene reaction are likely to be much more effective than existing compounds and will display catalytic radical-trapping activities at lower temperatures due to lower barriers to regeneration. This chapter is presented as it was published in the Journal of the American Chemical Society (*J. Am. Chem. Soc.* **2014**, 136, 16643-16650). The work was performed in conjunction with

fellow graduate student Ron Shah, who assisted with a portion of the alkoxyamine decomposition experiments and hexadecane autoxidations.

4.2 Introduction

Diarylamines are among the most commonly used radical trapping antioxidants (RTAs); compounds which inhibit the free radical chain oxidation of hydrocarbons by trapping chain carrying peroxyl radicals (eqs 4.1 and 4.2).[1,2]

$$Ar_2NH + ROO\bullet \longrightarrow Ar_2N\bullet + ROOH \qquad (4.1)$$

$$Ar_2N\bullet + ROO\bullet \longrightarrow \text{non-radical products} \qquad (4.2)$$

While diarylamines display similar efficacies to more prolific phenolic RTAs at ambient temperatures (typical k_1 values of 10^4–10^5 $M^{-1}s^{-1}$ and stoichiometric coefficients, n, of 2 based on eqs 4.1 and 4.2),[3] they have uniquely high efficacies at elevated temperatures (>120 °C), where 1 equiv of diarylamine can trap several chain-carrying peroxyl radicals. For example, as early as 1978 an unbelievable stoichiometry of n = 41 was reported from a diphenylamine-inhibited autoxidation of paraffin oil at 130 °C.[4] Some time ago, Korcek and co-workers proposed a mechanism accounting for these dramatic observations, shown in Scheme 4.1.[5] The large stoichiometric coefficients were ascribed to the observed regeneration of the diarylamine *in situ* during hexadecane autoxidation at 160 °C inhibited by the corresponding diarylnitroxide. Furthermore, the nitroxide proved to be as powerful an RTA as its parent amine. The amine was believed to be formed from a substrate-derived alkoxyamine – therefore *making use of the substrate as a stoichiometric reductant*.[6]

Elevated temperatures were presumed necessary to cleave the N–O bond of the alkoxyamine, which would lead to the diarylamine upon in-cage disproportionation of the diarylaminyl and alkoxyl radicals.[7] This idea was supported by the observation that heating of a mixture of alkoxyamines generated *in situ* from decomposition of *tert*-butyl peroxy-2-ethylhexanoate

in hexadecane in the presence of crude bis(*p*-octylphenyl)nitroxide gave 64% bis(*p*-octylphenyl)amine (among other products).[5] No further scrutiny of this mechanism is evident in the literature and no significant improvement in the chemistry behind diarylamine RTA technology has emerged since the 1950s.

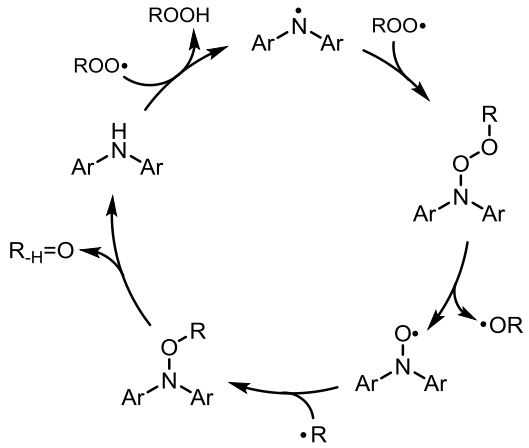

Scheme 4.1. Proposed mechanism of catalytic activity of diarylamine RTAs.

In recent years we have reported on the design and development of novel heterocyclic diarylamines,[8–10] some of which react up to 2 orders of magnitude faster with peroxyl radicals than conventional compounds at ambient temperatures (i.e., $k_1 > 10^7$ $M^{-1}s^{-1}$) due to their comparatively weaker N−H bonds (*ca*. 6 kcal/mol relative to diphenylamine). We anticipated that they would also be more efficient than conventional compounds at elevated temperatures since homolysis of the N−O bond in the intermediate alkoxyamines would also be much more facile. However, before setting out to investigate the properties of the new compounds any further, we sought more information about the mechanism proposed by Korcek and co-workers and present the results of our computational and experimental studies here.

4.3 Results and Discussion

4.3.1 Computational Results

The structures and energetics of the participants in the proposed catalytic cycle (Scheme 4.1) were computed at the CBS-QB3 level of theory[11] for the reaction between either diphenylamine (**4.1**) or 4,4'-dimethyldiphenylamine (**4.2**) and a model peroxyl radical, methylperoxyl (MeOO•). The former was chosen as it is the parent diarylamine, and the latter was chosen as a model for the industry-standard dialkylated diphenylamines. The key stationary points and their relative enthalpies were determined at 25 °C and are shown in Figure 4.1.

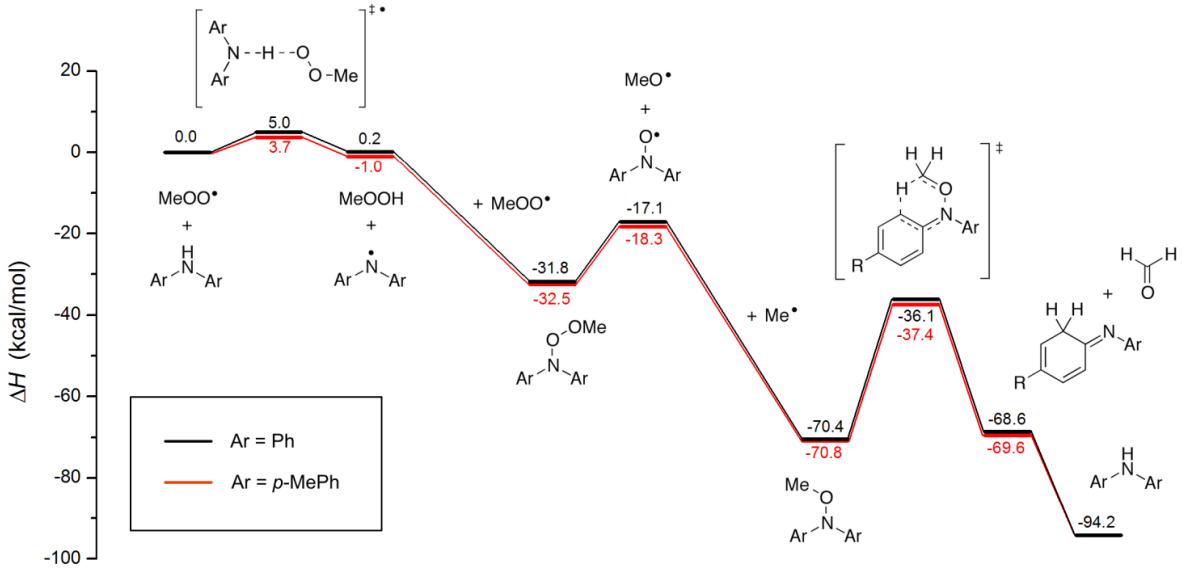

Figure 4.1. CBS-QB3-calculated enthalpies (at 25 °C) for relevant structures in Scheme 4.1.

The initial step, abstraction of the labile H-atom of diphenylamine by a peroxyl radical (eq 4.1), proceeds through a transition state characterized by proton transfer (roughly) within the plane of the aromatic rings, and simultaneous electron transfer from the π-system to the radical, consistent with its description as a proton coupled electron transfer (PCET) reaction.[8,12,13] The TS structure is shown in Figure 4.2 along with the highest (doubly) occupied molecular orbital, which clearly shows

electron delocalization from the π-HOMO of diphenylamine to the π*-LUMO of the methylperoxyl radical.

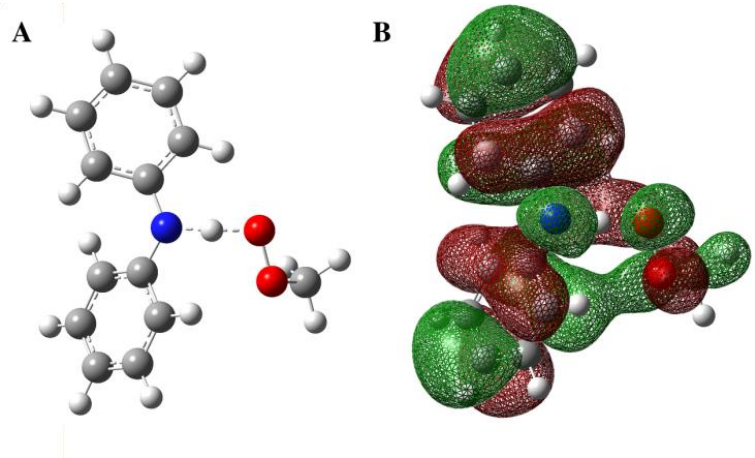

Figure 4.2. (A) Calculated TS structure for the reaction between diphenylamine and a methylperoxyl radical, and (B) the highest (doubly) occupied molecular orbital.

The enthalpic barrier to the reaction was calculated to be 5.0 kcal/mol, and the corresponding free energy barrier ($\Delta G^{\ddagger}$ = 16.2 kcal/mol) yields a rate constant of 1.8×10^4 $M^{-1}s^{-1}$ by application of transition state theory (at 25 °C), in good agreement with the experimental result of 1.5×10^4 $M^{-1}s^{-1}$ (at 50 °C).[3] It should be pointed out that the TS is preceded by a H-bonded prereaction complex and followed by a H-bonded postreaction complex with enthalpies of −4.2 and −9.0 kcal/ mol, respectively, relative to the separated starting materials (not shown in Figure 4.1). The phenyl rings in both the TS and product diphenylaminyl radical are oriented to maximize the delocalization of the radical throughout the π-system, although repulsion between the *ortho* hydrogens precludes complete planarization of the two rings.[14] Addition of *p*-methyl substituents to the rings drops the barrier 1.3 kcal/mol, °C (k = 1.5×10^5 $M^{-1}s^{-1}$), in good agreement with experiment (k = 1.8×10^5 $M^{-1}s^{-1}$ for 4,4'-dioctyldiphenylamine at 37 °C).[8,9] The substituent effect can be understood on thermodynamic grounds by the greater stability of the diarylaminyl radical,[15,16] and on kinetic grounds by the reduced energy gap between the higher energy π-HOMO of the substituted diphenylamine and π*-LUMO of the peroxyl radical.

Coupling of the diphenylaminyl radical to a methylperoxyl to yield an alkylperoxyamine is 32.0 kcal/mol downhill (enthalpically) and expected to be diffusion-controlled. N−O bond formation must compete with addition of a peroxyl radical to the aryl ring (the preferred pathway for reactions of peroxyl radicals with phenoxyl radicals[17]) as is shown in Scheme 4.2. The *para* and *ortho* adducts have C−O BDEs of 33.0 and 28.6 kcal/ mol, respectively. While, at first glance, it would seem that the preferred reaction of peroxyl radicals with diphenylaminyl radicals should therefore follow the *para*-coupling pathway, the follow-up reactions need to be considered. In the alkylperoxyamine intermediate the O−O bond is much weaker than the N−O bond (14.7 vs 32.0 kcal/mol), cleaving to yield the nitroxide and alkoxyl radical, whereas in the *para*-coupled adduct, the C−O bond is much weaker than the O−O bond (33.0 vs 41.3 kcal/mol), suggesting that, at elevated temperatures, the intermediates will be funneled toward the thermodynamic product: the nitroxide. (Should the O−O bond in the *para*- or *ortho*-coupled adduct be cleaved, in-cage disproportionation of the two oxygen-centered radicals is likely to proceed to give an *N*-phenyl iminoquinone. Alternatively, tautomerization of the adduct may occur, followed by very rapid O−O dissociation and in-cage disproportionation, to afford the same products.)[30]

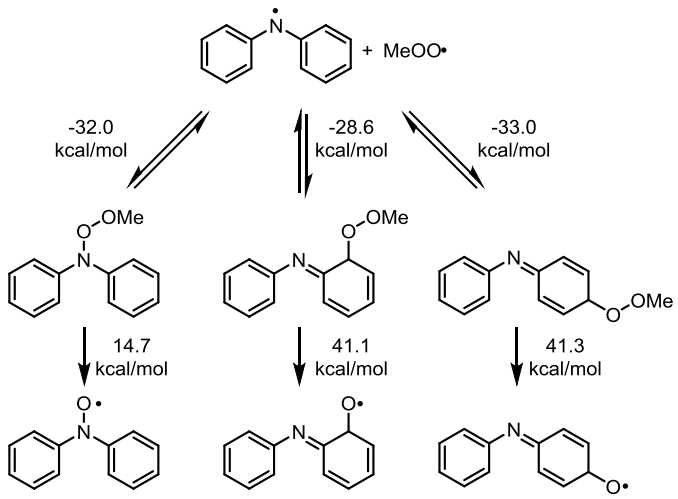

Scheme 4.2. Competing pathways (and associated ΔH values) for Ph_2N• + •OOMe.

The structure of the diphenylnitroxide is similar to that of the diphenylaminyl radical. Nitroxides can have up to *ca*. 30% of their spin density on the nitrogen atom,[18] and the aromatic rings in the diphenylnitroxide are oriented to maximize delocalization of the radical while minimizing the repulsion associated with planarizing the rings. Though the nitroxides derived from **4.1** and **4.2** are comparatively stable (the corresponding hydroxylamines have O−H BDEs of 71.4 and 70.8 kcal/mol, respectively), they can potentially react with peroxyl radicals via their aryl rings. (The *para* and *ortho* adducts from coupling diphenylnitroxide and methylperoxyl have C−O BDEs of 20.9 and 19.6 kcal/mol, respectively. While they are expected to fragment back to the nitroxide at elevated temperatures, competing tautomerization and subsequent O−O bond cleavage will yield *N*-oxides of the same *N*-phenyl iminoquinone products that arise from addition of peroxyl radicals to the rings of diphenylaminyl radicals, *vide supra*.)

Combination of an alkyl (methyl) radical to the diphenylnitroxide is exothermic (53.3 kcal/mol),[19] and the N−O bond dissociation enthalpy in the resultant alkoxyamine is 42.1 kcal/ mol (ΔG = 29.5 kcal/mol),[31] making it the rate-determining step in the regeneration of the diarylamine from its diarylaminyl radical upon disproportionation. Interestingly, we were able to locate a transition state for concerted N−O dissociation and disproportionation. The enthalpic cost to reach the transition state ($\Delta H^{\ddagger}$ = 39.4 kcal/mol) was slightly less than the N−O bond dissociation enthalpy and, given the small entropic cost associated with the process ($T\Delta S^{\ddagger} \sim 0$ kcal/mol at 298 K), suggested that the concerted pathway may be accessible. However, we subsequently found that this stationary point was unstable with respect to RHF → UHF transformation,[20] and while a stable UHF wave function could be obtained corresponding to the singlet biradical, no concerted TS structure could be located on this surface, with the structure collapsing directly to products.

While struggling with the foregoing calculations, we wondered whether another concerted process could intervene: a concerted six-electron pericyclic process – an unprecedented retro-

carbonyl-ene (hereafter RCE) reaction – which would give the same carbonyl product and an imino-tautomer of diphenylamine:

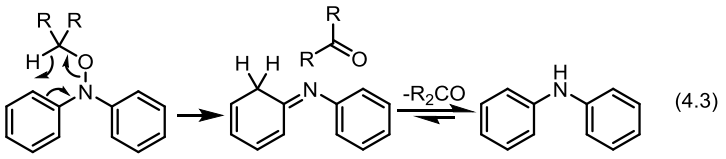

(4.3)

Indeed, we were able to find a transition state structure corresponding to this process (*cf.* Figure 4.3), and its enthalpic barrier, $\Delta H^{\ddagger}$ = 34.3 kcal/mol, was almost 8 kcal/mol lower than the N−O BDE. The HOMO of the TS structure is a mixture of the π-HOMO of the imino-tautomer of diphenylamine and the π*-LUMO of formaldehyde, the expected frontier MOs in the six-electron RCE pericyclic process. The low entropy of activation of $T\Delta S^{\ddagger}$ = 1.4 kcal/mol at 298 K suggests that this process could be competitive with N−O bond homolysis.

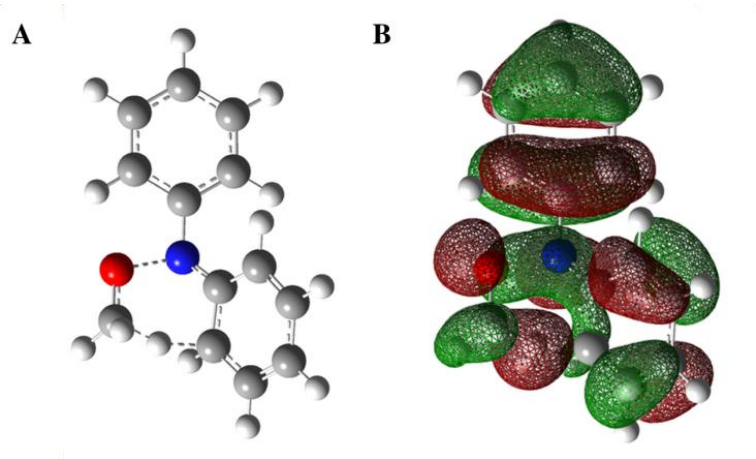

Figure 4.3. (A) Calculated TS structure for the retro-carbonyl-ene reaction of O-methyl N,N-diphenylhydroxylamine and (B) its HOMO.

Since the RCE mechanism involves concerted C−H cleavage, the ease with which it occurs should be dependent on the identity of the alkyl moiety. Indeed, when we replaced the methyl group with an isopropyl or allyl group, we found that the calculated N−O BDEs increased slightly (44.5 and 42.6 kcal/mol, respectively, compared to 42.1 kcal/mol), but the RCE reaction became more facile by 1.8 (32.5) and 4.0 (30.3) kcal/mol, respectively.

While the alkoxyamine derived from the 4,4'-dimethyldiphenylamine had an expectedly weaker N−O bond than in the diphenylamine-derived alkoxyamine owing to the ability of the electron-donating methyl substituents to better stabilize the electron-poor aminyl radical[15,16] (N−O BDE = 41.3 kcal/mol), a concerted RCE TS was also found for this reaction ($\Delta H^{\ddagger}$ = 33.4 kcal/mol), and again, it was lower in enthalpy than that for bond dissociation. These results suggest that the RCE reaction may be an accessible pathway for decomposition of diarylamine-derived alkoxyamines.[32]

4.3.2 Synthesis of *N*,*N*-Diarylalkoxyamines

Despite the proposed central role of *N*,*N*-diarylalkoxyamines in the catalytic activity of diarylamine radical-trapping antioxidants, there are only a handful of examples of their preparation and characterization and only one study of their reactivity – the seminal work of Korcek and coworkers relayed above.[5] We felt that our understanding of this reaction would be greatly bolstered by experiments employing authentic *N*,*N*-diarylalkoxyamines. As such, following Kelly's work,[21] we were able to prepare saturated and unsaturated alkoxyamines derived from diphenylamine and 4,4'-di-tertbutyldiphenylamine (**4.3**) as shown in Scheme 4.3. Briefly, the endoperoxide formed from photosensitized oxygenation of 1,3-cyclohexadiene[22] was treated with lithium diarylamide to prepare the unsaturated alkoxyamines **4.4** and **4.5**, and the corresponding saturated alkoxyamines **4.6** and **4.7** were obtained by the same chemistry, but following the precedented diimide reduction of the 1,3-cyclohexadiene-derived endoperoxide.[23] With these compounds in hand, we set out to determine the kinetics and mechanism of their decomposition by HPLC.

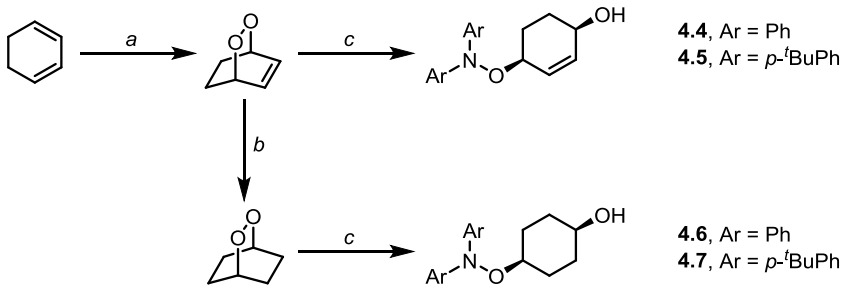

Scheme 4.3. Synthesis of *N*,*N*-diarylalkoxyamines. (a) O_2, *hv*, Rose Bengal, MeOH/CH_2Cl_2, 0 °C, 6 h, 46%; (b) $N_2(CO_2)_2K_2$, AcOH, MeOH, 0 °C, 2 h, 46%; (c) Ar_2NH, BuLi, Et_2O, −78°C, 10 min, 30% (**4.4**), 22% (**4.5**), 20% (**4.6**), 15% (**4.7**).

4.3.3 *N*,*N*-Diarylalkoxyamine Decomposition Experiments

In the event, the unsaturated alkoxyamine decomposed smoothly (*cf*. Figure 4.4A), and roughly six times faster than the saturated alkoxyamine at 120 °C, as monitored directly by HPLC ($k = 2.4 \times 10^{-4}$ s^{-1} vs $k = 4.1 \times 10^{-5}$ s^{-1}). Product analysis revealed near-quantitative formation of diphenylamine in both cases. However, subsequent experiments carried out at a variety of temperatures between 75 and 165 °C revealed markedly different Arrhenius parameters for the two substrates (*cf*. Figure 4.4B). The decomposition of the saturated alkoxyamine **4.6** was characterized by E_a = 35.1 ± 0.7 kcal/mol and log A = 15.1 ± 0.4, whereas the unsaturated alkoxyamine **4.4** decomposed with E_a = 30.2 ± 0.7 kcal/mol and log A = 13.2 ± 0.4. These results hint at different processes: the larger log A is consistent with a simple (N−O) bond dissociation in the transition state,[24] and the smaller log A is consistent with more organization in the transition state, perhaps due to concerted C−H cleavage such as in the computed RCE reaction. The alkoxyamines derived from the 4,4'-di-*tert*-butyldiphenylamine, **4.5** and **4.7**, decomposed faster than their diphenylamine-derived counterparts, **4.4** and **4.6**, by 2.4- and 3.7-fold at 120 °C, respectively. The activation energies for the substituted compounds (30.3 ± 0.3 kcal/mol for **4.5** and 33.5 ± 0.2 kcal/mol for **4.7**) were comparatively lower and also showed that the unsaturated alkoxyamine **4.5** had a significantly lower log$A$ (13.6 ± 0.2) than the saturated compound alkoxyamine **4.7** (14.8 ± 0.1), indicating that regardless of the

substitution of the diphenylamine, both unsaturated alkoxyamines decomposed through a pathway distinct from the saturated compounds.

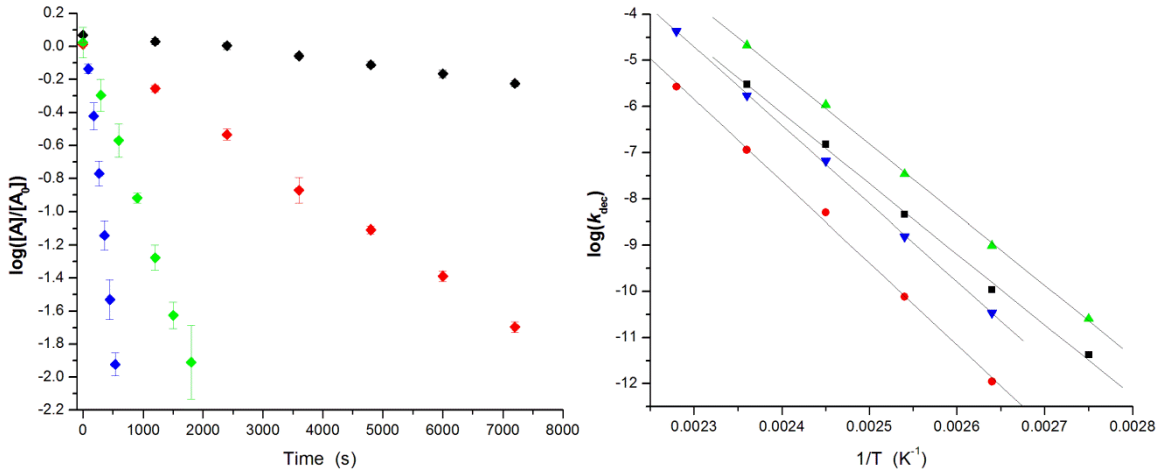

Figure 4.4. (A) Decomposition of **4.4** monitored by HPLC between 105 and 150 °C. (B) Temperature dependence of the decomposition of **4.4** (■),**4.5** (●),**4.6** (▲), and **4.7** (▼).

To provide further insight on the lower log *A* value for **4.4** compared to **4.6**, we synthesized the octadeuterated compounds **4.4**-d_8 and **4.6**-d_8 as in Scheme 4.3 (using ca. 94% perdeuterated 1,3-cyclohexadiene[25] as starting material) and measured their decomposition kinetics at 120 °C. These experiments revealed a kinetic isotope effect of 1.8 for **4.4** and 1.2 for **4.6**, which correspond to values of 2.1 and 1.3 at 25 °C – a primary kinetic isotope effect for **4.4**, suggesting some C−H bond cleavage in the transition state of the decomposition reaction, and a secondary kinetic isotope effect for **4.6**.

Direct evidence for the RCE mechanism was obtained upon examination of the products derived from the decomposition of **4.4**-d_8 and **4.6**-d_8; deuterium incorporation was observed in the *ortho* position of one of the phenyl rings of the diphenylamine derived from **4.4** (49% at 90 °C and decreasing with increasing temperature to 28% at 150 °C, as judged by the diminished integration of the signal in the ^{1}H NMR spectra relative to the *meta* and *para* proton signals), whereas the diphenylamine derived from decomposition of **4.6** contained no deuterium (see Supporting Information). These results, taken alongside the kinetic isotope effects and the Arrhenius parameters,

suggest a change in mechanism upon going from an "unactivated" (i.e., saturated) to "activated" (i.e., unsaturated) substrate. Incorporating the insights from the computations, our view is that "unactivated" alkoxyamines undergo N−O homolysis and disproportionation to yield diarylamines,[33] whereas suitably "activated" substrates can access the RCE pathway to yield the same products. Furthermore, a switch from the high-enthalpy/low-entropy N−O homolysis to the low-enthalpy/high-entropy RCE pathway with changing temperature is evident from the changing deuterium incorporation in the diphenylamine product.

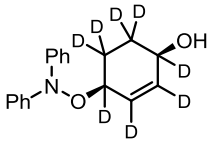

4-d_8

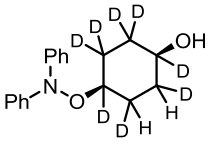

6-d_8

4.3.4 Inhibition of High Temperature Hexadecane Autoxidations

With the authentic alkoxyamines in-hand, we also evaluated their ability to inhibit the autoxidation of a hydrocarbon at elevated temperature relative to the corresponding diarylamines. We selected hexadecane because Korcek's suggested mechanism in Scheme 4.1 was derived largely from experiments carried out with this hydrocarbon.[5,26,27] Moreover, we employed the same temperature (160 °C) and the same type of stirred flow reactor as originally used by Korcek.[26] The stirred flow reactor makes use of a constant flow of O_2 to stir the reaction mixture and ensure that it is continuously oxygenated; a necessity at this temperature, otherwise, mass transfer of O_2 becomes rate-limiting.[26,27] In principle, since the half-lives of the unsaturated and saturated alkoxyamines at 160 °C (derived from the Arrhenius parameters given above) are only *ca*. 100 and 200 s, respectively, they should decompose largely to the diphenylamines in the first few minutes of the reaction, giving rise to inhibited autoxidations indistinguishable from those inhibited by the corresponding diphenylamines. The data, presented as the concentration of hydroperoxide determined as a function of time (using our previously described pro-fluorescent phosphine[28]), are shown in Figure 4.5. Interestingly, while the data from autoxidations inhibited by the unsaturated

alkoxyamines **4.4** and **4.5** were fully consistent with our expectations, the saturated alkoxyamines **4.6** and **4.7** were found to be less effective than either the unsaturated alkoxyamines or authentic diphenylamines.

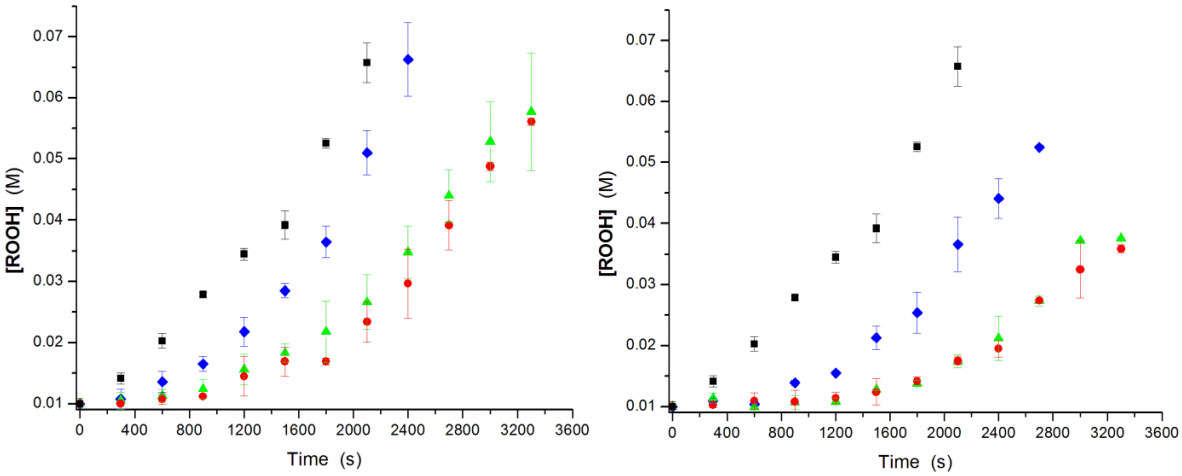

Figure 4.5. Hydroperoxide formation in the autoxidation of hexadecane at 160 °C initiated by 10 mM tetralin hydroperoxide (■) and inhibited by 100 μM of (A): diphenylamine **4.1** (●) n = 8.4, or alkoxyamines **4.4** (▲) n = 8.2, or **4.6** (◆) n = 5.8; (B): 4,4'-di-*tert*-butyldiphenylamine **4.3** (●) n = 9.5, or alkoxyamines **4.5** (▲) n = 9.1, or **4.7** (◆) n = 6.3.

These results imply that while the unsaturated alkoxyamines decompose to give diphenylamine quantitatively in hexadecane at 160 °C, the same cannot be said of the saturated alkoxyamines. This was hinted at in Korcek's original experiment, where he found that heating of a mixture of alkoxyamines generated *in situ* from decomposition of tert-butyl peroxy-2-ethylhexanoate in hexadecane in the presence of bis(*p*-octylphenyl)nitroxide gave 64% bis(*p*-octylphenyl)- amine.[5] If we consider this in the context of the foregoing mechanistic studies, the results highlight the competition that exists between disproportionation of the initially formed diphenylaminyl-alkoxyl radical pairs and other possible reactions, e.g. H-atom abstraction from hexadecane by the alkoxyl radical, which can initiate autoxidation. In contrast, the unsaturated alkoxyamines yield the same extent of inhibition as the corresponding diphenylamines because no radicals are formed in the RCE reaction, and the diphenylamines are produced quantitatively. This leads to the somewhat surprising

conclusion that *the catalytic radical-trapping antioxidant activities of diarylamines are likely to be highly substrate-dependent*. That is, while unsaturated hydrocarbons may be more oxidizable than saturated ones, when oxidized at elevated temperatures in the presence of diarylamines, they should give rise to alkoxyamines which are more efficiently converted back to the starting diarylamines, which will be characterized by higher stoichiometric numbers.

4.3.5 Retro-Carbonyl-Ene Reaction of Unactivated Alkoxyamines

While the foregoing results certainly provide insight into the mechanism of diarylamine regeneration and show that the efficacy of the diarylamine as an RTA is likely to be dependent on the substrate that is undergoing oxidation, it would arguably be more useful to know if the structure of the diarylamine could instead be altered to favor decomposition by the RCE reaction in lieu of N−O homolysis/disproportionation. We surmised that replacement of one of the phenyl rings in the diphenylamine-derived alkoxyamine with a naphthyl ring may decrease the enthalpic barrier for the RCE reaction sufficiently that an activated (i.e., unsaturated) alkyl element would no longer be required for the reaction to proceed in this way. CBS-QB3 calculations suggested that this would indeed be the case, predicting that the $\Delta H^{\ddagger}$ for the RCE reaction of the O-methyl alkoxyamine derived from *N*-phenyl-*β*-naphthylamine (**4.8**)[35] would be 6 kcal/mol lower than the corresponding alkoxyamine derived from diphenylamine. Gratifyingly, we were able to prepare the two corresponding *N*-phenyl-*β*-naphthylamine-derived alkoxyamines **4.9** and **4.10** as in Scheme 4.3.

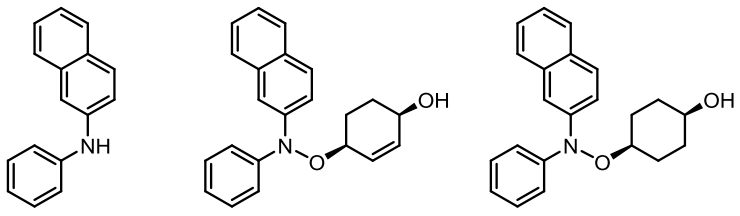

4.8 **4.9** **4.10**

The *β*-naphthyl-containing alkoxyamines **4.9** and **4.10** decomposed rapidly compared with the corresponding diphenylamine-derived compounds (at 120 °C, $k = 2.1 \times 10^{-3}$ and 6.4×10^{-4} s^{-1},

respectively). More interestingly, the temperature dependence of the rate constants for their disappearance yielded Arrhenius parameters of log A = 13.0 ± 0.3 and E_a = 28.2 ± 0.4 kcal/mol for **4.9** and log A = 12.9 ± 0.2 and E_a = 29.0 ± 0.4 kcal/mol for **4.10**, implying that both compounds decompose via the RCE pathway. Moreover, hexadecane autoxidations at 160 °C inhibited by **4.9** and **4.10** were indistinguishable from each other, and from hexadecane autoxidations inhibited by *N*-phenyl-*β*-naphthylamine35 (*cf*. Figure 4.5). Thus, by lessening the energetic penalty paid by the group on the amine to undergo the concerted process (the aromatic stabilization of the "second" ring of naphthalene is estimated to be 10−12 kcal/mol less than that in benzene),[29] we can favor this pathway even for "unactivated" (i.e., saturated) alkoxyamines.

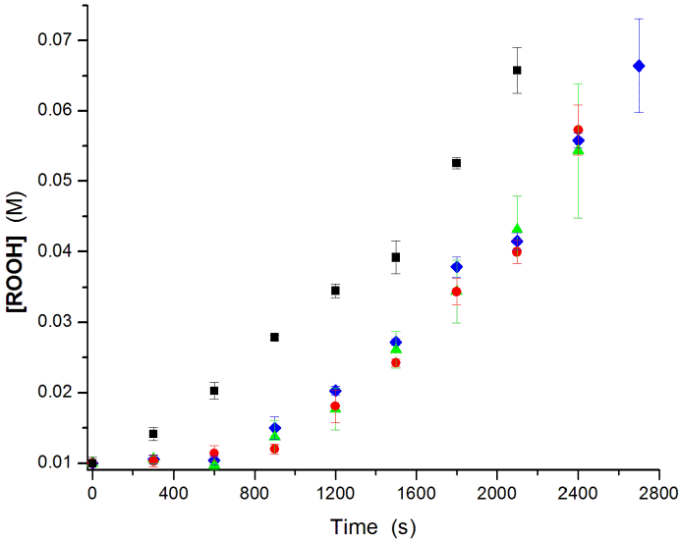

Figure 4.6. Hydroperoxide formation in the autoxidation of hexadecane at 160 °C initiated by 10 mM tetralin hydroperoxide (■), and inhibited by 100 μM of either *N*-phenyl-*β*-naphthylamine **4.8** (●) n = 5.2, unsaturated alkoxyamine **4.9** (▲) n = 5.2, or saturated alkoxyamine **4.10** (◆) n = 5.2.

Despite the greater reactivity of *N*-phenyl-*β*-naphthylamine[35] toward peroxyl radicals compared to diphenylamine (k = 1.1 × 10^5 $M^{-1}s^{-1}$ (**4.8**) vs 4.2 × 10^4 $M^{-1}s^{-1}$ (**4.1**) at 65 °C),[34] and significantly more favorable regeneration from its saturated alkoxyamine (*vide supra*), it is not as effective an inhibitor of hexadecane autoxidation (compare Figures 4.5A and 4.6 and stoichiometric factors derived from the data of n = 8.4 for the former and 5.2 for the latter). The likely explanation

is that addition of peroxyl radicals to the α-position of the naphthyl ring of the *N*-phenyl-*β*-naphthylaminyl radical intermediate will also be made easier compared to the diphenylaminyl radical due to the reduced aromaticity of the naphthyl ring. Indeed, the CBS-QB3-calculated C−O BDE of the adduct is 41.7 kcal/mol, which is 13.1 kcal/mol stronger than the analogous adduct of the diphenylaminyl radical (see Scheme 4.1), which makes peroxyl radical addition to the ring 9.7 kcal/mol more favorable than N−O bond formation (see Scheme 4.4). Although this reaction is reversible, it must compete with subsequent O−O bond homolysis (or tautomerization followed by homolysis), which requires roughly the same amount of energy as the reverse reaction (41.1 kcal/mol). Moreover, O−O bond homolysis is likely to be irreversible under the reaction conditions, as the resultant radicals can disproportionate to the iminoquinone and alcohol, products from which the diarylamine cannot be regenerated.

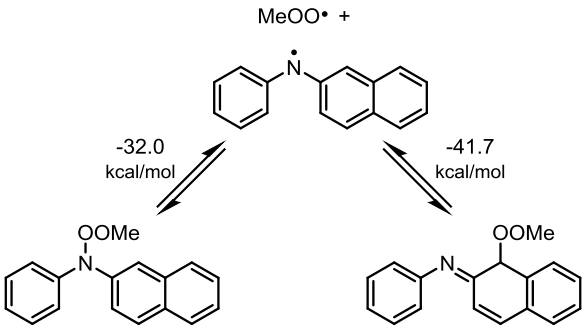

Scheme 4.4. Key competing pathways (and associated ΔH values) for phenyl *β*-naphthylaminyl + MeOO•.

The foregoing results have important implications with respect to the design of improved diarylamine radical-trapping antioxidants. They suggest that while optimization of the stability of the diarylaminyl radical may promote the initial H-atom transfer (proton-coupled electron transfer, eq 4.1) from the diarylamine to the peroxyl radical, this may not be helpful for promoting regeneration of the amine, since it could promote N−O bond homolysis and may facilitate cage escape. Instead, it would appear that diarylamines which are good H-atom donors and whose corresponding

alkoxyamines preferentially follow the retro-carbonyl-ene route to regenerate the diarylamine would be ideal radical-trapping antioxidants. We are currently exploring these ideas.

4.4 Conclusions

The synthesis of a series of *N*,*N*-diarylalkoxyamines has enabled kinetic and mechanistic experiments that clarify the mechanism of the catalytic behavior of diarylamine radical-trapping antioxidants. The determination of Arrhenius parameters, deuterium kinetic isotope effects, and isotope incorporation experiments confirm computational predictions that alkoxyamines derived from diphenylamines and saturated substrates decompose by N−O homolysis followed by disproportionation, whereas those derived from either diphenylamines and unsaturated substrates or *N*-phenyl-*β*-naphthylamine[35] and saturated substrates decompose by a concerted retro-carbonyl-ene reaction. This change in mechanism has significant implications in the use of diarylamine radical-trapping antioxidants, since they are expected to be comparatively better inhibitors of the autoxidation of unsaturated substrates owing to the more efficient regeneration of the diarylamine from its corresponding alkoxyamine. Moreover, it provides important insight into the design of the next generation of diarylamine radical-trapping antioxidants: compounds which turnover via the retro-carbonyl ene pathway will be far more effective than those that turnover via N−O homolysis and in-cage disproportionation, as do the industry-standard alkylated diphenylamines. While substitution of one of the phenyl rings for a naphthyl ring achieves this, it also makes deleterious (offcycle) reaction pathways more accessible. Limiting these reactions, while preserving the RCE pathway for diarylamine regeneration, should be the focus of future research.

4.5 Experimental

4.5.1 General Experimental

Reagents were purchased from commercial suppliers and used without further purification. 2,3-Dioxabicyclo[2.2.2]oct-5-ene was synthesized from the reaction of 1,3-cyclohexadiene with singlet oxygen according to the procedure of Ziegert and Brase.[22] The diimide reduction of the unsaturated endoperoxide was carried out according to the procedure of Coughlin, Brown, and Salomon.[23] Cyclohexadiene-d_8 was produced as a mixture of isomers via the procedure of Mugridge, Bergman, and Raymond,[25] and the crude mixture was subjected directly to singlet oxidation. Column chromatography was carried out using flash silica gel (40−63 μm, 230−400 mesh). ^{1}H and ^{13}C NMR were recorded on a Bruker AVANCE spectrmeter at 400 and 100 MHz, respectively, unless specified otherwise. High-resolution mass spectra were obtained on a Kratos Concept Tandem mass spectrometer.

4.5.2 General Procedure for the Synthesis of Diarylalkoxyamines

In a dry Schlenk flask under an inert atmosphere, 2.2 mmol of the appropriate diarylamine was dissolved in 15 mL of dry Et_2O (0.13 M) and cooled to −78 °C. Once cooled, 0.90 mL of *n*-BuLi in hexanes (2.5 M, 2.2 mmol) was added dropwise to the diarylamine solution, after which it was allowed to stir for 15 min at −78 °C. Endoperoxide (2.0 mmol) was dissolved in 1−2 mL of dry Et_2O and was added rapidly to the cooled reaction (over *ca*. 20 s; the color of the solution typically became a dark green). The reaction was allowed to stir for 10 min before an excess of water was added to quench the reaction, and the solution was allowed to warm to room temperature. The organic phase was separated, and the aqueous phase was extracted with Et_2O twice. The combined organic phases were washed with brine, then dried with MgSO4, filtered, and concentrated *in vacuo*. The alkoxyamines were purified by silica gel chromatography with 40% to 70% Et_2O/petroleum

ether, typically yielding a viscous oil which was crystallized from a small amount of Et_2O in hexanes at −20 °C overnight.

4-[N,N-Diphenyl(aminoxy)]-2-cyclohexen-1-ol (**4.4**). Yield: 30%. Off-white solid. ^{1}H NMR (400 MHz; $CDCl_3$): δ 7.31 (dd, J = 8.5, 7.4 Hz, 4H), 7.17−7.14 (m, 4H), 7.13−7.08 (m, 2H), 6.01−5.94 (m, 2H), 4.34 (m, 1H), 4.17 (br, 1H), 2.09−2.02 (m, 1H), 1.87−1.75 (m, 3H). ^{13}C NMR (100 MHz; $CDCl_3$): δ 149.4, 134.3, 128.9, 128.8, 124.4, 121.1, 74.8, 66.0, 28.4, 24.1. HRMS m/z: calcd $C_{18}H_{19}NO_2$, 281.1416; found, 281.1427.

4-[N,N-Di(4-tert-butylphenyl)aminooxy]-2-cyclohexen-1-ol (**4.5**). Yield: 22%. Off-white solid. ^{1}H NMR (400 MHz; DMSO-d_6): δ 7.34 (d, J = 8.8 Hz, 4H), 7.01 (d, J = 8.8 Hz, 4H), 5.86 (dd, J = 10.2, 1.7 Hz, 1H), 5.79 (dd, J = 10.5, 2.9 Hz, 1H), 4.86 (d, J = 5.5 Hz, 1H), 4.19 (m, 1H), 3.97 (m, 1H), 1.97−1.91 (m, 1H), 1.68−1.56 (m, 3H), 1.26 (s, 18H). ^{13}C NMR (100 MHz; $CDCl_3$): δ 147.04, 146.95, 134.0, 129.2, 125.6, 120.7, 74.4, 66.0, 34.3, 31.4, 28.5, 24.1. HRMS m/z: calcd $C_{26}H_{35}NO_2$, 393.2668; found, 393.2667.

4-[N,N-Diphenyl(aminooxy)]cyclohexanol (**4.6**). Yield: 20%. White solid. ^{1}H NMR (400 MHz; $CDCl_3$): δ 7.35−7.30 (m, 4H), 7.20−7.17 (m, 4H), 7.14−7.09 (m, 2H), 3.97 (m, 1H), 3.83−3.78 (m, 1H), 2.07−1.99 (m, 2H), 1.76−1.62 (m, 6H), 1.36 (br, 1H). ^{13}C NMR (100 MHz; $CDCl_3$): δ 149.7, 128.8, 124.2, 121.0, 77.5, 68.1, 30.8, 26.7. HRMS m/z, calcd $C_{18}H_{21}NO_2$, 283.1572; found, 283.1551.

4-[N,N-Di(4-tert-butylphenyl)aminooxy]-cyclohexanol (**4.7**). Yield: 15%. White solid. ^{1}H NMR (400 MHz; $CDCl_3$): δ 7.30 (d, J = 8.8 Hz, 4H), 7.08 (d, J = 8.8 Hz, 4H), 3.91 (m, 1H), 3.80−3.75 (m, 1H), 2.01 (m, 2H), 1.72−1.62 (m, 6H), 1.30 (s, 18H). ^{13}C NMR (100 MHz, $CDCl_3$) δ 147.3, 146.8, 125.6, 120.5, 68.2, 34.3, 31.4, 30.8, 26.8. HRMS m/z: calcd $C_{26}H_{37}NO_2$, 395.2824; found, 395.2849.

4-[N,N-Diphenyl(aminooxy)]-2-(1,2,3,4,5,5,6,6-d_8)-cyclohexen-1-ol (**4.4-d_8**). Yield: 29%. Off-white solid. *ca*. 94% D. ^{1}H NMR (300 MHz; $CDCl_3$): δ 7.31 (dd, J = 8.4, 7.2 Hz, 4H), 7.16 (dd, J = 8.7, 1.2 Hz, 4H), 7.13−7.08 (m, 2H), 5.97 (d, J = 9.7 Hz, 0.15H), 4.33 (s, 0.07H), 4.18−4.15 (m, 0.06H), 2.01 (s, 0.07H), 1.78 (d, J = 12.7 Hz, 0.21H), 1.51 (s, 1H). ^{13}C NMR (76 MHz, $CDCl_3$) δ 149.3, 128.9, 124.3, 121.1. HRMS m/z: calcd $C_{18}H_{11}D_8NO_2$, 289.1918; found, 289.1924.

4-[N,N-Diphenyl(aminooxy)]-2-(1,2,3,4,5,5,6,6-d_8)-cyclohexanol (**4.6-d_8**). Yield: 14%. White solid. *ca*. 93% D. ^{1}H NMR (300 MHz; $CDCl_3$): δ 7.30 (dd, J = 8.5, 7.2 Hz, 4H), 7.16 (d, J = 8.7 Hz, 4H), 7.09 (t, J = 7.3 Hz, 2H), 3.94−3.92 (m, 0.07H), 3.78− 3.76 (m, 0.07H), 3.40 (t, J = 6.6 Hz, 0.06H), 1.97 (br, 1H), 1.66 (br, 1H), 1.31 (s, 1H). ^{13}C NMR (76 MHz; $CDCl_3$): δ 149.7, 128.8, 124.1, 121.0. HRMS m/z: calcd $C_{18}H_{13}D_8NO_2$, 291.2074; found, 291.2096.

4-[N-2-Naphthyl-N-phenyl(aminooxy)]-2-cyclohexen-1-ol (**4.9**). Yield: 13%. Off-white solid. ^{1}H NMR (400 MHz; DMSO-d_6): δ 7.86 (m, 3H), 7.61 (d, J = 2.0 Hz, 1H), 7.47 (td, J = 13.6, 5.8 Hz, 2H), 7.37 (t, J = 7.9 Hz, 2H), 7.27 (dd, J = 8.8, 2.2 Hz, 1H), 7.16 (m, 3H), 5.92−5.84 (m, 2H), 4.89 (d, J = 5.6 Hz, 1H), 4.33 (m, 1H), 3.99 (m, 1H), 2.04−1.98 (m, 1H), 1.75−1.56 (m, 3H). ^{13}C NMR (100 MHz; DMSO-d_6): δ 149.0, 146.3, 136.9, 133.2, 130.4, 129.0, 128.8, 127.39, 127.37, 126.4, 125.8, 125.0, 124.4, 121.1, 120.7, 116.8, 74.4, 64.3, 27.7, 24.1. HRMS m/z: calcd $C_{26}H_{37}NO_2$, 331.1572; found, 331.1555.

4-[N-2-Naphthyl-N-phenyl(aminooxy)]cyclohexanol (**4.10**). Yield: 11%. Off-white solid. ^{1}H NMR (300 MHz; DMSO-d_6): δ 7.87 (m, 3H), 7.60 (s, 1H), 7.51−7.33 (m, 4H), 7.26 (d, J = 8.9 Hz, 1H), 7.18−7.11 (m, 3H), 4.44 (d, J = 3.6 Hz, 1H), 3.91 (m, 1H), 3.57 (m, 1H), 1.90 (m, 2H), 1.67−1.43 (m, 6H). ^{13}C NMR (76 MHz; DMSO-d_6): δ 149.2, 146.6, 133.2, 130.3, 128.9, 128.7, 127.4, 127.3, 126.4, 124.9, 124.2, 121.1, 120.7, 116.6, 77.9, 65.5, 30.4, 26.2. HRMS m/z: calcd $C_{26}H_{37}NO_2$, 333.1729; found, 333.1731.

4.5.3 Alkoxyamine Decomposition Experiments

n-Hexadecane (1.0 mL) was added to 0.015 mmol of alkoxyamine that was weighed into a glass vial. A magnetic Teflon coated stir bar was added, and the vial was capped with a rubber septum. The vial was then placed in a heating block at the appropriate temperature and allowed to stir for 30 s before the first sample was taken. Samples (100 μL) were taken at regular intervals and added to 900 μL of a 2.2 mM solution of benzyl alcohol in 2% isopropanol/hexanes (HPLC grade). Samples were analyzed using a Waters 2695 Alliance HPLC (gradient: 1−4 min: 1.2% ^{i}PrOH/hexanes, 0.8 mL min^{-1}; 5 min, 1.4% ^{i}PrOH/hexanes, 0.8 mL min^{-1}; 10 min 1.6% ^{i}PrOH/hexanes, 1.2 mL min^{-1}; 15−16 min:2.0%iPrOH/hexanes, 0.6 mL min^{-1}; 30 min; Sunfire Silica column (5 μm, 4.6 mm × 250 mm)) and analyzed by UV absorbance at 215 nm.

4.5.4 Hexadecane Autoxidations

n-Hexadecane (100 mL) was thoroughly degassed with argon and then heated to 160 °C while argon was continuously bubbled through the liquid. Once the temperature stabilized, 0.10 mmol of inhibitor (**4.1**, **4.3**−**4.10**) and 164 mg (1.0 mmol) of tetralin hydroperoxide were added to the solution, and the flow of argon was replaced with O_2. Aliquots (1.5 mL) were removed every 5 min and allowed to cool to room temperature for analysis. Four duplicates (30 μL) of each sample were loaded into separate wells of a 96-well microplate, and the automated reagent dispenser of a Biotek Synergy H1 microplate reader was used to dilute each sample with *tert*-amyl alcohol (200 μL) and a solution of a fluorgenic phosphine dye solution (20 μL of a 250 μM stock solution in acetonitrile) immediately before reading. The plate was stirred for 8 s and allowed to rest for 2 s more, and the fluorescence of each well was measured every second for 60 s (excitation = 340 nm; emission = 425 nm). The concentration of hydroperoxide was determined from the rate of phosphine oxidation using the rate constant for the reaction of the dye with secondary hydroperoxides in *tert*-amyl alcohol (k = 1.2 M^{-1} s^{-1}) assuming pseudo-first-order kinetics.[28]

4.6 References

(1) Ingold, K. U. *Chem. Rev*. **1961**, 61, 563.

(2) Ingold, K. U.; Pratt, D. A. *Chem. Rev*. **2014**, 114, 9022.

(3) Lucarini, M.; Pedrielli, P.; Pedulli, G. F.; Valgimigli, L.; Gigmes, D.; Tordo, P. *J. Am. Chem. Soc*. **1999**, 121, 11546−11553.

(4) Bolsman, T.; Blok, A. P.; Frijns, *J. Recl. Trav. Chim. Pays-Bas* **1978**, 97, 310.

(5) Jensen, R. K.; Korcek, S.; Zinbo, M.; Gerlock, J. L. *J. Org. Chem*. **1995**, 60, 5396.

(6) It has also been suggested that nitroxides can be catalytic RTAs because of reduction of their oxoammonium ions by substrate-derived alkyl radicals (see ref 2). The nitroxides are excellent RTAs when protonated by carboxylic acids; see: Amorati, R.; Pedulli, G. F.; Pratt, D. A.; Valgimigli, L. *Chem. Commun*. **2010**, 46, 5139. Carboxylic acids are known to be formed in autoxidations; see: Jensen, R. K.; Korcek, S.; Mahoney, L. R.; Zinbo, M. *J. Am. Chem. Soc*. **1981**, 103, 1742. Jalan, A.; Alecu, I. M.; Meana-Paneda, R.; Aguilera- Iparraguirre, J.; Yang, K. R.; Merchant, S. S.; Truhlar, D. G.; Green, W. H. *J. Am. Chem. Soc*. **2013**, 135, 11100.

(7) In contrast, the reaction of N,N-dialkylalkoxyamines with peroxyl radicals is believed to be the reaction responsible for the catalytic activities of the significantly less reactive hindered amine light stabilizers; see: Gryn'ova, G.; Ingold, K. U.; Coote, M. L. *J. Am. Chem. Soc*. **2012**, 134, 12979.

(8) Hanthorn, J. J.; Valgimigli, L.; Pratt, D. A. *J. Am. Chem. Soc*. **2012**, 134, 8306.

(9) Hanthorn, J. J.; Amorati, R.; Valgimigli, L.; Pratt, D. A. *J. Org. Chem*. **2012**, 77, 6895.

(10) Hanthorn, J. J.; Valgimigli, L.; Pratt, D. A. *J. Org. Chem*. **2012**, 77, 6895.

(11) Montgomery, J. A.; Frisch, M. J.; Ochterski, J. W.; Petersson, G. A. *J. Chem. Phys*. **1999**, 110, 2822.

(12) Isborn, C.; Hrovat, D. A.; Borden, W. T.; Mayer, J. M.; Carpenter, B. K. *J. Am. Chem. Soc*. **2005**, 127, 5794.

(13) DiLabio, G. A.; Johnson, E. R. *J. Am. Chem. Soc*. **2007**, 129, 6199.

(14) DiLabio, G. A.; Litwinienko, G.; Lin, S.; Pratt, D. A.; Ingold, K. U. *J. Phys. Chem*. A **2002**, 106, 11719.

(15) Pratt, D. A.; DiLabio, G. A.; Valgimigli, L.; Pedulli, G. F.; Ingold, K. U. *J. Am. Chem. Soc*. **2002**, 124, 11085.

(16) Pratt, D. A.; DiLabio, G. A.; Mulder, P.; Ingold, K. U. *Acc. Chem. Res*. **2004**, 37, 334.

(17) Boozer, C. E.; Hammond, G. S.; Hamilton, C. E.; Sen, J. N. *J. Am. Chem*. Soc. **1955**, 77, 3233.

(18) Stable Radicals: Fundamentals and Applied Aspects of Odd-Electron Compounds; Hicks, R. G., Ed.; John Wiley & Sons, Ltd.: **2010**.

(19) Beckwith, A.; Bowry, V. W.; Ingold, K. U. *J. Am. Chem. Soc*. **1992**, 114, 4983.

(20) Bauernschmitt, R.; Ahlrichs, R. *J. Chem. Phys*. **1996**, 104, 9047.

(21) Kelly, D. R.; Bansal, H.; Morgan, J. J. *Tetrahedron Lett*. **2002**, 43, 9331.

(22) Ziegert, R.; Brase, S. *Synlett* **2006**, 2119.

(23) Coughlin, D. J.; Brown, R. S.; Salomon, R. G. *J. Am. Chem. Soc*. **1979**, 101, 1533.

(24) Benson, S. W. Thermochemical Kinetics; John Wiley & Sons, Ltd.: **1976**.

(25) Mugridge, J. S.; Bergman, R. G.; Raymond, K. N. *Angew. Chem., Int. Ed*. **2010**, 49, 3635.

(26) Jensen, R. K.; Korcek, S.; Mahoney, L. R.; Zinbo, M. *J. Am. Chem. Soc*. **1979**, 101, 7574.

(27) Igarashi, J.; Jensen, R. K.; Lusztyk, J.; Korcek, S.; Ingold, K. U. *J. Am. Chem. Soc*. **1992**, 114, 7727.

(28) Hanthorn, J. J.; Haidasz, E.; Gebhardt, P.; Pratt, D. A. *Chem. Commun*. **2012**, 48, 10141.

(29) Schleyer, P. V. R.; Pühlhofer, F. *Org. Lett*. **2002**, 4, 2873.

(30) These are expected to hydrolyze to yield quinones, which are observed products in diphenylamine-inhibited autoxidations; see ref 4.

(31) In contrast, the O−C bond is significantly weaker than the N−O bond in N,N-dialkylalkoxyamines; see ref 7.

(32) It is difficult to determine $\Delta S^{\ddagger}$ for the N−O bond dissociation/in-cage disproportionation pathway for direct comparisons to the concerted process, or for comparison to our solution-phase experiments (*vide infra*).

(33) The small 'secondary' KIE observed for the decomposition of the saturated alkoxyamine likely reflects the commitment factor for the N−O homolysis given the subsequent in-cage disproportionation has to compete with radical recombination.

(34) Brownlie, I. T.; Ingold, K. U. *Can. J. Chem*. **1966**, 44, 861−868. The rate constants reported in this paper for *N*-phenyl-*β*-naphthylamine and diphenylamine were 5.0×10^4 and 2.0×10^4 M^{-1} s^{-1}, respectively at 65 °C, but these should be revised upward by a factor of 2.1 given the revised value of $2k_t$ for styrylperoxyl radicals, from which they are derived. See: Howard, J. A. In *Free Radicals*; Kochi, J. K., Ed.; Wiley: New Work, **1973**; Vol. 2, pp 3−62.

(35) *N*-Phenyl-*β*-naphthylamine was, at one time, among the most widely used diarylamine RTAs, but is now used sparingly owing to its carcinogenic potential. See: Weiss, T.; Brüning, T.; Bolt, H. M. *Crit. Rev. Toxicol*. **2007**, 37, 553.

4.7 Supporting Information

Optimized structures and energies (Gaussian 09) of the computationally calculated structures are provided in the Supporting Information section of the publication in the Journal of the American Chemical Society (*J. Am. Chem. Soc.* **2014**, 136(47), 16643-16650).

4.7.1 Alkoxyamine Decomposition Data – Arrhenius Plots

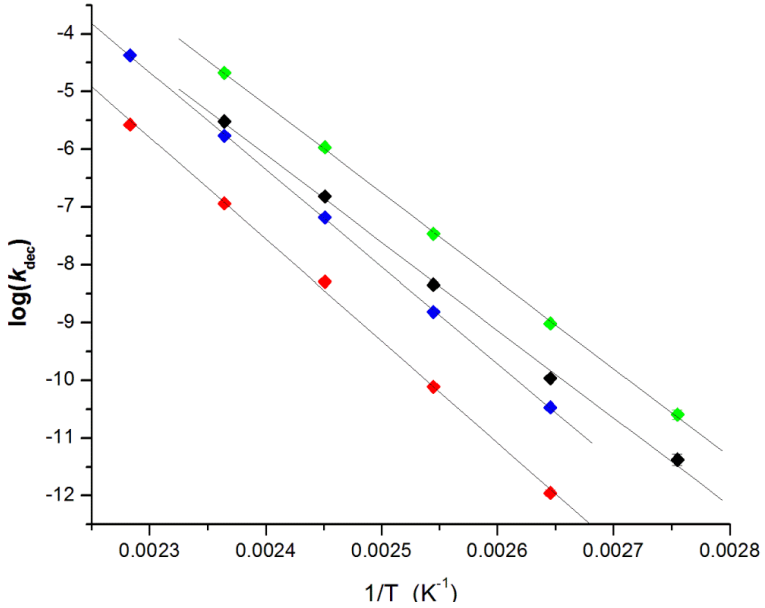

Figure S4.1. Temperature dependence of the decomposition of **4.4** (◆),**4.5** (◆),**4.6** (◆), and **4.7** (◆).

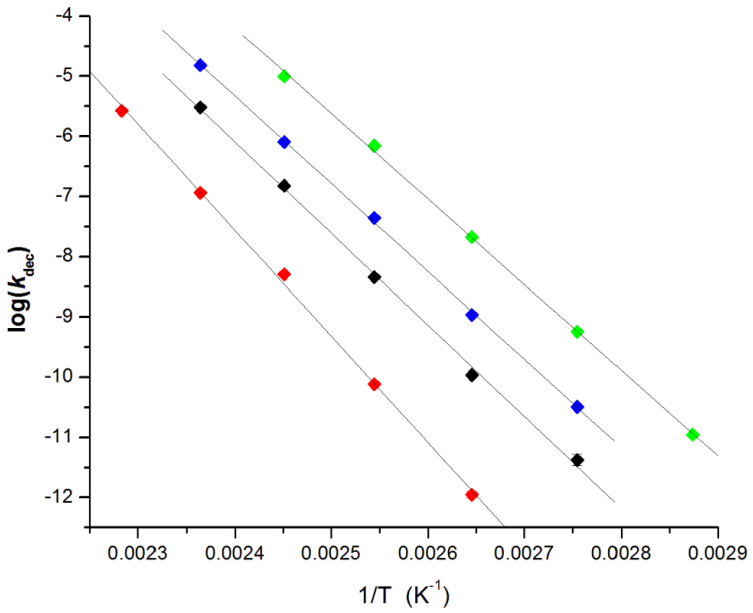

Figure S4.2. Temperature dependence of the decomposition of **4.4** (◆),**4.5** (◆),**4.9** (◆), and **4.10** (◆).

4.7.2 Alkoxyamine Decomposition Data – Decomposition Rates

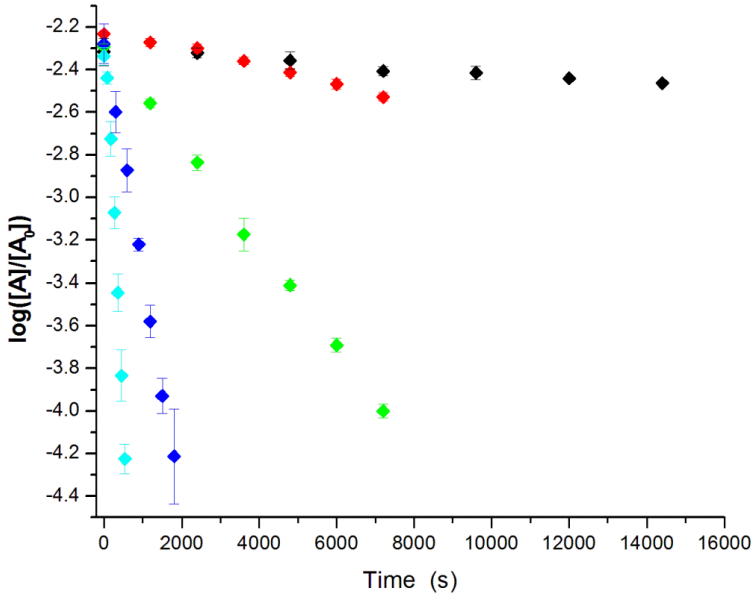

T (°C)	k_{dec} (s^{-1})
90	-1.15E-05
105	-4.71E-05
120	-2.38E-04
135	-1.09E-03
150	-4.01E-03

Figure S4.3. Decomposition of **4.4** monitored by HPLC at 90°C (◆), 105°C (◆), 120°C (◆), 135°C (◆), and 150°C (◆).

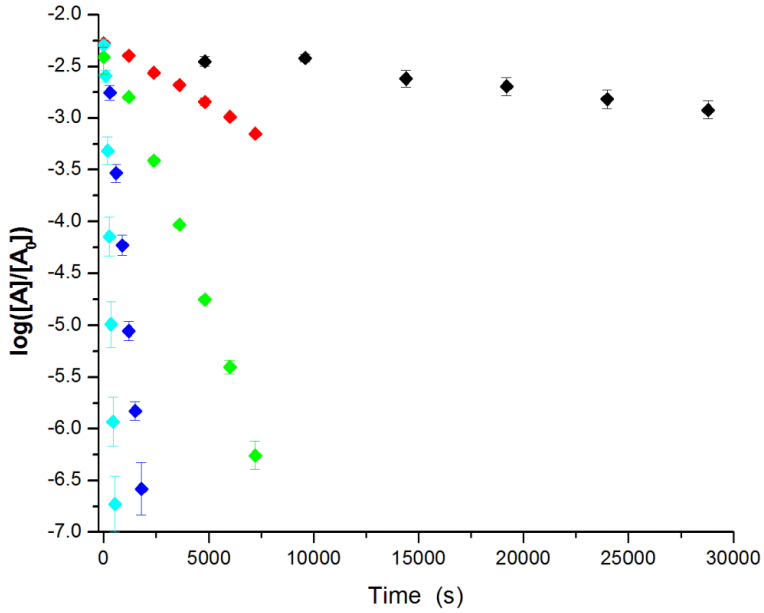

T (°C)	k_{dec} (s^{-1})
90	-2.51E-05
105	-1.22E-04
120	-5.72E-04
135	-2.56E-03
150	-9.33E-03

Figure S4.4. Decomposition of **4.5** monitored by HPLC at 90°C (◆), 105°C (◆), 120°C (◆), 135°C (◆), and 150°C (◆).

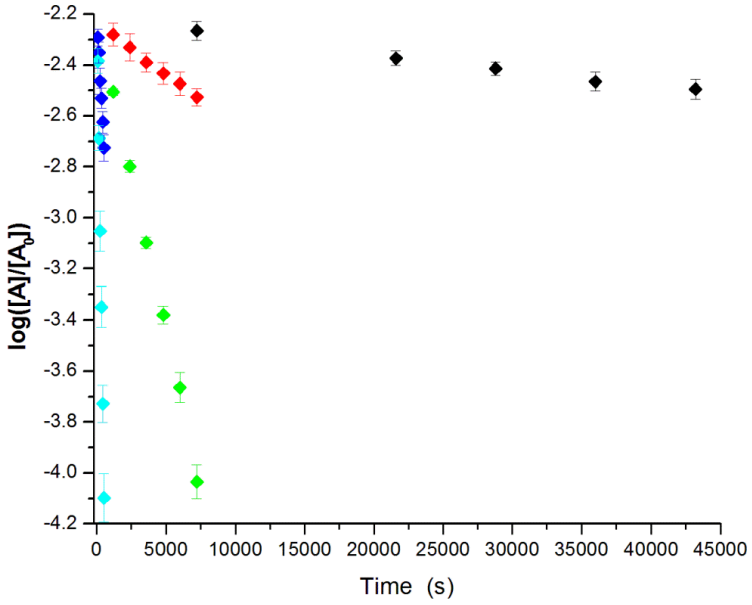

T (°C)	k_{dec} (s^{-1})
105	-6.45E-06
120	-4.06E-05
135	-2.51E-04
150	-9.69E-04
165	-3.81E-03

Figure S4.5. Decomposition of **4.6** monitored by HPLC at 105°C (◆), 120°C (◆), 135°C (◆), 150°C (◆), and 165°C (◆).

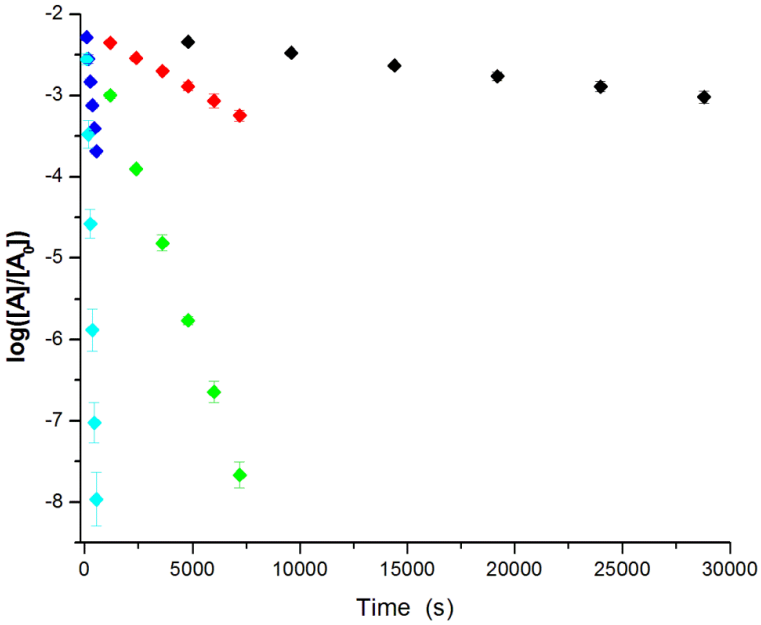

T (°C)	k_{dec} (s^{-1})
105	-2.84E-05
120	-1.49E-04
135	-7.62E-04
150	-3.13E-03
165	-1.27E-02

Figure S4.6. Decomposition of **4.7** monitored by HPLC at 105°C (◆), 120°C (◆), 135°C (◆), 150°C (◆), and 165°C (◆).

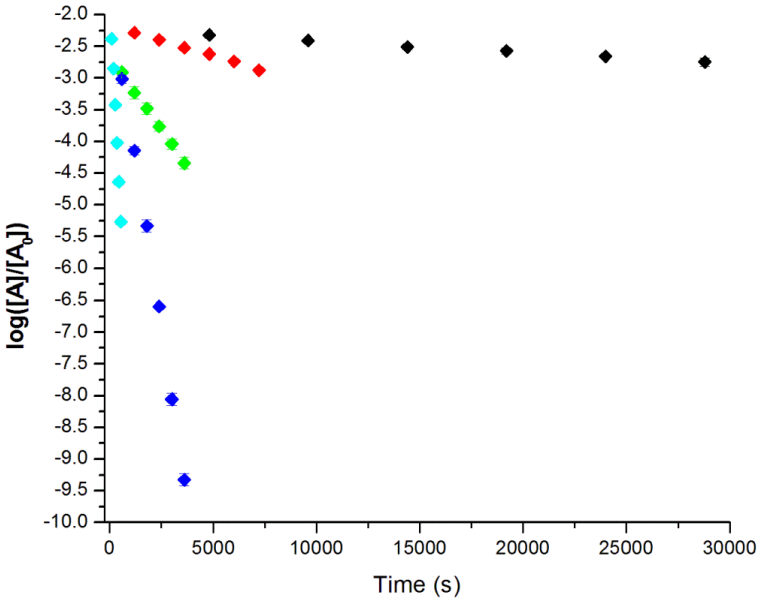

T (°C)	k_{dec} (s^{-1})
75	-1.75E-05
90	-9.72E-05
105	-4.64E-04
120	-2.12E-03
135	-6.73E-03

Figure S4.7. Decomposition of **4.9** monitored by HPLC at 75°C (◆), 90°C (◆), 105°C (◆), 120°C (◆), and 135°C (◆).

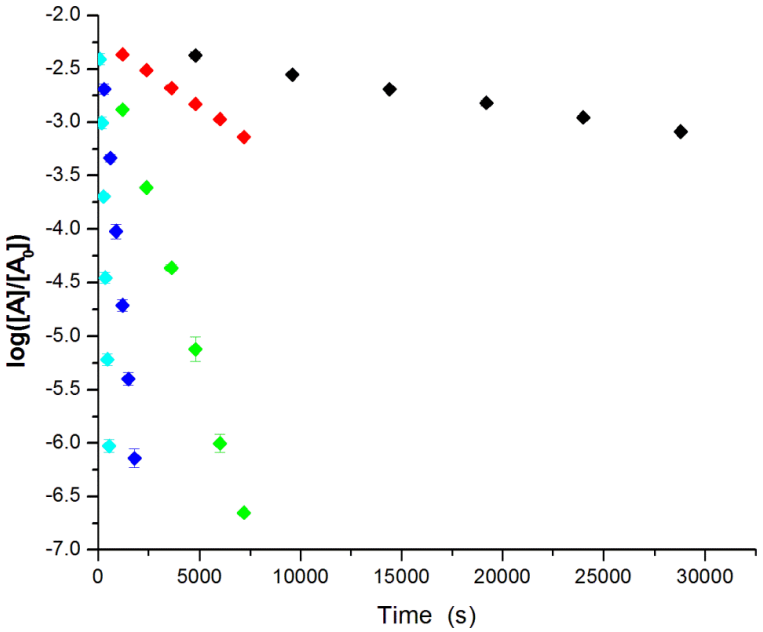

T (°C)	k_{dec} (s^{-1})
90	-2.77E-05
105	-1.29E-04
120	-6.38E-04
135	-2.26E-03
150	-8.09E-03

Figure S4.8. Decomposition of **4.10** monitored by HPLC at 90°C (◆), 105°C (◆), 120°C (◆), 135°C (◆), and 150°C (◆).

4.7.3 Deuterium Kinetic Isotope Effect – Alkoxyamine Decomposition

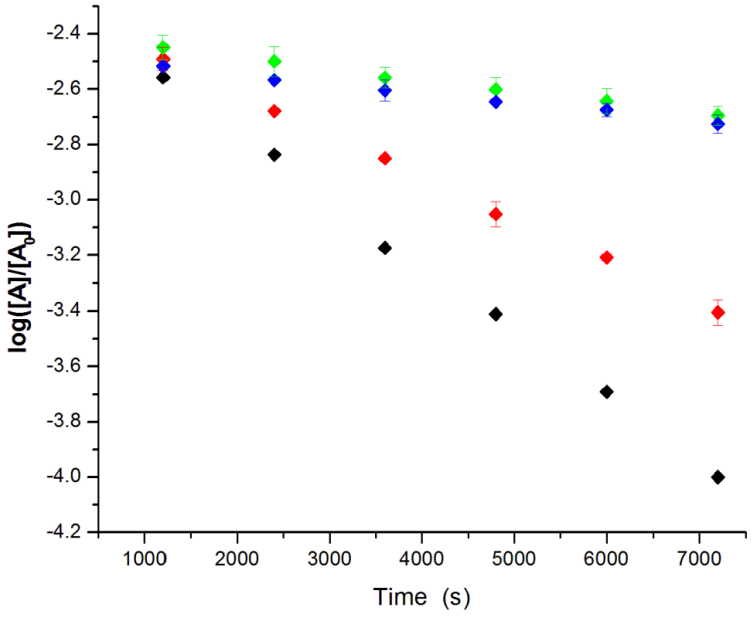

Figure S4.9. Deuterium kinetic isotope effect. Decomposition of **4.4** (◆),**4.4-*d*$_8$** (◆),**4.6** (◆), and **4.6-*d*$_8$** (◆) at 120°C in hexadecane, monitored by HPLC.

4.7.4 Deuterium Incorporation Experiments

Note: Longer ^{1}H NMR acquisition times did not have a significant effect on the relative peak integrations.

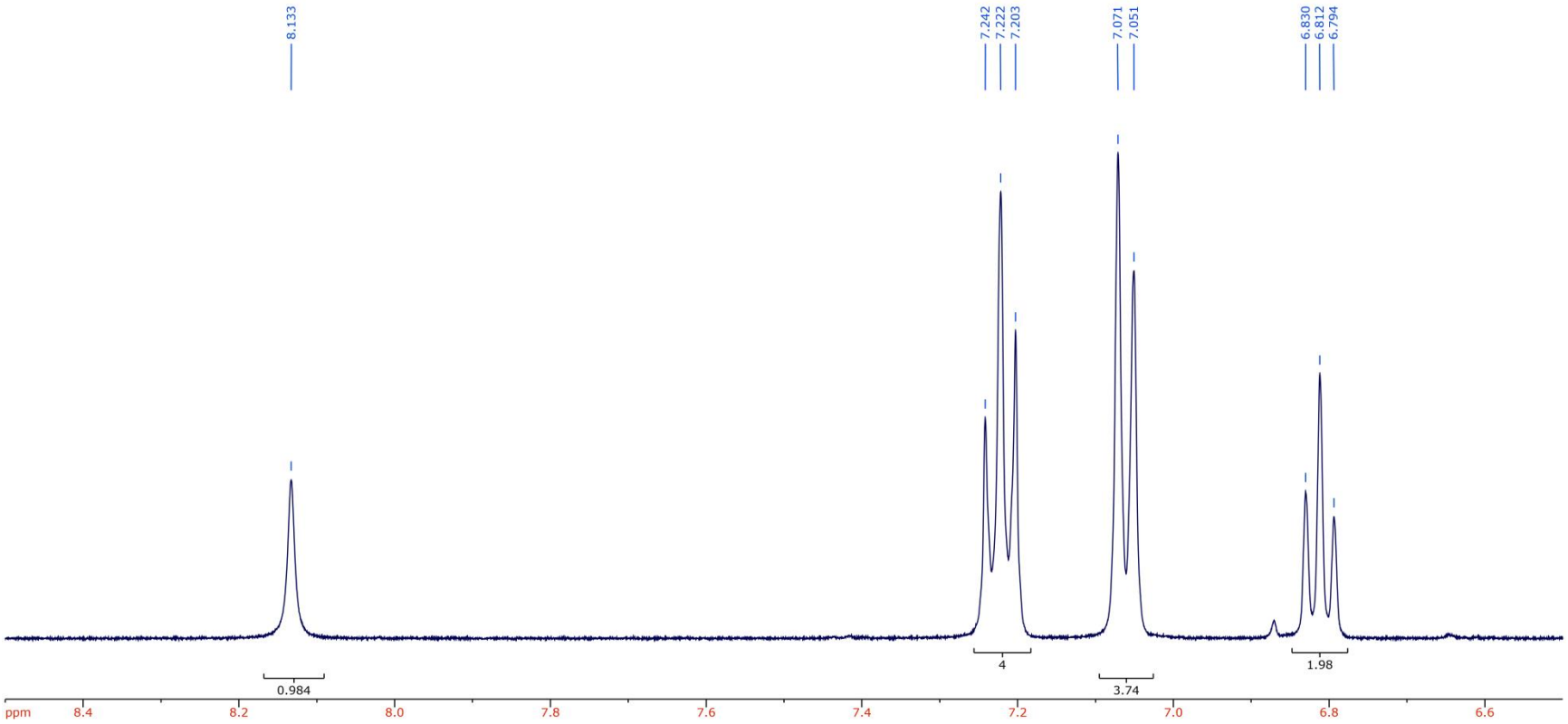

Figure S4.10. ^{1}H NMR of diphenylamine produced by decomposition of **4.4**-d_8 at 150°C in DMSO-d_6.

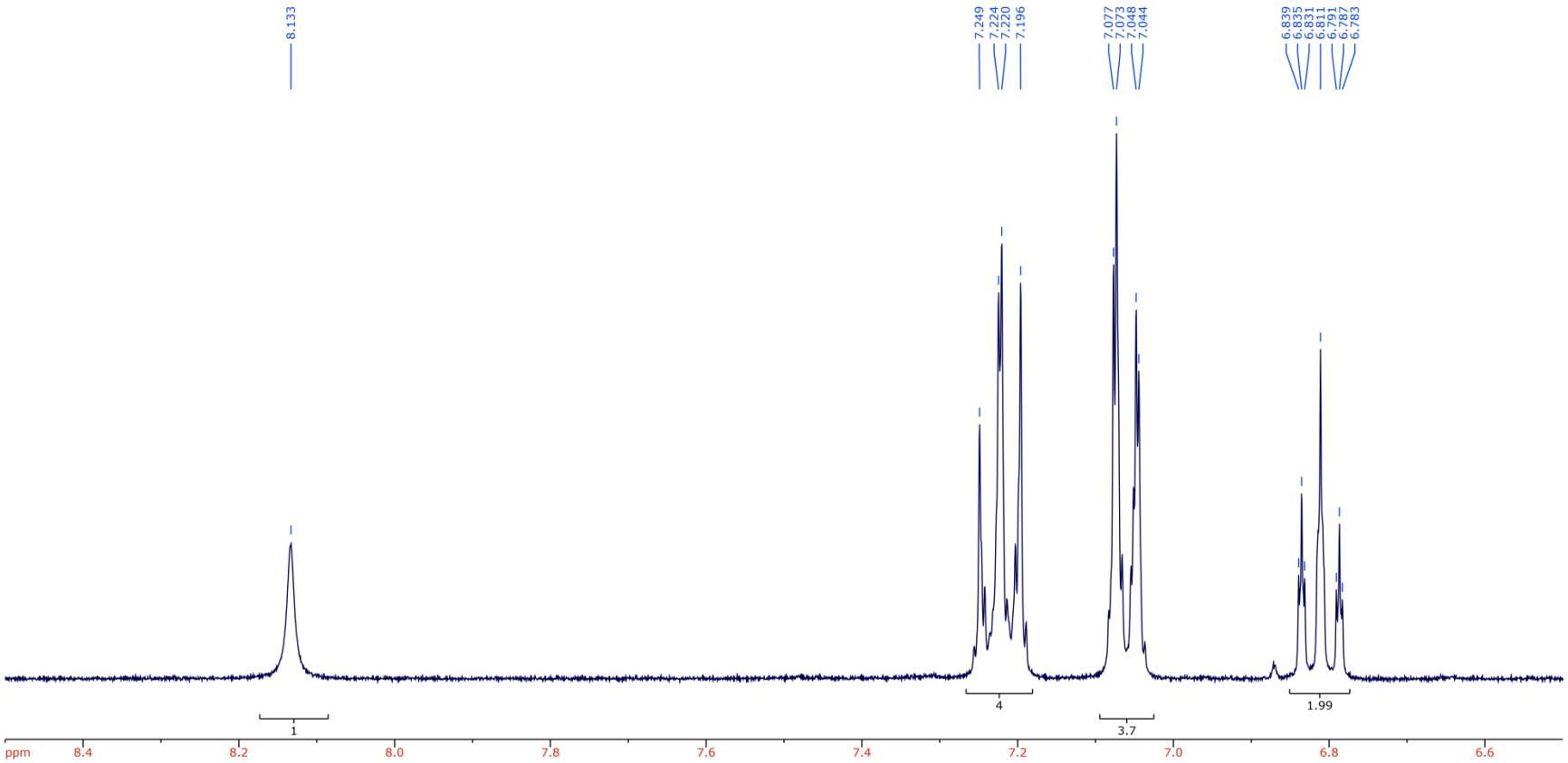

Figure S4.11. ^{1}H NMR of diphenylamine produced by decomposition of **4.4**-d_8 at 135°C in DMSO-d_6.

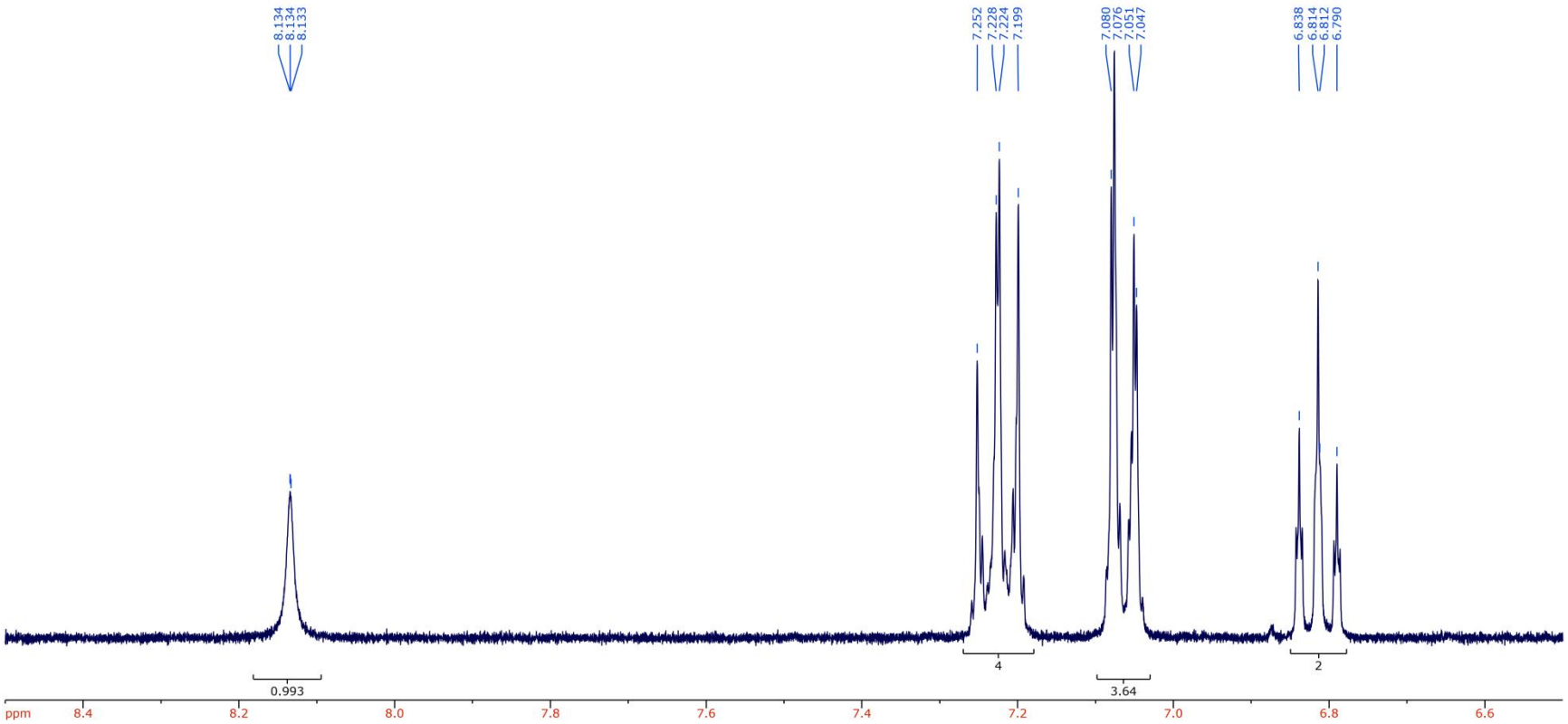

Figure S4.12. ^{1}H NMR of diphenylamine produced by decomposition of **4.4**-d_8 at 120°C in DMSO-d_6.

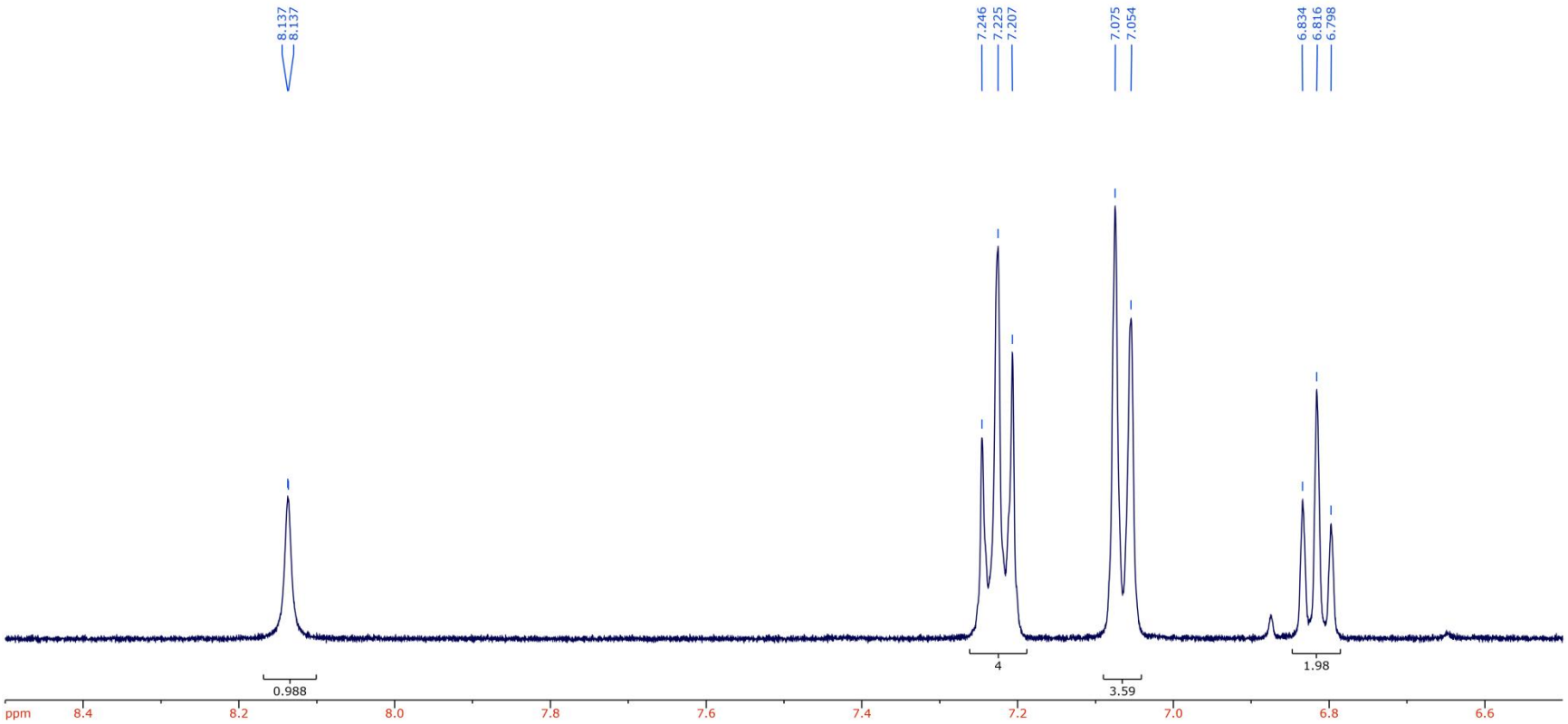

Figure S4.13. ^{1}H NMR of diphenylamine produced by decomposition of **4.4**-d_8 at 105°C in DMSO-d_6.

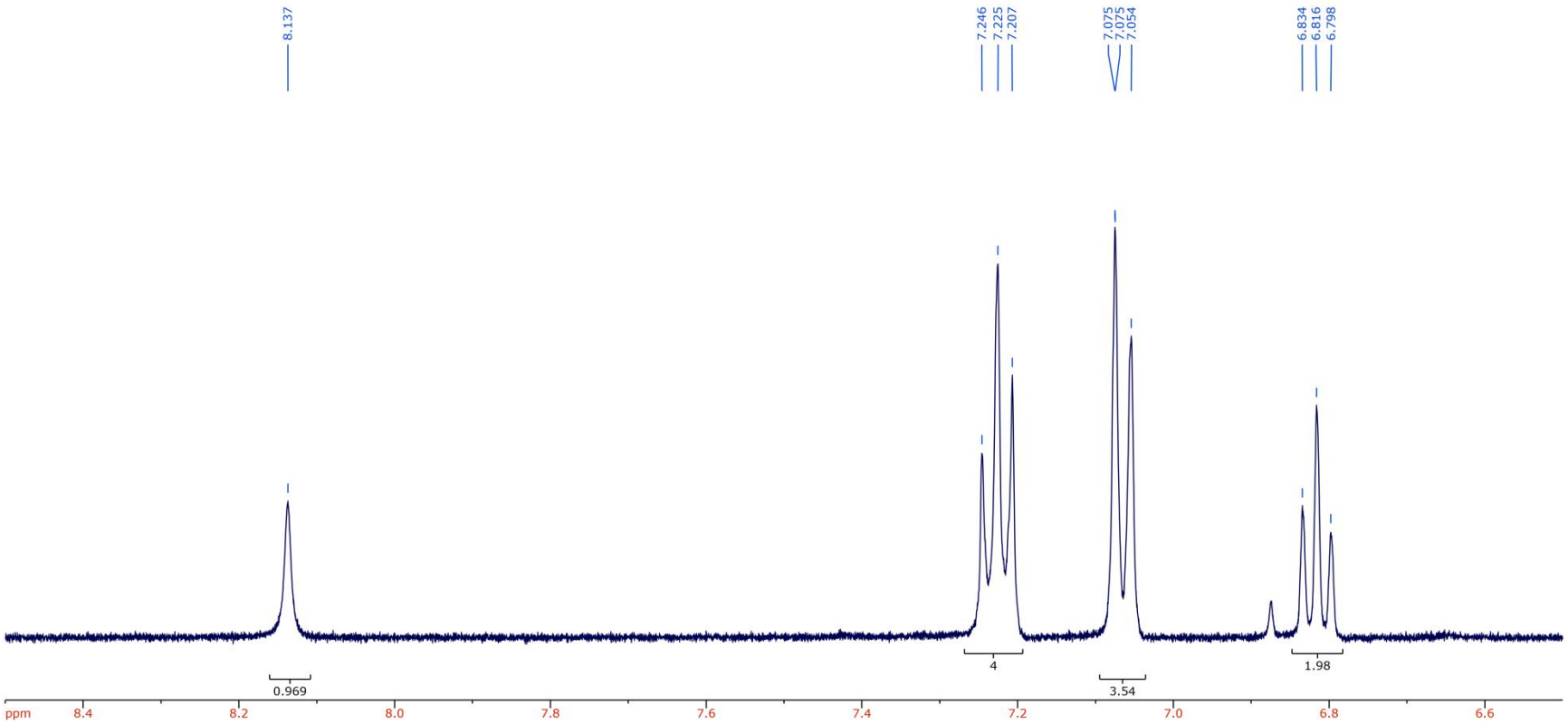

Figure S4.14. ^{1}H NMR of diphenylamine produced by decomposition of **4.4**-d_8 at 90°C in DMSO-d_6.

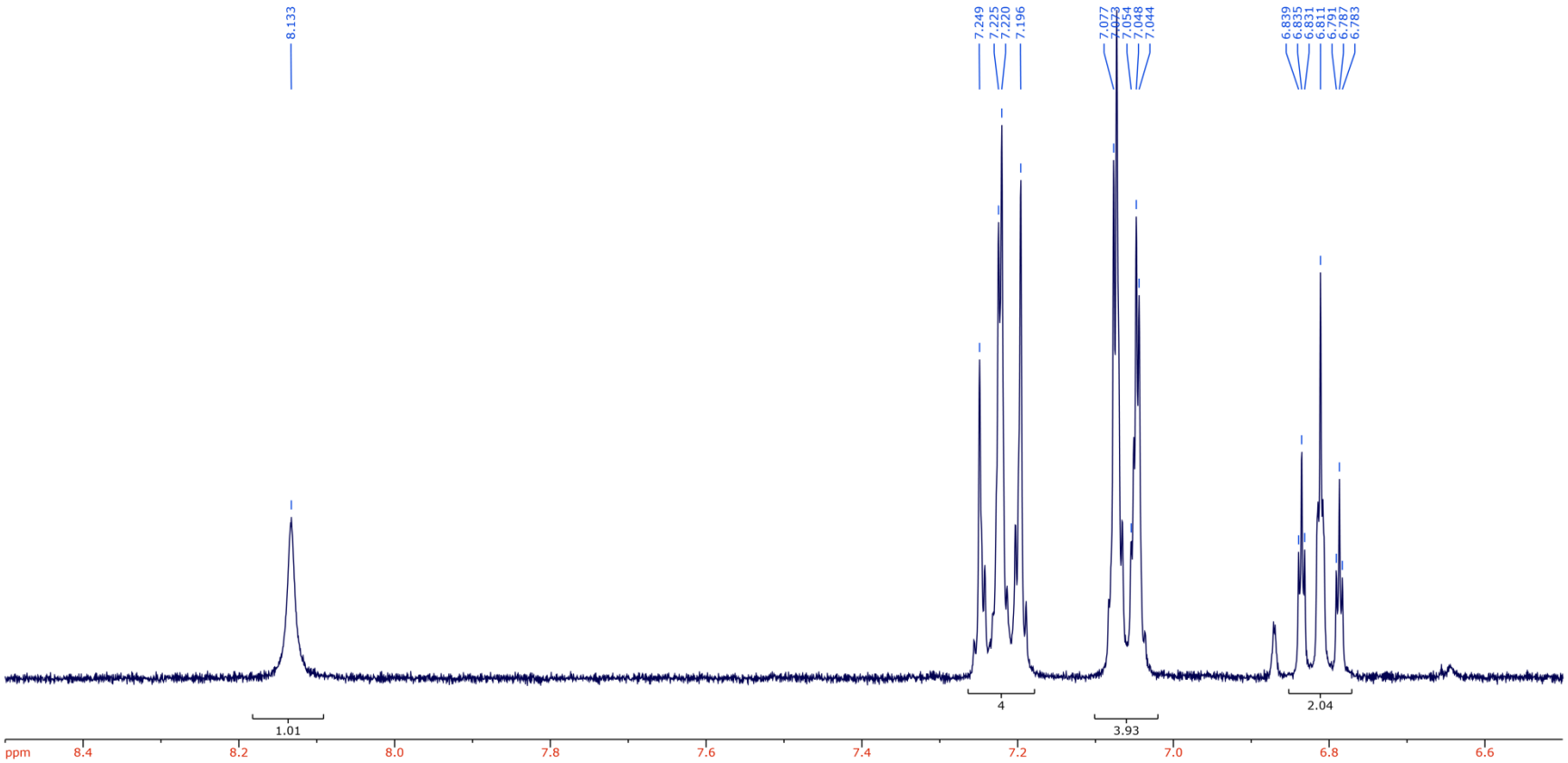

Figure S4.15. ^{1}H NMR of diphenylamine produced by decomposition of **4.6**-d_8 at 135°C in DMSO-d_6.

4.7.5 NMR Spectra of *N,N*-Diarylalkoxyamines

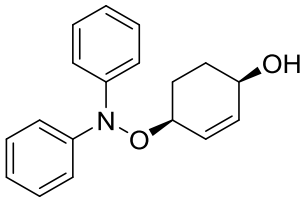

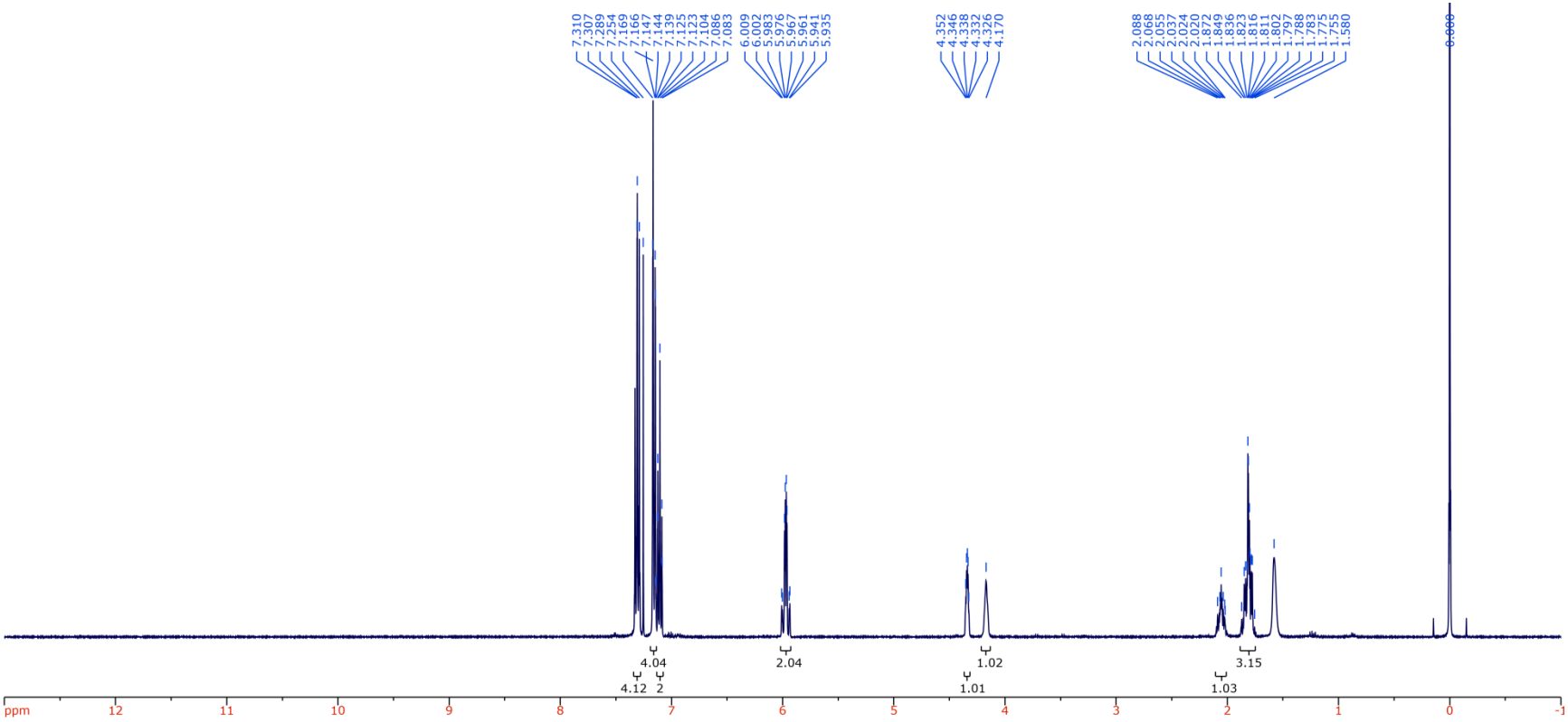

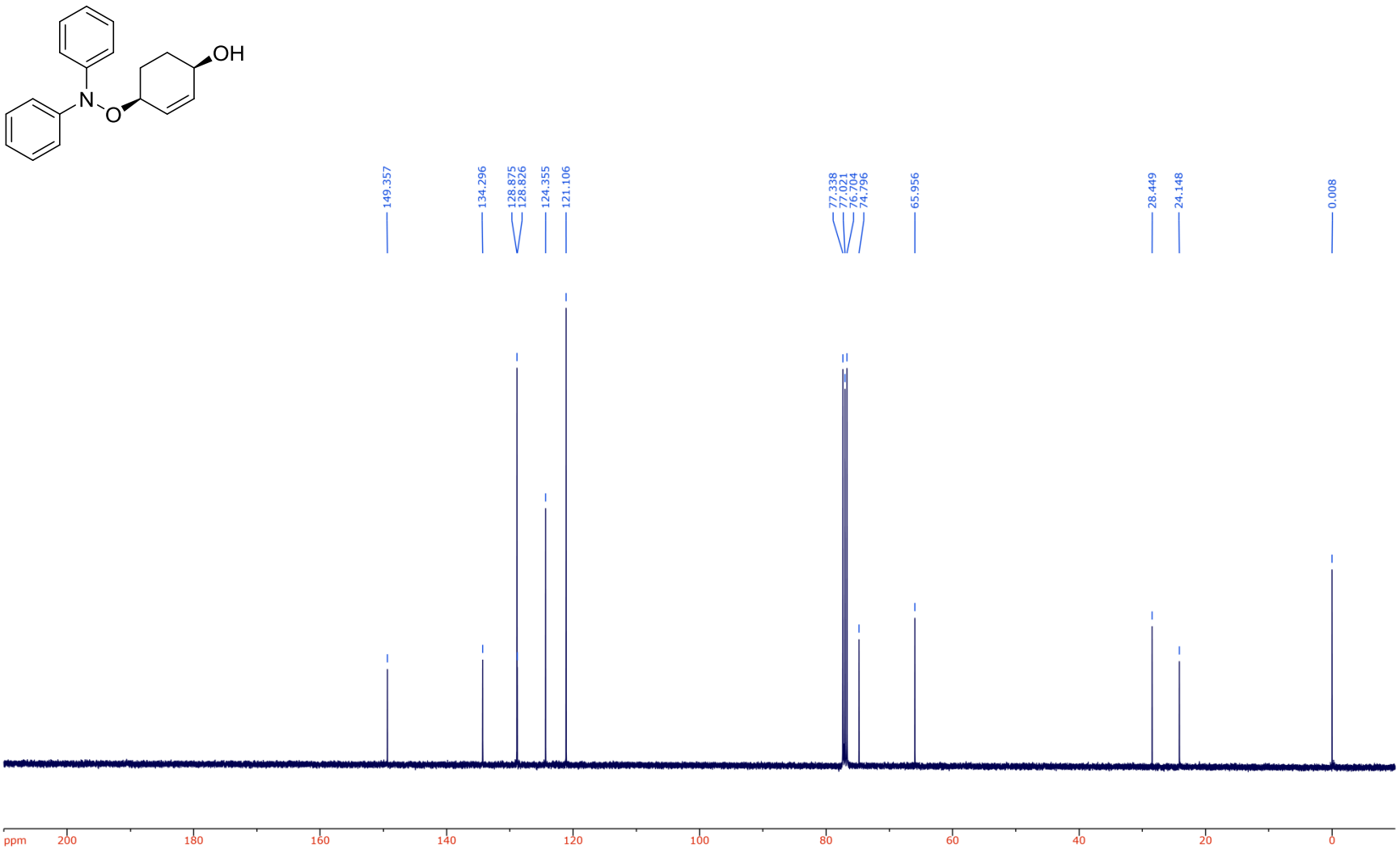
OH
N
O
149.357
134.296
128.875
128.826
124.355
121.106
77.338
77.021
76.704
74.796
65.956
28.449
24.148
0.008
ppm
200
180
160
140
120
100
80
60
40
20
0

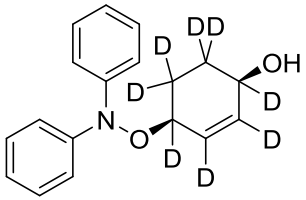
DD
D
OH
D
D
N
O
D
D
D

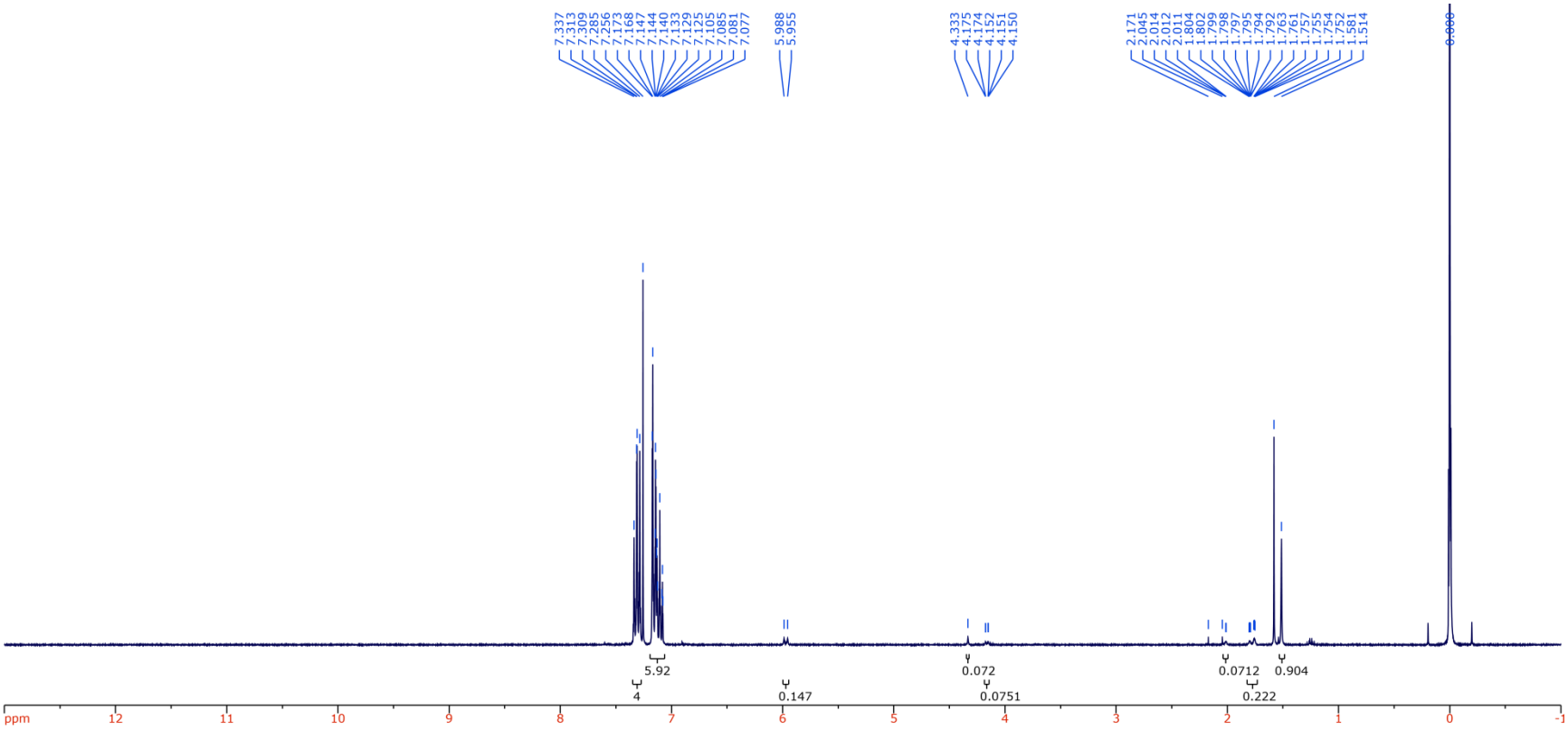
7.337
7.313
7.309
7.285
7.256
7.173
7.168
7.147
7.144
7.140
7.133
7.129
7.125
7.105
7.085
7.081
7.077
5.988
5.955
4.333
4.175
4.174
4.152
4.151
4.150
2.171
2.045
2.014
2.012
2.011
1.804
1.802
1.799
1.798
1.797
1.795
1.794
1.792
1.763
1.761
1.757
1.755
1.754
1.752
1.581
1.514
0.000
4
5.92
0.147
0.072
0.0751
0.0712
0.904
0.222
ppm
12
11
10
9
8
7
6
5
4
3
2
1
0
-1

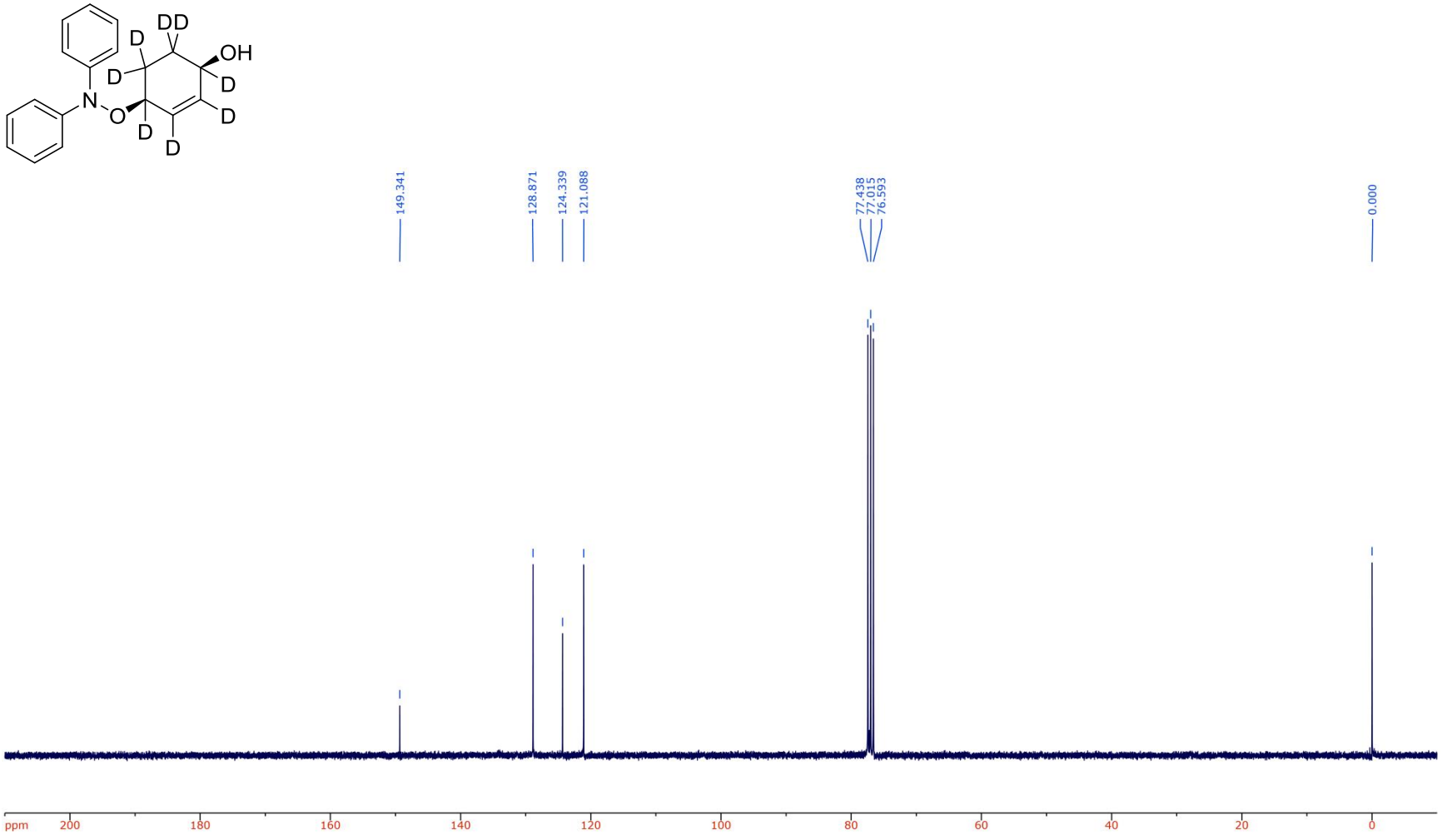
D
DD
OH
D
D
N
O
D
D
D
149.341
128.871
124.339
121.088
77.438
77.015
76.593
0.000
ppm
200
180
160
140
120
100
80
60
40
20
0

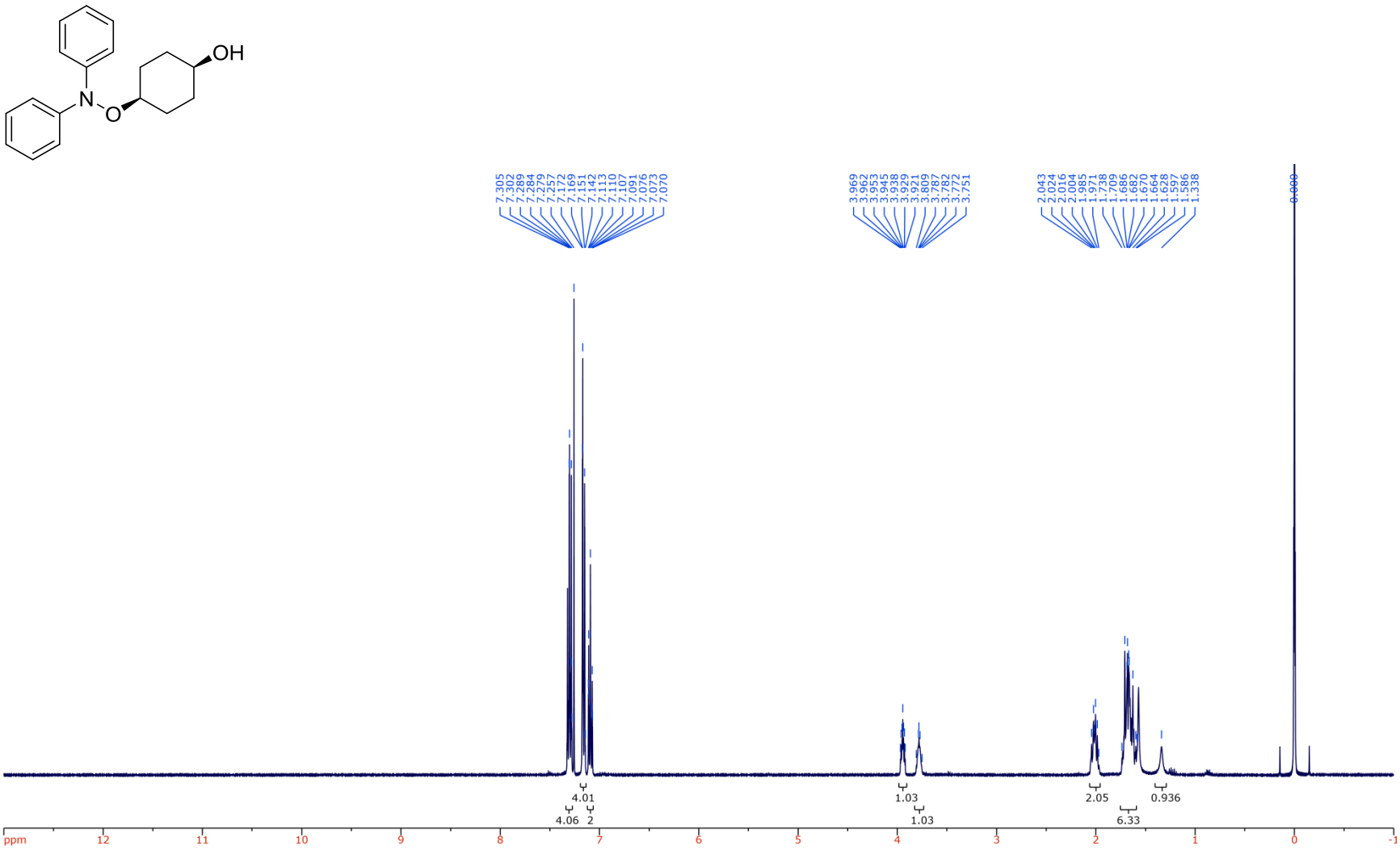
OH
N
O
7.305
7.302
7.289
7.284
7.279
7.257
7.172
7.169
7.151
7.142
7.113
7.110
7.107
7.091
7.076
7.073
7.070
3.969
3.962
3.953
3.945
3.938
3.929
3.921
3.809
3.787
3.782
3.772
3.751
2.043
2.024
2.016
2.004
1.985
1.971
1.738
1.709
1.686
1.682
1.670
1.664
1.628
1.597
1.586
1.338
0.000
4.01
4.06
2
1.03
1.03
2.05
6.33
0.936
ppm
12
11
10
9
8
7
6
5
4
3
2
1
0
-1

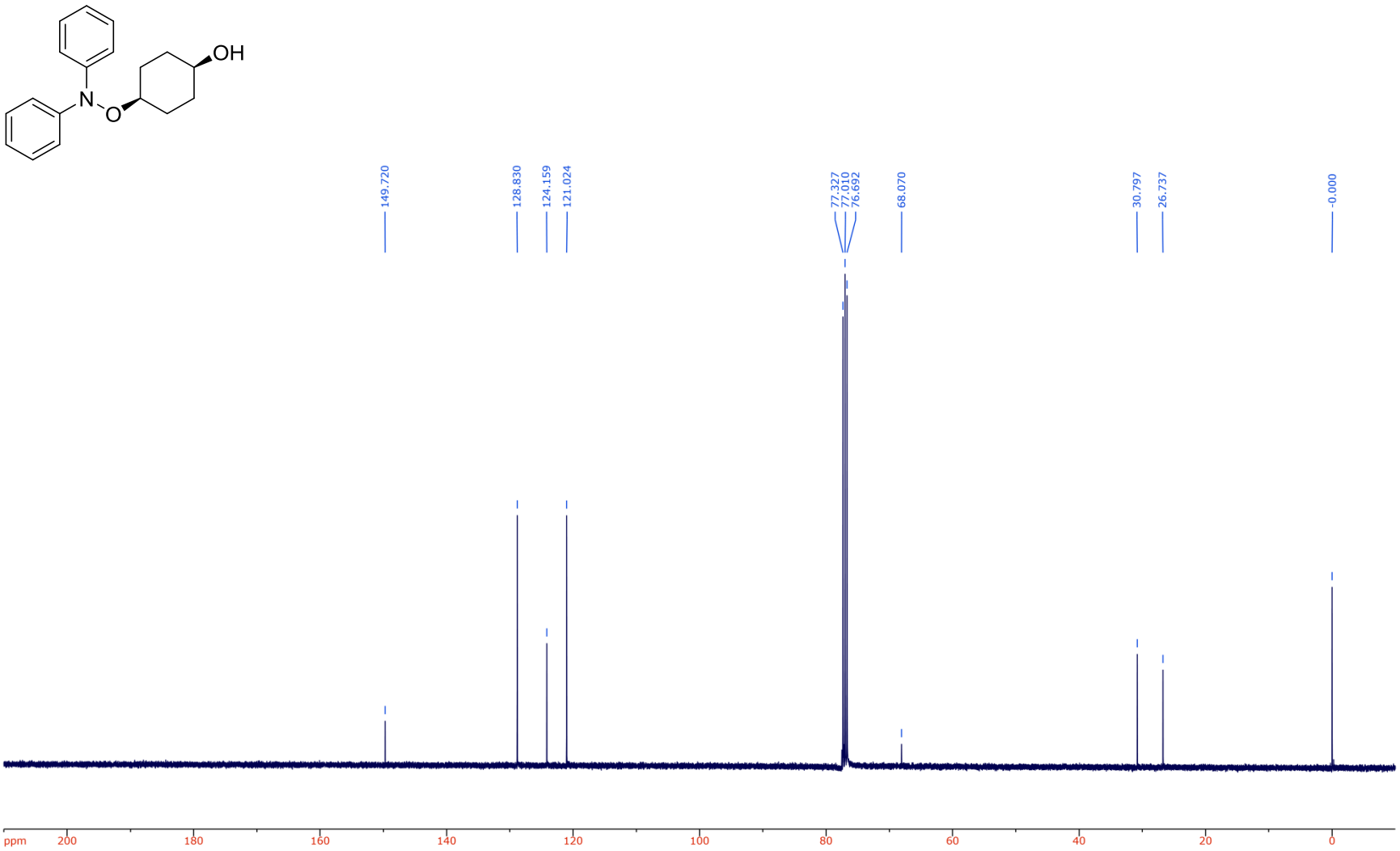
OH
N
O
149.720
128.830
124.159
121.024
77.327
77.010
76.692
68.070
30.797
26.737
-0.000
ppm
200
180
160
140
120
100
80
60
40
20
0

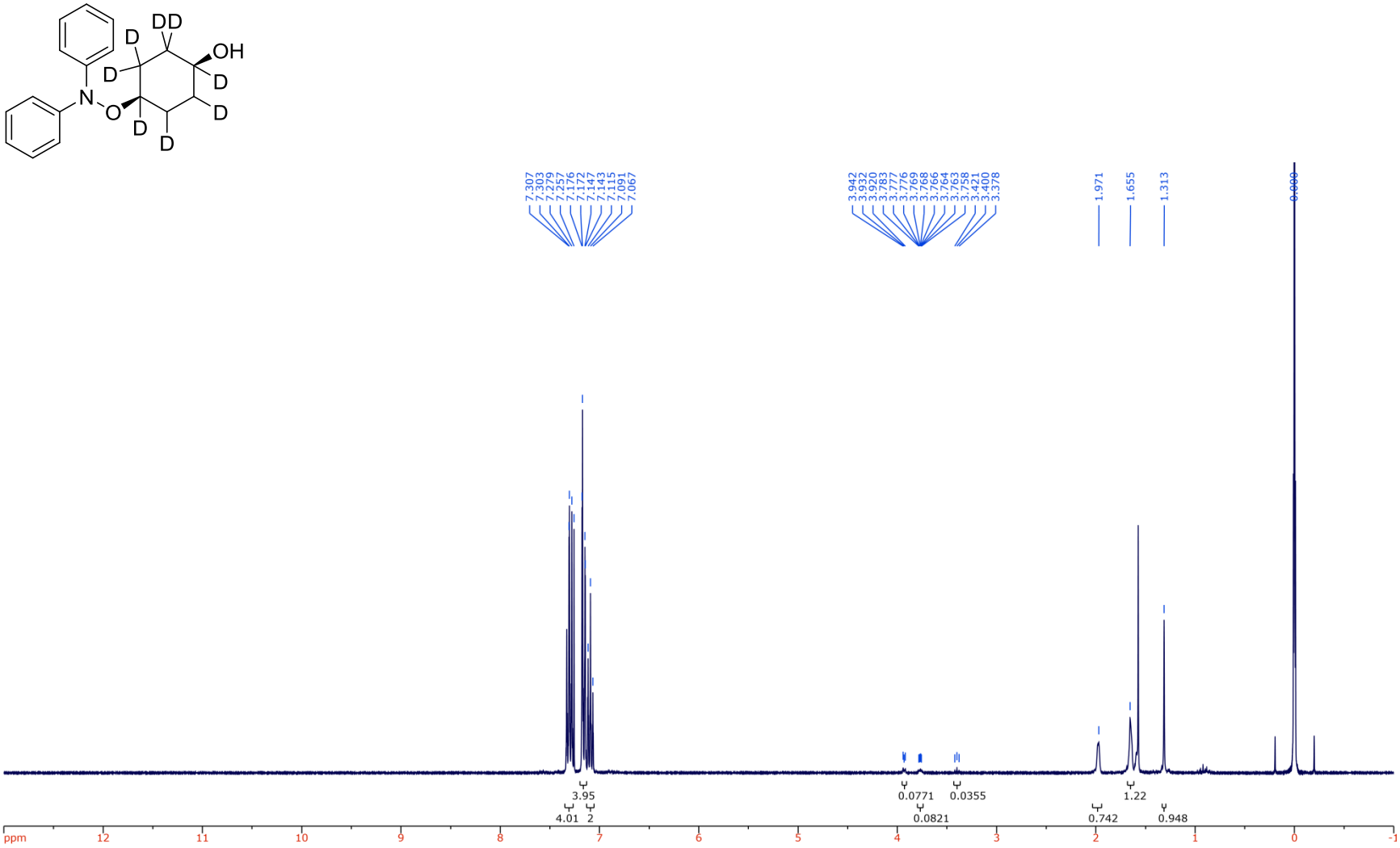
D
DD
OH
D
D
N
O
D
D
D
7.307
7.303
7.279
7.257
7.176
7.172
7.147
7.143
7.115
7.091
7.067
3.942
3.932
3.920
3.783
3.777
3.776
3.769
3.768
3.766
3.764
3.763
3.758
3.421
3.400
3.378
1.971
1.655
1.313
0.000
3.95
4.01
2
0.0771
0.0821
0.0355
1.22
0.742
0.948
ppm
12
11
10
9
8
7
6
5
4
3
2
1
0
-1

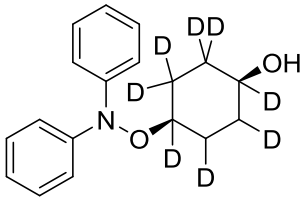
DD
D
OH
D
D
N
O
D
D
D

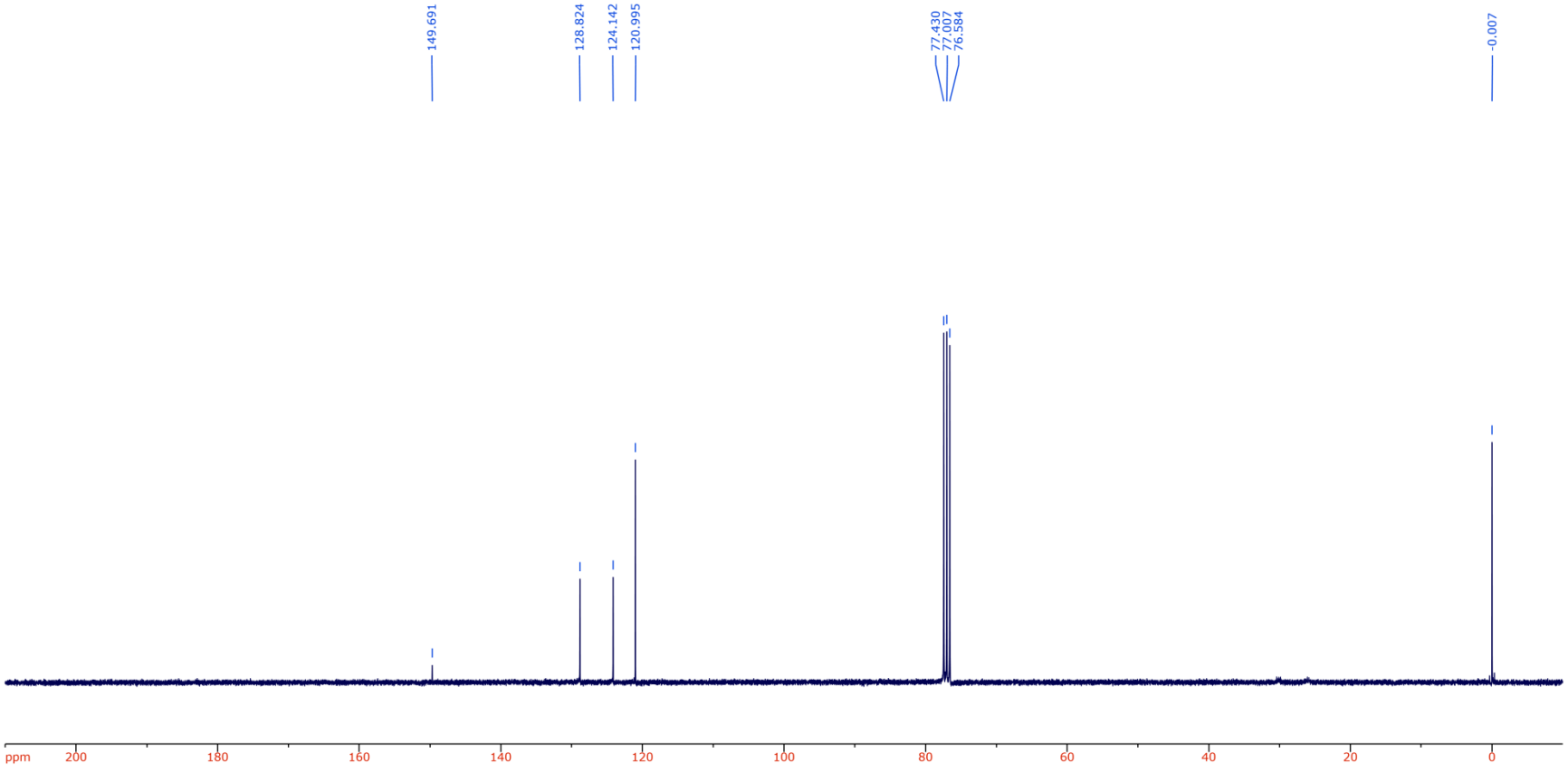
149.691
128.824
124.142
120.995
77.430
77.007
76.584
-0.007
ppm
200
180
160
140
120
100
80
60
40
20
0

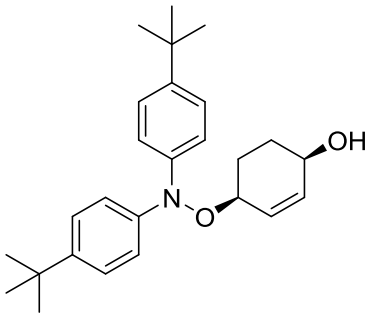
OH
N
O

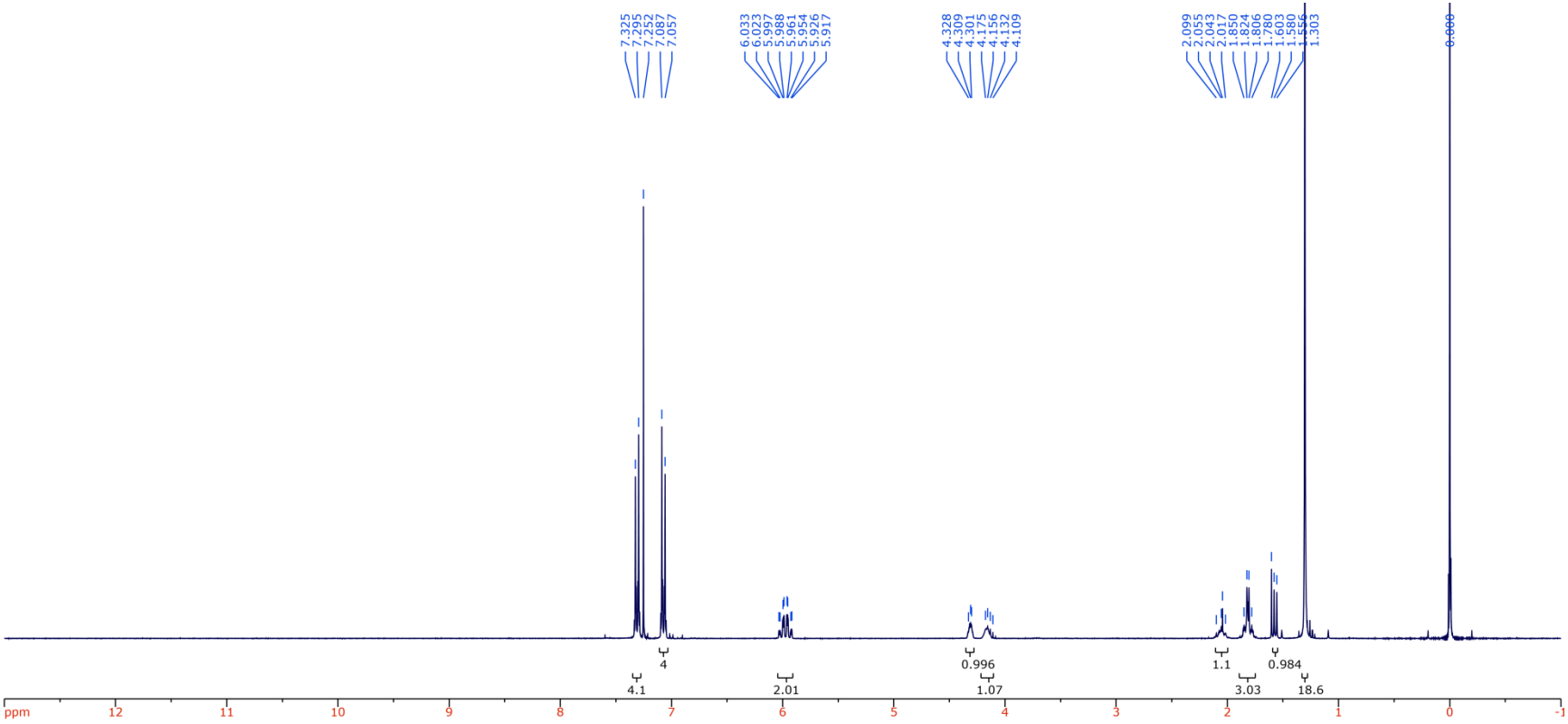
7.325
7.295
7.252
7.087
7.057
6.033
6.023
5.997
5.988
5.961
5.954
5.925
5.917
4.328
4.309
4.301
4.175
4.156
4.132
4.109
2.099
2.055
2.043
2.017
1.850
1.824
1.806
1.780
1.603
1.580
1.556
1.303
0.000
4.1
4
2.01
0.996
1.07
1.1
3.03
0.984
18.6
ppm
12
11
10
9
8
7
6
5
4
3
2
1
0
-1

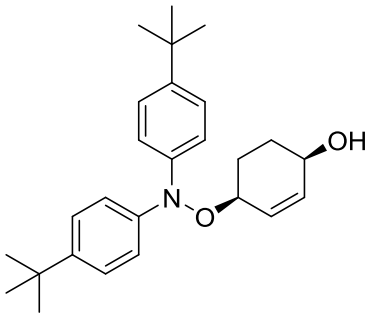
OH
N
O

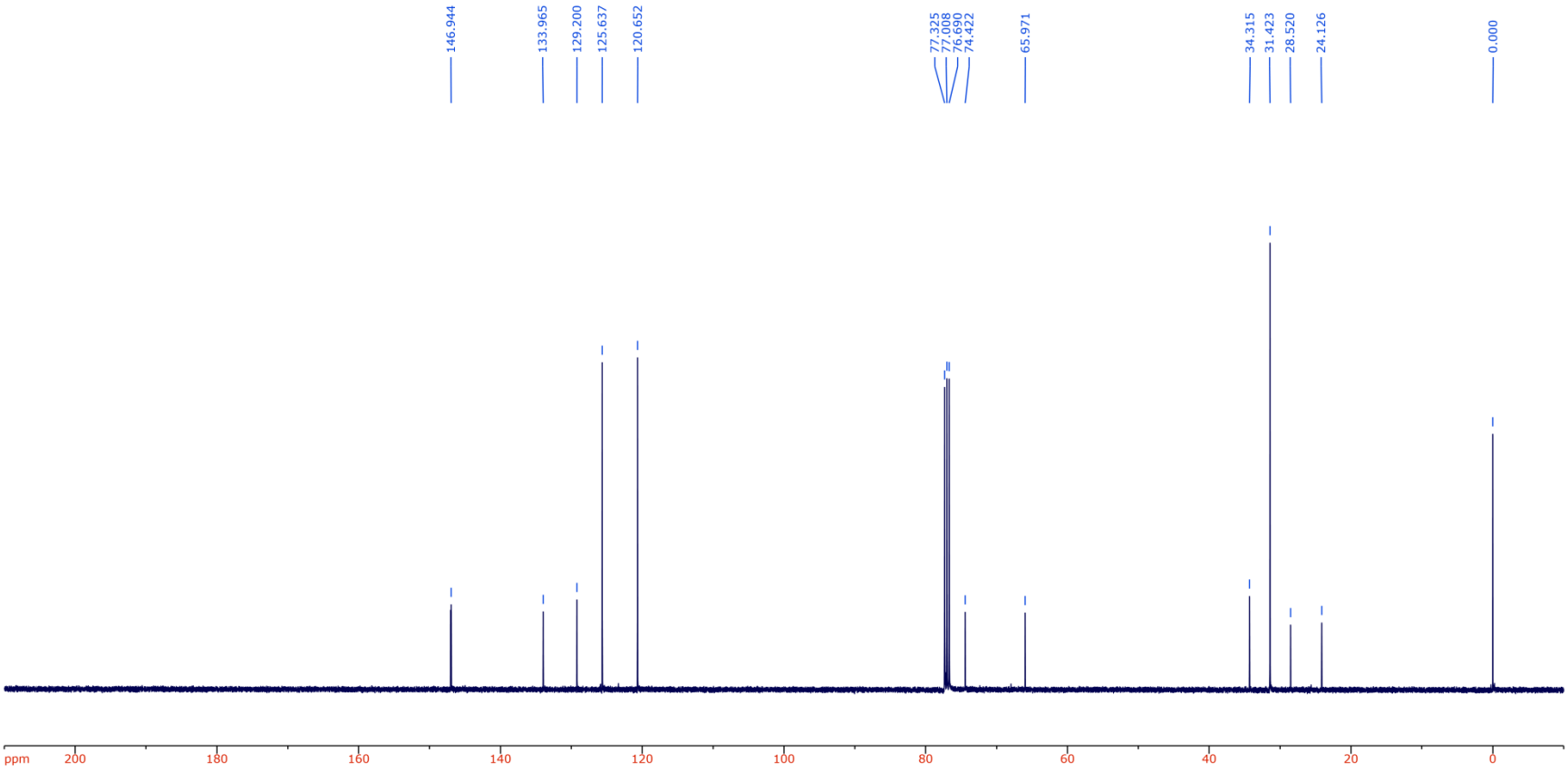
146.944
133.965
129.200
125.637
120.652
77.325
77.008
76.690
74.422
65.971
34.315
31.423
28.520
24.126
0.000
ppm
200
180
160
140
120
100
80
60
40
20
0

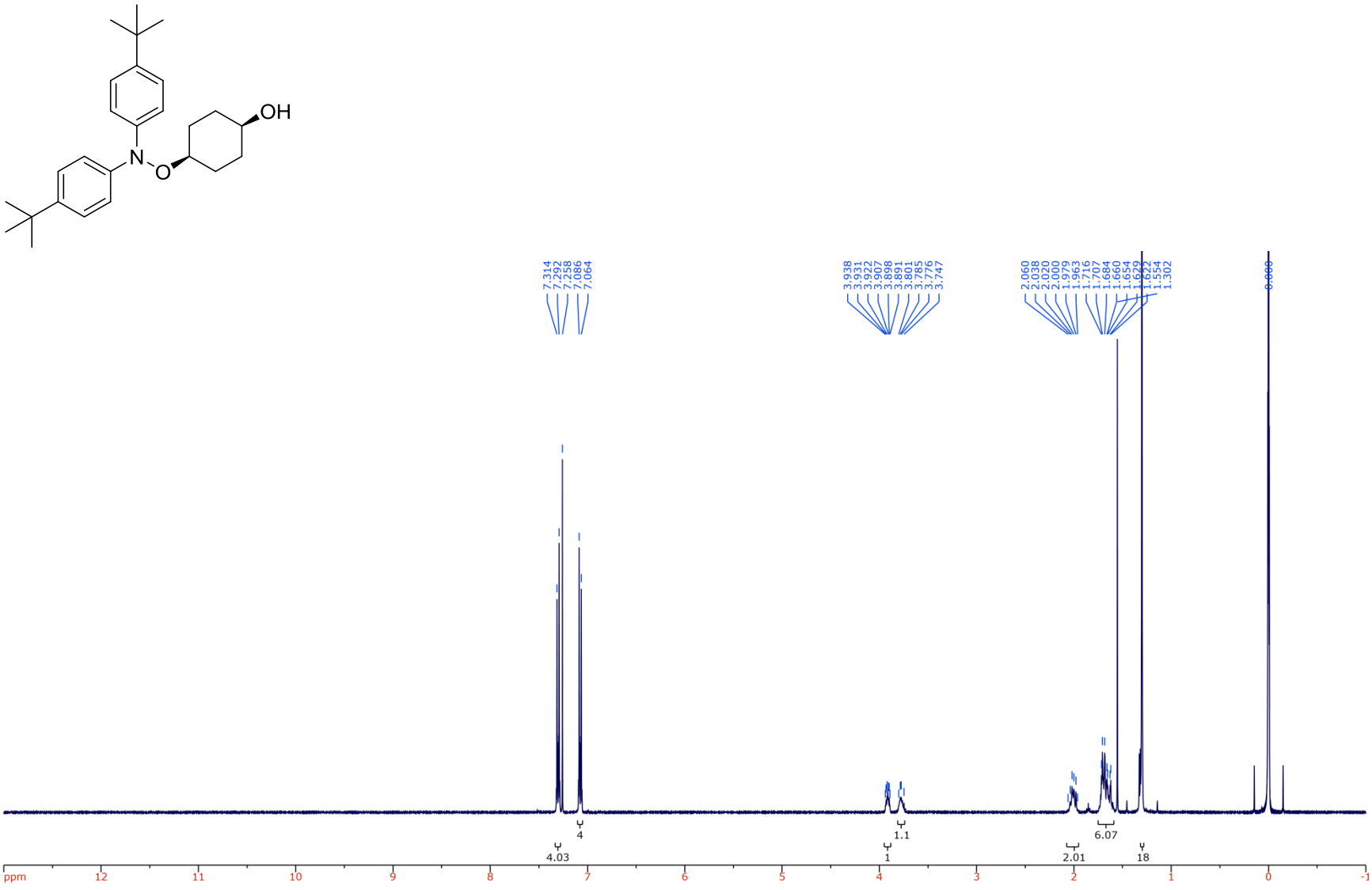
OH
N
O
7.314
7.292
7.258
7.086
7.064
3.938
3.921
3.907
3.898
3.891
3.801
3.785
3.776
3.747
2.060
2.038
2.020
2.000
1.979
1.963
1.716
1.707
1.684
1.660
1.654
1.629
1.622
1.554
1.302
0.000
4
1.1
6.07
4.03
1
2.01
18
ppm
12
11
10
9
8
7
6
5
4
3
2
1
0
-1

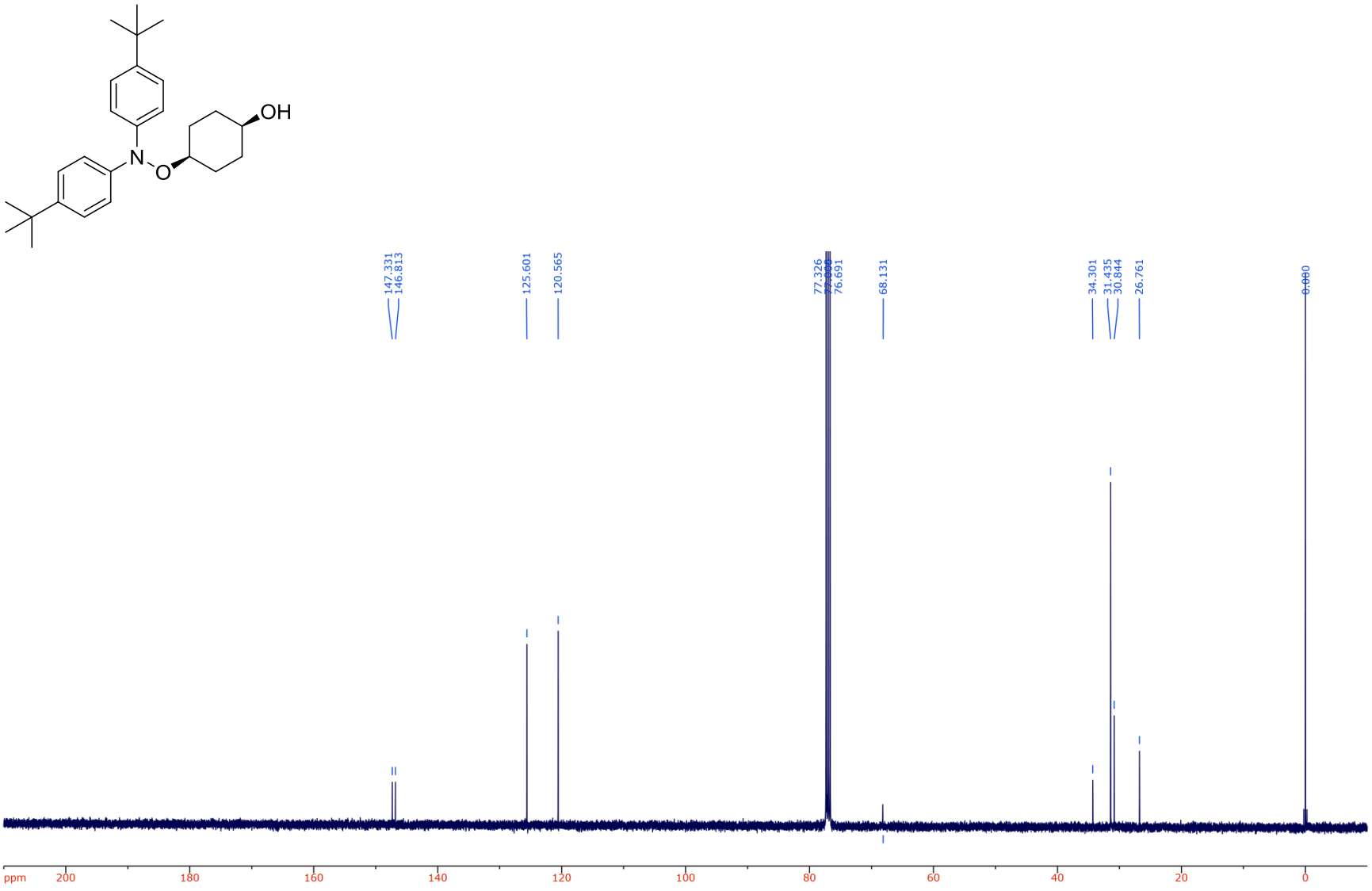
OH
N
O
147.331
146.813
125.601
120.565
77.326
76.691
68.131
34.301
31.435
30.844
26.761
0.000
ppm
200
180
160
140
120
100
80
60
40
20
0

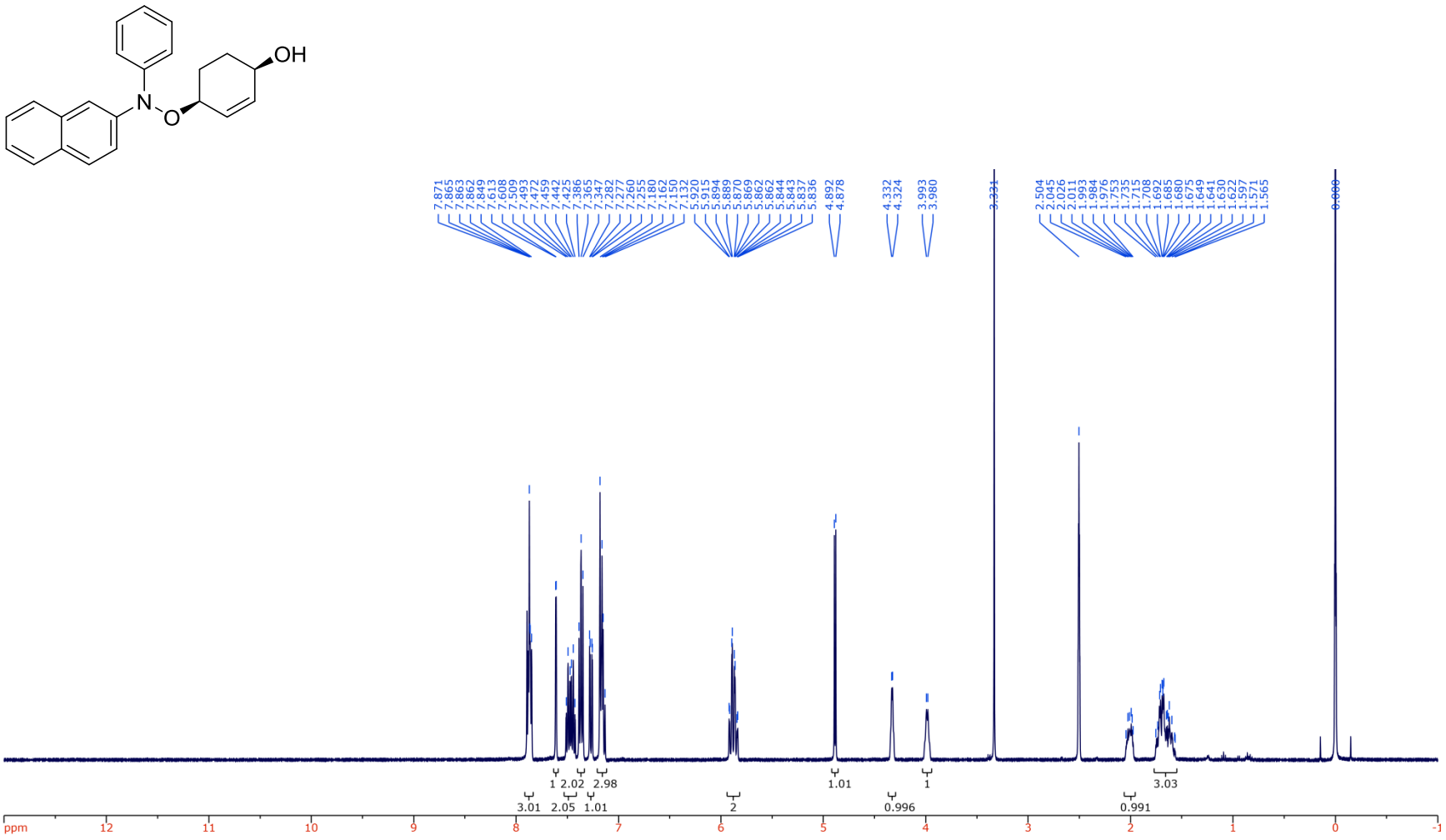
OH
N
O
7.871
7.865
7.863
7.862
7.849
7.613
7.608
7.509
7.493
7.472
7.459
7.442
7.425
7.386
7.365
7.347
7.282
7.277
7.260
7.255
7.180
7.162
7.150
7.132
5.920
5.915
5.894
5.889
5.870
5.869
5.862
5.862
5.844
5.843
5.837
5.836
4.892
4.878
4.332
4.324
3.993
3.980
3.331
2.504
2.045
2.026
2.011
1.993
1.984
1.976
1.753
1.735
1.715
1.708
1.692
1.685
1.680
1.675
1.649
1.641
1.630
1.622
1.597
1.571
1.565
0.000
1
2.02
2.98
1.01
2
1.01
1
3.03
3.01
2.05
1.01
0.996
0.991
ppm
12
11
10
9
8
7
6
5
4
3
2
1
0
-1

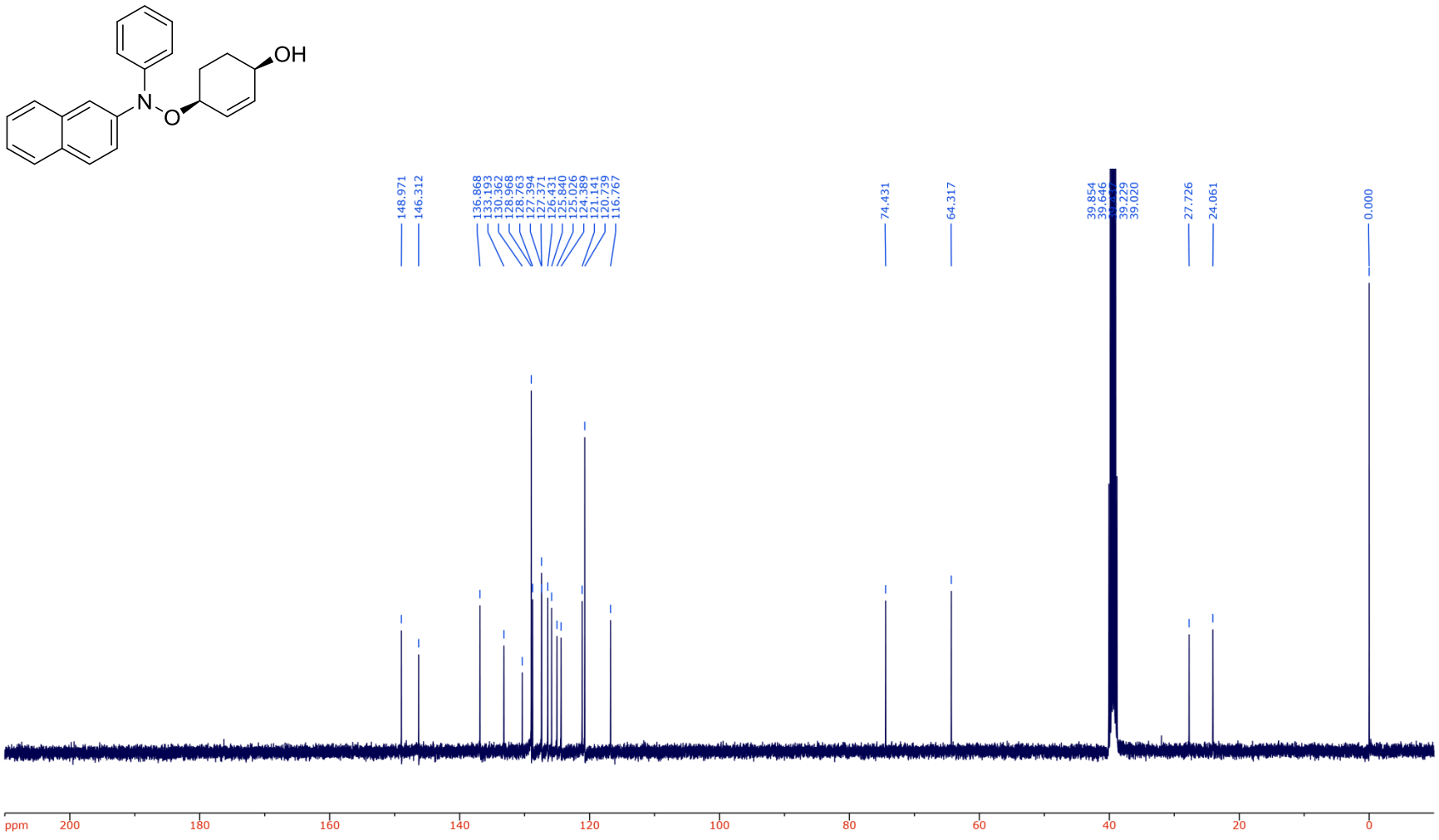
OH
N
O
148.971
146.312
136.868
133.193
130.362
128.968
128.763
127.394
127.371
125.431
125.340
125.026
124.389
121.141
120.739
116.767
74.431
64.317
39.854
39.646
39.229
39.020
27.726
24.061
0.000
ppm
200
180
160
140
120
100
80
60
40
20
0

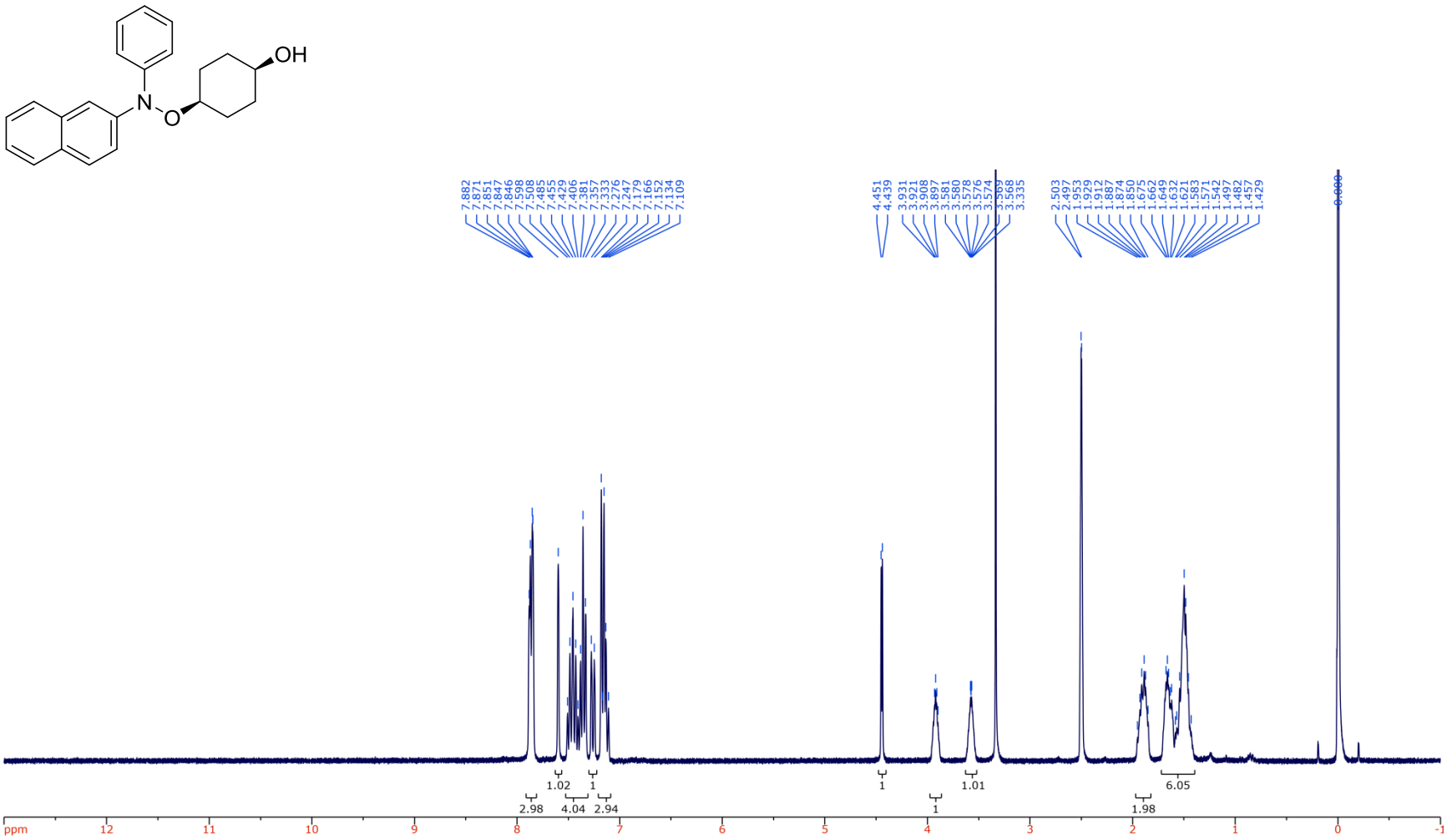
OH
N
O
7.882
7.871
7.851
7.847
7.846
7.598
7.588
7.485
7.455
7.429
7.406
7.381
7.357
7.333
7.276
7.247
7.179
7.166
7.152
7.134
7.109
4.451
4.439
3.931
3.921
3.908
3.897
3.581
3.580
3.578
3.576
3.574
3.569
3.568
3.335
2.503
2.497
1.953
1.929
1.912
1.887
1.874
1.850
1.675
1.662
1.649
1.632
1.621
1.583
1.571
1.542
1.497
1.482
1.457
1.429
0.000
1.02
1
2.98
4.04
2.94
1
1
1.01
1.98
6.05
ppm
12
11
10
9
8
7
6
5
4
3
2
1
0
-1

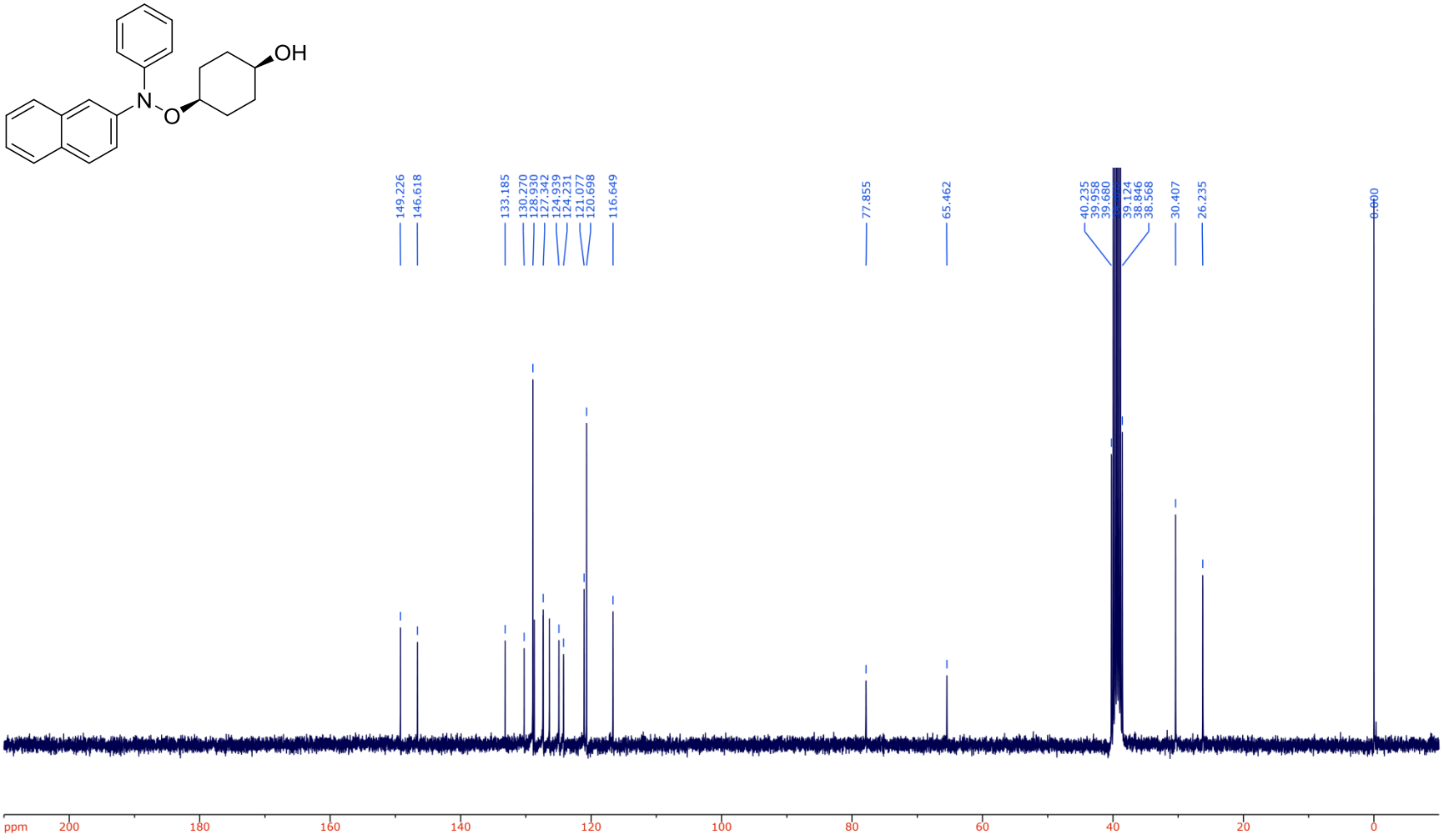
OH
N
O
149.226
146.618
133.185
130.270
128.930
127.342
124.939
124.231
121.077
120.698
116.649
77.855
65.462
40.235
39.958
39.680
39.124
38.846
38.568
30.407
26.235
0.000
ppm
200
180
160
140
120
100
80
60
40
20
0

CHAPTER 5: Acid Is Key to the Radical-Trapping Antioxidant Activity of Nitroxides

5.1 Preface

Persistent dialkylnitroxides (e.g., 2,2,6,6-tetramethylpiperidin-1-oxyl, TEMPO) play a central role in the activity of hindered amine light stabilizers (HALS)—additives that inhibit the (photo)oxidative degradation of consumer and industrial products. The accepted mechanism of HALS comprises a catalytic cycle involving the rapid combination of a nitroxide with an alkyl radical to yield an alkoxyamine that subsequently reacts with a peroxyl radical to eventually re-form the nitroxide.

Herein, we offer evidence in favor of an alternative reaction mechanism involving the acid-catalyzed reaction of a nitroxide with a peroxyl radical to yield an oxoammonium ion followed by electron transfer from an alkyl radical to the oxoammonium ion reforming the nitroxide. In preliminary work, we showed that TEMPO reacts with peroxyl radicals at diffusion-controlled rates in the presence of acids. Now, we show that TEMPO can be regenerated from its oxoammonium ion by reaction with alkyl radicals. We have determined that this reaction, which has been proposed to be a key step in TEMPO-catalyzed synthetic transformations, occurs with $k \sim 1–3 \times 10^{10}$ $M^{-1}s^{-1}$, thereby enabling it to compete with O_2 for alkyl radicals. The addition of weak acids facilitates this reaction, whereas the addition of strong acids slows it by enabling back electron transfer. The chemistry is shown to occur in hydrocarbon autoxidations at elevated temperatures without added acid due to the in situ formation of carboxylic acids, accounting for the long-known catalytic radical-trapping antioxidant activity of TEMPO that prompted the development of HALS. This chapter is presented as it was when published in the Journal of the American Chemical Society (*J. Am. Chem. Soc.*, **2016**, 138, 5290–5298). This work was performed with our collaborators Ricardo Amorati, Andrea Baschieri, and Luca Valgimigli, who are responsible for the inhibited autoxidation (O_2 consumption) and EPR data presented in this paper. Additionally, Derek Meng, who as an

undergraduate student under my supervision at the time, assisted in the collection of some of the model reaction and high temperature autoxidation data.

5.2 Introduction

Radical-trapping antioxidants (RTAs) inhibit the autoxidation of hydrocarbons by trapping the peroxyl radicals (ROO•) that propagate the chain reaction.[1,2] Phenols and diphenylamines are the archetype RTAs (represented by A-H in eqs 5.1 and 5.2); they undergo efficient formal H atom transfer to peroxyl radicals to yield stable RTA-derived radicals that do not propagate the chain reaction (A•, eq 5.1). Instead, A• reacts with another peroxyl to yield nonradical products (eq 5.2). Thus, the overall stoichiometry of the ROO•/A-H reaction is 2.

$$AH + ROO\bullet \longrightarrow A\bullet + ROOH \qquad (5.1)$$

$$A\bullet + ROO\bullet \longrightarrow \text{non-radical products} \qquad (5.2)$$

Nitroxides, such as 2,2,6,6-tetramethylpiperidin-1-oxyl (TEMPO, Scheme 5.1), have long been of interest as RTAs. Although early work by Brownlie and Ingold found TEMPO to be unreactive to peroxyl radicals at 65 °C,[3] later work showed that nitroxides were incredibly reactive at higher temperatures.[4,5] For example, a reaction stoichiometry of 510 was reported for the TEMPO-inhibited autoxidation of paraffin oil at 130 °C, making TEMPO (and related hindered nitroxides) the most efficacious RTA(s) ever reported.[5] This remarkable result coincided with the development of hindered amine light stabilizers (HALS) – technology now universally used to slow the (photo)oxidation of polymers and other petroleum-derived products. HALS generally comprise secondary or tertiary hindered amines that undergo in situ oxidation to nitroxides.[6] Related to this application, nitroxides have been explored as potential therapeutic and preventive agents against degenerative diseases in which lipid autoxidation (peroxidation) has been implicated.[7]

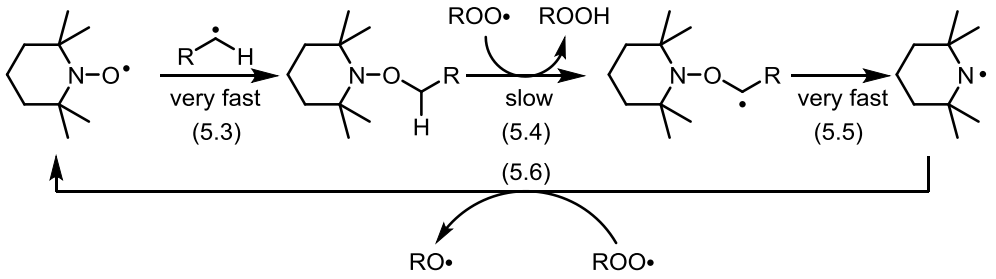

Scheme 5.1. Proposed mechanism of Hindered Amine Light Stabilizer activity.

Although nitroxides do not react directly with peroxyl radicals,[3,8] they react very quickly with alkyl radicals (eq 5.3).[9] At low concentrations of O_2 and sufficiently high concentrations of nitroxide, this reaction competes with addition of O_2 to alkyl radicals (which propagates autoxidation) to break one chain reaction. To account for the apparent catalytic RTA activity of TEMPO (or HALS), it is widely accepted that TEMPO is regenerated from the alkoxyamine.[6] Among the various mechanisms proposed for regeneration,[10] the most reasonable starts with H atom abstraction from the alkoxyamine by a chain-carrying peroxyl radical (eq 5.4, Scheme 5.1).[10,11] This reaction produces an alkyl radical that rapidly undergoes β-fragmentation to yield a carbonyl compound and aminyl radical (eq 5.5), from which TEMPO can be regenerated following reaction with a peroxyl radical (eq 5.6). This series of reactions completes a catalytic cycle wherein the substrate undergoing autoxidation serves as the stoichiometric reductant, and each pass through the cycle traps two chain-carrying radicals.

A short time ago, we found that the long-held dogma that nitroxides do not react with oxygen-centered radicals[12] must be applied with care. When autoxidations were carried out at ambient temperatures in the presence of added acid (e.g., acetic acid or trifluoroacetic acid), nitroxides were excellent radical-trapping antioxidants.[13] In our preliminary report, we showed that TEMPO, when protonated (eq 5.7), reacts with peroxyl radicals at rates approaching the diffusion-controlled limit (e.g., $k_{inh} \sim 1 \times 10^8$ M^{-1} s^{-1} with 10 mM *p*-TsOH) as in eq 5.8.[14]

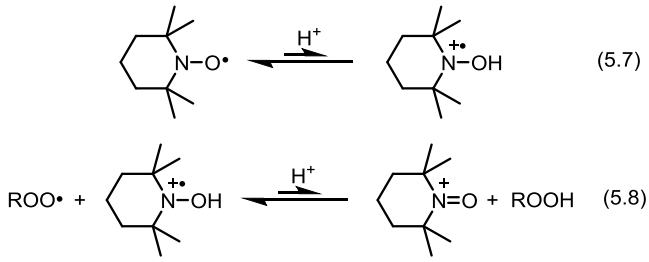

Furthermore, we showed that in the presence of weak carboxylic acids (e.g., acetic or benzoic acid), very long inhibited periods are observed, *during which the nitroxide is not consumed*—corresponding to massive stoichiometric numbers[13]—such as those observed in high-temperature autoxidations.[5] Thus, under weakly acidic conditions, TEMPO must be regenerated from its corresponding oxoammonium ion, $TEMPO^+$.[13] In sharp contrast, in the presence of strong acids (e.g., trifluoroacetic acid), only one peroxyl radical was trapped, suggesting that TEMPO could not be regenerated from $TEMPO^+$. At the time of our preliminary communication, the mechanism by which TEMPO was regenerated was elusive, as was the reason it occurred in the presence of weak acids but not stronger ones. Herein, we offer an explanation for these results and demonstrate that it accounts for the remarkable inhibition of autoxidation by nitroxides and, by extension, HALS.

5.3 Results

5.3.1 Mechanistic Possibilities

The oxoammonium ion derived from TEMPO is best known for its role as the catalytic oxidant in the oxidation of alcohols to carbonyl compounds.[15,16] This is believed to occur via a hydride transfer in a noncovalent prereaction complex (eq 5.9).

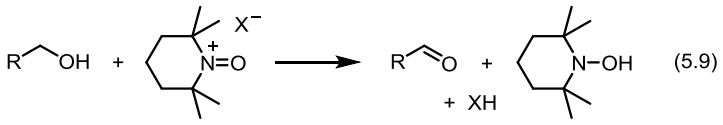

As such, at the conclusion of our preliminary work,[13] we wondered whether a (somewhat) similar reaction could occur with hydroperoxide products formed during an autoxidation. This

reaction would require hydride transfer from the β-carbon with concomitant formation of $^1O_2$ (eq 5.10):

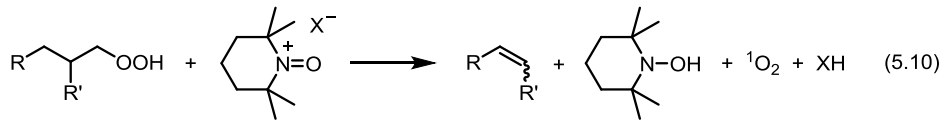

(5.10)

The resultant hydroxylamine could then react with a peroxyl radical to regenerate TEMPO – known to proceed readily with $k = 5 \times 10^5$ to 3×10^6 M^{-1} s^{-1}.[3,13] No precedent exists in the literature for this mechanism. However, the reaction of hydrogen peroxide with $TEMPO^+$ was suggested some time ago by Denisov as a key step in the TEMPO-inhibited autoxidation of ethylbenzene.[17] More recently, Goldstein *et al*. investigated the kinetics of this reaction in water.[7b] They found that the reaction was only particularly facile at alkaline pH, where electron transfer from the peroxide anion was possible, for example, $k = 5 \times 10^4$ M^{-1} s^{-1} at pH 8 and 5.1 M^{-1} s^{-1} at pH 4.[7b] Given that the latter value must represent the upper bounds in an acidified organic solvent, this mechanism would appear to be irrelevant in the current context. Moreover, the reductant in the current context must be a hydroperoxide, which is less acidic and therefore less reactive as an electron transfer reagent. Indeed, we found that the reaction between the tetrafluoroborate salt of the TEMPO-derived oxoammonium ion (hereafter $TEMPO^+BF_4^-$) and *t*-BuOOH proceeds with a rate constant of only $(4.5 \pm 0.5) \times 10^{-3}$ M^{-1} s^{-1} (in acetonitrile at 25 °C, see Supporting Information for details). This value, in light of the modest amount of hydroperoxides that are formed in the early stages of an (inhibited) autoxidation, suggests that this cannot be the mechanism of TEMPO regeneration.

Further consideration of all the species present in the inhibited autoxidations left only one possible candidate to reduce the oxoammonium ion: the chain-carrying alkyl radical, R• (eq 5.11):[18]

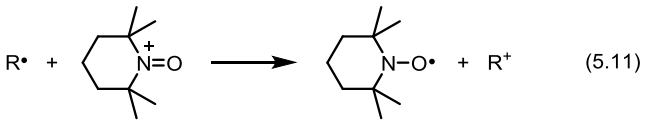

(5.11)

Computations carried out at the CBS-QB3 level of theory[19] suggest that this electron transfer reaction is exergonic, with $\Delta G°$ = −3.9 and −6.1 kcal/mol in the gas phase and acetonitrile, respectively, for R = cumyl (cumene was one of the substrates that we autoxidized in our previous studies).[13]

5.3.2 Product Studies in a Model Reaction

Since inhibited autoxidations are inherently complex, evidence for the reaction in eq 5.11 was initially sought in a model system. Cumyl radicals were generated from the thermal decomposition of azocumene in acetonitrile at 50 °C in the presence of $TEMPO^+BF_4^-$ and Me_4NOAc. The latter was included to produce the same $TEMPO^+AcO^-$ species that is expected to form in a TEMPO-inhibited autoxidation in the presence of acetic acid (as in our previous studies[13]). The reaction products were analyzed by HPLC with UV detection. The results are shown in Figure 5.1.

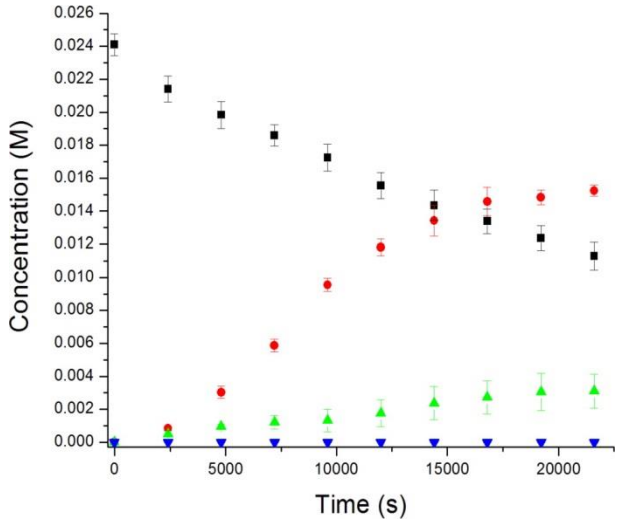

Figure 5.1. Decomposition of azocumene (■) and formation of the cumyl-TEMPO adduct in the presence of $TEMPO^+BF_4^-$ (25 mM) and $Me_4N^+AcO^-$ (25 mM) in acetonitrile at 50 °C under an atmosphere of argon (●), air (▲) or O_2 (▼).

In the absence of O_2 (via sparging the solutions extensively with argon), the cumyl-TEMPO adduct was the sole product formed and appeared at a rate roughly coinciding with the rate at which azocumene decomposed.[20] This is consistent with the expected reaction sequence shown in Scheme 5.2. Thus, decomposition of azocumene proceeds to yield two cumyl radicals – one of which reduces the oxoammonium ion to TEMPO, and the other reacts with TEMPO to give the observed alkoxyamine product. The same profile was observed in chlorobenzene (see Supporting Information). Similar results were obtained in experiments where azo(phenylethane), which yields secondary 1-phenylethyl radicals, was used in lieu of azocumene (see Supporting Information).

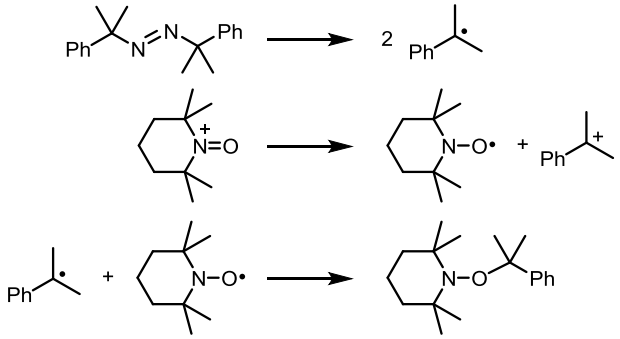

Scheme 5.2. Formation of the Cumyl-TEMPO adduct from azocumene and $TEMPO^+BF4^-$.

In the presence of air, the cumyl-TEMPO adduct was also formed, but at a much lower level, whereas when the reaction was carried out under an atmosphere of O_2, no adduct was observed. The lower yields of alkoxyamine in the presence of air were expected given the rapid reaction of cumyl radicals with O_2 ($k \sim 3 \times 10^9$ M^{-1} s^{-1}),[21] which outcompetes the reaction of cumyl radicals with TEMPO ($k = 1.2 \times 10^8$ M^{-1} s^{-1}).[9] This is underscored by the complete lack of alkoxyamine formed when the reaction was carried out in the presence of O_2. The addition of acetic acid (25 mM) had no effect on the reaction (see Supporting Information).[22]

5.3.3 Inhibited Autoxidations

If TEMPO is formed from $TEMPO^+$ in an autoxidation, the oxoammonium ion should inhibit the autoxidation similarly to the nitroxide from the outset. Thus, matched styrene autoxidations were carried out where either TEMPO or $TEMPO^+$ was added with or without acetic acid. The results are shown in Figure 5.2. Similar results were obtained in autoxidations of cumene (see Supporting Information).

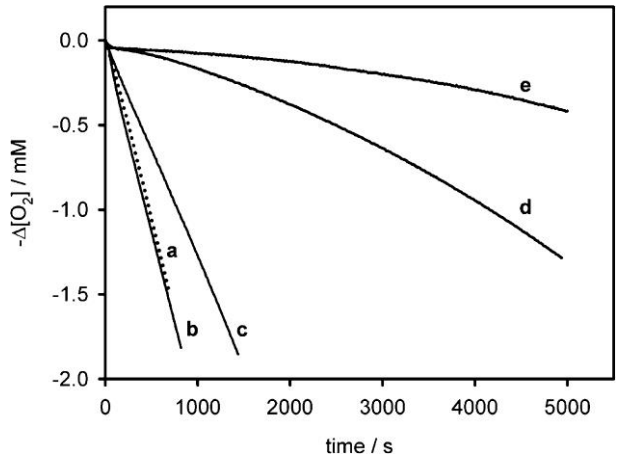

Figure 5.2. O_2 consumption during the autoxidation of styrene (4.3 M) in acetonitrile initiated by AIBN (0.05 M) at 30 °C (a, dotted line) and corresponding experiments carried out in the presence of 13 μM of either $TEMPO^+BF_4^-$ (b,d) or TEMPO (c,e) with (d,e) or without (b,c) acetic acid (43 mM).

As we reported in our preliminary communication,[13] TEMPO + AcOH gave rise to a lengthy inhibited period corresponding to a reaction stoichiometry of $n \gg 1$. When $TEMPO^+BF_4^-$ was used in place of TEMPO, the initial rate of autoxidation was not suppressed to the same extent as with TEMPO, but significant inhibition was still observed. Each of the TEMPO-inhibited and $TEMPO^+$-inhibited autoxidations could be modeled using the standard kinetic scheme for the inhibited autoxidation of styrene,[23] including the proposed inhibition reactions in eqs 5.7, 5.8, and 5.11, and fit by numerical integration to yield the unknown rate constant $k_{11} = (2.4 \pm 0.4) \times 10^{10}$ M^{-1} s^{-1} (see Supporting Information for details). The magnitude of this rate constant accounts for the successful competition of $TEMPO^+$ with O_2 for alkyl radicals necessary for this mechanism to be viable.

The combination of TEMPO and AcOH was also effective at inhibiting the autoxidation of styrene in chlorobenzene, but no significant inhibitory activity was observed past $n = 1$, implying that oxidation by $TEMPO^+$ cannot effectively compete with O_2 for alkyl radicals. Indeed, when used directly, $TEMPO^+BF_4^-$ had only a small effect on the autoxidation (Figure 5.3). Modeling the data as above yields the rate constant $k_{11} = 1.5 \times 10^9\ M^{-1}\ s^{-1}$, which is similar to the rate constant for the competing reaction of the styryl radicals with O_2 ($\sim 3 \times 10^9\ M^{-1}\ s^{-1}$). However, since $[O_2] = 2\ mM \gg [TEMPO^+] = 13\ \mu M$, this reaction is not competitive and no catalytic activity is observed.

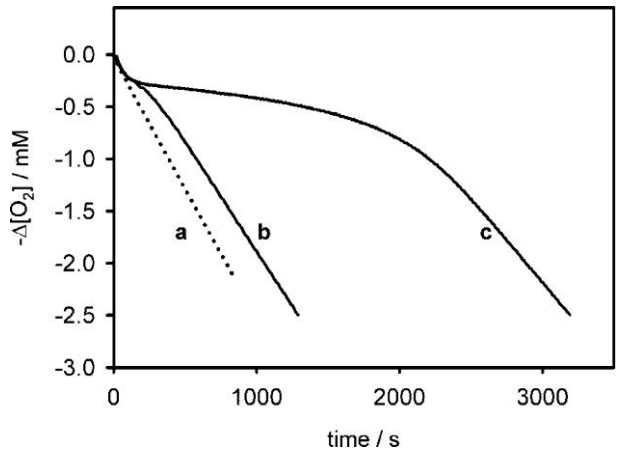

Figure 5.3. O_2 consumption during the autoxidation of styrene (4.3 M) in chlorobenzene initiated by AIBN (0.05 M) at 30 °C (a, dotted line) and corresponding experiments carried out in the presence of 13 μM of either $TEMPO^+BF_4^-$ (b) or TEMPO (c) and AcOH (44 mM).

5.3.4 Electron Paramagnetic Spectroscopy

To corroborate the foregoing product studies and inhibited autoxidation data, we sought to directly demonstrate that TEMPO is produced from $TEMPO^+$ under the conditions of a typical autoxidation. In fact, upon addition of $TEMPO^+BF_4^-$ to an air-saturated solution of either cumene or styrene in acetonitrile containing AIBN as the radical initiator, the formation of TEMPO could be observed directly by EPR (Figure 5.4A).

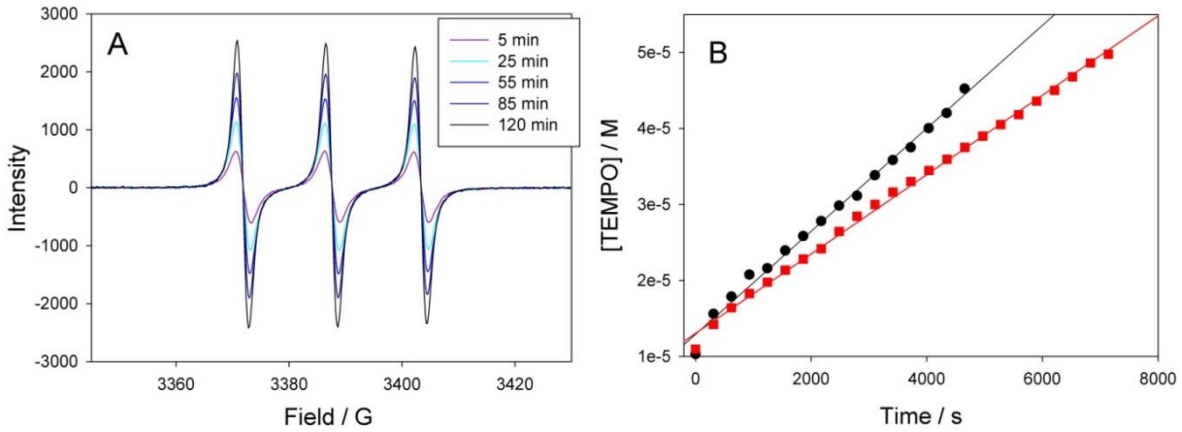

Figure 5.4. TEMPO formation during the autoxidation of styrene (4.3 M) in acetonitrile initiated by AIBN (50 mM) at 30 °C in the presence of $TEMPO^+BF_4^-$ (0.66 mM). A) Representative EPR spectra. B) Rate with (●) and without (■) added acetic acid (35 mM).

The evolution of the spectra revealed a rate of TEMPO formation (3.5×10^{-9} M s^{-1}) that was only slightly lower than the rate of radical initiation from AIBN decomposition ($R_i = 6.1 \times 10^{-9}$ M s^{-1}).[24] (The rate determined in a cumene autoxidation was 5.0×10^{-9} M s^{-1}; see Supporting Information.) As a result, since the rate constant for O_2 addition to the alkyl radicals derived from AIBN and styrene (or cumene) is $k \sim 3 \times 10^9$ M^{-1} s^{-1}, $[O_2] \sim 2$ mM and $[TEMPO^+ BF_4^-] = 0.66$ mM, we can estimate that under these conditions $k_{11} \sim 1 \times 10^{10}$ M^{-1} s^{-1}. Interestingly, when acetic acid (35 mM) was added to the reaction mixture, the formation of TEMPO was accelerated (compare data sets in Figure 5.4B), yielding an observed rate that was indistinguishable from the rate of radical initiation and implying that the rate constant for electron transfer had increased to $k_{11} \sim 3 \times 10^{10}$ M^{-1} s^{-1}, in excellent agreement with the rate constant derived from fitting the inhibited autoxidation data (vide supra). It is important to note that no TEMPO was observed in the absence of AIBN. Moreover, in the absence of either cumene or styrene, the formation of TEMPO due to reduction of $TEMPO^+$ by AIBN-derived radicals was determined to be much slower ($k_{11} \sim 1 \times 10^8$ M^{-1} s^{-1}; see Supporting Information).

In chlorobenzene, the rate of formation of TEMPO from $TEMPO^+BF_4^-$ in the presence of the same amount of acetic acid enables derivation of a rate constant of $k_{11} = 2.6 \times 10^9$ M^{-1} s^{-1} for the

electron transfer, which is just over an order of magnitude slower than that in acetonitrile and in excellent agreement with the kinetic data from the inhibited autoxidations.[25]

5.3.5 Addition of Strong Acids

Each of the three foregoing experiments were also carried out with TFA in place of AcOH. The data are presented in the Supporting Information. To summarize the results, (1) significantly lower yields of the cumyl-TEMPO adduct were observed when azocumene was decomposed in the presence of $TEMPO^+BF_4^-$ and TFA instead of AcOH, (2) the combination of $TEMPO^+BF_4^-$ and TFA did not inhibit the autoxidation of styrene in acetonitrile, and (3) no TEMPO was observed by EPR spectroscopy when AIBN was decomposed in the presence of $TEMPO^+BF_4^-$ and TFA instead of AcOH.

The simplest explanation for the lack of regeneration of TEMPO from $TEMPO^+$ in the presence of a strong acid is that it is destroyed under these conditions. Indeed, Ma and co-workers have suggested that $TEMPO^+$ is unstable in the presence of H_2SO_4 at elevated temperatures (100 °C, monitored by UV–vis spectroscopy),[26] where it is believed to eliminate HNO, eventually yielding unsaturated aliphatic products (Scheme 5.3). However, when we subjected $TEMPO^+BF_4^-$ (400 μM) to 10 mM TFA in acetonitrile at 50 °C, no change was observed in the UV–vis spectrum over the course of 1 h.[27]

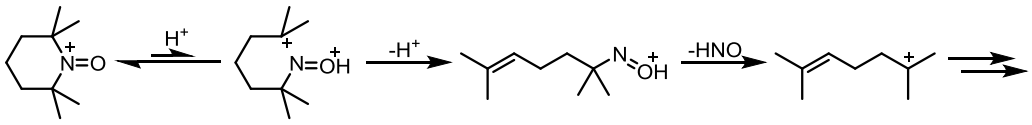

Scheme 5.3. Proposed mechanism for the decomposition of $TEMPO^+$ in the presence of strong acid.

Since the oxoammonium ion was stable under the reaction conditions, we next considered the possibility that the key electron transfer reaction (eq 5.11) was reversible. If so, the strength of

the acid and/or the nucleophilicity of its conjugate base are expected to influence the position of the key redox equilibrium in Scheme 5.4.

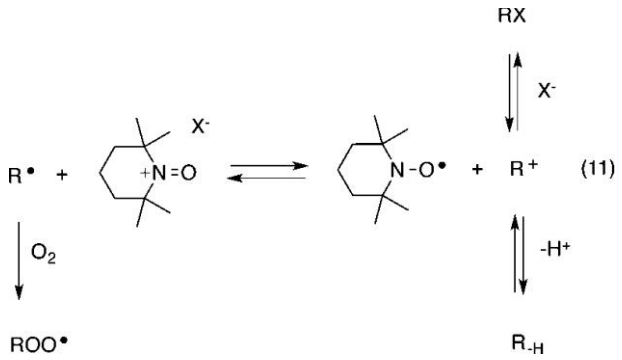

Scheme 5.4. Reactions influencing the reversibility of the electron transfer between $TEMPO^+$ and an alkyl radical.

Thus, the more acidic the medium, the less favorable the loss of a proton from the carbocation and/or the trapping of the carbocation by the less nucleophilic conjugate base. Indeed, if a strong acid (e.g., HBF_4) is added to a TEMPO/AcOH-inhibited autoxidation, the catalytic effect disappears (Figure 5.5).[28] Likewise, if an excess of the conjugate base of the strong acid (e.g., Oct_4NBF_4) is added, the catalytic effect decreases substantially (Figure 5.5). The latter result suggests that the oxidation potential of $TEMPO^+$ is also dependent on the identity of its counterion.

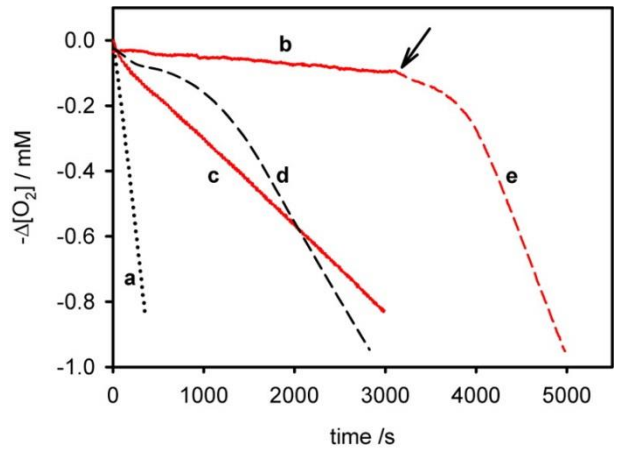

Figure 5.5. O_2 consumption during the autoxidation of styrene (4.3 M) in acetonitrile containing 1% H_2O initiated by AIBN (0.05 M) at 30 °C (a) and corresponding experiments carried out in the presence of TEMPO (13 μM) and acetic acid (43 mM) (b), acetic acid (43 mM) and Oct_4NBF_4 (0.13

M) (c), acetic acid (43 mM) and HBF_4 (43 mM) (d), and acetic acid (43 mM) with HBF_4 (43 mM) added at the time indicated by the arrow (e).

5.3.6 Autoxidations at Elevated Temperatures

Given the effect of weak acids on the RTA activity of nitroxides at ambient temperatures, we wondered whether the addition of a weak acid could bolster the activity of nitroxides at elevated temperatures, as well. Consequently, we examined the effect of a nitroxide/acid combination on the autoxidation of paraffin oil in a stirred flow reactor at 160 °C.[29,30] The reaction was initiated with a small amount of tetralin hydroperoxide (5 mM), and a dispersed stream of $O_2$was continuously passed through the solution to stir the medium and prevent mass transfer of O_2 from becoming rate-limiting. Aliquots were removed at regular time intervals, and the hydroperoxide concentration in each was determined using our previously described profluorescent phosphine (**5.1**).[31]

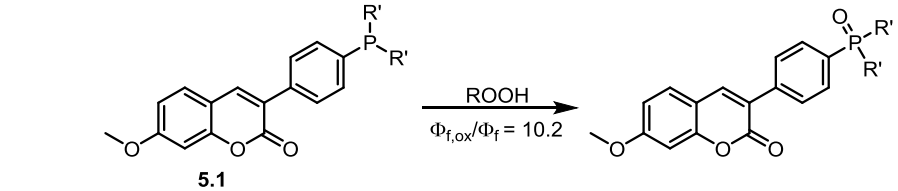

5.1

R' = *p*-Tolyl

Since TEMPO is somewhat volatile at 160 °C, a higher molecular weight analogue (**5.2**) was investigated, along with palmitic acid in lieu of the acetic acid used at ambient temperatures.[32] The results are shown in Figure 5.6A.

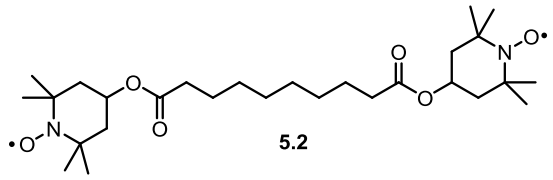

5.2

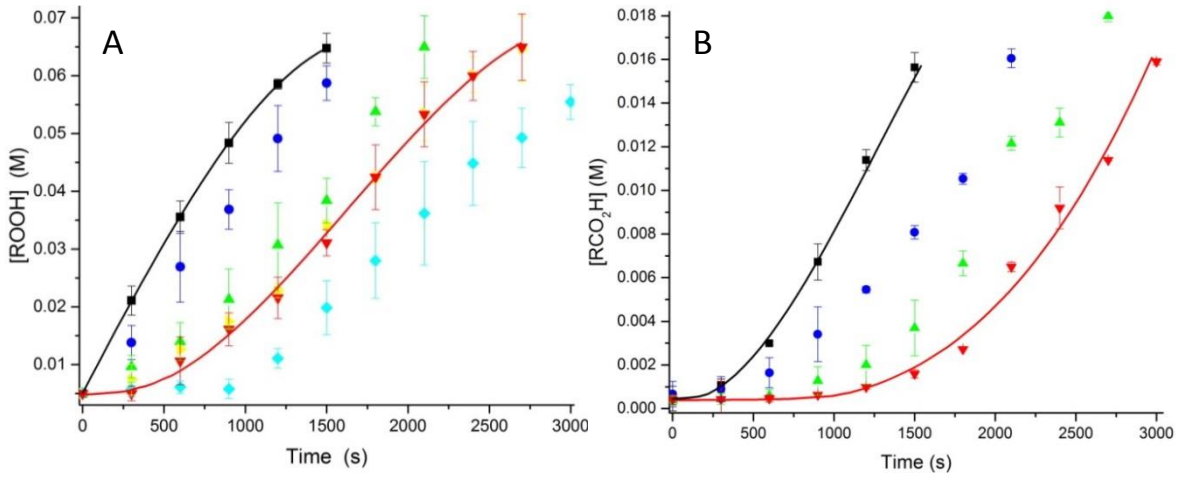

Figure 5.6. Hydroperoxide (A) and acid (B) formation in the autoxidation of light paraffin oil at 160 °C initiated by 5 mM tetralin hydroperoxide (■) and inhibited by 40 μM **5.2** (▼) with 4 mM palmitic acid (▶), 40 mM palmitic acid (◆), 4 mM 2,4,6-(*t*-Bu)$_3$pyridine (▲), or 40 mM 2,4,6-(*t*-Bu)$_3$pyridine (●).

Addition of the bis-nitroxide **5.2** to the paraffin autoxidation yielded the expected sigmoidal profile of hydroperoxide production in an inhibited autoxidation at elevated temperatures.[33] Although inclusion of 4 mM palmitic acid to the reaction mixture did not significantly improve the inhibitory activity of **2**, a higher loading (40 mM) produced a significant increase in the inhibited period. At first glance, the lack of effect of the lesser amount of acid and the fact that **5.2** is capable of inhibiting the autoxidation in the absence of added acid suggested that the acid-catalyzed reaction mechanism accounts for only a fraction of the activity of nitroxides at elevated temperatures. However, the autoxidation of paraffinic hydrocarbons is known to produce carboxylic acids (in addition to hydroperoxides) from the very early stages of the reaction.[34,35] Therefore, acids formed in situ may activate the nitroxide to react with peroxyl radicals. To probe this possibility, we added 4 and 40 mM of the nonvolatile, non-nucleophilic base 2,4,6-tri-*tert*-butylpyridine (TTBP) to autoxidations inhibited by **5.2** and found that it progressively diminished the RTA activity of the bis-nitroxide. Importantly, the addition of either acid or base had no effect on the rate of the uninhibited

autoxidation, suggesting that these additives play no role other than modulating the pH of the reaction (see Supporting Information for more data).

To confirm that carboxylic acids were present in the paraffin autoxidations, they were determined using the aminated coumarin derivative **5.3**, whose fluorescence is greatly enhanced (38-fold) upon protonation (see Supporting Information for details).[36] The results are shown in Figure 5.6B.

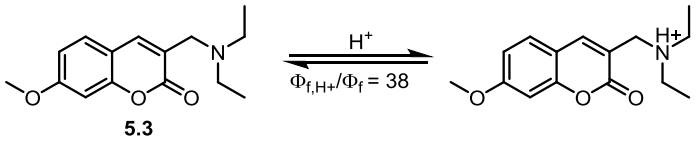

5.3

The commercially sourced light paraffin oil contained 0.14 mM carboxylic acid, and upon equilibration of the sample under a N_2 atmosphere and then heating to 160 °C, this increased to 0.5 mM.[37] Addition of the initiator and changing the atmosphere to O_2 led to a rapid accumulatation of acid, reaching 15 mM within 1500 s. In the inhibited autoxidations, the production of carboxylic acids mirrored the formation of hydroperoxides (albeit at lower absolute levels), consistent with the potent antioxidant activity of **5.2** and its diminution upon addition of base to the autoxidation.

5.4 Discussion

Despite the widespread use of HALS, their mechanism has remained a mystery since the suggestion that nitroxides must be the key intermediate in a catalytic radical-trapping cycle.[6] The commonly presented mechanism (Scheme 5.1) requires the nitroxide to compete with O_2 for alkyl radicals, but it is well known that the reaction of R• with TEMPO is 20−30-fold slower than the reaction of R• with O_2.[9,21] This is irrelevant if the TEMPO/O_2 concentration ratio is large, but in many of the experiments that established the unique reactivity of HALS, this condition is not fulfilled (likewise for the conditions under which HALS-containing materials are manipulated and/or used). For example, in the pioneering experiments carried out by Bolsman, Blok, and Frijns,[5] which showed a

stoichiometric number of 510 for the inhibition of paraffin oil autoxidation, only 1–4 μM TEMPO was used. Given that $[O_2] \sim 2$ mM,[38] *the rate of alkoxyamine formation must be at least 10000 times slower than the rate of peroxyl radical formation.*

Nevertheless, if alkoxyamines are indeed formed in these reactions, they must decompose to regenerate the nitroxide to complete the catalytic cycle. Recent computations and a reinterpretation of literature data led to the conclusion[10] that it must occur via the sequence of eqs 5.4, 5.5, and 5.6 in Scheme 5.1: H atom abstraction from the position adjacent the O atom in the alkoxyamine, followed by *β*-fragmentation of the resultant alkyl radical to give an aminyl radical, and then oxidation to give the nitroxide – as suggested earlier by Bolsman, Blok, and Frijns.[11] While it seems quite clear that this is the mechanism f an alkoxyamine with a peroxyl radical, it is unlikely to be kinetically relevant in an inhibited autoxidation. In fact, we have attempted to measure the rate constant for the reaction of a model alkoxyamine (*O*-allyl-TEMPO) with peroxyl radicals using the radical clock approach and found that it proceeds with $k \leq 1$ M^{-1} s^{-1} at 37 °C, expectedly similar to H atom abstraction from the α-CH_2 group of an ether.[39] Assuming log $A = 8$ for this H atom transfer[50] suggests that the rate constant could be as big as ~70 M^{-1} s^{-1}at 130 °C, but given that the alkoxyamine can be present at only 1–4 μM at most (assuming all of the TEMPO added in the first place is converted to the alkoxyamine), this means that *this reaction must be ca. 6 orders of magnitude too slow to compete with chain propagation* (which has k[substrate] ~ 90 s^{-1})[11,40] in the pioneering experiments of Bolsman, Blok, and Frijns.

Given our observation that TEMPO becomes a catalytic RTA in the presence of weak acid at ambient temperatures, it seemed reasonable to consider this as an alternative to the mechanism in Scheme 5.1. Indeed, the addition of acid to a paraffin oxidation at 160 °C improved the already catalytic RTA activity of bis(nitroxide) **5.2**, but more importantly, the addition of base was able to wipe it out in a dose-dependent manner (i.e., the activity of the nitroxide correlated with the amount of acid present). This must rule out the mechanism in Scheme 5.1 or any mechanism which invokes

H atom abstraction from the alkoxyamine in the turnover-limiting step since it cannot account for these observations. Moreover, the bis(oxoammonium) derived from **2** inhibited the paraffin oxidation similarly to **5.2** itself. Therefore, we suggest that the unique reactivity of nitroxides as RTAs (and HALS, in general) is better accounted for by the mechanism shown in Scheme 5.5.

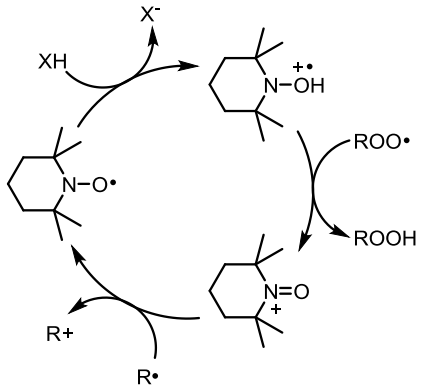

Scheme 5.5. Proposed mechanism of acid-catalyzed RTA activity of nitroxides.

Although this mechanism still requires the participation of an alkyl radical in the catalytic cycle, the reaction it undergoes is an electron transfer (to regenerate the nitroxide from the oxoammonium ion), which has been shown to compete effectively with its combination with O_2(*vide supra*).

Diarylamines are also common additives to petroleum-derived products, but because their oxidation products are highly colored, they are generally not used in applications where color changes are undesirable (e.g., in lightly colored plastics). Given that diarylamines are secondary amines whose catalytic activity also depends on the formation of a nitroxide intermediate (*cf.* Scheme 5.6),[41] it is possible that the mechanism in Scheme 5.5 could also contribute to their activity.[42,43] However, it is expected that (1) alkoxyamine formation will be slightly faster for Ar_2NO• + R• than for TEMPO• + R• due to reduced steric hindrance, (2) unimolecular decomposition of the resultant Ar_2NOR to regenerate Ar_2NH has a lower barrier than the return of the nitroxide,[42] (3) the diaryl nitroxide will be less basic than TEMPO, and (4) the

diaryloxoammonium ion will be a weaker oxidant than $TEMPO^+$. Moreover, in related work, we found that acid formation diminishes the activity of some Ar_2NH.[30]

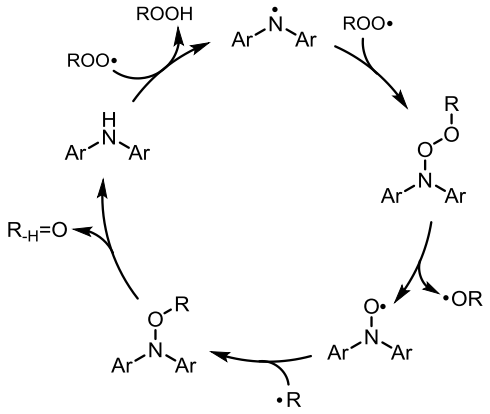

Scheme 5.6. Proposed mechanism of catalytic activity of diarylamine RTAs.

Although the secondary amines found in HALS are far less reactive toward peroxyl radicals than diarylamines, HALS have the distinct advantage that the nitroxide intermediate in their catalytic cycle is persistent and does not undergo deleterious reactions with peroxyl radicals. The same cannot be said for the nitroxides derived from diarylamines, which undergo competing reactions with peroxyl radicals at ring carbon atoms,[3] leading to complex mixtures of products[44] and precluding continuation of the cycle in Scheme 5.5.

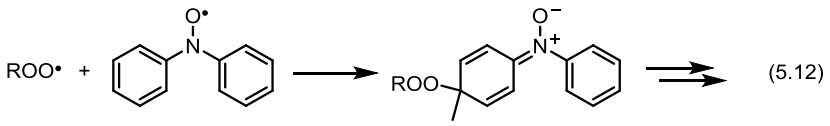

This fact underscores the unique reactivity of HALS but also prompts the question: what eventually leads to exit from the nitroxide's catalytic cycle? Why are nitroxides not infinitely reactive? The answer to this question may provide the key to the design of the ultimate hindered amine light stabilizers.

5.5 Conclusion

For the past 40 years, there has been widespread agreement that nitroxides are key intermediates in the catalytic activity of hindered amine light stabilizers, but the precise mechanism has been elusive. The formation of an alkoxyamine, and its subsequent decomposition to re-form a nitroxide, was believed to comprise the catalytic cycle. However, for the reasons discussed above, this cannot account for the reactivity of nitroxides as autoxidation inhibitors under most conditions. Instead, we have advanced the more plausible proposal that protonation of the nitroxide creates a potent formal H atom donor which reacts with a peroxyl radical[14] and the resultant oxoammonium ion oxidizes an alkyl radical, regenerating the nitroxide. The latter electron transfer has been shown to be competitive with O_2 addition in both model systems and authentic autoxidations (k_{11} = 1–3 × 10^{10} M^{-1} s^{-1}). This pathway provides a more plausible explanation for the catalytic activity of nitroxides as RTAs and also supports a role for this electron transfer reaction in TEMPO-mediated synthetic transformations. The ability of nitroxides to inhibit the autoxidation of hydrocarbons at high temperature is shown to depend on acid formation in situ. We have shown that the proposed catalytic cycle is also fully operative at ambient temperatures, suggesting that it may be of biological relevance and may contribute to the biological activity of TEMPO and related nitroxides.[7]

5.6 Experimental

5.6.1 General Experimental

Reagents and solvents were purchased from commercial sources and used without further purification unless otherwise indicated. $TEMPO^+BF_4^-$,[45] azocumene,[46] bis(nitroxide) **1**,[47] phosphine **2**,[31] and BODIPY **3**[36] were synthesized by literature precedent. Oxidizable substrates (cumene, styrene, paraffin oil) were carefully purified from stabilizers and hydroperoxides before use and were stored refrigerated under nitrogen.

5.6.2 Model Reactions

$TEMPO^{+}BF_4^{-}$ (12 mg, 50 μmol) and tetramethylammonium acetate (6.7 mg, 50 μmol) were added to a 3 mL vial. The contents were dissolved in acetonitrile (sparged with either argon or oxygen as necessary) and placed under the appropriate atmosphere. To this, azocumene (13 mg, 50 μmol) was added. The contents were heated and stirred at 50 °C. Aliquots (100 μL) were removed every 40 min and diluted to 1 mL with methanol containing 2.8 mM hexylbenzene. Samples were analyzed on a Waters Acquity H-Class UPLC equipped with a XTerra RP-18 column (5 μM × 4.6 mm × 150 mm) using 20% H_2O in methanol at a flow rate of 0.4 mL/min and detection at 216 nm.

5.6.3 Inhibited Autoxidations

Experiments were performed in a two-channel oxygen uptake apparatus, based on a Validyne DP 15 differential pressure transducer.[48] In a typical experiment, an air-saturated solution of either styrene or cumene containing AIBN was equilibrated with an identical reference solution containing excess 2,2,5,7,8-pentamethyl-6-hydroxychromane (PMHC) (25 mM). After equilibration, and when a constant O_2 consumption was reached, a stock solution of TEMPO or $TEMPO^{+}BF_4^{-}$ (final concentration = 5–50 μM) and a stock solution of the desired acid were injected in the sample flask. After calibration of the apparatus, the oxygen consumption in the sample was measured from the differential pressure recorded with time between the two channels. Rates of initiation, R_i, were determined for each condition in preliminary experiments by the inhibitor method using PMHC as the reference antioxidant: $R_i = 2\,[PMHC]/\tau$, where τ is the length of the induction period. Kinetic traces were analyzed by numerical fitting using GEPASI software.

5.6.4 EPR Measurements

EPR spectra were recorded with a X-band spectrometer with the following settings: microwave power = 6.3 mW, time constant and conversion time = 20.48 ms, modulation amplitude = 1.0 G. Typical samples contained $TEMPO^{+}BF_4^{-}$ (0.5–5 mM), AIBN (0.05 M), and styrene or cumene (40–50% v/v) in MeCN or PhCl and were air-saturated. Samples were transferred in a capillary glass tube and were placed in the thermostated instrument cavity at 303 K to cover the entire sensitive area. CH_3COOH and CF_3COOH (30–50 mM) were added to the sample as indicated. The absolute concentration of TEMPO formed in the sample was determined upon calibration with standard solutions in the corresponding solvent mixture. Time evolution of the EPR signal was monitored by an automated acquisition routine and analyzed using either the intensity of the first spectral line or the double integration of the whole spectrum.

5.6.5 Paraffin Autoxidations

Paraffin autoxidations were carried out using an analogous procedure to hexadecane autoxidations previously carried out by our group.[30,31,43] Light paraffin oil (100 mL) was thoroughly degassed with N_2 and then heated to 160 °C in a stirred flow reactor. Once the temperature stabilized, 0.04 mmol of bis(2,2,6,6-tetramethylpiperidin-1-oxyl-4-yl) decanedioate (**2**), the appropriate amount of either palmitic acid or 2,4,6-tri-*tert*-butylpyridine, and 82 mg (0.5 mmol) of tetralin hydroperoxide[49] were added to the solution. The flow of N_2 was replaced with 1 L/min O_2. Aliquots (0.5 mL) were removed every 5 min and allowed to cool to room temperature for analysis.

Four duplicates (30 μL) of each sample were loaded into a 96-well microplate.[50] Each well was read sequentially following manipulation as follows: an automated reagent dispenser was used to dilute the sample with *tert*-amyl alcohol (200 μL), and the plate was stirred for 28 s, after which a solution of fluorogenic phosphine **1** (20 μL of a 250 μM stock solution in acetonitrile) was injected

and the plate stirred for an additional 8 s and then allowed to rest for 2 more seconds. The fluorescence of each well was measured every 1.3 s for 30 s (excitation = 340 nm; emission = 425 nm). The concentration of hydroperoxide was determined from the rate of phosphine oxidation using the rate constant for the reaction of the dye with secondary hydroperoxides in *tert*-amyl alcohol (1.2 M^{-1} s^{-1}) assuming pseudo-first-order kinetics.[31]

In tandem, four duplicates (1.2 μL) of each sample were loaded into separate wells of a 96-well microplate; the automated reagent dispenser of the microplate reader was used to dilute each sample with 25% isopropyl alcohol in methanol (280 μL), and the plate was stirred for 15 s. Afterward, a solution of fluorogenic amine **3** (20 μL of a 630 μM stock in methanol) was added. The plate was stirred for 8 s, and the fluorescence of each well was measured every second for 10 s (excitation = 315 nm; emission = 395 nm) and the acid concentration was determined from the average fluorescence reading.

5.7 References

(1) Ingold, K. *Chem. Rev.* **1961**, 61, 563– 589.

(2) Ingold, K. U.; Pratt, D. A. *Chem. Rev.* **2014**, 114, 9022– 9046.

(3) Brownlie, I. T.; Ingold, K. U. *Can. J. Chem.* **1967**, 45, 2427– 2432

(4) Sudnik, M. V.; Romantsev, M. F.; Shapiro, A. B.; Rozantsev, E. G. *Bull. Acad. Sci. USSR, Div. Chem. Sci.***1975**, 24, 2702– 2704.

(5) Bolsman, T.; Blok, A.; Frijns, J. *Recl. des Trav. Chim. des Pays-Bas* **1978**, 97, 310– 312.

(6) See the following reviews on the subject: (a) Allen, N. S. *Chem. Soc. Rev.* **1986**, 15, 373– 404. (b) Gugumus, F. *Polym. Degrad. Stab.* **1993**, 40, 167– 215. (c) Pospisil, J. *Adv. Polym. Sci.* **1995**, 124, 87–189.

(7) See, for example: (a) Samuni, A. M.; Goldstein, S.; Russo, A.; Mitchell, J. B.; Krishna, M. C.; Neta, P. *J. Am. Chem. Soc.* **2002**, 124, 8719– 8724 (b)Goldstein, S.; Merenyi, G.; Russo, A.; Samuni,

A. *J. Am. Chem. Soc.* **2003**, 125, 789– 795 (c) Borisenko, G. G.; Martin, I.; Zhao, Q.; Amoscato, A. A.;Kagan, V. E. *J. Am. Chem. Soc.* **2004**, 126, 9221– 9232. (d) Wipf, P.; Xiao, J.; Jiang, J.; Belikova, N. A.; Tyurin, V.; Fink, M. P.; Kagan, V. E. *J. Am. Chem. Soc.***2005**, 127, 12460– 12461. (e) Dikalova, A. E.;Bikineyeva, A. T.; Budzyn, K.; Nazarewicz, R. R.; McCann, L.; Lewis, W.; Harrison, D. G.; Dikalov, S. I.*Circ. Res.* **2010**, 107, 106– 116. (f) Ji, J.; Kline, A. E.; Amoscato, A.; Samhan-Arias, A. K.; Sparvero, L. J.; Tyurin, V. A.; Tyurina, Y. Y.; Fink, B.;Manole, M. D.; Puccio, A. M.; Okonkwo, D. O.; Cheng, J. P.; Alexander, H.; Clark, R. S. B.;Kochanek, P. M.; Wipf, P.; Kagan, V. E.; Bayir, H. *Nat. Neurosci.* **2012**, 15, 1407– 1413. (g) Canistro, D.; Boccia, C.; Falconi, R.;

Bonamassa, B.;Valgimigli, L.; Vivarelli, F.; Soleti, A.; Genova, M. L.; Lenaz, G.; Sapone, A.; Zaccanti, F.;Abdel-Rahman, S. Z.; Paolini, M. *J. Gerontol. A Biol. Sci. Med. Sci.* **2015**, 70, 936–943.

(8) Kovtun, G. A.; Aleksandrov, A. L.; Golubev, V. A. *Bull. Acad. Sci. USSR, Div. Chem. Sci.* **1974**, 23, 2115–2121.

(9) (a) Bowry, V. W.; Ingold, K. U. *J. Am. Chem. Soc.* **1992**, 114, 4992– 4996.

(b) Sobek, J.; Martschke, R.; Fischer, H. *J. Am. Chem. Soc.* **2001**, 123, 2849–2857.

(10) Gryn'ova, G.; Ingold, K. U.; Coote, M. L. *J. Am. Chem. Soc.* **2012**, 134, 12979– 12988.

(11) Bolsman, T.; Blok, A.; Frijns, J. *Recl. des Trav. Chim. des Pays-Bas* **1978**, 97, 313– 319.

(12) This can be found throughout the literature, in particular, the two areas where nitroxide radical chemistry is particularly important. Radical polymerization: Matyjaszewski, K.; Davis, T. P. *Handbook of Radical Polymerization*; Wiley: Hoboken, NJ, **2002**. Spin-labeling: Kocherginsky, N.; Swartz, H. M.*Nitroxide Spin Labels: Reactions in Biology and Chemistry*; CRC Press: Boca Raton, FL, **1995**.

(13) Amorati, R.; Pedulli, G. F.; Pratt, D. A.; Valgimigli, L. *Chem. Commun. (Cambridge, U. K.)* **2010**, 46, 5139–5141.

(14) A role for the acid-mediated disproportionation of TEMPO to produce the corresponding hydroxylamine (and oxoammonium ion) was ruled out on kinetic grounds (see ref 13). However, it is also possible that the reaction takes place by a coupled proton–electron transfer, wherein a proton is transferred from the acid to the peroxyl radical concerted with the movement of an electron from TEMPO to the peroxyl. Since we found that there is a primary kinetic isotope effect on these reactions, a H atom must be in flight in the rate-determining step of the reaction, precluding any rapid pre-equilibrium between peroxyl and protonated peroxyl, such as that which is involved when phenols react with peroxyl radicals under acidic conditions. See: Valgimigli, L.; Amorati, R.; Petrucci, S.; Pedulli, G. F.; Hu, D.; Hanthorn, J. J.; Pratt, D. A.*Angew. Chem., Int. Ed.* **2009**, 48, 8348– 8351.

(15) Sheldon, R. A.; Arends, I. W. C. E.; ten Brink, G.-J.; Dijksman, A. *Acc. Chem. Res.* **2002**, 35, 774– 781 .

(16) (a) Bailey, W. F.; Bobbitt, J. M.; Wiberg, K. B. *J. Org. Chem.* **2007**, 72, 4504– 4509. (b) Hoover, J. M.; Ryland, B. L.; Stahl, S. S. *J. Am. Chem. Soc.* **2013**, 135, 2357– 2367. (c) Ryland, B. L.; McCann, S. D.; Brunold, T. C.; Stahl, S. S. *J. Am. Chem. Soc.* **2014**, 136, 12166– 12173.

(17) Denisov, E. T. *Polym. Degrad. Stab.* **1991**, 34, 325– 332.

(18) Baran has invoked this electron transfer in a mechanistic proposal for the guided desaturation of unactivated alkanes. See: Voica, A.-F.; Mendoza, A.; Gutekunst, W. R.; Fraga, J. O.; Baran, P. S. *Nat. Chem.* **2012**, 4, 629– 635.

(19) Montgomery, J. A.; Frisch, M. J.; Ochterski, J. W.; Petersson, G. A. *J. Chem. Phys.* **1999**, 110, 2822–2827.

(20) The induction period observed in the alkoxyamine formation is due to the necessary accumulation of TEMPO to outcompete the oxoammonium ion for the cumyl radicals.

(21) Maillard, B.; Ingold, K. U.; Scaiano, J. C. *J. Am. Chem. Soc.* **1983**, 105, 5095– 5099.

(22) Interestingly, corresponding reactions carried out in the absence of Me_4NAcO yielded lower amounts of alkoxyamine. The effect of couterions to the oxoammonuim ion will be discussed below.

(23) Burton, G. W.; Doba, T.; Gabe, E.; Hughes, L.; Lee, F. L.; Prasad, L.; Ingold, K. U. *J. Am. Chem. Soc*.**1985**, 107, 7053– 7065.

(24) Calculated from the inhibition time in O_2 uptake auotxidations inhibited by PMHC.

(25) In the absence of acid, the initial rate is noticeably lower and nonlinear, increasing with time, perhaps due to depletion of O_2 over the longer period of time and improving the competition with alkyl radicals.

(26) Ma, Y.; Loyns, C.; Price, B.; Chechik, V. *Org. Biomol. Chem.* **2011**, 9, 5573– 5578.

(27) It should be pointed out that the spectral characteristics ascribed to $TEMPO^+$ by Ma et al.(26) do not correspond to those reported by other investigators, e.g., Goldstein et al.[7b] or those determined in our own laboratory. See ref 7b for a discussion.

(28) Numerical fitting of the oxygen consumption traces from styrene autoxidations in MeCN (30 °C) inhibited by TEMPO (or $TEMPO^+$) in the presence of TFA (4.3 mM) and HBF_4 (4.3 mM) according to the proposed mechanistic scheme affords $k_{11} \sim 1 \times 10^9$ M^{-1} s^{-1} and $<10^9$ M^{-1} s^{-1}, respectively.

(29) Jensen, R. K.; Korcek, S.; Mahoney, L. R.; Zinbo, M. *J. Am. Chem. Soc.* **1979**, 101, 7574–7584.

(30) Shah, R.; Haidasz, E. A.; Valgimigli, L.; Pratt, D. A. *J. Am. Chem. Soc.* **2015**, 137, 2440– 2443.

(31) Hanthorn, J.; Haidasz, E.; Gebhardt, P.; Pratt, D. A. *Chem. Commun.* **2012**, 48, 10141– 10143.

(32) A sample of TEMPO heated in a vial to 160 °C lost *ca*. 60% of its mass over the course of 1 h.

(33) This arises due to the three distinct phases observable in the initial part of the reaction; the inhibited autoxidation, the uninhibited autoxidation where propagation proceeds at a constant rate, and the slowing of propagation in favor of termination with increasing concentration of hydroperoxides, which increase radical concentration upon thermolysis. Similar data were obtained when the corresponding bis-oxoammonium ion was added in lieu of **5.2** (see Supporting Information).

(34) Jensen, R. K.; Korcek, S.; Mahoney, L. R.; Zinbo, M. *J. Am. Chem. Soc.* **1981**, 103, 1742–1749.

(35) Jalan, A.; Alecu, I. M.; Meana-Pañeda, R.; Aguilera-Iparraguirre, J.; Yang, K. R.; Merchant, S. S.;Truhlar, D. G.; Green, W. H. *J. Am. Chem. Soc.* **2013**, 135, 11100– 11114.

(36) Shah, R.; Pratt, D. A. *J. Org. Chem.*, **2016**, *81* (15), pp 6649–6656.

(37) This increase is likely the result of thermal decomposition of γ-dihydroperoxides present at a concentration below those reliably determined by our method (ca. 1 mM).

(38) Bolsma, Blok, and Frijns suggest $[O_2] \sim 10^{-3}$ mM in paraffin at 130 °C under an atmosphere of O_2 but do not provide a reference or details of the measurement.[11] Korcek and co-workers report $[O_2]$ = 2.65 mM in hexadecane at 160 °C under an atmosphere of O_2, which they determined directly. See: Jensen, R. K.;Korcek, S.; Zinbo, M. *Oxid. Commun.* **1990**, 13, 258– 262.

(39) Up to 2.7 M of 2,2,6,6-tetramethyl-1-(2-propenyloxy)piperidine had no detectable influence on the product distribution in a methyl linoleate clocking experiment, which was carried out as described in: Roschek, B.;Tallman, K. A.; Rector, C. L.; Gillmore, J. G.; Pratt, D. A.; Punta, C.; Porter, N. A. *J. Org. Chem.* **2006**, 71,3527– 3532. The maximum rate constant for transfer from the H atom donor under these conditions is *ca*. 1 M^{-1} s^{-1}. For comparison, the propagation rate constant for H atom transfer from isopropyl *tert*-butyl ether (a similarly hindered ether) has been measured as k_p = 0.02 M^{-1} s^{-1}. See: Howard, J. A.; Ingold, K. U. *Can. J. Chem.* **1970**, 48, 873– 880.

(40) Bennett, J. E.; Eyre, J. A.; Summers, R. *J. Chem. Soc., Perkin Trans. 2* **1974**, 797– 800.

(41) Adamic, K.; Dunn, M.; Ingold, K. U. *Can. J. Chem.* **1969**, 47, 287– 294.

(42) Jensen, R. K.; Korcek, S.; Zinbo, M.; Gerlock, J. L. *J. Org. Chem.* **1995**, 60, 5396– 5400.

(43) Haidasz, E. A.; Shah, R.; Pratt, D. A. *J. Am. Chem. Soc.* **2014**, 136, 16643– 16650.

(44) Pospisil, J. *Polym. Degrad. Stab.* **1991**, 34, 85– 109.

(45) Holan, M.; Jahn, U. *Org. Lett.* **2014**, 16, 58– 61.

(46) Ikeda, H.; Hoshi, Y.; Namai, H.; Tanaka, F.; Goodman, J. L.; Mizuno, K. *Chem. - Eur. J.* **2007**, 13, 9207–9215.

(47) Valgimigli, L.; Pedulli, G. F.; Paolini, M. *Free Radical Biol. Med.* **2001**, 31, 708– 716.

(48) Amorati, R.; Pedulli, G. F.; Valgimigli, L. *Org. Biomol. Chem.* **2011**, 9, 3792– 3800.

(49) Knight, H. B.; Swern, D. *Org. Synth.* **1954**, 34, 90– 91.

(50) Benson, S. W. *Thermochemical Kinetics*, 2nd ed.; Wiley: New York, **1976**.

5.8 Supporting Information

5.8.1 Synthesis of Azocumene

Azocumene was synthesized through the procedure reported by Ikeda,[S1] and as had been previously synthesized by our lab.[S2]

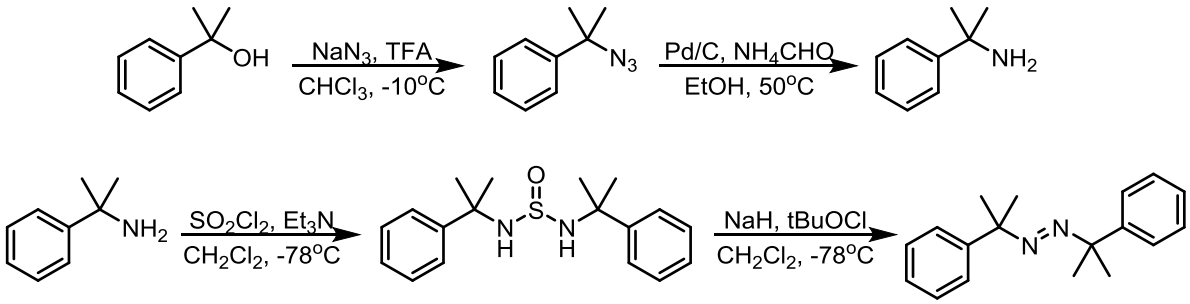

To a solution of cumyl alcohol (10 mmol) and sodium azide (22 mmol) in 10 mL $CHCl_3$ cooled to -10 °C was added TFA (55 mmol) dropwise as a solution in 10 mL $CHCl_3$. The solution was stirred overnight and upon completion was quenched with water. Following extraction with CH_2Cl_2, the organics were washed with brine, dried over MgSO4, and concentrated. The crude cumylazide was then dissolved in 50 mL EtOH and ammonium formate (50 mmol) and 10% Pd/C (100 mg) were added. The reaction was stirred at 50 °C overnight. Upon completion, the solution was diluted with ether and filtered through a pad of silica to afford cumylamine as a pale yellow oil. Yield: 72%. Spectral data are consistent with those in the literature.

To a solution of cumylamine (10 mmol) and dry Et_3N (11 mmol) in dry CH_2Cl_2 (10 mL) cooled to -78 °C was added sulfuryl chloride (5.1 mmol) dropwise. The reaction was maintained at -78 °C until completion, as determined by TLC. The reaction was quenched by addition of water, extracted with CH_2Cl_2 and the organics were washed with brine, dried over MgSO4, and concentrated. Recrystallization from EtOH afforded white needles. Yield: 71%. Spectral data are consistent with those in the literature.

To a suspension of NaH (2.1 mmol) in dry THF cooled to 0 °C was added N,N-bis(1-methyl-1- phenethyl)-sulfamide (3, 1.0 mmol) as a solution in THF dropwise. After 2 h, the solution was cooled to -78 °C and tert-butylhypochlorite (1.1 mmol) was added dropwise. The solution was allowed to warm to room temperature and then quenched with water and extracted with Et_2O. Organics were washed with brine, dried over MgSO4, and concentrated. Purification by column chromatography (Pet Ether/Et_2O) afforded azocumene which was then further purified by recrystallization from Hexanes/CH_2Cl_2 at -20 °C. Yield 11%. Spectral data are consistent with those in the literature.

5.8.2 Synthesis of $TEMPO^+BF_4^-$

$TEMPO^+BF_4^-$ was synthesized through the procedure of Holan and Jahn.[S3]

Isoamyl nitrite (1.0 mmol) was added slowly to a solution of BF_3-OEt_2 (1.3 mmol) in dry Et_2O (4.5 ml) under argon. The solution was stirred 5min before a solution of TEMPO (156 mg) in 0.5 ml Et_2O was added dropwise over 20 minutes. The solution was stirred an additional 10 minutes. The precipitate was filtered, washed thoroughly with Et_2O, and dried under vacuum. Yield 42%.

5.8.3 Synthesis of Cumyl-TEMPO Adduct

Azocumene (1.5 mmol) and TEMPO (3.0 mmol) were dissolved in thoroughly degassed MeCN (15 ml). The solution was stirred at 50°C, under argon, for 24h. The solvent was removed under vacuum, and the residue purified by column chromatography with Et_2O/hexanes to yield a white solid. Yield: 69%. Spectral data are consistent with those in the literature.[S4]

5.8.4 Azocumene Model Reaction Data

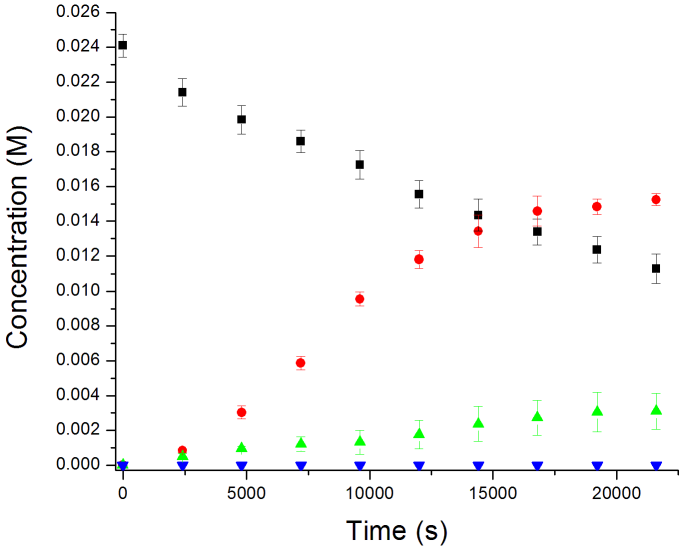

Figure S5.1. Decomposition of azocumene (■) and formation of the TEMPO-cumyl adduct (**5.2**) in the reaction between azocumene (25 mM) and $TEMPO^+BF_4^-$ (25 mM) in the presence of $Me_4N^+AcO^-$ (25 mM) in acetonitrile at 50°C, under argon (●), air (▲) or O_2 (▼).

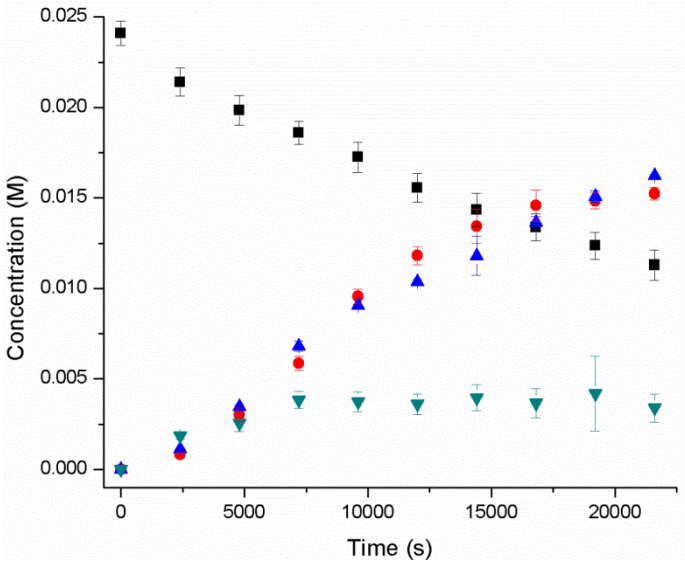

Figure S5.2. Decomposition of azocumene (■) and formation of the TEMPO-cumyl adduct (**5.2**) in the reaction between azocumene (25 mM) and $TEMPO^{+}BF_4^{-}$ (25 mM) in the presence of $Me_4N^{+}AcO^{-}$ (25 mM) in acetonitrile at 50°C, under argon, with no additive (●), 25mM AcOH (▲) or 25mM TFA (▼).

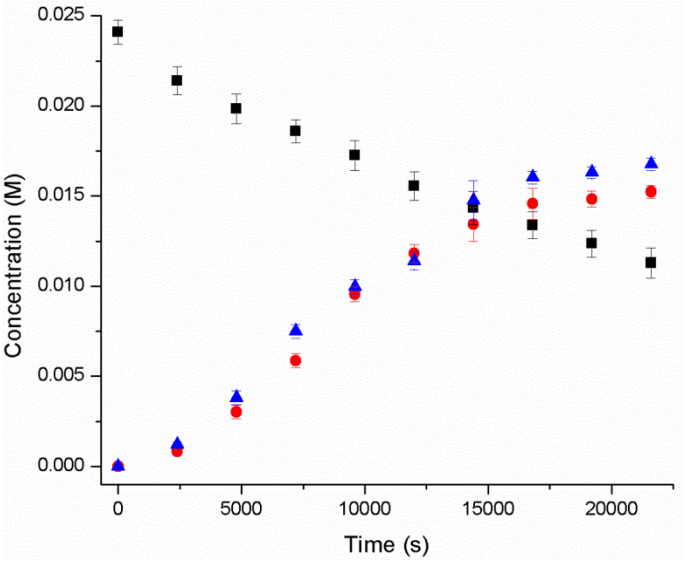

Figure S5.3. Decomposition of azocumene (■) and formation of the TEMPO-cumyl adduct (**5.2**) in the reaction between azocumene (25 mM) and $TEMPO^{+}BF_4^{-}$ (25 mM) in the presence of $Me_4N^{+}AcO^{-}$ (25 mM) in at 50°C, under argon, in acetonitrile (●), or in chlorobenzene (▲).

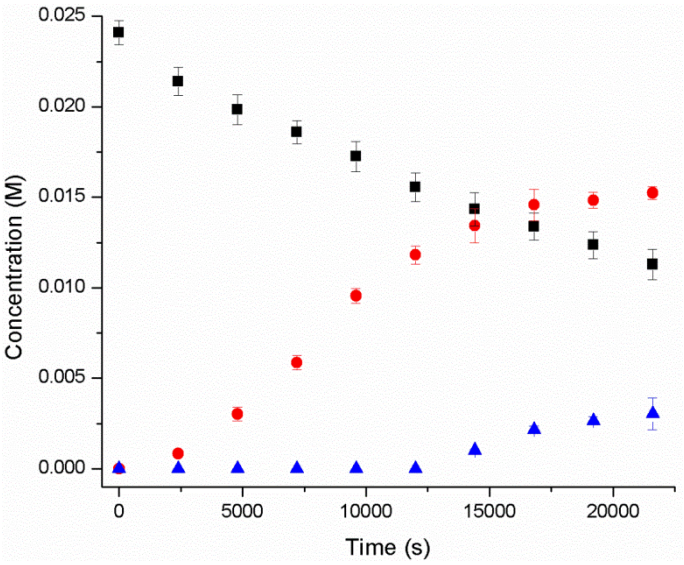

Figure S5.4. Decomposition of azocumene (■) and formation of the TEMPO-cumyl adduct (**5.2**) in the reaction between azocumene (25 mM) and $TEMPO^{+}BF_4^{-}$ (25 mM) at 50°C, under argon, in acetonitrile, in the presence of 25 mM $Me_4N^{+}AcO^{-}$ (●), without additives (▲).

5.8.5 $TEMPO^{+}BF_4^{-}$ Reactions by UV-Vis Spectroscopy

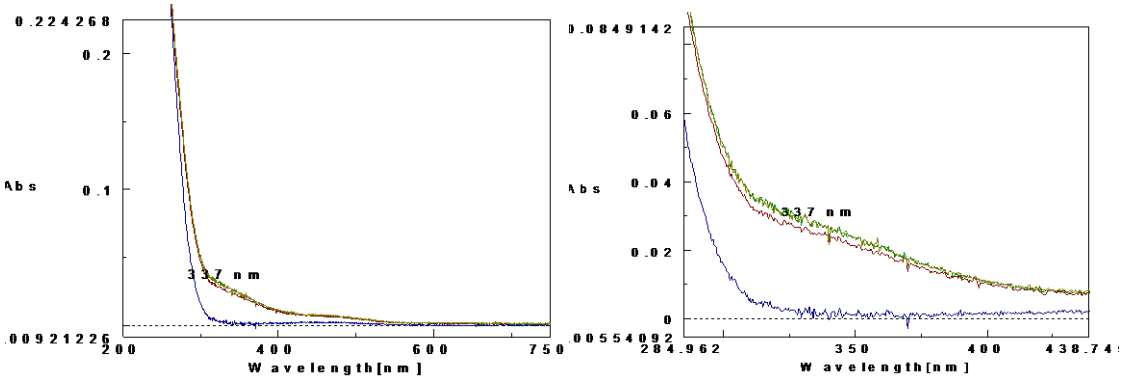

Figure S5.5. UV-Vis spectra in acetonitrile 20°C of the mixture $TEMPO^{+}BF_4^{-}$ **(**0.2mM) with *tert*-butyl hydroperoxide (3.3 mM) immediately after mixing (green) and after 137 min (red). The blue line shows the UV-Vis Spectrum of a reference solution of TEMPO (0.2 mM) in acetonitrile.

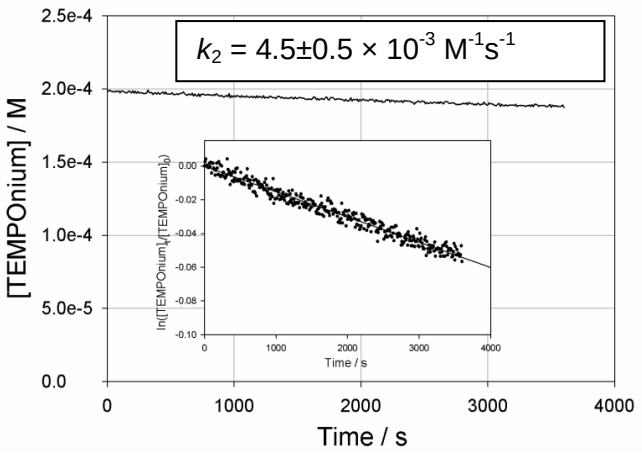

Figure S5.6. Time evolution of the concentration of TEMPO$^+$BF$_4^-$ (0.2mM) in acetonitrile at 20°C upon mixing with *tert*-butyl hydroperoxide (3.3 mM). The reaction was monitored at 337 nm, and the first-order plot of signal decay is shown in the insert.

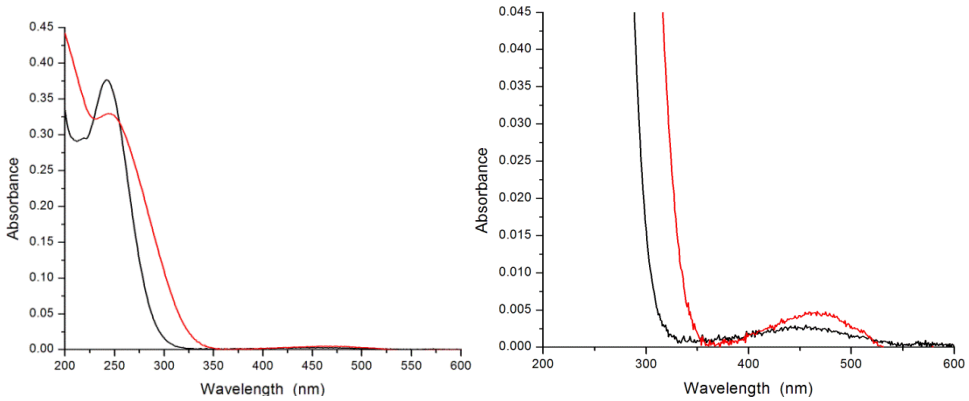

Figure S5.7. UV-Vis spectra of 0.4 mM TEMPO (Black) and TEMPO$^+$BF$_4^-$ (Red) in acetonitrile at 50°C.

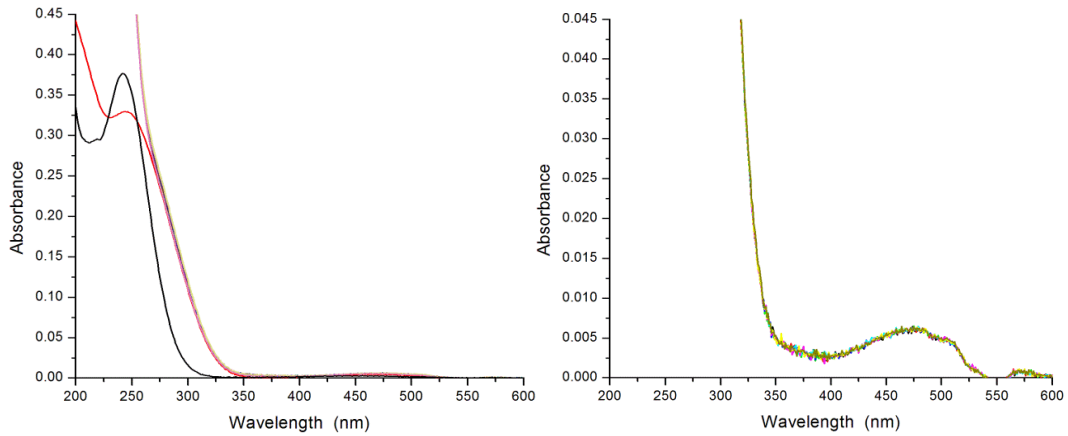

Figure S5.8. UV-Vis spectra of 400μM TEMPO (Black, left graph), or 400μM $TEMPO^{+}BF_4^{-}$ (Red, left graph) in 1% H_2O/MeCN. Decomposition of 400μM $TEMPO^{+}BF_4^{-}$ in 1% H_2O/MeCN with TFA (10mM) from 10-200 minutes (green through pink, indistinguishable).

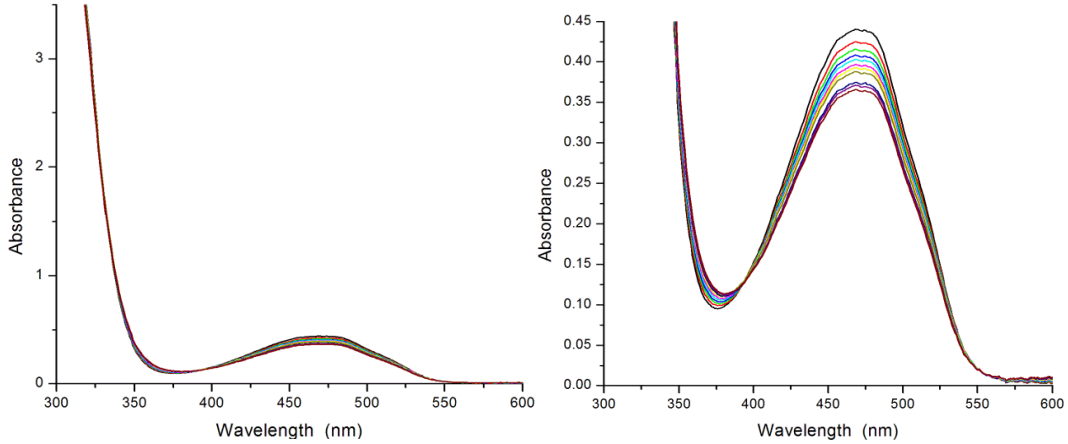

Figure S5.9. UV-Vis spectra of the decomposition of $TEMPO^{+}BF_4^{-}$ (20mM) in 1% H_2O/MeCN containing 0.1 M TFA, at 70°C. Spectra were taken every 4 minutes over the course of 40 minutes and yielded a decomposition rate of $R = 1.3 \times 10^{-6}$ Ms^{-1}.

5.8.6 Inhibited Autoxidation O_2-Uptake Data

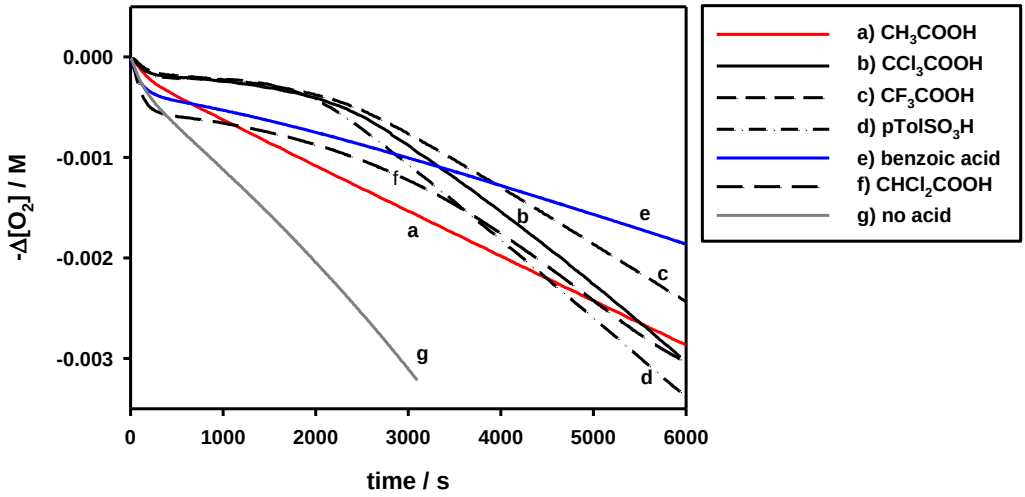

Figure S5.10. Oxygen consumption plot measured during the autoxidation of styrene (4.3 M) in MeCN (+ 1% H_2O) initiated by AIBN (0.05 M) at 30 °C in the presence of TEMPO (13 μM) and 4.3 mM of various acids.

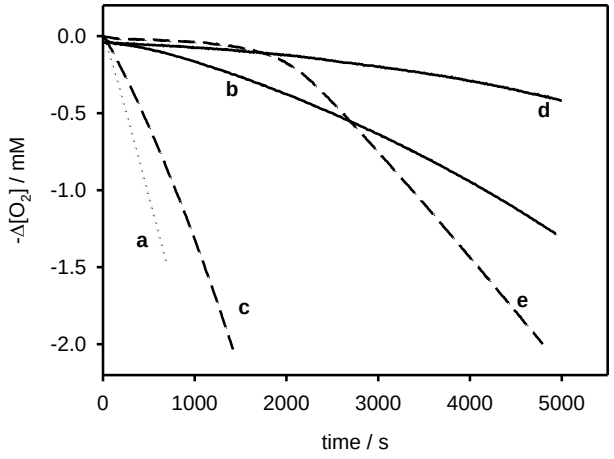

Figure S5.11. Inhibited autoxidation of styrene (4.3 M) initiated by AIBN (0.05 M) in MeCN with 1% H_2O in (a) the absence of inhibitors, and in the presence of 13 μM of either $TEMPO^+BF_4^-$ (b and c) or TEMPO (d and e) with added acetic acid (43 mM, solid lines) or trifluoroacetic acid (32 mM, dashed lines).

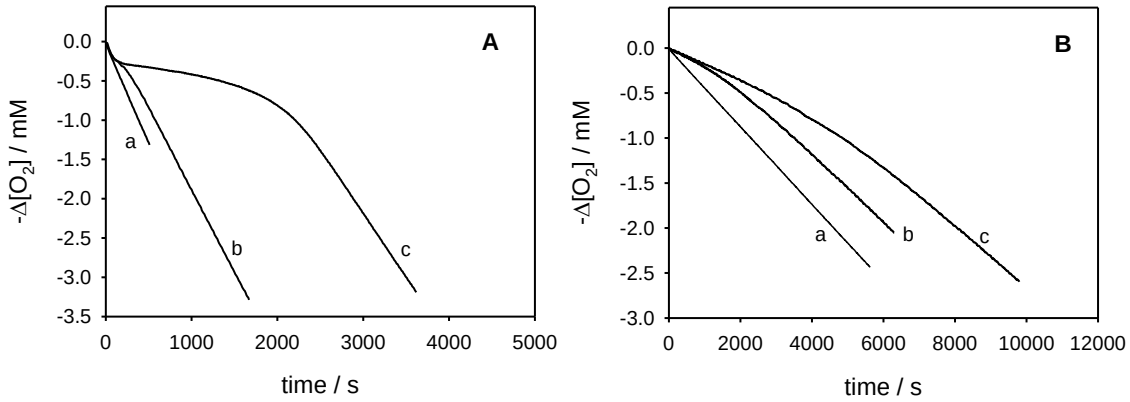

Figure S5.12. Oxygen consumption observed during the autoxidation of styrene (panel A) or of cumene (panel B) initiated by AIBN (0.05 M) at 30°C using in chlorobenzene. a) without inhibitors; b) $TEMPO^{+}BF_4^{-}$ (13 μM) and AcOH (44 mM); c) TEMPO (13 μM) and AcOH (44 mM).

The O_2 consumption plots were analyzed on the basis of the mechanism reactions 1-8 by using Gepasi software[S5] (see Figure S5.13). See the Supporting Information attached to the original publication (*J. Am. Chem. Soc.*, **2016**, *138* (16), pp 5290–5298) for information on the kinetic modeling and parameter fitting.

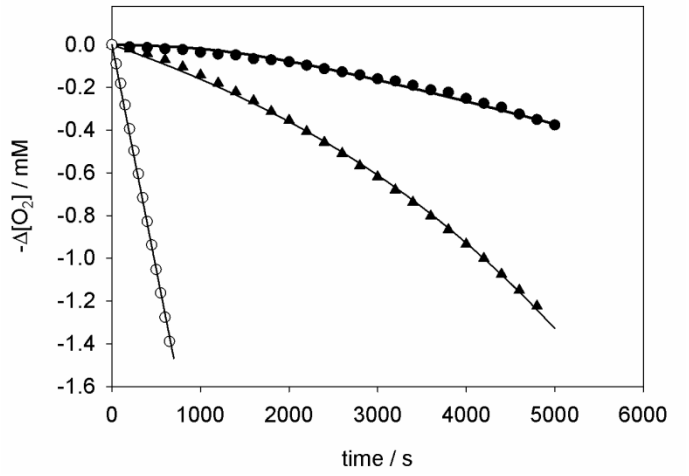

Figure S5.13. Inhibited autoxidation of styrene (4.3 M) initiated by AIBN (0.05 M) in MeCN with 1% of water and acetic acid (0.043 M), in the absence of inhibitors (○) or in the presence of TEMPO (13 μM, ●) or the TEMPOonium (13 μM, ▲). Lines represent the results from numerical fittings, see text.

5.8.7 Supporting Information References

S1.) Ikeda, H.; Hoshi, Y.; Namai, H.; Tanaka, F.; Goodman, J. L.; Mizuno, K. *Chem. Eur. J.* **2007**, 13, 9207–9215.

S2.) Hanthorn, J. J.; Synthesis, Thermodynamic and Kineic Studies of Novel Diarylamine Antioxidants & Development of a Fluorescent Probe for Quantifying Hydroperoxides and Measuring H-Atom Transfer Kinetics with Peroxyl Radicals. Ph.D. dissertation. Queen's University, Kingston, ON. 2012.

S3.) Holan, M.; Jahn, U. *Org. Lett.* **2014**, *16*, 58–61.

S4.) Connolly, T. J.; Baldoví, M. V.; Mohtat, N.; Scaiano, J. C. Tetrahedron Lett. 1996, 37, 4919–4922.

S5) Mendes, P. *Trends Biochem. Sci.* **1997**, 22, 361-363.

5.8.8 EPR Experiments

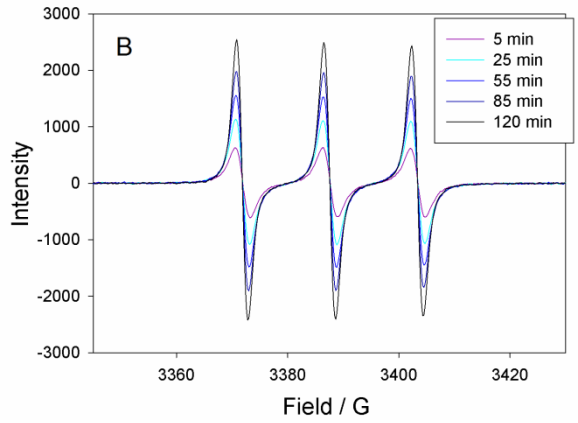

Figure S5.14. TEMPO formation during the autoxidation of 40% (v/v) styrene in acetonitrile at 30°C initiated by AIBN (50 mM) in the presence of $TEMPO^{+}BF_4^{-}$ **(**0.66 mM). Representative EPR spectra.

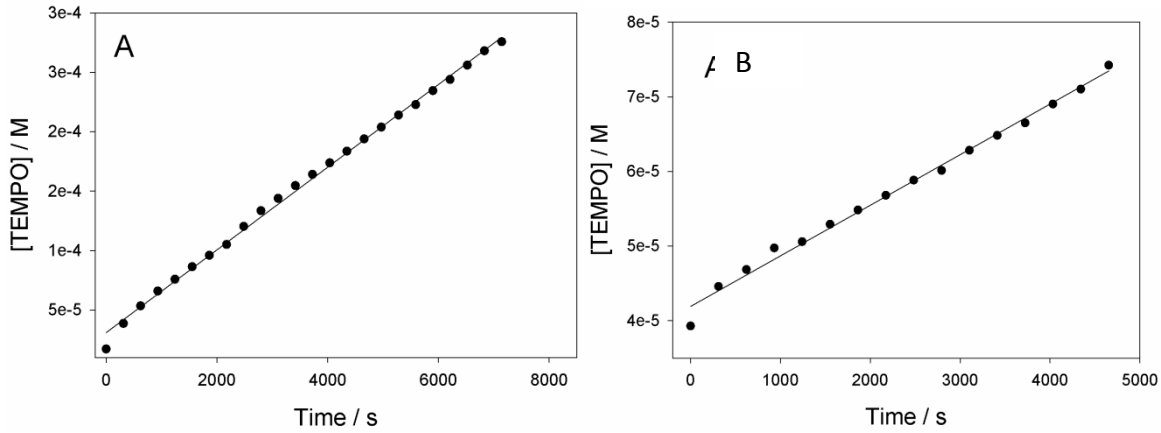

Figure S5.15. TEMPO formation during the autoxidation of 40% (v/v) styrene in acetonitrile at 30°C initiated by AIBN (50 mM) in the presence of $TEMPO^{+}BF_4^{-}$ **(**0.66 mM). Representative rate measurements without (A) and with (B) added acetic acid (35 mM).

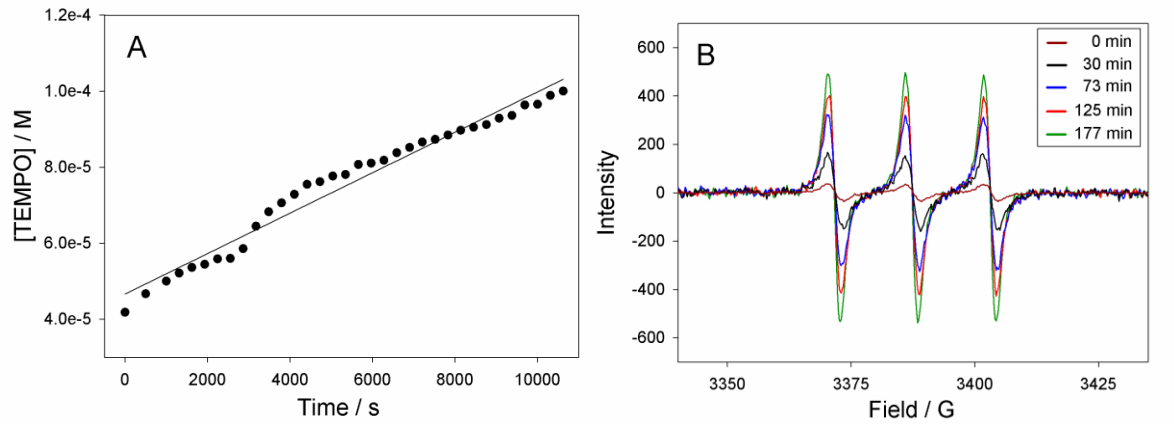

Figure S5.16. A) Time evolution of TEMPO during the autoxidation of 40% (v/v) cumene in acetonitrile at 303K initiated by AIBN (0.05M) in the presence of $TEMPO^{+}BF_4^{-}$ (0.66 mM). B) representative corresponding EPR spectra recorded at different times.

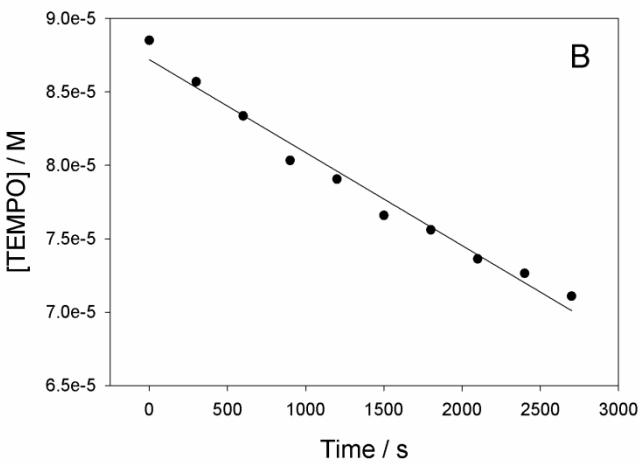

Figure S5.17. Time evolution of TEMPO concentation during the autoxidation (at 303K initiated by AIBN 0.05M) of 40% (v/v) cumene in acetonitrile in the presence of $TEMPO^{+}BF_4^{-}$ (0.66mM) upon addition of 26 mM trifluoroacetic acid after ~0.1mM TEMPO had already been formed.

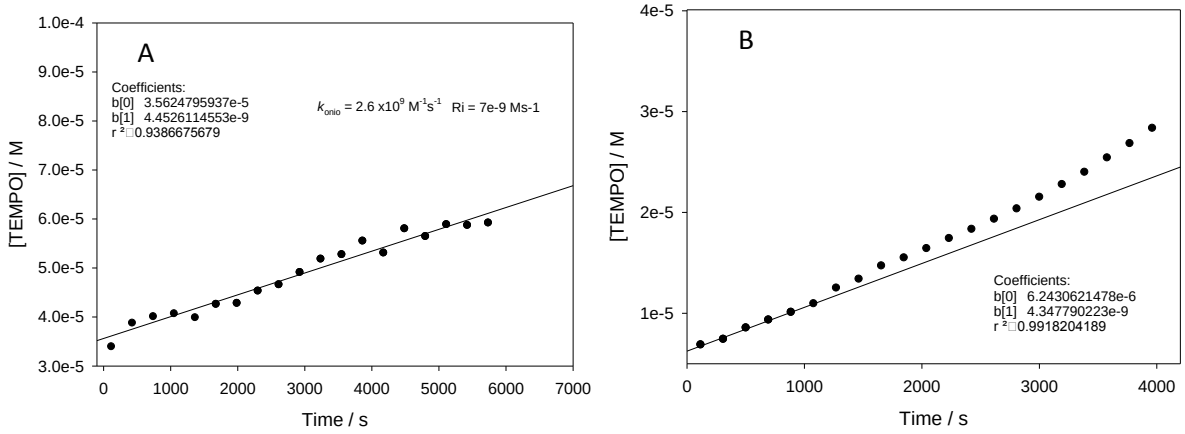

Figure S5.18. Time evolution of TEMPO concentation during the autoxidation (at 303K initiated by AIBN 0.055M) of 40% (v/v) cumene in chlorobenzene in the presence of $TEMPO^{+}BF_4^{-}$ (1.1mM) in the presence of 35 mM acetic acid (A) or without acid (B). In the absence of acid, the initial rate is noticeably slower and nonlinear – increasing with time, perhaps due to depletion of O_2 over the longer period of time, improving the competition with alkyl radicals.

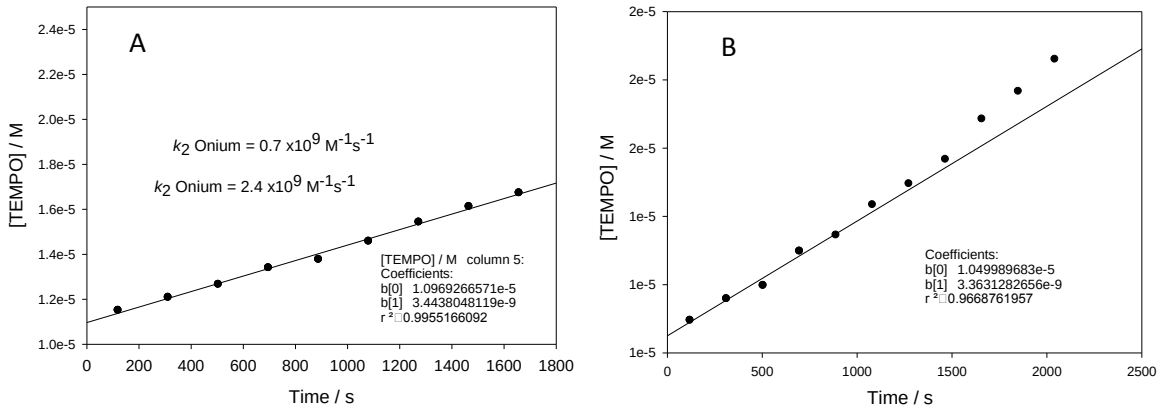

Figure S5.19. Time evolution of TEMPO concentation during the autoxidation (at 303K initiated by AIBN 0.055M) of 45% (v/v) cumene in chlorobenzene in the presence of $TEMPO^+BF_4^-$ (0.67 mM) in the presence of 35 mM acetic acid (A) or without acid (B).

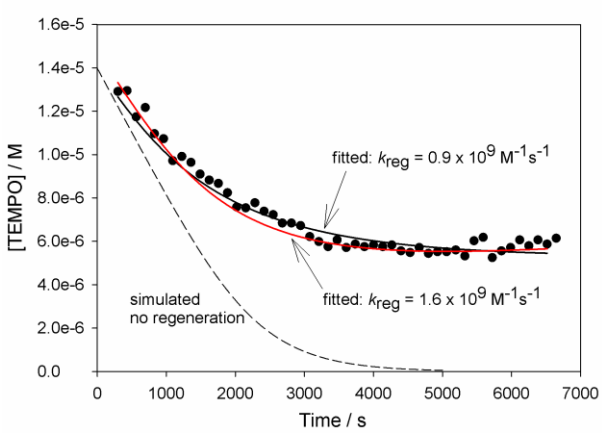

Figure S5.20. EPR detected time evolution of [TEMPO] during the autoxidation of cumene (45 % v/v)in Chlorobenzene initiated by AIBN 0.05M at 303K, in the presence of TEMPO 1.4 x 10-5 M and acetic acid 52 mM. Simulations show the expected decay in the absence of TEMPO regeneration from TEMPO+, and the fitted traces allowing regeneration with the indicated k_{reg} (= k_{onium}).

5.8.9 High Temperature Autoxidation Data

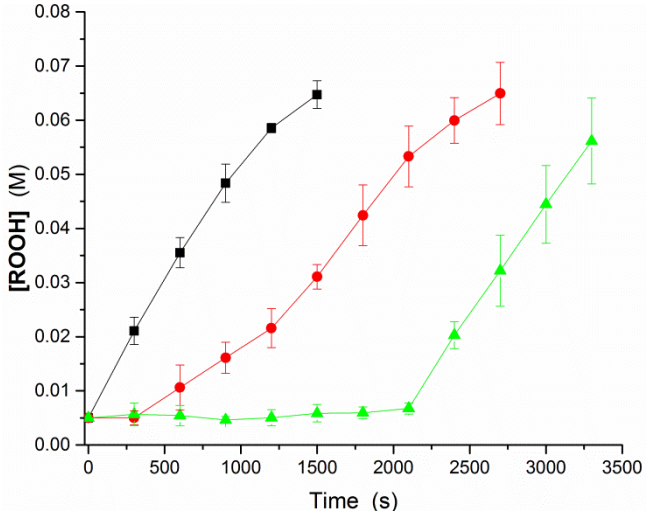

Figure S5.21. Inhibited autoxidation of light paraffin oil at 160°C, initiated by 5.0 mM tetralin hydroperoxide, uninhibited (■), or inhibited by either 1.0 mM BHT (▲) or 40 μM Bis(2,2,6,6-tetramethylpiperidin-1-oxyl-4-yl) decanedioate, **5.2** (●).

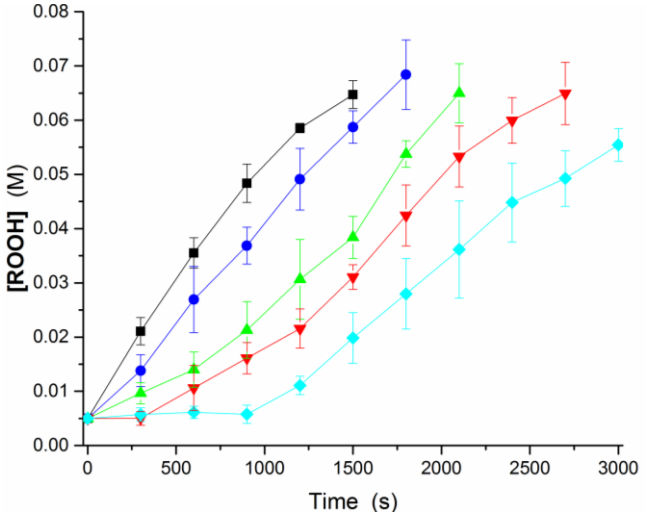

Figure S5.22. Hydroperoxide formation during the inhibited autoxidation of light paraffin oil at 160°C, initiated by 5.0 mM tetralin hydroperoxide, uninhibited (■), or inhibited by 40 μM **5.2** (▼) and either 40 mM palmitic acid (♦) or 4.0 (▲) or 40mM (●) tBu_3pyridine.

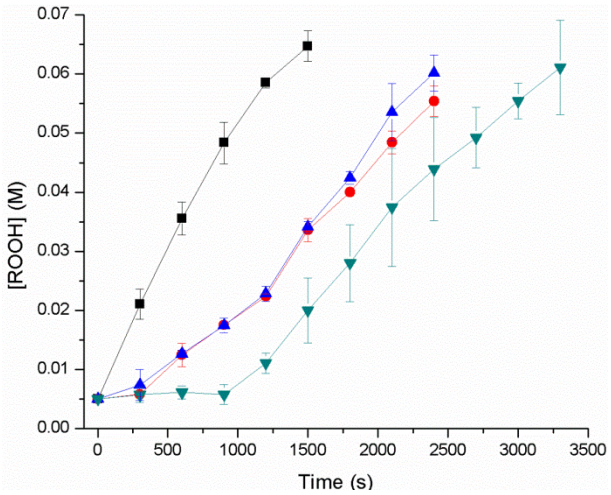

Figure S5.23. Hydroperoxide formation during the inhibited autoxidation of light paraffin oil at 160°C, initiated by 5.0 mM tetralin hydroperoxide, uninhibited (■), or inhibited by 40 μM **5.2** (●) and either 4mM (▲) or 40mM palmitic acid (▼).

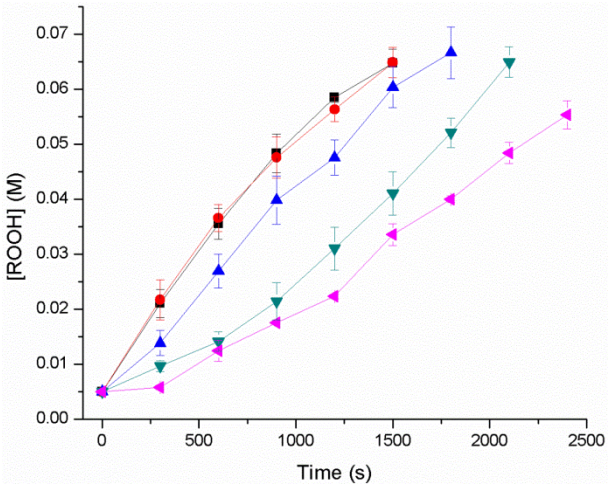

Figure S5.24. Hydroperoxide formation during the inhibited autoxidation of light paraffin oil at 160°C, initiated by 5.0 mM tetralin hydroperoxide, uninhibited without additives (■), or with 40 mM 2,4,6-tri-*tert*-butylpyridine (●); and inhibited with 40 μM **5.2** with no additive (◀) or either 4mM (▼) or 40mM 2,4,6-tri-*tert*-butylpyridine (▲).

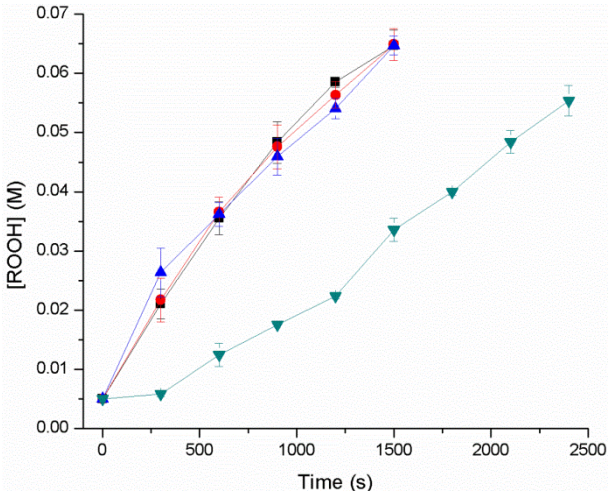

Figure S5.25. Hydroperoxide formation during the inhibited autoxidation of light paraffin oil at 160°C, initiated by 5.0 mM tetralin hydroperoxide, uninhibited without additives (■), or with 40 mM 2,4,6-tri-*tert*-butylpyridine (●) or palmitic acid (▲); or inhibited with 40 μM **5.2** with no additive (▼).

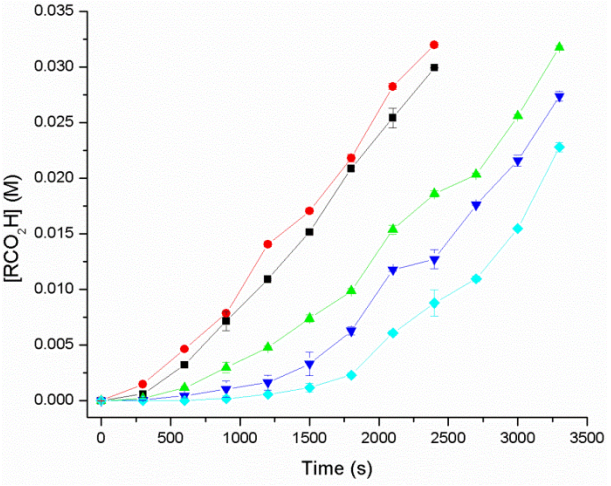

Figure S5.26. Carboxylic acid formation during the inhibited autoxidation of light paraffin oil at 160°C, initiated by 5.0 mM tetralin hydroperoxide, uninhibited without additives (■), or with 40 mM 2,4,6-tri-*tert*-butylpyridine (●); and inhibited with 40 μM **5.2** with no additive (♦) and 4.0 (▼) or 40mM (▲)2,4,6-tri-*tert*-butylpyridine.

CHAPTER 6: Diazaphenoxazines and Diazaphenothiazines: Synthesis of the 'Correct' Isomers Enables their Characterization as Extremely Potent Radical-Trapping Antioxidants

6.1 Preface

The preparation of 2,4-diazaphenothiazines and 2,4-diazaphenoxazines via a copper-catalyzed intramolecular amination is described. Literature approaches which utilize easily accessible (2'-aminophenyl) 4-pyri(mi)dyl sulfides undergo a Smiles rearrangement that gives rise to the 1,3-diaza derivatives instead – confirmed by x-ray crystallography. Inverting the polarity of the azine ring-forming reaction avoids the rearrangement and affords the desired products. Preliminary kinetic studies suggest that 2,4-diazaphenothiazines and 2,4- diazaphenoxazines, but not the corresponding 1,3-isomers, are potent radical-trapping antioxidants. This chapter is presented largely as it was when accepted for publication in Organic Letters (*Org. Lett.* **2017**, 19, 1854-1857).

6.2 Introduction

Phenoxazines and phenothiazines (i.e. **6.1** and **6.2**, Figure 6.1) figure prominently in medicinal chemistry,[1–5] and their photophysical properties have enabled their use in dye-sensitized solar cells,[6–8] organic light emitting diodes,[9–11] chemical probes,[12,13] and as photoredox catalysts.[14] Phenothiazines have also long been known to possess potent antioxidant activity,[15–17] and have been pursued as additives to protect petroleum-derived products, including lubricants, rubber and fuels from radical-mediated autoxidation. At ambient temperatures phenothiazine is 440-fold more reactive to autoxidation chain carrying peroxyl radicals than diphenylamine (**6.3**),[18] the base structure of the industry-standard alkylated diphenylamine (DPA) radical-trapping antioxidants (RTAs).[19,20] Phenoxazine is a further 3-fold more reactive under the same conditions.[18,21]

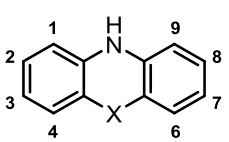

X	k_{inh}^{PhCl} ($M^{-1}s^{-1}$)	
O	2.9×10^7	(**6.1**)
S	8.8×10^6	(**6.2**)
H,H'	2.0×10^4	(**6.3**)

Figure 6.1. General structures of phenoxazine (**6.1**), and phenothiazine (**6.2**) and diphenylamine (**6.3**) and the rate constants for their reactions with peroxyl radicals (k_{inh}, in chlorobenzene).

Previous work by our group has shown that incorporation of heteroatoms at the 3- and/or 5-position of one or both of the aromatic rings of diarylamines greatly stabilizes them towards one electron oxidation.[22,23] This modification enables ring substitution with strongly electron-donating groups, which weaken the N-H bond and increase the rate of H-atom transfer to peroxyl radicals without compromising stability to one-electron oxidation. For example, diarylamine **6.4** is ~20-fold more reactive than the industry standard alkylated DPA at ambient temperatures;[22,23] a difference that was found to translate to the inhibition of high temperature autoxidations of heavy hydrocarbons by **6.5**.[24] Reasoning that phenoxazine and phenothiazine would present a better scaffold for further optimization, we sought to incorporate oxygen and sulfur into the structures of **6.4**, **6.5** and related heterocyclic diarylamines.

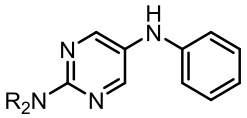

R = Me (**6.4**)
R = C_6H_{13} (**6.5**)

Although there has been some interest in aza-analogues of phenoxazine and phenothiazine,[25–33] 2-aza, 4-aza- and 2,4-diaza derivatives have received little attention.[34,35] Of particular relevance, Bakavoli and co-workers reported the preparation of phenothiazine analogs of **6.4**/**6.5** (Scheme 6.1) and their study as inhibitors of 15-lipoxygenase catalysis.[35–38]

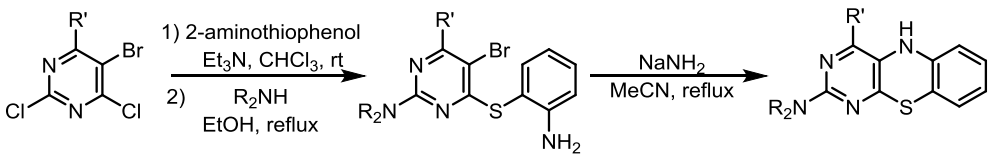

Scheme 6.1. Reported synthesis of 3-amino-2,4-diazapheno-thiazines analogous to **6.4**/**6.5**.

6.3 Results and Discussion

6.3.1 Synthesis of Diazaphenothiazine and Diazaphenoxazine Compounds

When we attempted to reproduce their reported synthesis of a representative 2,4-diazaphenothiazine (the 3-pyrrolidine-substituted derivative **6.6**), the crude material contained only trace amounts of the reported product.[37] However, upon recrystallization (as reported), a significant quantity of the major product was converted to the initially trace (reported) product. We surmised that our crude material may have undergone oxidation during recrystallization. Indeed, when the reaction was repeated and the crude material treated with a basic methanolic solution of iodine, the reported product was obtained. This product was characterized by us to be disulfide **6.7** (see Supporting Information) implying that the initial product was the corresponding thiol, and the difference between our experiment and that of Bakavoli was simply that *in situ* oxidation of the thiol(ate) was minimized in our hands. Thus, **6.8** undergoes a Smiles rearrangement under these conditions,[39] with the amide displacing the thiolate as in Scheme 6.2.

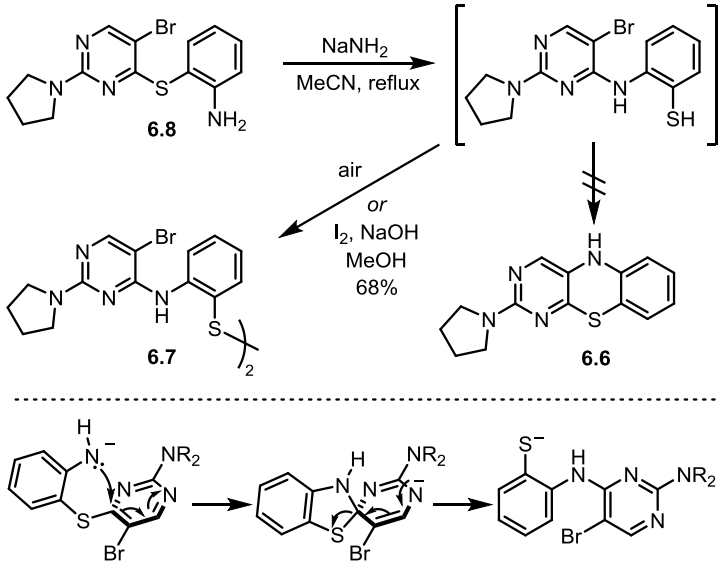

Scheme 6.2. Literature conditions for cyclization of **6.8** to **6.6** yields the rearranged thiol and corresponding disulfide **6.7**.

In an attempt to favour cyclization over the Smiles rearrangement, we converted the amine to the less nucleophilic acetamide (**6.9**) and subjected it to Ullmann-type conditions (Scheme 6.3). This afforded a new product whose structure was determined unambiguously by single crystal x-ray diffraction to be the 1,3-diazaphenothiazine **6.10**. Thus, although the cyclization proceeds (in good conversion, but poor yield after chromatography), it *follows* the Smiles rearrangement. Unfortunately, the same was true when the bromide was exchanged with an iodide. Evidently these substrates are too activated to the Smiles rearrangement – which the copper may even promote.[40]

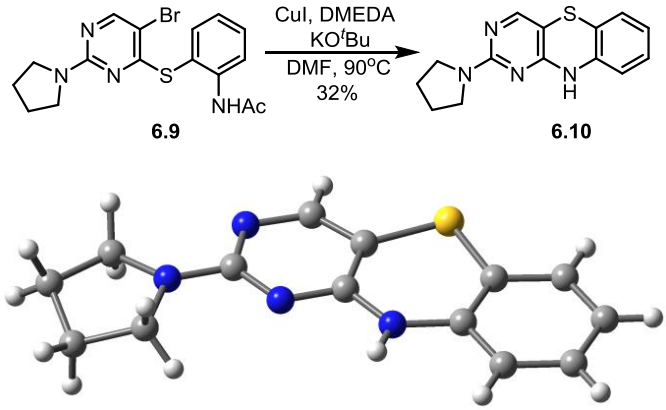

6.9 **6.10**

Scheme 6.3. Preparation of 1,3-diazaphenothiazine **6.10** and its structure as determined by single crystal x-ray diffraction.

In order to suppress the Smiles rearrangement, the polarity of the reaction was reversed; that is, the positions of the amine and bromide substituents on the pyrimidyl and phenyl rings were exchanged (i.e. **6.11** in Scheme 6.4).[41] Following acetylation to give **6.12**, the cyclization proceeded with excellent conversion, and subsequent deprotection provided the desired 2,4-diazaphenothiazine **6.6** in 86% (isolated) yield. Given that our ^{1}H and ^{13}C NMR spectral data were significantly different than those reported by Bakavoli *et al*. (which we have now shown correspond to disulfide **6.7**),[37] we determined the structure of our product unambiguously by single crystal x-ray diffraction in order to confirm that it was indeed **6.6**.

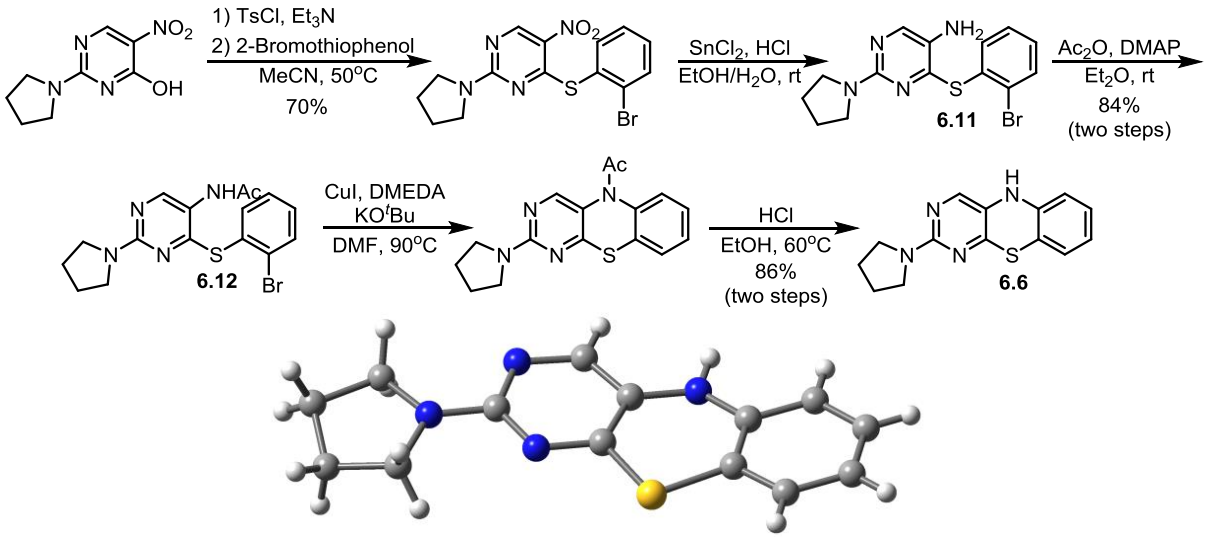

Scheme 6.4. Preparation of 2,4-diazaphenothiazine **6.6** and its structure as determined by single crystal x-ray diffraction.

The synthesis of the corresponding 2,4-diazaphenoxazine derivative was similarly problematic. The preparation of **6.13**, the diarylether analogous to diarylthioether **6.8** (Scheme 6.2), required explicit prior formation of the phenolate, and despite the poorer leaving group, the Smiles rearrangement preceded readily upon installation of the diethylamino substitutent to give a ~1:1 mixture of **6.13** and **6.14** (Scheme 6.5). Subsequent cyclization of **6.14** gave the 1,3-diazaphenoxazine **6.15**. However, as was the case with the sulfur analog, exchanging the amine and halide substituents provided the desired 2,4-diazaphenoxazine **6.16** (Scheme 6.6). To the best of our knowledge, **6.16** is the first reported 2,4-diazaphenoxazine.

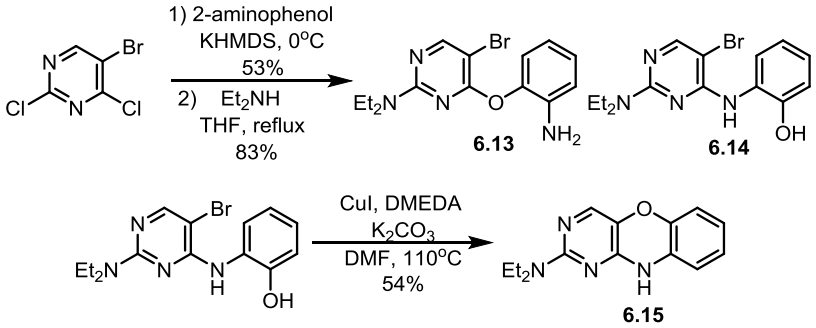

Scheme 6.5. Preparation of 1,3-diazaphenoxazine **6.15**.

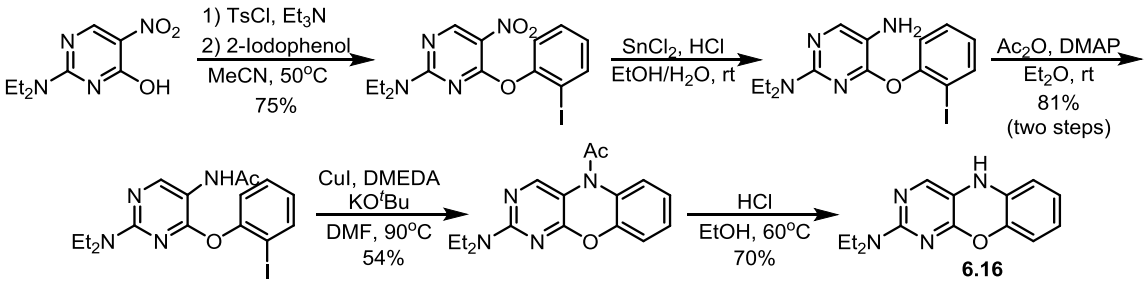

Scheme 6.6. Preparation of 2,4-diazaphenoxazine **6.16**.

6.3.2 Reactivity of Diazaphenothiazine and Diazaphenoxazines

With the two isomers of representative diazaphenothiazines and diazaphenoxazines in hand, the RTA activity of each was measured by the inhibited autoxidation of 1,4-dioxane. We monitored the autoxidations by following the consumption of PBD-BODIPY, a highly oxidizable and highly absorbing substrate which is added to the autoxidation to enable reaction monitoring by conventional spectrophotometry (eq 6.1).[42,43] The rate constants for the reaction of the amines with chain-carrying peroxyl radicals and the reaction stoichiometry (k_{inh} and n, respectively) can be calculated from the initial rate and inhibited period of PBD-BODIPY consumption through the use of equations 6.2 and 6.3, respectively. Representative autoxidation traces for **6.6**, **6.10**, **6.15**, and **6.16** are shown in Figure 6.2.

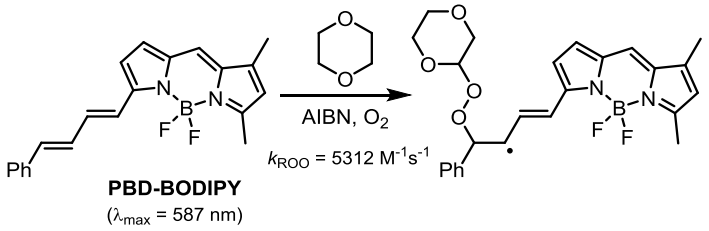

(6.1)

$$\frac{-d[\text{PBD-BODIPY}]}{dt} = \frac{k_{\text{ROO}}[\text{PBD-BODIPY}]R_{\text{i}}}{nk_{inh}[\text{RTA}]} \qquad (6.2)$$

$$t_{\text{inh}} = \frac{n[\text{RTA}]}{R_i} \qquad (6.3)$$

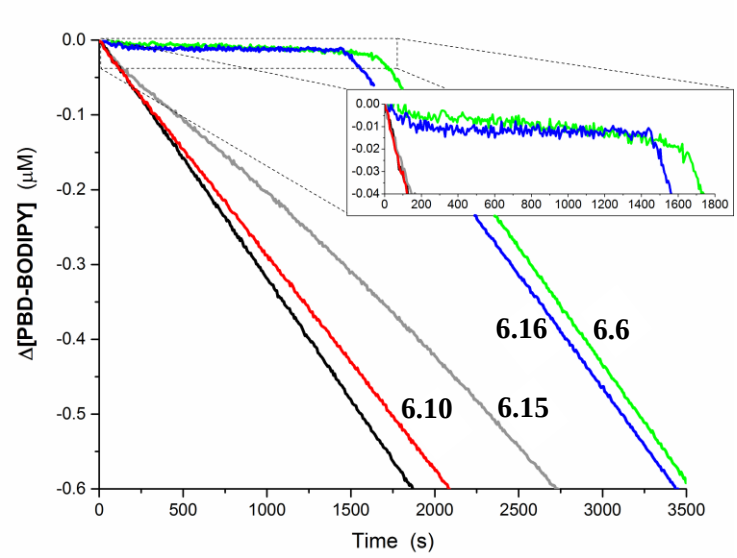

Figure 6.2. Co-autoxidation of 1,4-dioxane (2.9 M) and PBD-BODIPY (10 μM) initiated by AIBN (6 mM) in PhCl at 37 °C (black) and inhibited by 2 μM of **6.6** (green), **6.10** (red), **6.15** (grey), and **6.16** (blue). Reaction progress was monitored by absorbance at 587 nm (ε = 123,023 $M^{-1}cm^{-1}$).

Although the 1,3-diazaphenothiazine **6.10** barely inhibits the autoxidation and the 1,3-diazaphenoxazine **6.15** only retards it, the corresponding 2,4-diaza isomers **6.6** and **6.16** are remarkably effective. The stark difference in reactivity between the isomers is consistent with the trends we have observed in the simpler diarylamines, where nitrogen incorporation at tautomerizable positions is highly detrimental.[22] The inhibited periods (of *ca*. 1600 s) observed for the 2,4-diaza isomers correspond to the trapping of two chain-carrying peroxyl radicals – as is typical for diarylamine RTAs at ambient temperatures.[20,22,23] The very slight initial rate of the autoxidation inhibited by the 2,4-diazaphenothiazine **6.6** corresponds to a rate constant for its reaction with chain-carrying peroxyl radicals of $k_{\mathrm{inh}}^{\mathrm{dioxane}}$ = 5.0×10^6 $M^{-1}s^{-1}$; while the 2,4-diazaphenoxazine **6.16** is so reactive that it completely suppresses the autoxidation, precluding determination of a rate constant. To enable comparison of the reactivity of **6.6** with other diarylamines, its inhibition rate constant was corrected for the retarding effect of H-bonding of the aminic H-atom to dioxane using the Ingold-Abraham relationship (eq 4, where $\Delta\beta_2^{\mathrm{H}}$ = 0.26 is the difference in the H-bond accepting ability of the solvents and α_2^{H} = 0.44 is the H-bond donating ability of the H-atom donor, see Supporting

Information).[44,45] The corresponding value of k_{inh}^{PhCl} = 4.5×10^7 M^{-1}s^{-1} exceeds that of any diarylamine RTA ever reported.[23] Given that the 2,4-diazaphenoxazine **6.16** is an even better inhibitor than **6.6** (consistent with the difference between phenoxazine and phenothiazine)[18], its rate constant must be >10^8 M^{-1}s^{-1}, suggesting E_a ~ 0 since log$A$ for this H-atom transfer is likely to be around 8.[46]

$$\log(k_{inh}^{PhCl}) = \log(k_{inh}^{dioxane}) + 8.3\alpha_2^H\Delta\beta_2^H \qquad (4)$$

6.3.3 Synthesis of Monoazaphenothiazine and Monoazaphenoxazine Compounds

The 2-aza and 4-aza phenothiazines and phenoxazines can also be prepared using the approach described above.

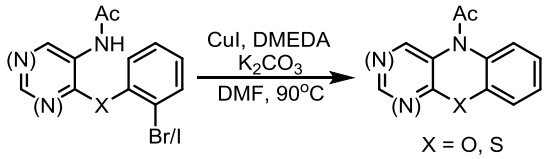

Although compounds of these types have previously been reported,[25,47] the conditions under which they have been prepared are often significantly harsher than those described above (e.g. 10 eq activated Cu, 160°C).[25,48] Moreover, many of the reported routes are vulnerable to the Smiles rearrangement – leading to the incorrect (undesired) isomer. For example, we have found that recent reports of the syntheses of substituted 4-azaphenothiazines[49] and 4-azaphenoxazines[50] lead to 1-azaphenothiazines and 1-azaphenoxazines, respectively (see Supporting Information for complete details). Not unexpectedly, it is difficult to assign the structures of these molecules simply from their NMR spectra – examples of which are included in Figure 6.3 for reference (see the Supporting Information for ^{13}C NMR spectra).[51] This underscores the need for multiple modes of characterization for structural elucidation.

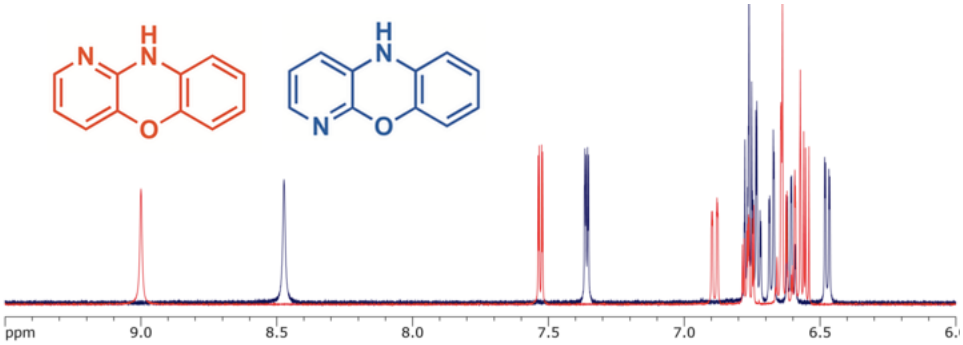

Figure 6.3. ^{1}H-NMR spectra of 1-azaphenoxazine and 4-azaphenoxazine in d_6-DMSO at 25°C.

6.4 Conclusions

In summary, we have developed a successful strategy to synthesize 2,4-diazaphenothiazine and 2,4-diazaphenoxazine derivatives. Some previously reported syntheses of these compounds have been mischaracterized because of a favorable Smiles rearrangement. Reversing the polarity of the intramolecular cross-coupling reaction suppresses the rearrangement and allows for successful construction of the central oxazine or thiazine ring. 1,3-Diazaphenoxazine and diazaphenothiazine derivatives have mediocre reactivity as radical-trapping antioxidants, while the corresponding 2,4-diaza derivatives are some of the fastest RTAs ever reported, trapping peroxyl radicals at rates approaching diffusion. Given these results, we anticipate more detailed studies on the synthesis and properties of azaphenoxazine and phenothiazine derivatives as RTAs.

6.5 References

(1) Dumitriu, G.-M.; Bîcu, E.; Belei, D.; Rigo, B.; Dubois, J.; Farce, A.; Ghinet, A. *Bioorg. Med. Chem. Lett.* **2015**, *25*, 4447–4452.

(2) Prinz, H.; Chamasmani, B.; Vogel, K.; Böhm, K. J.; Aicher, B.; Gerlach, M.; Günther, E. G.; Amon, P.; Ivanov, I.; Müller, K. *J. Med. Chem.* **2011**, *54*, 4247–4263.

(3) Rajagopalan, R.; Lin, T.-S.; Karwa, A. S.; Poreddy, A. R.; Asmelash, B.; Dorshow, R. B. *ACS Med. Chem. Lett.* **2012**, *3*, 284–288.

(4) Ramprasad, J.; Nayak, N.; Dalimba, U. *Eur. J. Med. Chem.* **2015**, *106*, 75–84.

(5) Marcu, A.; Schurigt, U.; Müller, K.; Moll, H.; Krauth-Siegel, R. L.; Prinz, H. *Eur. J. Med. Chem.* **2016**, *108*, 436–443.

(6) Karlsson, K. M.; Jiang, X.; Eriksson, S. K.; Gabrielsson, E.; Rensmo, H.; Hagfeldt, A.; Sun, L. *Chem. - A Eur. J.* **2011**, *17*, 6415–6424.

(7) Tian, H.; Yang, X.; Chen, R.; Hagfeldt, A.; Sun, L. *Energy Environ. Sci.* **2009**, *2*, 674–677.

(8) Tian, H.; Yang, X.; Chen, R.; Pan, Y.; Li, L.; Hagfeldt, A.; Sun, L. *Chem. Commun.* **2007**, *353*, 3741.

(9) Salunke, J. K.; Wong, F. L.; Feron, K.; Manzhos, S.; Lo, M. F.; Shinde, D.; Patil, A.; Lee, C. S.; Roy, V. A. L.; Sonar, P.; Wadgaonkar, P. P. *J. Mater. Chem. C* **2016**, *4*, 1009–1018.

(10) Data, P.; Pander, P.; Okazaki, M.; Takeda, Y.; Minakata, S.; Monkman, A. P. *Angew. Chemie - Int. Ed.* **2016**, *55*, 5739–5744.

(11) Wu, K.; Zhang, T.; Zhan, L.; Zhong, C.; Gong, S.; Jiang, N.; Lu, Z.-H.; Yang, C. *Chem. - A Eur. J.* **2016**, *22*, 10860–10866.

(12) Martinez, V.; Henary, M. *Chem. - A Eur. J.* **2016**, *22*, 13764–13782.

(13) Yang, X.-B.; Yang, B.-X.; Ge, J.-F.; Xu, Y.-J.; Xu, Q.-F.; Liang, J.; Lu, J.-M. *Org. Lett.* **2011**, *13*, 2710–2713.

(14) Pearson, R. M.; Lim, C.-H.; McCarthy, B. G.; Musgrave, C. B.; Miyake, G. M. *J. Am. Chem.*

Soc. **2016**, *138*, 11399–11407.

(15) Murphy, C. M.; Saunders, C. E. *Pet. Refin.* **1947**, *26*, 479–484.

(16) Murphy, C. M.; Ravner, H.; Smith, N. L. *Ind. Eng. Chem.* **1950**, *42*, 2479–2489.

(17) West, H. L. *J. Inst. Pet.* **1948**, *34*, 774.

(18) Lucarini, M.; Pedrielli, P.; Pedulli, G. F.; Valgimigli, L.; Gigmes, D.; Tordo, P. *J. Am. Chem. Soc.* **1999**, *121*, 11546–11553.

(19) Ingold, K. U. *Chem. Rev.* **1961**, *61*, 563–589.

(20) Ingold, K. U.; Pratt, D. A. *Chem. Rev.* **2014**, *114*, 9022–9046.

(21) It is important to point out that historically azaphenothiazine and azophenoxazine nomenclature differed in the American/British and German systems, e.g. 1-azaphenothiazine in the American/British nomenclature was 4-azaphenothiazine in the German system. Thus, great care must be taken upon consideration of literature data where structures are not explicitly shown. Current IUPAC nomenclature for these compounds is based on the American/British system (Figure 6.1).

(22) Hanthorn, J.; Valgimigli, L.; Pratt, D. *J. Am. Chem. Soc.* **2012**, *134*, 8306–8309.

(23) Hanthorn, J.; Amorati, R.; Valgimigli, L.; Pratt, D. *J. Org. Chem.* **2012**, *77*, 6895–6907.

(24) Shah, R.; Haidasz, E. A.; Valgimigli, L.; Pratt, D. A. *J. Am. Chem. Soc.* **2015**, *137*, 2440–2443.

(25) Ito, Y.; Hamada, Y. *Chem. Pharm. Bull.* **1978**, *26*, 1375–1383.

(26) Okafor, C. O. *Int. J. Sulfur Chem. Part B Q. Reports Sulfur Chem.* **1971**, *6*, 237–265.

(27) Okafor, C. O. *Int. J. Sulfur Chem. Part B Q. Reports Sulfur Chem.* **1971**, *6*, 345–360.

(28) Takahashi, T.; Yoneda, F. *Chem. Pharm. Bull.* **1958**, *6*, 46–49.

(29) Takahashi, T.; Yoneda, F. *Chem. Pharm. Bull.* **1958**, *6*, 378–381.

(30) Petrow, V. A.; Rewald, E. L. *J. Chem. Soc.* **1945**, 313–315.

(31) Schuler, W. A.; Klebe, H. *Justus Liebigs Ann. Chem.* **1962**, *653*, 172–180.

(32) Pluta, K.; Morak-Młodawska, B.; Jeleń, M. *J. Heterocycl. Chem.* **2009**, *46*, 355–391.

(33) Many of the previous reports – and much of the original work – on azaphenothiazine and azaphenoxazine derivatives are described in patent literature. See Supporting Information for a series

of examples.

(34) Saggiomo, A. J.; Craig, P. N.; Gordon, M. *J. Org. Chem.* **1958**, *23*, 1906–1909.

(35) Nikpour, M.; Mousavian, M.; Davoodnejad, M.; Alimardani, M.; Sadeghian, H. *Med. Chem. Res.* **2013**, *22*, 5036–5043.

(36) Bakavoli, M.; Nikpour, M.; Rahimizadeh, M.; Saberi, M. R.; Sadeghian, H. *Bioorg. Med. Chem.* **2007**, *15*, 2120–2126.

(37) Bakavoli, M.; Sadeghian, H.; Tabatabaei, Z.; Rezaei, E.; Rahimizadeh, M.; Nikpour, M. *J. Mol. Model.* **2008**, *14*, 471–478.

(38) Pooryaghoobi, N.; Bakavoli, M.; Alimardani, M.; Bazzazan, T.; Sadeghian, H. *Iran. J. Basic Med. Sci.* **2013**, *16*, 784–789.

(39) Bonvicino, G. E.; Yogodzinski, L. H.; Hardy, R. A. *J. Org. Chem.* **1962**, *27*, 4272–4280.

(40) Truce, W. E.; Kreider, E. M.; Brand, W. W.; Truce, W. E.; Kreider, E. M.; Brand, W. W. In *Organic Reactions*; John Wiley & Sons, Inc.: Hoboken, NJ, USA, 2011; pp. 99–215.

(41) A similar strategy has been employed to synthesize mono-azaphenoxazines;[25] although the conditions for the cross-coupling are considerably harsher, they do not report isomerization in the final product.

(42) Haidasz, E. A.; Van Kessel, A. T. M.; Pratt, D. A. *J. Org. Chem.* **2016**, *81*, 737–744.

(43) PBD-BODIPY consumption is too slow in autoxidations of more conventional substrates (e.g. styrene, cumene) that are inhibited by *very* reactive RTAs such as phenoxazine, prompting us to select dioxane as a substrate since it also slows H-atom transfer from good H-bond donors (i.e. amines) because of complex formation, see refs. 44 and 45.

(44) Snelgrove, D. W.; Lusztyk, J.; Banks, J. T.; Mulder, P.; Ingold, K. U. *J. Am. Chem. Soc.* **2001**, *123*, 469–477.

(45) Litwinienko, G.; Ingold, K. U. *Acc. Chem. Res.* **2007**, *40*, 222–230.

(46) H-atom transfer from diarylamines takes place with log$A$ ~ 7.[23] Since achieving the transition state for H-atom transfer from the tricyclc compounds does not require restricting the rotation of the

two N-aryl bonds, the log*A* is expected to be ~1 log unit greater.

(47) Poulenc, R. Azaphénothiazines. FRD1170119, 1955.

(48) The characterization of initially reported derivatives was generally based on IR, elemental analysis, and melting point determination.[25,47]

(49) Hu, W.; Zhang, S. *J. Org. Chem.* **2015**, *80*, 6128–6132.

(50) Shen, C.; Wu, X.-F. *Catal. Sci. Technol.* **2015**, *5*, 4433–4443.

(51) It should be noted that although the original NMR characterization for these compounds is often incomplete, melting points for 1- and 4-azaphenoxazine and azaphenothiazine have been reported, and are consistent with those measured by our group.

6.6 Supporting Information

6.6.1 Additional Patents on Azaphenoxazines and Azaphenothiazines

Poulenc, R. FRD1170119 (1958)

Poulenc, R. GB791190 (1958)

Clarke, F. H. US3118884 (1964)

Aiko, I. JP39000493 (1964)

Clarke, F. H. Jr. US3389136 (1968)

Westermann, A.; Bub, O.; Suranyi, L. DE1110651 (1958)

Schuler, W. A. US 3427312 (1969)

6.6.2 General Experimental

Reagents were purchased from commercial suppliers and used without further purification. Column chromatography was carried out using flash silica gel (40−63 μm, 230−400 mesh). UV−vis spectra and kinetics were measured on a Cary 100 UV−vis spectrophotometer equipped with a temperature

controller unit and a thermostated 6 × 6 multicell holder. ^{1}H and ^{13}C NMR were recorded on a Bruker AVANCE spectrometer at 600 and 125 MHz, respectively, unless specified otherwise. High-resolution mass spectra were obtained on a Kratos Concept Tandem mass spectrometer.

6.6.3 Inhibited Co-autoxidations of PBD-BODIPY/Dioxane

The co-autoxidations were carried out according to our previously published methodology,[S1] substituting 1,4-dioxane for styrene. The propagation rate constant for PBD-BODIPY autoxidation under these conditions was measured using the same procedure previously reported, and found to be $k^{\text{Dioxane}}_{\text{PBD-BODIPY}}$ = 5312 $M^{-1}s^{-1}$. The H-bonding acidity parameter for compound **6.6**, was measured using Abrahams NMR method,[S2–S4] modified for the use of d_6-benzene as the NMR solvent. The value was found to be α_2^{H} = 0.44. The H-bond basicity of the solvent mixture was determined to be β_2^{H} = 0.35, from the method of Gurka and Taft.[S5]

Briefly, unstabilzed 1,4-dioxane (0.620 mL) was loaded into a 3 mL cuvette along with 1.82 mL of PhCl. The cuvette was placed into the thermostated sample holder of a UV−vis spectrophotometer and allowed to equilibrate to 37 °C. A small aliquot (12.5 μL) of a 2.0 mM solution of PBD-BODIPY in 1,2,4-trichlorobenzene was added, followed by 50 μL of 0.3 M solution of AIBN in PhCl, and the solution was thoroughly mixed. The absorbance at either 587 nm (ε = 123,023 $M^{-1}cm^{-1}$) was monitored for 10-20 min to ensure that the reaction was proceeding at a constant rate, after which 10 μL of a 500 μM solution of the test antioxidant was added. The solution was thoroughly mixed and the absorbance readings resumed.

6.6.4 Synthesis of Disulfide 6.7

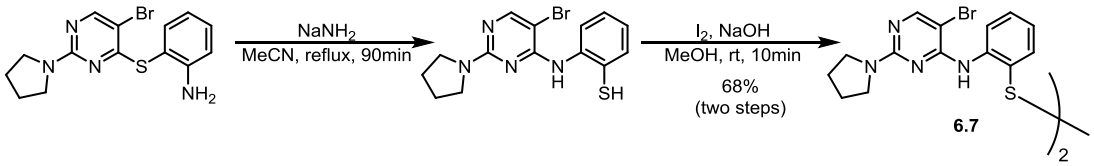

2-((5-Bromo-2-(Pyrrolidin-1-yl)pyrimidin-4-yl)amino)thiophenol and Disulfide (6.7). The procedure to produce the thiol was originally reported by Bakavoli *et. al.*[S6] Thus, 4-(2'-aminophenylthio)-5-bromo-2-(pyrrolidin-1-yl)pyrimidine [S6] (2.0 g, 5.7 mmol) and sodium amide (0.67 g, 17 mmol) were refluxed in dry MeCN under an inert atmosphere for 90 minutes. The solvent was evaporated under reduced pressure. The residue was dissolved in 20 ml H_2O, and AcOH was added dropwise until no more precipitate formed. The suspension was stirred for 10 minutes before the precipitate was filtered, washed with water, and then methanol. A small portion of the bright yellow solid was dried under high vacuum for crude NMR analysis (see Figure S6.1 for abridged spectrum). ^{1}H-NMR (400 MHz; $CDCl_3$): δ 8.58 (dd, *J* = 8.3, 1.3 Hz, 1H), 8.10 (d, *J* = 13.4 Hz, 2H), 7.54 (dd, *J* = 7.7, 1.5 Hz, 1H), 7.33-7.29 (m, 1H), 6.98 (td, *J* = 7.6, 1.3 Hz, 1H), 3.55 (t, *J* = 6.7 Hz, 4H), 2.00-1.97 (m, 4H).

Following the procedure of Bakavoli, [S6] the crude product could be recrystallized from EtOH/benzene. In this case the thiol could oxidize to form the disulfide. See below for the spectra of the mixture of compounds obtained from recrystallization. Instead, the crude product was suspended in 12 ml of MeOH and a 1M NaOH solution was added dropwise until the solid had dissolved. A solution of 0.74 g iodine (2.9 mmol) in 10 ml MeOH was added dropwise to the reaction until the colour from the iodine persisted, and no further precipitate formed. The residual iodine was quenched with a few drops of a saturated sodium thiosulfate solution. The precipitate was filtered, washed thoroughly with water, and then MeOH. The solid was dried under vacuum. Yield: 1.35 g of a light yellow solid, 68%. ^{1}H-NMR (600 MHz; $CDCl_3$): δ 8.61 (d, *J* = 8.4 Hz, 1H), 8.30 (s, 1H), 8.00 (s, 1H), 7.40 (d, *J* = 7.7 Hz, 1H), 7.33 (t, *J* = 7.8 Hz, 1H), 6.89 (t, *J* = 7.5 Hz, 1H), 3.54-3.46 (m,

4H), 2.01-1.96 (m, 4H). ^{13}C NMR (151 MHz; $CDCl_3$): δ 158.5, 156.8, 154.9, 141.1, 136.8, 131.5, 123.7, 122.6, 120.3, 92.6, 46.8 (br), 25.5 (br). HRMS(ESI+) calcd for $C_{28}H_{29}Br_2N_8S_2^+$ ($M+H^+$) 701.0297; found, 701.0306.

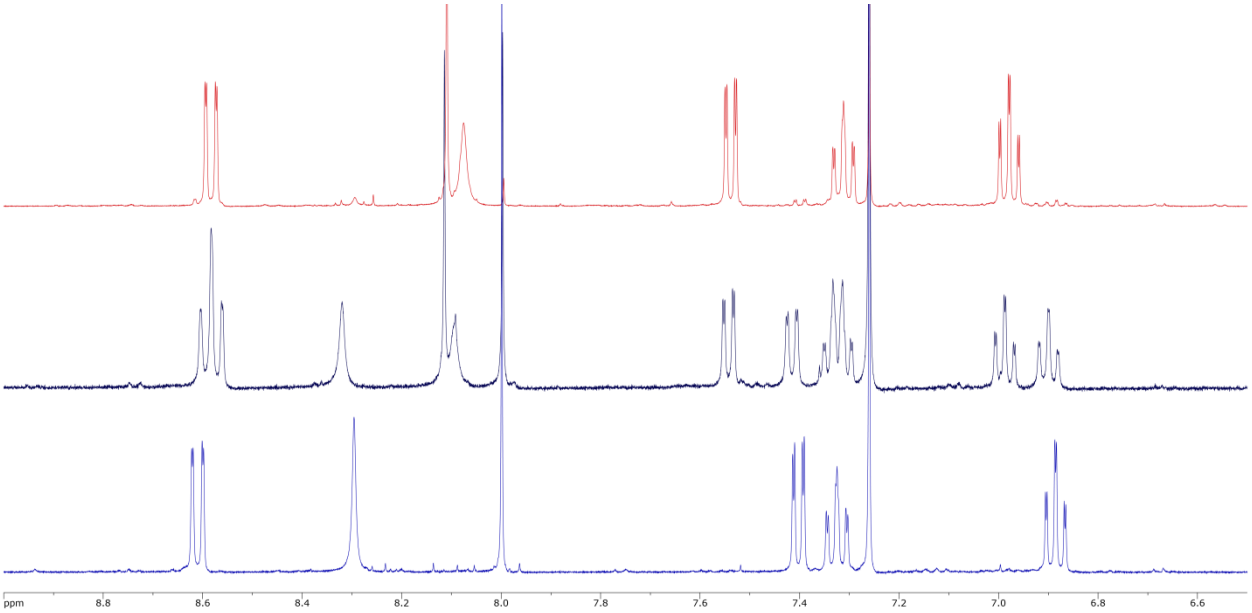

Figure S6.1. NMR spectra of crude thiol (red), the mixture obtained upon recrystallization of the thiol (black), and authentically prepared disulfide (blue).

6.6.5 Synthesis of 6.6 and 6.16

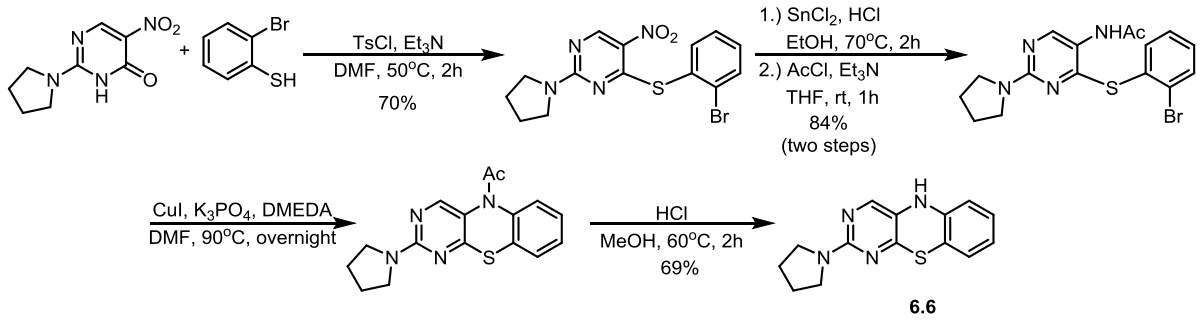

4-(2'-Bromophenylthio)-5-nitro-2-(pyrrolidin-1-yl)pyrimidine. *p*-Toluenesulfonyl chloride (1.4 g, 7.6 mmol) was added to a solution of 5-nitro-2-(pyrrolidin-1-yl)-4(3H)-pyrimidinone (1.6 g, 7.6 mmol) and triethylamine (2.5 ml, 18 mmol) in 38 ml MeCN under an inert atmosphere. The reaction

was stirred for 1h at 50 °C. The reaction was judged complete by TLC. The reaction was cooled to room temperature, and 2-bromothiophenol (0.92 ml, 7.6 mmol) was added to the reaction. The reaction was stirred for 1h at ambient temperature. The reaction mixture was poured in to 120 ml H_2O and stirred 10 minutes. The precipitate was filtered, washed with H_2O, and dried. The crude product was recrystallized from EtOAc/hexanes. Yield: 2.04 g of a yellow solid, 70%. ^{1}H-NMR (600 MHz; DMSO-d_6): δ 9.08 (s, 1H), 7.86 (dd, *J* = 7.8, 1.5 Hz, 1H), 7.73 (dd, *J* = 7.5, 1.8 Hz, 1H), 7.53-7.47 (m, 2H), 3.52 (t, *J* = 6.9 Hz, 2H), 2.87 (t, *J* = 6.9 Hz, 2H), 1.86 (quintet, *J* = 6.8 Hz, 2H), 1.76 (quintet, *J* = 6.9 Hz, 2H). 13-C NMR (151 MHz; DMSO): δ 166.5, 157.13, 157.00, 138.6, 133.6, 132.6, 131.3, 130.5, 130.2, 129.0, 47.4, 47.1, 25.2, 24.8 HRMS(EI) m/z: calcd $C_{14}H_{13}BrN_4O_2S$, 379.9942; found, 379.9953.

5-Acetamido-4-(2'-bromophenylthio)-2-(pyrrolidin-1-yl)pyrimidine. 4-(2'-Bromophenylthio)-5-nitro-2-(pyrrolidin-1-yl)pyrimidine (2.0 g, 5.3 mmol) and tin (II) chloride (4.06 g, 21.3 mmol) were dissolved in a mixture of 20 ml EtOH and 5 ml H_2O. $HCl_{(conc)}$ (3.7 ml) was added slowly to the reaction. The reaction was heated to 50°C for 2h, after which the reaction was judged complete by TLC. The reaction was poured into 1M NaOH and extracted twice with EtOAC. The organic phase was washed with H_2O, then brine. It was dried with $MgSO_4$, filtered, and evaporated under vacuum. [Note: The product is highly oxidizable and should be stored under vacuum or an inert atmosphere if kept for extended periods.] The crude material was dissolved in 25 ml of dry diethylether and acetic anhydride (1.0 ml, 10.6 mmol) was added. The reaction was stirred for 2h at room temperature. The precipitate was filtered, washed with 10% Et_2O/petroleum ether, and dried under s stream of air. Yield: 1.74 g of an off white solid, 84%. The material could be recrystallized from EtOAc/hexanes. ^{1}H-NMR (600 MHz; DMSO-d_6): δ 9.48 (s, 1H), 7.94 (s, 1H), 7.80 (dd, *J* = 7.9, 1.4 Hz, 1H), 7.66 (dd, *J* = 7.7, 1.7 Hz, 1H), 7.46 (td, *J* = 7.5, 1.5 Hz, 1H), 7.41 (td, *J* = 7.7, 1.8 Hz, 1H), 3.36 (s, 3H), 2.89 (s, 2H), 1.78 (s, 5H). 13-C NMR (151 MHz; DMSO): δ 169.9, 164.7, 157.7, 155.7, 138.6,

133.5, 131.8, 131.0, 130.1, 128.6, 118.2, 46.4 (br), 25.3 (br), 23.1 HRMS(EI) m/z: calcd $C_{16}H_{17}BrN_4O_1S$, 392.0306; found, 392.0298.

3-(Pyrrolidin-1-yl)-2,4-diazaphenothiazine (6.6). 5-Acetamido-4-(2'-bromophenylthio)-2-(pyrrolidin-1-yl)pyrimidine (1.56 g, 4.0 mmol), copper (I) iodide (0.15 g, 0.8 mmol), DMEDA (86 μL, 0.8 mmol), and potassium *tert*-butoxide (0.63 , 0.56 mmol) were added to 20 ml of dry DMF under an inert atmosphere. The reaction was stirred at 100°C overnight. The reaction was poured into water and extracted three times with EtOAC. The organic phase was washed twice with water, then once with brine. It was dried with $MgSO_4$, and filtered through a plug of silica gel. The filtrate was concentrated under vacuum. The dark oily solid was dissolved in 40 ml MeOH with 4 ml of concentrated HCl. The reaction was heated to 60 °C for 90 minutes, and the reaction was judged complete by TLC. The reaction was diluted with EtOAc, and extracted twice with 1M NaOH, then once with brine. The organic phase was dried with $MgSO_4$, filtered, and evaporated. The residue was dissolved in 50% EtOAc/hexanes, and filtered through a plug of silica. The filtrate was evaporated under vacuum. The material was recrystallized (under an inert atmosphere) from EtOAc/hexanes. Yield: 0.74 g of a yellow fluffy solid, 69%. ^{1}H-NMR (600 MHz; DMSO-d_6): δ 8.20 (s, 1H), 7.55 (s, 1H), 6.96-6.94 (m, 1H), 6.86 (dd, *J* = 7.7, 1.4 Hz, 1H), 6.67 (td, *J* = 7.5, 1.2 Hz, 1H), 6.58 (dd, *J* = 8.0, 1.2 Hz, 1H), 3.36-3.34 (m, 4H), 1.88-1.86 (m, 4H). 13-C NMR (151 MHz; DMSO): δ 156.1, 152.1, 140.7, 140.4, 128.0, 126.6, 125.4, 120.7, 114.3, 114.0, 46.4, 25.0 HRMS(EI) m/z: calcd $C_{14}H_{14}N_4S$, 270.0939; found, 270.0665.

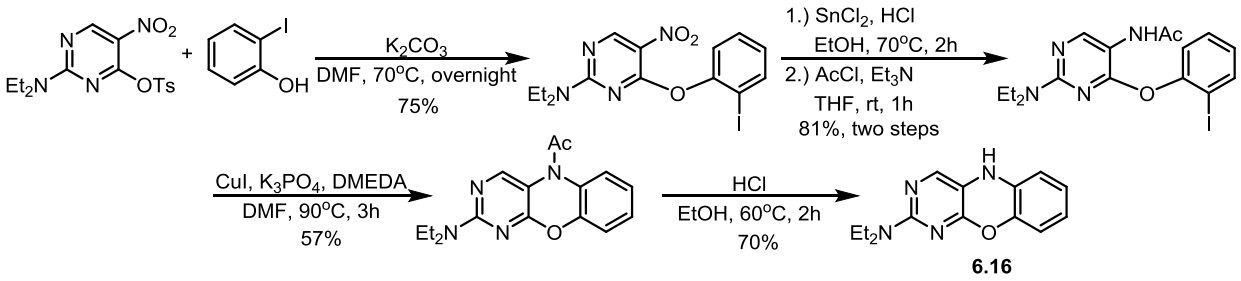

6.16

2-Diethylamino-4-(2'-iodophenoxy)-5-nitropyrimidine. (2-Diethylamino-5-nitropyrimidin-4-yl) *p*-toluenesulfonate (9.0 g, 24 mmol), 2-iodophenol (5.4 g, 24 mmol), and potassium carbonate (3.4 g, 24 mmol), were added to 60 ml of dry DMF under an inert atmosphere. The reaction was heated to 70°C, overnight. The reaction was poured into water, and extracted three times with diethylether. The organic phase was washed with water, and then once with brine. It was then dried with $MgSO_4$, filtered, and evaporated under vacuum. The residue was recrystallized from EtOAc/hexanes. Yield: 7.4 g of a yellow solid, 75%. ^{1}H-NMR (600 MHz; DMSO-d_6): δ 9.16 (s, 1H), 7.94 (dd, *J* = 7.9, 1.4 Hz, 1H), 7.51 (ddd, *J* = 8.1, 7.4, 1.5 Hz, 1H), 7.37 (dd, *J* = 8.1, 1.4 Hz, 1H), 7.12 (ddd, *J* = 7.9, 7.4, 1.5 Hz, 1H), 3.63 (q, *J* = 7.1 Hz, 2H), 3.11 (q, *J* = 7.0 Hz, 2H), 1.11 (t, *J* = 7.1 Hz, 3H), 0.78 (t, *J* = 7.0 Hz, 3H). 13-C NMR (151 MHz; DMSO): δ 161.6, 160.0, 159.2, 152.6, 139.5, 130.1, 128.5, 124.0, 122.6, 92.1, 43.4, 43.0, 13.3, 12.7 HRMS(EI) m/z: calcd $C_{14}H_{15}IN_4O_3$, 414.0189, found, 414.0197.

5-Acetamido-2-diethylamino-4-(2'-iodophenoxy)pyrimidine. 2-Diethylamino-4-(2'-iodophenoxy)-5-nitropyrimidine (1.0 g, 2.4 mmol) and tin (II) chloride (1.4g, 7.2 mmol) were dissolved in a mixture of 6 ml EtOH and 1.5 ml H_2O. 1.25 ml of $HCl_{(conc)}$ was added slowly to the reaction. The reaction was strred at room temperature for 3h, after which the reaction was judged complete by TLC. The reaction was poured into 1M NaOH and extracted three times with Et_2O. The organic phase was washed with H_2O, then brine. It was dried with $MgSO_4$, filtered, and evaporated under

vacuum. [Note: The product is highly oxidizable and should be stored under vacuum or an inert atmosphere if kept for extended periods.] The crude material was dissolved in 5 ml of dry THF and acetic anhydride (0.25 ml, 2.6 mmol) was added. The reaction was stirred overnight at room temperature. The solvent was evaporated, and the residue partitioned between EtOAc and water. The organic phase was washed with water, and then once with brine, dried with $MgSO_4$, and filtered through a plug of silica. The solvent was removed under vacuum. Yield: 0.83 g of a white solid, 81%. The material could be recrystallized from EtOAc/hexanes. ^{1}H-NMR (600 MHz; DMSO-d_6): δ 9.42 (s, 1H), 8.41 (s, 1H), 7.91 (dd, *J* = 7.9, 1.5 Hz, 1H), 7.46 (ddd, *J* = 8.0, 7.4, 1.6 Hz, 1H), 7.21 (dd, *J* = 8.1, 1.4 Hz, 1H), 7.06 (ddd, *J* = 7.8, 7.4, 1.5 Hz, 1H), 3.28 (br, 4H), 0.91 (br, 6H). 13-C NMR (151 MHz; DMSO): δ 169.3, 161.9, 157.7, 155.7, 153.3, 139.4, 129.9, 127.8, 124.0, 109.3, 92.7, 42.1, 23.4, 13.3 HRMS(EI) m/z: calcd $C_{16}H_{19}IN_4O_2$, 426.0552; found, 426.0594.

10-Acetyl-3-diethylamino-24-diazaphenoxazine. 5-Acetamido-2-diethylamino-4-(2'-iodophenoxy) pyrimidine (0.60 g, 1.4 mmol), copper (I) iodide (0.27 g, 1.4 mmol), DMEDA (0.15 ml, 1.4 mmol), and potassium *tert*-butoxide (0.22 g, 1.4 mmol) were added to 10 ml of dry DMF under an inert atmosphere. The reaction was stirred at 90°C for 3h. The reaction was poured into water and extracted twice with EtOAC. The organic phase was washed twice with water, then once with brine. It was dried with $MgSO_4$, and filtered through a plug of silica gel. The filtrate was concentrated under vacuum. The material was recrystallized from EtOAc/hexanes. Yield: 0.24 g of a brown solid, 57%. ^{1}H-NMR (600 MHz; DMSO-d_6): δ 8.50 (s, 1H), 7.64-7.63 (m, 1H), 7.31-7.28 (m, 2H), 7.23 (ddd, *J* = 8.0, 6.5, 2.4 Hz, 1H), 3.56 (s, 4H), 2.27 (br, 3H), 1.13 (t, *J* = 7.0 Hz, 6H). 13-C NMR (151 MHz; DMSO): δ 169.7, 162.7, 158.4, 154.5, 148.0, 128.9, 127.5, 125.5, 124.8, 117.7, 110.8, 42.1, 22.8, 13.4 HRMS(EI) m/z: calcd $C_{16}H_{18}N_4O_2$, 298.1430; found, 298.1462

3-Diethylamino-2,4-diazaphenoxazine (6.16). 10-acetyl-3-diethylamino-24-diazaphenoxazine (0.24 g, 0.80 mmol), was dissolved in 1.6 ml EtOH. $HCl_{(conc)}$ (0.40 ml) was added to the solution. The reaction was stirred at 60 °C for 2h, after which the reaction was judged complete by TLC. The

reaction was quenched by slow addition of sat. $NaHCO_{3(aq)}$, followed by 10 ml of water. The precipitate was filtered, washed with water, and dried under s stream of air. The solid was recrystallized from EtOAc/hexanes (under an inert atmosphere). Yield: brown solid, 70%. ^{1}H-NMR (500 MHz; DMSO-d_6): δ 8.01 (s, 1H), 7.47 (s, 1H), 6.80-6.74 (m, 2H), 6.56 (td, *J* = 7.7, 1.3 Hz, 1H), 6.47 (dd, *J* = 7.8, 1.3 Hz, 1H), 3.43 (q, *J* = 7.0 Hz, 4H), 1.06 (t, *J* = 7.0 Hz, 6H). 13-C NMR (126 MHz; DMSO): δ 158.0, 156.3, 141.7, 140.8, 132.6, 125.5, 119.9, 116.4, 115.8, 114.0, 41.7, 13.6 HRMS(EI) m/z: calcd $C_{14}H_{16}N_4O$, 256.1324; found, 256.1329.

6.6.6 Synthesis of 6.10 and 6.15

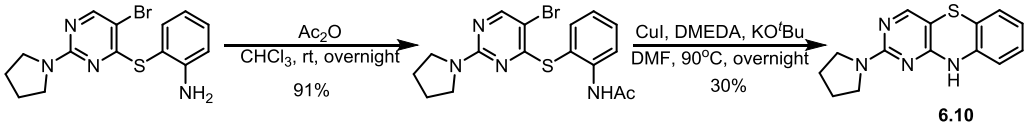

4-(2'-Acetamidophenylthio)-5-bromo-2-(pyrrolidin-1-yl)pyrimidine. 4-(2'-Aminophenylthio)-5-Bromo-2-(Pyrrolidin-1-yl)pyrimidine[6] (1.5 g, 4.3 mmol) and acetic anhydride (0.42 ml, 4.4 mmol) were added to 9 ml of $CHCl_3$, under an inert atmosphere. The reaction was stirred overnight, before it was diluted with CH_2Cl_2 and extracted with $NaHCO_{3(sat.)}$. The organic phase was dried with $MgSO_4$, filtered, and evaporated. The residual solid was dried under vacuum. Yield: 1.54 g of a white solid, 91%. ^{1}H-NMR (600 MHz; DMSO-d_6): δ 9.35 (s, 1H), 8.19 (s, 1H), 7.73 (d, *J* = 7.9 Hz, 1H), 7.55 (dd, *J* = 7.7, 1.3 Hz, 1H), 7.49 (td, *J* = 7.7, 1.2 Hz, 1H), 7.22 (t, *J* = 7.4 Hz, 1H), 3.37-3.27 (br, 2H), 2.81 (br, 2H), 2.00 (s, 3H), 1.76 (br, *J* = 51.6 Hz, 4H). 13-C NMR (151 MHz; DMSO): δ 169.0, 166.9, 157.7, 157.3, 141.5, 138.0, 130.9, 125.43, 125.41, 125.26, 102.3, 46.6, 46.4, 25.4, 25.1, 23.9 HRMS(EI) m/z: calcd $C_{16}H_{17}BrN_4OS$, 392.0306, found, 392.0323.

2-(Pyrrolidin-1-yl)-1,3-diazaphenothiazine (6.10). 4-(2'-acetamidophenylthio)-5-bromo-2-(pyrrolidin-1-yl)pyrimidine (0.24 g, 0.68 mmol), copper (I) iodide (26 mg, 0.14 mmol), DMEDA

(15 µl, 0.14 mmol), and potassium *tert*-butoxide (0.11 g, 0.95 mmol), were added to 2 ml dry DMF, under an inert atmosphere. The reaction was stirred at 90°C for overnight. The reaction was poured into water, and extracted twice with EtOAc. The organic phases were combined, and washed with water and once with brine. The solution was dried with $MgSO_4$, and filtered through a plug of silica gel. The material was purified by column chromatography with 40-70% Et_2O/pet. ether. Yield: 55 mg of a light yellow solid, 30%. The material could be recrystallized from EtOAc/hexanes. ^{1}H-NMR (400 MHz; DMSO-d_6): δ 9.45 (s, 1H), 7.63 (s, 1H), 7.02-6.97 (m, 1H), 6.92 (m, *J* = 1.2 Hz, 2H), 6.82 (td, *J* = 7.5, 1.2 Hz, 1H), 3.41 (m, 4H), 1.90-1.86 (m, 4H). 13-C NMR (76 MHz; DMSO): δ 159.4, 158.9, 152.1, 139.5, 127.7, 126.5, 123.6, 117.2, 116.4, 95.4, 46.8, 25.4 HRMS(EI) m/z: calcd $C_{14}H_{14}N_4S$, 270.0939; found, 270.0947.

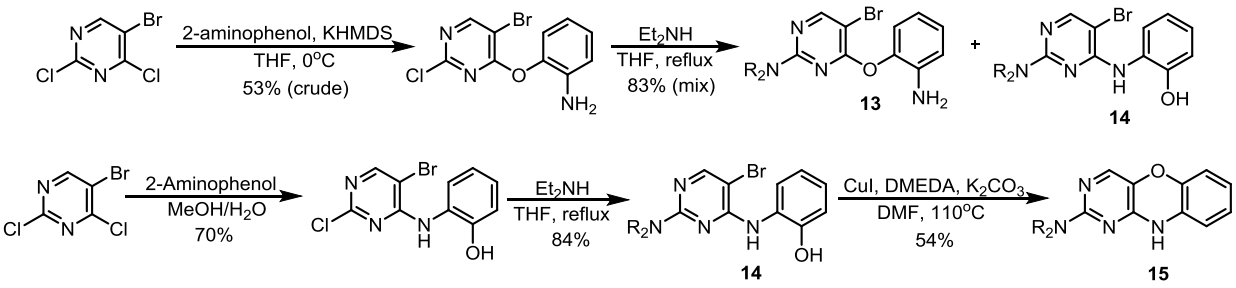

4-(2'-Aminophenoxy)-5-bromo-2-chloropyrimidine. A 1M KHMDS solution the THF(2.3 ml, 2.3 mmol), was added dropwise to a cooled solution of 2-aminophenol (0.25 g, 2.3 mmol) in 11 ml of dry THF, under an inert atmosphere. The solution was stirred for 10 minutes at 0°C. This solution was added dropwise to a solution of 5-bromo-2,4-dichloropyrimdiine (0.50 g, 2.2 mmol) in 11 ml dry THF at 0 °C, under an inert atmosphere. The reaction was allowed to stir for 2h. The reaction was poured into water and extracted twice with EtOAc. The organic layers were combined, washed with brine, and dried with $MgSO_4$. The solution was filtered, and concentrated under reduced pressure. The solid was washed thoroughly with hexanes, and dried under a stream of air. Crude

Yield: 0.35 g of a light brown powdery solid, 53%. See NMR section for full spectra. Crude ^{1}H-NMR (400 MHz; DMSO-d_6): δ 8.83 (s, 1H), 7.04-6.96 (m, 2H), 6.81 (dd, *J* = 8.0, 1.5 Hz, 1H), 6.58 (ddd, *J* = 8.0, 7.3, 1.5 Hz, 1H), 5.07 (s, 2H). Upon recrystallization of the material from EtOAc/hexanes approximately 10% of the material underwent a Smiles rearrangement to 4-((2'-hydroxyphenyl)amino)-5-bromo-4-chloropyrimidine. See NMR section for ^{1}H spectrum of mixture.

4-(2'-Aminophenoxy)-5-bromo-2-diethylaminopyrimidine (6.13). The crude 4-(2'-aminophenoxy)-5-bromo-2-chloropyrimidine (0.25 g, 0.83 mmol) and diethylamine (0.70 ml, 6.6 mmol), were refluxed in THF overnight. The solvent was evaporated, and the residue was diluted with EtOAc. The solution was washed twice with water and once with brine, dried with $MgSO_4$, and filtered through a short plug of silica. The filtrate was evaporated under reduced pressure. Crude ^{1}H NMR revealed a nearly 1:1 mixture of **6.13** and diarylamine **6.14**. See NMR section for complete spectra.

Note: Due to the favourability of the Smiles rearrangement, the diarylether derivatives were difficult to prepare and isolate in high yield and without contamination by the rearranged (diarylamine) product. In an attempt to prepare diazaphenoxazine **6.15** using a more practical synthetic route, we instead intentionally prepared the diarylamine derivatives as precursors to **6.15**.

4-((2'-Hydroxyphenyl)amino)-5-bromo-2-chloropyrimidine. 5-Bromo-2,4-dichloropyrimidine (0.50 g, 2.2 mmol) and 2-aminophenol (0.36 g, 3.3 mmol) were added to a mixture of 4.0 ml of MeOH and 2.0 ml H_2O. The reaction was stirred at room temperature for 2h. The reaction was diluted with 10 ml of H_2O, and acidified by dropwise addition of conc. $HCl_{(aq)}$. The precipitate was filtered, washed with water, and allowed to dry under a stream of air. Yield: 0.46 g of a brownish solid, 70%. ^{1}H-NMR (600 MHz; DMSO-d_6): δ 10.10 (s, 1H), 8.63 (s, 1H), 8.45 (s, 1H), 7.75 (d, *J* = 7.9 Hz, 1H), 7.07 (t, *J* = 7.1 Hz, 1H), 6.95 (d, *J* = 7.2 Hz, 1H), 6.87 (t, *J* = 7.6 Hz, 1H). 13-C NMR (151 MHz; DMSO): δ 158.34, 158.22, 158.0, 150.0, 126.5, 125.6, 124.2, 119.6, 115.8, 104.2 HRMS(EI) m/z: calcd $C_{10}H_7BrClN_3O$, 298.9461; found, 298.9490.

4-((2'-Hydroxyphenyl)amino)-5-bromo-2-diethylaminopyrimidine (6.14). 4-((2'-Hydroxyphenyl)-amino)-5-bromo-4-chloropyrimidine (1.85 g, 6.1 mmol) and diethylamine (3.8 ml, 37 mmol) were refluxed overnight in THF, under an inert atmosphere. The solvent was evaporated under reduced pressure. The residue was diluted with water, and extracted twice with EtOAc. The organic phases were combined, washed with brine, and dried with $MgSO_4$. The solution was filtered, and concentrated under vacuum. The material was recrystallized from EtOAC/hexanes. Yield: 1.73 g of a brown solid (84%). ^{1}H-NMR (600 MHz; DMSO-d_6): δ 10.24 (s, 1H), 8.31 (dd, *J* = 8.0, 1.5 Hz, 1H), 8.11 (s, 1H), 7.85 (s, 1H), 6.90 (dtd, *J* = 15.5, 7.8, 1.6 Hz, 2H), 6.82 (td, *J* = 7.6, 1.6 Hz, 1H), 3.53 (q, *J* = 7.0 Hz, 4H), 1.13 (t, *J* = 6.7 Hz, 6H). 13-C NMR (151 MHz; DMSO): δ 159.5, 157.2, 155.5, 146.9, 127.7, 123.3, 119.7, 119.5, 114.9, 91.6, 42.3 (br), 13.4 (br) HRMS(EI) m/z: calcd $C_{14}H_{17}BrN_4O$, 336.0585; found, 336.0592.

2-Diethylamino-1,3-diazpahenoxazine (6.15). 4-((2'-Hydroxyphenyl)amino)-5-bromo-2-diethyl-aminopyrimidine **14** (1.2g, 3.5 mmol), copper (I) iodide (0.13 g, 0.7 mmol), DMEDA (76 μl, 0.7 mmol), and potassium *tert*butoxide (0.69 g, 5.0 mmol) were added to 12 ml of dry DMF under an inert atmosphere. The reaction was heated to 90 °C, overnight. The reaction was poured into water and extracted twice with EtOAc. The organic phases were combined, washed twice with water and once with brine. The solution was dried with $MgSO_4$, filtered, and concentrated under reduced pressure. The crude material was purified via silica gel chromatography with 25% EtOAc/hexanes. Yield: 0.48 g of a white solid, 54%. ^{1}H-NMR (400 MHz; DMSO-d_6): δ 9.39 (s, 1H), 7.46 (d, *J* = 0.7 Hz, 1H), 6.77 (td, *J* = 7.4, 1.7 Hz, 1H), 6.72-6.65 (m, 3H), 3.45 (q, *J* = 7.0 Hz, 4H), 1.07 (t, *J* = 7.0 Hz, 6H). 13-C NMR (151 MHz; DMSO): δ 156.8, 151.1, 143.2, 139.1, 129.46, 129.26, 123.4, 122.3, 115.09, 114.89, 41.2, 13.3 HRMS(EI) m/z: calcd $C_{14}H_{16}N_4O$, 256.1324; found, 256.1353.

6.6.7 Synthesis of 4-Azaphenoxazine and 1-Azaphenoxazine

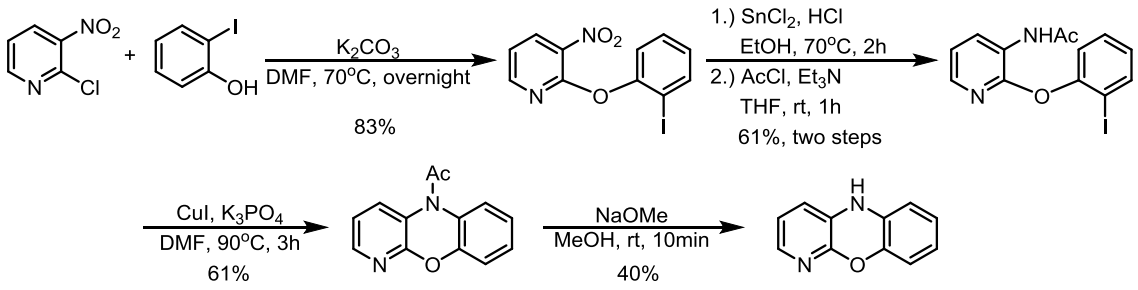

2-(2'-Iodophenoxy)-3-nitropyridine. 2-Chloro-3-nitropyridine (4.9 g, 31 mmol), 2-iodophenol (6.8 g, 31 mmol), and potassium carbonate (4.7 g 34 mmol), were added to 60 ml of dry DMF under an inert atmosphere. The reaction was stirred at 60 °C for 3h. The reaction was poured slowly into 400 ml of water, and stirred for 20 minutes. The precipitate was filtered, washed with water, and dried under a stream of air. Yield: 8.8 g of a yellow solid, 83%. The material can be recrystallized from EtOAc/hexanes. ^{1}H-NMR (600 MHz; DMSO-d_6): δ 8.64 (dd, *J* = 8.0, 1.7 Hz, 1H), 8.42 (dd, *J* = 4.8, 1.7 Hz, 1H), 7.93 (dd, *J* = 7.9, 1.5 Hz, 1H), 7.50 (ddd, *J* = 8.1, 7.4, 1.6 Hz, 1H), 7.42 (dd, *J* = 8.0, 4.8 Hz, 1H), 7.35 (dd, *J* = 8.1, 1.4 Hz, 1H), 7.11 (ddd, *J* = 7.8, 7.4, 1.5 Hz, 1H). 13-C NMR (151 MHz; DMSO): δ 154.5, 153.1, 152.5, 139.9, 136.7, 134.6, 130.4, 128.3, 124.2, 120.1, 92.1 HRMS(EI) m/z: calcd $C_{11}H_7IN_2O_3$, 341.9501; found, 341.9540.

3-Amino-2-(2'-iodophenoxy)pyridine. 2-(2'-Iodophenoxy)-3-nitropyridine (8.8 g, 25 mmol) and tin (II) chloride (19 g, 100 mmol) were dissolved in a mixture of 65 ml EtOH, and 12 ml water to which 17 ml of conc. $HCl_{(aq)}$ (200 mmol) was added slowly. The reaction was heated to reflux for 4h. Potassium carbonate was added until the reaction was neutral, and the solvent was evaporated under reduced pressure. 100 ml of benzene was added to the reaction, and the mixture heated to reflux, and stirred vigorously for 20 minutes. The organic phase of the reaction was decanted, and filtered to remove residual solids. The solvent was evaporated under reduced pressure. Yield: 5.9 g of a light pink solid, 73%. For analytical purposes, the material could be recrystallized from EtOAC/hexanes (under an inert atmosphere). ^{1}H-NMR (600 MHz; DMSO-d_6): δ 7.88 (dd, *J* = 7.9, 1.4 Hz, 1H), 7.43-

7.40 (m, 1H), 7.24 (dd, *J* = 4.8, 1.4 Hz, 1H), 7.12 (dd, *J* = 8.1, 1.3 Hz, 1H), 7.06 (dd, *J* = 7.6, 1.3 Hz, 1H), 7.00 (td, *J* = 7.6, 1.3 Hz, 1H), 6.85 (dd, *J* = 7.6, 4.8 Hz, 1H), 5.24 (br, 2H). 13-C NMR (151 MHz; DMSO): δ 154.6, 150.7, 139.5, 133.8, 132.9, 130.0, 126.8, 123.5, 121.3, 120.2, 92.3 HRMS(EI) calcd $C_{11}H_9IN_2O$, 311.9759; found, 311.9764.

3-Acetamido-2-(2'-iodophenoxy)pyridine. 3-amino-2-(2'-iodophenoxy)pyridine (1.0 g, 3.2 mmol), acetyl chloride (0.35 ml, 4.8 mmol), and triethylamine (0.83 ml, 6.0 mmol), were added to 12 ml of dry THF, under an inert atmosphere. The reaction was stirred at room temperature for 1h. The reaction was judged complete by TLC, and the mixture was poured into 50 ml DCM, and washed twice with water, and once with brine. The organic layer was dried with $MgSO_4$, filtered, and the solvent was removed under reduced pressure. The solid was recrystallized from benzene. Yield: 0.86 g, of a fluffy white solid, 76%. ^{1}H-NMR (600 MHz; DMSO-d_6): δ 9.76 (s, 1H), 8.50 (d, *J* = 7.1 Hz, 1H), 7.91 (dd, *J* = 7.9, 1.5 Hz, 1H), 7.74 (dd, *J* = 4.8, 1.5 Hz, 1H), 7.47-7.45 (m, 1H), 7.22 (dd, *J* = 8.0, 1.4 Hz, 1H), 7.09 (dd, *J* = 7.9, 4.8 Hz, 1H), 7.05 (td, *J* = 7.6, 1.4 Hz, 1H), 2.19 (s, 3H). 13-C NMR (151 MHz; DMSO): δ 170.0, 154.2, 153.1, 140.9, 139.7, 130.4, 130.1, 127.5, 124.3, 123.7, 119.4, 92.9, 24.3 HRMS(EI) m/z: calcd $C_{13}H_{11}IN_2O_2$, 353.9865; found, 353.9834.

10-Acetyl-4-azaphenoxazine. 3-Acetamido-2-(2'-Iodophenoxy)pyridine (0.40 g, 1.1 mmol), copper (I) iodide (0.11 g, 0.60 mmol), and potassium phosphate, tribasic (0.47 g, 2.2 mmol), were added to 8 ml of dry DMF, under an inert atmosphere. The mixture was heated to 90 °C for 3h, when it was judged to be complete by TLC. The mixture was poured into water, and extracted trice with EtOAc. The organic phase was washed with water, and then brine, dried with $MgSO_4$, filtered and concentrated under reduced pressure. The crude material was purified by silica gel chromatography, with 40% EtOAC/hexanes (+ 1% triethylamine). Yield: 0.15 g of a beige solid, 61%. ^{1}H-NMR (600 MHz; DMSO-d_6): δ 8.13 (dd, *J* = 4.8, 1.7 Hz, 1H), 8.07 (dd, *J* = 7.8, 1.7 Hz, 1H), 7.64-7.63 (m, 1H), 7.31-7.29 (m, 3H), 7.24 (ddd, *J* = 8.0, 6.2, 2.6 Hz, 1H), 2.29 (s, 3H). 13-C NMR (151 MHz; DMSO):

δ 169.7, 156.4, 149.3, 145.0, 134.8, 128.8, 127.8, 125.5, 124.6, 123.9, 120.9, 117.6, 23.1 HRMS(EI) m/z: calcd $C_{13}H_{10}N_2O_2$, 226.0742; found, 226.0708.

4-Azaphenoxazine. 10-Acetyl-4-Azaphenoxazine (0.16 g, 0.72 mmol), was added to 5 ml of a freshly prepared solution of sodium methoxide in MeOH (0.6 M). The reaction was stirred for 15 minutes under an inert atmosphere. The precipitate was filtered, washed with water, and dried under vacuum. The solid was recrystallized from benzene. Yield: 54 mg of a grey solid, 40%. ^{1}H-NMR (500 MHz; DMSO-d_6): δ 8.47 (s, 1H), 7.36 (dd, *J* = 4.8, 1.8 Hz, 1H), 6.78-6.72 (m, 3H), 6.68 (dd, *J* = 7.9, 1.4 Hz, 1H), 6.61 (td, *J* = 7.7, 1.4 Hz, 1H), 6.47 (dd, *J* = 7.7, 1.4 Hz, 1H). 13-C NMR (126 MHz; DMSO): δ 150.8, 143.2, 137.6, 131.7, 128.6, 124.9, 121.33, 121.17, 119.8, 116.0, 113.7 HRMS(EI) m/z: calcd $C_{11}H_8N_2O$, 184.0636; found, 184.0636.

1-Azaphenoxazine. This procedure, reported by Shen and coworkers [S7] for the synthesis of for the synthesis of 4-azaphenoxazine, was found instead to produce 1-aza derivatives. 2-Aminophenol (1.09 g, 10.0 mmol), 3-bromo-2-chloropyridine (1.93 g, 10.0 mmol), and cesium carbonate (3.25 g, 10 mmol), were added to 40 ml of DMSO under an inert atmosphere. The reaction was heated to 120 °C overnight. The reaction was diluted with acetone, and silica gel was added. The solvent was evaporated under vacuum. The residue was dry-loaded onto a silica gel column. The product was purified by silica gel chromatography using 40-100% EtOAC/hexanes for the mobile phase. Yield: 0.35 g of a pinkish solid, 19%. ^{1}H-NMR (500 MHz; DMSO-d_6): δ 9.01 (s, 1H), 7.53 (dd, *J* = 5.0, 1.4 Hz, 1H), 6.90-6.88 (m, 1H), 6.76 (ddd, *J* = 7.7, 6.9, 2.0 Hz, 1H), 6.65-6.61 (m, 2H), 6.59-6.54 (m, 2H). 13-C NMR (126 MHz; DMSO): δ 146.0, 142.3, 141.7, 139.0, 131.3, 124.2, 121.3, 120.6, 116.5, 115.0, 114.1 HRMS(EI) m/z: calcd $C_{11}H_8N_2O$, 184.0636; found, 184.0651.

6.6.8 Synthesis of Pyrimidine Precursors

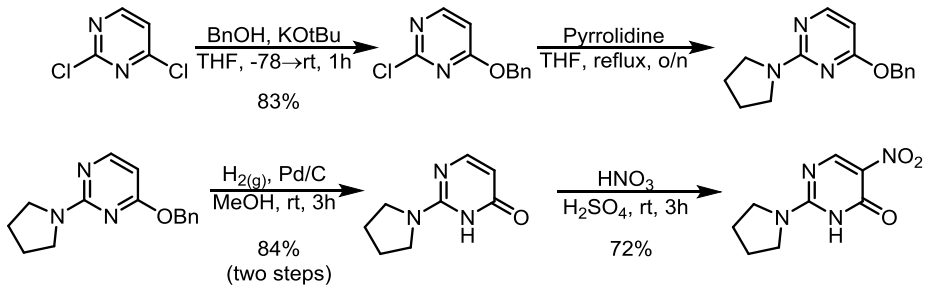

4-Benzyloxy-2-chloropyrimidine. Prepared using a previously described procedure.[S8] Potassium *tert*-butoxide (4.7 g, 42 mmol) was added to a solution of benzyl alcohol (8.3 ml, 80 mmol) in 20 ml THF and stirred until dissolved. This mixture was added dropwise to a solution of 2,4-dichloropyrimidine (5.9 g, 40 mmol) in 30 ml DMF cooled to -78 °C under an inert atmosphere. The mixture was allowed to warm slowly to ambient temperature, and stirred for 1h. The reaction mixture was poured slowly into 200 ml of water and stirred for several minutes. The precipitate was filtered and dried under vacuum. The product was recrystallized from hexanes in batches. Yield: 7.3 g of a white solid, 83%. ^{1}H-NMR (600 MHz; DMSO-d_6): δ 8.49 (d, *J* = 5.8 Hz, 1H), 7.48 (d, *J* = 7.1 Hz, 2H), 7.41 (t, *J* = 7.3 Hz, 2H), 7.37 (dd, *J* = 8.4, 6.0 Hz, 1H), 7.06 (d, *J* = 5.8 Hz, 1H), 5.42 (s, 2H). ^{13}C NMR (151 MHz; DMSO): δ 169.9, 160.1, 158.9, 135.4, 128.51, 128.50, 128.39, 107.7, 68.7 HRMS(EI) m/z: calcd $C_{11}H_9N_2OCl$, 220.0403; found, 220.0445.

4-Benzyloxy-2-(pyrrolidin-1-yl)pyrimidine. 4-Benzyloxy-2-chloropyrimidine (7.3 g, 33.4 mmol) and pyrrolidine (8.3 ml, 100 mmol) were refluxed in 66 ml THF for 5h. The reaction mixture was concentrated under vacuum, and the residue was dissolved in EtOAc, and washed with twice water and then once with brine. The organic phase was dried with $MgSO_4$, filtered, and concentrated under vacuum. The colourless oil was pure enough to be carried on crude to the next step.

2-(Pyrrolidin-1-yl)-4(3H)-pyrimidinone. The crude 4-benzyloxy-2-(pyrrolidin-1-yl)pyrimidine with 0.3g Pd/C were stirred in 100 ml MeOH, under one atmosphere of hydrogen gas. The reaction was

stirred overnight and filtered through a pad of celite, which was washed several times with hot methanol. The filtrate was evaporated and the product recrystallized from EtOAc/hexanes. Yield: 4.6 g of a beige solid, 85% over two steps. ^{1}H-NMR (600 MHz; DMSO-d_6): δ 10.91 (d, *J* = 0.2 Hz, 1H), 7.62 (d, *J* = 5.2 Hz, 1H), 5.51 (d, *J* = 5.9 Hz, 1H), 3.41 (s, 4H), 1.88 (s, 4H). ^{13}C NMR (151 MHz; DMSO): δ 163.9 (br), 156.7 (br), 153.9 (br), 101.4 (br), 47.0, 25.2 HRMS(EI) m/z: calcd $C_8H_{11}N_3O$, 165.0902; found, 165.0880.

5-Nitro-2-(pyrrolidin-1-yl)-4(3H)-pyrimidinone. 2-(Pyrrolidin-1-yl)-4(3H)-pyrimidinone (4.0 g, 24 mmol) was dissolved in 15 ml H_2SO_4 at room temperature and then cooled in an ice bath. Nitric acid (5 ml, 70%) was then added dropwise to the solution over several minutes. The reaction was allowed to stir at room temperature for 2h. The reaction was poured slowly over ice and stirred for several minutes before the precipitate was filtered, rinsed thoroughly with water, and allowed to under s stream of air. Yield: 3.6 g of a beige solid, 72%. ^{1}H-NMR (600 MHz; DMSO-d_6): δ 11.69 (s, 1H), 8.87 (s, 1H), 3.63 (t, *J* = 6.9 Hz, 2H), 3.49 (t, *J* = 6.9 Hz, 2H), 1.97 (quintet, *J* = 6.8 Hz, 2H), 1.89 (quintet, *J* = 6.8 Hz, 2H). ^{13}C NMR (151 MHz; DMSO): δ 159.0, 155.5, 154.2, 125.1, 49.0, 47.7, 25.5, 24.6 HRMS(EI) m/z: calcd $C_8H_{10}N_4O_3$, 210.0752; found, 210.0724.

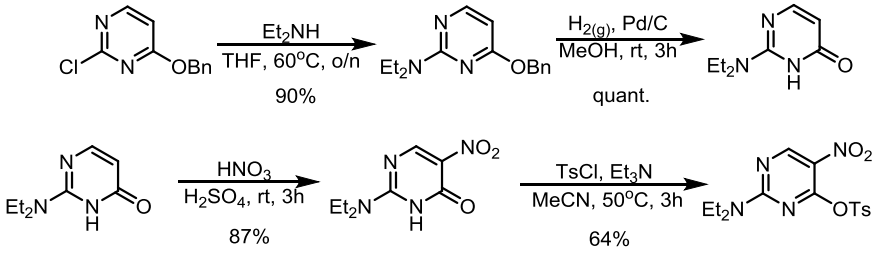

4-Benzyloxy-2-diethylaminopyrimidine. 4-benzyloxy-2-chloropyrimidine (3.80 g, 17.3 mmol) and diethylamine (26 ml, 250 mmol) were refluxed in 24 ml THF, overnight. The reaction mixture was concentrated under vacuum, and the residue was dissolved in CH_2Cl_2, and washed with twice water

and then once with brine. The organic phase was dried with $MgSO_4$, filtered through a plug of silica, and concentrated under vacuum. Yield: 4.0 g of a colourless oil, 90%. ^{1}H-NMR (600 MHz; DMSO-d_6): δ 8.07 (d, *J* = 5.6 Hz, 1H), 7.41 (d, *J* = 7.4 Hz, 2H), 7.37 (t, *J* = 7.6 Hz, 2H), 7.31 (t, *J* = 7.2 Hz, 1H), 6.04 (d, *J* = 5.6 Hz, 1H), 5.35 (s, 2H), 3.53 (q, *J* = 7.0 Hz, 4H), 1.08 (t, *J* = 7.0 Hz, 6H). 13-C NMR (151 MHz; DMSO): δ 169.1, 160.9, 159.0, 137.6, 128.8, 128.23, 128.21, 95.7, 66.9, 41.8, 13.5 HRMS(EI) m/z: calcd $C_{15}H_{19}N_3O$, 257.1528; found, 257.1507.

2-Diethylamino-4(3H)-pyrimidinone. 4-Benzyloxy-2-diethylaminopyrimidine (4.0 g) with 0.2g Pd/C were stirred in 45 ml MeOH, under one atmosphere of hydrogen gas. The reaction was stirred overnight, diluted with 50 ml EtOAc, and filtered through a pad of celite. The filtrate was concentrated under vacuum. Yield: 2.56 g of a white solid, quantitative. ^{1}H-NMR (600 MHz; DMSO-d_6): δ 10.90 (br, 1H), 7.67 (br, 1H), 5.54 (br, 1H), 3.49 (d, *J* = 7.0 Hz, 4H), 1.08 (t, *J* = 7.0 Hz, 6H). 13-C NMR (151 MHz; DMSO): δ 165.0 (br), 157.0 (br), 155.3 (br), 100.6 (br), 41.8, 13.4 HRMS(EI) m/z: calcd $C_8H_{13}N_3O$, 167.1059; found, 167.1061.

2-Diethylamino-5-nitro-4(3H)-pyrimidinone. 2-Diethylamino-4(3H)-pyrimidinone (11 g, 66 mmol) was dissolved in 35 ml H_2SO_4 at room temperature and then cooled in an ice bath. 12 ml of nitric acid (70%) was then added dropwise to the solution over several minutes. The reaction was allowed to stir at room temperature for 3h. The reaction was poured slowly over ice and stirred for several minutes before the precipitate was filtered, rinsed thoroughly with water, and allowed to under s stream of air. Yield: 12.2 g of a beige solid, 87%. ^{1}H-NMR (600 MHz; DMSO-d_6): δ 11.70 (br, 1H), 8.86 (s, 1H), 3.63 (br, 4H), 1.14 (t, *J* = 7.0 Hz, 6H). 13-C NMR (151 MHz; DMSO): δ 158.9, 155.9 (br), 155.3 (br), 124.9, 44.0 (br), 42.7 (br), 13.2 HRMS(EI) m/z: calcd $C_8H_{12}N_4O_3$, 212.0909; found, 212.0910.

(2-Diethylamino-5-nitropyrimidin-4-yl) p-toluenesulfonate. 2-Diethylamino-5-nitro-4(3H)-pyrimidinone (1.6 g, 7.5 mmol), *p*-toluenesulfonyl chloride (1.4 g, 7.5 mmol), and triethylamine (2.3

ml, 16 mmol) were added to 35 ml of dry MeCN, under an inert atmosphere. The reaction was heated to 50 °C for 3h. The reaction was judged complete by TLC. The solvent was removed by rotary evaporation, and the residue partitioned between CH_2Cl_2/1M $HCl_{(aq)}$. The organic phase was separated, washed once with water, and once with brine. It was dried by $MgSO_4$, filtered, and concentrated under vacuum. The product was recrystallized from benzene/hexanes. Yield: 1.75 g of a beige solid, 64%. ^{1}H-NMR (400 MHz; DMSO-d_6): δ 9.11 (s, 1H), 7.96 (d, *J* = 8.4Hz, 2H), 7.55 (d, *J* = 8.4Hz, 2H), 3.63 (q, *J* = 6.8Hz, 2H), 3.31 (q, *J* = 6.8Hz, 2H), 2.45 (s, 3H), 1.12 (t, *J* = 6.8 Hz, 3H), 0.97 (t, *J* = 6.8 Hz, 3H). 13-C NMR (76 MHz; DMSO): δ 159.1, 156.2, 146.0, 133.6, 130.2, 128.2, 127.7, 122.8, 42.8, 42.6, 21.1, 12.5, 12.3 HRMS(EI) m/z: calcd $C_{15}H_{18}N_4O_5S$, 366.0998; found, 366.1012.

6.6.9 Supporting Information References

(S1) Haidasz, E. A.; Van Kessel, A. T. M.; Pratt, D. A. *J. Org. Chem.* **2016**, *81*, 737–744.

(S2) Abraham, M. H.; Abraham, R. J.; Byrne, J.; Griffiths, L. *J. Org. Chem.* **2006**, *71*, 3389–3394.

(S3) Abraham, R. J.; Byrne, J. J.; Griffiths, L.; Perez, M. *Magn. Reson. Chem.* **2006**, *44*, 491–509.

(S4) Abraham, R. J.; Mobli, M. *Magn. Reson. Chem.* **2007**, *45*, 865–877.

(S5) Gurka, D.; Taft, R. W. *J. Am. Chem. Soc.* **1969**, *91*, 4794–4801.

(S6) Pooryaghoobi, N.; Bakavoli, M.; Alimardani, M.; Bazzazan, T.; Sadeghian, H. *Iran. J. Basic Med. Sci.* **2013**, *16*, 784–789.

(S7) Shen, C.; Wu, X.-F. *Catal. Sci. Technol.* **2015**, *5*, 4433–4443.

(S8) Wand, T.; Hanzelka, B.; Muh, U.; Bemis, G.; Zuccola, H. J. Pyrimidine Compounds as Tuberculosis Inhibitors. WO2011019405, 2011.

6.6.10 ^{1}H and ^{13}C-NMR spectra:

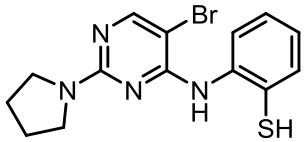

(Crude)

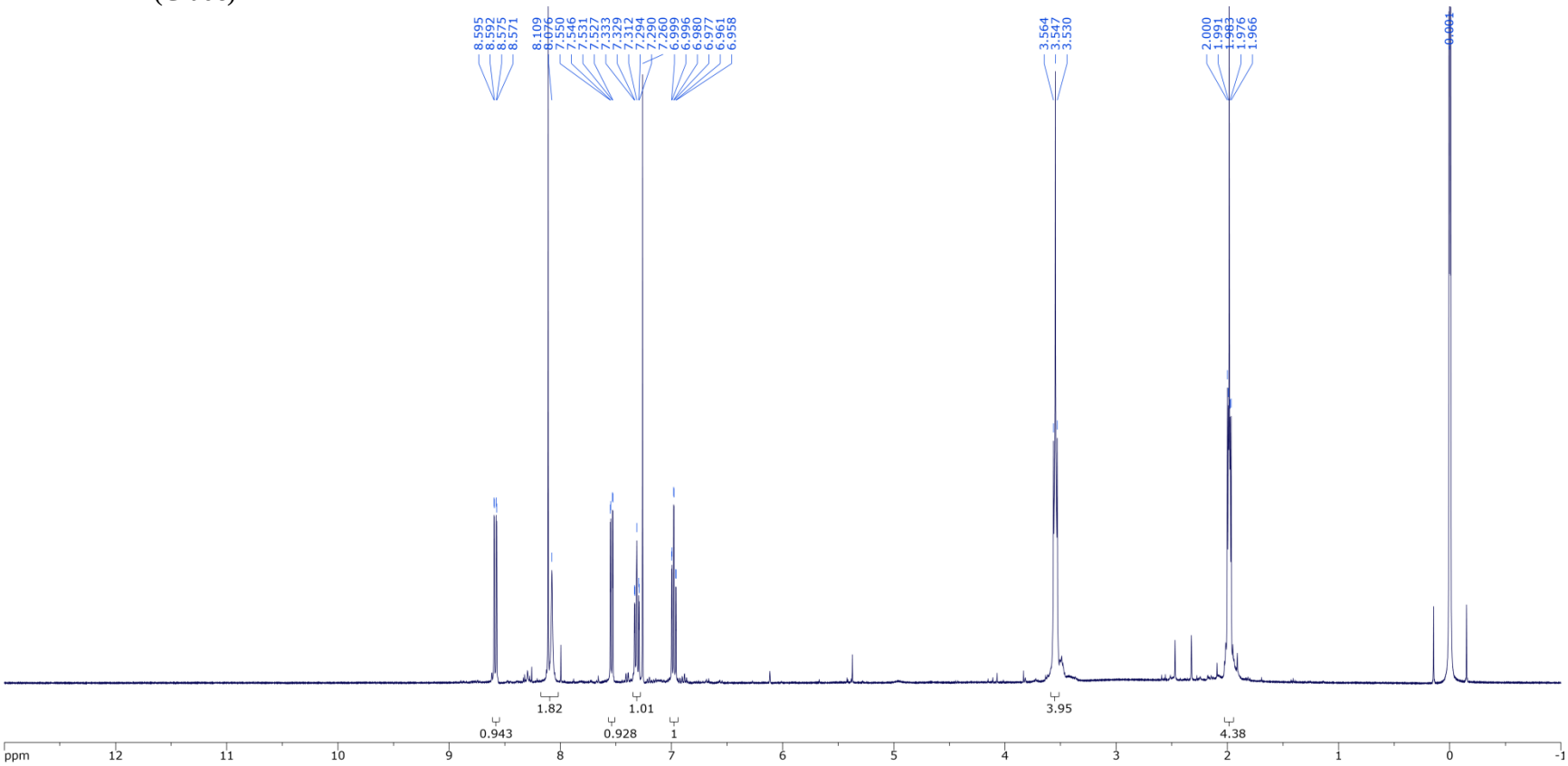

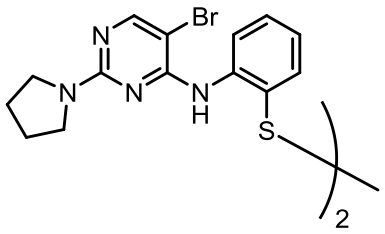
Br
N
N
N
H
N
S
2

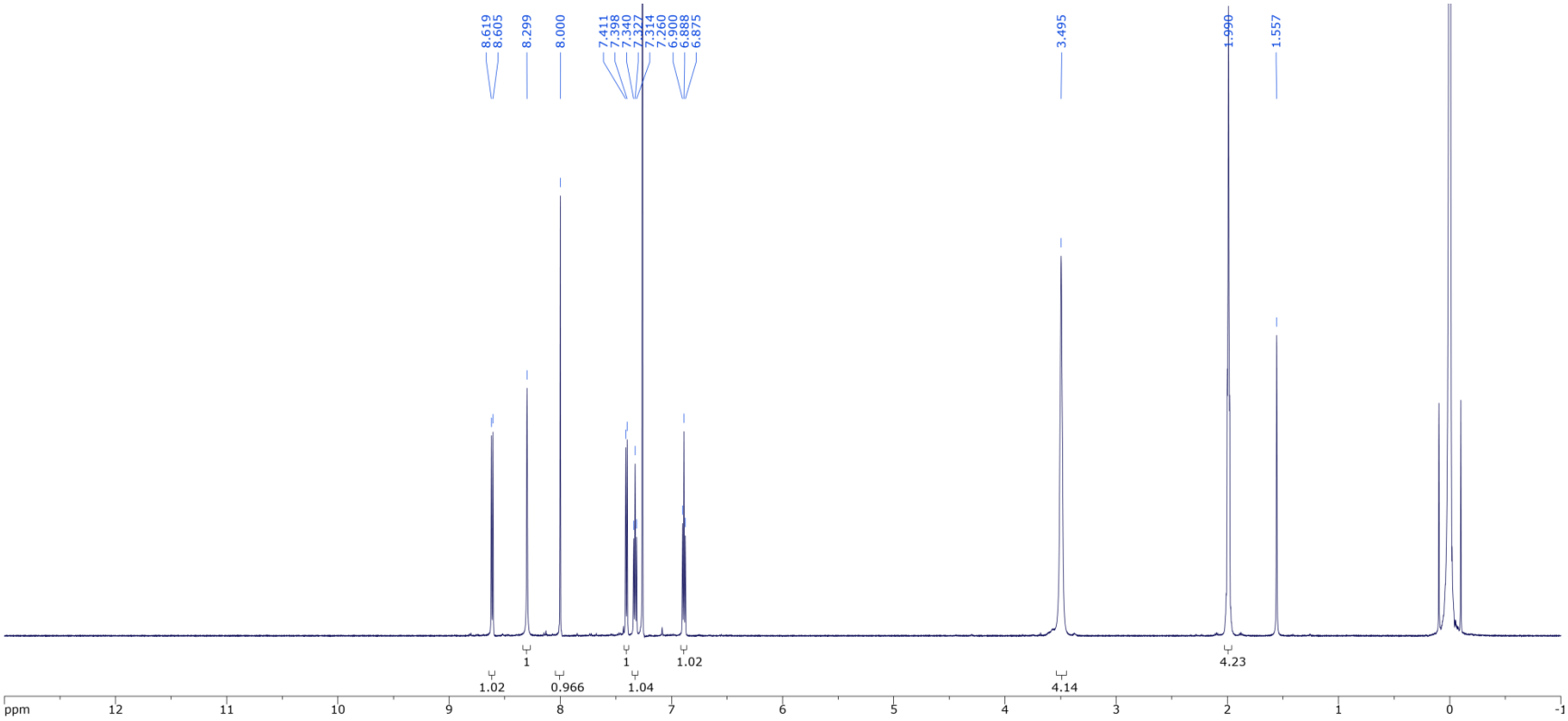
8.619
8.605
8.299
8.000
7.411
7.398
7.340
7.327
7.314
7.260
6.900
6.888
6.875
3.495
1.990
1.557
1.02
1
0.966
1
1.04
1.02
4.14
4.23
ppm
12
11
10
9
8
7
6
5
4
3
2
1
0
-1

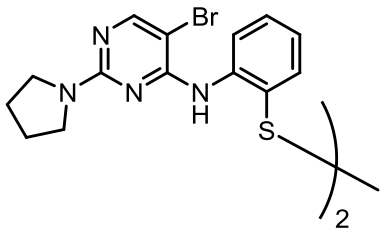
Br
N
N
N
H
S
2

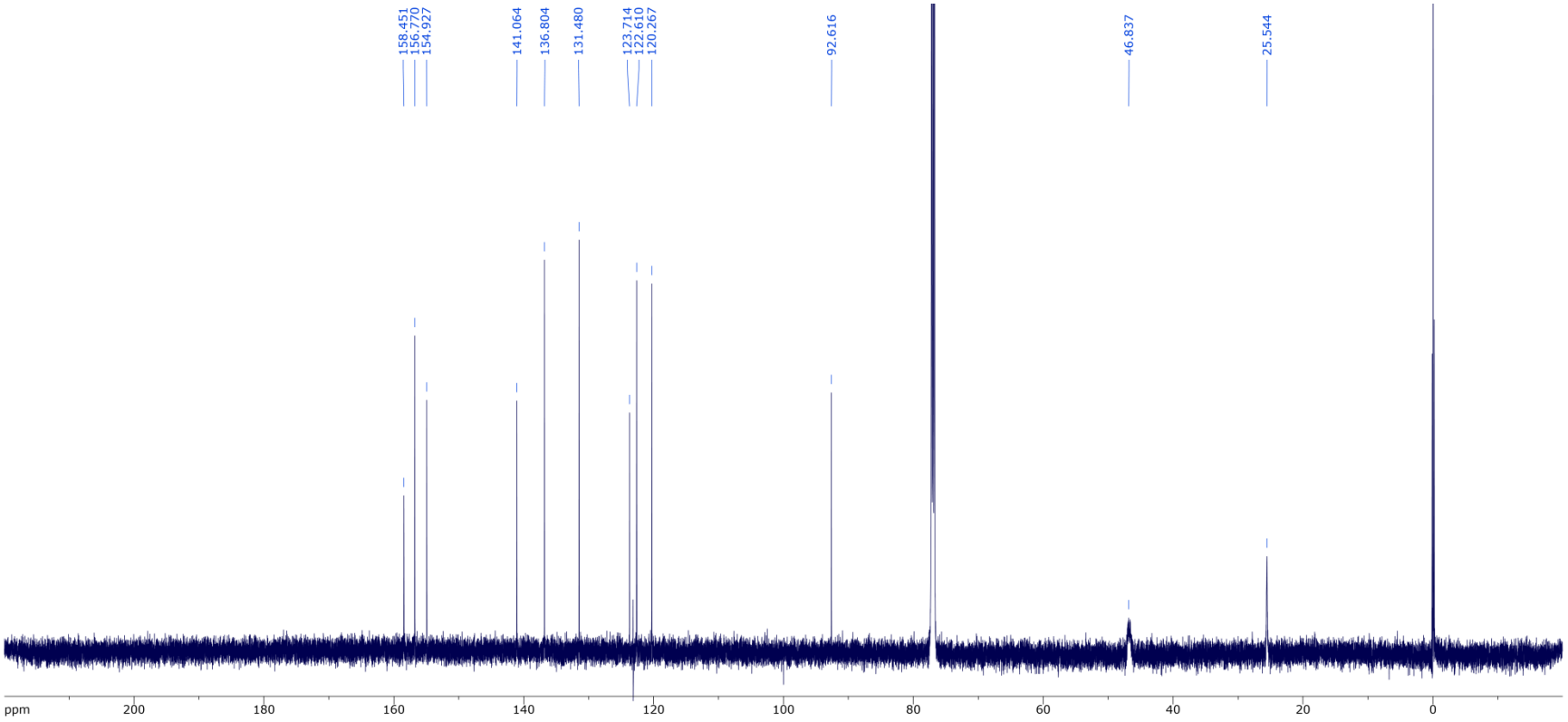
158.451
156.770
154.927
141.064
136.804
131.480
123.714
122.610
120.267
92.616
46.837
25.544
ppm
200
180
160
140
120
100
80
60
40
20
0

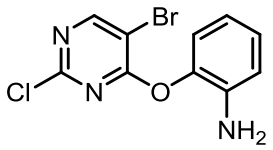
Br
N
Cl
N
O
NH2

Crude

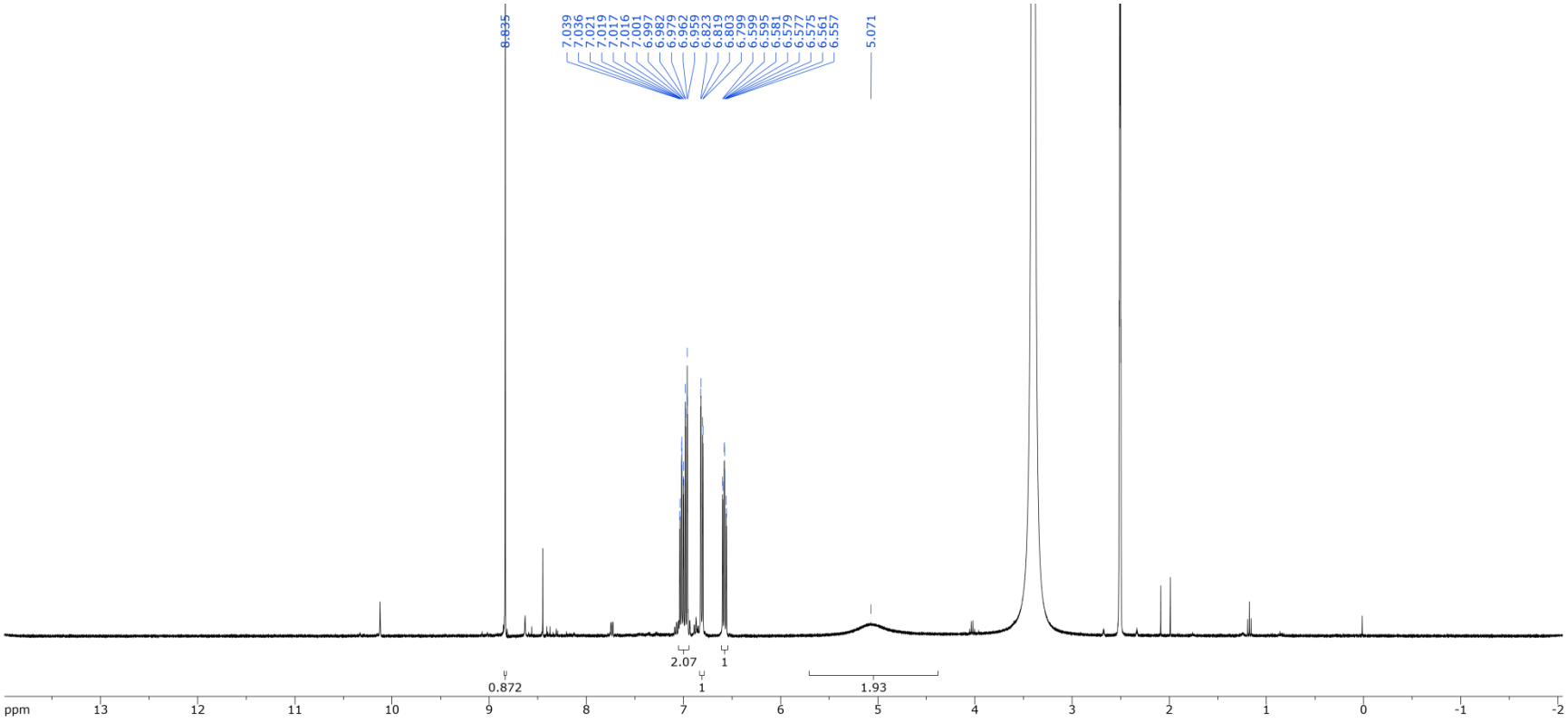
8.835
7.039
7.036
7.021
7.019
7.017
7.016
7.001
6.997
6.982
6.979
6.962
6.959
6.823
6.819
6.803
6.799
6.599
6.595
6.581
6.579
6.577
6.575
6.561
6.557
5.071
2.07
1
0.872
1
1.93
ppm
13
12
11
10
9
8
7
6
5
4
3
2
1
0
-1
-2

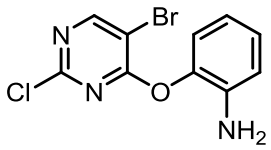

Recrystalized

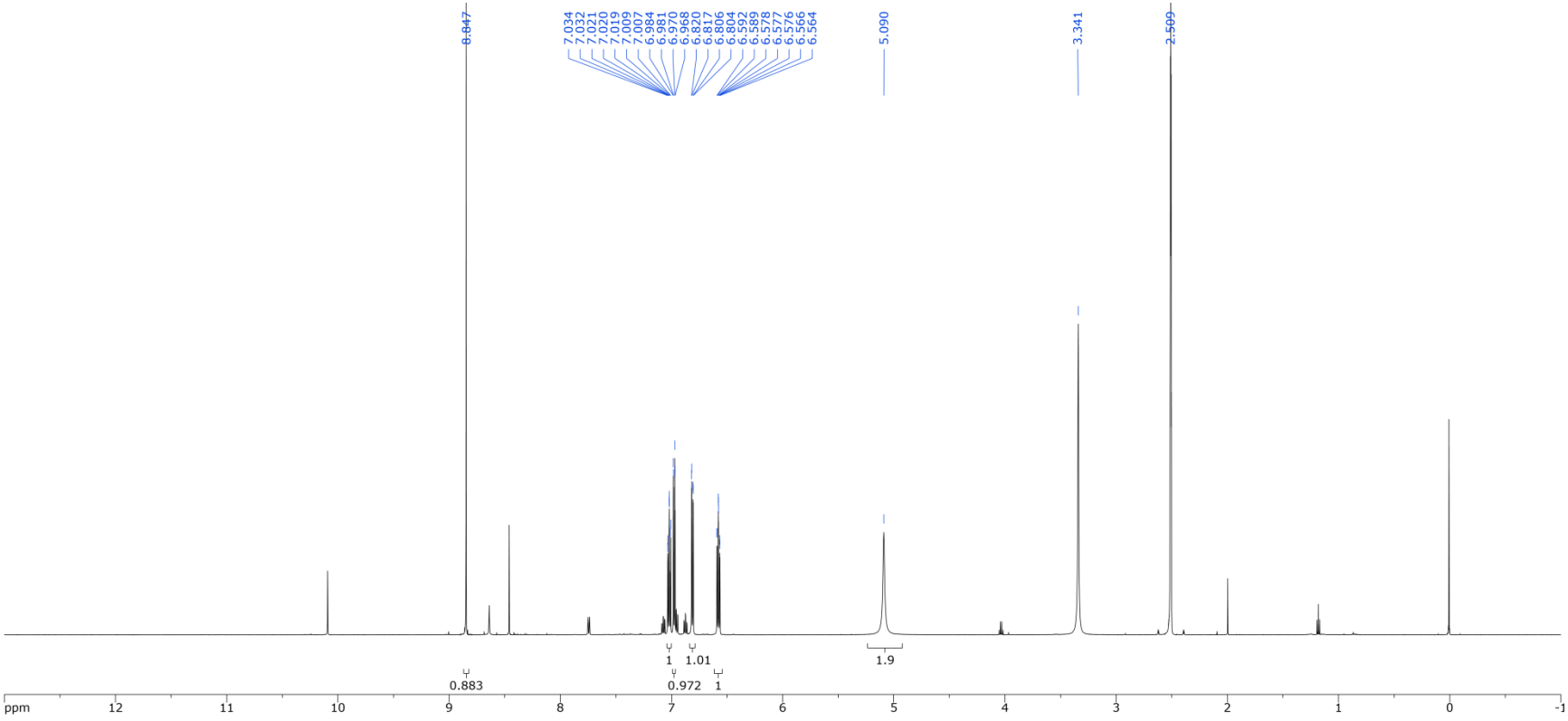

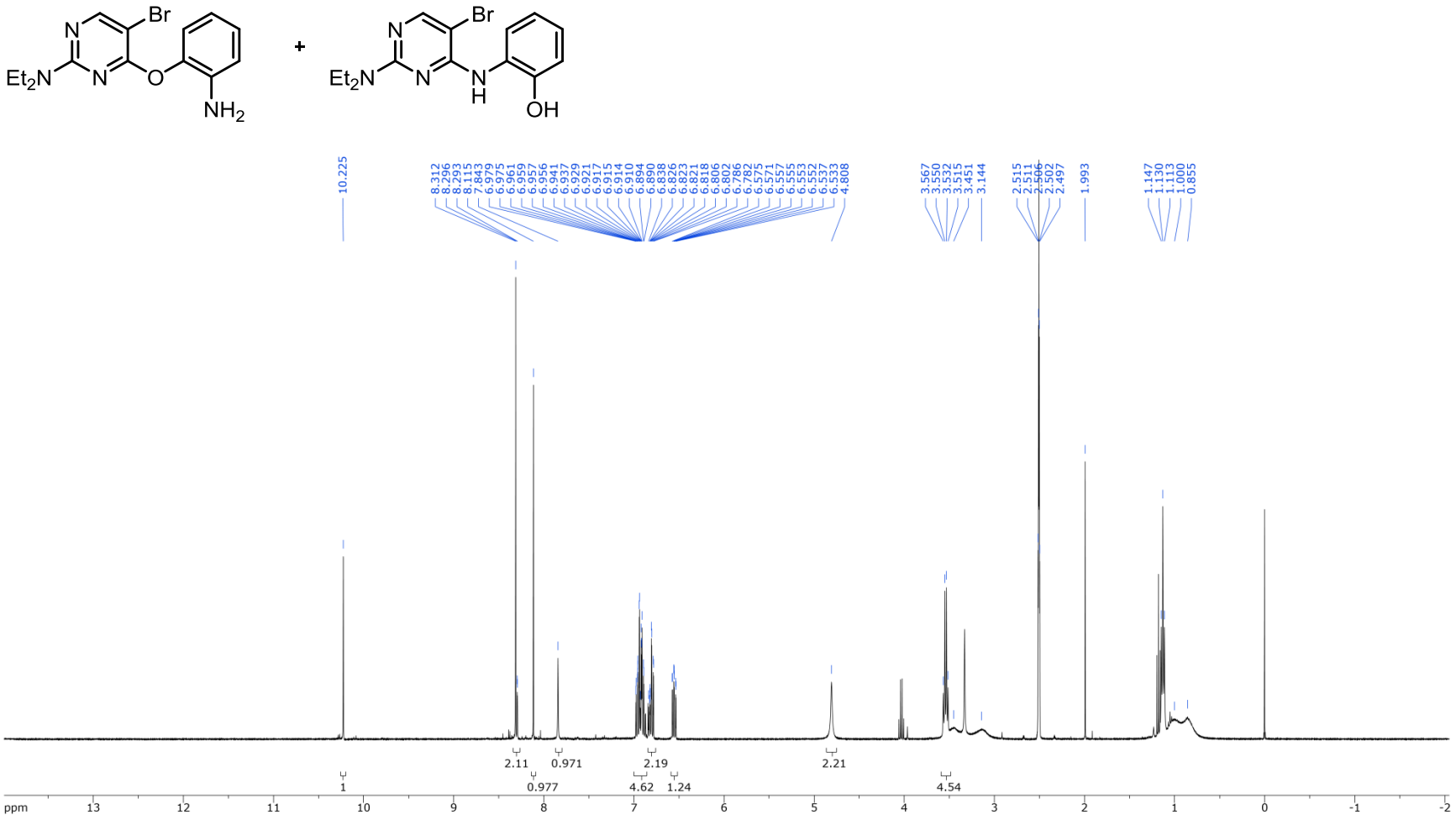
Br
N
Et2N
N
O
NH2
+
Br
N
Et2N
N
N
H
OH
10.225
8.312
8.296
8.293
8.115
7.843
6.979
6.975
6.961
6.959
6.957
6.956
6.941
6.937
6.929
6.921
6.917
6.915
6.914
6.910
6.894
6.890
6.838
6.826
6.823
6.821
6.818
6.806
6.802
6.786
6.782
6.575
6.571
6.557
6.555
6.553
6.552
6.537
6.533
4.808
3.567
3.550
3.532
3.515
3.451
3.144
2.515
2.511
2.506
2.502
2.497
1.993
1.147
1.130
1.113
1.000
0.855
2.11
0.971
2.19
2.21
1
0.977
4.62
1.24
4.54
ppm
13
12
11
10
9
8
7
6
5
4
3
2
1
0
-1
-2

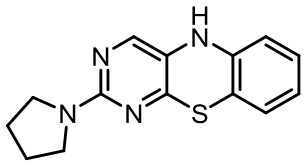
H
N
N
N
S
N

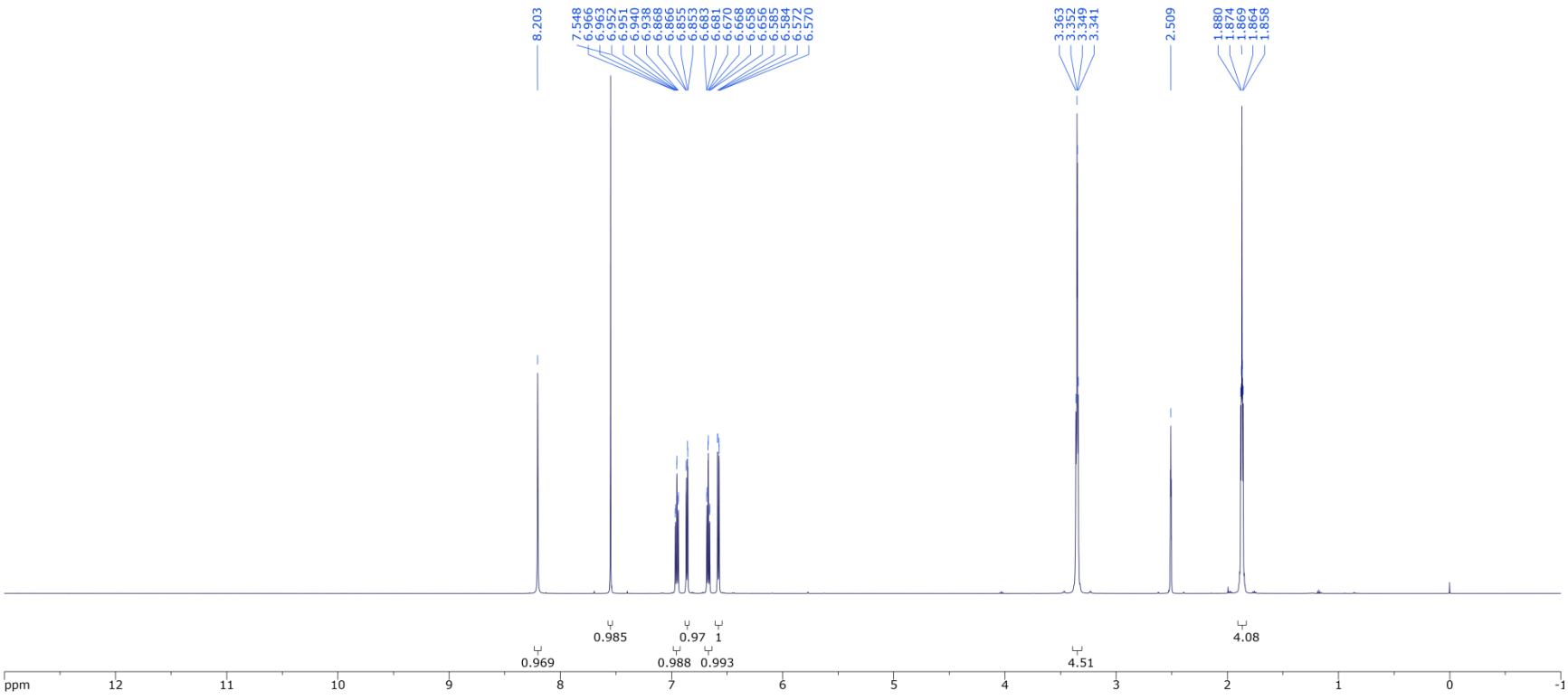
8.203
7.548
6.966
6.963
6.953
6.952
6.951
6.940
6.938
6.868
6.866
6.855
6.853
6.683
6.681
6.670
6.658
6.656
6.585
6.584
6.572
6.570
3.363
3.352
3.349
3.341
2.509
1.880
1.874
1.869
1.864
1.858
0.969
0.985
0.988
0.97
0.993
1
4.51
4.08
ppm
12
11
10
9
8
7
6
5
4
3
2
1
0
-1

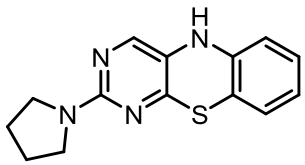
H
N
N
N
S
N

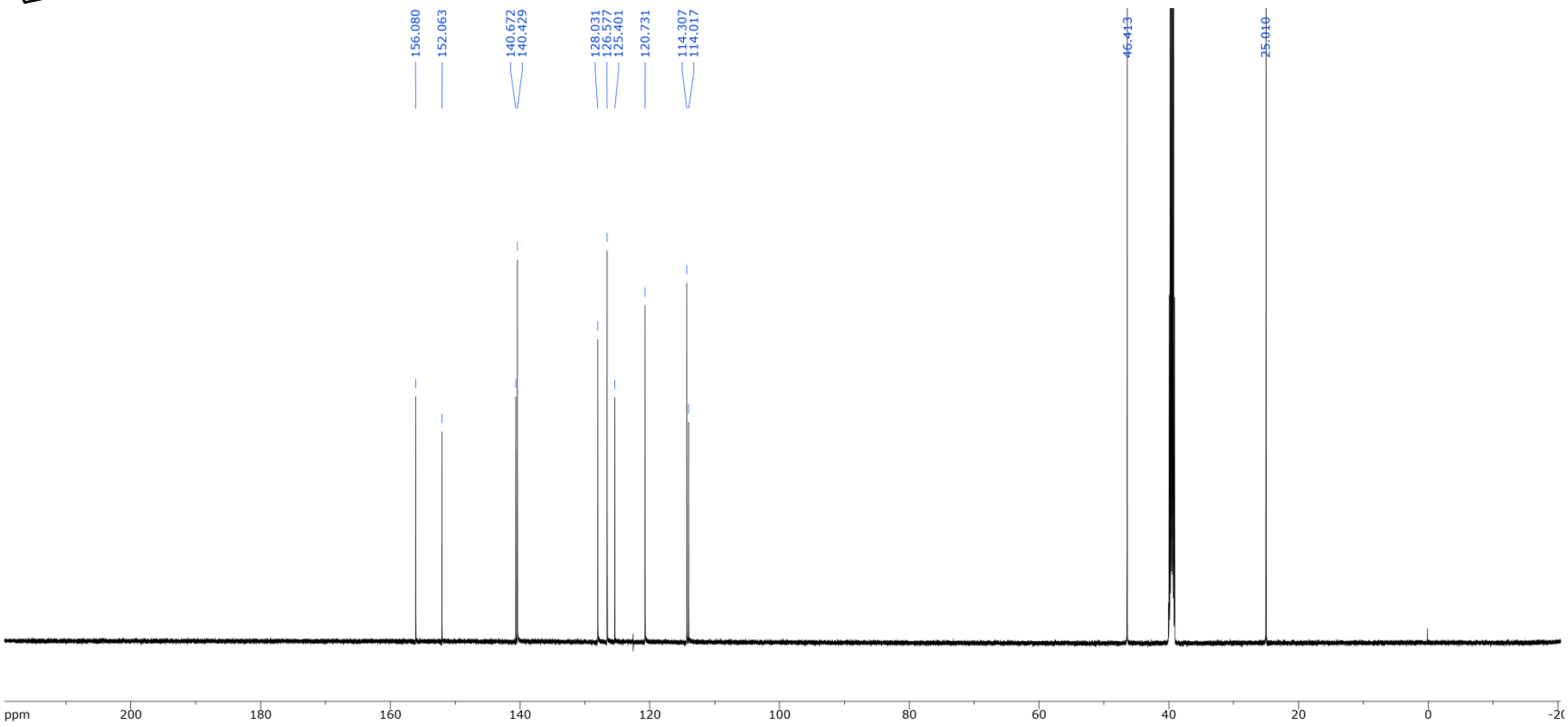
156.080
152.063
140.672
140.429
128.031
126.577
125.401
120.731
114.307
114.017
46.413
25.010
ppm
200
180
160
140
120
100
80
60
40
20
0

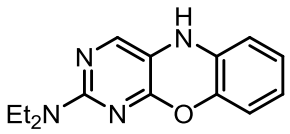
H
N
N
N
O
Et2N

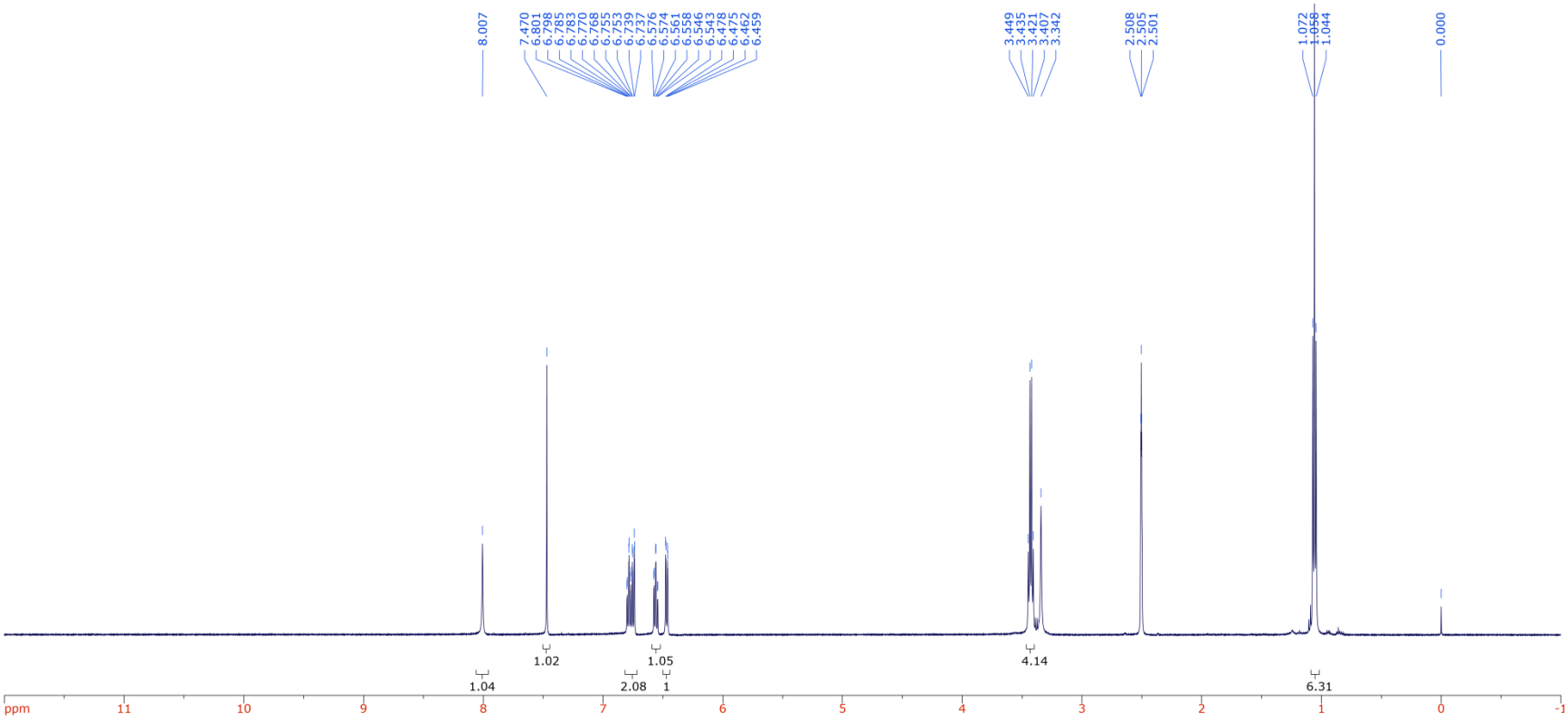
8.007
7.470
7.401
6.798
6.785
6.783
6.770
6.768
6.755
6.753
6.739
6.737
6.576
6.574
6.561
6.558
6.546
6.543
6.478
6.475
6.462
6.459
3.449
3.435
3.421
3.407
3.342
2.508
2.505
2.501
1.072
1.058
1.044
0.000
1.04
1.02
2.08
1.05
1
4.14
6.31
ppm
11
10
9
8
7
6
5
4
3
2
1
0
-1

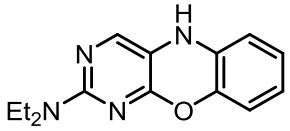
H
N
N
N
O
Et2N

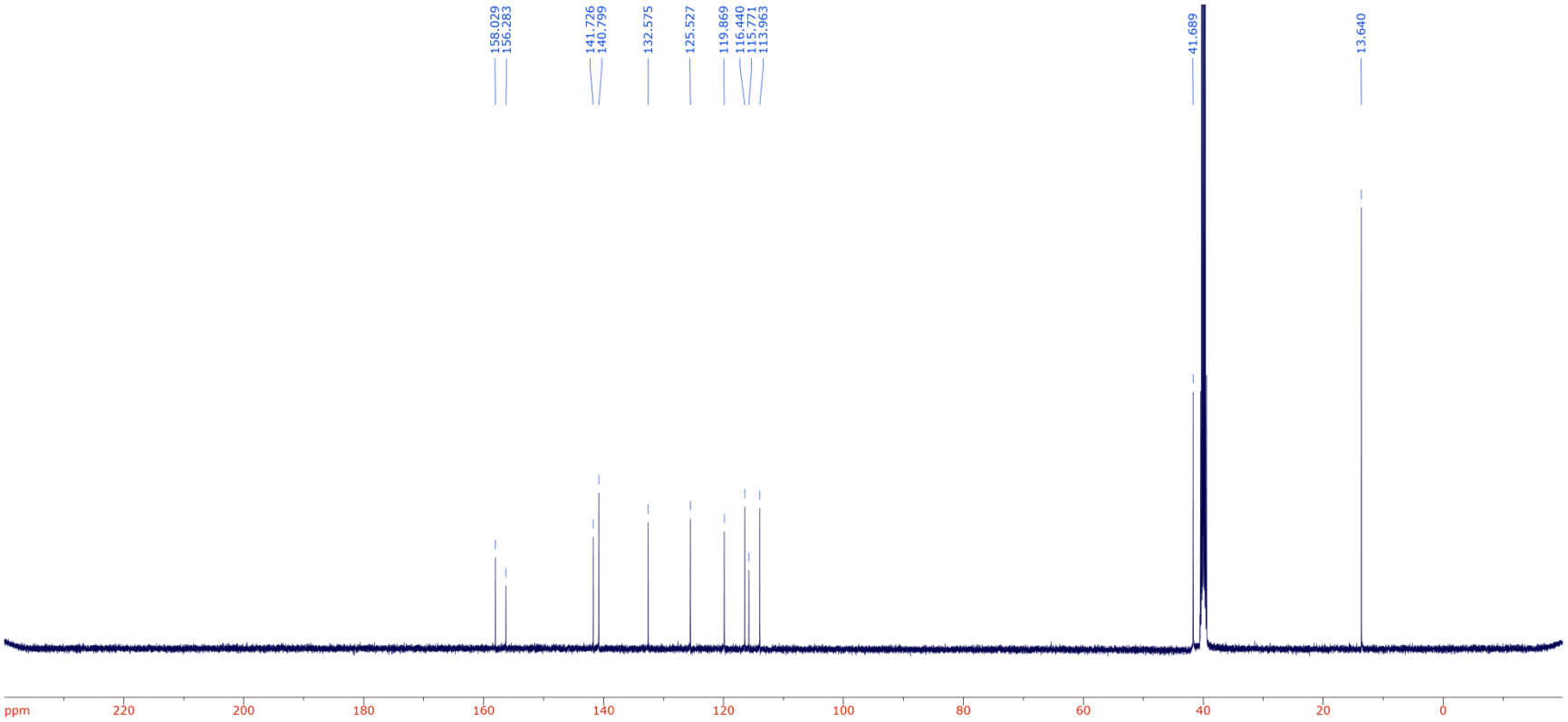
158.029
156.283
141.726
140.799
132.575
125.527
119.869
116.440
115.771
113.963
41.689
13.640
ppm
220
200
180
160
140
120
100
80
60
40
20
0

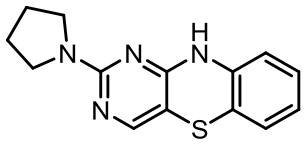

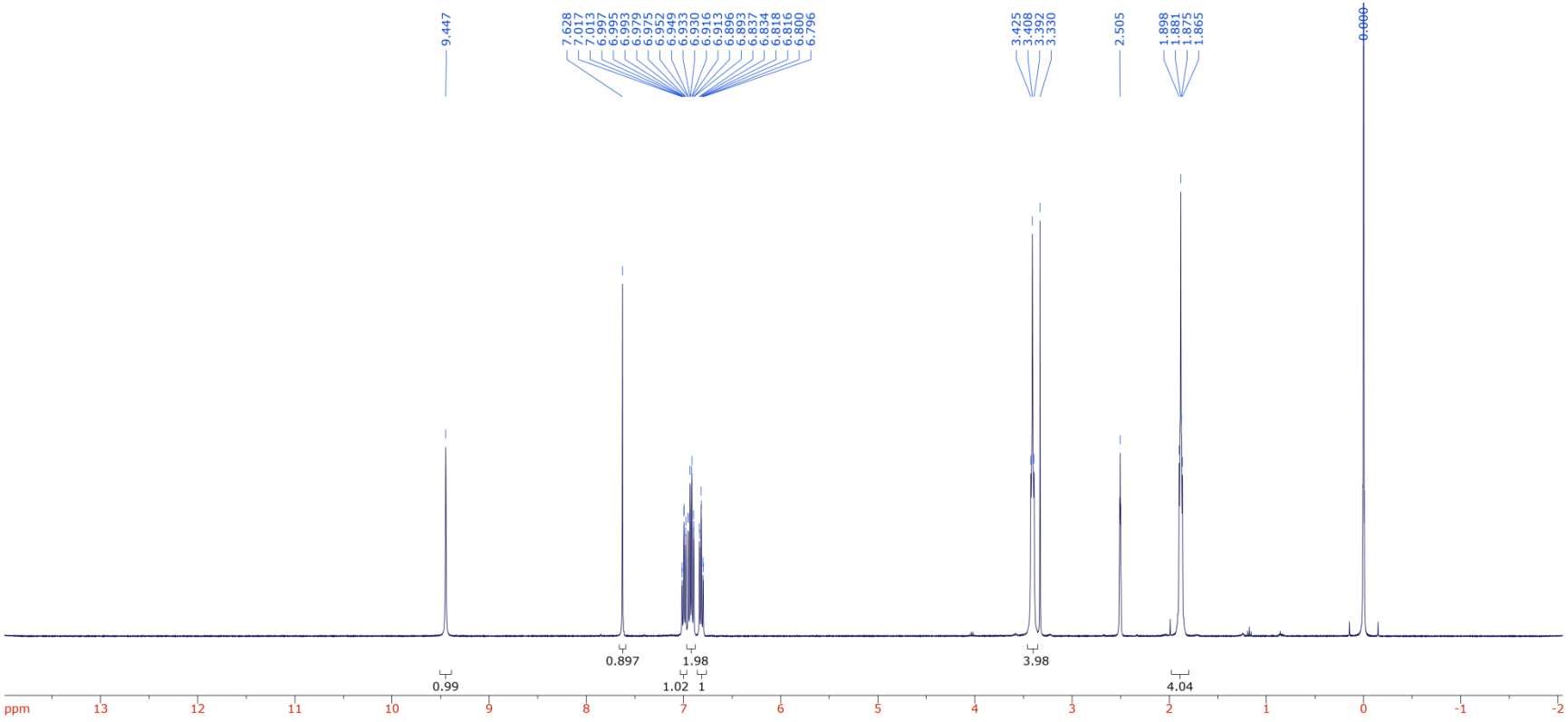
9.447
7.628
7.017
7.013
6.997
6.995
6.993
6.979
6.975
6.952
6.949
6.933
6.930
6.916
6.913
6.896
6.893
6.837
6.834
6.818
6.816
6.800
6.796
3.425
3.408
3.392
3.330
2.505
1.898
1.881
1.875
1.865
0.000
0.99
0.897
1.02
1.98
1
3.98
4.04
ppm
13
12
11
10
9
8
7
6
5
4
3
2
1
0
-1
-2

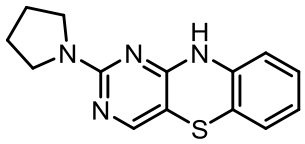

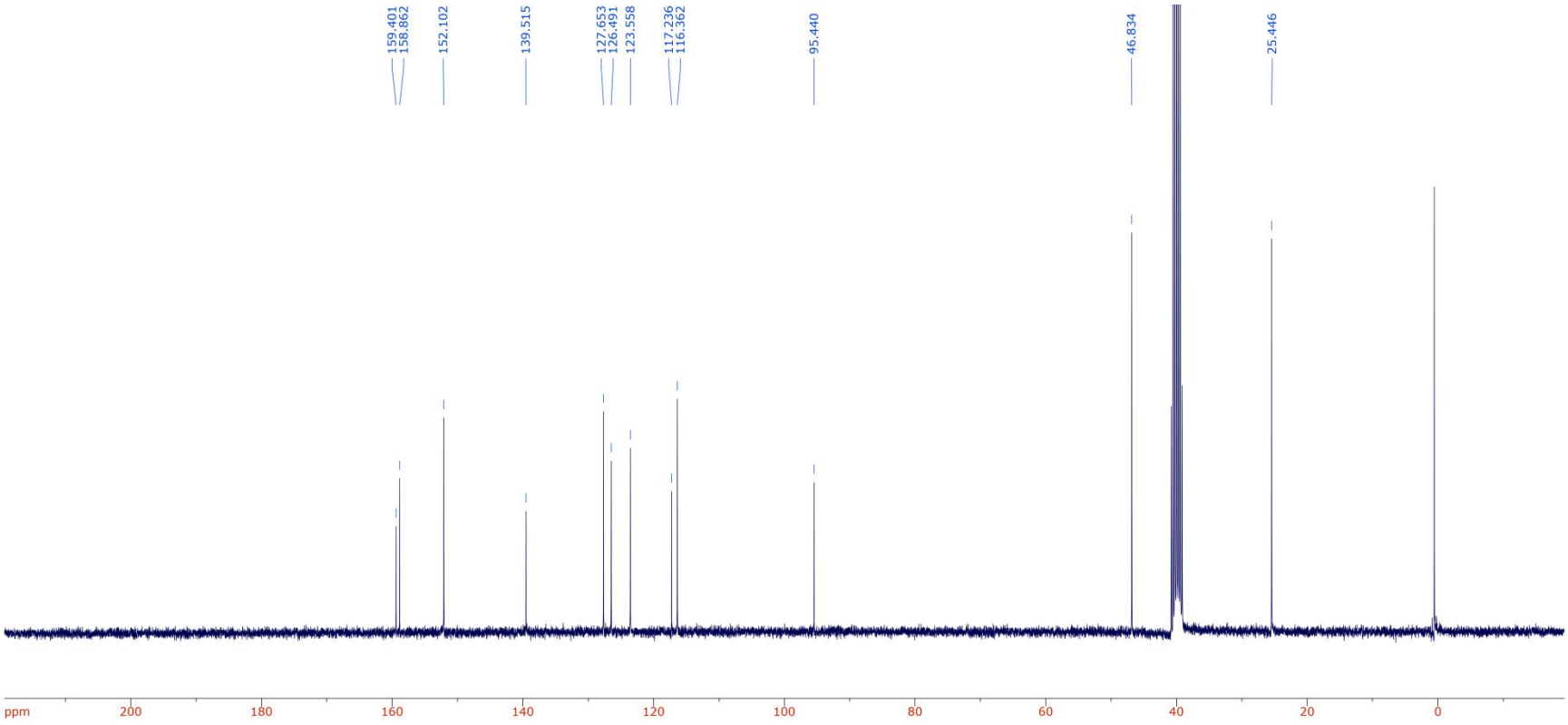
159.401
158.862
152.102
139.515
127.653
126.491
123.558
117.236
116.362
95.440
46.834
25.446
ppm
200
180
160
140
120
100
80
60
40
20
0

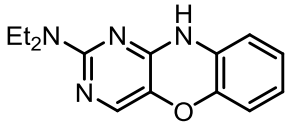
Et2N
N
H
N
N
O

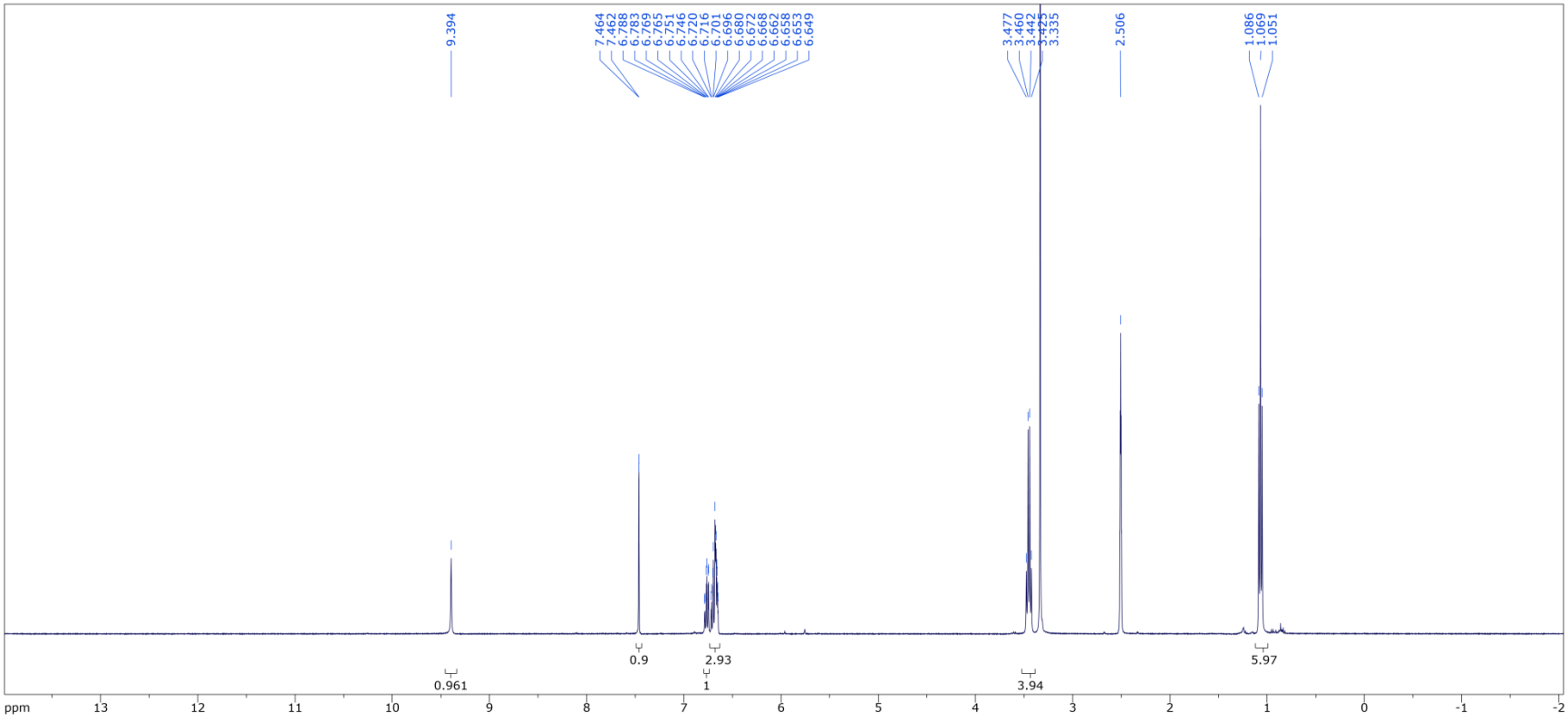
9.394
7.464
7.462
6.788
6.783
6.769
6.765
6.751
6.746
6.720
6.716
6.701
6.696
6.680
6.672
6.668
6.662
6.658
6.653
6.649
3.477
3.460
3.442
3.425
3.335
2.506
1.086
1.069
1.051
0.961
0.9
2.93
1
3.94
5.97
ppm
13
12
11
10
9
8
7
6
5
4
3
2
1
0
-1
-2

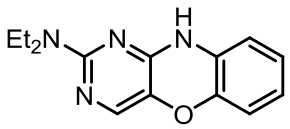
Et2N
N
H
N
N
O

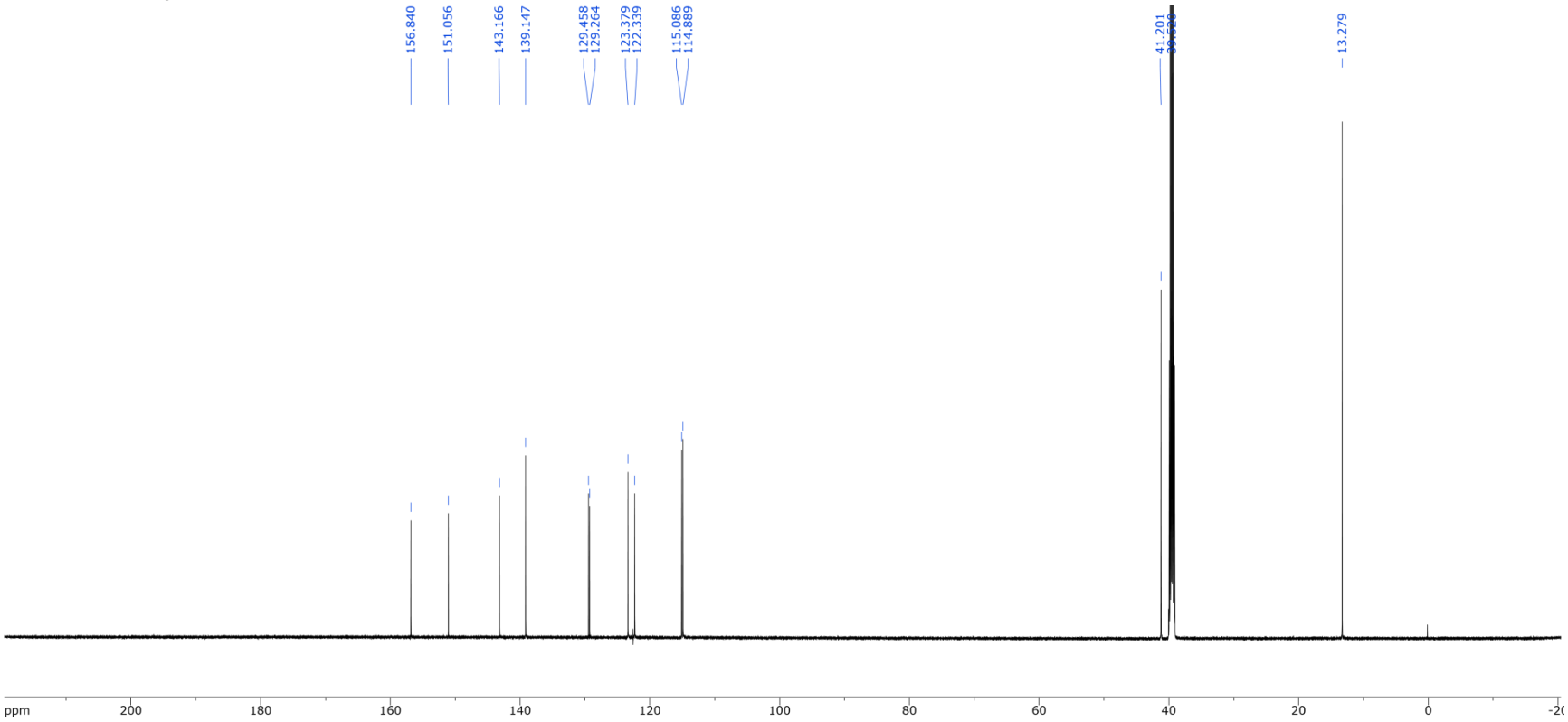
156.840
151.056
143.166
139.147
129.458
129.264
123.379
122.339
115.086
114.889
41.201
13.279
ppm
200
180
160
140
120
100
80
60
40
20
0

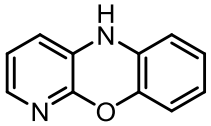
H
N
N
O

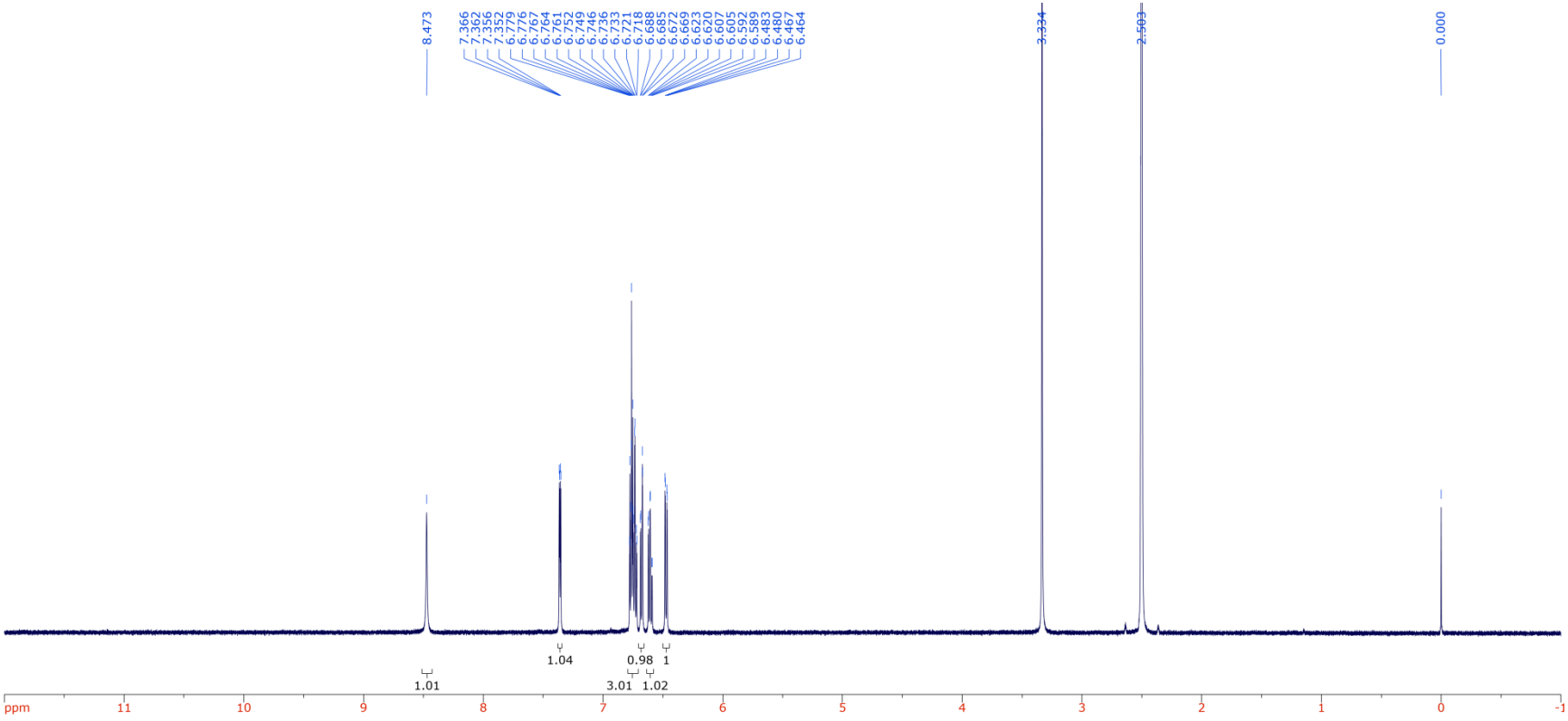
8.473
7.366
7.362
7.356
7.352
6.779
6.776
6.767
6.764
6.761
6.752
6.749
6.746
6.736
6.733
6.721
6.718
6.688
6.685
6.672
6.669
6.623
6.620
6.607
6.605
6.592
6.589
6.483
6.480
6.467
6.464
3.334
2.503
0.000
1.01
1.04
3.01
0.98
1.02
1
ppm
11
10
9
8
7
6
5
4
3
2
1
0
-1

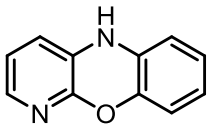
H
N
N
O

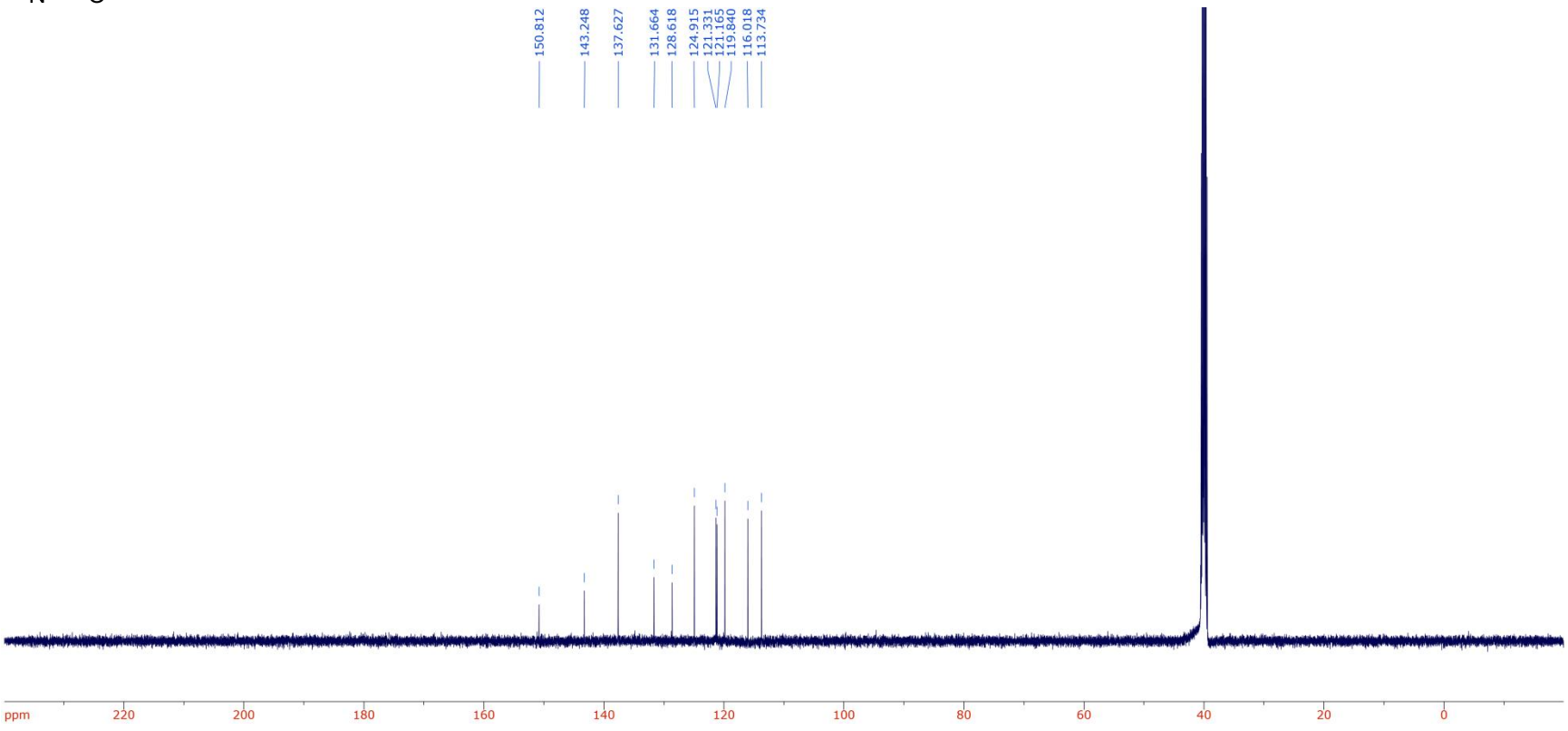
150.812
143.248
137.627
131.664
128.618
124.915
121.331
121.165
119.840
116.018
113.734
ppm
220
200
180
160
140
120
100
80
60
40
20
0

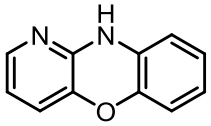

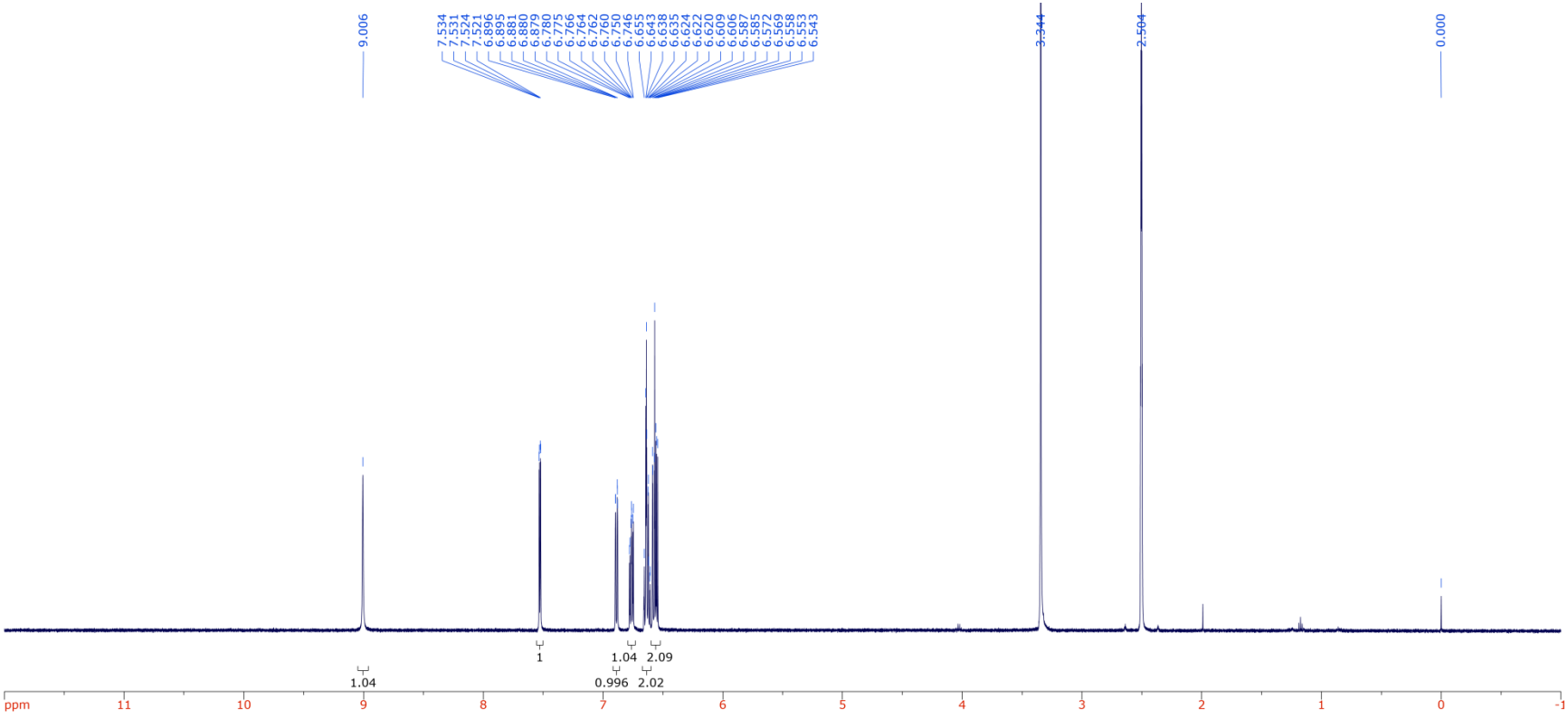
9.006
7.534
7.531
7.524
7.521
6.896
6.895
6.881
6.880
6.879
6.780
6.775
6.766
6.764
6.762
6.760
6.750
6.746
6.655
6.643
6.638
6.635
6.624
6.622
6.620
6.609
6.606
6.587
6.585
6.572
6.569
6.558
6.553
6.543
3.344
2.504
0.000
1.04
1
1.04
2.09
0.996
2.02
ppm
11
10
9
8
7
6
5
4
3
2
1
0
-1

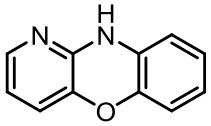
H
N
N
O

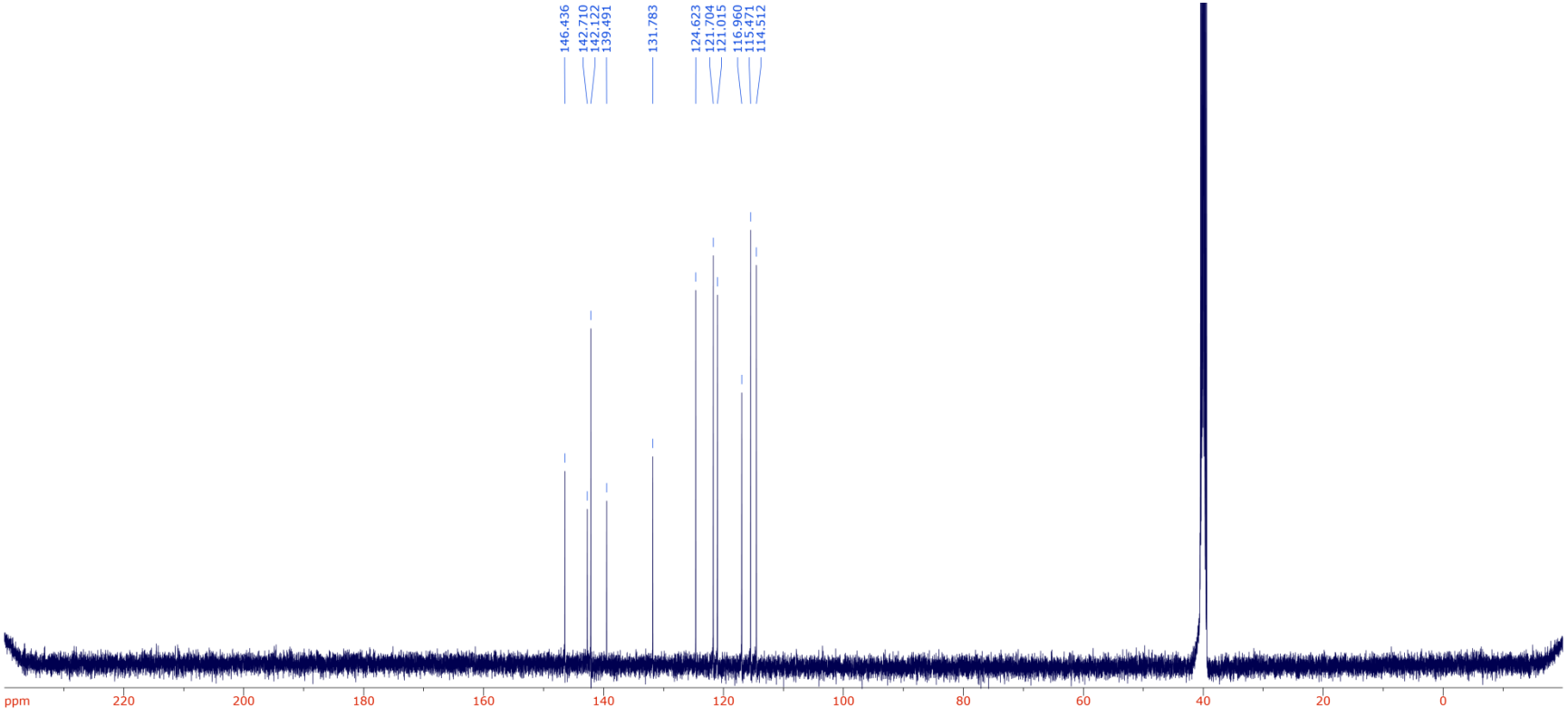
146.436
142.710
142.122
139.491
131.783
124.623
121.704
121.015
116.960
115.471
114.512
ppm
220
200
180
160
140
120
100
80
60
40
20
0

CHAPTER 7: Diffusion Controlled Radical-Trapping Antioxidants: The Reactivity of Azaphenoxazine and Azaphenothiazine Antioxidants

7.1 Preface

Recently, we reported the synthesis of a series of diazaphenoxazines and diazaphenothiazine radical-trapping antioxidants (RTAs). Preliminary attempts to measure second order rate constants for the reaction between these RTAs and peroxyl radicals found that there were among the fastest RTAs ever reported (*Org. Lett.* **2017**, 19, 1854-1857). Based on previous work, it was expected that these compounds would readily regenerate with an autoxidation, trapping the chain-carrying radicals catalytically. We have now expanded the scope of our investigation, including a range of mono- and diazaphenoxazines/phenothiazines, and studying their reactivity at a range of temperatures. These RTAs were found to be highly catalytically active between 70-100°C – temperatures well below those normally required for diarylamine regeneration. Furthermore, at elevated temperatures these RTAs greatly outperform industrially standard 4,4’-dialkyl-diphenylamines.

7.2 Introduction

Diarylamines (Ar_2NH) and phenols (ArOH) represent the two foremost classes of radical trapping antioxidants (RTAs), compounds that inhibit the autoxidative degradation of organic materials (oils, fuels, polymers, lipids, etc.)[1,2] by rapidly trapping the peroxyl radicals which propagate the radical chain reaction responsible for the process (Scheme 7.1).

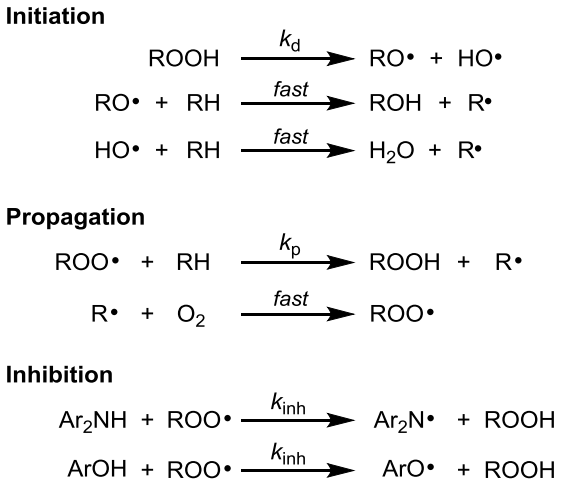

Scheme 7.1. Initiation, propagation, and inhibition reactions for the autoxidation of a hydrocarbon substrate.

They react by formal H-atom transfer from the weak N-H or O-H bond to the peroxyl radical, with an inhibition rate constant denoted k_{inh}.[3] Stabilization of the electron deficient RTA-derived aminyl or phenoxyl radical weakens the reactive bond of the RTA, and increases its reactivity to peroxyl radicals (Figure 7.1)[4,5] – a correlation described by the Evans-Polanyi relationship between k_{inh} and O-H BDE in phenols.[6,7] The kinetics of this inhibition reaction are fundamental to the efficacy of RTAs; faster trapping of the peroxyl radicals results in a shorter kinetic chain length to the oxidation and reduced buildup of hydroperoxides in the system. The importance of this last fact is magnified at elevated temperatures, where thermolysis of these product hydroperoxides is also the primary source of chain-initiating radicals. Under these conditions, the autoxidation (and thus degradation of the substrate) is autocatalytic.[8–10]

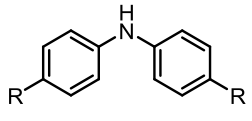

R	N-H BDE (kcal/mol)	k_{inh} ($M^{-1}s^{-1}$)
H	84.7	2.0×10^4
Me	82.2	1.8×10^5
OMe	80.7	3.7×10^6
NMe_2	78.4	-----[a]

Figure 7.1. N-H bond dissociation enthalpies and inhibition rate constants for a series of selectively substituted diphenylamines. [a)] Unstable under reaction conditions.

While it may seem that simply substituting RTAs with more strongly electron donating groups (thus weakening the reactive bond) would provide more effective antioxidants, this strategy can also compromise their stability to direct oxidation by either molecular oxygen or hydroperoxides.[5] Moreover, one-electron oxidation of these highly electron-rich compounds generates radical species in the reaction, further increasing the rate of oxidation and consuming additional RTA. For example, 4,4'-bis(dimethylamino)diphenylamine has an N-H BDE of 78.4 kcal/mol, significantly weaker than that of 4,4'-dialkyldiphenylamines, the major class of diarylamine RTAs used industrially (BDE = 82.2 kcal/mol, E^o = 1.02V vs. NHE).[5] However, in previous work,[4] an inhibition rate constant for 4,4'-bis(dimethylamino)diphenylamine couldn't be measured due to its instability (E^o = 0.34V vs. NHE), a result implying that it would be virtually useless as an antioxidant.

The problem of direct oxidation can be controlled via incorporation of heterocyclic rings into the RTA structures, increasing the oxidation potential of the molecule while having only a minor effect on reactivity (Figure 7.2).[4,11] Applying this strategy to stabilize highly electron rich phenolic and diarylaminic RTAs has led to the development of some of the most effective RTAs ever reported – compounds which often have reactivities approaching diffusion control.[5,12]

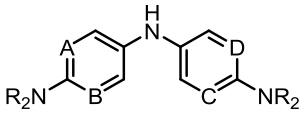

A	B	C	D	k_{inh} ($M^{-1}s^{-1}$)	E^o (V vs. NHE)
CH	CH	CH	CH	-----[a]	0.34
N	N	CH	CH	3.7×10^7	0.44
N	CH	N	CH	3.1×10^7	0.44
N	N	N	N	1.8×10^7	0.65

Figure 7.2. Inhibition rate constants and oxidation potentials for a series of diarylaminic RTAs.

Diarylamines possess a further advantage over phenolic antioxidants. While most RTAs at ambient temperatures can trap only two radicals – the first by formal H-atom transfer and the second by termination between a peroxyl and an RTA-derived radical (Scheme 7.2) – at elevated temperatures (>120°C), diarylamines have been shown to be catalytic.[13] This activity is believed to be the result of decomposition of an RTA-derived alkoxyamine to yield a carbonyl compound and

regenerate the amine.[13,14] Much like the N-H bond in the amine, stabilization of the aminyl radical weakens the N-O bond in the alkoxyamine, and promotes either the homolysis/disproportionation or retro-carbonyl-ene reaction responsible for the rate limiting turnover step in the catalytic cycle. This enhanced turnover can be seen in high temperature experiments where heterocyclic diarylamines, such as **7.1**, inhibit the autoxidation of n-hexadecane up to 12-fold more effectively than the industrial standard dialkyl-diphenylamines.[10]

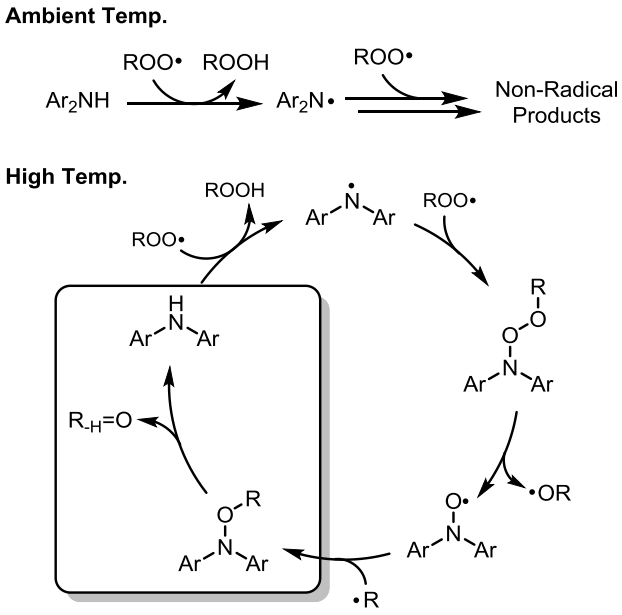

Scheme 7.2. Trapping of two peroxyl radicals by a diarylamine RTA at ambient temperatures and the catalytic cycle for diarylamine radical trapping at elevated temperatures.

Phenothiazine (**7.2**), an analogue of diphenylamine where the aromatic rings are bridged by a thioether, has long been known to be a potent antioxidant, and has been used industrially to inhibit the autoxidation of lubricants, rubbers, and fuels .[15–17] Similarly, phenoxazine (**7.3**), although not widely used as an RTA, is highly reactive to peroxyl radicals. These compounds have N-H BDEs as weak as many of the most reactive diarylamines (BDE = 79.3 and 77.2 kcal/mol, respectively) and correspondingly high inhibition rate constants (k_{inh} = 8.8×10^6 and 2.9×10^7 $M^{-1}s^{-1}$, respectively).[18] These results can be rationalized both based on the presence of a strong EDG, and the forced

planarity of the aromatic system, which further stabilizes the corresponding aminyl radicals relative to their diarylamine equivalents via increased overlap with the π-system.[19] Furthermore, in experiments studying the RTA activity of these compounds, Lucarini *et. al.* found that phenoxazine was able to inhibit styrene autoxidation catalytically; trapping on average 5 radicals per molecule (stoichiometric number, n = 5) at 50°C.[18] This activity implies that compounds with weaker N-H bonds (and correspondingly weaker N-O bonds in the intermediate) may regenerate effectively even at ambient temperatures.

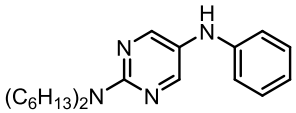

k_{inh} ($M^{-1}s^{-1}$)	
3.0×10^6	**(7.1)**

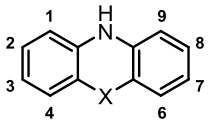

X	k_{inh} ($M^{-1}s^{-1}$)	
S	8.8×10^6	**(7.2)**
O	2.9×10^7	**(7.3)**

Remarkably, despite their weak BDEs, **7.2** and **7.3** both exhibit comparatively high stability towards direct oxidation (E^o = 0.87 and 0.85V vs. NHE, respectively, see Figure 7.3). In principle, the same attributes which stabilize aminyl radicals (and favour RTA reactivity) should also stabilize the RTA-derived radical cation and promote one-electron oxidation (as seen in the diarylamines and phenols), however, the innate stability of these compounds implies there must be another factor at play. Despite the impressive results seen in these initial studies, very little subsequent work has been done to understand the source of this behavior, or how it might be applied to the design of new generations of RTAs. Realizing that these molecules presented ideal scaffolds for further modification, we sought to combine these ideas, incorporating heterocyclic rings and strong EDGs in to the phenoxazine and phenothiazine framework, further pushing the limits of RTA reactivity. The results of our investigations are presented here.

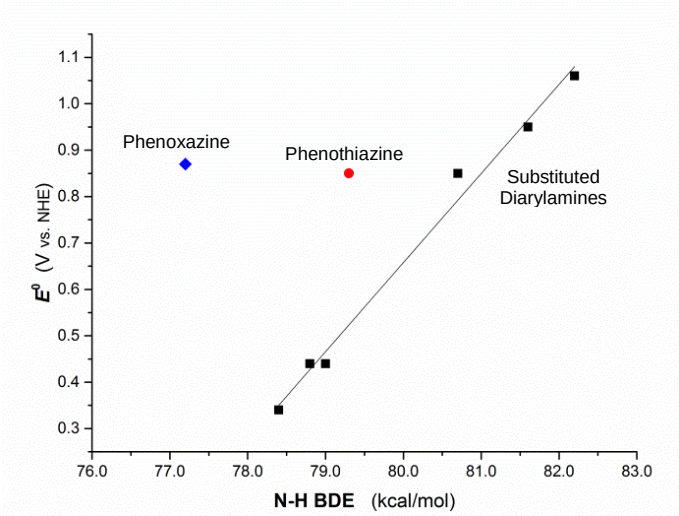

Figure 7.3. Oxidation potential (E^0) vs. N-H BDE for **7.2** (red), **7.3** (blue), and a series of diarylamine RTAs (black). The diphenylamines, listed in order of decreasing N-H BDE, are di-*p*-tolylamine, bis(6-methoxypyrdin-3-yl)amine, bis(4-methoxyphenyl)amine, N^5-(4-(dimethylamino) phenyl)-N^2,N^2-dimethylpyrimidine-2,5-diamine, N^5-(6-(dimethylamino)pyridin-3-yl)-N^2,N^2-dimethyl pyridine-2,5-diamine, and bis (4-dimethylaminophenyl)amine.

7.3 Results and Discussion

7.3.1 Computational Results

We first sought an explanation for the stability of phenoxazine and phenothiazine to one electron oxidation. The structures, N-H bond dissociation enthalpies (BDEs), and ionization potentials (IPs) of phenoxazine, phenothiazine, and 9,10-dihydroacridine were computed at the CBS-QB3 level of theory.[20]

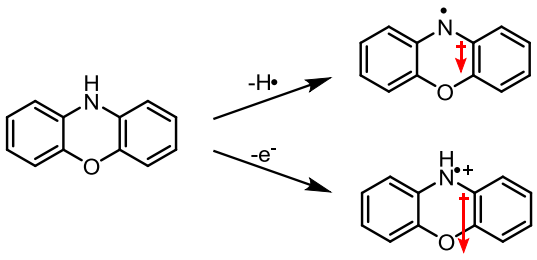

Although the -O- and -S- groups were strong electron donors into the π-system, it seemed plausible that the inductive/field effects from these electronegative atoms would destabilize the

RTA-derived radical cations more than the aminyl radicals resulting from loss of a H-atom. As such, morpholine, thiomorpholine, and piperidine were computed as models for the central ring without the influence of the π-system. Indeed, a slight trend was seen where the inductive effect from the oxygen in morpholine destabilized the aminyl radical cation without affecting its N-H BDE. This trend was even more apparent when the structures were forcibly planarized into a C_{2v} symmetric geometry resembling the central ring of the tricyclic systems (Figure 7.4). In these cases, field effects from the electronegative atom are responsible for a *ca.* 5.4 kcal/mol increase in the IP of (planarized) thiomorpholine, and a further 2.9 kcal/mol increase in the IP of morpholine, relative to piperidine. Simultaneously, these effects had virtually no influence on the N-H BDEs.

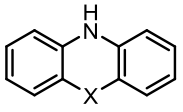

X	N-H BDE (kcal/mol)	IP (kcal/mol)
O	75.2	159.6
S	78.7	154.0
CH_2	84.0	164.1

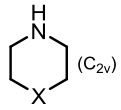

O	86.2	182.0
S	85.8	179.1
CH_2	86.7	173.7

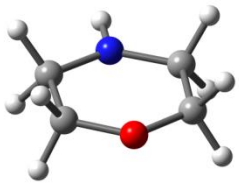

Figure 7.4. A) N-H BDEs and IPs of phenoxazine, phenothiazine, 9,10-dihydroacridine and the C_{2v} symmetric structures of morpholine, thiomorpholine, and piperidine calculated at the CBS-QB3 level of theory. B) Optimized C_{2v} symmetric geometry of morpholine.

The exceptional reactivity of phenoxazine, then, arises from the electron donating ability of the oxygen substituent, which stabilizes the aminyl radical through the π-system, but is balanced by inductive/field effects which destabilize the aminyl radical cation and disfavor direct oxidation.

We next examined if integration of heteroatoms into the rings would further stabilize the molecules towards oxidation (Table 7.1). When the nitrogen atoms were incorporated into positions in direct conjugation with the amine, the N-H bonds were significantly strengthened. Although both 1- and 3- azaphenoxazine showed appreciable increases in their ionization potentials (+4.4 and +9.0 kcal/mol, respectively), the BDEs of these compounds increased by 6.0 and 2.1 kcal/mol,

respectively, relative to phenoxazine. Alternatively, the bond strengths in 2- and 4-azaphenoxazine were virtually unchanged from that of phenoxazine (+0.5 and -0.5 kcal/mol, respectively), while they retained the higher IPs (+7.4 and +4.6 kcal/mol respectively) seen in the other isomers.

These trends were also seen in diaza-derivatives. While 1,3- and 1,4-diazaphenoxazine were significantly more stable to oxidation (+14.0 and +10.9 kcal/mol, respectively), this benefit is offset by the strengthened N-H bonds (+8.0 and +6.3 kcal/mol, respectively), which drastically cuts their reactivity to peroxyl radicals. 2,4-Diazaphenoxazine, on the other hand, maintained its weak N-H bond (+0.3 kcal/mol) and high IP (+12.2 kcal/mol), striking the best balance between increased IP and minimal BDE, and providing the most promising starting point for further optimization.

In theory, this substitution pattern can be applied to the other aromatic ring as well, yielding 2,4,6,8-tetrazaphenoxazine, a structure with a remarkably high ionization potential (+24.9 kcal/mol), relative to its N-H BDE (+0.2 kcal/mol), but which could only be studied *in silico* due to the difficulties associated with its synthesis (*vide infra*).

Table 7.1. Calculated N-H Bond Dissociation Enthalpies (BDEs) and Ionization Potentials (IPs) for a Series of Diazaphenoxazines Calculated at the CBS-QB3 Level of Theory.

	N-H BDE (kcal/mol)	IP (kcal/mol)		N-H BDE (kcal/mol)	IP (kcal/mol)
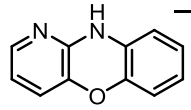	81.2	164.0	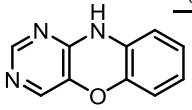	83.2	173.6
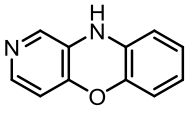	75.7	167.1	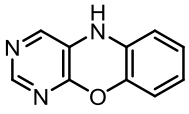	75.5	171.8
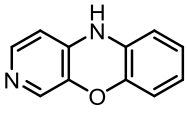	77.3	168.6	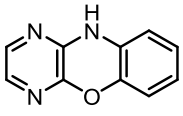	81.5	170.5
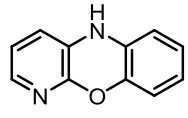	74.7	164.2	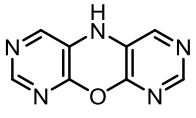	75.4	184.5

7.3.2 Synthesis of Azaphenoxazines and Azaphenothiazines

The 1-, 2-, 3-, and 4-aza derivatives of phenoxazine (**7.4-7.7**) and phenothiazine (**7.8-7.11**) have been previously described in the literature,[21–23] however their reactivity as RTAs has not previously been studied. Using a combination of literature procedures and those discussed in a recent article by our group,[24] each of the isomers of both phenoxazine, and phenothiazine were prepared (Figure 7.5).

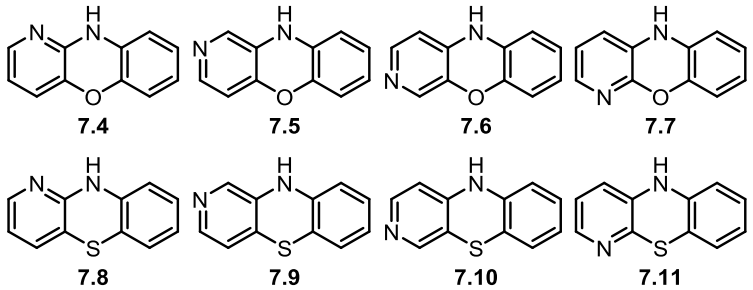

Figure 7.5. Structures of 1-, 2-, 3-, and 4-azaphenoxazine (**7.4-7.7**, respectively) and 1-, 2-, 3-, and 4-azaphenothiazine (**7.8-7.11**, respectively).

Additionally, a similar procedure was used to prepare 1,3- or 2,4-diaza derivatives. Briefly, either isomer could be prepared using a Cu-catalyzed cross coupling from the appropriate diaryl precursors, where the polarity of the amine and halide substituents determines the substitution pattern in the product (Scheme 7.3). This is based on either the presence or absence of an intramolecular Smiles rearrangement prior to the cross coupling. Through this approach we were able to synthesize a set of alkyl- and dialkylamino- substituted, 1,3- and 2,4-diazaphenoxazines and diazaphenothiazines **7.12-7.19** (Figure 7.6). These included the phenoxazine and phenothiazine analogues of diarylamine **7.1**, which were anticipated to have exceptional reactivity to peroxyl radicals.

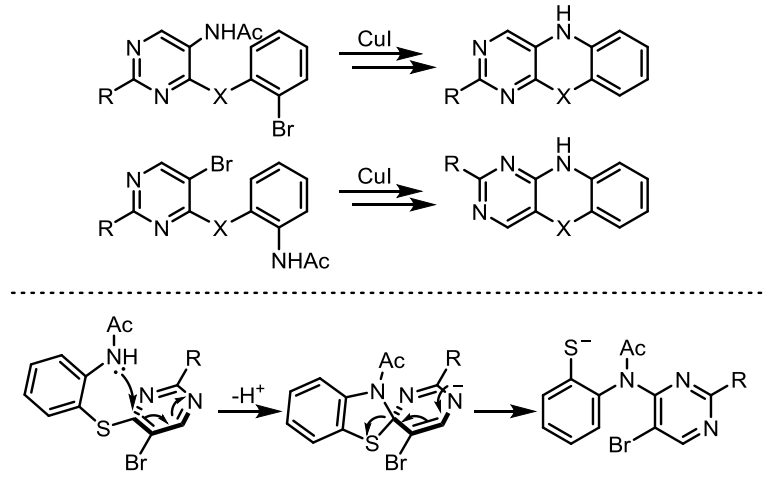

Scheme 7.3. A) Formation of either 1,3- or 2,4-diazaphenoxazines (X = O) or diazaphenothiazines (X = S) based on the polarity of the Cu-catalyzed cross coupling reaction. B) Mechanism of a representative smiles rearrangement.

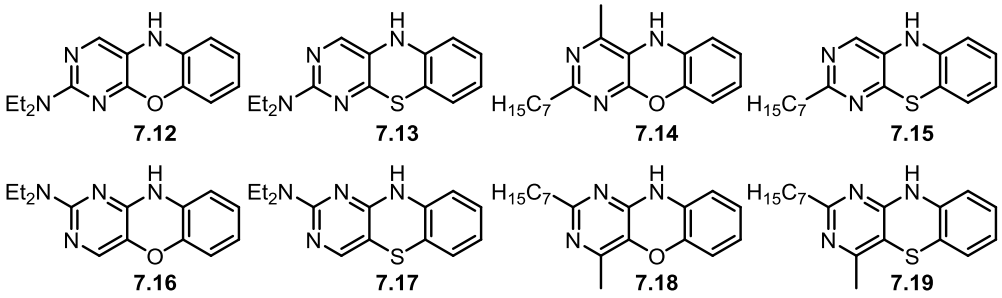

Figure 7.6. Structures of alkyl- and diethylamino-substituted diazaphenoxazine and diazaphenothiazine RTAs (**7.12-7.19**).

7.3.3 Electrochemistry

In order to measure the susceptibility of the RTAs to direct oxidation, the standard potentials (E^{o}) of each of the azaphenoxazines and azaphenothiazines were measured using cyclic voltammetry (CV, vs. $Ag/AgNO^{3}$). In the cases where the redox chemistry was irreversible, differential pulse voltammetry (DPV) was used to measure the anodic peak potentials (E^{pa}). Representative examples of these experiments are shown in Figure 7.7.

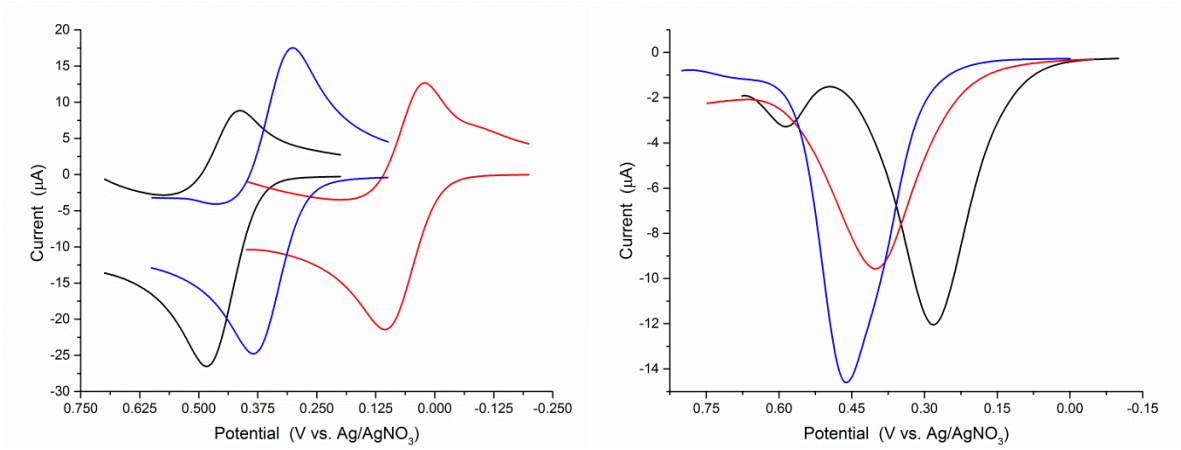

Figure 7.7. A) Representative cyclic voltammograms for **7.2** (blue), **7.8** (black), and **7.13** (red), in MeCN at 25°C. B) Representative differential pulse voltammograms for **7.9** (black), **7.10** (red), and **7.19** (blue) in MeCN at 25°C.

Incorporation of a single nitrogen atom into the aromatic increased the oxidation potential of the compounds relative to the unsubstituted derivatives (Table 7.2). The 1- and 4-aza derivatives, **7.4**, **7.7**, **7.8**, and **7.11**, had (quasi-)reversible electrochemistry, and consistently higher oxidation potentials that their parent structures (0.05-0.10 V vs. NHE). However, the 2- and 3-aza compounds, specifically **7.5**, **7.6**, and **7.9**, showed broad shallow (and irreversible) anodic peaks in both the CV and DPV experiments, implying that upon oxidation, these structures undergo further chemistry, likely generating other more oxidizable compounds.

Substitution of the molecules with dialkylamino-substituents, as in **7.12** and **7.13**, predictably lowers the redox potential of the RTAs (E^{o} = 0.54 and 0.59V, respectively). However, incorporation of the pyrimidine ring into the structures and the inductive/field effects from the chalcogen atoms both work to stabilize the molecule to one electron oxidation. Indeed both **7.12** and **7.13** are more stable to oxidation that many of the most reactive diarylamine RTAs (*cf.* Figure 7.2).[5]

The anodic peak potentials (E^{pa}) of the alkyl-substituted diaza-derivatives **7.14**, **7.15**, **7.18**, and **7.19**, were measured by differential pulse voltammetry due to the highly irreversible electrochemistry seen by CV. The E^{pa} of the compounds were quite high (0.99-1.05V), indicating

that the compounds were likely quite stable to direct oxidation. Indeed, the oxidation potentials of these compounds are comparable to that of the 4,4'-dialkyldiphenylamines used industrially.[5]

7.3.4 Inhibited Autoxidations at Ambient Temperatures

The efficacies of the antioxidants were measured using the spectrophotometric approach previously developed by our lab.[25] In this approach, the autoxidation of an oxidizable hydrocarbon is monitored by the addition of a highly absorbent probe, PBD-BODIPY, which oxidizes in parallel with the substrate. The consumption of the probe can be observed by conventional UV-Vis spectrophotometry and used to track the progress of the reaction. The second order inhibition rate constant for a given RTA can be calculated from the initial 'inhibited rate' in the autoxidation, and the stoichiometric numbers calculated from the length of the inhibited period.

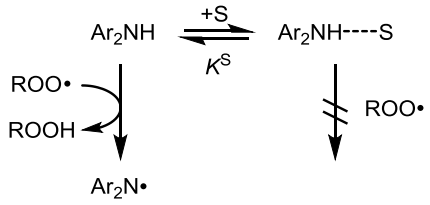

Scheme 7.4. H-bonding equilibrium between a diarylamine and solvent, and its effect on H-atom transfer reactions.

In order to directly compare the reactivity of the RTAs to the diarylamines and phenols reported previously, the kinetics of the RTAs must be measured at identical temperatures. However, the PBD-BODIPY/styrene system previously described at 37°C can only accurately measure rate constants up to *ca.* 10^7 $M^{-1}s^{-1}$.[25] Since **7.3** has a k_{inh} = 2.9×10^7 $M^{-1}s^{-1}$, the PBD-BODIPY/styrene system would very likely be insufficient to measure the reactivity of many of the azaphenoxazine and azaphenothiazine RTAs, and a different approach must be used. Since aminic or phenolic RTAs cannot react with radicals when hydrogen bonded (Scheme 7.4),[26,27] addition of an H-bond accepting solvent to the reaction lowers the effective concentration of RTAs in the system, and suppresses their

reactivity. In this case, these kinetic solvent effects (KSEs) could be exploited to reduce the reactivity of the RTAs to a measurable range. The effect of H-bonding KSEs on the reactivity of RTAs is well understood, and can be accounted for using the equations developed by Snelgrove *et. al.* (equation 8.1),[26] where α_2^{H} and β_2^{H} are the Abraham H-bond acidity and basicity values for the amine and solvent mixture, respectively.[28]

$$k_{\mathrm{inh}}^{\mathrm{Solvent}} = k_{\mathrm{inh}}^{0} - 8.3\alpha_2^{\mathrm{H}}\beta_2^{\mathrm{H}} \quad (8.1)$$

1,4-Dioxane was chosen as the oxidizable substrate due to its well characterized oxidation kinetics,[32] and moderate H-bond accepting ability.[33] The autoxidations were initiated by 6mM AIBN with 2μM antioxidant added after a steady rate of oxidation had been observed. Representative data for the dioxane autoxidations inhibited by **7.4**-**7.7** are shown in Figure 7.8.

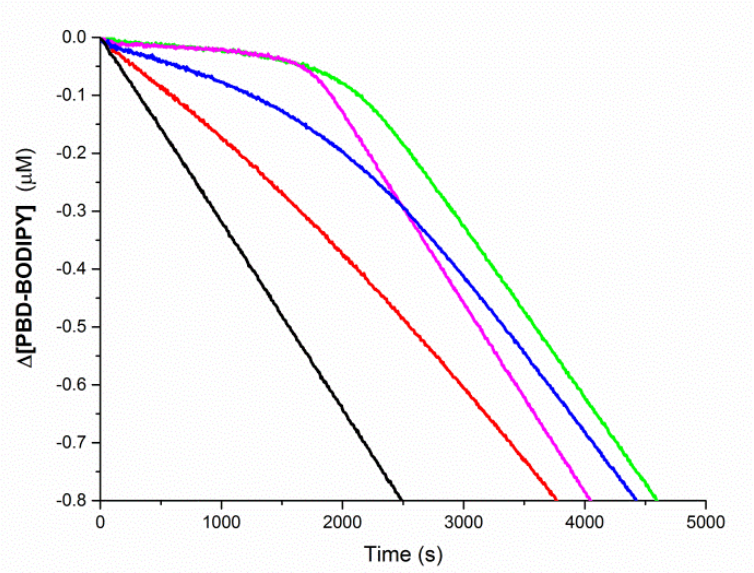

Figure 7.8. Co-autoxidation of 1,4-dioxane (2.9 M) and PBD-BODIPY (10 μM) initiated by AIBN (6 mM) in PhCl at 37°C monitored at 587nm (ε = 123,023 $M^{-1}cm^{-1}$). Uninhibited (black), and inhibited with 2 μM of **7.4** (red), **7.5** (green), **7.6** (blue), or **7.7** (magenta).

Under these conditions, **7.3** completely inhibited the reaction. This is likely the result of its weaker H-bonding acidity (α_2^{H} = 0.44), relative to its aza derivatives **7.4**-**7.7** (α_2^{H} = 0.50-0.55). Although the rate constants may be similar between the RTAs, **7.3** would be less affected by an H-

bonding solvent and its reactivity in the system would be higher. Alternatively, the corrected rate constant for **7.2**, k_{inh}^{PhCl} = 8.0×10^6 is in excellent agreement with the results obtained by Lucarini *et. al.*.[18]

The reactivity seen with RTAs **7.4**-**7.7** perfectly reproduce the trends predicted computationally. 1-Azaphenoxazine (**7.4**) was the least effective inhibitor, consistent with the largest projected increase in N-H BDE.[34] 3-Azaphenoxazine (**7.6**, k_{inh}^{PhCl} = 6.8×10^6 M^{-1}s^{-1}) performed better than **7.4**, although still showed a decrease in reactivity relative to phenoxazine itself (lit. k_{inh}^{PhCl} = 2.9×10^7 M^{-1}s^{-1}).[18] The 2- and 4- isomers, **7.5** and **7.6** (k_{inh}^{PhCl} = 2.5×10^7 and 4.2×10^7 M^{-1}s^{-1}, respectively) showed nearly identical reactivity to phenoxazine.

Table 7.2. Abraham H-Bond Acidity Parameters, Dioxane Inhibition Rate Constants, Chlorobenzene Inhibition Rate Constants, Standard Potentials, and Stoichiometries for Monoazaphenoxazine and Monoazaphenothiazine Antioxidants.

Compound	α_2^H	$k_{inh}^{Dioxane}$ (M^{-1}s^{-1})	k_{inh}^{PhCl} (M^{-1}s^{-1})	E^o (V $_{vs. NHE}$)	n
7.2	0.38	(1.2 ± 0.1) × 10^6	(8.0 ± 0.4) × 10^6	0.85	2.0
7.3	0.44	*too fast*	------	0.87	2.1
7.4	---[a]	(1.8 ± 0.1) × 10^5	------[a]	0.92	2.1
7.5	0.50	(2.1 ± 0.2) × 10^6	(2.5 ± 0.3) × 10^7	---[b]	2.5
7.6	0.55	(4.4 ± 0.2) × 10^5	(6.8 ± 0.3) × 10^6	---[b]	2.3
7.7	0.52	(3.1 ± 0.3) × 10^6	(4.2 ± 0.3) × 10^7	0.92	2.0
7.8	---[a]	*too slow*	------	0.97	---
7.9	0.41	(3.5 ± 0.2) × 10^5	(2.7 ± 0.2) × 10^6	---[b]	2.2
7.10	0.48	*too slow*	------	0.95[c]	---
7.11	0.46	(9.9 ± 0.1) × 10^5	(9.5 ± 0.1) × 10^6	0.93	2.1

[a)]Formation of H-bonded dimers in organic solution prevents accurate determination of α_2^H. [b)] Flat broad peak in DPV voltammograms. [c)] E^{pa} values from differential pulse voltammetry reported due to irreversible electrochemistry.

This same trend could be seen in the azaphenothiazine derivatives **7.8**-**7.11**, where the 2- and 4-aza derivatives (**7.9** and **7.11**, respectively) were effective RTAs, comparable to unsubstituted phenothiazine, while the 1- and 3-aza derivatives (**7.8** and **7.10**) were too slow to effectively inhibit the autoxidation.

The stoichiometry of the reaction was *ca.* 2 for each of the RTAs tested. This suggests that, in spite of the weak N-H bonds and heightened reactivity of the compounds, the antioxidants were all reacting stoichometrically and virtually no catalytic turnover was taking place.

Expecting that substitution of the azaphenoxazine and azaphenothiazine cores with electron donating groups would further increase the reactivity of the RTAs, we extended this approach to the alkyl- and dialkylamino-substituted diaza-derivatives (**7.12**-**7.15**). We found that, even when the autoxidations were performed in dioxane, the reactivity of the antioxidant often completely inhibited the autoxidation (i.e. consumption of the probe was too low to measure over the inhibited region of the reaction). In order to further suppress the reactivity of these RTAs, the reactions were run in a mixture containing an additional 3.5M DMSO. The stronger H-bond accepting ability of DMSO further reduces the effective k_{inh} of the antioxidant present in the reaction (Figure 7.9), allowing measurement of more reactive RTAs. Representative data for compounds **7.7**, **7.12**-**7.14** are shown in Figure 7.10.

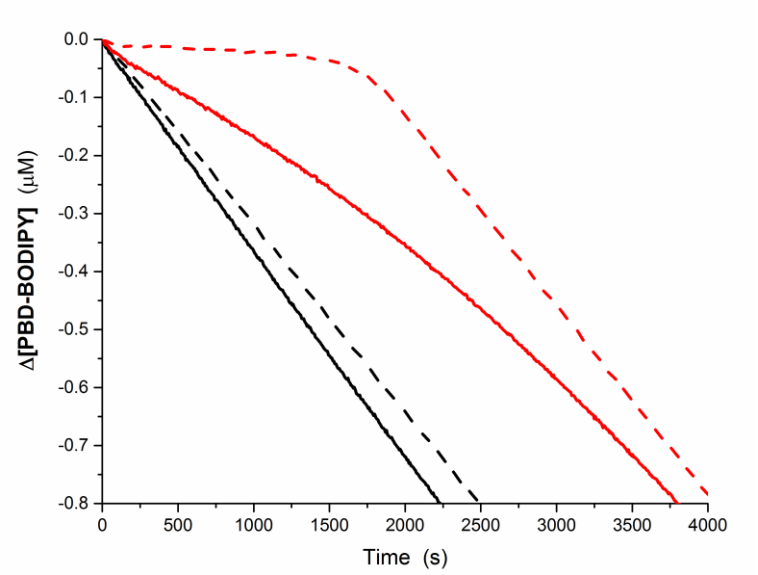

Figure 7.9. Co-autoxidation of 1,4-dioxane (2.9 M) and PBD-BODIPY (10 μM) initiated by AIBN (6 mM) in PhCl at 37°C, monitored at 587nm (ε = 123,023 $M^{-1}cm^{-1}$). Uninhibited (black), or inhibited with 2 μM **7.7** (red), with the reaction mixture containing no DMSO (dashed lines) or 3.5M DMSO (solid lines).

Addition of DMSO slowed the reactivity of compound **7.7** by a factor of *ca.*10 relative to its inhibition in dioxane (k_{inh} = 2.2×10^5 vs. 2.1×10^6 M^{-1}s^{-1}, respectively), however correcting the rate constants to account for the different H-bonding equilibria in the solutions results in nearly identical rate constants measured in either system. With the addition of DMSO, k_{inh} for **7.3** could be measured, and corrected to account for the KSE (k_{inh}^{DMSO} = 5.6×10^5, and k_{inh}^{PhCl} = 4.1×10^7 M^{-1}s^{-1}). The rate constant was again found to be in good agreement with the literature value.[18]

Even with DMSO added to the reaction, compounds **7.12** and **7.13** both almost completely inhibited autoxidation of the probe. Accounting for the KSE, the equivalent rate constants in chlorobenzene could be calculated as k_{inh}^{PhCl} = 5.2×10^8 and 1.3×10^8 M^{-1}s^{-1}, respectively, by far the most reactive aminic antioxidants ever measured! Moreover, compound **7.12** is faster than the most reactive phenolic antioxidants by a factor of two.[12]

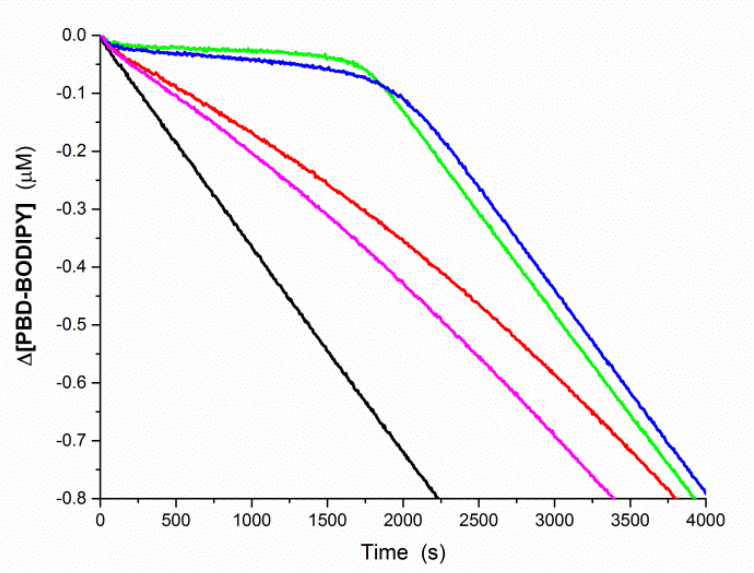

Figure 7.10. Co-autoxidation of 1,4-dioxane (2.9 M) and PBD-BODIPY (10 μM) initiated by AIBN (6 mM) in PhCl with DMSO (3.5 M) at 37°C, monitored at 587nm (ε = 123,023 M^{-1}cm^{-1}). Uninhibited (black), or inhibited with 2 μM of **7.7** (red), **7.12** (green), **7.13** (blue), or **7.14** (magenta).

The stoichiometry of the most reactive compound, **7.12**, was found to be slightly less than 2, possibly the result of minor background oxidation over the course of the reaction. However, even

7.13, which is nearly as oxidizable (Table 7.3), had a stoichiometry, n = 2.1, and showed no evidence of oxidative consumption over the reaction.

Table 7.3. Abraham H-Bond Acidity Parameters, Dioxane/DMSO Inhibition Rate Constants, Chlorobenzene Inhibition Rate Constants, and Stoichiometries for Selected Azaphenoxazine and Azaphenothiazine Antioxidants.

Compound	α_2^H	k_{inh}^{DMSO} ($M^{-1}s^{-1}$)	k_{inh}^{PhCl} ($M^{-1}s^{-1}$)	E^o ($V_{vs.\ NHE}$)	n
7.3	0.44	$(5.6 \pm 0.2) \times 10^5$	$(4.1 \pm 0.1) \times 10^7$	0.87	2.2
7.7	0.52	$(2.2 \pm 0.1) \times 10^5$	$(3.4 \pm 0.1) \times 10^7$	0.92	2.3
7.12	0.50	$(4.2 \pm 0.1) \times 10^6$	$(5.2 \pm 0.1) \times 10^8$	0.54	1.8
7.13	0.44	$(1.7 \pm 0.4) \times 10^6$	$(1.3 \pm 0.3) \times 10^8$	0.59	2.1
7.14	0.43	$(1.7 \pm 0.2) \times 10^5$	$(1.1 \pm 0.1) \times 10^7$	0.99	2.0
7.15	0.50	*too slow*	------	0.99	---

7.3.5 Inhibited Autoxidations at 100°C

Since no catalytic activity from the RTAs could be observed in dioxane at ambient temperatures, we next applied the PBD-BODIPY methodology to elevated temperature autoxidations of 1-hexadecene (chosen as a readily available, activated, non-volatile substrate).[35] As in the previous case, in the initial region of the reaction consumption of the probe is suppressed based on the reactivity of the RTA (Figure 7.11A), and could be used to determine k_{inh}. The RTAs which had nitrogen atoms in either the 1- or 3-positions were less effective inhibitors compared to the equivalent 2- and/or 4-aza isomers, consistent with the results at ambient temperature. After the inhibited region of the reaction (~1200s), which corresponds roughly to a stoichiometry of *ca*. n = 2 for each of the RTAs tested, we observed a 'secondary' inhibited region where the progress of the autoxidation was still slowed relative to the uninhibited rate. In many cases, this secondary inhibited phase lasted for many times the length of the initial region before returning to the true 'uninhibited rate' (Figure 7.11B). The length of inhibition corresponds to high stoichiometric numbers, similar to those seen at elevated temperatures where diarylamine RTAs are catalytic.

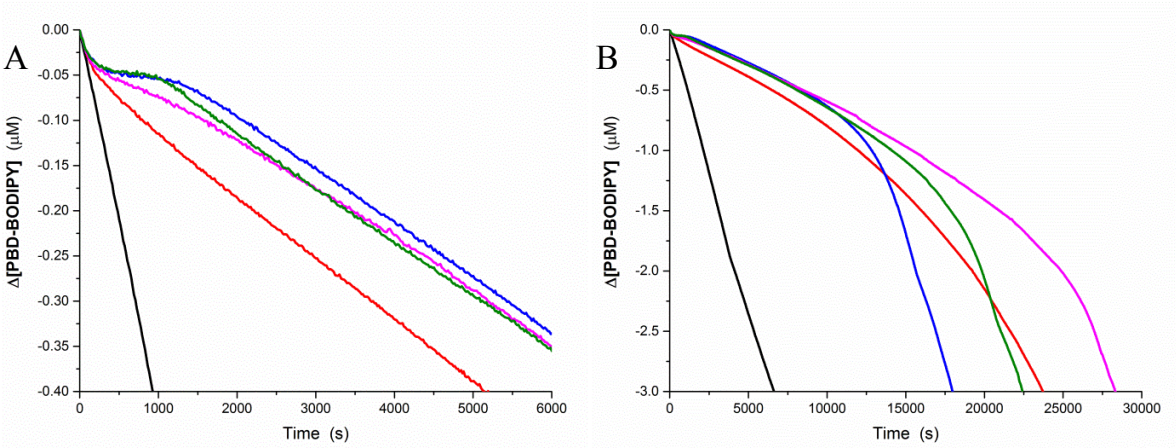

Figure 7.11. Co-autoxidation of 1-hexadecene (2.8 M) and PBD-BODIPY (10 μM) initiated by dicumyl peroxide (1 mM) in PhCl at 100°C, monitored at 587nm (ε = 131,972 $M^{-1}cm^{-1}$). Uninhibited (black), or inhibited with 600 nM of **7.4** (red), **7.5** (green), **7.8** (magenta), or **7.9** (blue). A) Initial phase of the reaction. B) Extended view.

Remarkably, it appears that the 'catalytic rate' (R_{cat}) of the reaction is roughly the same regardless of the structure of the antioxidant. This, coupled with the clear inflection point between the initial and catalytic regions of the reaction (for the most reactive RTAs), implies that under these conditions the rate limiting step in the catalytic cycle cannot significantly depend on the structure of the RTA. This would seem to rule out decomposition of the alkoxyamine intermediate as the key step in the process, as the strength of the N-O bond would depend heavily on the structure of the initial compound.

Additionally the stoichiometries of the antioxidants do not appear to follow a clear trend (Table 7.4). While the 2- and 4-azaphenoxazines (**7.5** and **7.7**) have faster inhibition rate constants – the result of a weaker N-H bond – they do not regenerate as effectively as the 1- and 3-aza isomers (**7.4** and **7.6**), which are similar in stoichiometry to unsubstituted phenoxazine. This trend seems to be reversed for the azaphenothiazine derivatives, where the 2- and 4-aza derivatives (**7.9** and **7.11**) regenerate more effectively than **7.10** (**7.8** is too slow to inhibit). Indeed, both **7.9** and **7.11** have almost twice the stoichiometry of the parent phenothiazine.

Table 7.4. Chlorobenzene Inhibition Rate Constants and Stoichiometries for Azaphenoxazine and Azaphenothiazine Antioxidants.

Compound	k_{inh}^{PhCl} ($M^{-1}s^{-1}$)	*n*
7.2	$(4.6 \pm 1.3) \times 10^6$	36 ± 3
7.3	$(2.1 \pm 0.4) \times 10^7$	61 ± 2
7.4	$(2.1 \pm 0.1) \times 10^6$	48 ± 1
7.5	$(1.7 \pm 0.5) \times 10^7$	31 ± 2
7.6	$(4.8 \pm 0.8) \times 10^6$	65 ± 1
7.7	$(1.3 \pm 0.6) \times 10^7$	46 ± 2
7.8	*too slow*	---
7.9	$(4.1 \pm 0.2) \times 10^6$	59 ± 1
7.10	$(2.0 \pm 0.1) \times 10^6$	25 ± 1
7.11	$(7.7 \pm 0.1) \times 10^6$	65 ± 2

The substituted diazaphenoxazines and diazaphenothiazines maintained their high reactivity at 100°C, with compounds **7.12** and **7.13**, again completely inhibiting consumption of the BODIPY probe. Similarly, the alkyl-substituted 2,4-diaza compounds **7.14** and **7.15**, proved to be capable inhibitors, with inhibition rate constants, $k_{inh}^{PhCl} = 1.0\times10^7$ and 4.4×10^6 $M^{-1}s^{-1}$, respectively. The 1,3-diaza isomers of phenoxazine were also surprisingly effective ($k_{inh}^{PhCl} = 1.2\times10^6$ and 1.1×10^6 $M^{-1}s^{-1}$, for **7.16** and **7.18**, respectively, Table 7.5). However, the 13-diazaphneothiazines **7.17** and **7.19**, were too slow to effectively inhibit the reaction.

Similar to the previous cases, for compounds reactive enough to inhibit the autoxidation, the inhibition time corresponds to a stoichiometry of roughly $n \approx 2$.However, despite the high reactivity of these compounds to peroxyls, they did not display nearly the catalytic activity of the unsubstituted or mono-aza derivatives. The consistent stoichiometry in the inhibited phase implies that, even at 100°C, the base compounds are reasonably stable towards direct oxidation, but that subsequent products – likely the nitroxide or alkoxyamine intermediates in the catalytic cycle – may still be susceptible to oxidation. Indeed, only **7.16** and **7.18**, compounds with the highest oxidation potentials and which were still effective inhibitors, displayed significant turnover. This suggests that

the stability of the intermediates likely has a more significant role in efficient turnover than a weak N-O bond in the alkoxyamine.

Table 7.5. Chlorobenzene Inhibition Rate constants and Stoichiometries for Diazaphenoxazine and Diazaphenothiazine Antioxidants.

Compound	k_{inh}^{PhCl} ($M^{-1}s^{-1}$)	*n*
7.12	*too fast*	4.8 ± 0.5
7.13	*too fast*	5.1 ± 0.5
7.14	$(1.0 \pm 0.1) \times 10^7$	8.1 ± 0.2
7.15	$(4.4 \pm 0.3) \times 10^6$	58 ± 3
7.16	$(1.2 \pm 0.1) \times 10^6$	3.2 ± 0.1
7.17	*too slow*	---
7.18	$(1.1 \pm 0.1) \times 10^6$	26 ± 1
7.19	*too slow*	---

7.3.6 Inhibited Autoxidations at Elevated Temperatures

Diarylamine antioxidants see the majority of their use well above 100°C, where they are known to be catalytically active.[13] To study the high temperature reactivity of these RTAs, we employed the autoxidation of *n*-hexadecane at 160°C. The experiments were run in a parallel stirred flow reactor, based on the design originally used by Jensen,[8] where a constant flow of oxygen is bubbled through the heated reaction in order to prevent mass transfer limitations from affecting the kinetics of the autoxidation. Samples were taken at regular intervals, and the hydroperoxides in the complex mixture were quantified using the pro-fluorescent phosphine previously developed by our lab.[36,37] Representative data from the autoxidations is shown in Figure 7.12.

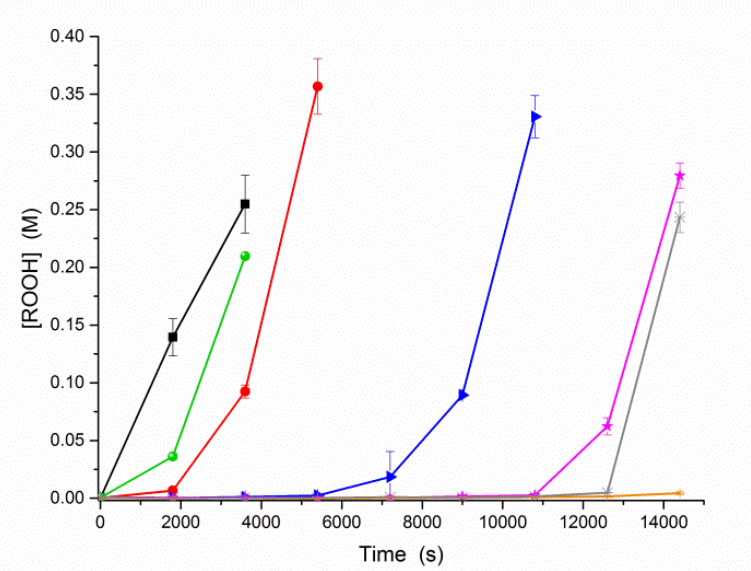

Figure 7.12. Hydroperoxide formation during the inhibited autoxidation of *n*-hexadecane at 160°C, no initiator, uninhibited (black), or inhibited with 100μM of diltolylamine (red), **7.4** (blue), **7.6** (magenta), **7.8** (green), **7.9** (orange), or **7.11** (grey).

Under these conditions, the concentration of hydroperoxides increase up to a maximum of *ca.* 0.3M, after which the yield decreases as the hydroperoxides decompose to form a complex mixture of ketones, alcohols, carboxylic acids, and esters.[8] Addition of 100μM of the RTAs to the autoxidizing mixture inhibited the formation of hydroperoxides for a given time based on the reactivity of the antioxidant. However, since at these temperatures thermolysis of hydroperoxides is the primary source of chain initiating radicals, the rate of initiation is variable as the reaction progresses. This prevents a simple kinetic analysis for determining the k_{inh} of the antioxidants, as well as calculation of the RTA stoichiometry. However, the relative efficacy of the antioxidants can still be approximated by the length of the inhibited period in the reaction (t_{inh}).

Table 7.6. Absolute and relative inhibition times of selected azaphenoxazine and azaphenothiazine RTAs.

Compound	t_{inh}	$t_{inh}/t_{inh\text{-}DTA}$
DTA	2020	1
7.2	9380	4.6
7.3	8910	4.4
7.4	7310	3.6
7.5	8860	4.4
7.6	11100	5.5
7.7	10800	5.4
7.8	390	0.2
7.9	>15000	>7.5
7.10	12510	6.2
7.11	12560	6.2

Both **7.2** and **7.3** were considerably more effective inhibitors than ditolylamine (DTA), the short chain analogue of the 4,4'-dialkyldiphenylamines used industrially – by factors of 4.4 and 4.6, respectively (Table 7.6).[38] As seen in the previous experiments the 1-aza derivatives, **7.4** and **7.8**, were the least effective inhibitors of the mono-aza compounds. While **7.4**, was moderately effective, preventing buildup of hydroperoxides for *ca.* 8900s, **7.8** scarcely inhibited at all, lasting *ca.* 390s before the autoxidation proceeded.

Compounds **7.5**, **7.6**, and **7.7**, inhibited the autoxidation well, preventing buildup of hydroperoxides for up to 5.5 times the length of time of ditolylamine. The differences between the isomers in hexadecene at 100°C are much larger than those seen in under these conditions, where the differences in activation energy between the isomers have less influence. The azaphenothiazines, **7.9**, **7.10**, and **7.11**, were incredibly effective inhibitors, performing amongst the best of all the compounds tested.

The autocatalytic nature of the autoxidation at these temperatures gives the phenothiazine derivatives an advantage over their phenoxazine counterparts. In the initial region of the autoxidation, the hydroperoxide concentration is quite low, resulting in a slow rate of initiation, after which the buildup of hydroperoxides (and thus R_i going forward) is inversely dependent on the k_{inh} of

the antioxidant. More effective RTAs trap peroxyl radicals faster, keeping [ROOH], and thus R_i, low. In the case of phenothiazines, not only can the antioxidant trap the peroxyl radicals which propagate the chain reaction, but the sulfide moiety can reduce the hydroperoxides which initiate them. In this way, phenothiazines both prevent the accumulation of hydroperoxides and decompose those already present – acting as both a radical-trapping and preventative antioxidant. This dual effect is responsible for the extreme efficacy seen by phenothiazine (relative to phenoxazine), and by many of the azaphenothiazine derivatives tested. In many applications, combinations of both radical trapping and preventative antioxidants are used together to take advantage of this effect.

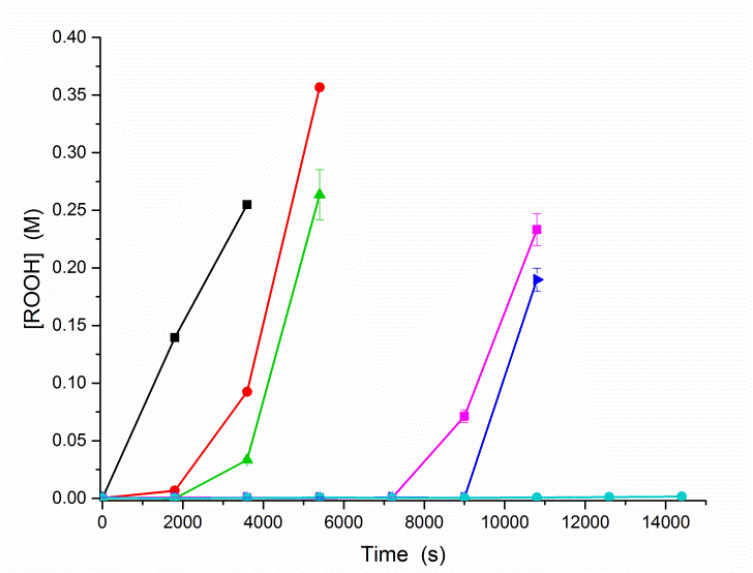

Figure 7.13. Hydroperoxide formation during the inhibited autoxidation of *n*-hexadecane at 160°C, no initiator, uninhibited (black), or inhibited with 100μM of diltolylamine (red), **7.12** (green), **7.13** (blue), **7.14** (magenta), or **7.15** (cyan).

Table 7.7. Absolute and Relative Inhibition Times of Selected Diazaphenoxazine and Diazaphenothiazine RTAs.

Compound	t_{inh}	$t_{inh}/t_{inh\text{-}DTA}$
7.12	2250	1.1
7.13	8990	4.5
7.14	7430	3.7
7.15	>15000	>7.5
7.17	3400	1.7
7.18	3530	1.7
7.19	160	0.08

Similar to the experiments at 100°C, the most electron rich compounds **7.12** and **7.13**, were only moderately effective inhibitors (Figure 7.13), likely owing to their low oxidation potentials. Exchange of the dialkylamino-substituents for the less electron rich alkyl chains improved the effectiveness of the RTAs, as in **7.14** and **7.15**, which inhibit more than twice the length of the more oxidizable compounds. Both the phenothiazines **7.13** and **7.15** inhibit more effectively than the corresponding phenoxazine derivatives, due to the mixture of radical-trapping and preventative antioxidant reactivity (Table 7.7).

Compounds **7.17** and **7.18**, which lack electron donating groups *ortho* or *para* to the reactive amine, only inhibited *ca.* 3500s – less than two fold more effectively than ditolylamine, and consistent with the poor reactivity seen by the majority of 1-aza or 1,3-diaza derivatives. While **7.8**, **7.17**, and **7.19** contain sulfide groups in their structures, and are likely to reduce hydroperoxides as preventative antioxidants, their strong N-H bonds (the result of the 1-aza substituent) prevent them from effectively terminating the radical chains responsible for the autoxidation.

Tricyclic azaphenoxazine and azaphenothiazine derivatives display remarkable reactivity as radical trapping antioxidants. The trends in reactivity across the compounds studied should provide useful structural and reactivity information for the design of highly effective, catalytically active RTAs based on these structural cores. The strength of their N-H bonds, and thus their reactivity to peroxyl radicals can be controlled by selective incorporation of heteroatoms and substitution of

electron donating groups into the aromatic rings. While the 2- and/or 4-aza isomers have the weakest N-H bonds (and thus highest reactivity to peroxyls), this does not necessarily translate to improved turnover of the RTAs. The 3-aza derivatives, in particular show increased turnover and more effective inhibition at elevated temperatures where they are catalytically active – a trend that is inconsistent with our current understanding of the catalytic mechanism. Alternatively, 1-aza isomers seem to be inferior in the majority of tests.

Much like diarylamines and phenols, the reactivity of these RTAs can be modulated by introduction of EDGs into the structure, however, this often seems to impede effective turnover of the RTA, rather than assist. Even though the electron rich the amines themselves appear stable to oxidation, it remains possible that intermediates in the catalytic cycle may be more prone to oxidation or off-cycle reactions as a result.

7.4 Conclusion

We have prepared a series of heterocyclic phenoxazine and phenothiazine analogues, which, based on computational predictions, were expected to have high reactivity as radical trapping antioxidants. Incorporation of heteroatoms into the rings increased the oxidation potential of the molecules and allowed substitution with electron donating groups, which weaken the reactive N-H bond. In order to measure the reactivity of these RTAs, we modified our previous spectrophotometric approach[25] to include H-bond accepting substrates/additives, which suppress the reactivity of the compounds, and allows for accurate measurement of their inhibition rate constants, k_{inh}. Incorporation of heteroatoms into the 1- and/or 3-positions in the ring system, reduce the reactivity of the RTA by strengthening the reactive bond, while the 2- and 4-aza derivatives have only a minor effect on k_{inh}. Substitution of the azaphenoxazine and azaphenothiazine core with electron donating groups can produce some of the most reactive RTAs ever reported.

We have further modified our spectrophotometric method to preform measurements at elevated temperatures, and have been able to observe catalytic turnover of these antioxidants at 70° and 100°C. Studies on the behavior and mechanism of this catalytic activity are the focus of future investigation. At 160°C, many of the phenoxazine and phenothiazine based RTAs outperform ditolylamine, and could provide enhanced stability to petroleum derived products in which they are used. Further work is currently underway to study the behavior of these compounds in industrially relevant applications.

7.5 References

(1) Ingold, K. *Chem. Rev.* **1961**, *61*, 563–589.

(2) Ingold, K. U.; Pratt, D. A. *Chem. Rev.* **2014**, *114*, 9022–9046.

(3) Brownlie, I. T.; Ingold, K. U. *Can. J. Chem.* **1966**, *44*, 861–868.

(4) Hanthorn, J.; Valgimigli, L.; Pratt, D. *J. Am. Chem. Soc.* **2012**, *134*, 8306–8309.

(5) Hanthorn, J.; Amorati, R.; Valgimigli, L.; Pratt, D. *J. Org. Chem.* **2012**, *77*, 6895–6907.

(6) Valgimigli, L.; Pratt, D. A. In *Encyclopedia of Radicals in Chemistry, Biology and Materials*; Chatgilialoglu, C.; Studer, A., Eds.; John Wiley & Sons, Ltd: Chichester, UK, 2012.

(7) Amorati, R.; Valgimigli, L. *Org. Biomol. Chem.* **2012**, *10*, 4147.

(8) Jensen, R. K.; Korcek, S.; Mahoney, L. R.; Zinbo, M. *J. Am. Chem. Soc.* **1979**, *101*, 7574–7584.

(9) Jensen, R.; Korcek, S.; Zinbo, M.; Johnson, M. *Int. J. Chem. Kinet.* **1990**, *22*, 1095–1107.

(10) Shah, R.; Haidasz, E. A.; Valgimigli, L.; Pratt, D. A. *J. Am. Chem. Soc.* **2015**, *137*, 2440–2443.

(11) Wijtmans, M.; Pratt, D. A.; Valgimigli, L.; DiLabio, G. A.; Pedulli, G. F.; Porter, N. A. *Angew. Chemie Int. Ed.* **2003**, *42*, 4370–4373.

(12) Wijtmans, M.; Pratt, D. A.; Brinkhorst, J.; Serwa, R.; Valgimigli, L.; Pedulli, G. F.; Porter, N. A. *J. Org. Chem.* **2004**, *69*, 9215–9223.

(13) Jensen, R. K.; Korcek, S.; Zinbo, M.; Gerlock, J. L. *J. Org. Chem.* **1995**, *60*, 5396–5400.

(14) Haidasz, E. A.; Shah, R.; Pratt, D. A. *J. Am. Chem. Soc.* **2014**, *136*, 16643–16650.

(15) West, H. L. *J. Inst. Pet.* **1948**, *34*, 774.

(16) Murphy, C. M.; Saunders, C. E. *Pet. Refin.* **1947**, *26*, 479–484.

(17) Murphy, C. M.; Ravner, H.; Smith, N. L. *Ind. Eng. Chem.* **1950**, *42*, 2479–2489.

(18) Lucarini, M.; Pedrielli, P.; Pedulli, G. F.; Valgimigli, L.; Gigmes, D.; Tordo, P. *J. Am. Chem. Soc.* **1999**, *121*, 11546–11553.

(19) The aromatic rings in diarylaminyl radicals are out of plane by *ca.* 40° in order to minimize steric repulsion between the 2- and 2'- hydrogen atoms, while maximizing delocalization of the

radical. See: DiLabio, G. A.; Litwinienko, G.; Lin, S.; Pratt, D. A.; Ingold, K. U. *J. Phys. Chem. A* **2002**, *106*, 11719–11725.

(20) Montgomery, J. A.; Frisch, M. J.; Ochterski, J. W.; Petersson, G. A. *J. Chem. Phys.* **1999**, *110*, 2822.

(21) Ito, Y.; Hamada, Y. *Chem. Pharm. Bull. (Tokyo).* **1978**, *26*, 1375–1383.

(22) Poulenc, R. Azaphénothiazines. FRD1170119, 1955.

(23) Okafor, C. O. *Int. J. Sulfur Chem. Part B Q. Reports Sulfur Chem.* **1971**, *6*, 237–265.

(24) Haidasz, E. A.; Pratt, D. A. *Org. Lett.* **2017**, submitted.

(25) Haidasz, E. A.; Van Kessel, A. T. M.; Pratt, D. A. *J. Org. Chem.* **2016**, *81*, 737–744.

(26) Snelgrove, D. W.; Lusztyk, J.; Banks, J. T.; Mulder, P.; Ingold, K. U. *J. Am. Chem. Soc.* **2001**, *123*, 469–477.

(27) Litwinienko, G.; Ingold, K. U. *Acc. Chem. Res.* **2007**, *40*, 222–230.

(28) The α_2^H values for the each of the amines were measured using a version of Abrahams procedure modified for the use of d_6-benzene as an NMR solvent (see Supporting Information).[29-31]

(29) Abraham, R. J.; Byrne, J. J.; Griffiths, L.; Perez, M. *Magn. Reson. Chem.* **2006**, *44*, 491–509.

(30) Abraham, M. H.; Abraham, R. J.; Byrne, J.; Griffiths, L. *J. Org. Chem.* **2006**, *71*, 3389–3394.

(31) Abraham, R. J.; Mobli, M. *Magn. Reson. Chem.* **2007**, *45*, 865–877.

(32) Howard, J. A.; Ingold, K. U. *Can. J. Chem.* **1969**, *47*, 3809–3815.

(33) Abraham, M. H.; Grellier, P. L.; Prior, D. V.; Morris, J. J.; Taylor, P. J. *J. Chem. Soc. Perkin Trans. 2* **1990**, 521.

(34) In the cases of 1 and 5 the α_2^H value for the amines couldn't be measured, likely due to the formation of H-bonded dimers in the d_6-benzene NMR solvent. The H-bonding in solution influences the shifts of the N-H peaks in the spectrum and results in an inaccuracy in α_2^H measurement.

(35) The kinetics of PBD-BODIPY at elevated temperatures could be characterized in a similar

fashion to the ambient temperature experiments with both styrene and dioxane.[25]

(36) Hanthorn, J.; Haidasz, E.; Gebhardt, P.; Pratt, D. *Chem. Commun.* **2012**, *48*, 10141–10143.

(37) Shah, R.; Pratt, D. A. *J. Org. Chem.* **2016**, *81*, 6649–6656.

(38) For comparison, diarylamine **1**, the most effective of the heterocyclic diarylamines previously reported by our group inhibits the autoxidation for 7450 s.

7.6 Supporting Information

7.6.1 General Experimental

Reagents were purchased from commercial suppliers and used without further purification. Mono- and diazaphenoxazines and phenothiazines were prepared according to procedures previously reported by our lab.[S1] Column chromatography was carried out using flash silica gel (40−63 μm, 230−400 mesh). UV−vis spectra and kinetics were measured on a Cary 100 UV−vis spectrophotometer equipped with a temperature controller unit and a thermostated 6 × 6 multicell holder. ^{1}H and ^{13}C NMR were recorded on a Bruker AVANCE spectrometer at 600 and 125 MHz, respectively, unless specified otherwise. High-resolution mass spectra were obtained on a Kratos Concept Tandem mass spectrometer.

7.6.2 Inhibited Co-autoxidations with PBD-BODIPY

The co-autoxidations were carried out according to our previously published methodology.[S2] The rate constants for addition of peroxyl radicals onto PBD-BODIPY in 1-hexadecene autoxidations at elevated temperatures were evaluated by the same method as those previously reported,[S2] and found to be $k_{\text{PBD-BODIPY}}$ = 7633 $M^{-1}s^{-1}$ and 17,802 $M^{-1}s^{-1}$ at 70° and 100°C, respectively, and the corresponding extinction coefficients ε = 131,972 M^{-1} cm^{-1} (587 nm), and ε =

119,116 M^{-1} cm^{-1} (586 nm), respectively. Autoxidations in 1,4-dioxane were carried out using the same methodology described in a previous publication.[S1] Autoxidations of 1,4-dioxane containing 3.5M DMSO, were carried out in an otherwise identical manner. The rate constants in these cases were determined to be $k_{PBD\text{-}BODIPY}$ = 5312 $M^{-1}s^{-1}$ and 5902 $M^{-1}s^{-1}$ in dioxane and dioxane/DMSO, respectively, and the corresponding extinction coefficients ε = 123,023 M^{-1} cm^{-1} (587 nm), and ε = 118,217 M^{-1} cm^{-1} (587 nm), respectively.

Briefly, substrate (1-2 mL) was loaded into a 3 mL cuvette along with the appropriate volume of PhCl, such that the final volume of the reaction is 2.5 ml. The cuvette was placed into the thermostated sample holder of a UV−vis spectrophotometer and allowed to equilibrate to the appropriate temperature. A small aliquot (12.5 μL) of a 2.0 mM BODIPY solution in 1,2,4-trichlorobenzene was added, followed by 50-100 μl of a solution of initiator in PhCl. The solution was thoroughly mixed. The consumption of the probe was monitored for 10-20 min to ensure that the reaction was proceeding at a constant rate, after which 10 μL of a 500 μM solution of the test antioxidant was added. The solution was thoroughly mixed and the absorbance readings resumed.

7.6.3 General Procedure for *n*-Hexadecane Autoxidations

n-Hexadecane (5 mL) was loaded into separate test tubes compatible with the heating block of a parallel reactor. Solutions of the RTA were added to the appropriate wells (10 μl of a 50 mM solution in dioxane).[S3] The test tubes were loaded into the pre-heated block of the parallel synthesizer, and connected to a capillary bubbling tube. Aliquots (0.5 mL) were removed every 30 minutes, and allowed to cool to room temperature for analysis. Four duplicates (30 μL) of each sample were loaded into separate wells of a 96-well microplate and the automated reagent dispenser of the microplate reader was used to dilute each sample with *tert*-amyl alcohol (200 μL) and a solution of a fluorgenic phosphine dye solution (20 μL of a 250 μM stock solution in acetonitrile)

immediately before reading. The plate was stirred for 8 seconds, and allowed to rest for 2 more seconds, and the fluorescence of each well was measured every second for 60 seconds (absorption 340; emission 425). The concentration of hydroperoxide was determined from the rate of phosphine oxidation using the rate constant for the reaction of the dye with secondary hydroperoxides in *tert*-amyl alcohol (k = 1.2 $M^{-1}s^{-1}$) assuming pseudo-first-order kinetics.[S4]

7.6.4 Characterization Data

***1-Azaphenoxazine* (1):** ^{1}H-NMR (500 MHz; DMSO-d_6): δ 9.01 (s, 1H), 7.53 (dd, J = 5.0, 1.4 Hz, 1H), 6.90-6.88 (m, 1H), 6.76 (ddd, J = 7.7, 6.9, 2.0 Hz, 1H), 6.65-6.61 (m, 2H), 6.59-6.54 (m, 2H). ^{13}C NMR (126 MHz; DMSO): δ 146.4, 142.7, 142.1, 139.5, 131.8, 124.6, 121.7, 121.0, 117.0, 115.5, 114.5 HRMS (EI): Calc'd for $C_{11}H_8N_2O$: 184.0636, Found: 184.0651, Mp = 209-211 °C.

***2-Azaphenoxazine*:** ^{1}H-NMR (600 MHz; DMSO-d_6): δ 8.38 (s, 1H), 8.38 (s, 1H), 7.75 (d, J = 5.2 Hz, 1H), 7.75 (d, J = 5.2 Hz, 1H), 7.65 (s, 1H), 7.65 (s, 1H), 6.77 (td, J = 7.6, 1.5 Hz, 1H), 6.77 (td, J = 7.6, 1.5 Hz, 1H), 6.65-6.59 (m, 3H), 6.65-6.59 (m, 3H), 6.48 (dd, J = 7.8, 1.5 Hz, 1H), 6.48 (dd, J = 7.8, 1.5 Hz, 1H). ^{13}C NMR (151 MHz; DMSO): δ 149.6, 143.7, 142.2, 134.9, 132.3, 130.1, 125.3, 121.3, 116.0, 114.4, 110.7 HRMS (EI): Calc'd for $C_{11}H_8N_2O$: 184.0636, Found: 184.0615. Mp = 207-210 °C

***3-Azaphenoxazine* (3):** ^{1}H-NMR (400 MHz; DMSO-d6): δ 8.80 (s, 1H), 7.78 (d, J = 5.1 Hz, 1H), 7.69 (s, 1H), 6.79-6.75 (m, 1H), 6.66-6.64 (m, 2H), 6.50 (dt, J = 7.4, 0.7 Hz, 1H), 6.39 (d, J = 5.1 Hz, 1H). ^{13}C NMR (151 MHz; DMSO): δ 146.6, 143.5, 140.7, 139.4, 135.7, 130.9, 124.7, 122.3, 116.0, 114.6, 108.2 HRMS (EI): Calc'd for $C_{11}H_8N_2O$: 184.0636, Found: 184.0646. Mp = 243-244 °C

***4-Azaphenoxazine* (1):** ^{1}H-NMR (500 MHz; DMSO-d_6): δ 8.47 (s, 1H), 7.36 (dd, J = 4.8, 1.8 Hz, 1H), 6.78-6.72 (m, 3H), 6.68 (dd, J = 7.9, 1.4 Hz, 1H), 6.61 (td, J = 7.7, 1.4 Hz, 1H), 6.47 (dd, J = 7.7, 1.4 Hz, 1H). ^{13}C NMR (126 MHz; DMSO): δ 150.8, 143.2, 137.6, 131.7, 128.6, 124.9, 121.3,

121.1, 119.8, 116.0, 113.7 HRMS (EI): Calc'd for $C_{11}H_8N_2O$: 184.0636, Found: 184.0636 Mp = (dec.) 217-220 °C

***1-Azaphenothiazine* (2):** ^{1}H-NMR (300 MHz; C_6H_6): δ 9.20 (s, 1H), 7.81 (dd, *J* = 4.9, 1.6 Hz, 1H), 7.27 (ddd, *J* = 7.5, 1.6, 0.5 Hz, 1H), 7.00 (ddd, *J* = 8.0, 7.2, 1.5 Hz, 1H), 6.92 (dd, *J* = 7.7, 1.5 Hz, 1H), 6.84-6.76 (m, 2H), 6.73 (dd, *J* = 7.5, 4.9 Hz, 1H). ^{13}C NMR (76 MHz; DMSO): δ 153.0, 145.5, 140.7, 133.7, 127.6, 125.8, 122.4, 117.8, 115.1, 115.0, 112.0 HRMS (EI): Calc'd for $C_{11}H_8N_2S$: 200.0408, Found: 200.0400. Mp = 116 °C

2-Azaphenothiazine : ^{1}H-NMR (600 MHz; DMSO-d_6): δ 8.73 (s, 1H), 7.84 (d, *J* = 4.9 Hz, 1H), 7.80 (s, 1H), 7.01 (t, *J* = 7.6 Hz, 1H), 6.92 (dd, *J* = 16.8, 6.2 Hz, 2H), 6.77 (t, *J* = 7.5 Hz, 1H), 6.67 (d, *J* = 7.9 Hz, 1H). 13-C NMR (151 MHz; DMSO): δ 143.0, 141.5, 138.4, 135.2, 128.6, 127.3, 127.0, 122.8, 121.1, 115.4, 114.8 HRMS (EI): Calc'd for $C_{11}H_8N_2S$: 200.0408, Found: 200.0388. Mp = 169 °C

***3-Azaphenothiazine* (4):** ^{1}H-NMR (400 MHz; DMSO-d_6): δ 9.10 (s, 1H), 7.98 (d, *J* = 5.4 Hz, 1H), 7.88 (s, 1H), 7.02 (td, *J* = 7.6, 1.3 Hz, 1H), 6.94 (dd, *J* = 7.7, 1.2 Hz, 1H), 6.81 (td, *J* = 7.5, 1.2 Hz, 1H), 6.68 (dd, *J* = 7.9, 1.1 Hz, 1H), 6.55 (d, *J* = 5.4 Hz, 1H). ^{13}C NMR (151 MHz; DMSO): δ 149.2, 148.5, 146.1, 140.2, 128.3, 127.2, 123.5, 116.2, 115.6, 113.6, 109.2, 40.0 HRMS (EI): Calc'd for $C_{11}H_8N_2S$: 200.0408, Found: 200.0414. Mp = 247-248 °C

***4-Azaphenothiazine* (2):** ^{1}H-NMR (400 MHz; DMSO-d_6): δ 8.61 (s, 1H), 7.75 (dd, *J* = 4.7, 1.5 Hz, 1H), 6.99-6.91 (m, 2H), 6.88 (dd, *J* = 7.7, 1.4 Hz, 1H), 6.83 (dd, *J* = 8.0, 1.5 Hz, 1H), 6.74 (td, *J* = 7.5, 1.3 Hz, 1H), 6.62 (dd, *J* = 7.9, 1.1 Hz, 1H). ^{13}C NMR (76 MHz; DMSO): δ 141.5, 140.2, 139.7, 137.5, 127.6, 126.3, 122.5, 121.8, 119.4, 116.2, 114.3 HRMS (EI): Calc'd for $C_{11}H_8N_2S$: 200.0408, Found: 200.0383. Mp = 248-250 °C

***3-Diethylamino-2,4-Diazaphenoxazine* (3):** ^{1}H-NMR (500 MHz; DMSO-d_6): δ 8.01 (s, 1H), 7.47 (s, 1H), 6.80-6.74 (m, 2H), 6.56 (td, *J* = 7.7, 1.3 Hz, 1H), 6.47 (dd, *J* = 7.8, 1.3 Hz, 1H), 3.43 (q, *J* = 7.0

Hz, 4H), 1.06 (t, *J* = 7.0 Hz, 6H). ^{13}C NMR (126 MHz; DMSO): δ 158.0, 156.3, 141.7, 140.8, 132.6, 125.5, 119.9, 116.4, 115.8, 114.0, 41.7, 13.6 HRMS(EI) m/z: calcd $C_{14}H_{16}N_4O$, 256.1324; found, 256.1329. Mp = 155-156 °C

***3-Diethylamino-2,4-Diazaphenothiazine* (4):** ^{1}H-NMR (500 MHz; DMSO-d_6): δ 8.21 (s, 1H), 7.54 (s, 1H), 6.95 (td, *J* = 7.6, 1.4 Hz, 1H), 6.86 (dd, *J* = 7.7, 1.3 Hz, 1H), 6.67 (td, *J* = 7.5, 1.2 Hz, 1H), 6.58 (dd, *J* = 8.0, 1.2 Hz, 1H), 3.44 (q, *J* = 7.0 Hz, 4H), 1.05 (t, *J* = 7.0 Hz, 6H). ^{13}C NMR (126 MHz; DMSO): δ 156.8, 152.6, 141.17, 140.99, 128.5, 127.0, 125.7, 121.2, 114.8, 114.5, 41.7, 13.5 HRMS (EI): Calc'd for $C_{14}H_6N_4S$: 272.1095, Found: 272.1079. Mp = (dec.) 180°C

***3-Heptyl-1-Methyl-2,4-Diazaphenoxazine*:** ^{1}H-NMR (400 MHz; DMSO-d_6): δ 7.84 (s, 1H), 6.83-6.79 (m, 1H), 6.69 (td, *J* = 8.1, 1.5 Hz, 2H), 6.63 (ddd, *J* = 7.8, 7.4, 1.6 Hz, 1H), 2.50-2.47 (m, 2H), 2.18 (s, 3H), 1.60 (quintet, *J* = 7.3 Hz, 2H), 1.26 (t, *J* = 4.6 Hz, 8H), 0.86 (t, *J* = 6.7 Hz, 3H). ^{13}C-NMR (76 MHz; DMSO): δ 161.0, 156.6, 147.9, 142.5, 132.0, 125.5, 121.6, 121.3, 116.3, 114.9, 37.8, 31.6, 29.06, 28.96, 28.3, 22.5, 19.5, 14.4 HRMS: Calc for $C_{18}H_{23}N_3O$, 297.1841; Found: 297.1839. Mp = 91-92 °C

***3-Heptyl-2,4-Diazaphenothiazine* (7):** ^{1}H-NMR (300 MHz; DMSO-d_6): δ 8.64 (s, 1H), 7.65 (s, 1H), 7.00-6.94 (m, 1H), 6.87 (dd, *J* = 7.7, 1.4 Hz, 1H), 6.74 (dd, *J* = 7.5, 1.2 Hz, 1H), 6.58 (dd, *J* = 8.0, 1.2 Hz, 1H), 2.56 (t, *J* = 7.6 Hz, 2H), 1.60 (m, 2H), 1.24 (m, 8H), 0.85 (t, *J* = 6.7 Hz, 3H). ^{13}C NMR (76 MHz; DMSO): δ 163.1, 151.4, 139.7, 138.7, 133.7, 128.8, 127.2, 122.5, 115.3, 114.9, 37.7, 31.6, 28.97, 28.91, 28.3, 22.5, 14.4 HRMS (EI): Calc'd for $C_{17}H_{21}N_3S$: 299.1456, Found: 299.1444. Mp = 123 °C

2-Diethylamino-1,3-Diazaphenoxazine: ^{1}H-NMR (400 MHz; DMSO-d_6): δ 9.39 (s, 1H), 7.46 (d, *J* = 0.7 Hz, 1H), 6.77 (td, *J* = 7.4, 1.7 Hz, 1H), 6.72-6.65 (m, 3H), 3.45 (q, *J* = 7.0 Hz, 4H), 1.07 (t, *J* = 7.0 Hz, 6H). ^{13}C NMR (151 MHz; DMSO): δ 156.8, 151.1, 143.2, 139.1, 129.46, 129.26, 123.4, 122.3, 115.09, 114.89, 41.2, 13.3 HRMS(EI) m/z: calcd $C_{14}H_{16}N_4O$, 256.1324; found, 256.1353. Mp = 130-131 °C

***2-Diethylamino-1,3-Diazaphenothiazine* (7):** ^{1}H-NMR (500 MHz; DMSO-d_6): δ 9.39 (s, 1H), 7.63 (s, 1H), 7.02-6.98 (m, 1H), 6.93 (dd, *J* = 20.3, 7.8 Hz, 2H), 6.84-6.80 (m, 1H), 3.50 (q, *J* = 7.0 Hz, 4H), 1.09 (t, *J* = 7.0 Hz, 6H). ^{13}C NMR (126 MHz; DMSO): δ 159.9, 158.9, 152.2, 139.6, 127.7, 126.5, 123.5, 117.2, 116.4, 95.2, 41.5, 13.7 HRMS (EI): Calc'd for $C_{14}H_6N_4S$: 272.1095, Found: 272.1084. Mp = 112 °C

***2-Heptyl-4-methyl-1,3-Diazaphenoxazine* (5):** ^{1}H-NMR (400 MHz; DMSO-d6): δ 9.52 (s, 1H), 6.78 (ddd, J = 7.7, 5.5, 3.3 Hz, 1H), 6.72-6.69 (m, 2H), 6.59 (d, J = 7.1 Hz, 1H), 2.45 (t, J = 7.7 Hz, 2H), 2.10 (s, 3H), 1.61 (dd, J = 7.9, 7.1 Hz, 2H), 1.27-1.25 (m, 8H), 0.86 (t, J = 6.9 Hz, 3H). ^{13}C NMR (151 MHz; DMSO): δ 164.2, 150.9, 147.4, 143.7, 133.7, 130.3, 124.6, 123.0, 115.9, 115.3, 38.2, 31.7, 29.16, 29.01, 28.4, 22.6, 17.4, 14.4 HRMS (EI): Calc'd for $C_{18}H_{23}N_3O$: 297.1841, Found: 297.1829. Mp = 124 °C

***2-Heptyl-4-methyl-1,3-Diazaphenothiazine* (6):** ^{1}H-NMR (400 MHz; DMSO-d6): δ 9.60 (s, 1H), 7.01-6.93 (m, 2H), 6.82-6.77 (m, 2H), 2.49 (d, J = 9.5 Hz, 2H), 1.65-1.61 (m, 2H), 1.26 (t, J = 5.3 Hz, 8H), 0.87-0.84 (m, 3H). ^{13}C NMR (151 MHz; DMSO): δ 167.6, 158.9, 157.9, 139.1, 128.2, 126.6, 123.8, 116.40, 116.27, 105.6, 38.3, 31.6, 29.2, 29.0, 28.3, 22.5, 21.6, 14.4 HRMS (EI): Calc'd for $C_{18}H_{23}N_3S$: 313.1612, Found: 297.1634.

7.6.5 UV–Vis Spectra and Extinction Coefficients for PBD-BODIPY

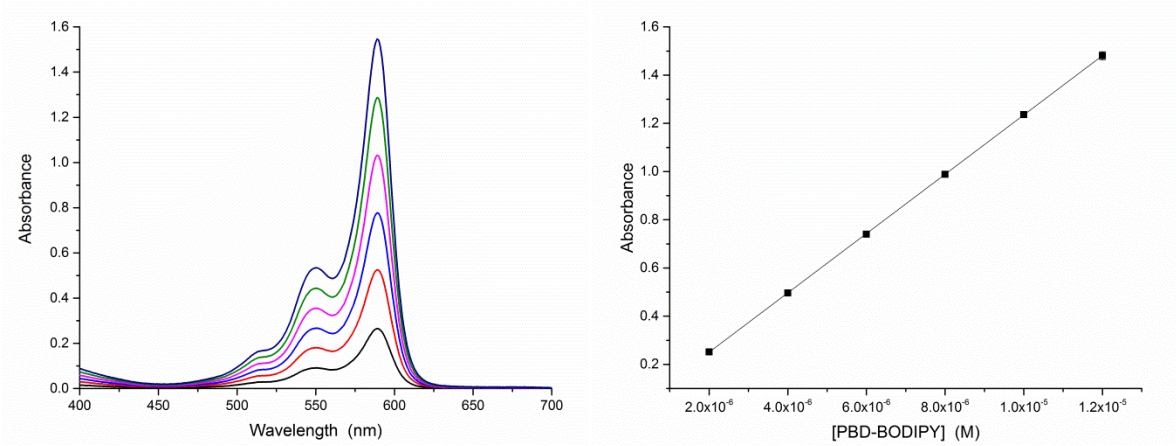

Figure S7.1. (A) Uv-Vis spectra for 2-14 μM PBD-BODIPY. (B) Extinction coefficient for STY-BODIPY in 2.9 M 1,4-dioxane/PhCl (37°C), λ_{max} = 587 nm, ε = 123,023 $M^{-1}cm^{-1}$. Average of three measurements (error bars are too small to be resolved from the data points).

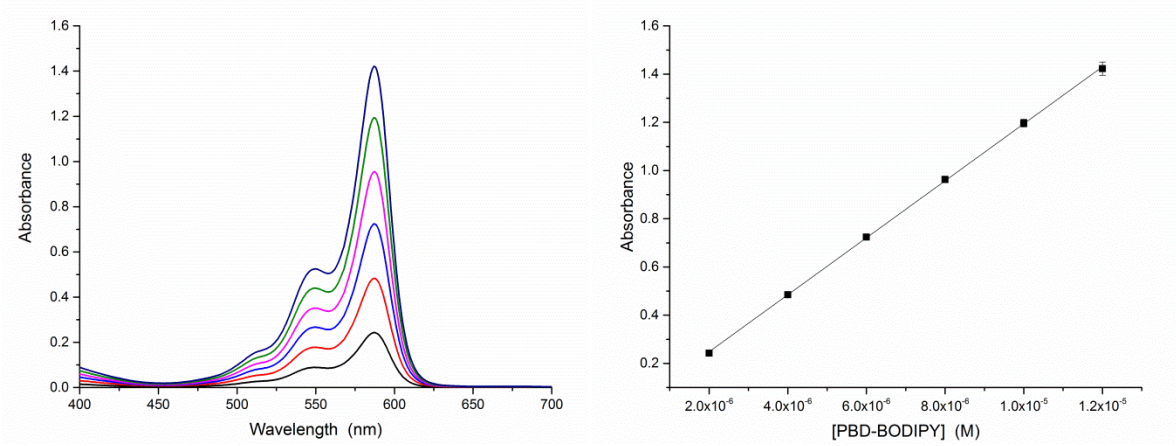

Figure S7.2. (A) Uv-Vis spectra for 2-14 μM PBD-BODIPY. (B) Extinction coefficient for STY-BODIPY in 2.9 M 1,4-dioxane/PhCl with 3.5 M DMSO (37°C), λ_{max} = 587 nm, ε = 118,217 $M^{-1}cm^{-1}$.

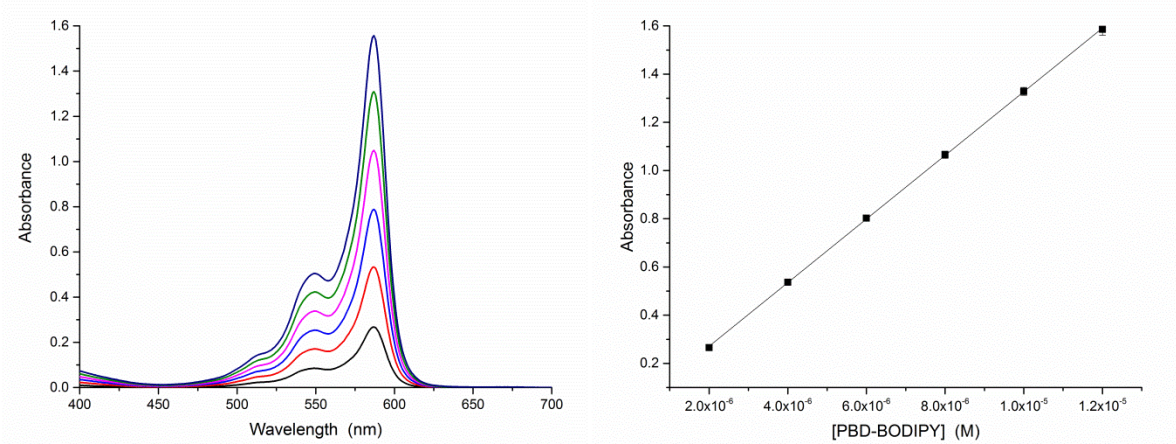

Figure S7.3. (A) Uv-Vis spectra for 2-14 μM PBD-BODIPY. (B) Extinction coefficient for STY-BODIPY in 2.8M 1-hexadecene/PhCl (70°C), λ_{max} = 587 nm, ε = 131,972 $M^{-1}cm^{-1}$. Average of three measurements (error bars are too small to be resolved from the data points).

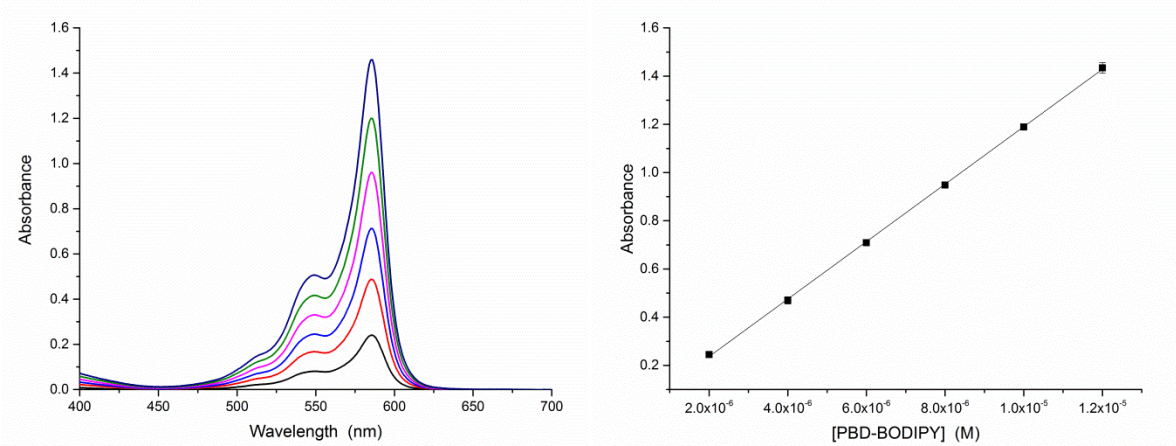

Figure S7.4. (A) Uv-Vis spectra for 2-14 μM PBD-BODIPY. (B) Extinction coefficient for STY-BODIPY in 2.8M 1-hexadecene/PhCl (100°C), λ_{max} = 586 nm, ε = 119,166 $M^{-1}cm^{-1}$. Average of three measurements (error bars are too small to be resolved from the data points).

7.6.6 Uninhibited PBD-BODIPY Consumption Rates

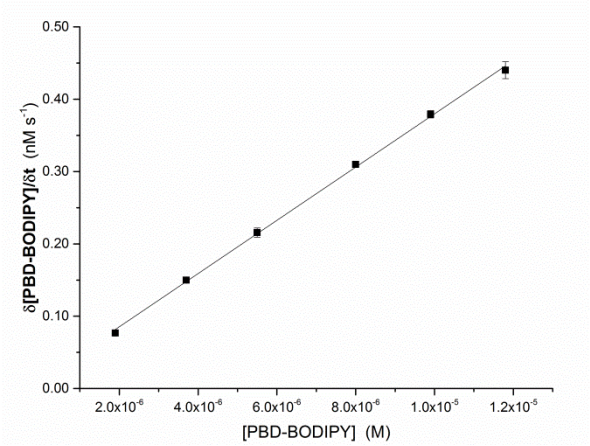

Figure S7.5. Rate of PBD-BODIPY consumption as a function of PBD-BODIPY concentration in AIBN-initiated (6 mM) co-autoxidations of PBD-BODIPY and 1,4-dioxane (2.9 M) in PhCl at 37 °C.

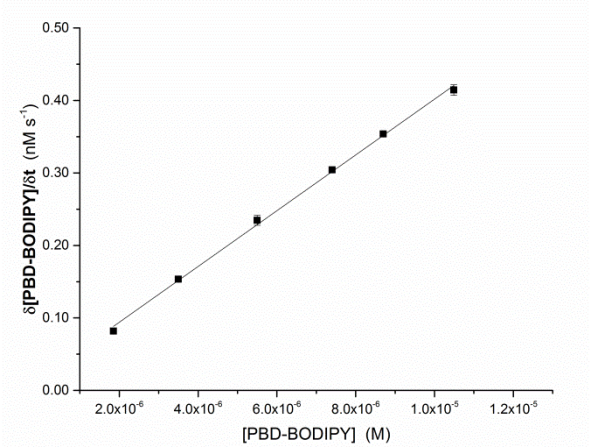

Figure S7.6. Rate of PBD-BODIPY consumption as a function of PBD-BODIPY concentration in AIBN-initiated (6 mM) co-autoxidations of PBD-BODIPY and 1,4-dioxane (2.9 M) with 3.5 M DMSO in PhCl at 37 °C.

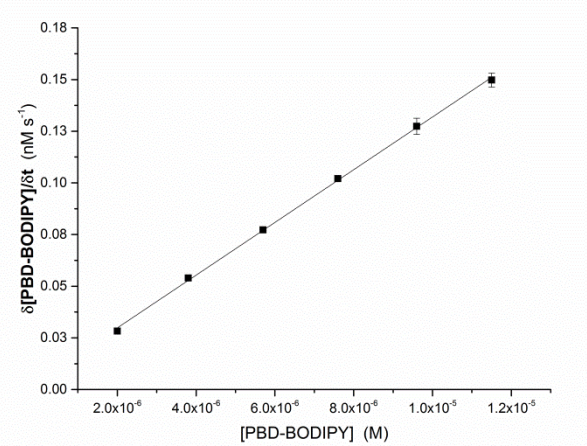

Figure S7.7. Rate of PBD-BODIPY consumption as a function of PBD-BODIPY concentration in di-*tert*-butylperoxide-initiated (87 mM) co-autoxidations of PBD-BODIPY and 1-hexadecene (2.8 M) in PhCl at 70 °C.

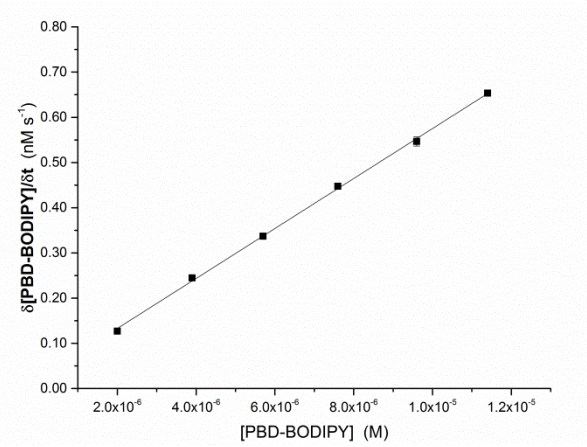

Figure S7.8. Rate of PBD-BODIPY consumption as a function of PBD-BODIPY concentration in dicumylperoxide-initiated (1.0 mM) co-autoxidations of PBD-BODIPY and 1-hexadecene (2.8 M) in PhCl at 100 °C.

7.6.7 1-Hexadecene Autoxidations at 70°C

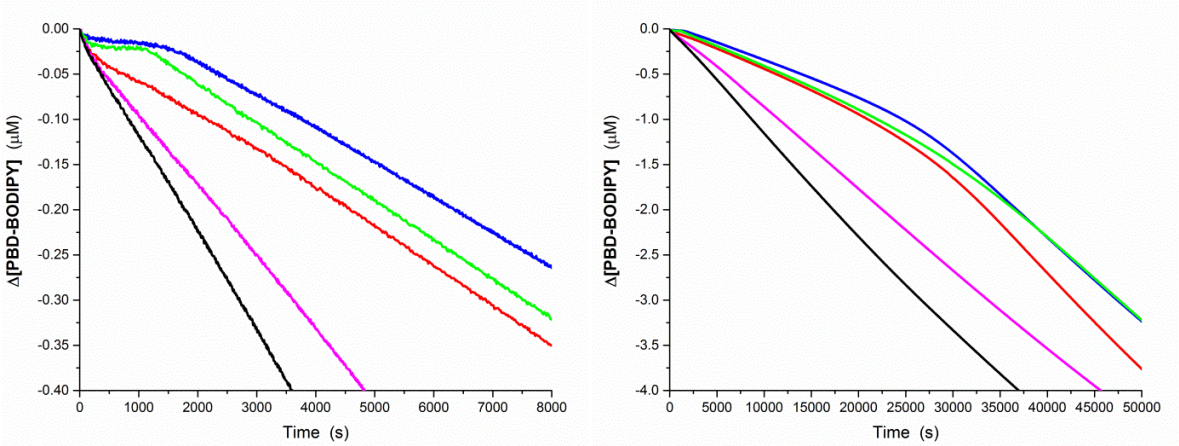

Figure S7.9. Representative co-autoxidation of 1-hexadecene (2.8 M) and PBD-BODIPY (10 μM) initiated by $^{t}Bu_2O_2$ (87 mM) in PhCl at 70°C, monitored at 587nm (ε = 131,972 $M^{-1}cm^{-1}$). Uninhibited (black), or inhibited with 600 nM of **7.4** (red), **7.7** (green), **7.8** (magenta), or **7.11** (blue).

Table S7.1 Inhibition Rate Constants and Stoichiometries of Azaphenoxazine and Azaphenothiazine RTAs in 1-Hexadecene Autoxidations in PhCl at 70°C.

Compound	k_{inh}^{PhCl} ($M^{-1}s^{-1}$)	*n*
7.2	$(3.6\pm0.1)\times10^{6}$	116±8
7.3	$(6.7\pm0.6)\times10^{6}$	53±2
7.4	$(6.8\pm0.2)\times10^{5}$	50±1
7.5	$(1.5\pm0.3)\times10^{7}$	23±1
7.6	$(5.3\pm0.3)\times10^{6}$	122±1
7.7	$(1.2\pm0.2)\times10^{7}$	53±1
7.8	$(2.8\pm0.1)\times10^{5}$	10±2
7.9	$(3.3\pm0.2)\times10^{6}$	30±1
7.10	$(1.9\pm0.1)\times10^{6}$	34±1
7.11	$(3.3\pm0.6)\times10^{6}$	52±2
7.12	*too fast*	2.3±0.1
7.13	*too fast*	6.6±0.3
7.14	*too fast*	7.8±0.8
7.15	$(6.6\pm0.3)\times10^{6}$	53±1
7.16	$(2.4\pm0.4)\times10^{6}$	11±1
7.17	$(2.0\pm0.2)\times10^{5}$	------
7.18	$(3.0\pm0.1)\times10^{6}$	109±3
7.19	$(3.3\pm0.2)\times10^{5}$	------

7.6.8 Supporting Information References

S1) Haidasz, E. A.; Pratt, D. A.; *Org. Lett.*, **2017**, Submitted.

S2) Haidasz, E. A.; Van Kessel, A. T. M.; Pratt, D. A. *J. Org. Chem.* **2016**, *81*, 737–744.

S3) Shah, R.; Pratt, D. A. *J. Org. Chem*. **2016**, 81, 6649–6656.

S4) Hanthorn, J.; Haidasz, E.; Gebhardt, P.; Pratt, D. *Chem. Commun.* **2012**, *48*, 10141–10143.

CHAPTER 8: The Substrate-Dependence of Nitroxide-based Radical Trapping Antioxidants

8.1 Preface

Aminic radical trapping antioxidants (RTAs) are common additives added to hydrocarbon materials (e.g. rubbers, plastics, lubricating oils, etc.) – particularly those which are used at elevated temperatures. These RTAs inhibit the radical chain reaction responsible for oxidative degradation in a catalytic fashion. Over the course of our studies on the mechanism of aminic RTAs, we have found that nitroxides – which are key intermediates in the reactivity of both diarylamine RTAs and hindered amine light stabilizers (HALS) – are potent catalytic inhibitors in olefinic substrates (styrene, cyclooxtene, hexadecene), even at temperatures too low for the accepted mechanism to operate. However, the same nitroxides were found to be poor inhibitors in substrates lacking unsaturation (cumene, ethylbenzene, dioxane). Herein, we describe our observations relating to this intriguing catalytic RTA activity. This work was done in conjunction with fellow graduate student Kareem Harrison, who is responsible for the results with the d-*tert*-ialkyl and aryl *tert*-alkyl amine/nitroxide derivatives, cyclooctene autoxidations, the inhibited autoxidations under acidic and basic conditions, and the forthcoming isotope effect experiments.

8.2 Introduction

Autoxidation, the spontaneous, radical-mediated oxidation of hydrocarbons to their corresponding hydroperoxides (Scheme 8.1), can be inhibited through the addition of radical-trapping antioxidants (RTAs). These compounds trap the chain carrying peroxyl radicals (ROO•) responsible for propagating the reaction – often by proton coupled electron transfer (PCET) from a weak N-H or O-H bond.[1,2]

Initiation

$$In_2 \longrightarrow 2\ In\bullet$$
$$In\bullet + RH \longrightarrow InH + R\bullet$$

Propagation

$$ROO\bullet + RH \longrightarrow ROOH + R\bullet$$
$$R\bullet + O_2 \longrightarrow ROO\bullet$$

Termination

$$ROO\bullet + ROO\bullet \longrightarrow \text{non-radical products}$$

Scheme 8.1. Radical chain mechanism of hydrocarbon autoxidation.

Although both substituted phenols and diarylamines are commonly used RTAs, diarylamines are particularly effective inhibitors at elevated temperatures (>120°C) because they can be regenerated *in situ*. Thus, where phenolic RTAs are typically capable of trapping only two radicals per molecule (first by formal H-atom transfer, then by termination with the RTA-derived radical), very high stoichiometric numbers (*n*) have been reported for the reactions of diarylamine RTAs.[3] A mechanism which accounted for these observations was first proposed by Korcek *et. al.* in 1995 (Scheme 8.2),[4] and invokes the formation of an RTA/substrate-derived N,N-diarylalkoxyamine (eq 8.3). Decomposition of this intermediate to regenerate the amine is thought to be the rate limiting step in the cycle (eq 8.4). Originally, this reaction was believed to occur through a homolysis/disproportionation mechanism – an explanation that was consistent with the high temperatures required to homolyse the N-O bond before turnover could occur.[4] More recently, our group has provided evidence that a pericyclic retro-carbonyl-ene (RCE) reaction may be responsible – particularly in the presence of unsaturated substrates (Scheme 8.3).[5]

Catalytic

$$Ar_2NH + ROO\bullet \longrightarrow Ar_2N\bullet + ROOH \qquad (8.1)$$
$$Ar_2N\bullet + ROO\bullet \longrightarrow Ar_2NO\bullet + RO\bullet \qquad (8.2)$$
$$Ar_2NO\bullet + R\bullet \longrightarrow Ar_2NOR \qquad (8.3)$$
$$Ar_2NOR \longrightarrow Ar_2NH + R_{\text{-H}}{=}O \qquad (8.4)$$

Off-Cycle

$$Ar_2N\bullet + ROO\bullet \longrightarrow \text{non-radical products} \qquad (8.5)$$
$$Ar_2NO\bullet + ROO\bullet \longrightarrow \text{non-radical products} \qquad (8.6)$$

Scheme 8.2. Proposed Diarylamine Catalytic Cycle and Potential Off-Cycle Reactions.

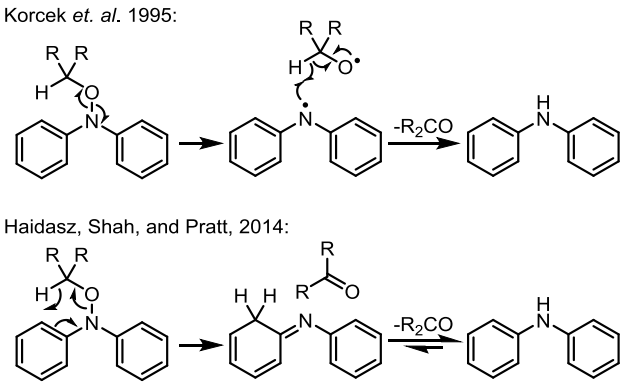

Scheme 8.3. Proposed mechanisms for decomposition of *N*,*N*,-diarylalkoxyamines (eq 8.4).

Although either the substrate or amine fragment could be modified to favor the more efficient RCE pathway, unactivated derivatives (i.e. those alkoxyamines composed of simple diphenylamines and saturated alkanes) widely react through homolysis/disproportionation. In either case, the activation energies for the regeneration reaction are quite high (30-35 kcal/mol),[5] consistent with their expected role as the rate limiting step, and justification for the elevated temperatures required for catalytic turnover.

Subsequently, during the report of our spectrophotometric approach for monitoring hydrocarbon autoxidation,[6] we reported that suitably activated diarylamines can display modest catalytic activity (n = 3.1– 3.9) as low as 37°C in styrene, and more recently, that highly activated (aza)phenoxazine derivatives turnover readily between 70 and 100°C in 1-hexadecene, *where some compounds react with stoichiometric numbers up to 120!* While these compounds are highly activated compared to diphenylamines, the calculated enthalpic barriers for the RCE reaction (using the reliable CBS-QB3 method[7]) are still predicted to be greater than 28 kcal/mol for both of these – suggesting that the regeneration reactions would be far too slow to be kinetically competitive with autoxidation at these temperatures.

$$Ar_2NOR \xleftarrow[k = 1.8 \times 10^9\ M^{-1}s^{-1}]{Ar_2NO\bullet\ (2\ \mu M)} R\bullet \xrightarrow[k \sim 3 \times 10^9\ M^{-1}s^{-1}]{O_2\ (2\ mM)} ROO\bullet$$

Moreover, a kinetic analysis of alkoxyamine formation reveals inconsistencies between kinetic information and the proposed cycle. The Korcek mechanism requires trapping of an alkyl radical with an RTA-derived nitroxide, necessitating that the nitroxide compete with O_2. While alkyl radicals react rapidly with both O_2 (~3×10^9 $M^{-1}s^{-1}$)[8] and diaryl nitroxides (1.8×10^9 $M^{-1}s^{-1}$, see Supporting Information), under the conditions employed in our autoxidation studies, oxygen is present in roughly a 1000-fold excess over the nitroxide (~2 mM vs. 2 μM), meaning that formation of the alkoxyamine – much less regeneration of the diarylamine derived therefrom – would be orders of magnitude too slow to compete with propagation of the autoxidation.

Considering the above, the origins of the unexpected catalytic activity seen at moderate temperatures are a mystery. The details of our investigations into this peculiar reactivity are described below.

8.3 Results

8.3.1 Inhibition by Diarylamines and Diarylnitroxides in Styrene and Cumene

In order to examine the plausibility of alkyl radical trapping by diarylnitroxides at moderate temperatures, a model 4,4'-dialkyldiphenylamine and its corresponding nitroxide were prepared. Bis(4-*tert*-butylphenyl)amine (**8.1**) was synthesized through Buchwald amination from the appropriate arylamine and bromide precursors,[9] and was then oxidized to its nitroxide (**8.2**) according to literature procedures (Scheme 8.4).[10]

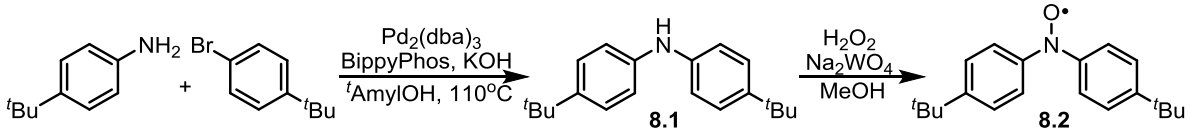

Scheme 8.4. Synthesis of bis(4-*tert*-butylphenyl)amine (**8.1**) and bis(4-*tert*-butylphenyl)nitroxide (**8.2**).

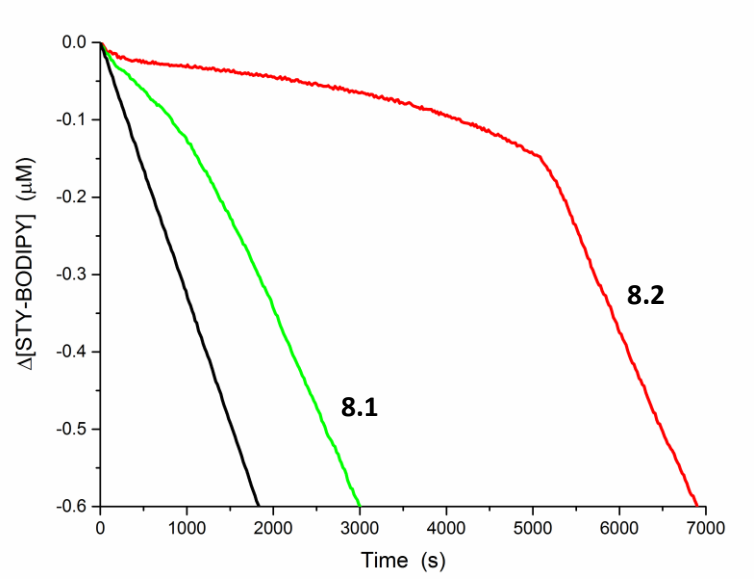

Figure 8.1. Co-autoxidations of styrene (3.5 M) and STY-BODIPY (10 μM) initiated by $^{t}Bu_2O_2$ (218 mM) at 70 °C. Uninhibited (black), or inhibited by 2.0 μM of **8.1** (green) or **8.2** (red).

Upon addition of 2μM of **8.1** or **8.2** to a co-autoxidizing mixture of styrene and STY-BODIPY[6] at 70°C, a wholly unexpected result was observed (Figure 8.1). Not only was nitroxide **8.2** a highly efficient RTA capable of catalytically trapping peroxyl radicals (n = 10.6 ± 0.2), but *it greatly outperformed its precursor amine **1**!* (n = 2.1 ± 0.1). Early work by the groups of Thomas[11] and Ingold[12] has previously shown that diarylnitroxides are effective RTAs capable of reacting both with peroxyl and alkyl radicals,[13] although both reports state that the nitroxides are less effective than their amine precursors. Furthermore, Thomas reports that in the autoxidation of cumene at 68.5°C, diphenylnitroxide is non-catalytic (n = 1.1),[11] consistent with trapping only a single radical per molecule as it is consumed. At first glance, these results seem entirely at odds with the observations in our experiments. However, both Thomas and Ingold monitored their respective autoxidation experiments via O_2 consumption measurements. With this method, the reaction is performed in a sealed system and progress is monitored by differential pressure measurements of the atmosphere over the reaction. Unfortunately, this requires very high rates of autoxidation in order to guarantee a significant (measurable) change in the partial pressure of O_2. This is often ensured by the very high

rates of initiation ($R_i \sim 10^{-7}$ M s^{-1}) used in these experiments, which necessitate high concentrations of RTA as a result. Alternatively, co-autoxidations with STY-BODIPY are generally run at much slower R_i (1-4 × 10^{-9} M s^{-1}), more representative of autoxidation in applied systems.

When STY-BODIPY co-autoxidations inhibited by **8.1** and **8.2** were performed in cumene under Thomas' conditions (Figure 8.2A), our observations are largely consistent with theirs.[11] Diarylnitroxide **8.2** was roughly 2-fold less reactive than its amine **8.1**. Moreover, the stoichiometries measured for **8.1** (n = 2.3 ± 0.1) and **8.2** (n = 1.1 ± 0.1) matched those reported for diphenylnitroxide, and indicated that no turnover was taking place for either compound.

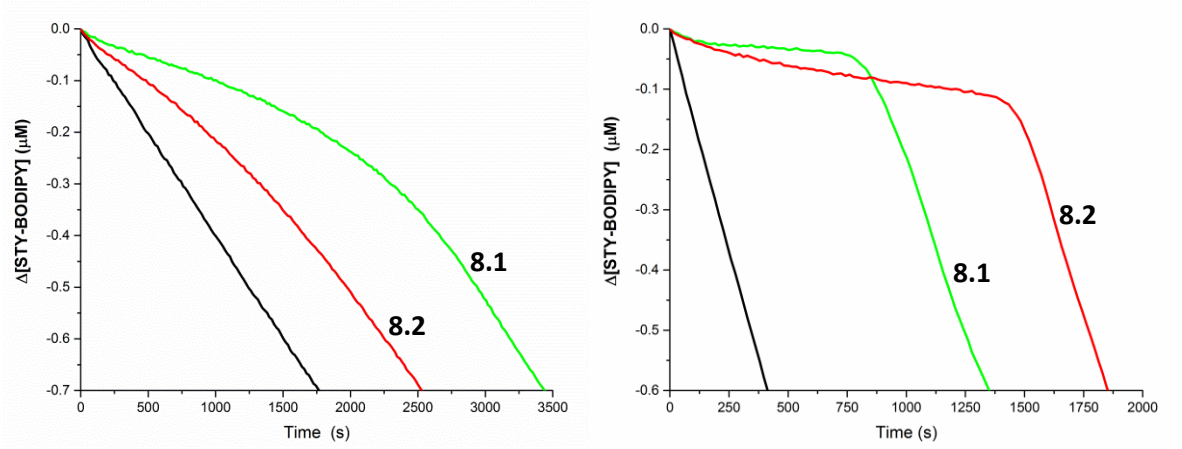

Figure 8.2. Co-autoxidations of A) cumene (0.29 M) or B) styrene (3.5 M), with STY-BODIPY (10 μM) initiated by AIBN (1.0 mM) at 70°C. Uninhibited (black), or inhibited by 50 μM of **8.1** (green) or **8.2** (red).

Repeating the experiments with styrene (Figure 8.2B) saw a similar initial profile between **8.1** and **8.2**, where the amine remained the more effective inhibitor (consistent with the results of Ingold,[12] whose experiments were performed in styrene at 65°C). However, even in this case nitroxide **8.2** trapped more radicals than **8.1** (n = 1.8 ± 0.2 vs. 0.8 ± 0.2, respectively), implying that, even with very rapid R_i, the same catalytic inhibitory effect is at play as in the above examples. Unfortunately, the high concentration of RTA in Ingold's experiments (4.3 mM) precluded determination of stoichiometries under their conditions, and as such, the presence of catalytic activity

would not have been detected. The reduced stoichiometries of either RTA under these conditions are likely caused by an increase in non-productive radical-radical reactions of either the aminyl radical or nitroxide that would take place at higher R_i (eqs 8.5 and 8.6).

8.3.2 Inhibition by Hydroxylamines and Alkoxyamines

Since both the homolysis/disproportionation and RCE reactions are predicted to be too slow at these temperatures, it seemed prudent to conclusively confirm or refute the relevance of *N*,*N*-diarylalkoxyamines in the catalytic activity described above. However, despite their proposed central role in the behaviour of diarylamine RTAs there are very few examples of their preparation, and fewer still of their reactivity.[4,5] In our previous publication, we used Kelly's method[15] to synthesize these compounds by treatment of a lithium diarylamide with a strained endoperoxide. However, in order to prepare alkoxyamines whose alkoxy substituent resembles the substrate as closely as possible, an alternative approach was needed. Work by Meyer[16] had shown that phenylhydrazine is capable of reducing diarylnitroxides selectively to their hydroxylamines, subsequently Sen'[17] developed a similar procedure using hydrazine hydrate. Stirring a solution of the nitroxide in THF with 1 equiv of hydrazine, followed by careful evaporation of the solvent gave crude hydroxylamine **8.3**, which could be recrystallized to purity, or treated with potassium HMDS and an alkyl halide at -78°C to afford the alkoxyamines **8.4** and **8.5** (Scheme 8.5).

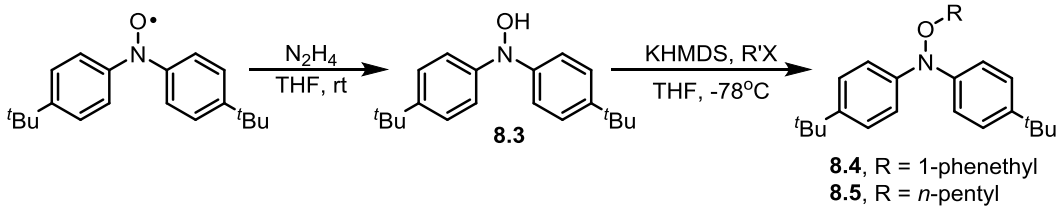

Scheme 8.5. Synthesis of hydroxylamine **8.3**, and diarylalkoxyamines **8.4** and **8.5**.

Hydroxylamine **8.3** was also a potent inhibitor in styrene autoxidations, inhibiting the autoxidation very similarly to nitroxide **8.2** (Figure 8.3). Hydroxylamines are known to rapidly trap

peroxyl radicals by PCET from their O-H bond (k_{inh} ~ 10^6 $M^{-1}s^{-1}$),[12,18] yielding the nitroxide. This similarity would then be the result of near quantitative formation of **8.2** from **8.3** after trapping one additional peroxyl radical (n = 11.7 ± 0.1). Alternatively, the 2° phenethyl alkoxyamine **8.4** did not appear to inhibit the autoxidation at all under these conditions. While **8.4** is activated towards the RCE reaction that regenerates the diarylamine,[5] this rearrangement appears far too slow at 70°C to effectively inhibit the reaction. A mixture of equal amounts of **8.1**, **8.2**, and **8.4** inhibited the autoxidation in a strictly additive fashion, verifying that there are no alternative kinetic effects based on the presence of mixtures of amine, nitroxide, and/or alkoxyamine.

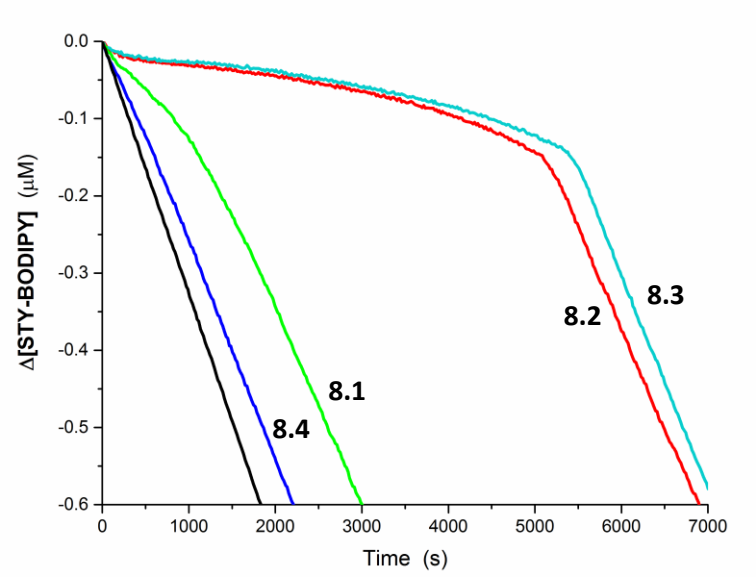

Figure 8.3. Co-autoxidations of styrene (3.5 M) and STY-BODIPY (10 μM) initiated by $^tBu_2O_2$ (218 mM) at 70 °C. Uninhibited (black), or inhibited by 2.0 μM of **8.1** (green), **8.2** (red), **8.3** (cyan), or **8.4** (blue).

8.3.3 Inhibition in Ethylbenzene, Hexadecene, Cyclooctene, and Dioxane

When the substrate was exchanged for ethylbenzene, the catalytic inhibitory activity of the nitroxide disappeared (Figure 8.4). Diarylamine **8.1** remained moderately effective, inhibiting the autoxidation for *ca.* 3000s, however, neither nitroxide **8.2** nor its alkoxyamine **8.4** had any effect on the reaction.

Since **8.2** does not appear to inhibit under these conditions, the stoichiometry of amine **8.1** (n = 2.3 ± 0.1) implies that the majority of the aminyl radicals terminate with ROO• through the aryl rings (eq 8.5) before they can be oxidized further (eq 8.2). The hydroxylamine **8.3** was a highly effective inhibitor for the first 900s of the reaction (n = 0.7 ± 0.05), however once it had been consumed (and oxidized to **8.2**) no further activity was seen. The stoichiometry of n < 1, suggests that a certain amount of **8.3** is oxidized directly by oxygen over the course of the reaction.

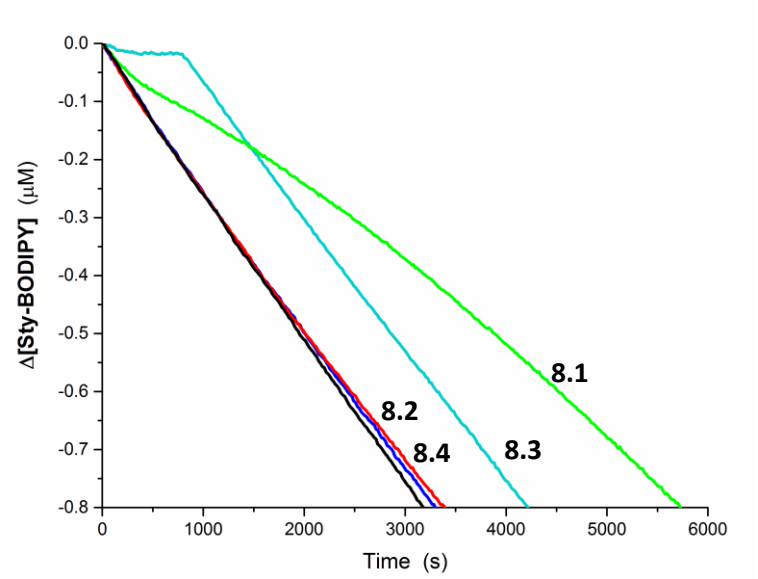

Figure 8.4. Co-autoxidations of ethylbenzene (3.3 M) and STY-BODIPY (10 μM) initiated by $^{t}Bu_2O_2$ (87 mM) at 70 °C. Uninhibited (black), or inhibited by 2.0 μM of **8.1** (green), **8.2** (red), **8.3** (cyan), or **8.4** (blue).

The difference between the catalytic activity in styrene and ethylbenzene suggests that the unsaturation in the former is vital to nitroxide catalytic activity under these conditions. Further evidence of this was obtained by using either 1-hexadecene or cyclooctene as the substrate. In 1-hexadecene (at 100°C in order facilitate autoxidation of this less activated substrate, Figure 8.5),[19] nitroxide **8.2** (n = 117 ± 7) showed catalytic activity well above that observed for the corresponding amine **8.1** (n = 23 ± 3). The discrepancy, again, likely results from low yielding conversion of **8.1** to **8.2** (eq 8.2). Consistent with the previous results at lower temperatures, diarylalkoxyamine **8.5** showed little activity even at the higher temperatures used in these experiments.[20] Similar results

were obtained in cyclooctene autoxidations (70°C), where **8.2** remained catalytically active, while **8.1** was a far less effective inhibitor (see Supporting Information).

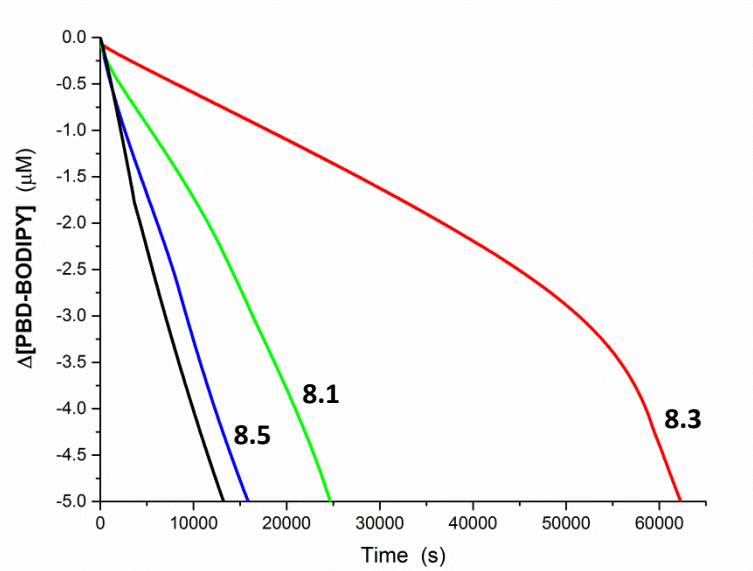

Figure 8.5. Co-autoxidations of 1-hexadecene (2.8 M) and PBD-BODIPY (10 μM) initiated by dicumylperoxide (1.0 mM) at 100 °C. Uninhibited (black), or inhibited by 2.0 μM of **8.1** (green), **8.3** (red), **8.5** (blue).

No inhibitory activity from **8.2** was seen when 1,4-dioxane, chosen as an activated non-benzylic saturated substrate, was used in the autoxidations (Figure 8.6). While **8.1** still inhibited the autoxidation in dioxane, it is much slower than in the previous cases since H-bonding of its reactive N-H bond impedes the radical trapping PCET reaction (eq 8.1).[21,22] While this kinetic solvent effect (KSE) reduces the effective k_{inh} of the reaction between **8.1** and ROO•, it is not expected to have as significant of an effect on the kinetics of nitroxide radical trapping.[23] The poor reactivity of **8.2,** then, is consistent with the previous experiments where an unsaturation is necessary for inhibition by the nitroxide. Consistent with the above examples, diarylalkoxyamine **8.4** had no effect on the reaction and the autoxidation proceeded essentially uninhibited.

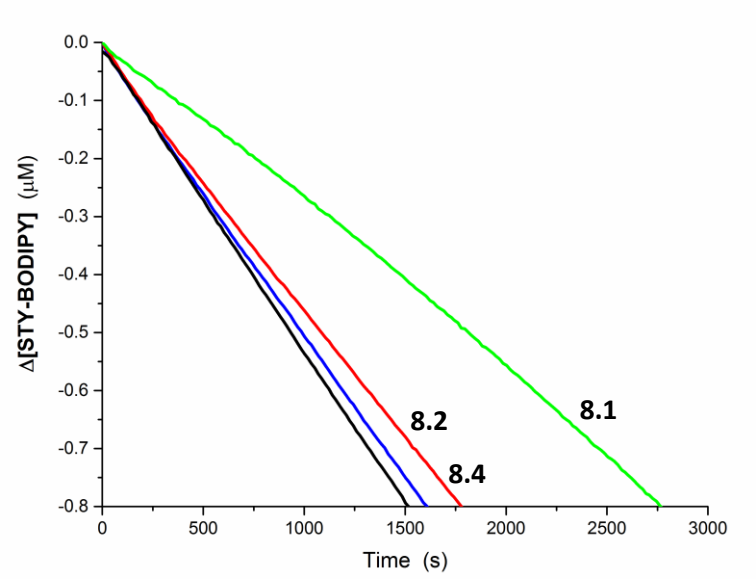

Figure 8.6. Co-autoxidations of 1,4-dioxane (2.9 M) and STY-BODIPY (10 μM) initiated by $^{t}Bu_2O_2$ (218 mM) at 70 °C. Uninhibited (black), or inhibited by 2.0 μM of **8.1** (green), **8.2** (red), **8.4** (blue).

8.3.4 Inhibition by Other Amines and Nitroxides

The autoxidations were repeated using a series of amines and nitroxides bearing di-*tert*-alkyl, aryl *tert*-alkyl, and diaryl substituents. 2,2,6,6-Tetramethylpiperidine (**8.6**) and TEMPO (**8.7**) were available commercially, while (4-*tert*-butylphenyl) *tert*-butylamine (**8.8**), bis(4-methoxyphenyl)-amine (**8.10**),[9] their analogous nitroxides (**8.9** and **8.11**, respectively)[24] and phenethyl alkoxyamine (**8.12**)[25] were prepared through literature procedures. The O-allyl alkoxyamine (**8.13**) was prepared from reduction and alkylation of **8.11**, using the method described above.

Chart 8.1. Structures of amines **8.6**, **8.8**, and **8.10**, their corresponding nitroxides **8.7**, **8.9**, **8.11**, and alkoxyamines **8.12** and **8.13**.

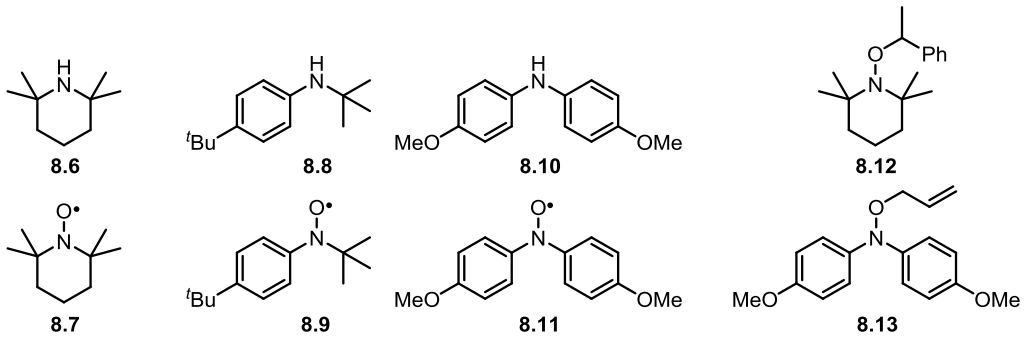

Like compound **8.2**, nitroxides **8.7**, **8.9**, and **8.11** all inhibited styrene autoxidations catalytically (Figure 8.7), with **8.11** being the most effective (n = 10.8 ± 0.2), followed by **8.7** (n = 9.4 ± 1.8) and **8.9** (n = 6.0 ± 0.9). Of the amines, only **8.10** was able to significantly inhibit the autoxidation, consistent with its known effectiveness as a RTA (lit. k_{inh} = 3.3 × 10^5 $M^{-1}s^{-1}$).[26] Its stoichiometry (n = 6.1 ± 0.6) further suggests that there is significant (although not quantitative) formation of **8.11** as the amine/aminyl radical is oxidized (eqs 8.1 and 8.2). The lack of clear inhibition seen by **8.6** and **8.8** is consistent with little peroxyl radical trapping activity – a result of their high N-H BDEs[27] and low k_{inh}[26] – and virtually no oxidation to their nitroxides under the experimental conditions. In line with the results from **8.4** and **8.5**, neither of the alkoxyamines **8.12** or **8.13** inhibited the autoxidation to a significant degree.

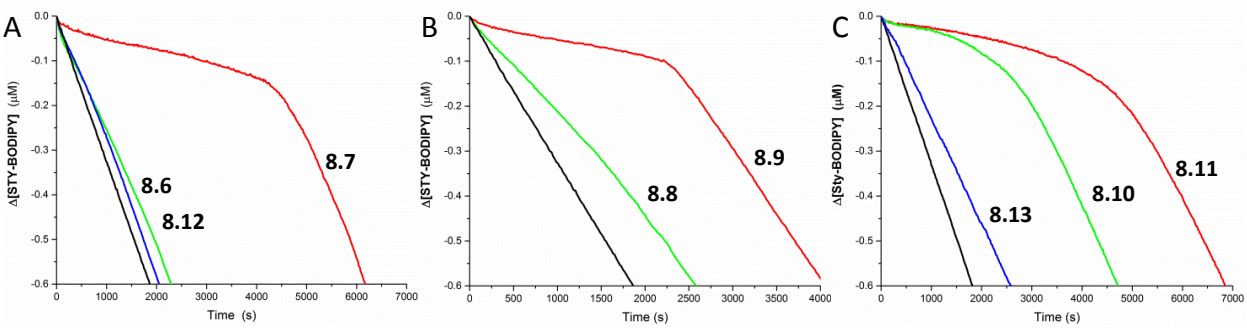

Figure 8.7. Co-autoxidations of styrene (3.5 M) and STY-BODIPY (10 μM) initiated by $^tBu_2O_2$ (218 mM) at 70 °C. A) Uninhibited (black), or inhibited by 2.0 μM of **8.6** (green), **8.7** (red), or **8.12** (blue). B) Uninhibited (black), or inhibited by 2.0 μM of **8.8** (green), or **8.9** (red). C) Uninhibited (black), or inhibited by 2.0 μM of **8.10** (green), **8.11** (red), or **8.13** (blue).

When cyclooctene autoxidations were carried out in the presence of **8.6**-**8.11**, the results were analogous to those seen in styrene (see Supporting Information). The nitroxides were all highly active RTAs, inhibiting the autoxidation for extended periods of time, while the amines were less effective.

8.4 Discussion

8.4.1 Mechanistic Possibilities

When first examining the mechanism of diarylamine regeneration, Korcek and co-workers found that when hexadecane autoxidations (at 160°C) were inhibited with bis(4-octylphenyl)nitroxide that the corresponding amine accumulated as the nitroxide was consumed. This was among the primary evidence for regeneration of the amine in the catalytic cycle (Scheme 8.6A). However, despite their proposed key intermediacy, diarylalkoxyamines were never detected within the reaction mixture and evidence for their rearrangement to diarylamines is based on explicitly prepared samples.[4,5] The lack of direct evidence for alkoxyamine formation within the reaction is odd considering that the rate determining step in the proposed cycle is its decomposition – if this were the case, the alkoxyamine would be expected to accumulate as the reaction proceeds.

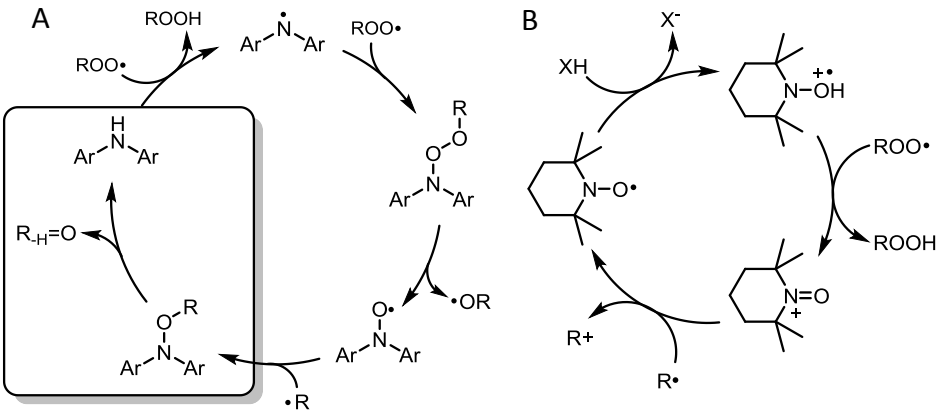

Scheme 8.6. A) Proposed catalytic cycle for diarylamine regeneration (Korcek Cycle). B) Proposed catalytic cycle for acid-catalyzed nitroxide RTAs.

In the presence of weak acids, dialkylnitroxides such as TEMPO are also known to trap oxygen centered radicals catalytically (Scheme 8.6B).[18,28] Upon protonation, nitroxides become potent H-atom donors, capable of trapping peroxyl radicals at rates approaching diffusion control (k_{inh} = 3.1 × 10^7 $M^{-1}s^{-1}$).[18] The resulting oxoammonium salt is then capable of directly oxidizing the chain-carrying alkyl radicals competitively with oxygen addition (k_{ox} = 1-3 × 10^{10} $M^{-1}s^{-1}$),[28] reducing the oxoammonium ion back to the nitroxide in the process.

8.4.2 Catalytic Activity of Diarylnitroxides and Amines

The high stoichiometry measured for inhibition of styrene autoxidation by **8.2** indicates that some type of catalytic inhibitory activity is taking place in the reaction. Furthermore, the drastic difference in stoichiometry between **8.1** and **8.2** implies incomplete oxidation of the amine to the nitroxide, consistent with independent results by Ingold and Korcek (maximum instantaneous yield of nitroxide ~ 3.1% in styrene at 65°C,[29] and ~ 7.8% in *n*-hexadecane at 160°C[4]), As such, amine **8.1** (n = 2.1 ± 0.1) traps radicals first by formal H-atom transfer (eq 8.1), followed by direct coupling of its aminyl radical through the aryl rings (eq 8.5), with very little oxidation to **8.2** occurring throughout the reaction (eq 8.2). Similarly, the more electron rich aminyl derived from diarylamine **8.10** is more oxidizable, and appears to yield a modest amount of **8.11** which is responsible for its catalytic activity (although lower relative to authentic **8.11**). The discrepancy between the amines and nitroxides is even greater for the dialkyl and alkyl-aryl compounds, **8.6**-**8.9**, where the amines are even poorer RTAs compared to diarylamines **8.1** and **8.10**. Taken together, these results suggest that, while the amines are precursors to the nitroxides, they are not directly involved in the catalytic activity under these conditions (i.e. even if the nitroxide were *quantitatively* converted to the amine and traps one radical in the process, it would then still be subject to low yielding conversion back to the nitroxide, such that the total stoichiometry would only increase by ~1).

Work by Thomas and Tolman originally suggested that diarylnitroxides are not catalytically active at 68.5°C.[11] Their experiments with cumene showed stoichiometries of $n \sim 2$ for diphenylamine and $n \sim 1$ for diphenylnitroxide, both of which are consistent with formal H-atom transfer from the diarylamine (eq 8.1),[30] followed by termination of either the aminyl or nitroxide with ROO• (eqs 8.5 and 8.6). Importantly, it should be noted that 3° hydrocarbons, such as cumene, would yield alkoxyamines which lack the crucial α-H-atom needed to regenerate the diarylamine through either potential mechanism for the Korcek cycle. As such, even if the diarylalkoxyamine were formed, it could not regenerate the diarylamine (Scheme 8.7). However, the lack of catalytic activity under Tolmans' conditions still cannot rule out that the catalytic activity observed in styrene is the result of diarylalkoxyamine formation.

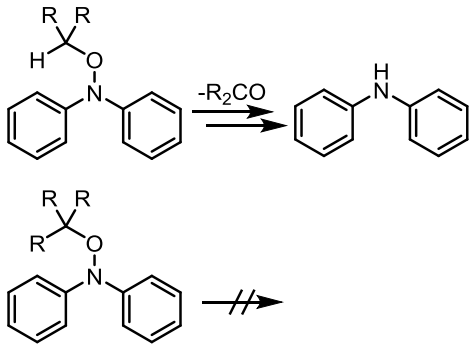

Scheme 8.7. Regeneration of a diarylamine from a primary or secondary diarylalkoxyamine.

Styrene autoxidations inhibited by hydroxylamine **8.3** were nearly identical to those inhibited by **8.2**; however, this similarity doesn't necessarily imply its presence in the nitroxide catalytic cycle. Since the reaction between **8.3** and ROO• is rapid ($k_{inh} \sim 10^6$ $M^{-1}s^{-1}$) and returns the nitroxide after a single peroxyl radical is trapped[12,18] – consistent with the difference in *n* between **8.2** and **8.3** – the catalytic inhibition seen after the initial stages of the reaction may be only due to the nitroxide without further involvement by the hydroxylamine.

The lack of inhibition seen from any of the alkoxyamines, **8.4**, **8.5**, **8.12**, or **8.13**, confirms that they cannot be involved in the catalytic activity seen under these conditions. These results rule

out turnover through the Korcek cycle, regardless of the mechanism invoked to decompose the diarylalkoxyamine. This is in alignment with the results described above, which suggest that the amines themselves do not directly participate in the catalytic cycle responsible for this activity. As the temperature of the reaction increases, regeneration of the amine through the Korcek cycle will eventually become feasible, however, formation of the alkoxyamine will still require the nitroxide to successfully compete with oxygen for alkyl radicals, and the amine will still suffer from poor conversion to the nitroxide.

Catalytic inhibition by nitroxides was only observed in olefinic substrates. When autoxidations were performed in cumene, ethylbenzene, or 1,4-dioxane no inhibition was seen from **8.2**, **8.7**, **8.9**, or **8.11**; whereas the same compounds in either styrene, 1-hexadecene, or cyclooctene showed pronounced inhibition well beyond that seen by their parent amines. While the lack of catalytic activity in cumene might be related to the 3° peroxyl radicals which propagate the autoxidation in that substrate, the same is not true for ethylbenzene whose chain carrying radical is nearly identical to the poly(styryl)peroxyl radicals which propagate the reaction in styrene (Figure 8.8). At the same time, inhibition by the nitroxides was even more prominent in 1-hexadecene and cyclooctene autoxidations. The presence of the double bond appears essential for the RTA activity of nitroxides, although the explanation behind this is still under investigation.

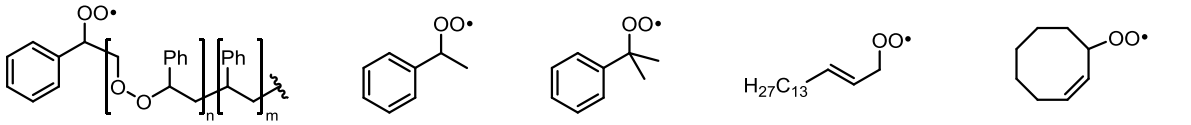

Figure 8.8. Peroxyl radicals derived from different substrates.

Similar inhibitory activity was seen by each of the nitroxides, **8.2**, **8.7**, **8.9**, and **8.11** in styrene regardless of the presence or absence of aromatic rings in the nitroxide structure, indicating that direct involvement of an aryl ring in the inhibition reaction is unlikely. Alternatively, the presence of aryl rings on the amines favors oxidation of the N-H bond and stabilizes the aminyl

radical,[31] which is expected to improve conversion to the catalytically active nitroxide. Considering the largely structure-independent inhibition by these nitroxides, we next considered the possibility of acid-catalyzed RTA activity[18,28] which could potentially be extended to include diaryl and aryl *tert*-alkyl nitroxides in addition to the dialkylnitroxides responsible for the activity of hindered amine light stabilizers (HALS).[32] The activity of the nitroxides, then, would vary both based on their pK_a and the ability of their analogous oxoammonium ions to oxidize chain carrying radicals and regenerate the nitroxide. To test this theory a 50-fold excess of 2,4,6-tri-*tert*-butylpyridine (TTBP) was added as a base to styrene autoxidations inhibited by **8.2** or **8.7**. In either case the addition of base had only a minor effect on the catalytic activity of the compounds under these conditions, suggesting that the availability of acid wasn't directly linked to the inhibition (see Supporting Information). We next prepared authentic **8.14**, the oxoammonium salt derived from **8.11**, by controlled nitration of anisole using the procedure of Meyer (Scheme 8.8).[33,34]

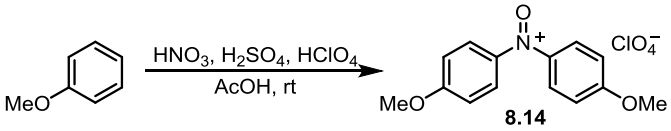

Scheme 8.8. Synthesis of diaryloxoammonium perchlorate **8.14**.

When **8.14** was added to styrene autoxidations no inhibition was observed (see Supporting Information), indicating either that the oxoammonium salt was unable to oxidize the alkyl radicals in the reaction, or the material was unstable under the reaction conditions. Indeed, the intense colour of the oxoammonium salt disappeared upon adding a small volume of styrene to a solution of **8.14** in PhCl, suggesting that any oxoammonium salt added or produced in the reaction would rapidly degrade. The lack of inhibition seen in the autoxidations further suggests that whatever products arise from either decomposition or direct reaction of **8.14** with styrene have no further inhibitory effect. The acid-catalyzed pathway would be expected to be more favorable in dioxane, where the more polar solvent would favor protonation of **8.11**, and electron rich α-alkoxy alkyl radicals would

be expected to be readily reduce **8.14**. However, no inhibition was seen by either **8.11** or **8.14** in dioxane (see Supporting Information).

Furthermore, invoking the acid catalyzed mechanism does not explain the requirement for olefinic substrates. Indeed, much of the original work on this mechanism was performed in cumene autoxidations,[18,28] where protonated nitroxides readily trapped cumylperoxyl radicals, and were then reduced by electron transfer from cumyl radicals. [35] It is expected that the similar behaviour would be seen in cumene, ethylbenene, and dioxane, and without the necessity of an olefinic substrates. Moreover, the source of the acid required for this pathway is unclear. The substrates (except dioxane) used in these studies were purified by percolation through *basic* alumina prior to the experiments, and while hydrocarbon autoxidation is known to produce carboxylic acids at high temperatures from γ-ketohydroperoxides,[36,37] neither these hydroperoxides nor the acids derived therefrom would be produced by autoxidation of substrates used in these experiments. Considering the above, it appears unlikely that the protonation/electron transfer mechanism is related to the RTA activity seen from the nitroxides under these conditions.

As both regeneration through the Korcek cycle and the acid-catalyzed pathway appear to be inconsistent with the results obtained thus far, alternative mechanisms must be explored. Since inhibition by nitroxides in unsaturated substrates appears to be catalytic, a stoichiometric reductant is necessary for turnover of the RTA – one which is either already present in the reaction or generated over the course of the autoxidation.

Mechanisms invoking addition of the nitroxides across the olefinic double bond can likely be ruled out based on the work of Ruban and co-workers, who measured the addition of nitroxides to styrene at temperatures up to 120°C.[38] The addition of TEMPO to styrene is too slow, even at 120°C (k_{add} = 2.6 × 10^{-5} $M^{-1}s^{-1}$), to account for the inhibition observed from nitroxides in our experiments. Furthermore, unlike styrene, where addition of a radical to the double bond forms a stabilized benzylc radical, addition of nitroxides across the double bonds in 1-hexadecene and cyclooctene

generate an unstabilized 2° alkyl radical as the product which would further disfavor addition reactions.

Styrene is known to dimerize slowly upon heating.[39,40] The product, a dearomatized tetralin derivative referred to as the 'Mayo Dimer', has an exceptionally weak C-H bond at the ring junction – H-atom transfer from which has been implicated in the thermal initiation of styrene polymerization by a reverse radical disproportionation reaction (Scheme 8.9).[41] The weakness of this bond suggests that it would be capable of reducing nitroxides to their hydroxylamines. Indeed, evidence for this reaction was presented by Moad,[42] who found a roughly 1:1 mixture of hydroxylamine and alkoxyamine products arising from TEMPO in styrene polymerization at 100°C.

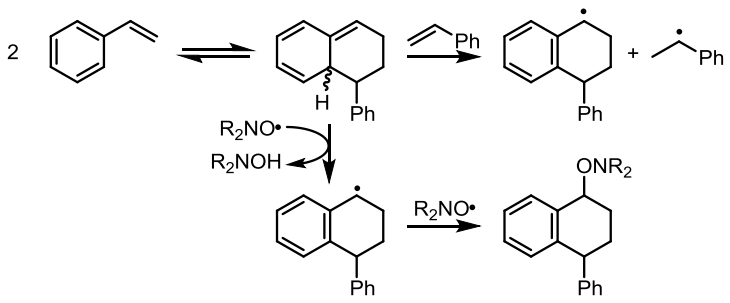

Scheme 8.9. Formation of the Mayo dimer, its reverse radical disproportionation with styrene, and H-atom abstraction by a nitroxide.

Computations carried out at the CBS-QB3 level of theory[7] suggest that abstraction of the relevant H-atom by dimethylnitroxide has $\Delta G^{\ddagger}$ = 19.8 kcal/mol, which corresponds to a second order rate constant of k = 4.6 $M^{-1}s^{-1}$ at 70°C by application of transition state theory. Given the low concentrations of both the dimer[40] and the nitroxide within an autoxidation, this suggests that this reaction would likely be too slow to account for the inhibition observed in our experiments.

It has been observed that phenolic antioxidants, such as α-tocopherol (α-TOC), can behave catalytically in autoxidations of 1,4-cyclohexadiene.[43] In this substrate, the autoxidation is known to be propagated by hydroperoxyl radicals (HOO•) rather than substrate-derived alkylperoxyl radicals.[19,44] The O-H bond in HOO• (BDE = 49.2 kcal/mol)[45] is much weaker than that of α-TOC

(O-H BDE = 77.2 kcal/mol)[46] and serves as a reductant for the α-TOC derived phenoxyl radical (eqs 8.7 and 8.8).

$$ArOH + HOO\bullet \longrightarrow ArO\bullet + H_2O_2 \qquad (8.7)$$
$$ArO\bullet + HOO\bullet \longrightarrow ArOH + O_2 \qquad (8.8)$$

The O-H bonds in hydroxylamines are weaker than that of α-TOC, although still more than 20 kcal/mol greater than the O-H bond in HOO• (e.g. 69.7 kcal/mol for TEMPO-H,[47] and calculated as 70.8 kcal/mol for bis(4-methylphenyl)hydroxylamine[5]). The nitroxides, then, should be capable of abstracting an H-atom from HOO•, to produce hydroxylamines, which are effective RTAs and reform the nitroxide upon trapping another (hydro)peroxyl radical (eqs 8.9 and 8.10).[12]

$$R_2NO\bullet + HOO\bullet \longrightarrow R_2NOH + O_2 \qquad (8.9)$$
$$R_2NOH + ROO\bullet \longrightarrow R_2NO\bullet + ROOH \qquad (8.10)$$

The only requirement for these reactions would be formation of HOO• in the autoxidations of styrene, 1-hexadecene, and cyclooctene – something which has not previously been observed. While the autoxidation of 1-hexadecene has not been studied in great detail, it is expected to be analogous to 1-hexene.[48,49] In the cases of either 1-hexadecene or cyclooctene, a mechanism can be drawn for the production of HOO• from allylic peroxyl radicals (Scheme 8.10), where intramolecular H-atom abstraction via a 7-membered cyclic transition state eliminates HOO• and forms a conjugated diene.

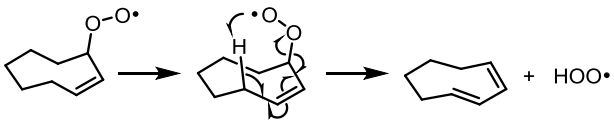

Scheme 8.10. Intramolecular H-atom abstraction and elimination of HOO• from cyclooctene.

Likewise, a mechanism could be drawn for formation of HOO• from autoxidation of the Mayo dimer, involving intramolecular H-atom abstraction from the activated bis(benzylic) C-H bond with concomitant elimination of the radical (Scheme 8.11).

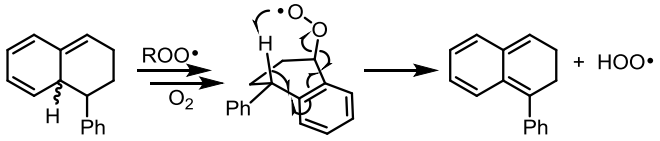

Scheme 8.11. Possible mechanism for formation of HOO• from autoxidation of the Mayo dimer.

While a transition state for the intramolecular H-atom abstraction in cyclooctene was readily located, the free energy of the reaction and the corresponding rate constant ($\Delta G^{\ddagger}$ = 22.4 kcal/mol, k = 4.0 × 10^{-2} $M^{-1}s^{-1}$) were found to be very slow relative to propagation of the autoxidation. Nonetheless, production of only a small amount of HOO• would be necessary to account for the inhibition by nitroxides in the above experiments (e.g. only ~11μM of HOO•, produced over ~5000s, would be necessary to reduce **8.2** and provide the inhibition in Figure 8.1). Computational studies on similar mechanisms within the Mayo dimer, and 1-hexene (as a model for 1-hexadecane) are ongoing. However, it should be noted that during Moss' product analyses from the autoxidation of 1-hexene, no products arising from 1,3-hexadiene (the proposed by-product of HOO• elimination) were observed.[48] Furthermore, rather than forming the allylic peroxyl radicals required for the above mechanism, cyclooctene is known to autoxidize predominantly by peroxidation of the alkene – specifically by addition of a peroxyl radical across the double bond, followed by an intramolecular homolytic substitution as in Scheme 8.12.[50,51]

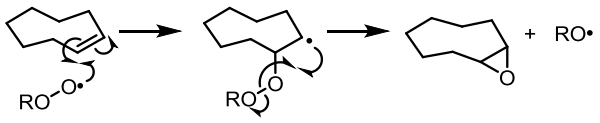

Scheme 8.12. Peroxidation of cyclooctene by peroxyl radicals.

In order to provide evidence for the intramolecular H-atom transfer reaction shown in Scheme 8.10, we conducted inhibited autoxidations using norbornene (bicyclo[2.2.1]hept-2-ene) as the oxidizable substrate. Unlike those in cyclooctene or 1-hexadecene, the allylic hydrogen atoms in norbornene are held perpendicular to the alkene by the bicyclic structure and cannot be easily abstracted – as a result, norbornene autoxidizes exclusively by radical addition (Scheme 8.13).[52] This

pathway, in addition to the lack of accessible allylic hydrogen atoms in norbornene-derived peroxyl radicals, should preclude HOO• formation by the mechanism described above.

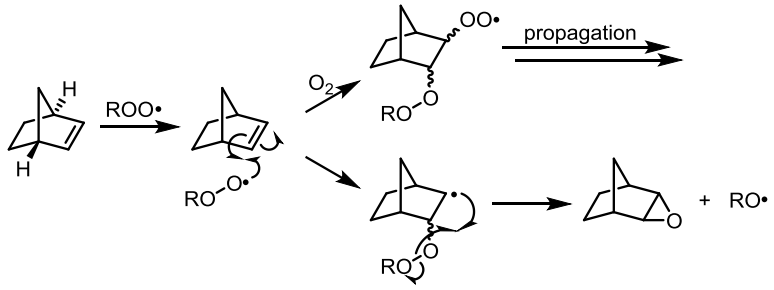

Scheme 8.13. Autoxidation of norbornene (bicyclo[2.2.1]hept-2-ene).

When the experiments were performed, however, it was found that the nitroxides **8.2** and **8.7** maintained their heightened reactivity over their amine precursors **8.1** and **8.6**, respectively (Figure **8.9**), implying that if HOO• is formed, it would be through a pathway arising from addition of oxygen centered radicals to an alkene – a process which is accessible to all the previous olefinic substrates as well, including styrene.

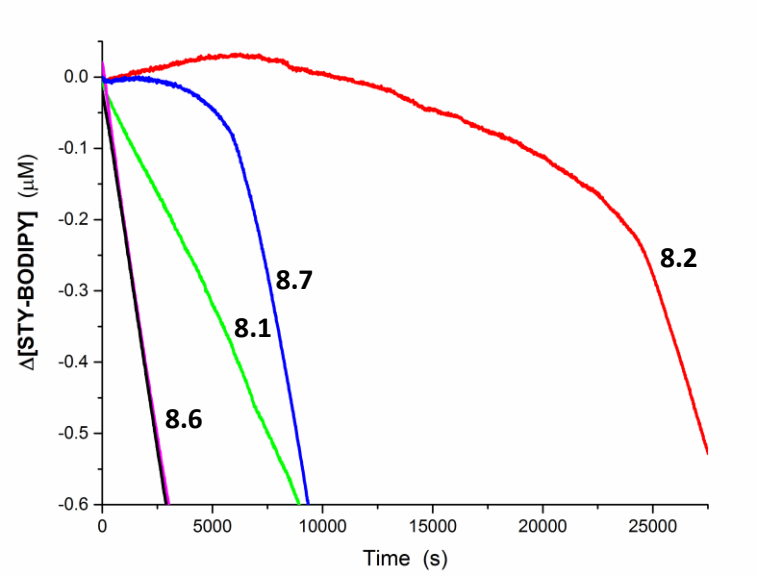

Figure 8.9. Co-autoxidations of norbornene (1.0 M) and STY-BODIPY (10 μM) initiated by $^{t}Bu_2O_2$ (218 mM) at 70 °C. Uninhibited (black), or inhibited by 2.0 μM of **8.1** (green), **8.2** (red), **8.6** (magenta), or **8.7** (blue).[53]

As C-H bonds α to heteroatoms are also activated towards abstraction by radicals (e.g. in dioxane autoxidations),[54,55] it seemed conceivable that the β-peroxy peroxyl radical might abstract its own activated β-H-atom in a five membered transition state, yielding an alkyl radical which would likely β-fragment, releasing either HOO• or RO• (Scheme 8.14). While this may seem a peculiar reaction, a transition state was, nonetheless, readily located computationally. The free energy required for the reaction ($\Delta G^{\ddagger}$ = 29.4 kcal/mol) was higher than that for the similar 7-membered variant (*vide supra*) and yields a predicted rate constant of $k = 1.0 \times 10^{-8}$ $M^{-1}s^{-1}$ upon application of transition state theory – far too slow to be relevant in the current context. However, the high vibrational frequency calculated for the transition state (-2181 cm^{-1}) suggests a very narrow reaction barrier on the potential energy surface – an indicator that tunneling may be an important factor in the reaction. Indeed, upon application of the tunneling corrections developed by Truhlar,[56] the predicted rate constant increased by more than six orders of magnitude ($k = 2 \times 10^{-1}$ $M^{-1}s^{-1}$) – suggesting that it may indeed be a viable pathway.

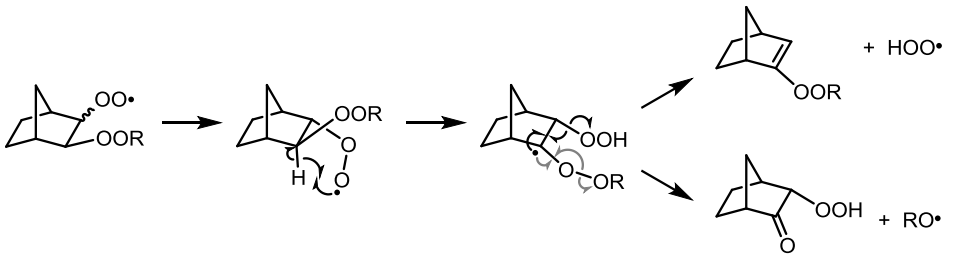

Scheme 8.14. Intramolecular H-atom abstraction by a β-peroxy peroxyl radical, followed by possible β-fragmentation to form either HOO• or RO•.

Computational studies on this reaction specifically, and in the context of the overall autoxidation are currently ongoing. Additionally, given the potential importance of tunneling in this process, deuterium kinetic isotope effects (DKIEs) would serve as important evidence in favor of or against this mechanism. Deuteration of the vinylic positions on styrene or cyclooctene would greatly slow the intramolecular H-atom abstraction, while only having minimal effect on the overall autoxidation of the substrates. The DKIEs in arising from the use of these deuterated substrates will

provide important information on if/how the substrate may be producing HOO•. Furthermore, experiments including the addition of ~1% MeOH/MeOD to the autoxidation have recently been carried out. The DKIEs for inhibition by nitroxides **8.2** and **8.7** in styrene have been found to be k_H/k_D = 4.0 and 4.1, respectively – suggesting that the active RTA in the system involves transfer of an exchangeable H-atom in the transition state (consistent with the suggestion that the hydroxylamines are the active RTAs). Additionally, electron paramagnetic resonance (EPR) spectroscopy could be used to monitor the formation and consumption of nitroxides over the course of the autoxidation.

8.5 Conclusion

Diaryl-, aryl-alkyl-, and dialkylnitroxides all display catalytic RTA activity in autoxidations of olefinic hydrocarbons, while the same compounds are completely inactive in other 2° or 3° oxidizable substrates. Based on the experiments described above, it seems doubtful that either regeneration through the Korcek cycle or acid-catalyzed pathways are related to this activity. The former can be ruled out based on the lack of activity from the alkoxyamines and poor conversion of the amines to their nitroxides, while the latter can be excluded based on the activity under basic conditions, the instability of the oxoammonium salts, and the selectivity towards olefinic substrates. The above results underscore the important relationship between substrate and RTA activity, although the specific mechanism behind this remarkable inhibitory activity remains unclear. More importantly, the potential relevance of this process to RTA catalytic activity under applied conditions needs to be carefully examined. Many of the hydrocarbons used industrially in polymers and lubricating oils (where aminic RTAs are commonly used) contain varying amounts of unsaturation, and this effect may be responsible for some or even most of the catalytic RTA activity responsible for protecting these products from degradation. Moreover, an understanding of this mechanism may open other avenues of research towards designing even more effective radical-trapping antioxidants.

8.6 References

(1) Ingold, K. U. *Chem. Rev.* **1961**, *61*, 563–589.

(2) Ingold, K. U.; Pratt, D. A. *Chem. Rev.* **2014**, *114*, 9022–9046.

(3) Bolsman, T.; Blok, A.; Frijns, J. *Recl. des Trav. Chim. des Pays-Bas* **1978**, *97*, 310–312.

(4) Jensen, R. K.; Korcek, S.; Zinbo, M.; Gerlock, J. L. *J. Org. Chem.* **1995**, *60*, 5396–5400.

(5) Haidasz, E. A.; Shah, R.; Pratt, D. A. *J. Am. Chem. Soc.* **2014**, *136*, 16643–16650.

(6) Haidasz, E. A.; Van Kessel, A. T. M.; Pratt, D. A. *J. Org. Chem.* **2016**, *81*, 737–744.

(7) Montgomery, J. A.; Frisch, M. J.; Ochterski, J. W.; Petersson, G. A. *J. Chem. Phys.* **1999**, *110*, 2822.

(8) Maillard, B.; Ingold, K. U.; Scaiano, J. C. *J. Am. Chem. Soc.* **1983**, *105*, 5095–5099.

(9) Hanthorn, J. J.; Valgimigli, L.; Pratt, D. A. *J. Org. Chem.* **2012**, *77*, 6908–6916.

(10) Golubev, V. A.; Sen', V. D. *Russ. J. Org. Chem.* **2013**, *49*, 555–558.

(11) Thomas, J. R.; Tolman, C. A. *J. Am. Chem. Soc.* **1962**, *84*, 2930–2935.

(12) Brownlie, I. T.; Ingold, K. U. *Can. J. Chem.* **1967**, *45*, 2427–2432.

(13) The reaction of aryl nitroxides with peroxyl radicals takes place at the 2- or 4-positions the aryl ring[14] and, while reversible, likely competes with tautomerization to an aryl peroxide.[5]

(14) Boozer, C. E.; Hammond, G. S.; Hamilton, C. E.; Sen, J. N. *J. Am. Chem. Soc.* **1955**, *77*, 3233–3237.

(15) Kelly, D.; Bansal, H.; Morgan, J. *Tetrahedron Lett.* **2002**, *43*, 9331–9333.

(16) Meyer, K. H.; Reppe, W. *Berichte der Dtsch. Chem. Gesellschaft (A B Ser.* **1921**, *54*, 327–337.

(17) Golubev, V. A.; Tkachev, V. V.; Sen', V. D. *Russ. J. Org. Chem.* **2014**, *50*, 678–684.

(18) Amorati, R.; Pedulli, G. F.; Pratt, D. A.; Valgimigli, L. *Chem. Commun.* **2010**, *46*, 5139–5141.

(19) Howard, J.; Ingold, K. *Can. J. Chem.* **1967**, *45*, 793–802.

(20) Control experiments were run with **2**, under identical conditions but in the absence of initiator. No change was observed in the reaction over several hours.

(21) Snelgrove, D. W.; Lusztyk, J.; Banks, J. T.; Mulder, P.; Ingold, K. U. *J. Am. Chem. Soc.* **2001**, *123*, 469–477.

(22) Litwinienko, G.; Ingold, K. U. *Acc. Chem. Res.* **2007**, *40*, 222–230.

(23) Beckwith, A. L. J.; Bowry, V. W.; Ingold, K. U. *J. Am. Chem. Soc.* **1992**, *114*, 4983–4992.

(24) Tokumaru, K.; Sakuragi, H.; Simamura, O. *Tetrahedron Lett.* **1964**, *5*, 3945–3948.

(25) Willenbacher, J.; Wuest, K. N. R.; Mueller, J. O.; Kaupp, M.; Wagenknecht, H.-A.; Barner-Kowollik, C. *ACS Macro Lett.* **2014**, *3*, 574–579.

(26) Brownlie, I. T.; Ingold, K. U. *Can. J. Chem.* **1967**, *45*, 2419–2425.

(27) Lalevée, J.; Allonas, X.; Fouassier, J.-P. *J. Am. Chem. Soc.* **2002**, *124*, 9613–9621.

(28) Haidasz, E. A.; Meng, D.; Amorati, R.; Baschieri, A.; Ingold, K. U.; Valgimigli, L.; Pratt, D. A. *J. Am. Chem. Soc.* **2016**, *138*, 5290–5298.

(29) Adamic, K.; Dunn, M.; Ingold, K. U. *Can. J. Chem.* **1969**, *47*, 287–294.

(30) Brownlie, I. T.; Ingold, K. U. *Can. J. Chem.* **1966**, *44*, 861–868.

(31) Pratt, D. A.; DiLabio, G. A.; Valgimigli, L.; Pedulli, G. F.; Ingold, K. U. *J. Am. Chem. Soc.* **2002**, *124*, 11085–11092.

(32) Allen, N. S. *Chem. Soc. Rev.* **1986**, *15*, 373.

(33) Meyer, K. H.; Gottlieb-Billroth, H. *Berichte der Dtsch. Chem. Gesellschaft (A B Ser.* **1919**, *52*, 1476–1489.

(34) Kehrmann, F.; Decker, H. *Berichte der Dtsch. Chem. Gesellschaft (A B Ser.* **1921**, *54*, 2427–2435.

(35) It should also be noted that in nonpolar solvents such as PhCl, electron transfer from the alkyl radicals to the oxoammonium salt was disfavored, and precluded turnover of the nitroxide RTA.[28].

(36) Jensen, R. K.; Korcek, S.; Mahoney, L. R.; Zinbo, M. *J. Am. Chem. Soc.* **1981**, *103*, 1742–1749.

(37) Jalan, A.; Alecu, I. M.; Meana-Pañeda, R.; Aguilera-Iparraguirre, J.; Yang, K. R.; Merchant, S. S.; Truhlar, D. G.; Green, W. H. *J. Am. Chem. Soc.* **2013**, *135*, 11100–11114.

(38) Ruban, L. V.; Buchachenko, A. L.; Neiman, M. B. *Polym. Sci. U.S.S.R.* **1967**, *9*, 1750–1758.

(39) Mayo, F. R. *J. Am. Chem. Soc.* **1953**, *75*, 6133–6141.

(40) Kothe, T.; Fischer, H. *J. Polym. Sci. Part A Polym. Chem.* **2001**, *39*, 4009–4013.

(41) Thickett, S. C.; Gilbert, R. G. *Macromolecules* **2008**, *41*, 4528–4530.

(42) Moad, G.; Rizzardo, E.; Solomon, D. H. *Polym. Bull.* **1982**, *6*, 589–593.

(43) Cedrowski, J.; Litwinienko, G.; Baschieri, A.; Amorati, R. *Chem. - A Eur. J.* **2016**, *22*, 16441–16445.

(44) Howard, J. A.; Ingold, K. U. *Can. J. Chem.* **1967**, *45*, 785–792.

(45) Warren, J. J.; Tronic, T. A.; Mayer, J. M. *Chem. Rev.* **2010**, *110*, 6961–7001.

(46) Lucarini, M.; Pedulli, G. F. *Chem. Soc. Rev.* **2010**, *39*, 2106–2119.

(47) Mahoney, L. R.; Mendenhall, G. D.; Ingold, K. U. *J. Am. Chem. Soc.* **1973**, *95*, 8610–8614.

(48) Moss, S. J.; Steiner, H. *J. Chem. Soc.* **1965**, 2372–2377.

(49) Howard, J. A.; Ingold, K. U. *Can. J. Chem.* **1966**, *44*, 1119–1130.

(50) Van Sickle, D. E.; Mayo, F. R.; Arluck, R. M. *J. Am. Chem. Soc.* **1965**, *87*, 4824–4832.

(51) Lauterbach, G.; Pritzkow, W. *J. Prakt. Chem.* **1995**, *337*, 237–238.

(52) Van Sickle, D. E.; Mayo, F. R.; Arluck, R. M. *J. Org. Chem.* **1967**, *32*, 3680–3681.

(53) The slight increase in the absorbance reading is a result of slow evaporation of the norbornene (b.p. = 96 °C) evaporating over the course of the reaction at 70 °C. The difference in the reading roughly corresponds to 0.3% of the total reaction volume over the first 7000 s.

(54) Howard, J. A.; Ingold, K. U. *Can. J. Chem.* **1969**, *47*, 3809–3815.

(55) Howard, J. A.; Ingold, K. U. *Can. J. Chem.* **1970**, *48*, 873–880.

(56) Skodje, R.T.; Truhlar, D.G. *J. Phys. Chem.* **1981**, 85, 3021.

8.7 Supporting Information

8.7.1 General Experimental

Reagents were purchased from commercial suppliers and used without further purification. Column chromatography was carried out using flash silica gel (40−63 μm, 230−400 mesh). UV−vis spectra and kinetics were measured on a Cary 100 UV−vis spectrophotometer equipped with a temperature controller unit and a thermostated 6 × 6 multicell holder. ^{1}H and ^{13}C NMR were recorded on a Bruker AVANCE spectrometer at 600 and 125 MHz, respectively, unless specified otherwise. High-resolution mass spectra were obtained on a Kratos Concept Tandem mass spectrometer.

8.7.2 Inhibited Co-autoxidations with STY-BODIPY and PBD-BODIPY

The co-autoxidations were carried out according to our previously published methodology,[S1] substituting substrates and initiators as needed. Briefly, substrate (1-2 mL) was loaded into a 3 mL

cuvette along with the appropriate volume of PhCl, such that the final volume of the reaction is 2.5 ml. The cuvette was placed into the thermostated sample holder of a UV−vis spectrophotometer and allowed to equilibrate to the appropriate temperature. A small aliquot (12.5 μL) of a 2.0 mM BODIPY solution in 1,2,4-trichlorobenzene was added, followed by 50-100 μl of a solution of initiator in PhCl. The solution was thoroughly mixed. The consumption of the probe was monitored for 10-20 min to ensure that the reaction was proceeding at a constant rate, after which 10 μL of a 500 μM solution of the test antioxidant was added. The solution was thoroughly mixed and the absorbance readings resumed.

8.7.3. General Procedure for the Reduction/Alkylation of Diarylnitroxides

The diarylnitroxide (1.0 mmol) was dissolved in degassed THF (7 ml, 0.15 M), under a nitrogen atmosphere. Hydrazine hydrate (62 μl, 1.0 mmol) was added to the solution. The reaction was stirred at room temperature until dark red colour of the nitroxide had disappeared (*ca.* 10-15 mins). The solution was carefully evaporated under reduced pressure by rotovap (~20 °C), followed by drying under high vacuum. If needed, the hydroxylamines could be recrystallized from EtOAc/hexanes with gentle heating while under an inert atmosphere.

The crude hydroxylamine was dissolved in degassed THF (7ml ml, 0.15 M), under an inert atmosphere, and cooled to -78 °C in a dry ice/acetone bath. A 1.0 M solution of KHMDS in THF (1.0 ml, 1.0 mmol) was added dropwise, and the reaction stirred for 15 mins. The alkyl halide was added dropwise to the reaction, and the solution allowed to warm to room temperature overnight. TLC showed that the alkoxyamines were not stable to chromatography. The reaction was extracted twice with Et_2O/H_2O. The organic phases were combined, washed with brine, dried with Mg_2SO_4, and filtered. The solvent was evaporated under reduced pressure (~20 °C). The crude material was crystalized from EtOAc/hexanes with gentle heating, under an inert atmosphere.

Bis(4-tert-butylphenyl)hydroxylamine (8.3): Beige solid, 72%. ^{1}H-NMR (400 MHz; DMSO-d_6): δ 9.73 (s, 1H), 7.31 (d, *J* = 8.6 Hz, 4H), 7.04 (d, *J* = 8.6 Hz, 4H), 1.27 (s, 18H). 13-C NMR (76 MHz; DMSO): δ 147.7, 145.2, 125.3, 119.3, 33.9, 31.3

O-(1-phenylethyl)-N,N-bis(4-tert-butylphenyl)hydroxylamine (8.4): Light yellow solid, 46%. ^{1}H-NMR (400 MHz; DMSO-d_6): δ 7.39-7.27 (m, 9H), 6.94 (d, *J* = 8.7 Hz, 4H), 4.86 (q, *J* = 6.4 Hz, 1H), 1.50 (d, *J* = 6.5 Hz, 3H), 1.26 (s, 19H). 13-C NMR (76 MHz; DMSO): δ 146.8, 146.5, 142.0, 128.1, 127.7, 126.9, 125.5, 120.5, 79.2, 34.0, 31.2, 21.0

O-(1-pentyl)-N,N-bis(4-tert-butylphenyl)hydroxylamine (8.5): Yellow solid, 50%. ^{1}H-NMR (400 MHz; DMSO-d_6): δ 7.35 (d, *J* = 8.8 Hz, 5H), 6.99 (d, *J* = 8.7 Hz, 4H), 3.85 (t, *J* = 6.6 Hz, 2H), 1.60 (quintet, *J* = 7.1 Hz, 2H), 1.35-1.27 (m, 23H), 0.85 (t, *J* = 7.1 Hz, 3H). 13-C NMR (75 MHz; DMSO): δ 146.38, 146.24, 125.6, 120.0, 72.9, 34.0, 31.2, 27.8, 27.6, 21.9, 13.8

O-allyl-N,N-bis(4-methoxyphenyl)hydroxylamine (8.13): Light brown solid. 63% ^{1}H-NMR (400 MHz; DMSO-d_6): δ 6.98 (d, *J* = 9.1 Hz, 4H), 6.90 (d, *J* = 9.1 Hz, 4H), 5.99 (ddt, *J* = 17.3, 10.4, 6.0 Hz, 1H), 5.31 (dd, *J* = 17.3, 1.8 Hz, 1H), 5.22-5.19 (m, 1H), 4.34 (d, *J* = 6.0 Hz, 2H), 3.73 (s, 6H). 13-C NMR (76 MHz; DMSO): δ 156.3, 142.6, 134.0, 122.3, 118.4, 114.2, 73.6, 55.2

8.7.4 Cyclooctene Autoxidations

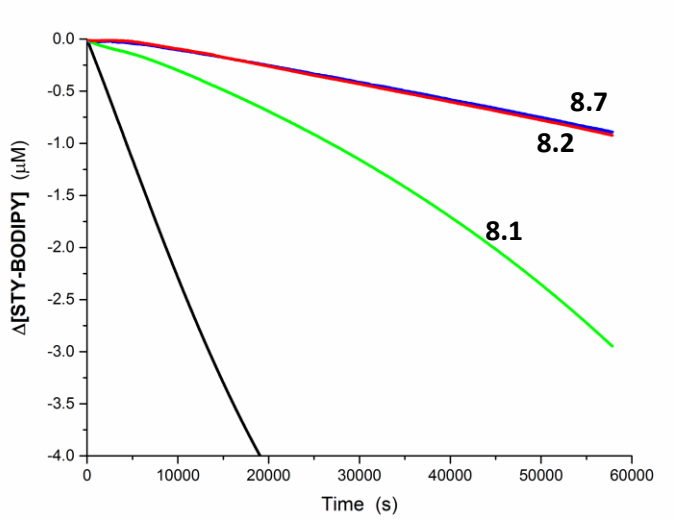

Figure S8.1. Co-autoxidations of cyclooctene (3.1 M) and STY-BODIPY (10 μM) initiated by $^{t}Bu_2O_2$ (218 mM) at 70 °C. Uninhibited (black), or inhibited by 2.0 μM of **8.1** (green), **8.2** (red) or **8.7** (blue).

8.7.5 Autoxidations Containing Tri-*t*-Butylpyridine

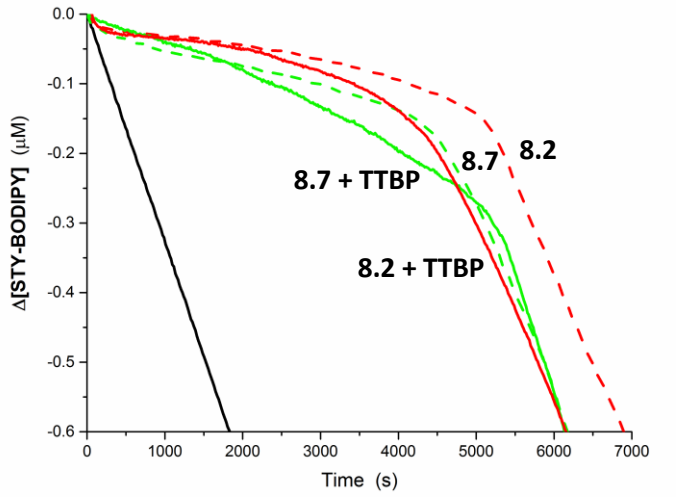

Figure S8.2. Co-autoxidations of styrene (3.5 M) and STY-BODIPY (10 μM) initiated by $^{t}Bu_2O_2$ (218 mM) at 70 °C. Uninhibited (black), or inhibited by 2.0 μM of **8.2** (red) or **8.7** (blue). Without added base (dashed lines), or with 0.1 mM TTBP (solid lines).

8.7.6. Autoxidations Inhibited by 4,4'-Dimethoxydiphenyl Oxoammonium Perchlorate

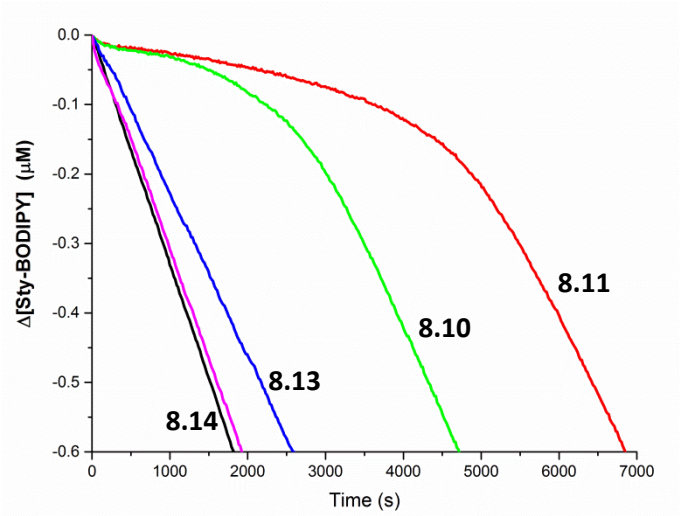

Figure S8.3. Co-autoxidations of styrene (3.5 M) and STY-BODIPY (10 μM) initiated by $^{t}Bu_2O_2$ (218 mM) at 70 °C. Uninhibited (black), or inhibited by 2.0 μM of **8.10** (green), **8.11** (red), **8.13** (blue), or **8.14** (magenta).

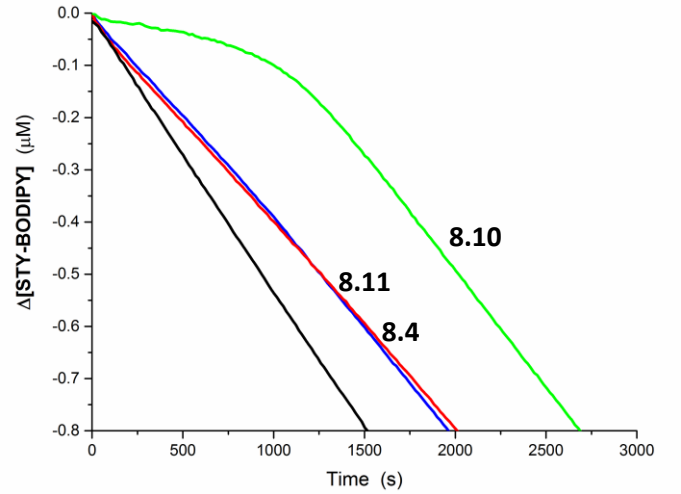

Figure S8.4. Co-autoxidations of 1,4-dioxane (2.9 M) and STY-BODIPY (10 μM) initiated by $^{t}Bu_2O_2$ (218 mM) at 70 °C. Uninhibited (black), or inhibited by 2.0 μM of **8.10** (green), **8.11** (red), **8.14** (blue).

8.7.7 Alkyl Radical Clocking Experiments for Bis(4-*tert*-butylphenyl)nitroxide

Alkyl radical clocking experiments were carried out by the method of Ingold[S2] at 70°C. The product ratios arising from the reaction of bis(4-*tert*-butylphenyl)nitroxide with the alkyl radical clock yielded the second order rate constant k = 1.9 $M^{-1}s^{-1}$.

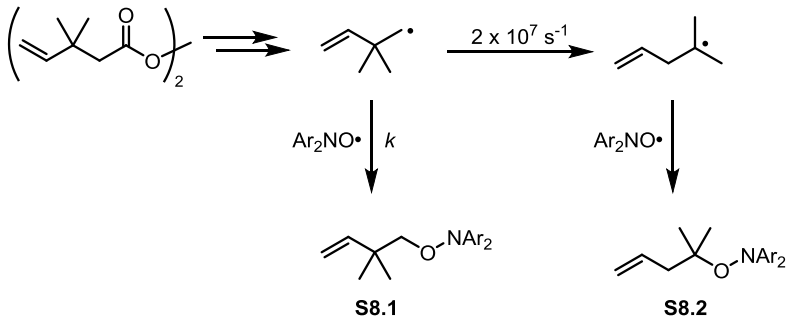

Scheme S8.1. Alkyl radical clock from decomposition of a diacylperoxide precursor.

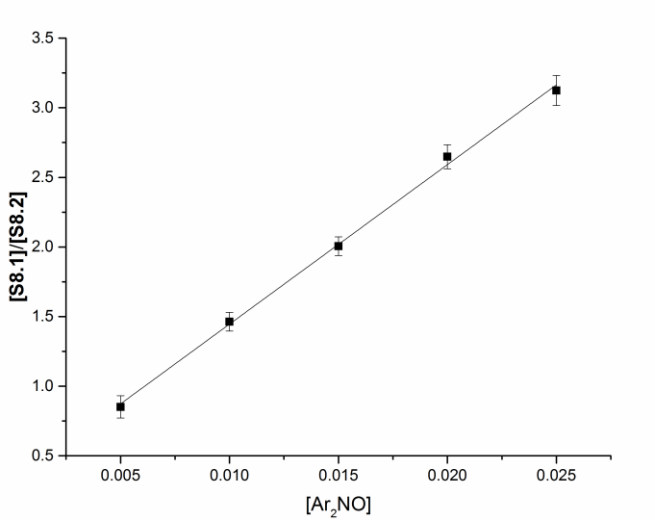

Figure S8.5. Product ratios arising from the reaction of bis(4-*tert*-butylphenyl)nitroxide with 2,2-dimethylbut-3-enyl radicals.

8.7.8 Supporting Information References

S1) Haidasz, E. A.; Van Kessel, A. T. M.; Pratt, D. A. *J. Org. Chem.* **2016**, *81*, 737–744.

S2) Beckwith, A. L. J.; Bowry, V. W.; Ingold, K. U. *J. Am. Chem. Soc.* **1992**, *114*, 4983–4992.

8.7.9 ^{1}H and ^{13}C-NMR Spectra

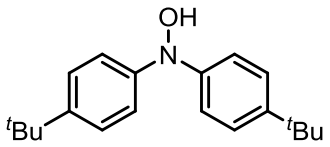

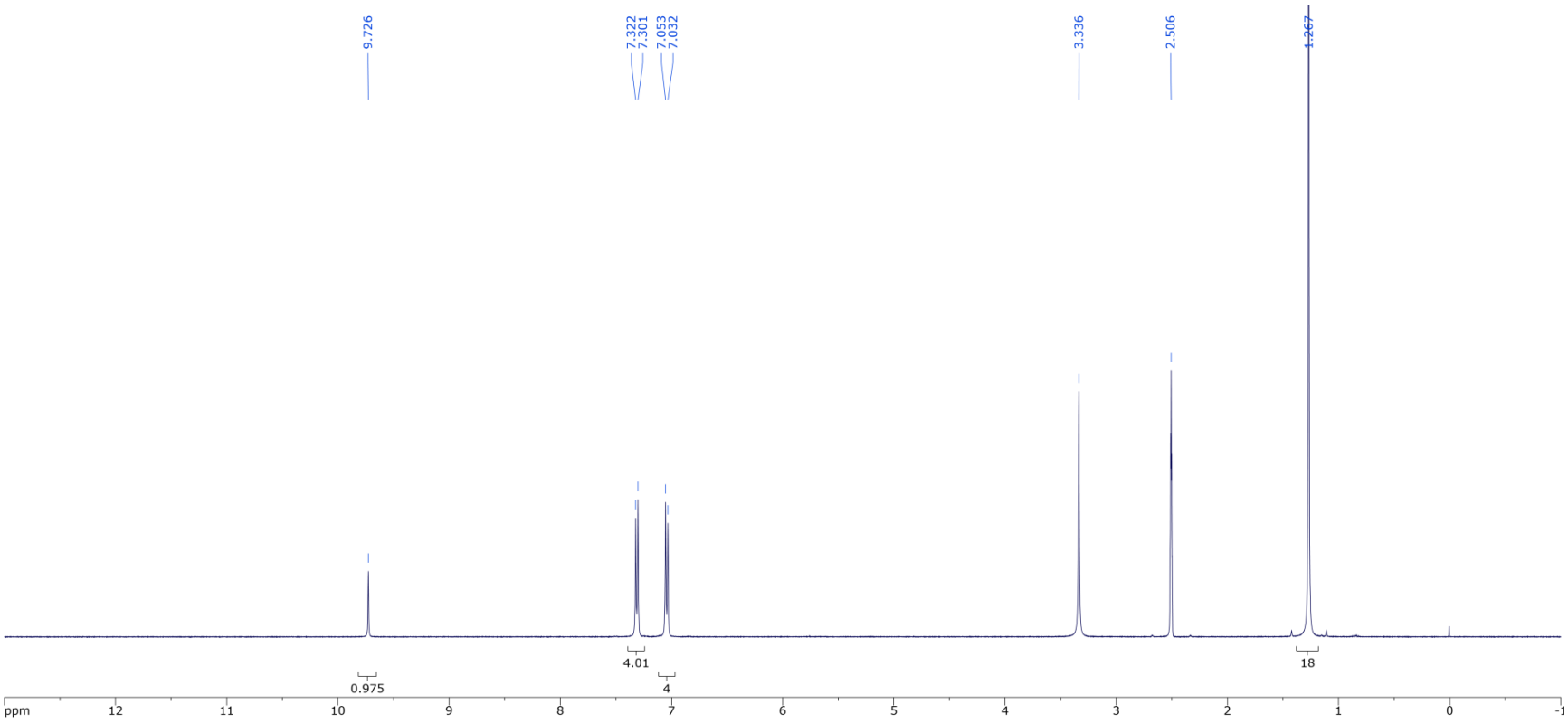

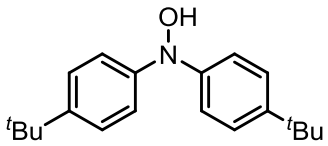
OH
N
tBu
tBu

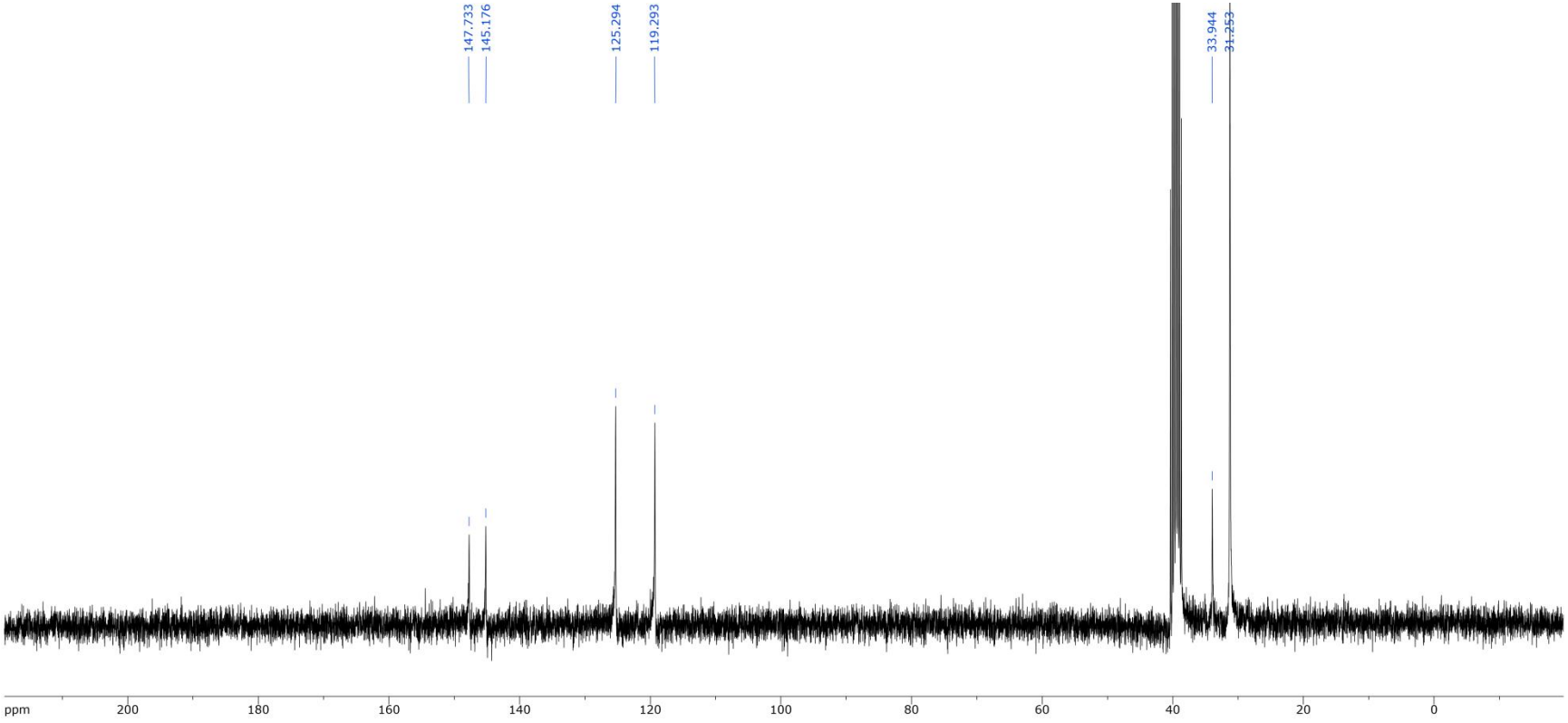
147.733
145.176
125.294
119.293
33.944
31.253
ppm
200
180
160
140
120
100
80
60
40
20
0

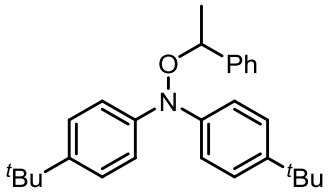
O
Ph
N
tBu
tBu

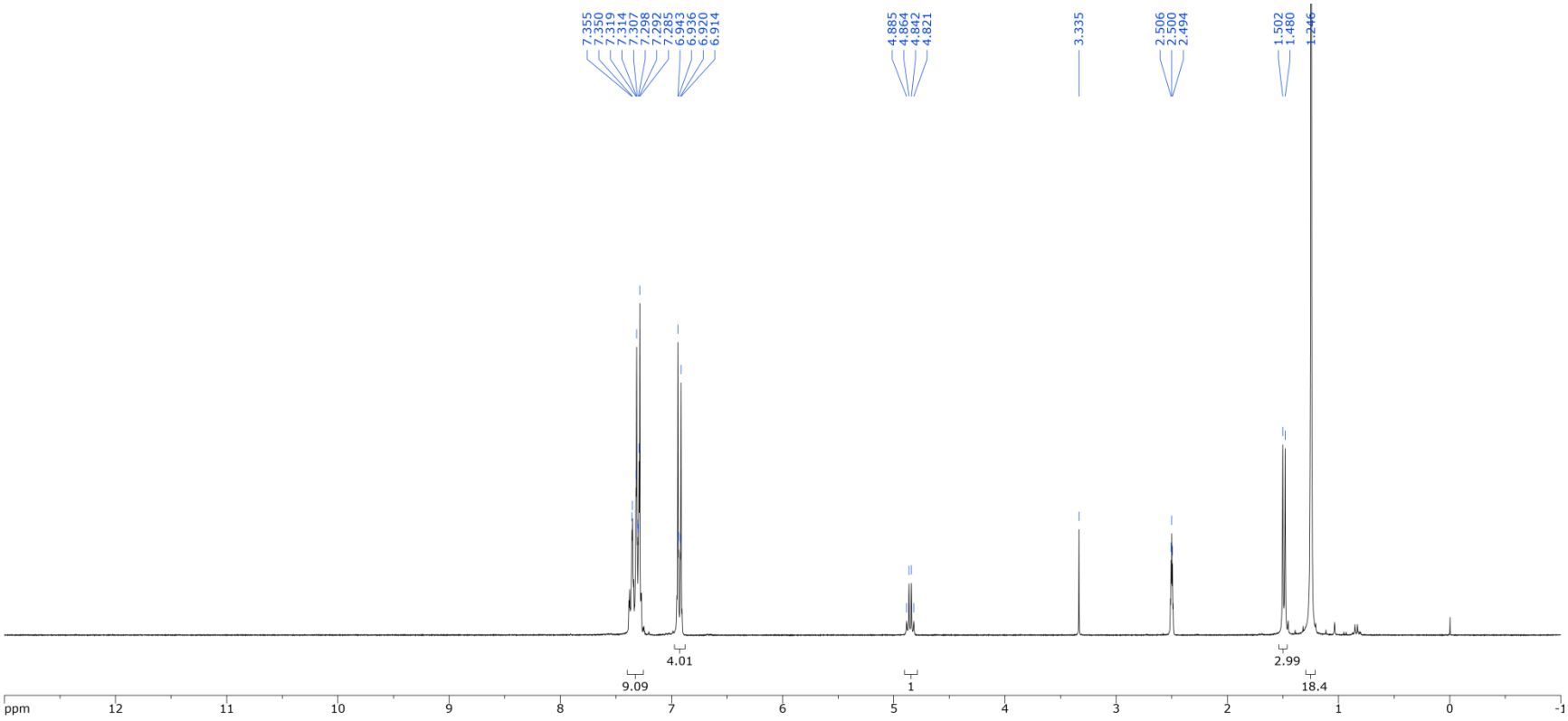
7.355
7.350
7.319
7.314
7.307
7.298
7.292
7.285
6.943
6.936
6.920
6.914
4.885
4.864
4.843
4.821
3.335
2.506
2.500
2.494
1.502
1.480
1.246
9.09
4.01
1
2.99
18.4
ppm
12
11
10
9
8
7
6
5
4
3
2
1
0
-1

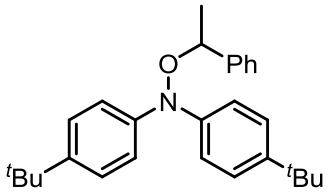
O
Ph
N
tBu
tBu

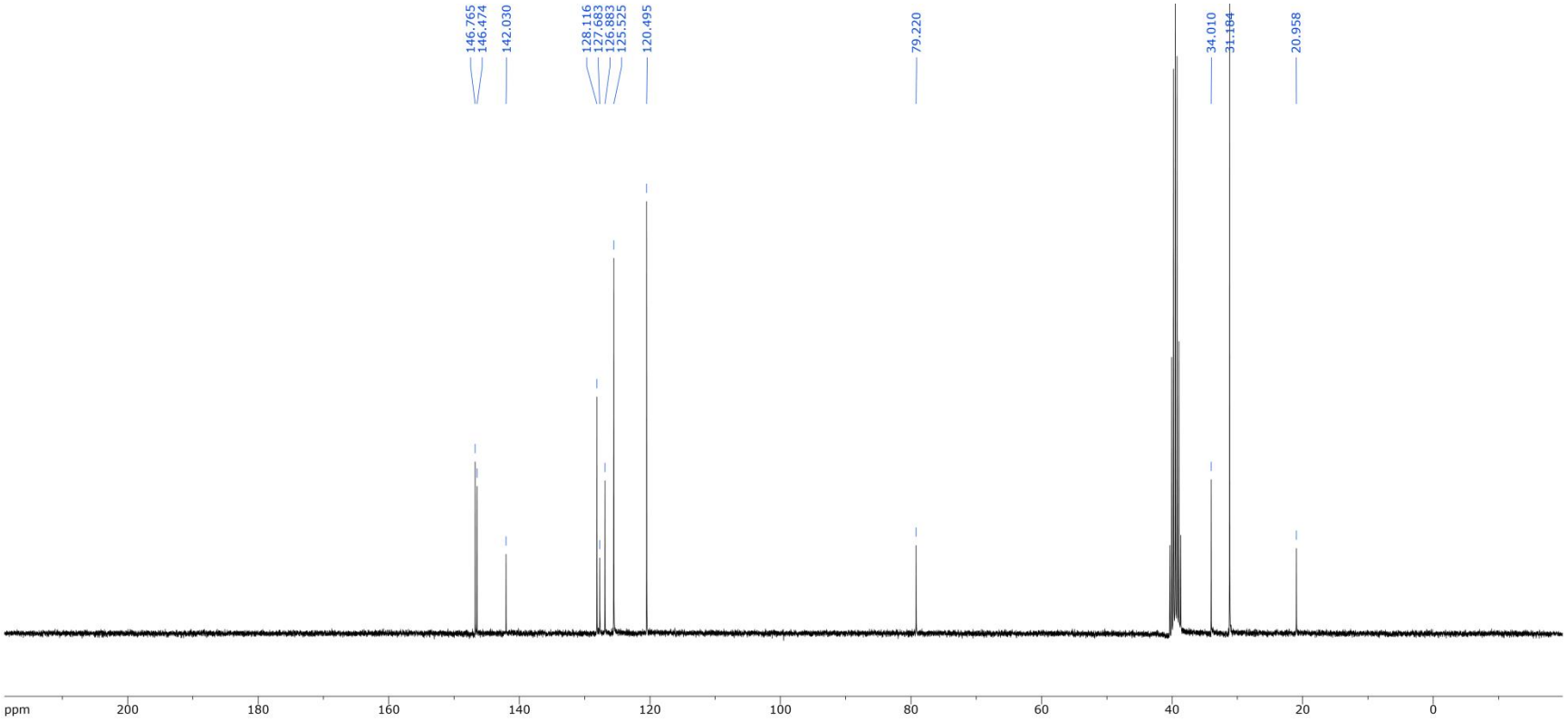
146.765
146.474
142.030
128.116
127.683
126.883
125.525
120.495
79.220
34.010
31.184
20.958
ppm
200
180
160
140
120
100
80
60
40
20
0

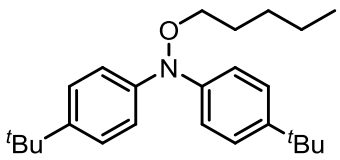
O
N
tBu
tBu

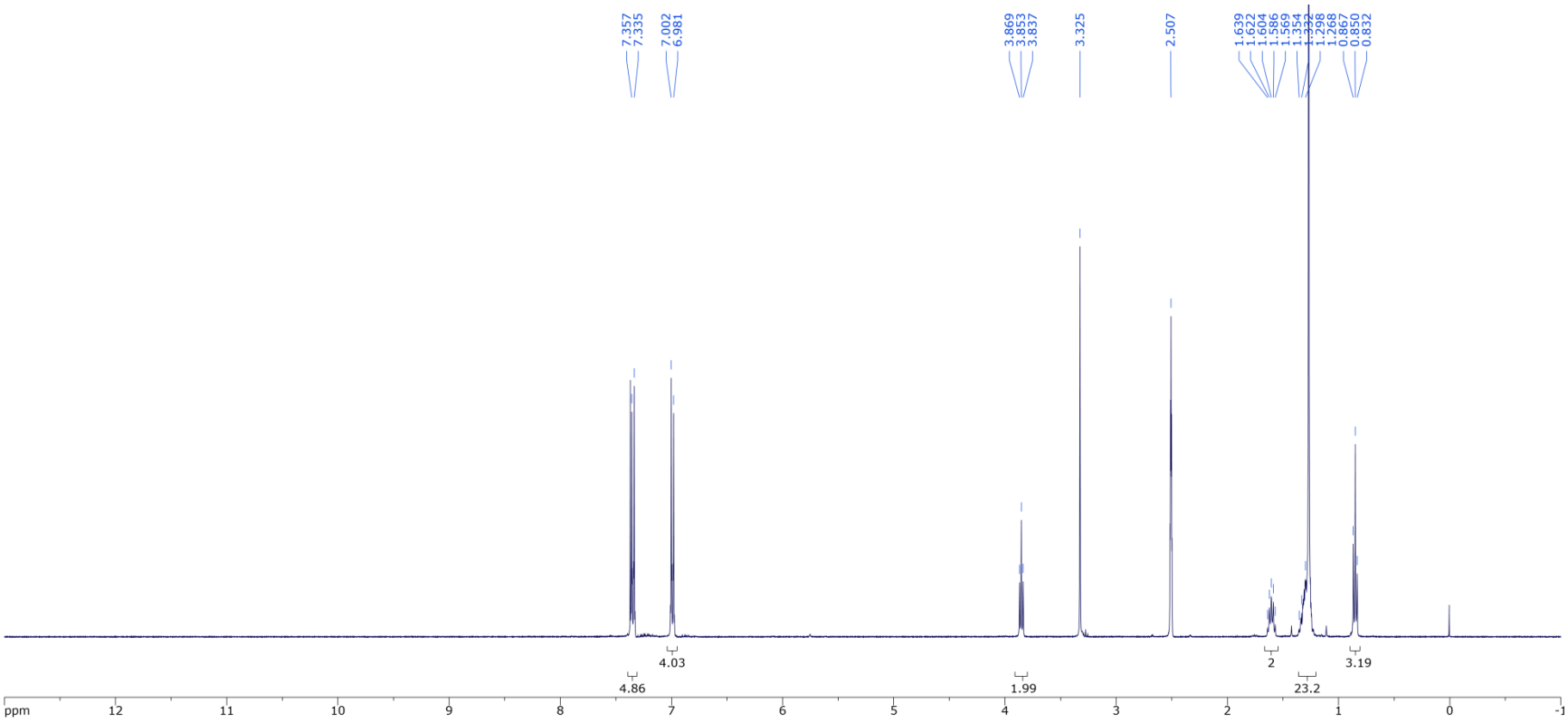
7.357
7.335
7.002
6.981
3.869
3.853
3.837
3.325
2.507
1.639
1.622
1.604
1.586
1.569
1.334
1.298
1.268
0.867
0.850
0.832
4.86
4.03
1.99
2
23.2
3.19
ppm
12
11
10
9
8
7
6
5
4
3
2
1
0
-1

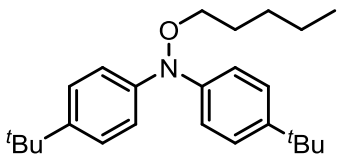
O
N
tBu
tBu

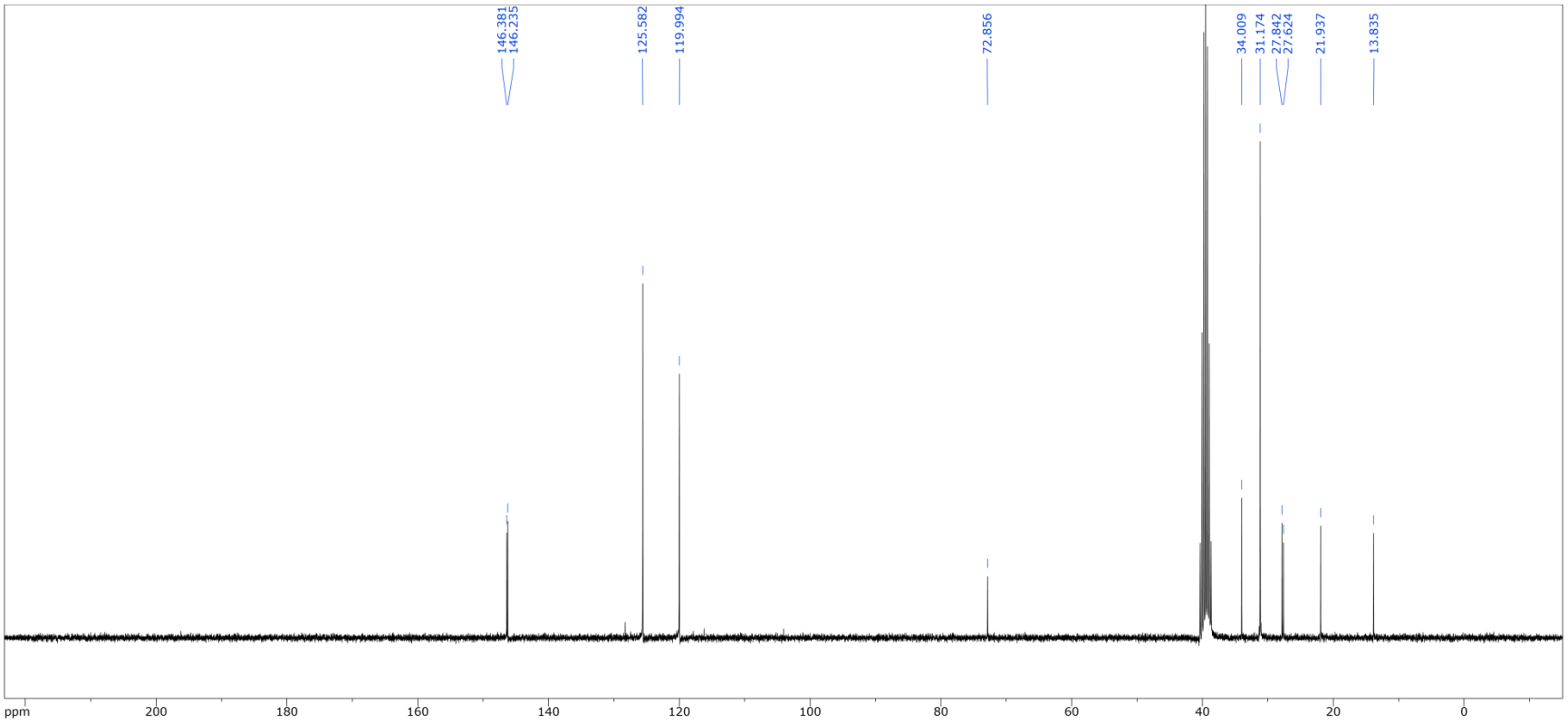
146.381
146.235
125.582
119.994
72.856
34.009
31.174
27.842
27.624
21.937
13.835
ppm
200
180
160
140
120
100
80
60
40
20
0

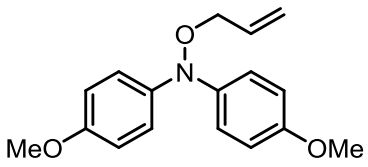
O
N
MeO
OMe

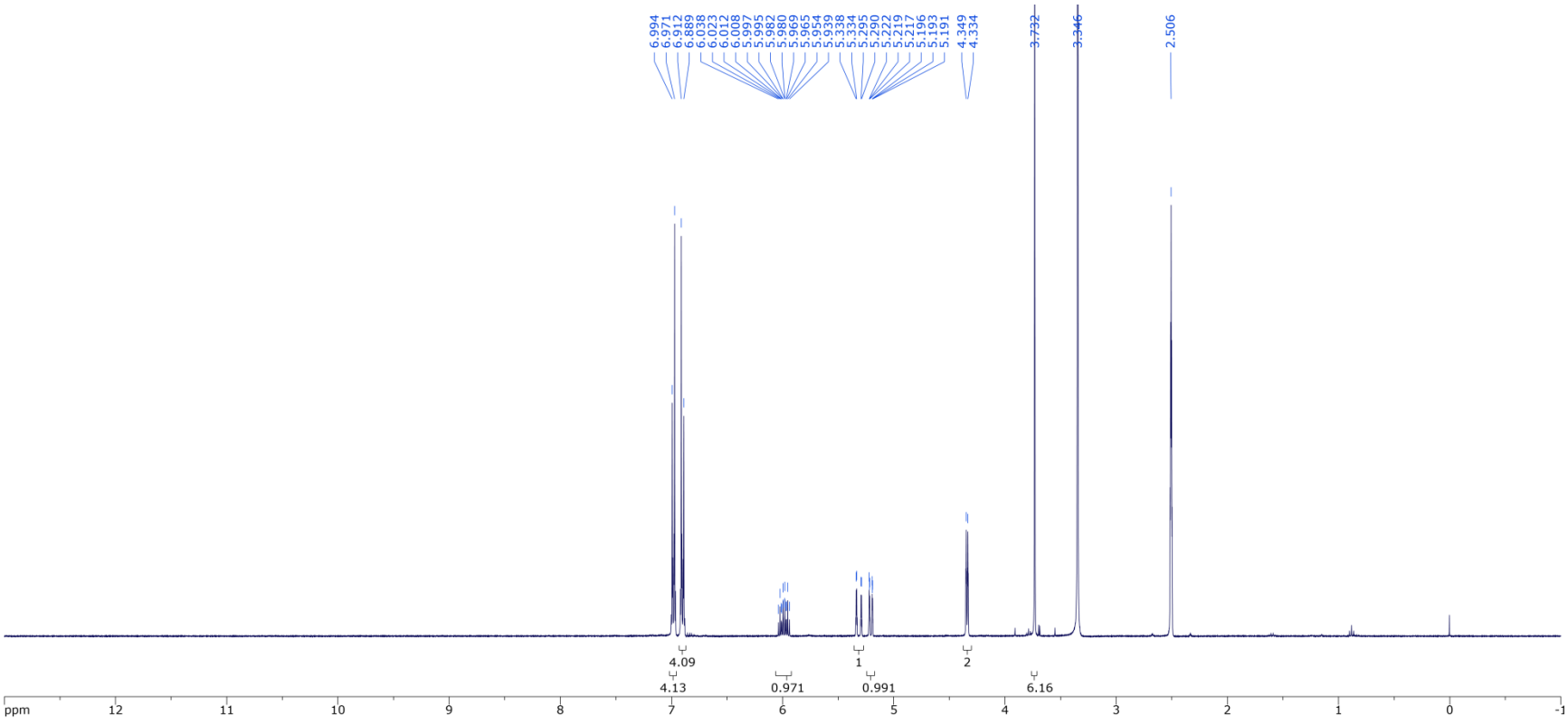
6.994
6.971
6.912
6.889
6.038
6.023
6.012
6.008
5.997
5.995
5.982
5.980
5.969
5.965
5.954
5.339
5.338
5.334
5.295
5.290
5.222
5.219
5.217
5.196
5.193
5.191
4.349
4.334
3.732
3.346
2.506
4.09
4.13
0.971
1
0.991
2
6.16
ppm
12
11
10
9
8
7
6
5
4
3
2
1
0
-1

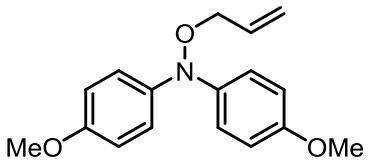
O
N
MeO
OMe

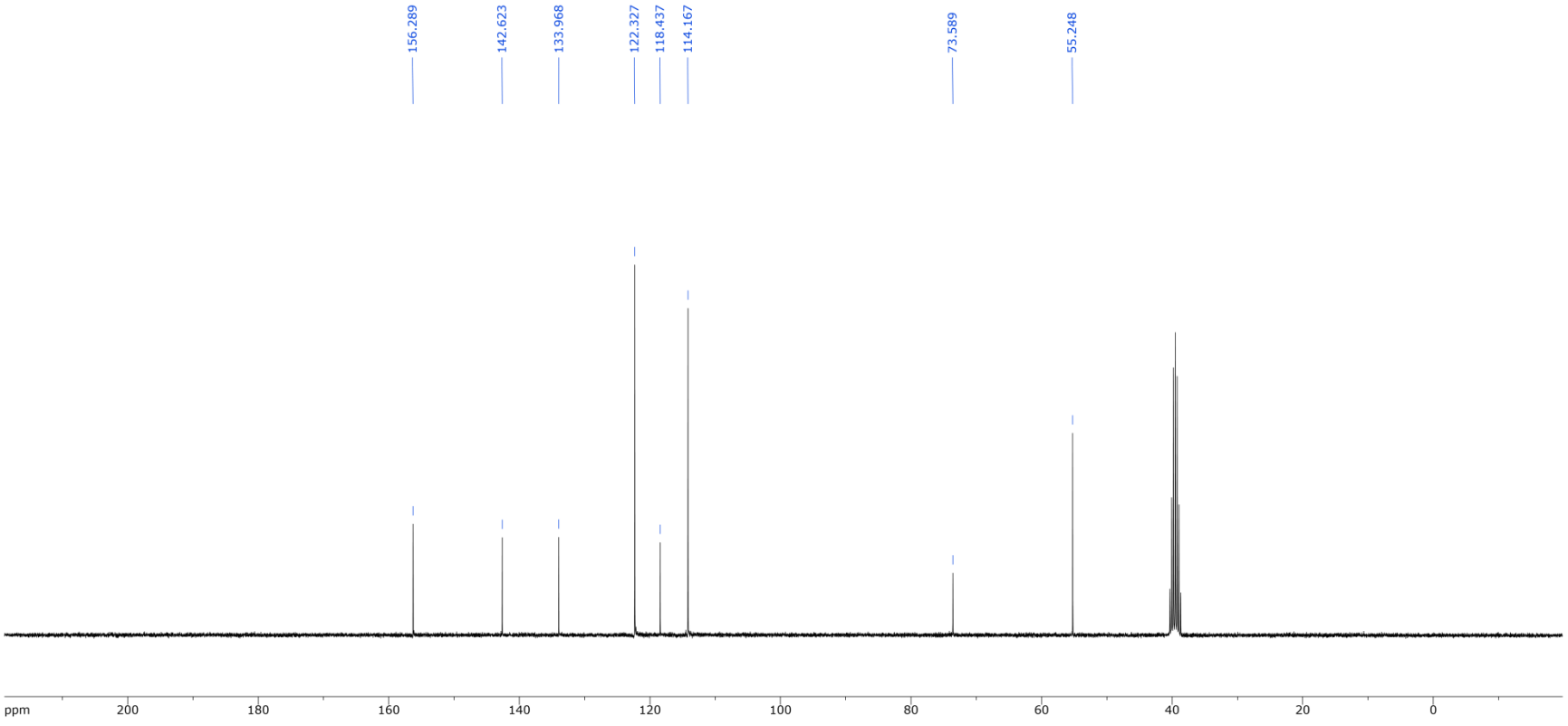
156.289
142.623
133.968
122.327
118.437
114.167
73.589
55.248
ppm
200
180
160
140
120
100
80
60
40
20
0

CHAPTER 9: Summary and Prospectus

The work described in thesis provides a clear step forward for both the study – and further development – of radical-rapping antioxidants (RTAs). New methodology has been developed for rapid and accurate measurements of the reactivity of RTAs at both ambient temperatures and in high temperature applications where they are often used industrially.[1,2] New mechanistic insights into the catalytic turnover of aminic RTAs have identified potential strategies for the development of even more effective oxidation inhibitors.[3,4] Syntheses of heterocyclic analogues of phenoxazine and phenothiazine have contributed to an understanding of the underlying reactivity behind these tricyclic RTAs, and has led to the development of the most reactive series of aminic antioxidants ever reported.

Development of the pro-fluorescent phosphine described in Chapter 2 has greatly simplified determination of hydroperoxides, the primary oxidation products formed in the autoxidation of hydrocarbons.[1,5] This has been used to evaluate the industrial potential of a series of heterocyclic diarylamines developed by our group (ch. 2),[6] turnover of both diarylamine (ch. 4)[3] and HALS-derived RTAs (ch. 5),[4] and the reactivity of a novel series of azaphenoxazine and azaphenothiazine RTAs (ch. 7). In addition to the work published in this thesis, this methodology has been subsequently adapted as part of an automated procedure to simultaneously quantify both hydroperoxides and carboxylic acids (another key autoxidation product)[7] – replacing laborious and time-consuming titrations for either product. The ability to monitor autoxidation and its inhibition in these complex systems may provide a valuable tool for deconvoluting the myriad interactions between RTAs, substrates, acids/bases, and the numerous other additives commonly present in lubricating oils (e.g. detergents, viscosity modifiers, etc.).

The PBD- and STY-BODIPY probes described in Chapter 3 allow accurate measurements of RTA reactivity under a range of experimental conditions. This method is easily adaptable to a wide

variety of substrates, temperatures, solvents, and rates of initiation, as well as mechanistic studies (i.e. kinetic solvent effect, kinetic isotope effect, and antioxidant co-operativity).[2] The approach has been used to study the kinetics of novel azaphenoxazines and azaphenothiazines (ch. 6 and 7),[8] polysulfide-1-oxide,[9] and hydropersulfide[10] RTAs, as well as performing mechanistic experiments on the unusual activity of nitroxide RTAs (ch. 8). Furthermore, application of this method in biphasic mixtures – namely egg phosphatidylcholine liposomes – has allowed the direct study of autoxidation and RTA activity under conditions representative of the cellular membranes in biological systems.[11,12] Given the versatility of this method over the more laborious O_2 consumption experiments historically used for RTA measurements, the PBD-/STY-BODIPY approach should continue to provide a rapid and accessible means for the study of autoxidation and RTA behaviour.

Kinetic and mechanistic studies on the decomposition of *N*,*N*-diarylalkoxyamines has revealed a novel mechanism for the proposed rate-limiting step in the Korcek catalytic cycle for diarylamine turnover.[3] This retro-carbonyl-ene (RCE) reaction is accessible to alkoxyamines activated on either the substrate- or amine-fragments of their structure, and is typically more rapid and higher yielding than the alternative N-O homolysis/disproportionation pathway. Despite previous studies performed by Korcek[13] and our group,[3] many questions remain concerning their proposed mechanism. Despite the proposed rate-limiting step being decomposition of RTA-derived diarylalkoxyamines, these compounds have not previously been detected in amine-inhibited autoxidations. Furthermore, there is currently no explanation of how formation of these alkoxyamines (let alone their decomposition into diarylamines) would be able to compete with propagation of the autoxidation. While both O_2 and diarylnitroxides react with alkyl radicals at approximately the same rate (~3×10^9 vs. 1.8×10^9 $M^{-1}s^{-1}$, see ch. 8), during the inhibited autoxidation reactions oxygen is often present in 50-100 fold excess over the nitroxide[3,6] – suggesting that O_2 addition (and thus propagation of the autoxidation) should be the predominant fate of alkyl radicals.

The discovery that nitroxides are capable of (catalytically) trapping oxygen centered radicals in the presence of carboxylic acids[14] represents a significant shift in the understanding of nitroxide antioxidant activity. The mechanistic investigations described in ch. 5 support this by identifying the stoichiometric reductant (namely the chain-carrying alkyl radicals), determining that the proposed electron transfer reaction is kinetically competent for inhibition, and confirming that carboxylic acids generated *in situ* are responsible for this activity in high-temperature autoxidation.[4] The viability of this mechanism at ambient temperatures suggests that it could play a role in the biological activity of nitroxides, as well. In fact, it has subsequently been invoked in the biological activities of ferroptosis inhibitors, liproxstatin-1 and ferrostatin-1 which are expected to oxidize to nitroxides as they trap radicals.[11] The significance of this mechanism to understanding nitroxide RTA activity suggests that it will remain important both in biological and industrial settings.

The synthesis and kinetic characterization of novel azaphenoxazine and azaphenothiazine RTAs, as described in chapters 6 and 7, has revealed that they are among the most reactive class of antioxidants ever reported.[8] The key to the synthesis of the more reactive 2- and/or 4-aza isomers lies in obtaining the correct amide/halide polarity for the Cu-catalyzed ring-forming reaction. Easily accessed (2'-aminophenyl)-4-pyrimidyl ethers/sulfides undergo a favorable Smiles rearrangement, leading to the unreactive 1- and/or 3-aza isomers instead. The high reactivity of these compounds was subsequently found to translate to high temperatures as well, where they were found to be catalytically active and often outperformed even the most reactive diarylamine RTAs previously reported by our group.[6] Catalytic turnover of these RTAs was not limited to very high temperature autoxidations. Extended inhibition times were observed in 1-hexadecene autoxidations at 70 and 100°C – often corresponding to stoichiometric numbers between 60 and 120. The remarkable activity of these compounds at elevated temperatures underscores the important balance between the reactivity and stability required to maximize RTA efficacy in these systems. Additional work is currently underway in our lab to explore the efficacy of substituted phenoxazine RTAs in high

temperature applications.[15] Taken together with this work, we hope to establish a model that will assist in understanding the influence of the both of these factors, and enable the design of RTAs with the optimal balance between reactivity and stability.

Both di-*tert*-alkyl and diarylnitroxides are catalytic inhibitors in autoxidations of olefinic substrates (e.g. styrene, 1-hexadecene, cyclooctene, norbornene), inhibiting far longer and more effectively than their precursor amines. In substrates without alkenes (e.g. cumene, ethylbenzene, 1,4-dioxane), however, these same nitroxides show very little inhibitory activity. Under identical conditions, *N*,*N*-diarylalkoxyamines and oxoammonium salts – key intermediates in the previously explored catalytic cycles (ch. 4 and 5)[3,4] – also had no effect, indicating that this inhibition likely occurs through another path. Our hypothesis is that small concentrations of hydroperoxyl radicals (HOO•) are produced during autoxidation of alkenes. HOO• is a capable reductant,[16] and is believed to reduce nitroxides to the hydroxylamines which function as the RTA. The mechanism behind the formation of HOO• is currently being explored both computationally and through mechanistic experiments designed to identify the key steps in the process, and is believed to arise from the *β*-alkylperoxy peroxyl radicals formed from addition of peroxyl radicals to alkenes. The formation of HOO• would represent a minor *but critically important* pathway in alkene autoxidation. If formed, RTAs (such as nitroxides) which utilize HOO• as a stoichiometric reductant could be designed as incredible effective inhibitors. Furthermore, as many polymers and lubricating oils already contain varying amounts of unsaturation, HOO• formation may already be occurring in these systems, and may already be responsible for catalytic turnover of nitroxide RTAs in these applications.

References

(1) Hanthorn, J.; Haidasz, E.; Gebhardt, P.; Pratt, D. *Chem. Commun.* **2012**, *48*, 10141–10143.

(2) Haidasz, E. A.; Van Kessel, A. T. M.; Pratt, D. A. *J. Org. Chem.* **2016**, *81*, 737–744.

(3) Haidasz, E. A.; Shah, R.; Pratt, D. A. *J. Am. Chem. Soc.* **2014**, *136*, 16643–16650.

(4) Haidasz, E. A.; Meng, D.; Amorati, R.; Baschieri, A.; Ingold, K. U.; Valgimigli, L.; Pratt, D. A. *J. Am. Chem. Soc.* **2016**, *138*, 5290–5298.

(5) Jensen, R. K.; Korcek, S.; Mahoney, L. R.; Zinbo, M. *J. Am. Chem. Soc.* **1979**, *101*, 7574–7584.

(6) Shah, R.; Haidasz, E. A.; Valgimigli, L.; Pratt, D. A. *J. Am. Chem. Soc.* **2015**, *137*, 2440–2443.

(7) Shah, R.; Pratt, D. A. *J. Org. Chem.* **2016**, *81*, 6649–6656.

(8) Haidasz, E. A.; Pratt, D. A. *Org. Lett.* **2017**, *19*, 1854–1857.

(9) Chauvin, J.-P. R.; Haidasz, E. A.; Griesser, M.; Pratt, D. A. *Chem. Sci.* **2016**, *7*, 6347–6356.

(10) Chauvin, J.-P. R.; Griesser, M.; Pratt, D. A. *J. Am. Chem. Soc.* **2017**, *139*, 6484–6493.

(11) Zilka, O.; Shah, R.; Li, B.; Friedmann Angeli, J. P.; Griesser, M.; Conrad, M.; Pratt, D. A. *ACS Cent. Sci.* **2017**, *3*, 232–243.

(12) Van Kessel, A. T. M.; Shah, R.; Haidasz, E. A.; Pratt, D. A.; *Manuscript in praparation*.

(13) Jensen, R. K.; Korcek, S.; Zinbo, M.; Gerlock, J. L. *J. Org. Chem.* **1995**, *60*, 5396–5400.

(14) Amorati, R.; Pedulli, G. F.; Pratt, D. A.; Valgimigli, L. *Chem. Commun.* **2010**, *46*, 5139–5141.

(15) Farmer, L.; Haidasz, E. A.; Griesser, M.; Pratt, D. A.; *Manuscript in preparation*.

(16) Cedrowski, J.; Litwinienko, G.; Baschieri, A.; Amorati, R. *Chem. - A Eur. J.* **2016**, *22*, 16441–16445.